National Library
of Canada

Bibliothèque nationale
du Canada

Canadian Theses Service

Service des thèses canadiennes

Ottawa, Canada
K1A 0N4

NOTICE

The quality of this microform is heavily dependent upon the quality of the original thesis submitted for microfilming. Every effort has been made to ensure the highest quality of reproduction possible.

If pages are missing, contact the university which granted the degree.

Some pages may have indistinct print especially if the original pages were typed with a poor typewriter ribbon or if the university sent us an inferior photocopy.

Previously copyrighted materials (journal articles, published tests, etc.) are not filmed.

Reproduction in full or in part of this microform is governed by the Canadian Copyright Act, R.S.C. 1970, c. C-30.

AVIS

La qualité de cette microforme dépend grandement de la qualité de la thèse soumise au microfilmage. Nous avons tout fait pour assurer une qualité supérieure de reproduction.

S'il manque des pages, veuillez communiquer avec l'université qui a conféré le grade.

La qualité d'impression de certaines pages peut laisser à désirer, surtout si les pages originales ont été dactylographiées à l'aide d'un ruban usé ou si l'université nous a fait parvenir une photocopie de qualité inférieure.

Les documents qui font déjà l'objet d'un droit d'auteur (articles de revue, tests publiés, etc.) ne sont pas microfilmés.

La reproduction, même partielle, de cette microforme est soumise à la Loi canadienne sur le droit d'auteur, SRC 1970, c. C-30.

NL-339 (r. 88/04)

Canada

THE UNIVERSITY OF ALBERTA

PETROGENESIS OF QUATERNARY ALKALINE LAVAS IN WELLS GRAY PROVINCIAL PARK, B.C. AND CONSTRAINTS ON THE PETROLOGY OF THE SUBCORDILLERAN MANTLE

by

Paul Metcalfe

A THESIS

SUBMITTED TO THE FACULTY OF GRADUATE STUDIES AND RESEARCH

IN PARTIAL FULFILMENT OF THE REQUIREMENTS FOR THE DEGREE

OF Doctor of Philosophy

Department of Geology

EDMONTON, ALBERTA

Fall 1987

Permission has been granted to the National Library of Canada to microfilm this thesis and to lend or sell copies of the film.

The author (copyright owner) has reserved other publication rights, and neither the thesis nor extensive extracts from it may be printed or otherwise reproduced without his/her written permission.

L'autorisation a été accordée à la Bibliothèque nationale du Canada de microfilmer cette thèse et de prêter ou de vendre des exemplaires du film.

L'auteur (titulaire du droit d'auteur) se réserve les autres droits de publication; ni la thèse ni de longs extraits de celle-ci ne doivent être imprimés ou autrement reproduits sans son autorisation écrite.

ISBN 0-315-41165-1

University of Alberta
Edmonton

Department of Geology

Canada T6G 2E3

158 Earth Sciences Building, Telephone (403) 432-3265

Ph. (403)432-3583
1st June, 1987.

British Columbia Ministry of the Environment
Surveys and Resource Mapping Department
Parliament Buildings
Victoria, B.C.
V8V 1X5

Dear Sir,

I am a graduate student at the University of Alberta, currently completing my Ph.D. thesis in geology. The thesis addresses the volcanoes of the Wells Gray-Clearwater area in east-central British Columbia and includes physiographic descriptions of ten of the volcanoes in the area. The descriptions in the thesis would be greatly enhanced by reproductions of several stereographic aerial photographs published by your department. The pertinent photographs are numbers BC7324-63, BC7324-64, BC7324-65, BC7323-221, BC7323-222, BC78099-131, BC78099-132, BC1744-10, BC1744-11, BC1744-12, BC5049-72, and BC5049-73.

I would be grateful, therefore, if you could permit me to reproduce these photographs in my thesis in order to illustrate more clearly these features. I hereby declare that these reproductions will not be used for financial gain, that no will subsequent use will be made of them without further written permission from your department and that their source will be acknowledged, both in the plate captions and in the appropriate section in the thesis text.

I trust that I have given you sufficient information about the aerial photographs. My thesis will be defended on June 4th and will be complete shortly afterwards. Please do not hesitate to contact me, should you require additional information.

Yours sincerely,

P. Metcalfe

Paul Metcalfe

Province of
British Columbia

Ministry of
Environment
and Parks
SURVEYS AND
RESOURCE MAPPING

Parliament Buildings
Victoria
British Columbia
V8V 1X5

87-06-09

Mr. Paul Metcalfe
Department of Geology
University of Alberta
158 Earth Science Building
Edmonton, Alberta
T6G 2E3

Dear Mr. Metcalfe:

Thank you for your letter dated June 1st, requesting permission to reproduce Province of British Columbia aerial photographs as part of your thesis. The statement in paragraph two of your letter promising an appropriate credit line is acceptable and permission is granted for you to reproduce the requested photographs.

Good luck in the defense of your thesis.

Yours truly

Chris Reich

Chris D. Reich
Head, Distribution Services
MAPS-B.C.

CDR:mb

THE UNIVERSITY OF ALBERTA

RELEASE FORM

NAME OF AUTHOR Paul Metcalfe

TITLE OF THESIS **PETROGENESIS OF QUATERNARY ALKALINE LAVAS IN WELLS GRAY PROVINCIAL PARK, B.C. AND CONSTRAINTS ON THE PETROLOGY OF THE SUBCORDILLERAN MANTLE**

DEGREE FOR WHICH THESIS WAS PRESENTED Doctor of Philosophy

YEAR THIS DEGREE GRANTED Fall 1987

Permission is hereby granted to THE UNIVERSITY OF ALBERTA LIBRARY to reproduce single copies of this thesis and to lend or sell such copies for private, scholarly or scientific research purposes only.

The author reserves other publication rights, and neither the thesis nor extensive extracts from it may be printed or otherwise reproduced without the author's written permission.

(SIGNED) P Metcalfe

PERMANENT ADDRESS:

c/o The Castlemans' Society
University College, The Castle
DURHAM, England

DATED October 9th 1987

THE UNIVERSITY OF ALBERTA

FACULTY OF GRADUATE STUDIES AND RESEARCH

The undersigned certify that they have read, and recommend to the Faculty of Graduate Studies and Research, for acceptance, a thesis entitled **PETROGENESIS OF QUATERNARY ALKALINE LAVAS IN WELLS GRAY PROVINCIAL PARK, B.C. AND CONSTRAINTS ON THE PETROLOGY OF THE SUBCORDILLERAN MANTLE** submitted by Paul Metcalfe in partial fulfilment of the requirements for the degree of Doctor of Philosophy.

C.M. Scarfe for
Supervisor

H. Baadsgaard

G.L. Cumming

R.A. Burwash

External Examiner

Date ....

To my father, who taught me the first R; to my mother, who taught me the third R and to Lyn, who prodded me to finish the second R.

Abstract

Basaltic volcanism in the area of Wells Gray Provincial Park, east-central British Columbia, represents some of the youngest volcanic material in the Canadian Cordillera. Basalts were erupted from eleven of the centres in the area over a period of time from 0.3 Ma to as little as 300 a B.P.. The centres are pre-, syn- and postglacial, are usually polygenetic and are, with one exception, of central type. The maximum volume of lava erupted from any centre is 0.3 km^3, suggesting that the volcanoes separated by greater than 10 km have discrete source regions. Lavas erupted from these later centres are mainly alkaline and olivine-clinopyroxene phyric and contain olivine and clinopyroxene xenocrysts. One centre has erupted lavas of transitional tholeiitic composition which are olivine-plagioclase phyric.

The alkaline lavas contain abundant xenoliths of Cr-spinel lherzolite, spinel clinopyroxenite and, rarely, ferroan websterite and spinel wehrlite. Clinopyroxene xenocrysts within the alkaline lavas are of four discrete compositions, similar to those found in xenoliths. This indicates the presence of mineralogical and chemical heterogeneity in the subcordilleran mantle.

One spinel clinopyroxenite xenolith from the area contains kaersutite in equilibrium with the clinopyroxene. The kaersutite is interpreted as a primary mineral in this assemblage and part of a possible source assemblage for the host lava. The occurrence is the second reported for the Canadian Cordillera. A small inclusion of websterite contains the one of the first reported occurrences of primary apatite in a mantle assemblage. The apatite occurs as sealed inclusions, 50 µm in size, in clinopyroxene.

Mg numbers in most of the Wells Gray lavas vary between 60 and 66. There is no systematic increase in Rb/Sr with alkali content and Cr, Ni and Co are relatively high, indicating that the lavas are near-primary in composition. Their slight enrichment in Fe may indicate derivation from a relatively iron-rich source. The incompatible element

compositions of the alkaline lavas are strongly enriched relative to chondritic abundances and show as much as 30% variation in lavas from earlier and later phases of activity at a single centre, a variation which is too great to be produced by crystal fractionation. The variation is interpreted as being the result of partial melting of slightly different source volumes, a later partial melting event taking place in a source region which includes the region of residuum from a previous event.

The concentrations of incompatible elements and the $^{143}Nd/^{144}Nd$ and $^{87}Sr/^{86}Sr$ ratios of the lavas define two lava types. Type 1 is enriched in Ba and $^{87}Sr/^{86}Sr$ and depleted in Zr and $^{143}Nd/^{144}Nd$ relative to Type 2. The isotopic variation is subparallel to the array of ocean island basalts and is interpreted as the result of mixing between a mid-ocean ridge basalt isotopic component and an undepleted mantle isotopic component. In at least one centre of each lava type, the Sm/Nd and $^{143}Nd/^{144}Nd$ ratios show an inverse correlation with P_2O_5, suggesting that the ratios are controlled, at least in part, by melting of, or equilibration of the lavas with, a phosphate phase in the mantle.

The chemical, mineralogical and isotopic heterogeneity of the Wells Gray alkaline lavas is interpreted as being representative of heterogeneity in the subcordilleran mantle. The discovery of volatile rich phases indicates that at least one metasomatic event has enriched the source regions in incompatible elements and has probably resulted in the formation of an amphibole source phase. This enrichment is a necessary precursor to the generation of lavas with high concentrations of these elements, from small, discrete source volumes in the subcordilleran mantle.

Acknowledgements

Many people have contributed to every aspect of this thesis. First and foremost, I thank my parents who did everything possible to encourage me in my career in geology.

Grant-in-aid number 55-30135 from the Boreal Institute for Northern Studies funded the entirety of the fieldwork for the thesis, as well as being almost the sole contributor in preparation of the thesis. My sincerest thanks go to the staff of the Institute, in particular Anita Moore, Lyn Frasch and Simonne Rogianni, for their administration of this grant. I am grateful to the B.C. Ministry of Parks and Environment, both for their granting of permission to work in Wells Gray Park and for their courtesy in permitting the reproduction of the aerial photographs which are included in the photographic plates. Funding for part of the whole rock chemical analyses is from contract DSS EMR 0SB83 00319. I am indebted to Drs. F.J. Longstaffe, R.A. Burwash and R.D. Morton for their financial assistance through teaching contracts and assistantships during the final part of the study. I wish to thank, also, the members of my thesis defence committee, particularly Dr. J.N. Ludden of the Université de Montréal. Sincere thanks are also due to Terry Krissie of the department of International Student Services, for arranging the bursary which helped me to finish, and to Dr. F. Chia of the Faculty of Graduate Studies for his aid at a crucial time.

This thesis would never have been finished without the help of the following people. Foremost are Lyn Frasch, for the encouragement and help which she gave me in the preparation of the thesis itself, and Pat Cavell and Jan Wijbrans for their thorough, yet encouraging, reviews of the manuscript. The isotope work would not have been started, far less completed, without the guidance of Alan Smith. Dr. T. Yanagi contributed greatly to the research during his stay at the university. I also thank Drs. H. Baadsgaard and R. St.J. Lambert for allowing me the use of their laboratory facilities. Dr. G.L. Cumming of the Department of Physics was courteous in letting me work on the final stages of my thesis in the mass spectrometer lab; Dragan Krstic even more so in putting up with me for 18 months in his work space.

Fieldwork could not have been conducted in Wells Gray Park without the help of B.C. Parks, particularly Pat Rogers, the warden of Wells Gray Park, and Trevor Goward, the park naturalist. Catherine M. Elléon, Jennifer Gibbs and Dennis R. Bull, my field assistants over the course of three different field trips, were indefatigable in their pursuit of all peaks from Pyramid Mountain upward. My thanks also go to Catherine J. Hickson and Jack Souther of the Geological Survey of Canada for their help and advice both in the field and in discussion of the Wells Gray lavas.

I extend my sincerest thanks to the entire isotope research group here in Physics, for their help in the isotope lab and their subsequent adoption of me and also to Dave Tomlinson and Steve Launspach for their help and advice during the course of my work with the electron microprobe. Todd Dunn was extremely generous with his time in the building and initial calibration of the vacuum fusion system. Garth Milvain and Ron Stewart helped with computer account funds. My thanks for their moral support also go to Paul and Fiona Lhotka and my other friends among the alumni from the University of Manitoba. Doug, Brenda, Maxine, Adam, Drew, Maria, Jim, Jackie and, of course, Marvin and Elrod formed the surroundings which made the system bearable. Last of all, I would like to thank my supervisor, Dr. C.M. Scarfe.

Table of Contents

Chapter Page

1\.

INTRODUCTION 1

A. Tectonostratigraphic History 2

B. Present tectonic setting 6

C. Lithospheric structure and constraints on the nature of the source region from geophysical studies 7

Gravity studies 7

Natural seismicity 8

Seismic refraction studies 9

Magnetotelluric studies 10

D. Geochemical and petrological constraints on the nature of the source region 11

E. Summary 13

2\.

PHYSICAL VOLCANOLOGY 15

A. Spanish Creek area 15

Spanish Mump 17

Spanish Bonk 17

Hyalo Ridge 17

Spanish Lake Centre 19

Flourmill Centre 21

B. Pyramid Mountain 22

C. Ray Lake area 23

Ray Mountain 23

Pointed Stick Cone and Ray Ridge 28

Dragonhead Centre 29

D. Kostal Lake Area 31

Kostal Lake 31

E. Summary and age relations 34

3.

PETROGRAPHY 36

A. Descriptive petrography by centre 36

Spanish Mump 36

Spanish Bonk 37

Hyalo Ridge 38

Spanish Lake Centre 39

Flourmill Centre 40

Pyramid Mountain 41

Ray Mountain 42

Ray Ridge 45

Pointed Stick Cone 46

Dragonhead Centre 46

Kostal Lake Centre 48

Summary of lava petrography 51

B. Ultramafic xenoliths 51

Spinel lherzolite assemblage 52

Clinopyroxenites 54

Plagioclase clinopyroxenites 54

Cumulate xenoliths 55

Summary of ultramafic xenolith petrography 55

C. Volatile bearing phases 56

Phlogopite 56

Kaersutite 56

Apatite 56

4.

MINERAL CHEMISTRY 58

A. Analytical procedure 58
Electron microbeam analysis 58
Analytical precision 59
B. Analytical results 59
Clinopyroxene 59
Olivine 73
Plagioclase 77
Oxide minerals 80
Orthopyroxene 83
Amphibole 84
Apatite 87
Sulphide minerals 87
C. Xenolith thermometry 87
D. Summary 89
5.
WHOLE ROCK CHEMISTRY 91
A. Analytical procedure 91
Sample selection 91
Sample preparation 92
Whole rock chemical analysis 92
Analytical precision and uncertainty 92
Determination of ferric iron 93
B. Analytical results 93
Normative mineralogy and chemical classification 93
Major elements 95
Trace element variation 101
C. Generation of the Wells Gray lavas 115
D. Summary 122

6.
ISOTOPIC ANALYSIS 124
A. Analytical procedure 124
Sample selection 124
Sample preparation 125
Isotopic analysis 126
Analytical precision and reproducibility 126
B. Analytical results 126
Isotopic ratios of Sr and Nd 126
Sm and Nd concentrations 137
C. Summary 144
7.
VOLATILE CONCENTRATIONS 146
A. Analytical procedure 147
Sample selection 147
Petrography of volcanic glass 147
Petrography of glass inclusions 148
Sample preparation 150
Apparatus 150
Analytical precision and error 152
B. Analytical results 155
C. Summary 157
8.
CONCLUSION 159
A. Results 159
B. Possible sources for magma 163
C. Petrogenesis of the Wells Gray lavas 165
LIST OF REFERENCES 168
PHOTOGRAPHIC PLATES 176

APPENDIX A
ELECTRON MICROBEAM ANALYSIS 189

Sample selection 189

Sample preparation 189

Analytical procedure 189

Analytical results 190

APPENDIX B
MINERAL CHEMISTRY 195

APPENDIX C
CHEMICAL AND ISOTOPIC ANALYSIS 355

A. Sample selection 355

B. Sample preparation 355

C. Whole rock chemical analysis 355

D. Isotopic analysis 364

Sample preparation 364

Mass spectrometry 365

APPENDIX D
WHOLE ROCK CHEMISTRY 367

APPENDIX E
VACUUM FUSION APPARATUS 391

Construction 391

Problems in operation and sources of contamination 391

Present operating procedure of the vacuum fusion system 392

List of Tables

Table Page

1 Symbols and sample suffixes used for centres described in the text 8

2 Predicted and observed partition coefficients (χ(amphibole)/χ(pyroxene)) for two xenoliths in British Columbia 117

3 Concentrations of major elements in amphibole mass-balance calculation 119

4 Results of isotopic analyses 127

5 Major oxide, H_2O and CO_2 concentrations in volcanic glasses 154

A-1 Mineral standards used for analysis by electron microprobe 192

A-2 Chemical compositions of mineral standards used 193

A-3 Analytical precision in microprobe analysis 194

B-1 Major element concentrations in clinopyroxene 196

B-2 Major element concentrations in incognate clinopyroxene 223

B-3 Major element concentrations in olivine 236

B-4 Major element concentrations in incognate olivine 275

B-5 Major element concentrations in plagioclase 279

B-6 Major element concentrations in incognate plagioclase 296

B-7 Major element concentrations in oxide 302

B-8 Major element concentrations in incognate oxide 333

B-9 Major element concentrations in incognate orthopyroxene 340

B-10 Major element concentrations in amphibole 344

B-11 Major element concentrations in incognate apatite 346

B-12 Major element concentrations in sulphide 347

B-13 Major element concentrations in whole glass 349

C-1 Analytical results for U.S.G.S. whole rock standards 357

C-2 Replicate whole rock analyses 359

C-3 Analytical precision in whole rock analyses 363

Table Page

D-1 Major oxide and trace element concentrations in samples of whole rock 368

List of Figures

Figure Page

1 Tectonic setting of the Canadian Cordillera 3

2 Volcanoes and lava flows studied in the Wells Gray area 16

3 Spanish Creek area, showing the five volcanic centres 18

4 Ray Mountain area, showing the four areas studied 24

5 Detailed map of the Ray Mountain centre 25

6 Cross section through the Ray Mountain centre 26

7 Kostal Lake area, showing the volcanic centre 32

8 Clinopyroxenes from Spanish Bonk 61

9 Clinopyroxenes from Hyalo Ridge 62

10 Clinopyroxenes from Spanish Lake 63

11 Clinopyroxenes from Flourmill Centre 64

12 Clinopyroxenes from Ray Mountain 65

13 Clinopyroxenes from Pointed Stick Cone and Ray Ridge 66

14 Clinopyroxenes from Dragonhead 67

15 Clinopyroxenes from Kostal Lake 68

16 Clinopyroxenes from the xenoliths 69

17 Na_2O against TiO_2 in clinopyroxenes 70

18 Summary of clinopyroxene compositions from Wells Gray Park 71

19 Pyroxene quadrilateral showing pairs selected for thermometry 72

20 Range of olivine and orthopyroxene compositions for each centre 75

21 Compositional ranges of plagioclase in Wells Gray Park 78

22 Compositional ranges of plagioclase in Wells Gray Park 79

23 T - fO_2 diagram from co-existing oxide pairs 81

24 Cr against Al for xenophyric and xenolith spinels 82

25 TiO_2 against K_2O for the Dragonhead amphiboles 86

Figure Page

26 Weight % SiO_2 against weight percent total alkalies 94

27 Weight % MgO against weight % Al_2O_3 97

28 Total Fe, as weight percent FeO, against MgO 98

29 Weight % K_2O against weight percent Na_2O 100

30 MgO against Ni for the Wells Gray lavas 102

31 Weight percent MgO against Cr for the Wells Gray lavas 104

32 CaO against V in the Wells Gray lavas 105

33 Sr against Nb for the Wells Gray lavas 106

34 Ba against Sr for the Wells Gray lavas 108

35 Zr against Ba for the Wells Gray lavas 109

36 Zr against Nb for the Wells Gray lavas 110

37 Ba against Nb for the Wells Gray lavas 111

38 Weight % P_2O_5 against Sr for the Wells Gray lavas 112

39 Cl against P_2O_5 for the Wells Gray lavas 113

40 Cl against Nb for the Wells Gray lavas 114

41 Structure of an amphibole, viewed along the z axis 121

42 Sr and Nd isotopic compositions of the Wells Gray lavas 128

43 Comparison of isotopic data with those from other basaltic rocks 130

44 $1/P_2O_5$ against Nd isotopic composition 134

45 P_2O_5 against Nd isotopic composition 135

46 Maximum Cl for a sample suite against Nd isotopic composition 138

47 P_2O_5 (wt.%) against Sm in the Wells Gray lavas 140

48 P_2O_5 (wt.%) against Nd in the Wells Gray lavas 141

49 $1/P_2O_5$ (wt.%) against Sm/Nd in the Wells Gray lavas 142

50 Vacuum fusion apparatus used in volatile analysis 151

51 Schematic time-pressure diagram of a vacuum fusion analysis 153

Figure Page

52 CO_2 against H_2O for volcanic glasses 156

53 H_2O against P_2O_5 for volcanic glasses 158

54 The subcordilleran mantle of British Columbia 164

55 Possible methods of generation of the Wells Gray lavas 166

List of Plates

Plate Page

1A Hyalo Ridge, seen from the south across Spanish Lake 177

1B Section exposed on the east flank of Hyalo Ridge 177

1C View along the section through the Hyalo Ridge lava cap 177

1D Pillow lavas in the distal portion of a flow on Hyalo Ridge 177

1E Blast pit in the easternmost crater of the Spanish Lake centre 177

1F Lava flow from a flank eruption in Spanish Lake centre 177

3 Stereographic aerial photograph of the Spanish Lake centre 178

4 Stereographic aerial photograph of the Flourmill centre 179

4A Layered cinders and agglutinate in Flourmill centre 180

4B Lava squeeze-up in the southwest crater of Flourmill centre 180

4C Drained lava lake in the northwest cone of the Flourmill centre 180

4D Explosion pit surrounded by a ring of scoria 180

4E Volcanic bombs from the northwest part of the Flourmill centre 180

4F Pyramid Mountain seen from the south 180

5A The fissure structure in the Ray Mountain centre 181

5B View southward along the Ray Mountain fissure towards Key Puy 181

5C Dyke intruded during the earlier phase of activity 181

5D Basal contact of Ray Mountain hyaloclastite 181

5E Stratigraphic section through Ray Mountain 181

7 Stereographic aerial photograph of the Dragonhead centre 182

7A Dragonhead cone from the air across the Falls Creek valley 183

7B Dragonhead cone from the northeast 183

7C Breach in Dragonhead cone 183

7D Vertical contact of distal Dragonhead flow with mica schist 183

7E Tree mould in the distal portion of the Dragonhead flow 183

Plate		Page
7F	Section from the base of the Dragonhead flow, distal portion	183
9	Stereographic aerial photograph of the Kostal Lake centre	184
9A	Kostal Lake centre from the air	185
9B	Kostal Lake centre from the air	185
9C	View across the flow from the north cone at Kostal Lake	185
9D	The south cone of the Kostal Lake centre, seen from the air	185
9E	The south cone of the Kostal Lake centre from the northwest	185
9F	The breach in the south cone	185
10A	Photomicrograph of hyaloclastite from Spanish Mump	186
10B	Clinopyroxene xenocrysts in lava from Spanish Bonk	186
10C	Hyaloclastite from Hyalo Ridge	186
10D	Olivine xenocryst showing embayed margins	186
10E	Glass fragment from Pyramid Mountain showing oxidation	186
10F	Hyaloclastite from Ray Mountain	186
11A	Protoclastic aluminous spinel wehrlite	187
11B	Porphyroclastic Cr-spinel lherzolite	187
11C	Cr-spinel wehrlite, exhibiting tabular equigranular texture	187
11D	Cr-spinel lherzolite, exhibiting mosaic equigranular texture	187
11E	Protoclastic Al-spinel clinopyroxenite	187
11F	Porphyroclastic wehrlite	187
12A	Kaersutitic amphibole in an aluminous spinel clinopyroxenite	188
12B	Kaersutitic amphibole in an aluminous spinel clinopyroxenite	188
12C	Websterite with primary apatite enclosed in clinopyroxene	188
12D	Primary apatite grains in clinopyroxene	188
12E	Electron photomicrograph of apatite grain analysed	188
12F	Devitrified melt inclusion in an olivine phenocryst	188

Table 1

Symbols and sample suffixes used for centres described in the text

Unit	Suffix	Symbol
Spanish Mump	SM	[‡]
Spanish Bonk	SB	[‡]
Hyalo Ridge	ST	⍓
Spanish Lake Centre	SL	⊠
Flourmill Centre	SC	⊞
Pyramid Mountain	PY	+
Spahats (Second Canyon dyke)	SP	X
Ray Mountain	RM	🄨
Ray Ridge	RR	‡
Pointed Stick Cone	RC	‡
Dragon's Tongue	R	Δ
Dragon's Tongue (proximal)	RP	Δ
Dragon's Tongue (distal)	RD	Δ
Kostal Lake	KL	O
Kostal Lake (older lavas)	KP	O
Kostal Lake (north cone)	KN	O
Kostal Lake (south cone)	KS	O
Kostal Lake (lava tube)	KT	O

INTRODUCTION

The purpose of this study is to determine the petrogenesis of alkaline lavas in an intraplate tectonic setting near a continental margin. The area selected for study is centred on 52°N, 120°W, in the Quesnel Highlands of British Columbia. The lavas are of small erupted volume, and are of Quaternary age, sufficiently young as to preclude even moderate weathering or alteration, permitting analysis for major and trace element concentrations, Sr and Nd isotopic compositions, mineral compositions and whole rock volatile concentrations. The lavas are easily accessible, well exposed and represent some of the youngest volcanic activity in North America.

Little work has been done on lavas of this type in the Canadian Cordillera. The present study concentrates on the northern part of the Wells Gray area and provides a morphologic description of the eleven centres in the study area. The textural relationships of phenocrysts, xenocrysts and xenoliths in the lavas are described, prior to a discussion of their mineral chemistry. These, together with the whole rock chemical and isotopic compositions of the lavas are then used to determine their petrogenetic history. Lastly, the concentrations of H_2O and CO_2 in selected samples from the study area are described and compared with other published volatile concentrations from basalts.

The study area is almost entirely enclosed within the boundaries of Wells Gray Provincial Park and covers approximately 800 km^2. The field area was mapped and sampled in relevant areas during the summers of 1982, 1983 and 1984; previous mapping in the area was conducted by Campbell (1963a, 1963b), and Campbell and Tipper (1971).

The basement of the study area comprises metamorphic rocks of the Omenica Crystalline Terrane, with Jurassic metamorphic ages. The area has been glaciated and is deeply incised by rivers. Pre- and synglacial volcanism resulted in valley-filling lava piles which were eroded by the rivers to produce spectacular canyons and waterfalls. The older pre- and synglacial volcanism was the subject of a morphologic and petrogenetic study at the University of British Columbia (Hickson 1987). The older lavas are the precursors of those studied here.

The lavas studied herein erupted from a group of small isolated centres during and since the last glaciation. Major element compositions for four of the eruptive events were determined by Fiesinger and co-workers (1975, 1977); they also determined phenocryst and groundmass compositions using an electron microprobe. With the exception of this study and that conducted by Hickson (1987), no other data exist for the Quaternary centres.

The western Canadian continental margin has a history of tectonic accretion, magmatism and metamorphism for as much as 200 Ma. During this time the potential source region has developed characteristics which have been described by previous workers. It is therefore convenient, as an introduction to the volcanology of the Wells Gray area, to give a brief description of some of the tectonic, geophysical and geochemical constraints on magmatism in the Canadian Cordillera.

A. Tectonostratigraphic History

The area of volcanic activity in Wells Gray Park lies near the eastern end of the Quaternary Anahim volcanic belt of British Columbia (Fig. 1). This belt of volcanoes is one of three active, although quiescent, belts present in the central and southern parts of the Canadian Cordillera, with a history of volcanism ranging in age from the Miocene to as little as 300 years (Souther 1977). The complexity of the structure and tectonic history of the Canadian Cordillera permits only a simplified account to be given here; the reader is referred to previous works (Monger *et al.* 1972, 1982, Monger and Price 1979, Tempelman-Kluit 1979) for a more detailed overview and for an introduction to more specific regional studies.

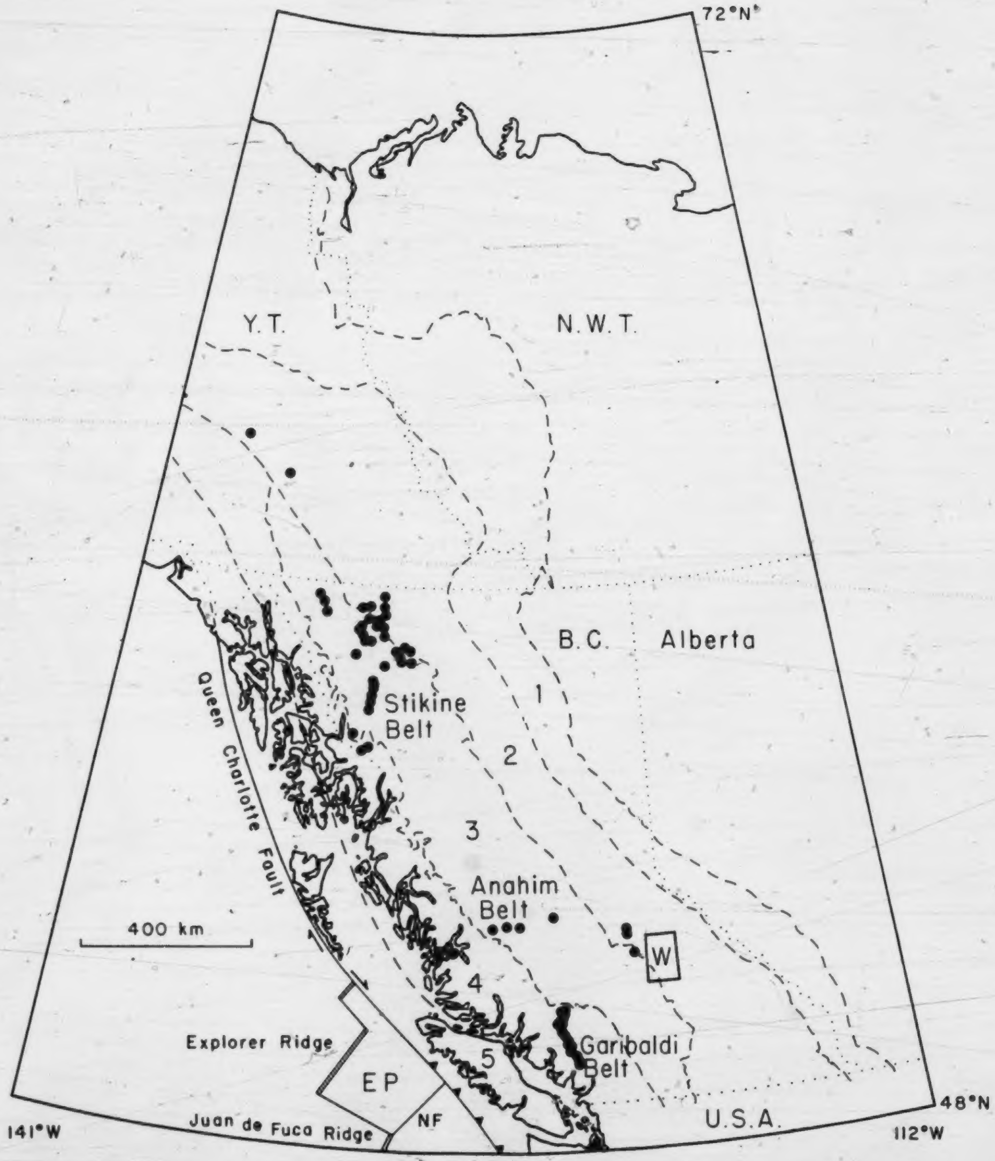
72°N
Y.T.
N.W.T.
B.C.
Alberta
1
2
3
4
5
Stikine Belt
Anahim Belt
Garibaldi Belt
W
Queen Charlotte Fault
400 km
Explorer Ridge
EP
NF
Juan de Fuca Ridge
U.S.A.
48°N
141°W
112°W

Fig. 1. Tectonic setting of the Canadian Cordillera, showing the locations of the three volcanic belts. Volcanoes are shown by circles. The present-day subduction and transform plate boundaries at the edge of the North American continent are from Keen and Hyndman (1979). Triangles mark the location of present-day subduction at the plate boundary. The tectonostratigraphic boundaries within the Canadian Cordillera (Monger *et al.* 1982) are shown by dashed lines. The tectonostratigraphic regions are: 1. Rocky Mountain fold and thrust belt; 2. Omenica Crystalline Terrane, merging in the north with the Yukon Crystalline Terrane and the Yukon Cataclastic Complex; 3. Intermontane Belt; 4. Coast Plutonic Complex; 5. Insular Belt. The Wells Gray area, shown in Fig.2, has bold outlines and is labelled "W". EP = Explorer Plate; NF = Nootka Fault.

Fig.1 shows the areal distribution of the five major tectonostratigraphic divisions of the Cordillera. These are, outboard (westward) from the North American continental margin, the Rocky Mountain Miogeocline, the Omenica Crystalline Terrane, the Intermontane Belt, the Coast Plutonic Belt and the Insular Belt. These tectonostratigraphic assemblages represent *in toto* the result of repeated accretion of allochthonous terranes onto the North American continental margin during and since the Triassic period.

The Rocky Mountain Belt comprises a thick sequence of sedimentary rocks, ranging in age from Proterozoic to Cretaceous. Lithologies are dominantly carbonates and clastic rocks derived from the craton until the middle to late Jurassic and are overlain by clastic sedimentary rocks derived from the uplifting orogen to the west (Monger *et al.* 1972, Price *et al.* 1981). The edge of the stable North American craton was overridden in the middle to late Triassic by allochthonous terranes, forming imbricate listric thrust faults. The extent of the resultant crustal shortening and the volume constraints on basement and cover suggest that a "ledge" of lower crustal material extends under the Omenica Crystalline Terrane to the west (Tempelman-Kluit and Wanless 1975).

The Omenica Crystalline Terrane is a belt of medium to high grade metamorphic rocks, immediately outboard of the Rocky Mountain thrust and fold belt and separated from the latter by the Rocky Mountain and Tintina Trenches. The assemblages present in the Terrane comprise mid-Proterozoic to mid-Palaeozoic miogeoclinal sedimentary rocks and Palaeozoic and lower Mesozoic volcanic and pelitic sedimentary rock (Monger *et al.* 1982). Locally, inliers of Precambrian basement occur, which were deformed and metamorphosed to high grades in the middle Mesozoic to early Tertiary. Intrusions of Mesozoic and Tertiary age intrude the metamorphic rocks. The Omenica Crystalline Terrane is interpreted as one of two structural welts in the Canadian Cordillera (Monger *et al.* 1982), marking the zone of suture between the North American Continent and a collage of allochthonous terranes obducted onto the continental margin during the early to mid-Jurassic.

The Intermontane Belt is an area of upper Palaeozoic to middle Mesozoic marine volcanic and sedimentary rock and middle Mesozoic to upper Tertiary marine and non-marine sedimentary and volcanic rocks. These assemblages have been cut by comagmatic intrusions and deformed at various times since the early Mesozoic (Monger *et al.* 1982). Terranes within the belt are interpreted as allochthonous fragments of continental crust, obducted onto the North American continental margin. Four main terranes are recognised (Coney *et al.* 1980); these are the Quesnel, Stikine, Eastern and Cache Creek terranes; Stikinia and Quesnellia occupy the greatest areas within the belt.

The Coast Plutonic Complex is a highly deformed metamorphic and plutonic belt lying outboard of the Intermontane Belt. Assemblages contained within the belt comprise sedimentary and volcanic strata of late Palaeozoic to Tertiary age (Monger *et al.* 1982). The rocks have been metamorphosed, in places to high grade, and are intruded by granitoid intrusions of Cretaceous and Tertiary age. The metamorphism is, at least in part, contiguous with the intrusive phase. Monger *et al.* (1982) interpreted the Coast Plutonic Complex as the second of the two structural welts marking the accretion of allochthonous terranes presently lying to the west of the plutonic belt. Monger and Price (1979) interpreted the belt as being related to the eastward subduction of oceanic lithosphere, followed by collision and subsequent accretion of the terranes which presently form the Insular Belt.

The Insular Belt includes the Alexander, Wrangell and Gravina-Nutzotin terranes (Monger *et al.* 1982). Assemblages present in the terranes comprise Upper Cambrian to Cainozoic volcanic and sedimentary strata, cut by granitic rocks in part comagmatic with the volcanics. The terranes were deformed at various times from the Palaeozoic to the Quaternary. The Insular Belt is interpreted as the more outboard of the two "superterrane" collages accreted during the course of Cordilleran evolution (Monger *et al.* 1982). The terranes were juxtaposed by the late Jurassic or early Cretaceous, as indicated by the stratigraphic overlap of the Gravina-Nutzotin assemblage (Coney *et al.* 1980). The whole belt was accreted onto the North American continental margin during the late Cretaceous or early Tertiary.

Monger and Price (1979) cite the earliest phase of Cordilleran evolution as being the formation of an Atlantic-type wedge of miogeoclinal sediments from 1500 Ma to 380 Ma. The time span from the late Devonian to late Triassic saw closure of the ocean basin to the west of the stable North American craton through westerly-dipping subduction beneath the terranes which form Superterrane I (Tempelman-Kluit 1979). Final closure of the Anvil Ocean (Tempelman-Kluit 1979) followed by obduction of the collage of terranes comprising Superterrane I onto the North American continental margin occurred at the end of the Triassic period.

During the latter part of the Jurassic period, closure of an ocean basin brought the components of Superterrane II into proximity with the "prograded" North American continental margin. Eastward-dipping subduction during this period and extending into the Cretaceous formed the Coast Range Plutonic Complex (Monger and Price 1979). The present configuration of terranes was complete by the end of the Cretaceous period.

Following the accretion of Superterrane II on the western margin of the Cordillera, the processes attendant on subduction and accretion continued into the Tertiary. Major dextral faults, initiated in the late Cretaceous and early Tertiary, run along the length of the Cordillera, reflecting anticlockwise rotation and flexure of the North American continental margin.

B. Present tectonic setting

The tectonic setting of the Cordillera since the Miocene has been dominated by the current plate boundaries with the adjacent oceanic lithosphere and by the relative motions of the plate system. The tectonic elements are reviewed in Fig. 1. The margin of the North American craton (the Insular Belt) is in contact with Pacific Ocean lithosphere, the latter comprising two plates, the Pacific and Juan de Fuca plates separated by the Juan de Fuca mid-ocean ridge. At the northern end of the Juan de Fuca ridge, where the ridge abuts against the continental margin, the Juan de Fuca plate has fractured to form a daughter plate, called the Explorer plate, which is separated from the Juan de Fuca plate by the Nootka fracture zone.

Dextral strike-slip movement along the Queen Charlotte Fault is active at the present time. In the south the Juan de Fuca and Explorer plates are probably undergoing subduction (Riddihough and Hyndman 1976); the "triple point" for ocean ridge-trench-transcurrent fault has shifted position during the past 10 Ma (Keen and Hyndman 1979). Presently, the triple point is assumed to lie off the coast of northern Vancouver Island.

Three loose associations of volcanoes, interpreted as volcanic belts, cut across the tectonostratigraphic boundaries of the Cordillera, and have been active since the late Tertiary (Fig. 1). The southernmost, Garibaldi-Cascade Belt is an extension of the calc-alkaline volcanism in the United States, associated with subduction on the continental margin. The Stikine (alkaline) Belt in northern British Columbia is associated with east-west tension in the North American Plate.

The Anahim Belt, with a maximum age of 14.5 Ma, runs from west to east across the Cordillera, at a latitude of 52°N and is assumed to be the trace of a hot spot in the underlying mantle (Bevier *et al.* 1979). Movement of the North American plate over a stationary hot spot in the underlying mantle would produced the apparent movement calculated from age measurements; however, the Wells Gray area lies away from the main Anahim trend (Fig. 1, Hickson and Souther unpubl. data) and may be unrelated to the presumed plume trace.

C. Lithospheric structure and constraints on the nature of the source region from geophysical studies

Reviews of geophysical studies in the Canadian Cordillera are given by Keen and Hyndman (1979) and by Clowes (1980); geophysical evidence supporting subduction off the southwestern coast of British Columbia is summarised by Riddihough and Hyndman (1976).

Gravity studies

Gravity studies have been used to interpret deep structure both on the continental margin (Riddihough 1979) and across the Cordillera to the stable craton (Stacey 1973). Riddihough recognised a pattern on the continental margin similar to that noted by Watts and Talwani (1975) for island arcs of the western Pacific; a negative gravity anomaly is correlated with the trench outboard from Vancouver Island and a positive gravity anomaly occurs along the length of Vancouver Island itself, 100 km inboard from the negative anomaly. Riddihough, noting a disparity between the gravity and seismic data for the continental margin, also proposed that the downgoing slab be assigned the physical properties consistent with mafic and ultramafic rocks metamorphosed to amphibolite or granulite grades.

Stacey (1973), using Airy-type compensation, related the observed residual anomalies in the inland gravity data to lateral density variations in the crust and in the upper mantle. The density of both crust and mantle decreases westward across the Rocky Mountain Trench, possibly at the edge of the Precambrian basement. Large residual anomalies in Vancouver Island were interpreted as the effect of a "light" crust overlying a dense mantle; the underthrust plate being at relatively shallow depth. Stacey suggested that the northern limit of the underthrust Juan de Fuca plate occurred at 51°N.

Natural seismicity

The natural seismicity of British Columbia has been reviewed by Milne *et al.* (1978). Most earthquakes occur on the continental margin of British Columbia, along the Queen Charlotte Fault. P-node fault-plane solutions along the Queen Charlotte Fault and in the region of the Straits of Georgia and Puget Sound give strike-slip movement in a dextral sense (Weichert and Hyndman 1981), with strike-slip rates of 5.2 cm a^{-1}, which are in good agreement with rates predicted from plate movements (Milne *et al.* 1978, Weichert and Hyndman 1981). Earthquake fault solutions in the Puget Sound region give a component of thrust motion but the amount of thrust is an order of magnitude lower than that predicted by plate movements (Rogers 1979). The oceanic lithosphere in this region is relatively young (approximately 9 Ma) and hot (Parsons and Sclater 1977); such hot lithosphere might account for the absence of a Benioff zone and for the low strain release in the thrust earthquakes. Rogers (1979) discovered that earthquakes beneath Vancouver Island did not have a significant thrust component. Fault-plane solutions are consistent with either dextral strike-slip on northwesterly-trending faults or sinistral strike-slip on northeasterly-trending faults. The latter solution is consistent with Keen and Hyndman (1979) who inferred differential subduction beneath Vancouver Island; subduction rates were estimated as 1 cm a^{-1} in the north and 3 to 4 cm a^{-1} in the south.

Milne *et al.* (1978) report an isotropic distribution of earthquakes in the interior of the Cordillera. An "inlier" of moderate strain release at the eastern end of the Anahim Belt is interpreted by Rogers (1981) as evidence for an Anahim hotspot.

Seismic refraction studies

Seismic refraction studies in the Canadian Cordillera have been conducted by Chandra and Cumming (1972), Cumming *et al.* (1979), Forsyth and Berry (1974), Mereu *et al.* (1977) and Hales and Nation (1973). The Mohorovicic discontinuity dips gently eastward from a depth of 25 km beneath the Insular Belt to 30 km beneath the Intermontane Belt and to depths of 37-48 km beneath the Rocky Mountains and 50 km beneath the Great Plains. Hales and Nation (1973) report a 7 km thickness of lithospheric mantle beneath the Cordillera; this abnormally low value is in agreement with the estimate of Berry and Forsyth (1975: 8 km).

Seismic P-wave velocities in the mantle have been calculated by Cumming *et al.* (1979) (7.8 km s^{-1}); by Forsyth and Berry (1974) (8.06 km s^{-1}); by Spence *et al.* (1977) (8.22 km s^{-1}) and by Mereu *et al.* (1977) (8.0 to 8.1 km s^{-1}). Both Chandra and Cumming (1972) and Forsyth and Berry (1974) noted a decrease in upper mantle velocity by as much as 0.3 km s^{-1} westward across the Cordillera. Mereu *et al.* (1977) discovered a high velocity layer *beneath* the base of the continental lithosphere, at a depth of 55 to 70 km.

Wickens (1971, 1977), using surface waves and crustal refraction with Rayleigh and Love waves, found that the craton is characterised by high velocity lithospheric mantle to a depth of 90 km, with an underlying low velocity zone. The Cordilleran region is characterised by lower overall mantle velocities; the high velocity lithospheric mantle is thin or absent. An abnormally low velocity zone extends from the base of the lithospheric mantle to a depth of 90 km. Beneath this zone is "normal" asthenospheric mantle.

Seismic refraction and reflection studies on Vancouver Island (Ellis *et al.* 1983) show that crustal seismic velocities increase gradually from 5.3 km s^{-1} at the surface to 6.75 km s^{-1} at a depth of 15.5 km. A sharp transition occurs at this depth to a seismic velocity of 7 km s^{-1}. The preferred model for the thickness of the crust incorporates a crustal low velocity zone; crustal thickness is estimated as 37 km. The basement dips eastward at 1.4°, increasing to 4° at the continental rise. The oceanic Moho dips eastward at an angle of 6° to the centre of Vancouver Island; here the crust thickens by 10 km, with a flat-lying Moho to the east.

Magnetotelluric studies

Magnetotelluric studies in the Canadian Cordillera have been carried out by Caner (1971), Caner *et al.* (1971), Porath *et al.* (1971), Dragert (1973), Camfield and Gough (1975), Bingham *et al.* (1981) Gough (1986) and Gough *et al.* (1982). The Cordillera lying to the west of the Rocky Mountain Trench is characterised by high conductivity in the lower crust and/or upper mantle; this agrees with interpretations of seismic refraction data.

Bingham *et al.* (1981) and Gough *et al.* (1982) located two anomalies in British Columbia. The first, beneath southeastern British Columbia and southwestern Alberta, was interpreted as a discontinuity in the Precambrian basement. The second anomaly is consistent with a region of high conductivity beneath Tete Jaune Cache, 100 km northeast of the Wells Gray volcanoes. This anomaly is possibly related to a geothermal area. Dragert and Clarke (1977) reported a band of high conductivity associated with the Rocky Mountain Trench. The anomaly may be resolved into a near-surface conductive zone interpreted as wet sediments and a conductive band at a depth of 40 to 50 km, interpreted as a possible zone of partial melting; a conductive zone perpendicular to the Rocky Mountain Trench may be interpreted as a basement discontinuity. A more recent study of the Trench anomaly (Gough 1986) suggests that the anomaly is related to a conductive band beneath the Main Ranges of the Rocky Mountains.

Dragert (1973) noted that a simple conductor model was insufficient to account for the anomaly in the close vicinity of the Rocky Mountain Trench and proposed that a conductive band was present beneath the active volcanic belts of the Cordillera. Studies by Ngoe and Boyer (1978) in the Stikine volcanic belt revealed a zone of enhanced conductivity in the mantle beneath the belt, interpreted as evidence of partial melting. Ngoe and Boyer interpreted their results as indicative of a thin (19 km) crust in the belt, underlain by a zone of partial melting. No such study has been carried out for the Anahim Belt.

D. Geochemical and petrological constraints on the nature of the source region

The nature of the sublithospheric mantle and its role in the generation of alkali basalts must be considered as a necessary precursor to an understanding of the petrogenesis of the intraplate alkaline lavas in Wells Gray Park. The composition of the source region and the scale and extent of compositional heterogeneity must first be considered. Initial estimates of upper mantle composition from modelling of major and trace elements in chondritic meteorites (e.g. Sun 1982, Palme and Nickel 1985) give compositions which agree with estimates of mantle density. The pyrolite model (Clark and Ringwood 1964, Green and Ringwood 1967) also has this approximate composition. These models are intended to represent the composition of homogeneous, undepleted mantle and must be regarded as a base from which to develop the proposed constraints for magmatism in the cordillera.

Three types of sample are assumed to provide tangible information on the composition of the mantle; these are ophiolite complexes, assumed to represent depleted oceanic mantle, Alpine-type ultramafic units, such as the Anvil Allochthon (Tempelman-Kluit 1979) and nodules of ultramafic rock entrained as xenoliths in alkaline lavas. These last are of greatest interest to this study because the entrained lithologies are a representative sample of the upper mantle transected by the ascending magma, if not of the source rock itself.

Studies of the subcordilleran mantle in British Columbia and throughout the North American Cordillera have, therefore, concentrated upon incognate material included in alkaline lavas. Wilshire and Shervais (1975) identified two assemblages in lavas from the southwestern U.S.A.; a chromiferous variety, bearing Cr-spinel and Cr-diopside, and an aluminous assemblage, bearing Al-spinel and Al-augite, of which a significant number were clinopyroxenites. The nodule assemblage transported to the surface in B.C. is dominantly of Cr-spinel bearing lherzolites (Fujii and Scarfe 1982, Brearley *et al.* 1984, Brearley 1986) with smaller populations of other chromium-bearing ultramafic rocks. The aluminous assemblage is, however, also represented by significant quantities of xenoliths.

Garnet-bearing ultramafic assemblages are unknown in the Canadian Cordillera. Spinel-bearing assemblages, either Cr-rich or Al-rich, are the most abundant xenoliths and are therefore possible candidates for a source rock. However, whole rock chemical analyses conducted by Smith (1986) on samples of the nodules indicated that the majority were depleted in some incompatible elements, such as Rb, Ti and Y, relative to chondritic abundances. Such rocks are unlikely to produce the concentrations of incompatible elements observed by Bevier (1978, 1983a) in the Rainbow Range, of western B.C..

The subcordilleran mantle, as reviewed earlier, is exceptional in its tectonic setting and history. The Canadian Cordillera lacks a root of lithospheric mantle; the top of the low velocity zone lies just beneath the Moho. Three major subduction events have occurred during the last 200 Ma, possibly causing the decoupling of crust and lithospheric mantle and contributing oceanic material to the mantle. Ancient oceanic crust is proposed (Hofmann and White 1982, White and Hofmann 1982, Zindler *et al.* 1984) as a contaminant for the upper mantle, producing chemical and isotopic heterogeneity in mid-ocean ridge basalts. It may be inferred that material from the subducted plates has contributed, in the same way, to the source regions for the cordilleran lavas (Carlson 1984, Hart 1985). The scale of these heterogeneities is unknown.

Heterogeneities on a smaller scale are found in ultramafic xenoliths throughout the North American Cordillera. Francis (1976) described amphibole and phlogopite in ultramafic xenoliths from Nunivak Island, Alaska . Brearley and Scarfe (1984) described the first occurrence, in Canada, of a pargasitic amphibole in a spinel lherzolite classified as Wilshire and Shervais' (1975) Cr-diopside bearing assemblage. An abundance of data exists (Wilshire and Trask 1971, Best 1974, Wilshire *et al.* 1980, Menzies and Murthy 1980a, Menzies *et al.* 1985) for phlogopite and amphibole, of a variety of compositions, in the southwestern U.S.A.. These occurrences indicate the presence of mesoscopic chemical and mineralogical heterogeneity and the presence of volatiles in the subcordilleran mantle; the latter will be discussed later. The origin of the hydrous phases is interpreted as the result of metasomatism (Lloyd and Bailey 1975, Menzies and Murthy 1980b, Boettcher and O'Neil 1980, Wilshire 1984, Schneider and Eggler 1986), increasing the concentrations of incompatible elements in the putative source rocks to those suitable for generation of alkali basalts.

In a volatile-free source, of fixed composition, the composition of the melt produced by partial melting will depend upon the depth at which melting takes place and the extent of partial melting. Alkali basalts can be generated (e.g. Takahashi and Kushiro 1983) by equilibrium partial melting of a spinel peridotite, under dry conditions, at pressures greater than 15 to 20 kbar. Frey *et al.* (1978), using concentrations of K_2O and P_2O_5 in chondritic mantle and in derived magma, calculated that basanites were generated by as little as 1% partial melting of a lherzolite mantle. Sleep (1974) suggested that such a small fraction could not escape from the source rock; more recent calculations (McKenzie 1985) indicate that as little as 0.1% partial melt can escape efficiently.

As noted above, volatile-bearing phases do exist in or near the source regions of the cordilleran alkaline magmas. Consequently, the role of volatiles in the generation of alkaline magmas has received considerable study (Brey and Green 1975, Bryan 1976, 1977, Eggler 1974, 1975, Eggler *et al.* 1976, Green 1973b, Kushiro 1970, 1971, Kushiro *et al.* 1975, Mysen 1976, 1977, 1979, Mysen *et al.* 1975, Mysen and Boettcher 1975a, 1975b, Ngoe and Boyer 1978). The species H_2O and CO_2 have opposite effects on magmas generated from a lherzolite source. The presence of H_2O in the source region drives magma compositions towards the field of silica-saturation; CO_2 drives compositions towards the silica-undersaturated field (Mysen and Boettcher 1975a, 1975b). Knowledge of the concentrations of the two components in an intraplate alkaline magma, relative to concentrations in a tholeiitic basalt will test the importance of these components to alkaline magma genesis.

A dependence upon P_2O_5 is observed in the concentration of rare-earth elements in primary mantle-derived magmas by Beswick and Carmichael (1978), Chauvel and Jahn (1984) and by McDonough *et al.* (1985). This is interpreted as the effect of a phosphate phase which is present at or near the source regions of the alkaline magmas.

E. Summary

The Canadian Cordillera is a tectonostratigraphic collage, formed by the accretion of two terrane assemblages (superterranes), with associated subduction of oceanic lithosphere, during and since the beginning of the Jurassic period. Pacific oceanic lithosphere is currently subducting aseismically beneath Vancouver Island. The crust of the cordillera lacks a lithospheric mantle root; the base of the crust is 30 to 35 km beneath the surface of the earth. The asthenosphere beneath the base of the crust contains a zone characterised by high seismic velocity, which may be either a decoupled part of the lithosphere or the subducted oceanic crust. The subcordilleran mantle has, therefore, a history of magmatism and tectonism which may have led to the formation of heterogeneities.

Studies of the subcordilleran mantle, using ultramafic xenoliths, indicate that the mantle comprises a Cr-rich assemblage, typically spinel lherzolite, and an Al-rich assemblage, typically spinel clinopyroxenite. Both assemblages may host volatile-bearing minerals such as kaersutitic or pargasitic amphibole and phlogopite. The presence of these phases strongly suggest that the mantle is heterogeneous on a mesoscopic, and possibly macroscopic, scale. For these reasons, the alkaline lavas of the Wells Gray area were studied to determine their variation in major and trace element concentrations, to evaluate the extent of enrichment of incompatible elements and the differences in their ^{143}Nd/^{144}Nd and ^{87}Sr/^{86}Sr ratios, and to determine the source mineralogy for magma of these compositions in the subcordilleran mantle.

2.

PHYSICAL VOLCANOLOGY

The purpose of this part of the study is to describe the morphology of each of the volcanic centres in the study area and to determine their sequence of eruption. This was completed in order to correlate possible variations in texture, in mineral and whole rock chemistry and in isotopic composition with geographic location and time of eruption. This study addresses the syn- and postglacial volcanoes in the north-central and west-central area of the park because these volcanoes are alkaline in whole rock chemistry (Fiesinger 1975, Fiesinger and Nicholls 1977) and represent small erupted volumes. The petrogeneses of lavas from these centres are the primary focus of this study.

Preliminary work in the area, describing the volcanic centres, was carried out by the Geological Survey (Campbell 1961, 1963a, 1963b, 1967, Campbell and Tipper 1971). Preliminary results from a more recent study are given by Hickson and Souther (1984) and are the subject of a Ph.D. thesis at the University of British Columbia (Hickson 1987).

Ten centres are located in the study area, together with an outlier of a lava flow which has no explicit source, but is related by morphology to nearby centres. The centres are grouped, for convenience, into four main areas, shown in Fig.2. The first of these is the Spanish Creek area, on the western boundary of Wells Gray Park, which contains five centres. The second comprises the edifice of Pyramid Mountain, described by Hickson (1987). The third is the area around Ray Lake, containing four volcanic features and the fourth and last is the Kostal Lake area. The areas will be described in the sequence above. However, it is stessed that a complete overlap in ages of centres exists between areas. The sequence of description is not related to any stratigraphic succession.

A. Spanish Creek area

The Spanish Creek area lies on the western margin of the park (Fig.2). Five main centres of volcanic activity were identified in the field and from aerial photographs. These form a linear chain, from the most northerly centre near the head of Daniel Creek

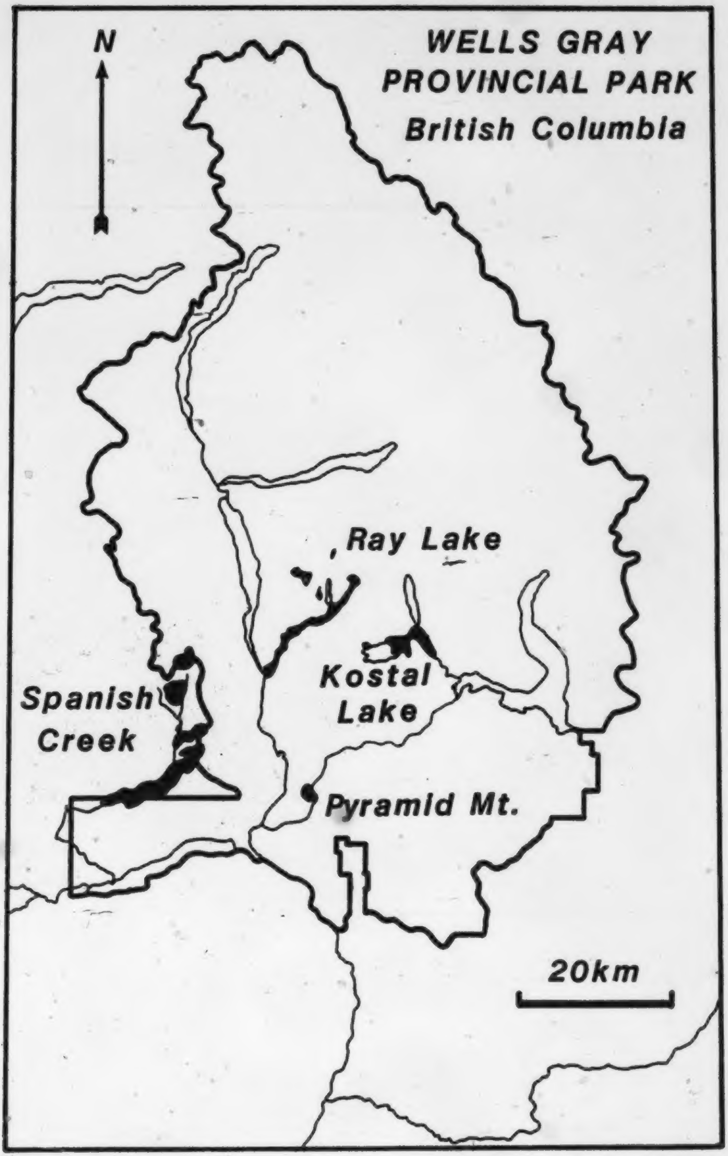
N
WELLS GRAY
PROVINCIAL PARK
British Columbia
Ray Lake
Kostal Lake
Spanish Creek
Pyramid Mt.
20km

Fig. 2. Volcanoes and lava flows studied in the Wells Gray area. The area shown is that labelled "W" in Fig. 1. The three main areas studied are the Spanish Creek, Ray Lake and Kostal Lake areas. In addition, the hyaloclastite mound of Pyramid Mountain was also sampled.

to the most southerly, at the head of Flourmill Creek (Fig.3).

The centres in the Spanish Creek area are the most closely related in space and, possibly, the most diverse in their eruption time; there is no relationship between the position of any centre in the chain and its morphologic type. The oldest of the centres appears to be the volcanic neck of Spanish Bonk, which has been glaciated. Hyalo Ridge and Spanish Mump are synglacial centres but may have evolved during different periods of glaciation. The two postglacial centres, Flourmill and Spanish Lake are located in a complex magnetic anomaly and may share a common conduit; these last are the only two centres studied whose chemistry and age relations are sufficiently similar for this to have occurred.

Spanish Mump

Spanish Mump is the most northerly volcano in the Spanish Creek area and lies at the headwaters of Spanish Creek and Daniel Creek, 6 km east-northeast of Mica Mountain, at 52°9'N 120°20'30"W. The location is shown in Fig.3. The centre comprises an overgrown mound, 150 m in elevation and 5 km^2 in area, with gently sloping sides. Float found on the south slope of the mound indicates that the mound is of hyaloclastite and is similar in morphology to Pyramid Mountain; the mound is therefore interpreted as a subglacial mound or SUGM (Hickson 1987).

Spanish Bonk

Spanish Bonk, 2.5 km southwest of Spanish Mump is a small, probably monogenetic, vent on the west side of the Spanish Creek valley at 52°8'N 120°22'W. The location is shown in Fig.3. The centre comprises a small dome of basaltic lava, 70 m in height and 0.25 km^2 in basal area. The dome has been glaciated, forming a crag and tail. The absence of a cinder cone is probably due to glaciation. Removal of unconsolidated cinders from the cone by a glacier eventually exposed a volcanic neck.

Hyalo Ridge

Hyalo Ridge lies 4 km to the north of Spanish Lake at 52°7'N 120°21'30"W. (Fig.3). It is a steep-sided edifice surmounting the east end of the Mica Mountain ridge

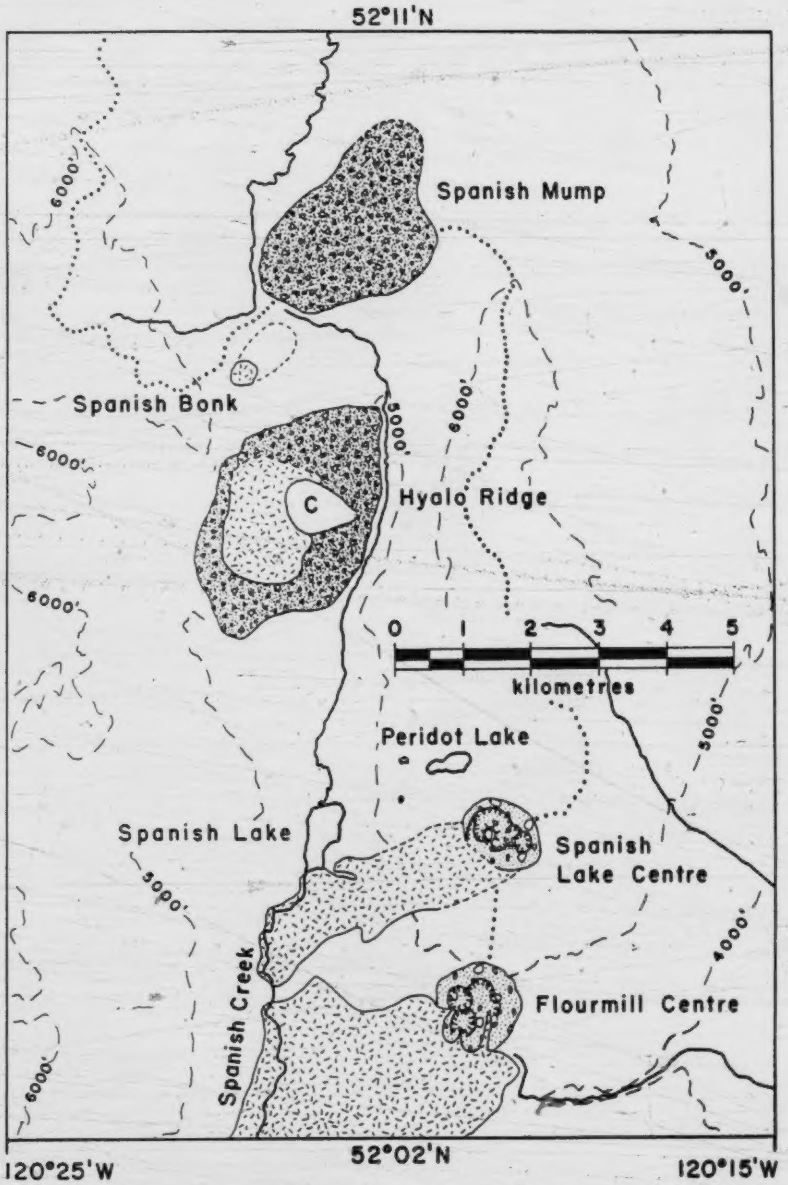
52°11'N
Spanish Mump
Spanish Bonk
Hyalo Ridge
C
Peridot Lake
Spanish Lake
Spanish Lake Centre
Flourmill Centre
Spanish Creek
6000'
5000'
4000'
0 1 2 3 4 5
kilometres
120°25'W
52°02'N
120°15'W

Fig. 3. Spanish Creek area, showing the five volcanic centres. Subaerial ejecta are shown by circles, hyaloclastite by triangles and lava flows by hachuring. Spanish Mump is a hyaloclastite mound or SUGM, Spanish Bonk is a glaciated subaerial cone, Hyalo Ridge is a tuya and Spanish Lake and Flourmill are postglacial cinder cones which have erupted valley-filling lava flows.

and is a prominent topographic feature, 600 m high, when seen from the air. Plate 1A shows the southern aspect of the edifice. The volcano lacks an eruption crater. Despite the topographic prominence of Hyalo Ridge, it has been glaciated.

The volcano comprises a steep-sided cone of yellow-weathering hyaloclastite surmounted by five flat-lying lava flows. The flows are very limited in area and act as a protective cap to the hyaloclastite mound (Plates 1B, C). A cirque has been cut on the eastern flank of the edifice. At four flow margins, exposed in the cirque, are well-developed pillow lavas (Plates 1C, D); these are interpreted as being a contact with an intraglacial lake. Immediately beneath the lowermost lava flow are pillow breccias, grading downward into the hyaloclastite pile. The lake level estimated from these water-contact features is at an elevation of approximately 1820 m above sea level. This elevation is some 600 m above the present valley bottom and 500 m above the passes into the Clearwater valley. Either the watershed between Spanish Creek and the Clearwater valley was considerably higher at the time of formation of Hyalo Ridge or, more probably, the outlets to the Spanish Creek valley were blocked by ice.

The steep sides and greater height of Hyalo Ridge and the spatially restricted nature of its lava flows are in contrast with the postglacial lavas from the Spanish Lake and Flourmill centres. Similar occurrences have been reported from northern British Columbia (Mathews 1947) where lava emerged from a subglacial vent and was shattered by rapid cooling, forming a volcaniclastic pile beneath the melting glacier. An intraglacial lake formed and the volcanic pile grew such that the vent was eventually clear of the water. A lava cap formed and the resulting flat-topped edifice remained after the ice receded. Such a mountain is called a tuya (after Mathews 1947).

Spanish Lake Centre

Spanish Lake Centre lies 2.5 km to the east of Spanish Lake at 52°4'30"N 120°19'W (Fig.3, Plate 2). Three water-filled, steep-sided depressions 1 km to the northeast of the volcano are interpreted by Hickson and Souther (1984) as pit craters resulting from a subterranean phreatomagmatic explosion, followed by subsidence. Volcanic ejecta and lava are absent from the vicinity of these craters.

The Spanish Lake centre is entirely postglacial. One major and two satellite cones have formed, the major cone being the most westerly and the oldest. The major part of the edifice comprises two nested cinder cones with a central resurgent lava dome 30 m in height (Plate 1F). The outer cone is the older and is breached in the southwest by two lava flows which have destroyed approximately 60° circumference of its wall. The inner, younger cinder cone is intact for nearly all of its margin; it is breached, on its northern wall, by a lava flow from a flank eruption which flows back into the central crater (Plate 1F). Both inner and outer cones are of unconsolidated irregular blocks with little agglutinate; the inner cone incorporates weathered bipolar fusiform bombs. The particle size of the ejecta is as much as 1 m. Crustal xenoliths, as much as 5 cm in diameter, commonly occur in the ejecta fragments.

The older of the satellite cones is situated on the eastern rim of the major cone. Ejecta from its vent cover the eastern walls of both nested cones. The younger cone lies on the eastern edge of the volcano and developed on the eastern flank of the older satellite cone (Fig.3). Both satellite cones contain a higher proportion of agglutinate material than the main cone. The younger satellite cone has a central blast pit, 20 m deep (Plate 1E), which formed during the final phase of activity of the centre.

Lava flows from two flank eruptions flowed westward into the Spanish Creek valley. That on the northern rim of the centre flowed out of a breach in the outer wall, to the west, and inward, through a breach in the north wall of the inner cone, to inundate the area around the resurgent dome (Plate 1F). A stream section through the flow on the valley side indicates that it is 7 to 10 m thick, with a flow top comprising blocky scoria, as much as 1 m in size, and larger rafts, as much as 5 m wide. The flow contains xenoliths of spinel lherzolite, as much as 3 cm in size. The second, more extensive flow originated from the southwest wall of the inner cone and destroyed a large portion of the outer cone. The flow is of a thickness comparable to the north flow, with a similar flow top and xenoliths of identical size and lithology. The flows were probably synchronous.

Lava from the Spanish Lake Centre dams the Spanish Creek valley, forming Spanish Lake. The lavas do not come into contact with flows from the Flourmill centre. The relative ages of eruption of the two centres are therefore not known.

Flourmill Centre

Flourmill Centre is the most southerly of the volcanic centres in the Spanish Creek area and lies at the headwaters of Flourmill Creek (52°3'N 120°19'W), on the drainage divide between Spanish Creek and the Clearwater River valley (Fig.3, Plate 3). The cinder cone is complex, comprising three overlapping cinder cones of slightly differing ages. The highest part of the cone rises to 250 m above its base.

The oldest part of the cone lies on the northeastern side, comprising a partially preserved cinder cone. The southeastern portion was destroyed or covered by ejecta from subsequent eruptions. The cone is composed of irregular blocks and rare bipolar fusiform bombs interlayered with vesicular agglutinate. A breach on the southeast side of the cone drained the central lava lake. The lava flowed southwest into the Spanish Creek valley, carrying rafts of agglutinate from the wall of the cone. The flow is rich in inclusions of pyroxenite and megacrysts of pyroxene, as much as 10 cm and 1 cm, respectively, in diameter.

Cessation of eruptions on the eastern part of Flourmill Centre was succeeded by the construction of a satellite cone on what is now the southwestern flank of the volcano. This part of the cinder cone is well-preserved and is composite in nature, comprising loosely consolidated vesicular blocks, interlayered with agglutinate and protected by a resistant cap of the same material (Plate 4A) Several well-preserved regular bombs occur with the irregular blocks. These are of the spherical and breadcrust types, with some poorly preserved bipolar fusiform varieties. All blocks and bombs are poorly vesicular. Scoriaceous material is rare (<5%) and is pervasively interlayered with poorly vesicular agglutinate.

The wall of the southwest cone was breached on the south side, permitting draining of lava from the lava lake in the crater into the Spanish Creek valley. The crust of the lava lake is fractured and a number of upwellings of lava through these fissures (Plate 4B) occur on the crust of the lava lake and in a north-northwesterly trending line up the north wall of the cone.

The most recently-formed part of the volcano lies on its northwest flank, in part built on the deposits from the southwestern vent. It is a complete and remarkably well-preserved composite cone comprising at least three deposition cycles of loosely consolidated bombs, pervasively interlayered with agglutinate. The second layer contains a number of excellently preserved bipolar fusiform and ribbon bombs (Plate 4E). All ejecta are moderately to poorly vesicular; scoria is rare or absent.

The cone is breached by a lava flow on the southwest side; remnants of a lava lake persist in the crater (Plate 4C). The crust of the relict lake is fractured, forming rafted blocks as much as 10 m in width. The last activity in the crater formed a small ring of scoriaceous ejecta, now extensively weathered, on the northwest inner wall of the main crater (Plate 4D).

Three lava flows erupted from Flourmill Centre have flowed into the Spanish Creek Valley. The thickness of each flow, estimated from a stream section in Spanish Creek, is 7 to 10 m. The lava beds extend approximately 15 km down the valley of Spanish Creek, with a breadth of 2 km. The total volume of the lavas is therefore 0.3 km^3, by far the largest of the four postglacial volcanoes. By contrast, the volume of the source cone is, at most, 0.09 km^3, the volume of scoriaceous material far less (5000 m^3)

Basal sections of the lava flows along Spanish Creek are not common and no carbon has yet been discovered for isotopic analysis. Both the Flourmill and Spanish Lake centres rest on unweathered glacial till (Hickson 1987). It is probable that the centres are nearly contemporaneous and are older than either the Dragonhead or Kostal Lake centres.

B. Pyramid Mountain

Pyramid Mountain, a volcanic edifice in the southern portion of the park, at 51°59'40"N 120°6'10"W (Fig.2), and is a landmark in the centre of the Helmcken Plateau (Plate 4F). The area has already been mapped (Hickson and Souther 1984, Hickson 1987); only a summary of the morphology will be given here.

Pyramid Mountain is a steep-sided cone, 250 m in height, comprising yellow-weathering hyaloclastite. The cone is steeper and better exposed than Spanish Mump, the only other hyaloclastite mound studied. Subaerial eruption products are absent. Layering is present in the hyaloclastite at the summit and on a subsidiary summit on the eastern flank of the cone. Hickson (1987) interprets the subsidiary summit as a landslide remnant of the true summit of the cone; this landslide would also have formed the broken terrain on the north flank of the cone. Hickson proposes that the cone is the first phase of subglacial volcanism, forming a subglacial mound or SUGM. Accumulation of the mound ceased before the mound could break the surface of the intraglacial lake and further volcanism could add a lava cap to form a tuya (after Mathews 1947).

C. Ray Lake area

The Ray Lake area lies approximately 10 km east of Clearwater Lake (Figs.2 and 4). Three main centres of volcanic activity are present in the area, together with a lava flow from an unknown vent (Ray Ridge). The centres studied are the Ray Mountain fissure, the glaciated cinder cone of Pointed Stick Cone and the Dragonhead postglacial cinder cone and Dragon's Tongue lava flow.

Ray Mountain

The Ray Mountain fissure is located 6 km to the east of Clearwater Lake, at the summit of Ray Mountain at 52°15'N 120°7'W. The location of the centre is shown in Fig.4; a larger-scale map and a section are presented in Figs.5 and 6, respectively. The centre contains at least two vents, in the form of fissures; this mode of eruption differs from those of the other centres in the Wells Gray area. The edifice was dissected by glaciation, during and following the later of two phases of activity, permitting examination of a section through the erupted material.

The peripheral contact of eruption products with bedrock is exposed at both the north and south ends of the Ray Mountain ridge, although a complete section is present only in the vicinity of the summit (Fig.6). The peripheral deposits to the north represent the later eruption phase of the Ray Mountain centre and are not representative of the earliest activity at the centre. The central and southern portions of the centre, from the summit of Ray Mountain southward to the southern margin of the edifice, are of greater thickness and incorporate subaerial material older than the peripheral glacial contact unit. The contact between products from the two eruptive events is marked by the peripheral hyaloclastite unit (Fig.6, Plate 5E). At the summit of Ray Mountain the hyaloclastite rests paraconformably on layered subaerial agglutinate from the earlier eruptive phase.

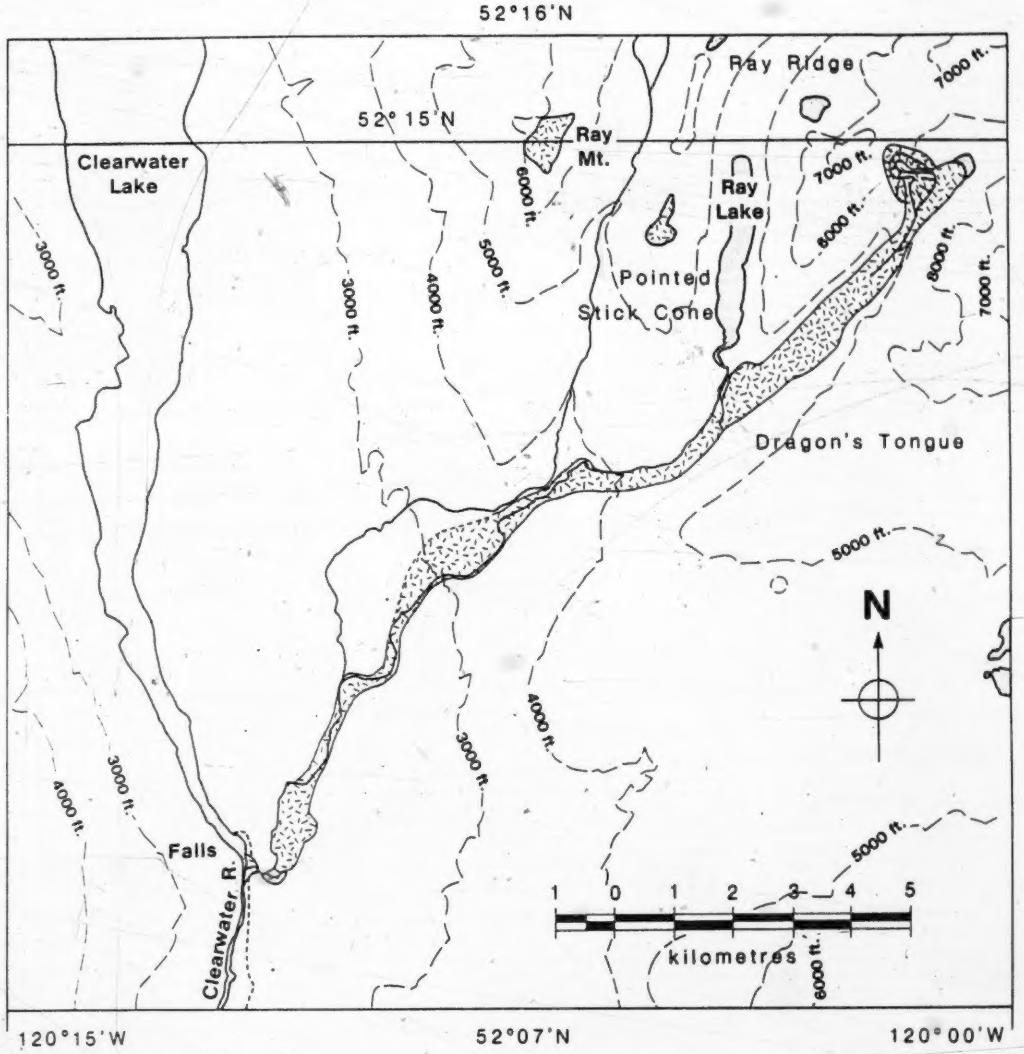
52°16'N
Ray Ridge
7000 ft.
52° 15'N
Ray Mt.
Clearwater Lake
6000 ft.
Ray Lake
7000 ft.
8000 ft.
3000 ft.
3000 ft.
4000 ft.
5000 ft.
Pointed Stick Cone
8000 ft.
7000 ft.
Dragon's Tongue
5000 ft.
N
4000 ft.
3000 ft.
3000 ft.
4000 ft.
Falls
5000 ft.
1 0 1 2 3 4 5
kilometres
6000 ft.
Clearwater R.
120°15'W
52°07'N
120°00'W

Fig. 4. Ray Mountain area, showing the four areas studied. Ray Mountain is a fissure volcano which has undergone two phases of activity. Ray Ridge comprises a lava flow dissected by glaciation, without a vent. Pointed Stick Cone is a glaciated, weathered cinder cone without lava flows. Dragonhead and the Dragon's Tongue comprise a postglacial cinder cone and a long lava flow, erupted from the latter, which extends to Clearwater Lake. The age of the Dragonhead centre is 7500 a.

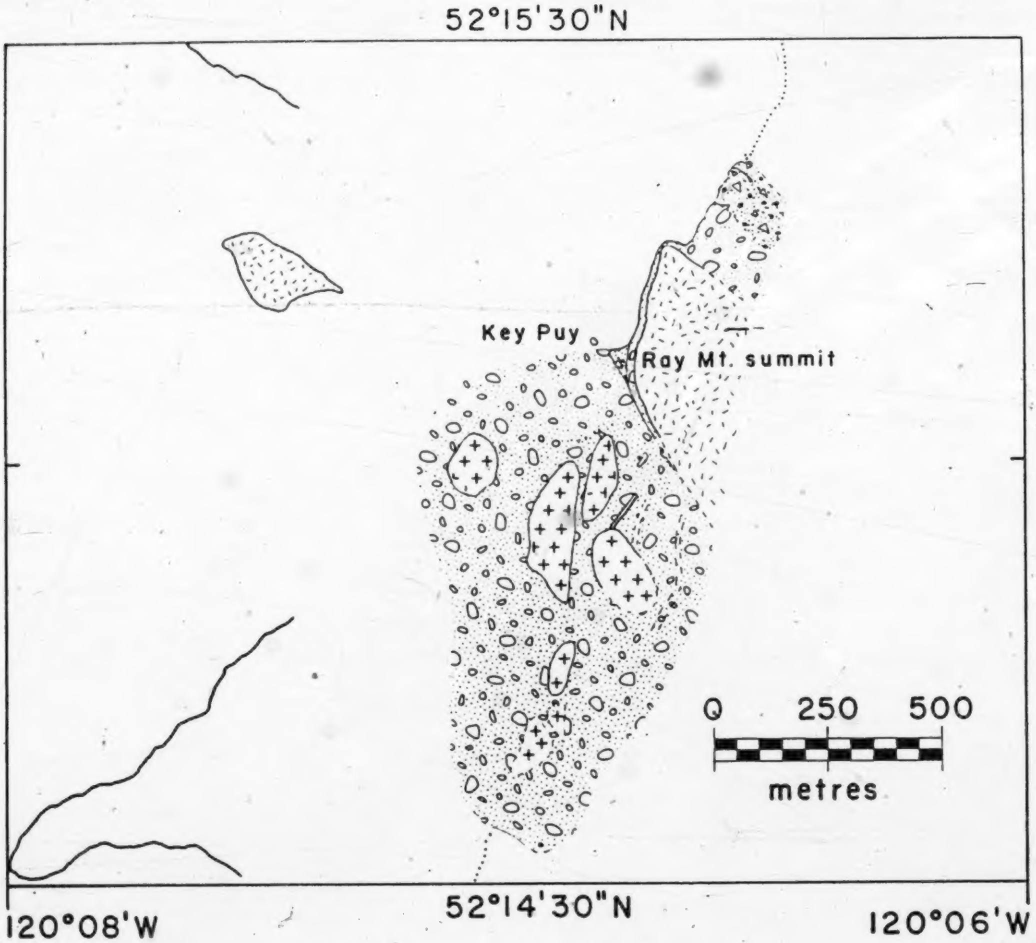
52°15'30"N
Key Puy
Ray Mt. summit
0
250
500
metres
52°14'30"N
120°08'W
120°06'W

Fig. 5. Detailed map of the Ray Mountain centre. The centre comprises products of two phases of fissure eruption, the younger phase lying on the north flank of the older. Subaerial ejecta are shown by circles, intrusions by crosses, dykes by solid lines, hyaloclastite by triangles and lava flows by hachuring.

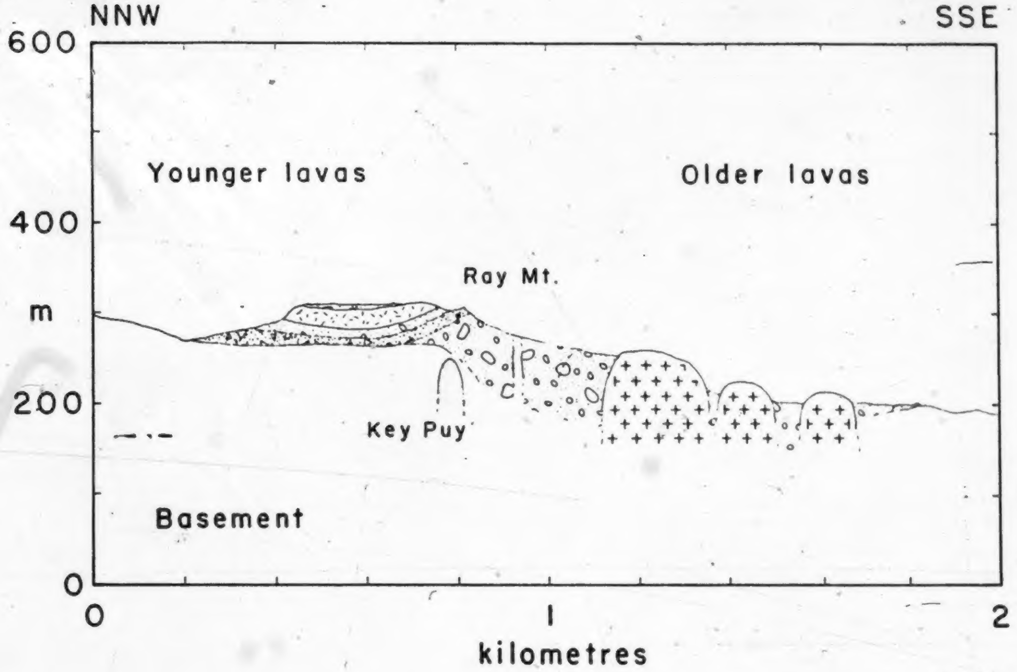
NNW
SSE
600
400
m
200
0
Younger lavas
Older lavas
Ray Mt.
Key Puy
Basement
0
1
2
kilometres

Fig. 6. Cross section through the Ray Mountain centre. Symbols used for the various units are as for Fig.5. The section is taken from NNW to SSE along the western edge of the exposure shown in Fig.5 and in Plate 5E. Vertical exaggeration is 2.

The earlier phase of activity at the Ray Mountain centre was exclusively subaerial in style. Two fissures or synvolcanic faults have been exposed by erosion in the central and southern portions of the centre (Plate 5A). Products of the fissure eruptions comprised blocky irregular scoria and vesicular basalt, now deeply weathered. The maximum particle size is approximately 0.5 m. Layering of the ejecta dips gently away from the fissure system, to east and west (Plate 5B). The base of the unit, in the central portion of the edifice, is not exposed but the unit is at least 100 m thick.

Erosion along the two synvolcanic fissures has exposed domes of massive, poorly vesicular lava (Plate 5A). These domes exhibit vertical baked contacts against agglutinate and are interpreted as subvolcanic plugs lying along or close to the fissures which acted as conduits for the magma. Several northward-trending dykes originate at the largest dome (Plate 5A) and show chilled margins against the agglutinate (Plate 5C). A large part of the fissure system is covered by loose material, fallen from the slopes above, but the *in situ* agglutinate, where exposed, exhibits disturbed layering in the vicinity of the fissures (Plate 5B).

A small *puy*, 300 m west of the summit of Ray Mountain (Plate 5B), is the probable source of a lava flow which flowed west from the centre towards Clearwater Lake. The flow has been glaciated and the distal portions are covered by drift, but the flow may extend as far as the basalt plateau at the margin of Clearwater Lake.

The basal units from the second phase of activity at this centre are subaqueous and ice-contact deposits which are in sharp contrast with the subaerial deposits beneath the paraconformity. The basal unit oversteps the unconformity between the subaerial deposits of the earlier phase and the Shuswap basement (Fig.6). At the northern margin of the centre, the base of the hyaloclastite rests unconformably upon quartz-feldspar-mica gneiss, the latter containing pegmatites. The unit comprises 1 to 2 m of black weathered gravel containing hyaloclastite and glacial debris (Plate 5D). Country rock fragments present in the basal gravel are of similar composition to that of the underlying country rock.

The basal gravel grades upward into a 15 m thick hyaloclastite unit which lacks fragments of country rock. The unit is yellow-weathering and similar in appearance to that found at Pyramid Mountain. It is overlain by 5 to 10 m of red-weathering subaerial agglutinate and scoria. The section is capped by a 5 m thick lava flow, fine grained and poorly vesicular, and by 2 m of red-weathering agglutinate overlying the flow. The top of this section has been eroded; the units above and including the basal hyaloclastite dip eastwards from the fissure, north from Ray Mountain and south from the northern contact (Fig.6, Plate 5E), creating a bowl-like structure, interpreted as the result of peripheral ice or water contact.

A high-precision K-Ar age obtained by Hickson (1987) gives a closure age of 0.3 Ma for the largest dome in the central complex. It is certain that Ray Mountain had more than one phase of activity, extending through at least one glaciation; the age is therefore an approximate age for the earlier phase of fissure activity.

Pointed Stick Cone and Ray Ridge

Two volcanic features, Pointed Stick Cone and Ray Ridge, occur along the ridge immediately to the west of Ray Lake. Neither are reported by the Geological Survey but were noted during an earlier survey by Mathews and are described by Hickson (1987). Locations for the features are shown in Figs.2 and 4.

Ray Ridge, the more northerly of the features, is a portion of a glaciated lava flow (52°16'30"N 120°4'30"), unassociated with any vent, and overlies a hyaloclastite unit (Hickson 1987). The flow is 4 to 5 m thick and weakly vesiculated with horizontal shear fractures 5 to 50 cm apart, penetrative on a mesoscopic scale. The vesicles are elongated, suggesting plastic flow. This outcrop is rich in ultramafic xenoliths, as much as 3 cm in size, suggesting proximity to a vent. The vent itself is not exposed.

Pointed Stick Cone, the second volcanic feature along the ridge, is a glaciated subaerial cinder cone at 52°14'N 120°5'W. It comprises unconsolidated irregular blocks of vesicular lava, as much as 1 m in size, interlayered with agglutinate. All rocks are pervasively weathered and subangular fragments of pegmatite are found atop the cone, suggesting that they were deposited by glacial or periglacial action.

The cone rises to a height of 40 m above its base and covers an area of 0.2 km^2. The southern wall is heavily dissected and there is a breach in the eastern wall. Lava flows are absent; either none were erupted or, more probably, those flowing into the Ray Lake valley were later eroded by a valley glacier. The central crater is partially filled with sediment and hosts a small saline lake; any remnant of a central lava lake is covered by sediment.

An outcrop of lava, 30 m wide and 50 m long, of unknown thickness extends northward along Ray Ridge from the base of Pointed Stick Cone. The flow has been glaciated and is overgrown; it is not explicitly associated with the cone. The basalt is fine-grained and poor in both vesicles and phenocrysts.

Dragonhead Centre

One centre in the Ray Lake area is postglacial. It is located 12 km east of Clearwater Lake, in the centre of the park at 52°14'30"N 120°1'W and has erupted a valley-filling lava flow extending 16 km downvalley to the foot of Clearwater Lake (Fig.4, Plate 6).

The volcano is a cinder cone constructed on the north side of the upper Falls Creek valley (Fig.4, Plates 6, 7A). The cone comprises interlayered agglutinate and irregular blocky scoria, 0.1 to 1.0 m in size; both are deeply weathered. One central crater is present, breached on the valley side in two places to permit egress of lava flows to the valley floor. The final stage of activity created a blast pit, now largely infilled by blocks fallen from the inner walls of the cone.

Layering of agglutinate, exposed in the inner wall of the cone, dips towards the valley at angles of as much as 50°. The dip of the layering is consistent, not with confocal slumping of the cone towards the blast pit, but with slumping in the direction of the valley floor (Plate 7B). A knoll, comprising agglutinate and blocky cinders occurs at the junction of the two breaches in the cone and is interpreted as the slumped portion of the cone (Plate 7C); the lava pond in the central crater was probably drained as a result of slumping of the south side of the cone in the direction of the valley. The lava flows from the two breaches are contemporaneous and coalesce in the valley.

Lava erupted from the cinder cone extends 16 km down the Falls Creek valley. The depth of valley fill in the proximal portion of the flow is not known but is in excess of 15 m; stream erosion has not as yet exposed a flow base. The flow surface is of *aa*, comprising rafted blocks as large as 5 m in length and 2 m in thickness. The flow is sparsely reforested but comparatively little soil formation has taken place on the flow surface.

The distal portion of the flow is a valley fill with a flow bottom exposed by stream erosion on the north side of the valley. The knickpoint of Falls Creek at present lies 2 km upstream from its junction with the Clearwater river. The stream, prior to the eruption, had cut a canyon in metamorphic rocks 400 m east of the junction. Lava filled the valley, dammed Falls Creek and overflowed the valley down the canyon on the south side of the valley (Plate 7D). Falls Creek was constrained to flow along the northern edge of the lava flow and, at the distal lava pond, flowed across the northern lobe of the flow and cut a new canyon to the north of the old (Fig.4).

Abundant tree moulds are present in the flow surface (Plate 7E) and one mould was discovered in the flow base, exposed by stream erosion. Only one mould examined, in the flow surface, showed clear bark impressions, indicating that the tree entrapped was a poplar. The presence of a mature forest indicates that the recession of the glaciers in this valley occurred a significant time prior to the eruption of the Dragonhead Centre and suggest that the Dragonhead Centre is younger than the Flourmill and Spanish Lake centres, which both rest upon unweathered glacial material. The volcanism in Spanish Creek, however, occurred at a higher elevation; the three centres may, therefore, be contemporaneous.

The northern edge of the Dragon's Tongue has been exposed by stream erosion. The flow rests on unconsolidated micaceous sand, deposited by the stream, in all locations save one. The exception is a three-metre exposure of the flow base by Falls Creek. At this location the flow is 5 to 7 m in thickness and rests on intercalated clay and silt with one 3 to 5 cm thick peat horizon (Plate 7F). The location is interpreted as an overgrown sandbank in the pre-lava Falls Creek which silted over. The silt and clay overlie normal stream sands.

Isotopic analysis of carbon from the peat gives an age of 7560±110 a for the horizon (sample GSC-3944); this is a maximum age for the lava flow. The Dragonhead centre was therefore active shortly after recession of ice from the Fraser advance (*ca.* 8000 a). The centre probably postdates the Flourmill and Spanish Lake centres and certainly precedes the latter phase of activity at Kostal Lake.

D. Kostal Lake Area

Kostal Lake

The Kostal Lake centre is the youngest and the most easterly of the centres in the study area. The centre is situated 18 km to the east of Clearwater Lake, at 52°10′30″N 119°57′W, on the northeast shore of Kostal Lake. The centre comprises at least two vents which have been active since the last glaciation. A map of the centre is shown in Fig.7 and a stereographic aerial view is presented in Plate 8. Volcanic edifices comprise one perfectly preserved cinder cone and a second, less well-preserved cone to the north. There is no evidence of pre- or synglacial activity, although older lavas are probably obscured by the most recent eruption.

At least two phases of activity have occurred at the Kostal Lake centre. The first is represented by overgrown mounds of agglutinate to the east of the two recent cinder cones (Plate 9A), surrounded and in part covered by lava flows and ejecta from the later eruption. The extent of the older lavas is shown in Fig.7. It is probable that the second phase of activity destroyed any existing volcanic edifices, leaving relict rafts of agglutinate included within and at the margins of the younger flows.

Lava fountains during the second phase of activity constructed two cinder cones which have been preserved. The more northerly (Plates 9B, 9C) is poorly preserved and probably formed first; part of the cone was destroyed by later lava flows. The cone is constructed from loose blocks which range in size from 10 to 50 cm, interlayered with agglutinate, some of which exhibits ropy texture. The height of the north cone is approximately 70 m above its base.

The more southerly, younger cone is a perfectly preserved cinder cone rising to a height of 200 m above its base (Plates 9A, 9D, 9E). The cone exhibits two phases of formation, each phase depositing alternate layers of cinder blocks, 10 to 50 cm, and agglutinate. The first phase of cone formation is visible as a shelf on the inner wall of the central crater. The later part of the cone, on the northeast side, has been dislocated by a lava flow; the cone is breached on the east side. A lava boss, remnant of a lava lake, is present in the central crater.

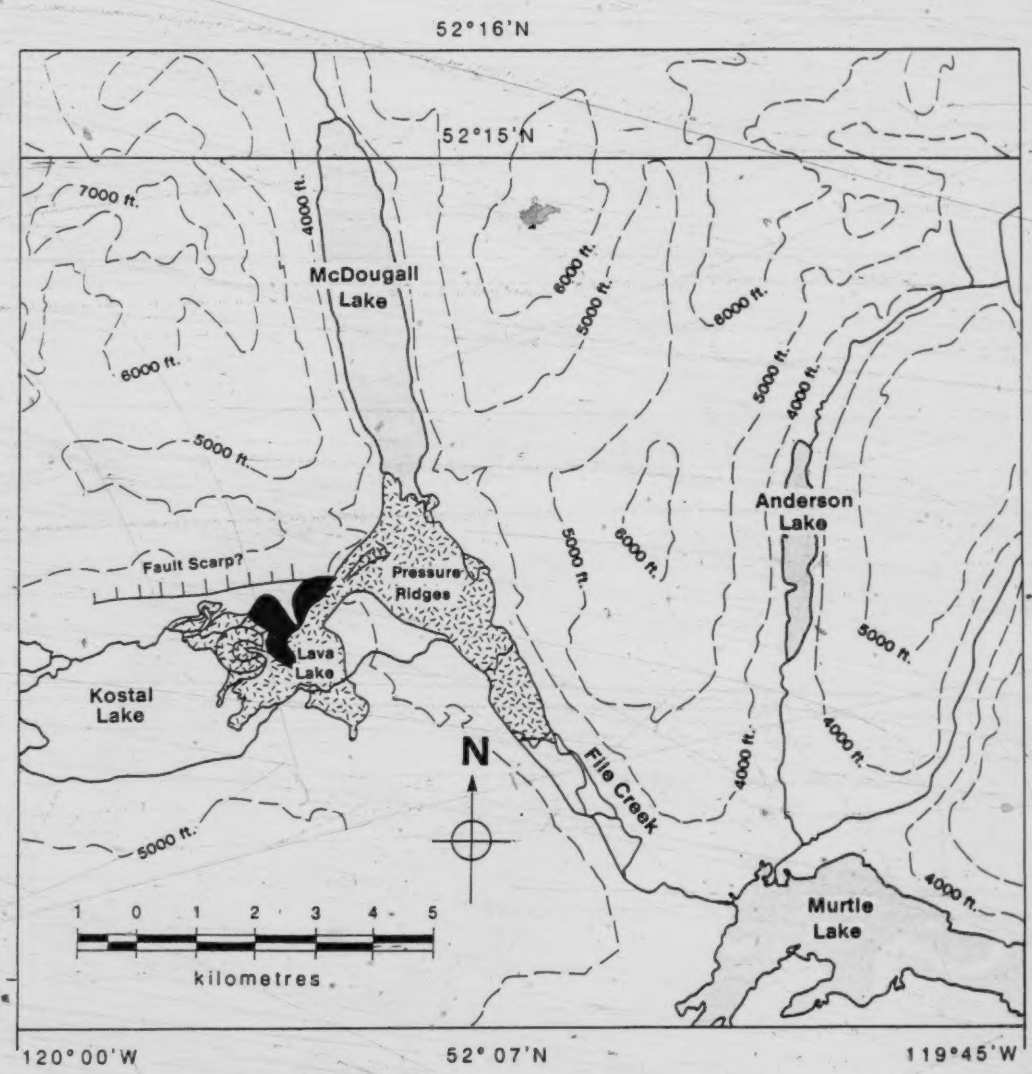
52°16'N
52°15'N
7000 ft.
4000 ft.
McDougall Lake
6000 ft.
5000 ft.
6000 ft.
6000 ft.
5000 ft.
5000 ft.
4000 ft.
Anderson Lake
Fault Scarp?
Pressure Ridges
5000 ft.
6000 ft.
Lava Lake
Kostal Lake
N
File Creek
5000 ft.
4000 ft.
4000 ft.
5000 ft.
4000 ft.
Murtle Lake
1 0 1 2 3 4 5
kilometres
120°00'W
52°07'N
119°45'W

Fig. 7. Kostal Lake area, showing the volcanic centre. Lavas from the earlier phase of activity (solid area) are surrounded by products of the later eruption (hachured area). The two volcanic cones and three valley-filling flows are products of the later eruption.

The flow bases are not exposed in the proximal portions of the Kostal Lake Centre, therefore carbon for an isotopic ^{14}C age could not be obtained. A minimum age of 300 a for the more recent phase of activity was estimated, based on the extent of reforestation of the flow surfaces.

Three lava flows emerge, from breaches in the south wall of the north cone (Plates 9B, 9C), the east wall of the south cone (Plates 9A, 9D, 9F) and from a lava tube on the north side of the south cone (Plates 9B, 9E). The flow from the north cone appears to be the earliest; the flow trends westward for a distance of at least 500 m into what is now Kostal Lake. The flow surface is of *aa*, comprising numerous rafted blocks as much as 10 m wide, diminishing in size towards the distal portions of the flow. Lava squeeze-ups are rare. The flow base is not exposed but from surface topography in the area, the flow's thickness is approximately 10 m.

The flows from the lava tube and from the central vent of the south cone appear to have been synchronous. The lava flow from the tube emerges from the broken terrain to the northeast of the south cone and exhibits three lobes, two of which abut against the valley side to the north and older agglutinate to the east, respectively. The third lobe flows westward until diverted southwestward by the flow from the north cone (Fig.7) The flow base is not exposed; the flow has a maximum thickness of 15 m. The flow surface proximal to the vent comprises rafted blocks of *aa*, as much as 5 m in width. The distal portion of the western lobe includes some pyroclastic material; the flow surface block size decreases to 0.5 m and well-developed pressure ridges are present. That portion closest to Kostal Lake is of hummocky relief, although the block size in the flow surface does not change significantly.

The flow from the central crater is bounded by the lakeshore and by older agglutinate to the north. Water contact features are absent, suggesting that Kostal Lake did not exist until after the last eruptive phase had ended. The proximal portion comprises rafted blocks of *aa*, as large as 20 m in width, decreasing to 5 m in width at a distance of 300 m from the vent, where the flow forms a small lava lake of unknown depth (Plate 9A), damming the valley to form Kostal Lake.

The centre lies in a depression bounded by the sides of the valley; only the flow from the south cone has overflowed the valley's wall and flowed down File Creek, to the east (Fig.7). It is possible that the depression is caused by subsidence associated with deflation of a magma chamber underlying the volcano.

E. Summary and age relations

Eleven volcanic features, comprising ten volcanic centres and a glaciated lava flow, were investigated. The volcanoes are, with one exception, central-type and are not related to any overt structural trend in the basement metamorphic rocks. The exception is the Ray Mountain centre which has been active along two north-south fissures, possibly related to a pre-existing fault system.

Erupted volumes are, with one exception, less than 0.3 km^3. The exception is Hyalo Ridge, which has erupted a volume of as much as 0.8 km^3; this volume is more comparable to those of the lavas forming Hickson and Souther's (1984) valley-filling assemblage. Over 2 km^3 form the Helmcken Plateau alone. Despite the small erupted volumes, Kostal Lake, Spanish Lake, Flourmill and Ray Mountain have been active more than once. In the case of Ray Mountain, a change from subaerial to subaqueous eruption products indicates that the time intervening between events was sufficiently long as to allow the onset of glaciation.

The centres examined have, without exception, developed in the Quaternary. Four of the centres, Spanish Bonk, Hyalo Ridge, Ray Mountain and Pointed Stick Cone, formed prior to the Fraser glacial advance and have been glaciated. Hyalo Ridge, part of Ray Mountain, Pyramid Mountain and Spanish Mump are partly or totally composed of hyaloclastite, indicating that they were active during a period or periods of glaciation. The remaining four centres are entirely postglacial in eruption history. Of these, the Flourmill and Spanish Lake centres overlie unweathered glacial till (Hickson 1987) and the Dragonhead centre incorporates trees into its distal portion. Carbon from a peat layer overlain by the Dragon's Tongue has a ^{14}C age of 7550±110 a. The excellent preservation of the Kostal Lake centre suggests a younger age; the age of the youngest cone, constrained by the cedar trees growing on the cone, could be as young as 300 a.

Assignation of relative ages to the centres studied in Wells Gray Park is seriously hindered by the topographic relief of the area, the resultant variation in glacial history, the scarcity of sources of carbon for ^{14}C measurements, the low erupted volumes and the relative isolation of the centres from each other. Hickson and Souther (1984) and Hickson (unpubl. data) have high precision K-Ar age measurements for the Hyalo Ridge, Pyramid Mountain and Ray Mountain centres of 0.1 Ma, 0.1 Ma and 0.3 Ma, respectively. This author proposes the following tentative eruption sequence, based upon Hickson's work and upon the extent of preservation of each of the centres: Ray Mountain (lower sequence), Hyalo Ridge, Ray Ridge, Spanish Bonk, Pointed Stick Cone, Spanish Mump, Pyramid Mountain, Flourmill, Spanish Lake, Kostal Lake (earlier lavas), Dragonhead and Kostal Lake (later lavas). It is stressed here that the phases of activity of near-synchronous centres almost certainly overlap in time.

It is concluded that volcanic activity in the central area of Wells Gray Park took place from approximately 0.3 Ma to the present day, over an area of approximately 600 km². It is evident, from the sequence given above and from Figs.2, 3 and 4, that the eruption sequence is not related to geographic location. The centres studied exhibit no trend of decreasing age, despite the fact that the most easterly centre, Kostal Lake, is also the youngest. The volumes of magma produced from each centre do not exceed 0.3 km³. The source volume for melt generation in the mantle, even allowing for the 0.1% partial melting suggested by McKenzie (1985) would therefore be 300 km³. Although the geometry of the source is not known, it can be modelled by a spherical volume, 9 km in diameter for 0.1% partial melting and 4 km in diameter for 1% partial melting. The spatial separation of the areas, even given these source volumes and a low degree of partial melting, strongly suggests the existence of several discrete source regions, rather than a single source.

3.

PETROGRAPHY

The purpose of this part of the study is to describe in detail the textural and mineralogical features of the Wells Gray lavas, with emphasis on the syn- and postglacial centres in the more northerly part of the study area. The preglacial and many of the synglacial lavas are, as noted above, the subject of a study by Hickson (1987). Observation of textural and mineralogical features in the lavas facilitates interpretation of their mineral and whole rock compositions. The phenocryst assemblages of the Wells Gray lavas are therefore of particular interest, as are their xenocryst and xenolith assemblages. Consequently, the petrographic studies are a necessary precursor to mineralogical analysis by electron microbeam.

Samples were collected, during mapping of the areas described in Chapter 2, of material representing each eruptive event. Representative samples from each event were taken and a total of 187 thin sections and 45 polished thin sections were prepared, the latter for analysis by electron microprobe. Details of the microprobe analysis are given in Chapter 4. In this chapter, detailed descriptions of the various lavas are followed by a general description of ultramafic xenoliths from the centres.

A. Descriptive petrography by centre

Spanish Mump

The location of Spanish Mump is shown in Fig.3. Samples from the centre are porphyritic vesicular hyaloclastites with fragments of fresh yellow glass and black oxidised glass which vary in size from 0.1 to 6 mm. Several fragments of glass have leached rims; such fragments also contain a higher proportion of crystals in the glassy groundmass. Vesicles in all fragments are small and spherical (0.5 mm maximum). Vesicles in leached groundmass are infilled with fine grained zeolite. Darker areas of oxidation are present in the yellow glass, particularly in flow banded samples. The latter have vesicles streaked out parallel to the flow banding.

Groundmasses in the hyaloclastite fragments vary in crystallinity from 10% to as much as 50%, of grain size 0.01 to 0.1 mm. Plagioclase microlites comprise most of the groundmass with intersertal clinopyroxene and anhedral Fe-Ti oxide. The only phenocryst phase is olivine, 0.1 to 0.3 mm in size. Skeletal growth of olivine occurs in several fragments.

Xenocrysts and xenoliths comprise quartz, quartzite and biotite schist, derived from the crust, and several mantle-derived minerals. Olivine is coarse grained, being 0.5 to 2.0 mm in size. In one occurrence the olivine is associated with Cr-spinel in a fragment of a xenolith (Plate 10A). Orthopyroxene is anhedral, 0.3 to 0.5 mm in size and bordered with a reaction rim of olivine. Clinopyroxene is subhedral and, in one case, occurs in a clinopyroxenite xenolith.

Spanish Bonk

The location of Spanish Bonk is shown in Fig.3. Lavas from this centre are non-vesicular, medium grained and strongly olivine-clinopyroxene phyric, contain olivine- and clinopyroxene-bearing xenoliths. The groundmass is almost holocrystalline and comprises 15% anhedral isogranular Fe-Ti oxide, 0.01 to 0.03 mm in size; 35% subhedral plagioclase in subtrachytic orientation, 0.05 to 0.2 mm and 15% anhedral intersertal clinopyroxene, 0.05 to 0.1 mm. Traces of residual glass are also present. The groundmass plagioclase is seriate and as much as 0.2 mm in length.

The phenocryst assemblage includes 5% subhedral plagioclase, as much as 0.8 mm in length. Olivine and clinopyroxene comprise the balance (15% each) of the phenocryst assemblage. Both are euhedral and range in size from 0.3 to 5.0 mm; clinopyroxene usually forms slightly larger crystals. Olivine is weakly zoned and, rarely, strained. Clinopyroxene is strongly zoned, frequently has a corroded core and often has a marked change of composition from its interior to a 0.1 to 0.2 mm phyric rim. Oscillatory zoning is common in the cores of such crystals and especially common in the phyric rims. Significant compositional changes frequently occur over distances as small as several μm. Rare xenocrysts of clinopyroxene of comparable size occur without phyric rims and are extensively corroded (Plate 10B).

Hyalo Ridge

The location of Hyalo Ridge is shown in Fig.3. The lavas are olivine ± plagioclase phyric, in contrast to the other volcanoes which are usually olivine + clinopyroxene phyric. Both stages of tuya formation (Chapter 2) have similiar phenocryst assemblages.

The initial subglacial, subaequeous eruptive event, formed a hyaloclastite mound. The poor thermal conductivity of ice possibly resulted in frequent underwater steam flashes, fracturing lava more efficiently and precluding the formation of pillow lavas. The hyaloclastite produced during eruption is a medium grained, matrix-supported breccia (Plate 10C). The fragments are as much as 5 mm in size and are angular to subrounded with a texture ranging from holocrystalline to as much as 80% glass. The rock typically comprises 30% yellow glass fragments, 10% black glass fragments and 10% devitrified basalt fragments. The matrix comprises 5% anhedral olivine, 0.3 to 2.0 mm in size, and hydrated glass.

All glass fragments are non-vesicular. The height of the column of water or ice above the vent cannot have exceeded 800 m, (the height of the lava cap above the valley floor), therefore the maximum hydrostatic pressure on the fragments examined did not exceed 4 atmospheres. The absence of vesicles is, therefore, probably due to low initial concentrations of volatiles dissolved in the magmas.

Fragments of yellow glass are closest to holohyaline. The fragments are olivine-plagioclase phyric and comprise 10% euhedral to subhedral olivine, 0.1 to 1.0 mm in size; 10 to 20% subhedral plagioclase, 0.1 to 0.5 mm, in trachytic or felted texture; 70 to 80% non-vesicular yellow glass, rarely flow banded, with streaks of oxidation marked by "variolites" of Fe-Ti oxide. Clinopyroxene and incognate crystals or inclusions are absent. Olivine in the matrix is rounded but not explicitly incognate.

The second phase of activity is represented by at least 4 lava flows, with distal pillow lavas and pillow breccias at the margin of the plateau. Pillow lavas are moderately vesicular with a 2 cm quenched rim, becoming more oxidised towards the interior of the pillows. The phenocryst mineralogy of the pillow lavas is in all respects similar to that of the subaerial portion of the flows. The main portions of the flows forming the lava cap are poorly vesicular, fine grained hypocrystalline and olivine-phyric. Xenocrysts and xenoliths are absent. Vesicles are irregular, 0.1 to 0.3 mm in size and comprise less than 5% of the lavas.

Olivine, the first formed phenocryst, is euhedral to anhedral, 0.2 to 4.0 mm in size and comprises as much as 15 to 20% of the whole rock. Plagioclase phenocrysts, where present, comprise as much as 15% of the rock, are seriate, subhedral, as much as 0.8 mm in length, and with trachytic texture. The groundmass comprises 40% felted subhedral plagioclase, 0.1 to 0.2 mm in size 10% subhedral Fe-Ti oxide, 0.01 mm in size; 5% isogranular olivine, 0.1 to 0.2 mm in size and 10% intersertal clinopyroxene with intersertal black glass.

Spanish Lake Centre

The location of Spanish Lake Centre is shown in Fig.3. Samples from the two phases of activity identified at Spanish Lake are identical in their phenocryst and groundmass mineralogy and do not differ significantly either in their xenocryst content or xenocryst type. The samples vary in vesicularity from 50%, in scoria from various portions of the cone, to 10 to 20% in the lava flows.

The lavas are olivine-clinopyroxene xenophyric and olivine-clinopyroxene phyric, comprising 10 to 15% euhedral to subhedral olivine, 0.1 to 3.0 mm in size, rarely exhibiting skeletal growth, and 10 to 15% subhedral to anhedral clinopyroxene, 0.1 to 0.5 mm in size, forming glomerophenocrysts, 1.0 to 1.5 mm in size. The groundmass comprises 20 to 35% subhedral plagioclase, 0.05 to 0.2 mm in length, exhibiting trachytic texture; 10 to 15% subhedral Fe-Ti oxide, 0.01 to 0.1 mm in size; 5% isogranular olivine, 0.1 to 0.2 mm in size, 15 to 20 % intersertal clinopyroxene, 0.1 to 0.2 mm in size and 5 to 20 % intersertal glass.

Xenocrysts and xenoliths are common in proximal lavas. Crustal xenoliths comprise fragments of quartzite, as much as 2 cm in size with a grain size of 0.3 mm and show a sharp reaction rim, comprising microcrystalline olivine and pyroxene. Ultramafic xenoliths comprise Cr-spinel lherzolites and clinopyroxenites; xenocrysts comprise as much as 10% anhedral olivine, 0.5 to 10 mm in size, with rims of phyric olivine; as much as 15% anhedral clinopyroxene, 0.3 to 7.0 mm in size, with a thick, zoned rim of phyric clinopyroxene, 0.1 to 0.2 mm wide.

At least two varieties of clinopyroxene are present. The first is pervasively corroded with a narrower phyric clinopyroxene rim; the second exhibits peripheral corrosion and a thicker phyric rim. Both varieties form clinopyroxenites, described in detail in the second part of this chapter. Olivine xenocrysts infrequently have inclusions either of Cr-spinel or green Al-spinel. Phlogopite occurs in one xenolith and is described in detail below.

Flourmill Centre

The location of Flourmill Centre is shown in Fig.3. Two phases of activity in the Flourmill Centre are identified on the basis of petrography, differing in their xenocryst and xenolith assemblages. Field relations (Chapter 2) are indistinct because ejecta from the later event overlie, and are confused with, ejecta from the earlier. Older lavas are both olivine-clinopyroxene xenophyric and olivine-clinopyroxene phyric. They comprise 10% euhedral to subhedral olivine phenocrysts, 0.2 to 1.0 mm in size, exhibiting skeletal growth, and 10% subhedral clinopyroxene, 0.2 to 0.5 mm in size, forming radial glomerophenocrysts as much as 1.5 mm in diameter. The groundmass comprises 20 to 35% subhedral plagioclase, 0.05 to 0.2 mm in length, in weak trachytic orientation; 10 to 15% subhedral to anhedral Fe-Ti oxide, 0.02 to 0.05 mm in size; 5 to 10% isogranular olivine, 0.1 mm in size; 20% isogranular clinopyroxene, 0.01 to 0.1 mm in size and 5 to 15% intersertal glass.

The younger flows exhibit phenocryst and groundmass modes identical to those present in the older phase of activity. Vesicles in samples from either phase vary in shape from rounded to irregular. Vesicularity varies from as much as 70% in ejecta to as little as 20% in rafted blocks in the more recent flows.

Earlier and later phases differ mainly in their incognate material. Samples from the earlier phase are significantly olivine and clinopyroxene xenophyric, comprising as much as 20% of the latter mineral and a significant percentage of clinopyroxenite xenoliths. Olivine xenocrysts are rounded, strained, and vary in size from 0.5 mm to as much as 1 cm (Plate 10D); they are often with phyric overgrowths. Trace amounts of xenophyric olivine, of similar size and texture, are present in the more recent lavas with trace amounts of xenophyric clinopyroxene, 0.5 to 4.0 mm in size, corroded and zoned with a strongly zoned phyric rim, 0.5 mm in width.

The abundance of xenocrysts of clinopyroxene in the earlier lavas from the Flourmill Centre permits identification of at least two varieties. The first is a pervasively corroded clinopyroxene with only a vestigial phyric rim; this type is generally the smaller, possibly as a result of corrosion. The second type is far less pervasively corroded; in some cases corrosion is restricted to a thin layer immediately inside the phyric rim. The differing textures suggest at least two sources for the xenophyric material; similar diversities in xenophyric clinopyroxene were noted by Wass (1979) and by Duda and Schminke (1985).

Xenoliths, with one exception, are described below. The exception is 7 mm in size. and comprises 20% subhedral plagioclase, 1 mm in size; 40% isogranular clinopyroxene and 40% subhedral olivine, both 0.3 mm in size. The mode is identical to that observed in the sample; the sample is therefore interpreted as a fragment of vent lining.

Pyramid Mountain

The location of Pyramid Mountain is shown in Fig.2. Samples from spatter on the southwest side of the mountain are fine-grained, non-vesicular, nearly holohyaline and olivine phyric, comprising 15% anhedral olivine phenocrysts, 0.1 to 4 mm in a groundmass comprising 40% subhedral plagioclase, 0.05 to 0.1 mm exhibiting felted texture; 10% subhedral Fe-Ti oxide, 0.01 to 0.05 mm; 20% intersertal clinopyroxene, 0.1 to 0.2 mm and 10% anhedral olivine. The remainder of the groundmass is residual glass. Xenocrysts and xenoliths are absent.

Hyaloclastite from the summit of Pyramid Mountain differs in texture from that taken from Spanish Mump and from any other glasses. The sample is a fresh fragmental rock composed exclusively of fragments of olivine phyric glass. Fragment size is as much as 1 cm; smaller, altered, fragments comprise the matrix. The fragments are vesicular; vesicles are spherical and range in size from 0.1 to 3 mm, comprising approximately 40% of the whole rock.

Phenocrysts are exclusively of euhedral to anhedral olivine, of grain-size 0.1 to 0.3 mm and frequently form glomerophenocrysts. Xenocrysts are absent. The groundmass comprises yellow glass.

Larger glass fragments show a progressive oxididation, over a depth range of 40 mm, from the quenched rim inwards. Such larger fragments are vesicular; vesicles are rounded, 0.5 to 5.0 mm in diameter and comprise 30% of the whole fragment. The rim of the fragment is olivine phyric; the olivine phenocrysts are euhedral and comprise 10% of the rock. Phenocryst size varies from 0.1 to 1.5 mm. The groundmass comprises yellow glass with rare plagioclase microlites, 0.05 to 0.1 mm in length.

Five millimetres from the edge of larger fragments, "variolites" of Fe-Ti oxide occur as discrete, small clusters in the glassy groundmass (Plate 1.0E). These clusters increase in concentration with depth until, at a depth of 4 mm, the entire groundmass is affected. No other change in mode is observed. Xenocrysts and xenoliths are absent in the glass fragments.

Ray Mountain

The location of Ray Mountain is shown in Figs.4 and 5. Two main eruptive events occurred at Ray Mountain. The older of these is exposed both as an extrusive and as an intrusive phase, the latter including several altered dykes, as described in Chapter 2.

Samples from the earlier event are very poorly vesicular and are olivine and clinopyroxene phyric, comprising 15 to 20% euhedral to subhedral olivine, of grain size 0.1 to 2.0 mm and 5 to 10% euhedral to subhedral clinopyroxene, 0.1 to 1.0 mm, showing strong zoning and, rarely, resorbed cores. The groundmass varies little in grain size from intrusive to extrusive phases, suggesting that the intrusions are little more than volcanic necks. The groundmass minerals comprise 30 to 35% subhedral plagioclase, 0.01 to 0.1 mm in size, frequently seriate with microphenocrysts as much as 0.6 mm in length; 15% subhedral to anhedral Fe-Ti oxide 0.01 to 0.02 mm; 5% anhedral olivine 0.01 to 0.1 mm; 15% anhedral intersertal clinopyroxene, 0.01 to 0.1 mm and a intersertal residual brown glass.

At least 10% of each sample from this group comprises incognate material. Xenoliths with significant olivine are rare. One wehrlite comprising 10 to 20% anhedral olivine, poikilitically enclosed by crystals of clinopyroxene, 1 to 2 mm in size, was observed. In addition, a harzburgite, comprising one orthopyroxene grain and several olivine grains with a 0.2 mm reaction rim, was also observed. Olivine xenocrysts are more abundant, comprising 5 to 10% of the whole assemblage. These are rounded and occasionally have phyric rims. They are compositionally similar to the phyric olivine (see Chapter 4) and differ only in their shape.

Clinopyroxene is the dominant xenocryst phase in this earlier group of lavas, comprising as much as 20% of any sample. At least two varieties of xenocryst are present, the first almost completely resorbed by the melt, 0.5 to 1.0 mm in size and anhedral without any phyric rim. The second type is larger, 1 to 2 mm in size, compositionally zoned and has a rim of strongly zoned "normal" phyric clinopyroxene, 0.1 to 0.3 mm wide. The cores of the latter variety are less strongly resorbed.

Xenoliths composed exclusively of clinopyroxene are common and range in size from 3 to 15 mm. Each xenolith exhibits a different degree of resorption, estimated from the resorption observed in individual grains; the extent of resorption is dependent mainly upon the degree of magma influx along grain boundaries. The latter feature may be related to composition; insufficient data exist for comparison of the different xenoliths.

Products of the younger eruptive event rest on an erosional unconformity described in Chapter 2. The basal unit is an ice contact feature and incorporates a significant proportion of glacial material. The rock is a medium-grained, matrix-suspended breccia with fragments as large as 1.2 cm (Plate 10F). The fragments are predominantly of basaltic glass and basalt which comprise 30 to 45% of the whole rock.

The basaltic fragments are hypocrystalline, vesicular and porphyritic, comprising 40% spherical vesicles, 0.1 to 2.1 mm; 10% euhedral to subhedral olivine, 0.1 to 0.3 mm; 10% subhedral clinopyroxene, 0.1 to 0.3 mm and 15% subhedral plagioclase in trachytic orientation, 0.1 to 0.4 mm, all in a glassy groundmass. All fragments are angular to subangular with no evidence of reworking.

The fragments of country rock comprise 3% rounded to subrounded fragments of quartz-feldspar-muscovite schist and blastomylonite. The fragments are as much as 5 mm in size. The grain size of the schist ranges from 0.3 mm to 0.5 mm; the mode comprises 10 to 20 % anhedral muscovite, in lepidoblastic orientation; 10% plagioclase (anhedral, of composition of An_{20}) and the remainder 60% anhedral quartz; both tectosilicates have sutured boundaries. The cataclasite is of finer grain size, 0.01 to 0.2 mm and exhibits a well developed mortar texture, almost a flaser fabric.

Approximately 30% of the rock comprises clastic grains of olivine and clinopyroxene, 0.1 to 2 mm in size. The grains have been reworked and rounded either by water or by glacial action. Euhedral crystals are rare and it is impossible to distinguish phenocryst from xenocryst on the basis of texture. The remainder of the rock comprises fine grains of hydrated glass.

Samples from 5 m higher in the section have far less extraneous material, fewer crystals and are more glassy. The rock comprises vesicular glass shards; the vesicles are 0.1 to 1 mm in radius, spherical and comprise 40% of a whole shard. The glass forms subrounded globules, peripherally hydrated but not devitrified. The hydration margin of the globules is 0.1 to 0.2 mm wide. Hydration has also taken place along radial cracks in the globules. Globule size is approximately 1 to 5 mm. Phenocrysts comprise olivine (5%) clinopyroxene (5%) and plagioclase Rare microphenocrysts of plagioclase occur in the larger fragments.

Samples still higher in the section have approximately the same crystal and xenolith abundance but less hydration of the glass has taken place. Fragments are coarser grained and vesicles are larger and slightly more abundant. Glass fragments are angular to subangular, ranging in size from 0.1 to 1.0 mm. The hydration rim on the glass fragments is 0.2 to 0.3 mm in width. Vesicles are spherical and range in size from 0.1 to 3.0 mm. Phenocrysts in the glass are olivine and clinopyroxene, each ranging in size from 0.05 to 2.0 mm and with abundances of 10% and 5% respectively. Plagioclase is absent except as rare microlites.

The most recent extrusive rocks exposed on Ray Mountain include the uppermost lava flow (see Chapter 2). The two samples taken from the flow are nearly identical in their texture and their modal mineralogy. The flow is hypocrystalline and porphyritic, with a fine-grained, partly devitrified groundmass. Vesicles are rare or absent.

The groundmass is inhomogeneous and comprises a felted intergrowth of 40% plagioclase microlites, 0.01 to 0.05 mm; 20% anhedral isogranular Fe-Ti oxide, 0.03 to

0.10 mm, and 25% altered ferromagnesian minerals. The groundmass exhibits a felted texture, although plagioclase microphenocrysts exhibit trachytic orientation.

The phenocryst assemblage comprises 10% subhedral olivine, 0.1 to 2.0 mm; 5% subhedral to anhedral titaniferous clinopyroxene, 0.1 to 0.5 mm, rarely as 1 mm glomerophenocrysts, and 5% subhedral plagioclase, 0.1 to 0.3 mm in length, exhibiting trachytic texture.

One anhedral xenocryst of clinopyroxene, 2 mm in size, is present in sections examined and exhibits alteration to biotite and Fe-Ti oxide. Plagioclase fills the alteration embayments. Olivine is anhedral and 0.5 to 2.0 mm in size, comprising less than 5% of the mode. The xenocrysts all exhibit straining and rounding by resorption. Ultramafic xenoliths are absent.

Rare fragments of quartz and quartzite, 0.1 to 3.0 mm in size, are present, and represent material included in the flow during passage through the crust. All fragments have reaction rims of fine grained olivine and pyroxene.

Ray Ridge

The location of Ray Ridge is shown in Fig.4. The single sample sectioned, from this exposure, is nearly holocrystalline, fine-grained, porphyritic, and poorly vesicular. Vesicles are irregular and approximately 1 mm in size. Phenocrysts comprise 15% euhedral olivine, 0.3 to 2.0 mm, exhibiting peripheral zoning. Phyric clinopyroxene is rare, occuring as a rim to clinopyroxene xenocrysts. Both phenocryst phases are seriate. The groundmass comprises 35% subhedral plagioclase, 0.1 to 0.3 mm, strongly trachytic; 15% anhedral to subhedral Fe-Ti oxide, 0.05 to 0.1 mm; 25% anhedral isogranular clinopyroxene, 0.2 to 0.3 mm; 15% anhedral isogranular olivine, 0.2 to 0.3 mm.

Xenocrysts are rare, comprising rounded and embayed olivine, 2 mm in size, and corroded clinopyroxene, 0.5 to 1.0 mm in size. Both phases exhibit zoned phyric rims. A xenolith of spinel lherzolite, of grain size 1 to 5 mm, was observed in thin section; other xenoliths, noted in outcrop, are of similar grain size and comprise Cr-diopside, Cr-spinel, orthopyroxene and olivine.

Pointed Stick Cone

The location of Pointed Stick Cone is shown in Fig.4. Lava flows are absent (Chapter 2). Ejecta from the cone are porphyritic, poorly vesicular and fine grained; the groundmass glass is all devitrified. Vesicles are irregular, 0.5 to 2 mm in size, and comprise 15% of the whole rock. The rock comprises 10% olivine phenocrysts, occuring as euhedral to subhedral crystals 0.3 to 1.0 mm in size and less than 5% subhedral to anhedral clinopyroxene, 0.3 to 0.5 mm in size. The groundmass comprises 40% subhedral plagioclase, 0.1 mm in size; 20% subhedral Fe-Ti oxide, 0.03 to 0.1 mm; 30% anhedral intersertal clinopyroxene, 0.03 to 0.1 mm and 5% anhedral isogranular olivine 0.03 to 0.1 mm.

Xenocrysts are infrequent and comprise olivine and clinopyroxene, the latter with a 0.1 mm-wide phyric rim. One xenocryst of Fe-Ti oxide is present.

Dragonhead Centre

The location of Dragonhead Centre is shown in Fig.4. Scoria forming the cinder cone are highly vesicular. Vesicles are rounded, 0.4 to 5.0 mm in size and comprise 40% of the rock volume. The whole rock is olivine + clinopyroxene ± plagioclase phyric. Olivine occurs as euhedral to subhedral crystals, 0.2 to 1.0 mm in size, which exhibit skeletal growth. Entrapped melt inclusions are present. Some of the smaller inclusions are glassy. Inclusions of Cr-spinel, 0.01 mm in size, are common. The olivine phenocrysts comprise 10% of the whole rock.

Clinopyroxene phenocrysts are euhedral to subhedral, 0.1 to 1.0 mm in size and comprise 10% of the whole rock; phyric clinopyroxene is also present as an overgrowth on xenocrysts of clinopyroxene. Glomerophenocrysts of clinopyroxene, 0.5 to 1.0 mm are rare and do not exhibit any reaction texture with the enclosing melt. Such phenocrysts are, without exception, strongly zoned and compositional changes occur over a distance of only a few μm.

Plagioclase comprises 10% of the whole rock, occurring as 0.3 to 0.5 mm subhedral microphenocrysts with seriate and felted textures. The groundmass comprises 35% subhedral plagioclase, 0.03 to 0.1 mm in length, exhibiting trachytic texture; 20% isogranular clinopyroxene, 0.1 mm in size; 10% isogranular Fe-Ti oxide, 0.01 mm in size; and 5% isogranular olivine, 0.1 mm in size. Intersertal glass may comprise as much as 40% of the whole rock, at the expense of the other groundmass phases.

Incognate material comprises 5 to 10 % xenocrysts of olivine, 1 to 2 mm in size. The xenocrysts are rounded and peripherally zoned with skeletal phyric olivine occuring along their rims. Xenophyric clinopyroxene comprises 5 to 10% of the rock. The clinopyroxene is subhedral and 1 to 2 mm in size with a 0.1 mm rim of phyric clinopyroxene.

Xenocrysts derived from the crust are rare and comprise subhedral to anhedral quartz with a 0.1 mm-wide reaction rim of fine grained olivine and pyroxene.

Two xenoliths were observed in the scoria. The first is a cordierite-sillimanite gneiss, derived from the crust, with a grain size 0.1 to 0.5 mm, and a negligible reaction rim. The second is a plagioclase clinopyroxenite with plagioclase enclosing clinopyroxene grains 1.0 mm in size. The latter is described in detail below.

Two flows from breaches in the cone formed the proximal portion of the Dragon's Tongue. The flows coalesced to form the valley-filling flow described in Chapter 2. Samples are moderately vesicular. Vesicles, comprising 10 to 20% of the whole rock, are rounded to irregular and 0.1 to 10.0 mm in size. The lavas are olivine-clinopyroxene phyric and olivine-clinopyroxene xenophyric. Cognate material comprises 15% euhedral to subhedral olivine phenocrysts 0.3 to 4.0 mm in size, exhibiting skeletal growth, and as much as 10% subhedral to anhedral clinopyroxene, 0.3 to 1.0 mm in size. The groundmass comprises 20 to 35% subhedral plagioclase, 0.05 to 0.3 mm in size; 10 to 20% anhedral to subhedral Fe-Ti oxide, 0.01 to 0.03 mm in size; 5 to 10% isogranular olivine, 0.05 to 0.2 mm in size; 15 to 20% anhedral isogranular and intersertal clinopyroxene and 10 to 25% intersertal glass.

Xenocrysts comprise 10% anhedral olivine, 0.5 to 5.0 mm in size, exhibiting straining and phyric overgrowths; olivine xenocrysts often form aggregates. Three types of xenophyric clinopyroxene were identified. The first is colourless, 0.5 to 1.0 mm in size, and is pervasively corroded with little or no development of a phyric rim. The second, most common variety, is green to dark green in colour, peripherally corroded and also lacks a phyric rim. The third type is brown in colour, peripherally corroded, and has a 0.1 to 0.2 mm phyric rim, the latter strongly zoned.

Xenoliths of granodiorite, derived from the crust, occur in the proximal lavas. These exhibit narrow 0.1 mm reaction rims with the enclosing melt. The reaction rims are very fine-grained and comprise olivine, pyroxene and strongly-zoned plagioclase.

The second type of xenolith is that of the plagioclase clinopyroxenite already described from the scoria. Such xenoliths include rare primary kaersutite. Xenoliths of both these types are described in detail below.

Samples from the distal portion of the flow have identical groundmass mineralogy to that of samples from the proximal portion. Clinopyroxene phenocrysts are less common (5%) and attain only 0.5 mm in size. Xenocrysts and phenocrysts of olivine are as abundant and as large as in the proximal portions of the flow. Clinopyroxene xenocrysts are rare and more pervasively corroded, although of comparable size to those in the proximal portions. One xenolith of spinel lherzolite was found and is described below.

Kostal Lake Centre

The location of Kostal Lake Centre is shown in Fig.7. The Kostal Lake lavas comprise six eruptive units separated by an unknown, although probably brief, time (Chapter 2). The lack of extensive ash deposits on the most recent flows suggests that lava fountain activity ceased prior to cooling to the flows. Only one unit has soil formed on it. The soil is rich in ash and probably represents a significantly earlier event.

Samples from the earliest phase of activity are moderately vesicular, xenophyric and porphyritic. Vesicles are rounded to irregular, range in size from 0.1 to 5.0 mm and comprise approximately 15% of the whole rock.

Olivine is the dominant phenocryst phase, comprising 15% of the whole rock and occurring as euhedral and subhedral crystals 0.1 to 2.0 mm in size. Skeletal growth is common. Subhedral clinopyroxene, 0.2 to 0.5 mm in size, is a subordinate phenocryst phase comprising, at most, 5% of the whole rock. Plagioclase occurs only as a microphenocryst and exhibits seriate texture. The groundmass comprises 35% subhedral plagioclase, 0.05 to 0.2 mm in size; 20% subhedral to anhedral Fe-Ti oxide, 0.01 to 0.03 mm in size; 15% intersertal clinopyroxene, 0.05 to 0.2 mm; 5% euhedral to subhedral olivine, 0.05 to 0.2 mm in size and 15% intersertal glass.

All xenocrysts of olivine are rounded, 0.5 to 5.0 mm in size and are optically strained and zoned. Xenocrysts of clinopyroxene are 0.3 to 2.0 mm in size, anhedral and corroded, with a 0.1 mm wide rim of strongly zoned phyric clinopyroxene. The latter xenocryst is not abundant save in one sample where it comprises as much as 10% of the whole rock. A clinopyroxenite xenolith occurs in the same sample. Xenoliths derived from the crust comprise granodiorite of grain size 0.5 to 2.0 mm.

Samples from both north and south cones are highly vesicular; spherical vesicles, 0.1 to 6.0 mm in size comprise 50 to 70% of the whole rock. The cinders are olivine and clinopyroxene phyric, comprising 15% euhedral to subhedral olivine, 0.2 to 4.0 mm in size, exhibiting skeletal growth; 5% subhedral to anhedral clinopyroxene, 0.1 to 0.3 mm in size, and minor microphenocrysts of subhedral plagioclase 0.1 to 0.3 mm in length, exhibiting seriate and weak trachytic textures. the groundmasses comprise 30% subhedral plagioclase, 0.05 to 0.3 mm in size; 15% subhedral to anhedral Fe-Ti oxide, 0.01 to 0.05 mm in size; 5 to 10% isogranular olivine, 0.05 to 0.2 mm in size; 15% isogranular and intersertal clinopyroxene, 0.02 to 0.2 mm in size and 20 to 25% intersertal glass.

Samples from the north and south cones are nearly identical in their phenocryst and groundmass modes and textures but differ slightly in their xenocryst content. Olivine xenocrysts are not common in either cone; they are anhedral, 0.5 to 5.0 mm in size, often with overgrowths of phyric olivine. Pervasive optical straining and peripheral zoning are present.

Clinopyroxene xenocrysts are rare, anhedral, 0.5 to 2.0 mm in size and are pervasively corroded with only a thin (0.02 to 0.05 mm) rim of phyric clinopyroxene. One orthopyroxene grain 0.5 mm in size, rimmed with olivine, and a fragment of wehrlite with a grain size of 2 mm occur in a sample from the south cone.

The lava flow from the north cone is homogeneous for its observed length, in both phenocryst and groundmass mineralogy, but not in xenocryst abundance. Samples are moderately vesicular, vesicles ranging in size from 0.1 to 7.0 mm and in shape from spherical to irregular. Phenocrysts comprise 15 to 20% euhedral olivine, 0.2 to 3.0 mm in size, exhibiting skeletal growth, and 5 to 10% euhedral to subhedral clinopyroxene, 0.2 to 0.5 mm in size, forming glomerophenocrysts. Microphenocrysts of plagioclase are rare and exhibit seriate texture. The groundmass comprises 25% subhedral plagioclase in weak trachytic orientation, 0.05 to 0.2 mm in length; 5 to 15% anhedral to subhedral Fe-Ti oxide, 0.01 to 0.05 mm in size; 5% anhedral olivine, 0.05 to 0.2 mm in size; 20% intersertal clinopyroxene, 0.05 to 0.3 mm in size and 15% intersertal glass.

Xenocrysts in the flow occur in significant quantity only in the flow margins and in its distal portions. Here, xenophyric clinopyroxene comprises as much as 15% of the whole rock. Olivine xenocrysts comprise 5% of the whole rock throughout the flow. The olivine xenocrysts are anhedral, strained and 0.5 to 4.0 mm in size, with overgrowths of phyric olivine. Clinopyroxene xenocrysts are anhedral and occur in various stages of corrosion. The degree of corrosion is apparently independent of grain size. The xenocrysts are 0.5 to 3.0 mm in size with only a thin (0.05 mm) phyric rim.

The lava flow from the south cone is similar in nearly all respects to that from the north cone; the groundmass and phenocryst assemblages are identical. Olivine xenocrysts, as in the flow from the north cone, are rounded, strained, and 0.5 to 5.0 mm in size, with a thin overgrowth of phyric olivine. The main differences are in the ubiquity of clinopyroxene xenocrysts and in the presence of plagioclase xenocrysts. Clinopyroxene xenocrysts are anhedral, strongly zoned and corroded with a 0.05 mm-wide phyric rim. The plagioclase xenocrysts are peripherally corroded, anhedral and vary in size from 1.0 to 5.0 mm. The plagioclase is probably derived from a granodiorite.

The remaining flow is extruded from a lava tube and is described in Chapter 2. It is probably part of the lava pulse which produced the south lava lake. Samples from the tube flow are identical in vesicularity, phenocryst and groundmass assemblages to the flows from the north and south cones. The xenocryst assemblage is identical to that of the southern flow, except that the proportions of olivine and clinopyroxene are slightly higher. In addition, xenoliths of spinel lherzolite, clinopyroxenite and granodiorite occur. The granodiorite contains plagioclase crystals similar to those found in the south flow. The ultramafic xenoliths are described in detail below.

Summary of lava petrography

Lavas erupted from centres in the Wells Gray area, during and since the last glaciation comprise ice/water-contact and subaerial extrusive rocks. The ice/water-contact lavas are near-holohyaline; subaerial lavas are hypocrystalline. Both morphologic types fall into the following three mineralogical classes. Lavas from Hyalo Ridge are unique in this study but are typical of the earlier lavas in the area (Hickson 1987, Hickson and Souther 1984) They are olivine + plagioclase phyric; clinopyroxene is absent from the phenocryst assemblage and xenoliths are rare or absent.

The second mineralogical type is represented by lavas from the Spanish Lake and Flourmill centres. The distinctive feature of these centres is the presence of glomerophenocrysts of clinopyroxene, in quantities sufficient to identify the lavas as ankaramites after Fiesinger and Nicholls (1975).

The third mineralogical type, which grades into the second, is represented by the remaining centres in the study area and is identified by the phenocryst assemblage olivine ± clinopyroxene. The presence or absence of clinopyroxene is usually dependent upon the degree of quenching in the lava; probably all lavas of this type are potentially clinopyroxene-phyric. Both the second and third types contain abundant xenocrysts of olivine and, especially, clinopyroxene. Xenoliths of spinel lherzolite and clinopyroxenite are also common.

The first type of lava differs markedly from the second and third types, not only in the phenocryst assemblage but also in the paucity of xenoliths and in non-vesicular character. It is possible, therefore, on the basis of mineral assemblage, that these lavas have a petrogenetic history which differs from the other, clinopyroxene-bearing lavas in the study area.

B. Ultramafic xenoliths

Xenoliths bearing clinopyroxene ± olivine ± spinel ± orthopyroxene are common in all lavas with titaniferous augite phenocrysts (see above). Small ultramafic inclusions are ubiquitous and, in sectioning samples, a bias was given to examining the textures present in the incognate material.

Two mineral assemblages are common in the Wells Gray xenoliths. The first is a Cr-spinel lherzolite assemblage, comprising olivine, clinopyroxene, orthopyroxene and spinel. The second assemblage comprises Al-spinel and clinopyroxene. The small size of most of the xenoliths may result in the absence of one or more phases from any one xenolith.

Xenoliths vary in their degree of preservation from those which have remained sealed against invasion of the melt to those where pervasive invasion of melt has occurred along grain boundaries and corrosion has taken place. Ubiquitous xenocrysts represent the extreme case where a xenolith has disintegrated. Xenoliths of the first type are typically rounded, with a narrow reaction rim and are usually of Cr-spinel lherzolite (see below). Xenoliths of the second type are typically angular, fractured and deeply corroded; these are dominantly Al-spinel clinopyroxenites, described below. It is probable, therefore that the Cr-spinel bearing assemblage either represents a more refractory composition, less amenable to dissolution by the enclosing magma, or that the Cr-spinel bearing xenoliths have been entrained for a significantly shorter time. The two hypotheses are not mutually exclusive.

In the following descriptions the terminology of Mercier and Nicolas (1975) will be used as far as possible. The textures of the inclusions are frequently perturbed by corrosion but a general classification is usually possible.

Spinel lherzolite assemblage

Xenoliths of the Cr-spinel lherzolite assemblage are common in the most recent phase in Spanish Lake and in the south cone and tube flow at Kostal Lake. In the latter centre the xenoliths are as much as 9.0 cm in length. Spinel lherzolite is less common, but present, in the Ray Ridge flow, in the distal, more recent, portion of the Dragon's Tongue and in the most recent phase of activity at the Flourmill centre. Xenocryst assemblages typical of this lherzolite also occur in the Spanish Mump and Pyramid Mountain centres, although xenoliths are absent. It is possible that the xenoliths disintegrate upon quenching.

Nearly all xenoliths of this type examined contain Cr-spinel and are related to the Cr-diopside type described by Wilshire and Shervais (1975). The exception is an

Al-spinel bearing wehrlite collected from a locality on the Trophy Range, to the south of the field area. Those collected within the study area are, without exception, Cr-spinel lherzolites. Corrosion occurs only on the margins of the xenoliths. Negligible invasion by the melt has taken place and the xenoliths are typically rounded.

The Al-spinel bearing wehrlite from Trophy Mountain (Plate 11A) is an example of Mercier and Nicolas' (1975) protoclastic texture. The rock comprises 30% anhedral strained olivine, of grain size 1.0 to 2.0 mm, in porphyroclastic aggregates, as much as 6 mm in size, in approximate optical continuity and 5 to 10% green spinel, in vermicular and equigranular habits and 0.5 to 1.0 mm in size, enclosed in a matrix of clinopyroxene, 0.5 to 1.5 mm in size. Porphyroclasis has commenced in the clinopyroxene grains but preferred orientation is not visible, within the constraints imposed by the single section cut.

The Cr-spinel bearing xenoliths and related types, such as websterite and lherzolite fragments, exhibit fabrics ranging from protoclastic to equigranular. The least deformed of the xenoliths exhibit a protoclastic texture.

Xenoliths exhibiting at least minor amounts of deformation are more common. Porphyroclastic xenoliths comprise porphyroclasts of olivine (Plate 11B) or, less commonly clinopyroxene and orthopyroxene, as much as 7 mm in size, enclosed in a matrix of smaller, unstrained granoblastic olivine and pyroxene. The grain size of the granoblastic matrix ranges from 0.5 to 1.5 mm. Spinel grains, of similar size, often retain the vermicular form characteristic of protogranular xenoliths; in other cases they are equant.

The tabular and mosaic equigranular textures are typical of a spinel wehrlite fragment from the Trophy Range (Plate 11C) and a Cr-spinel lherzolite fragment from the Spanish Lake Centre (Plate 11D), respectively. The tabular equigranular xenoliths have grain sizes of 1.0 to 2.0 mm; the mosaic equigranular xenoliths are finer grained, with a range of 0.5 to 1.0 mm. This is in agreement with the descriptions given by Mercier and Nicolas (1975). Within the limited number of xenoliths examined, there is no gradation of xenolith deformation with area. Each textural type is represented at each of the centres listed above.

Clinopyroxenites

Clinopyroxenite xenoliths are abundant in lavas at Kostal Lake, Flourmill and in the Dragon's Tongue; they are present, in reduced numbers, at the Spanish Lake centre and in the earlier-erupted lavas on Ray Mountain. Fewer samples were taken than of spinel lherzolite, precluding an accurate assessment by areas, but, as with spinel lherzolite, the textural distribution appears the same for all centres. Equigranular textures are absent in all centres. Porphyroclastic textures are less common than in the spinel lherzolite assemblage; protoclastic textures are far more common (Plate 11E).

Xenoliths with protoclastic textures comprise coarse-grained allotriomorphic aggregates. Clinopyroxene grains range in size from 3 to 10 mm in size, show optical straining and contain inclusions of sulphide. Spinel, where present, is green in colour and occurs as vermicular anhedra, 0.5 to 1.5 mm in size. The mineral comprises less than 5% of any sample. Where porphyroclasis has commenced, the porphyroclastic aggregates are 7 to 10 mm in size, in a matrix comprising clinopyroxene or, less commonly, olivine. The matrix grain size is 0.5 to 2.0 mm in size. Straining of the fabric is clearly visible in some samples (Plate 11F).

Plagioclase clinopyroxenites

Two samples from the proximal portion of the Dragon's Tongue are spinel plagioclase clinopyroxenites, comprising 80 to 90% rounded anhedral clinopyroxene, 0.5 to 10 mm in size; 5 to 10% intersertal hercynitic spinel 0.5 to 3.0 mm in size and 5 to 10% intersertal plagioclase. All phases exhibit a sharp reaction rim with the enclosing melt, suggesting that the material, despite the presence of plagioclase, is not cognate. The spinel commonly exhibits the intersertal texture described by Mercier and Nicolas (1975) as characteristic of their porphyroclastic texture and the clinopyroxene grains occur in 4 to 5 mm porphyroclastic clusters with optical near-continuity. The plagioclase, as reported in Chapter 4, is somewhat more sodic than that crystallised from the host magma and is possibly of post-deformational origin. Accessory phases in these xenoliths are discussed below.

Cumulate xenoliths

Wehrlite cumulates occur in the tube flow at Kostal Lake, in one sample from a parasitic cone at Spanish Lake and in several samples from the Flourmill centre. The wehrlites comprise 20 to 30% anhedral olivine, 0.5 to 2.0 mm in size, enclosed, completely or partially, by anhedral crystals of clinopyroxene, 1.0 to 6.0 mm in size. The clinopyroxene is frequently pervasively corroded by the host lava; olivine is peripherally corroded. The cumulates are therefore incognate and are possibly derived from locations at or near the base of the crust.

Three xenoliths from the lavas erupted during the earlier phase of activity at Ray Mountain are gabbro cumulates. They are coarse grained and allotriomorphic, comprising 2 to 20% rounded anhedral olivine, 1 to 2 mm in size; 10 to 15% anhedral Fe-Ti oxide, 0.5 mm in size; 30 to 40% anhedral corroded clinopyroxene, 1.0 to 2.0 mm in size, poikilitically enclosed by plagioclase, as much as 12 mm in size. All xenoliths are rounded and 2 to 3 cm in size. The plagioclase exhibits a weak reaction texture with the enclosing magma. These xenoliths are interpreted as the product of a high-level fractionation process; the morphology of this volcano (fissure type) is unique in the Wells Gray area.

One xenolith in the distal portion of the Dragon's Tongue is a fine-grained wehrlite, comprising 50% subhedral olivine and 50% subhedral clinopyroxene, both 0.3 to 0.5 mm in size. Layering is absent. The xenolith is 10 mm in size and is interpreted as the result of high-level crystal fractionation.

Summary of ultramafic xenolith petrography

Three ultramafic xenolith assemblages are present in the clinopyroxene-bearing lavas of the Wells Gray area. The first comprises olivine ± clinopyroxene ± plagioclase cumulates which occur at the Flourmill centre, in the distal portion of the Dragon's Tongue, in the earlier phases of activity at Ray Mountain and at Kostal Lake. The second and third types are a spinel lherzolite and a clinopyroxenite assemblage. Both second and third types are assumed to be derived from the upper mantle. The spinel lherzolite assemblage is characterised by Cr-spinel, the clinopyroxenite assemblage by Al-spinel. This division is analogous to that established by Wilshire and Shervais (1975) for the southwestern United States.

Textural studies on the xenoliths indicate that the Cr-spinel lherzolite assemblage exhibits the porphyroclastic and equigranular textures described by Mercier and Nicolas (1975). Xenoliths of the Al-spinel clinopyroxenite assemblage are more pervasively corroded and exhibit the less deformed protoclastic and porphyroclastic textures. The better preservation of the spinel lherzolites suggests a shorter immersion time in the host magmas. The degree of corrosion of the spinel clinopyroxenites suggests a longer residence time in the host magmas and, possibly a greater depth of origin.

C. Volatile bearing phases

Phlogopite

Two wehrlite cumulates at Kostal Lake contain inclusions of phlogopite 0.05 to 0.1 mm in length, enclosed by a clinopyroxene grain. The inclusions are primary and occur in trains parallel to the b crystallographic axis of the clinopyroxene and parallel to the (001) face.

Kaersutite

One spinel clinopyroxenite xenolith in the proximal portion of the Dragon's Tongue includes kaersutite, in amounts as much as 5% and as much as 2.0 mm in size. The kaersutite is subhedral to anhedral, is rarely enclosed by clinopyroxene grains and also intergrown with the clinopyroxene, suggesting an equilibrium relationship (Plates 12A, 12B). Where the amphibole is in contact with the host magma, oxidation and dissolution of the former have occurred, forming rims of fine-grained Fe-Ti oxide. The amphibole is clearly incognate.

Apatite

Apatite occurs as several primary inclusions, 0.01 to 0.05 mm in size, in a clinopyroxene grain in a clinopyroxene + orthopyroxene aggregate hosted by a lava flow erupted during the older phase of activity at the Flourmill centre (Plates 12C, D, E). The aggregate has a grain size of 0.5 mm and an overall size of 3.0 mm. Its small size, relative to its grain size, precludes accurate classification on the basis of modal mineralogy; the aggregate could easily represent a pyroxene-rich vein or glomerocryst in a spinel lherzolite. The inclusion is rimmed with strongly zoned phyric clinopyroxene and is clearly incognate. The texture, after Mercier and Nicolas (1975) is mosaic equigranular.

The apatite grains are subhedral to anhedral and occur in a clinopyroxene grain near the centre of the inclusion (Plates 12C, 12D). The clinopyroxene grain has been fractured, apparently after inclusion of the apatite; however, at least two of the apatite inclusions are still sealed. The average size of the inclusions is 20 µm. This is the first recorded occurrence of primary apatite in a mantle assemblage in Canada.

4.

MINERAL CHEMISTRY

Analysis of the major mineral phases present in the Wells Gray basalts was carried out in order to discover the extent of mineralogical variation in the lavas. Petrographic analysis, described in Chapter 3, indicates that many of the lavas contain olivine and clinopyroxene xenocrysts of several different types. These xenocrysts probably represent mineral assemblages present near the source regions of the alkali basalts and were analysed to determine their differences in composition from those of the phenocrysts and to estimate the extent to which the isotopic and chemical compositions of the lavas have been altered by the xenocryst material.

A. Analytical procedure

Electron microbeam analysis

Samples were prepared as polished thin sections, permitting detailed textural studies in addition to detailed chemical analysis by microbeam. Fragments of glass and crystals from hyaloclastite samples were prepared as polished grain mounts. Glass fragments to be analysed for their volatile concentrations were polished on both sides, prior to microbeam analysis. Seven such grain mounts were prepared. Petrographic descriptions of all rock samples are given in Chapter 3.

A detailed description of analytical procedure using the electron microprobe is given in Appendix A. Major mineral phases, accessory minerals and groundmass glass were analysed for major elements using an ARL SEMQ electron microprobe with an ORTEC energy dispersive system. Accelerating voltage during each run was 15 kV and the sample current was 0.39 nA. The ratio of sample current to aperture current was measured at the beginning and end of each run; aperture current was monitored throughout a run.

Analytical standards for each element analysed in each phase are listed in Table A-1 (Appendix A). The concentrations of constituent elements in all standards are listed in Table A-2. Care was taken, where possible, to choose standards of a similar matrix to that of the phase to be analyzed.

All spectra were collected over a period of four minutes live time. Olivine, pyroxene, oxide minerals and sulphide minerals were analysed using a point beam in a single location. Plagioclase was also analysed in this manner after measurements indicated that prolonged bombardment did not significantly alter the Na Kα counts obtained using a wavelength dispersive spectrometer. For apatite and volcanic glass each spectrum was obtained over several points, using a 30 second (live time) acquisition period and a beam rastered over an area of 400 μm^2.

A minimum of 10^6 counts (full spectrum) were obtained for each sample analysed. Data were stored on floppy discs. Data processing was carried out with the EDATA2 data reduction programme of Smith and Gold (©1976). Results were examined for totals and, where appropriate, stoichiometry.

Analytical precision

Estimates of analytical precision for all microbeam analyses are based upon the analytical precision of element concentrations in the analytical standards, and upon the counting statistics for both standard and sample, for each element analysed (Smith 1976). Precisions (2σ) for each element are listed in Table A-3 (Appendix A), as a percentage of the total concentration of that element in each phase analysed.

Comparison of the analyses in this study with analyses obtained using the wavelength dispersive system was not possible, due to technical difficulties encountered when using the gas-flow counters in that system. However, Brearley (1986) reports close agreement between analyses obtained using either system.

B. Analytical results

Clinopyroxene

Analytical results for all clinopyroxenes analysed are presented in Tables B-1 and B-2 in Appendix B. Table B-1 lists the compositions of all phenocrysts and xenocrysts analysed and Table B-2 lists the compositions of grains in xenoliths. In both cases, ferric iron is calculated using stoichiometry and the end member percentages are calculated using the method of Lindsley (1983). All analyses in Tables B-1 and B-2 are plotted on a portion of the pyroxene quadrilateral, in Figs.8 to 15. Xenolith pyroxene compositions from Table B-2 are plotted in Fig.16. Samples selected for rudimentary two-pyroxene geothermometry are plotted on Fig.19.

Samples from Hyalo Ridge do not contain clinopyroxene phenocrysts. The groundmass pyroxenes are augites with moderate Al_2O_3 and low TiO_2 and Na_2O concentrations (Figs.9 and 17), with lower Wo concentrations than the pyroxenes in the clinopyroxene-phyric lavas. The pyroxenes are small in size and are unzoned.

Clinopyroxenes analysed, from all clinopyroxene-phyric lavas in the Wells Gray area, range in composition from diopside to augite. None exceed 22 mol.% ferrosilite (Fig.18). The clinopyroxenes analysed comprise four main types. The first of these is a cognate phase, frequently occuring either as discrete phenocrysts or as phyric rims on clinopyroxene xenocrysts. As noted in Chapter 3, the phenocrysts are frequently zoned on a very fine scale (approximately 1 to 10 μm) and considerable caution was exercised in the selection of homogeneous volumes for analysis. The zoning follows the trend labelled "cognate" in Fig.18 to more ferroan varieties at phenocryst margins for all centres where a significant population was analysed. Examples of this trend, for individual centres, are seen in data from all the postglacial centres (Figs.10, 11, 14 and 15).

The second variety of pyroxene is xenophyric and occurs as extensively corroded xenocrysts in the alkaline lavas (Plate 10B). Their composition is that of ferroan augite, poor in Al_2O_3. Such compositions are represented in Fig.8 (which includes the compositions of the grains shown in Plate 10B) and in Figs.10, 11, 12, 13 and 15. Xenocrysts of this type are frequently zoned, with a still more ferroan rim (Figs.10, 11 and 15). Where the corrosion is less pervasive, there are frequently overgrowths of phyric pyroxene, with compositions in the cognate range.

The third variety of pyroxene is the most common of the xenocrysts. This variety is rich in Al_2O_3 and is more magnesian than the ferroan augites; this type is less corroded and frequently has a rim of phyric clinopyroxene (Plate 10B). Zoned cores in xenocrysts of this type are far less common, but occasionally zonation to more ferroan compositions has taken place prior to corrosion and the addition of a phyric rim (Fig.15).

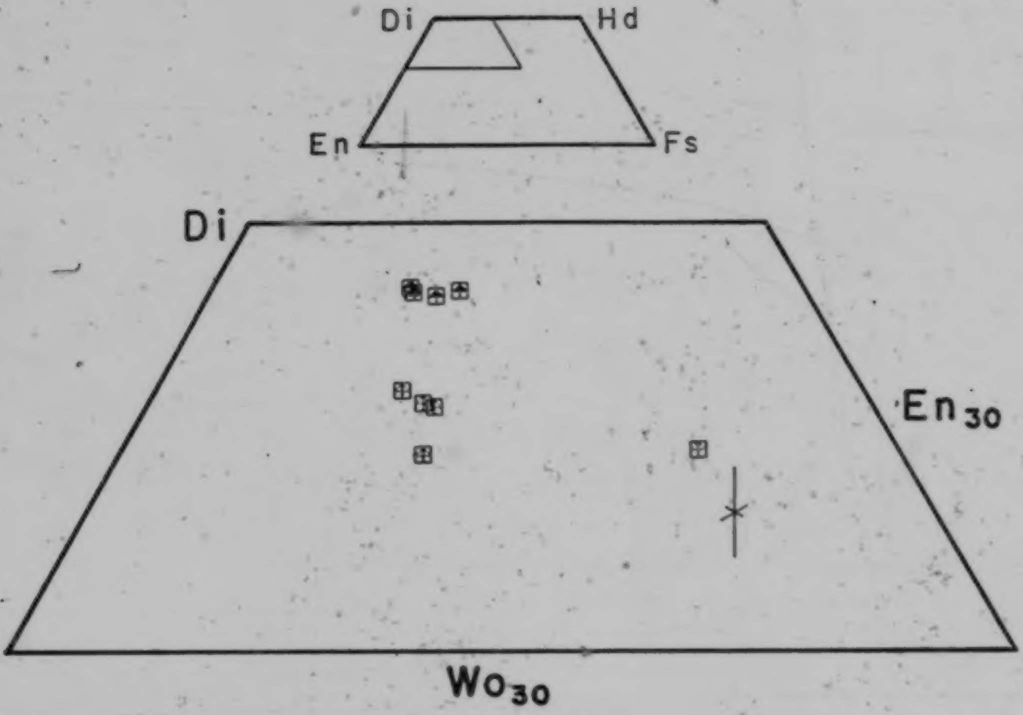

Fig. 8. Clinopyroxenes from Spanish Bonk. Analyses are recalculated after the method of Lindsley (1983) and are plotted on a part of the pyroxene quadrilateral, shown above. Figs. 9 to 16 and Fig. 18 show the same part of the quadrilateral. Symbols used are solid for cognate crystals, open for xenocrysts. Error bars are given at the 2σ confidence level based on the maximum observed concentrations of each component. Two types of xenocryst, one Fe-rich, the other Al-rich (Plate 10B) are present.

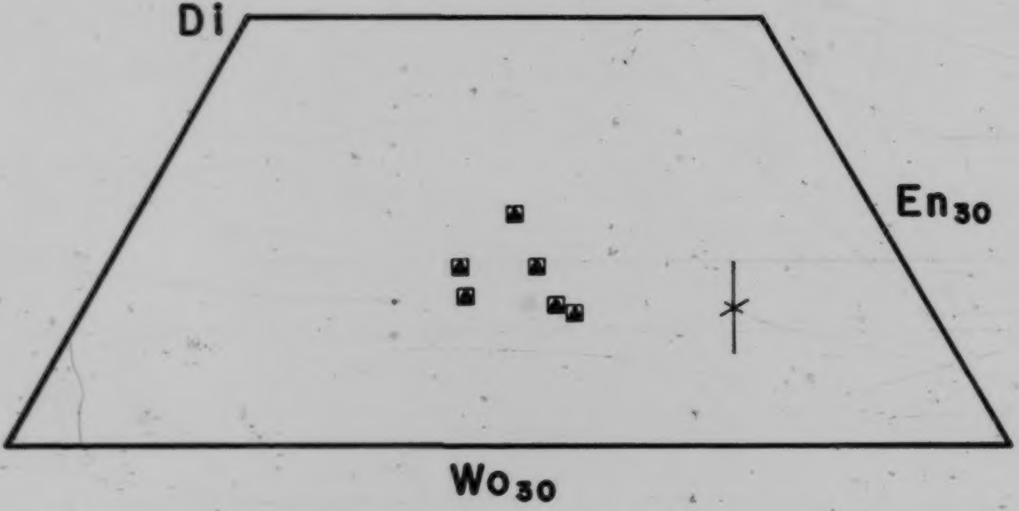

Fig. 9. Clinopyroxenes from Hyalo Ridge. Analyses are recalculated after the method of Lindsley (1983) and are plotted on a part of the pyroxene quadrilateral, shown in Fig.8. Symbols used are solid; all crystals are cognate. Error bars are given at the 2σ confidence level based on the maximum observed concentrations of each component.

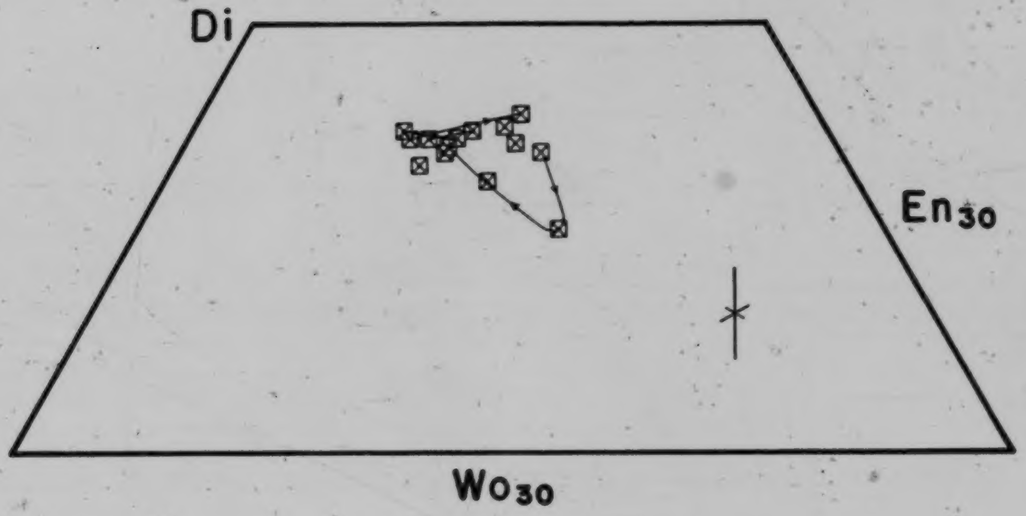

Fig. 10. Clinopyroxenes from Spanish Lake. Analyses are recalculated after the method of Lindsley (1983) and are plotted on a part of the pyroxene quadrilateral, shown in Fig.8. Error bars are given at the 2σ confidence level based on the maximum observed concentrations of each component. Only one xenocryst was analysed, giving a composition which was zoned towards an Fe-rich corroded surface, overgrown by phyric clinopyroxene. Change in composition by zonation, from core to rim, is shown by arrows.

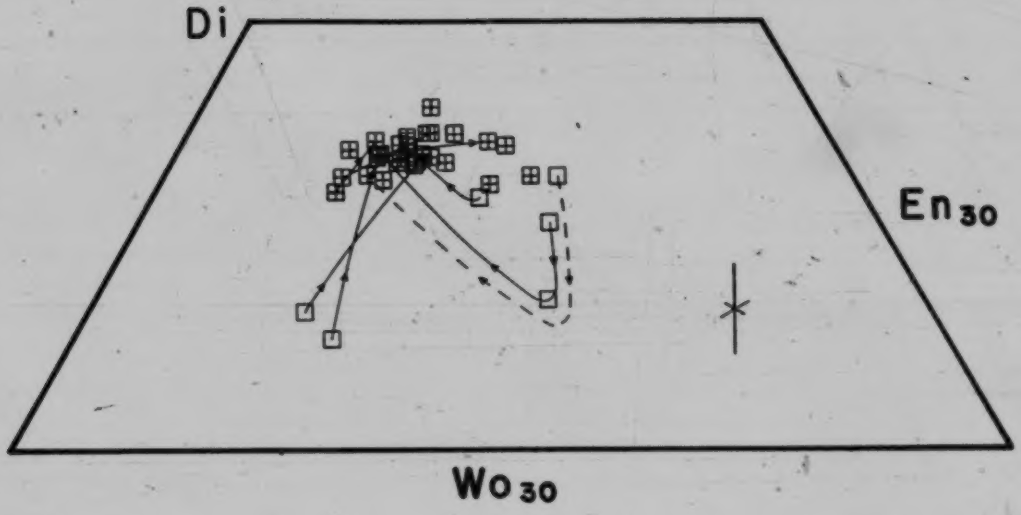

Fig. 11. Clinopyroxenes from Flourmill Centre. Analyses are recalculated after the method of Lindsley (1983) and are plotted on a part of the pyroxene quadrilateral, shown in Fig.8. Symbols used are solid for cognate crystals, open for xenocrysts. Error bars are given at the 2σ confidence level based on the maximum observed concentrations of each component. Two types of xenocryst, Fe-rich and Al-rich, were analysed. Arrowed lines indicate compositional variation from core to cognate rim.

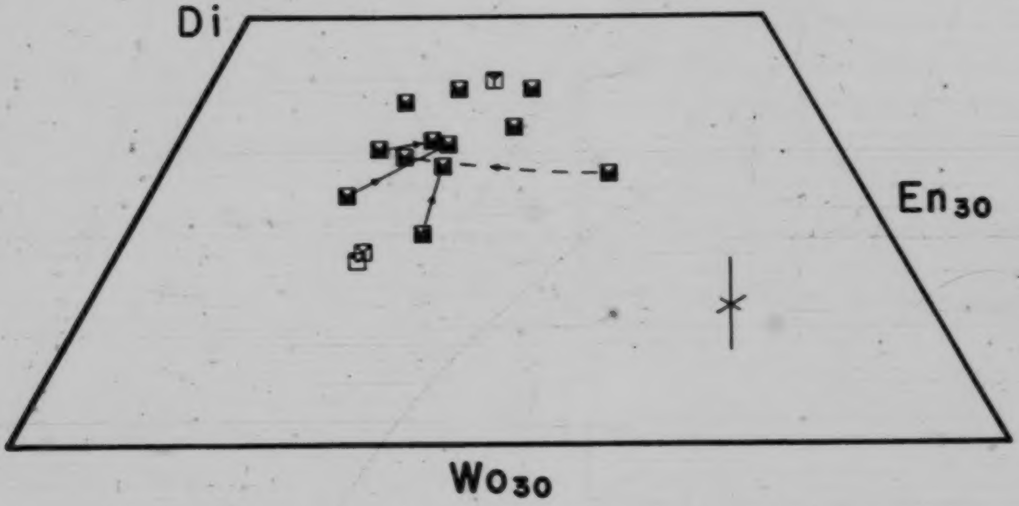

Fig. 12. Clinopyroxenes from Ray Mountain. Analyses are recalculated after the method of Lindsley (1983) and are plotted on a part of the pyroxene quadrilateral, shown in Fig.8. Symbols used are solid for cognate crystals, open for xenocrysts. Error bars are given at the 2σ confidence level based on the maximum observed concentrations of each component. Change in composition by zonation, from core to rim, is shown by arrows.

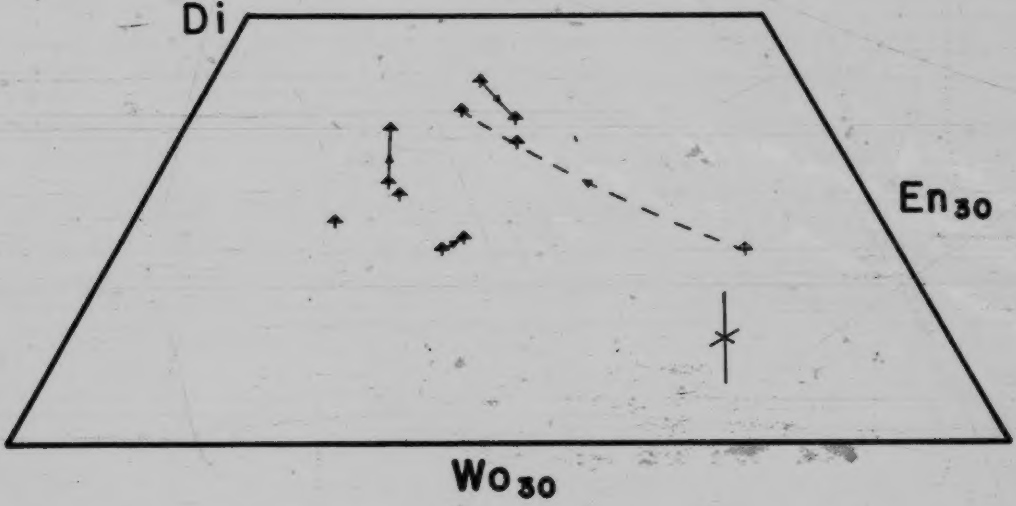

Fig. 13. Clinopyroxenes from Pointed Stick Cone and Ray Ridge. Analyses are recalculated after the method of Lindsley (1983) and are plotted on a part of the pyroxene quadrilateral, shown in Fig.8. Symbols used are solid for cognate crystals, open for xenocrysts. Error bars are given at the 2σ confidence level based on the maximum observed concentrations of each component. The single xenocryst is Fe-rich. Change in composition by zonation, from core to rim, is shown by arrows.

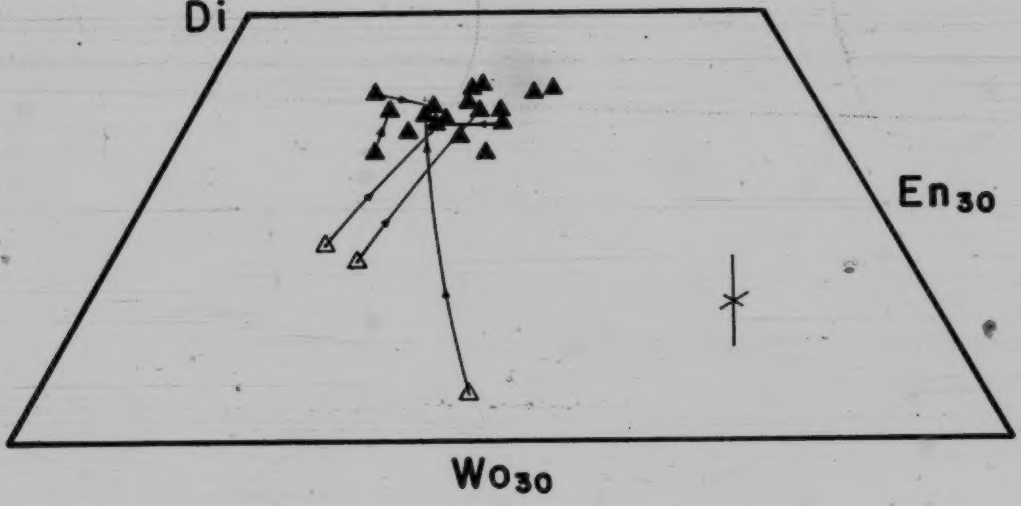

Fig. 14. Clinopyroxenes from Dragonhead. Analyses are recalculated after the method of Lindsley (1983) and are plotted on a part of the pyroxene quadrilateral, shown in Fig.8. Symbols used are solid for cognate crystals, open for xenocrysts. Error bars are given at the 2σ confidence level based on the maximum observed concentrations of each component. The xenocrysts analysed are exclusively Al-rich. Change in composition by zonation, from core to rim, is shown by arrows.

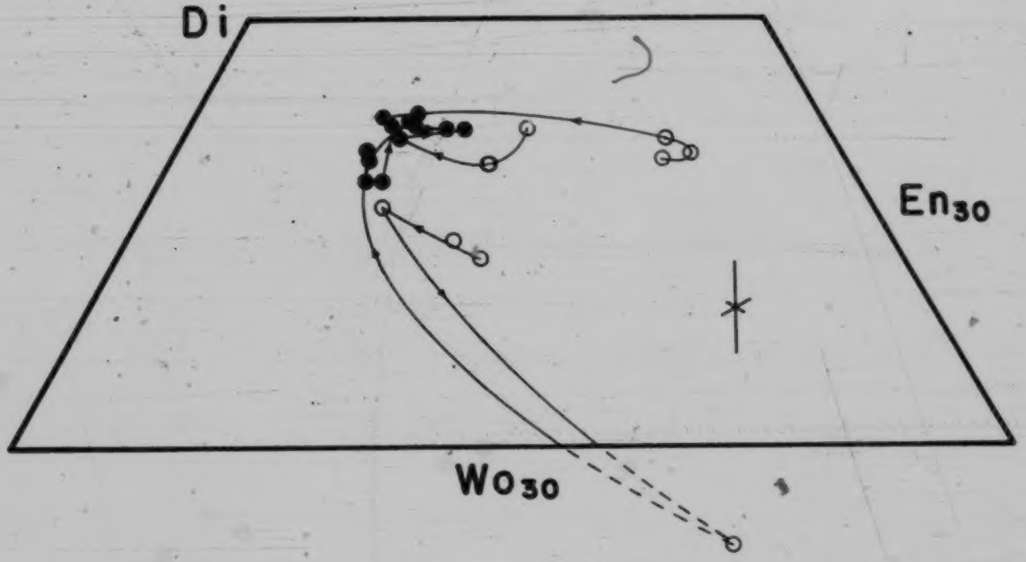

Fig. 15. Clinopyroxenes from Kostal Lake. Analyses are recalculated after the method of Lindsley (1983) and are plotted on a part of the pyroxene quadrilateral, shown in Fig.8. Symbols used are solid for cognate crystals, open for xenocrysts. Error bars are given at the 2σ confidence level based on the maximum observed concentrations of each component. The xenocrysts analysed include both Al-rich and Fe-rich types and are strongly zoned. Change in composition by zonation, from core to rim, is shown by arrows.

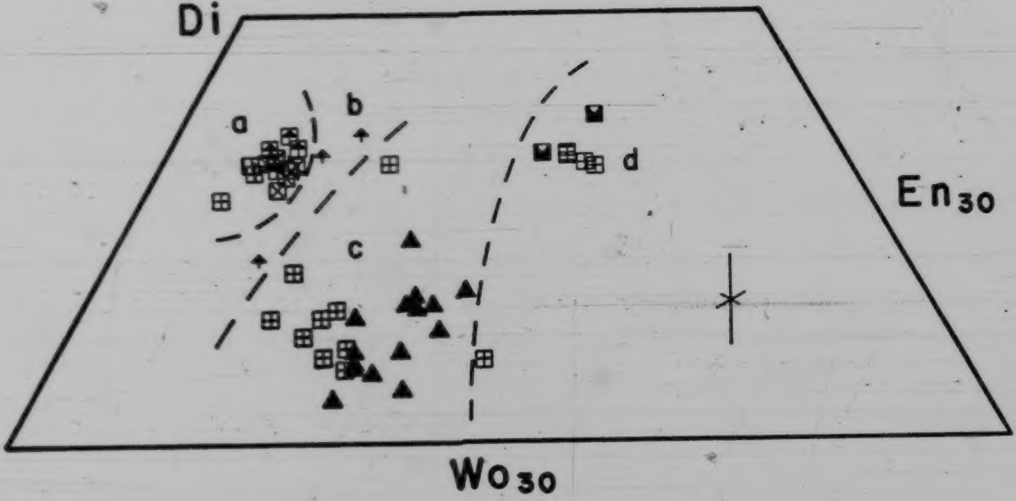

Fig. 16. Clinopyroxenes from the xenoliths. Analyses are recalculated after the method of Lindsley (1983) and are plotted on a part of the pyroxene quadrilateral, shown in Fig.8. Symbols used for each centre are listed in Table 1. Error bars are given at the 2σ confidence level based on the maximum observed concentrations of each component. a = Cr-rich spinel lherzolite assemblage; b = Fe-rich spinel lherzolite found on Ray Ridge; c = Al-rich spinel clinopyroxenite; d = Fe-rich websterite and clinopyroxenite.

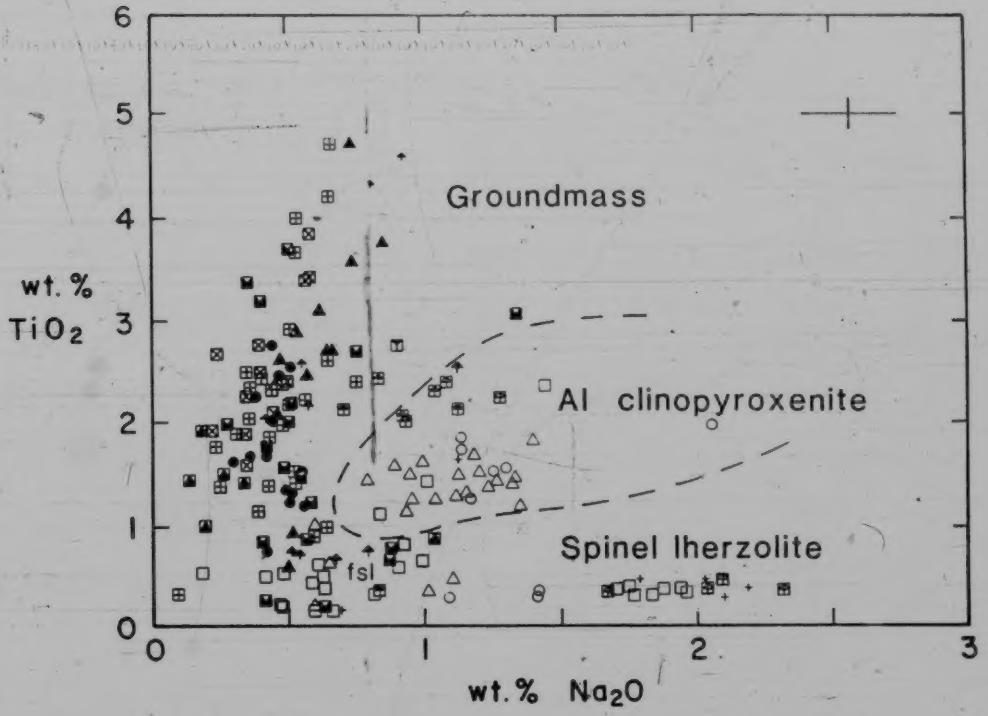

Fig. 17. Na_2O against TiO_2 in clinopyroxenes. Symbols used are solid for cognate crystals, open for xenocrysts; symbols used for each centre are listed in Table 1. Error bars are given at the 2σ confidence level based on the maximum observed concentrations of each component. The three main fields of composition are shown; clinopyroxenes from the Fe-rich spinel lherzolite lie in the field labelled fsl, intermediate between spinel lherzolite and the less titaniferous groundmass clinopyroxenes.

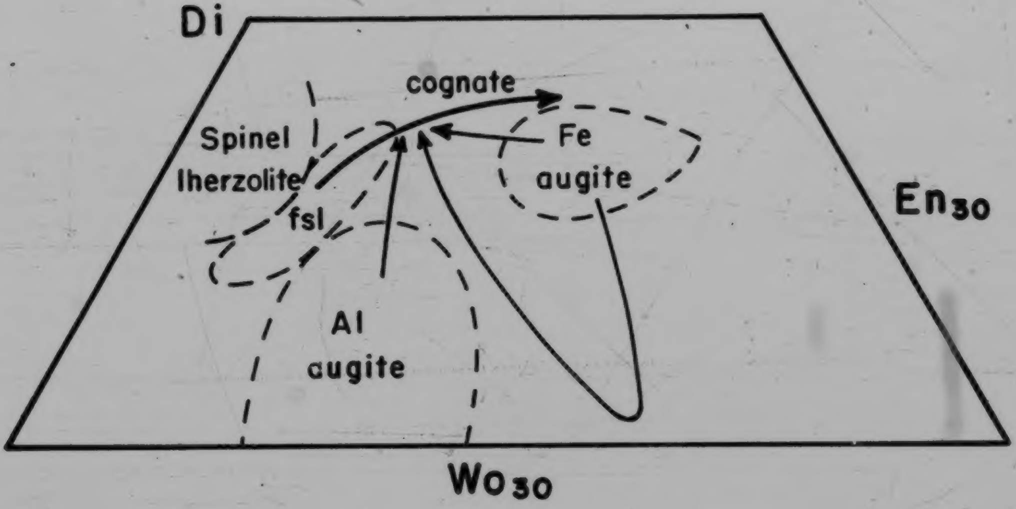
Di
cognate
Spinel
lherzolite
fsl
Fe
augite
En30
Al
augite
Wo30

Fig. 18. Summary of clinopyroxene compositions from Wells Gray Park. The fields of composition and zonation trends for each major group are shown on a part of the pyroxene quadrilateral, shown in Fig.8.

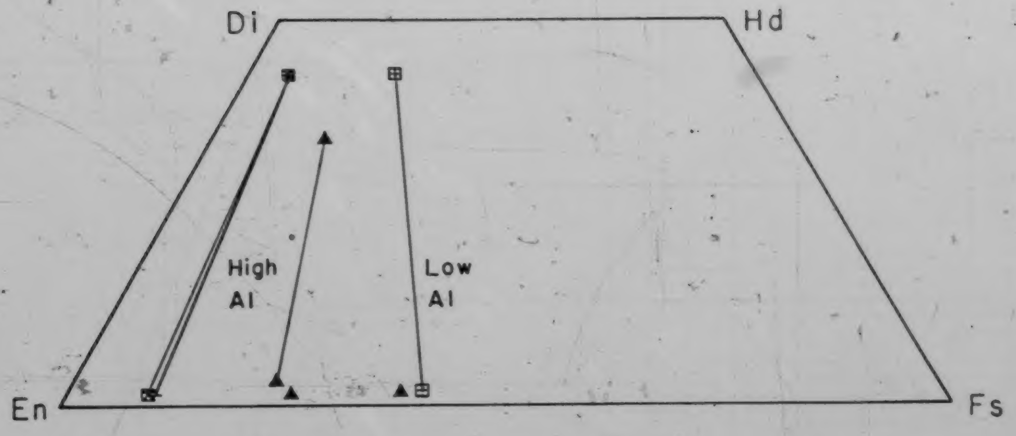

Fig. 19. Pyroxene quadrilateral showing pairs selected for thermometry. Symbols used for each centre are listed in Table 1. The mineral pairs are chosen from Pyramid Mountain (13/8/10), Spanish Lake (24/8/13X), Dragonhead (14/8/1X) and from Flourmill (2/8/6X3).

The fourth variety of clinopyroxene, occuring as a very rare xenocryst, is chrome diopside, associated with a spinel lherzolite assemblage in the hyaloclastites of Spanish Mump and Pyramid Mountain. The compositional range of this variety is shown in Fig.16. These xenocrysts are far less pervasively corroded than the other varieties and are rounded, with negligible phyric rims. Their compositions and textures are identical to those of the Cr-rich diopside crystals found in xenoliths of Cr-spinel lherzolite throughout the study area.

Xenoliths in the study area also contain clinopyroxene grains from any of four different types (Fig.16). Three of the types are identical to those identified as xenocrysts. The fourth type occurs in an iron-rich spinel wehrlite nodule with a mosaic equigranular texture, found in the Ray Ridge lava flow. The size of the nodule is sufficiently small as to preclude accurate classification of the rock type; conceivably, the xenolith is from a spinel lherzolite assemblage. The clinopyroxene is similar in composition to the other Cr-diopsides but is significantly richer in ΣFe and Cr.

The Al-rich augite crystals occur in association with Al-rich spinel in spinel clinopyroxenite xenoliths. This type of xenolith is most common in the proximal portions of the Dragon's Tongue. The xenoliths in this flow also contain kaersutite in association with the clinopyroxene (Plates 12A, 12B). It is possible that clinopyroxene xenocrysts of this type were formed by reaction of the kaersutite.

Iron-rich augite crystals occur in a small ultramafic xenolith from the older lavas erupted from the Flourmill Centre. The xenolith is a websterite with a mosaic equigranular texture (Plate 12C) and contains, included within the clinopyroxene, grains of primary apatite (Plates 12C, D, E). The compositions are typical of apatite (Table B-11). The augite is homogeneous, has a reaction rim and is overgrown with phyric clinopyroxene.

Olivine

Olivine is the predominant phenocryst phase in all the lavas, comprising as much as 20% of the mode. In addition, optically strained and partially resorbed olivine xenocrysts are ubiquitous (Plate 10D). Analyses of olivine crystals from all the lavas are presented in Table B-3 in Appendix B. A summary of the compositional ranges, for each centre, is given in Fig.20.

The lavas from Hyalo Ridge are olivine-plagioclase phyric and are poor in xenocrysts and xenoliths, in contrast to the xenocryst- and xenolith-rich olivine-clinopyroxene phyric lavas from the other centres. Olivine crystals were analysed in samples from the hyaloclastite mound (23/8/2), the basal flow of the lava cap (23/8/12) and from the uppermost flow (23/8/6) in the tuya structure. The two samples from the lower part of the edifice have more Fo-rich values ranging from Fo_{85} to Fo_{74}. The sample from the upper part has olivines ranging in composition from Fo_{80} to Fo_{63}.

Three compositional ranges of olivine occur in the clinopyroxene-phyric lavas. The first is a narrow compositional range from Fo_{90} to Fo_{91}, occuring in xenocrysts from Spanish Mump, Spanish Lake, and Pyramid Mountain (Fig.20). All olivine grains separated from hyaloclastite at Spanish Mump and Pyramid Mountain have Fo contents close to 90 and "primary" NiO contents of 0.4 to 0.5 weight percent. These magnesian olivines, in thin section, exhibit straining and resorbed margins (Plate 10D). They are interpreted as xenocrysts, separated from a lherzolite parent rock. Olivine compositions from spinel lherzolite xenoliths (Table B-4, Fig.20) are nearly identical to this variety of xenocryst.

The second compositional range comprises "normal" phyric olivine which occurs in most lavas, including all those from post-glacial centres. The compositional range is from Fo_{86} to Fo_{74}; crystals of this composition are invariably normally zoned.

Olivine compositions in the sample from Spanish Bonk range from Fo_{82} at their core to Fo_{70} at their rims and in the groundmass olivine (Fig.20). Both phases of activity at the Flourmill and Spanish Lake centres have erupted lavas containing xenophyric and phyric olivine; the former is most abundant in the older lavas from Flourmill Centre and has caused the observed Mg enrichment in whole rock analyses (see Chapter 5). Phenocryst and xenocryst compositions range from Fo_{86} in the cores of crystals to Fo_{76} at their rims in Flourmill and from Fo_{86} to a groundmass value of Fo_{60-69} at Spanish Lake. Normal zoning is present in all grains analysed. No compositional difference exists between xenocrysts and phenocrysts.

The Dragon's Tongue is both olivine xenophyric and olivine phyric for its entire length. Phenocrysts have compositions ranging from Fo_{82} at their cores to Fo_{76} at their

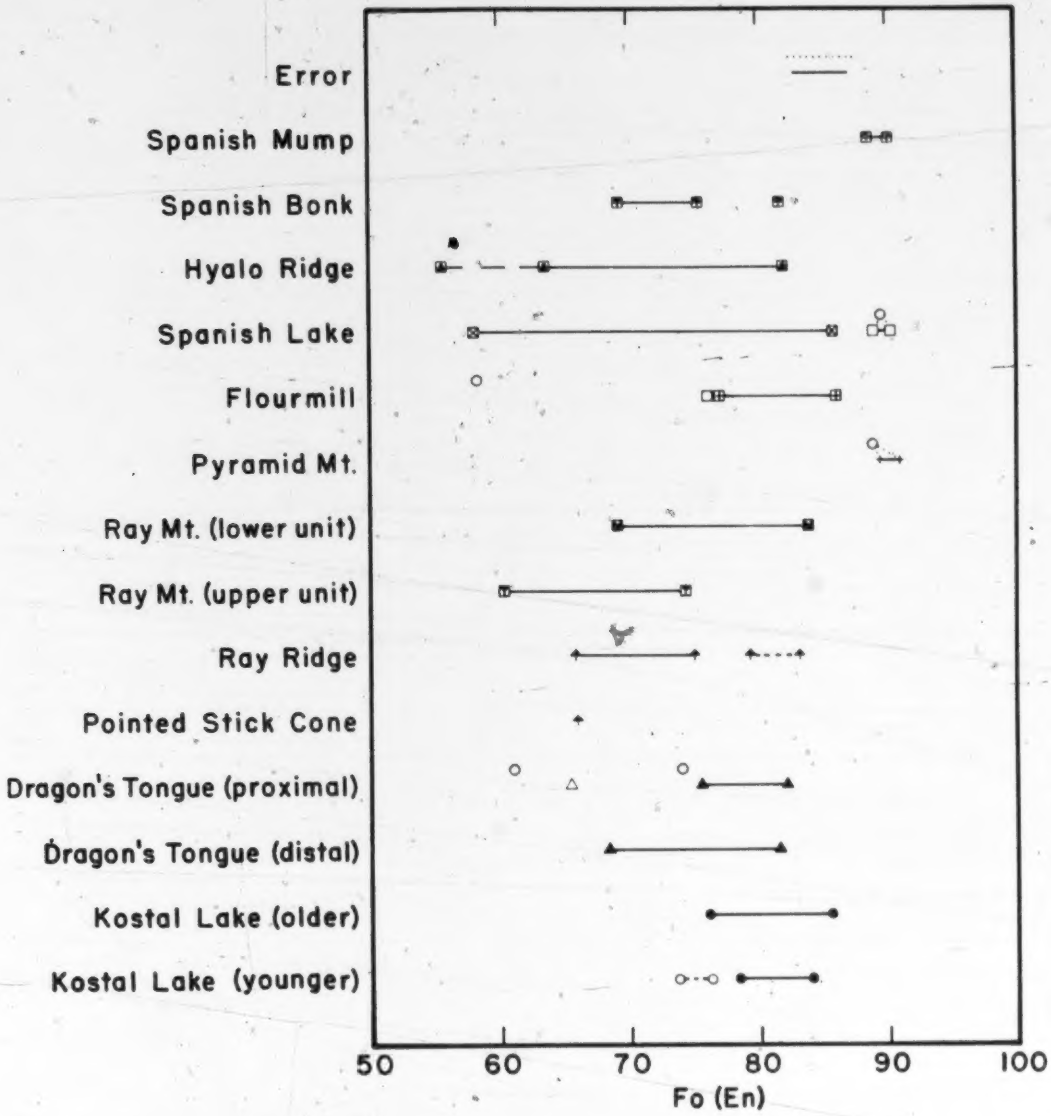

Fig. 20. Range of olivine and orthopyroxene compositions for each centre. Symbols used for each centre are listed in Table 1. Open symbols refer to olivine xenocryst ranges. Orthopyroxene xenocryst ranges are represented by diamonds in circles, offset from the olivine compositions. Where appropriate, dotted tie lines are drawn from the orthopyroxene to xenolith olivine compositions. Error bars are given at the 2σ confidence level based on the maximum observed concentrations of each component.

rims. Only moderate compositional zoning is present. Compositions analysed in samples from the distal part of the flow are identical to those from the proximal portions.

One xenocryst in the Dragon's Tongue has a core composition of Fo_{68}. This crystal exhibits reverse zoning to a rim of composition Fo_{76}, consistent with the composition of the groundmass olivine. This xenocryst is of the third compositional type, described below.

All six eruptive units at Kostal Lake have phenocryst and xenocryst compositions in the range Fo_{82} to Fo_{76}. Although xenocrysts may be identified texturally, their compositions are identical to those phenocrysts analysed, with one exception. This latter is a xenocryst with a core composition of Fo_{68}, reversely zoned to a rim composition identical to that of the groundmass. This xenocryst is identical to that analysed from the Dragon's Tongue.

The third type of olivine spans the compositional range Fo_{70} to Fo_{60} and occurs as phenocrysts in Ray Ridge, Pointed Stick Cone and in the second phase of activity in the Ray Mountain centre. This type of olivine also occurs as rare xenocrysts in the Kostal Lake and Dragon's Tongue lavas, as described above.

The two phases of activity at the Ray Mountain centre contain different compositional ranges in olivine. The earlier phase contains the second type (Fo_{86} to Fo_{72}) and the later phase the third type (Fo_{70} to Fo_{60}). Olivine xenocrysts are absent in both phases of activity. Phenocryst compositions range from Fo_{85} at phenocryst cores to Fo_{72} at their rims in lavas from the earlier phase. The later phase of activity contains phenocrysts ranging from Fo_{74} to Fo_{60} in composition. The abrupt break in petrographic and mineralogical composition coincides with a comparable break in whole rock chemical compositions (see Chapter 5).

The lava flow exposed on Ray Ridge is xenophyric and olivine phyric. Phenocrysts range in composition from Fo_{69} to Fo_{66}. The only xenocryst analysed has a composition of Fo_{76}. Three olivine crystals in a xenolith of spinel lherzolite have an average composition of Fo_{83} (Table B-4, Fig.20). This composition is unusually poor in forsterite for a spinel lherzolite.

Olivines of all three types are almost ubiquitously low in nickel, suggesting that the olivine was not formed from a primary magma. However, sulphide inclusions in clinopyroxene crystals may be responsible for removal of Ni from the melt prior to crystallisation of olivine.

Plagioclase

Plagioclase is an abundant groundmass phase in the Wells Gray lavas but, as noted in Chapter 2, occurs as a phenocryst only in lavas from Hyalo Ridge. Analytical results for cognate plagioclase are presented in Table B-5, in Appendix B. Analyses of incognate plagioclase, from xenoliths, are presented in Table B-6. Analyses were recalculated on the basis of 8 oxygens, using Fe^{3+} to augment deficiencies in Al and Si. A graphic comparison of compositional ranges is given in Figs.21 and 22. The plagioclase is both normally and reversely zoned; core compositions may be as calcic as An_{73} and as sodic as An_{61}. Rim compositions vary from An_{64} to An_{53}. The phenomenon of reverse zoning may be apparent only; the skeletal growth of many crystals may in fact produce normal zoning in embayments. In addition, the apparent zonation may lie within the precision of the microprobe analyses for Na and Ca.

Two generalised populations are apparent, despite the textural and analytical problems described above. Plagioclase from Spanish Bonk, Spanish Lake, Flourmill, Dragonhead and the earlier phase of activity on Ray Mountain has core compositions as calcic as An_{73} with average core compositions of approximately An_{68}.

The second population of plagioclase is slightly more sodic. Plagioclase crystals from Kostal Lake, Ray Ridge, Pointed Stick Cone and the earlier phase of activity at Ray Mountain all have compositions as calcic as An_{63} with a mean composition of An_{59}. Plagioclase in hyaloclastite samples from Pyramid Mountain is too fine in grain size for zoning to be detected by microprobe analyses. The composition of the plagioclase is An_{53}.

The two plagioclase-bearing xenoliths found in the park were taken from the Flourmill and from the Dragonhead centres; plagioclase in the latter xenolith occurs in association with aluminous spinel, aluminous clinopyroxene and kaersutitic amphibole (Plates 12A, 12B). The compositions in either xenolith are shown in Fig.22c, together with representative compositions of groundmass plagioclase in the enclosing lavas. Plagioclase compositions are as sodic as An_{35} and show a strong reaction relationship

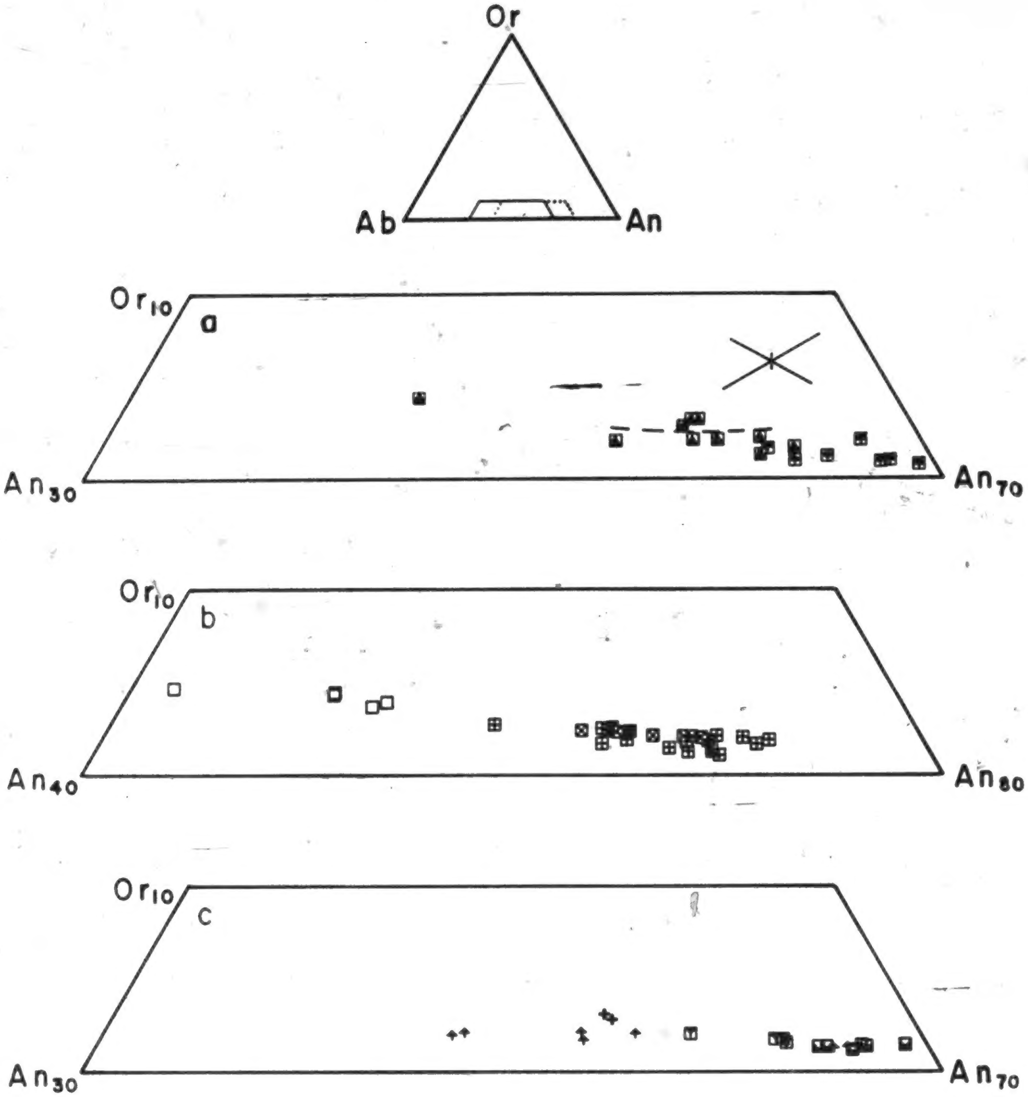

Fig. 21. Compositional ranges of plagioclase in Wells Gray Park. Analyses are plotted on a part of the plagioclase ternary diagram (see inset). Note that (b) displays a slightly different compositional range. Symbols used are solid for cognate crystals, open for xenocrysts and are listed in Table 1. Error bars are given at the 2σ confidence level. a = Spanish Bonk and Hyalo Ridge; b = Spanish Lake and Flourmill; c = Pyramid Mountain, Ray Mountain, Ray Ridge and Pointed Stick Cone.

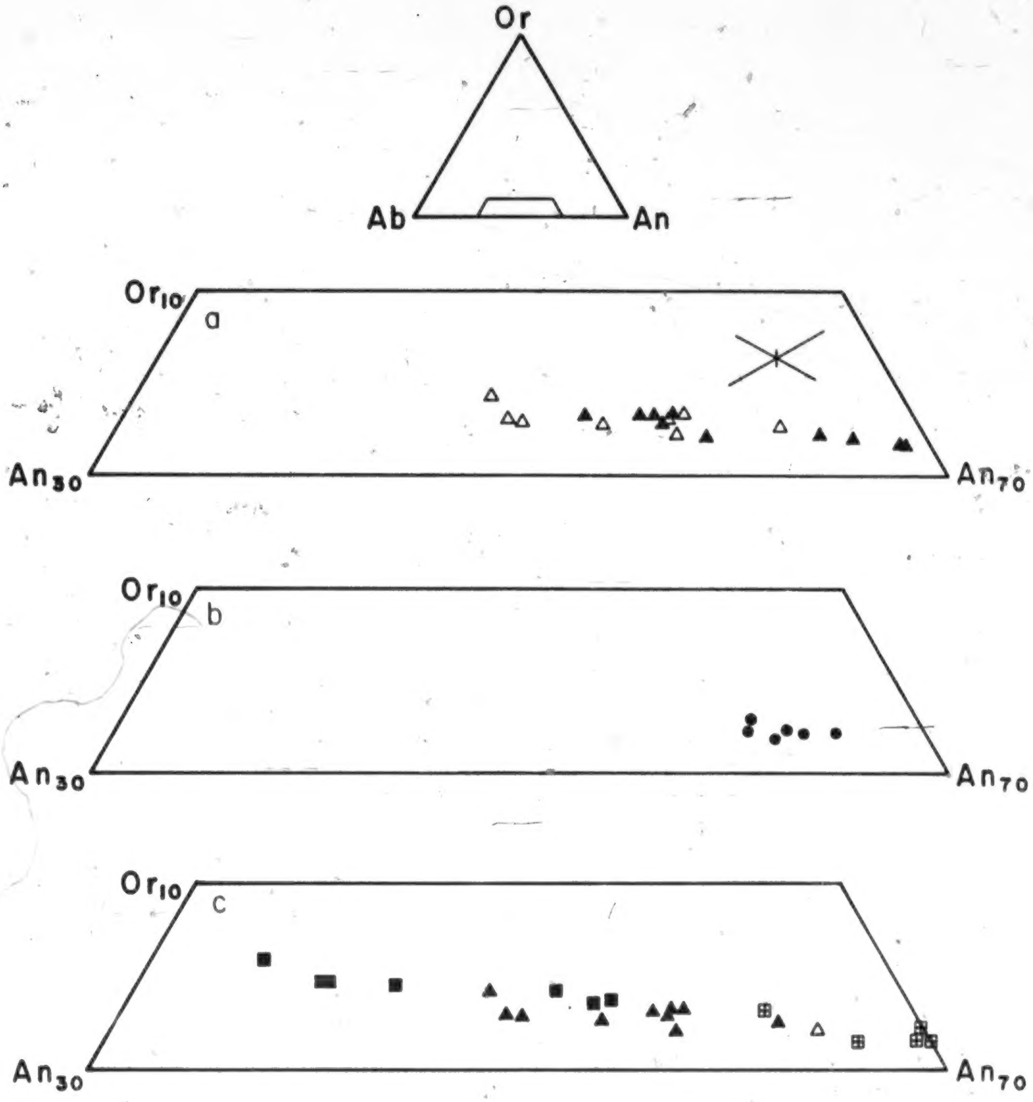

Fig. 22. Compositional ranges of plagioclase in Wells Gray Park. Analyses are plotted on a part of the plagioclase ternary diagram (see inset). Symbols used are solid for cognate crystals, open for xenocrysts and are listed in Table 1. Error bars are given at the 2σ confidence level. a = Dragon's Tongue; b = Kostal Lake; c = Xenolith plagioclase from Flourmill and the Dragon's Tongue.

with the host lava. Neither occurrence can be interpreted as a mantle-derived phase, despite the coexistence with high-Al clinopyroxene; the thickness of the continental crust constrains the modal composition of mantle-derived xenoliths to the stability field of spinel. The intersertal plagioclase in both cases is therefore interpreted as a reaction product, formed during ascent of the entrained xenoliths.

Oxide minerals

Two types of cognate oxide, magnetite and ilmenite, are present in the Wells Gray lavas. Magnetite occurs as a groundmass phase, with or without ilmenite. In lavas from Flourmill, Spanish Lake, Dragonhead, and the earlier phase of activity on Ray Mountain, magnetite is the only oxide phase. An exception is the occurrence of ilmenite in equilibrium with magnetite in sample W3-17/8/13-RM from Ray Mountain. The other lavas contain both oxide phases but the two are not necessarily in equilibrium. Analyses are presented in Table B-7, in Appendix B. Ferric iron was calculated from total iron on the basis of stoichiometry. x(usp) and x(ilm) were calculated using the method of Spencer and Lindsley (1981).

Fig.23 is a diagram of equilibration temperature against f(O_2) for oxide pairs analysed from the Wells Gray lavas (Spencer and Lindsley 1981). The oxide pairs analysed for each sample lie along curves through T-f(O2) space between the QFM and Ni-NiO buffers. The earlier phase of activity on Ray Mountain, represented by W3-17/8/13-RM formed under the most oxidised conditions while the lavas from from Hyalo Ridge (upper unit), Spanish Bonk, Ray Mountain (upper unit), Ray Ridge and the lower unit on Hyalo Ridge formed under less oxidised conditions.

Spinel occurs as xenocrysts or in xenoliths at all centres studied. Analyses of the xenocrysts are included in Table B-7; analyses of spinel crystals from xenoliths are presented in Table B-8. A graph of Cr against Al for all incognate spinels (Fig.24) shows an inverse correlation between Cr and Al, which is normal for spinels from the upper mantle (Brearley *et al*. 1982). The spinel minerals have undergone alteration by soaking in the melt, resulting in peripheral oxidation (Plate 10A). Depletion in Cr and Al takes place at all surfaces exposed to the host magma with corresponding enrichment in FeO and TiO_2.

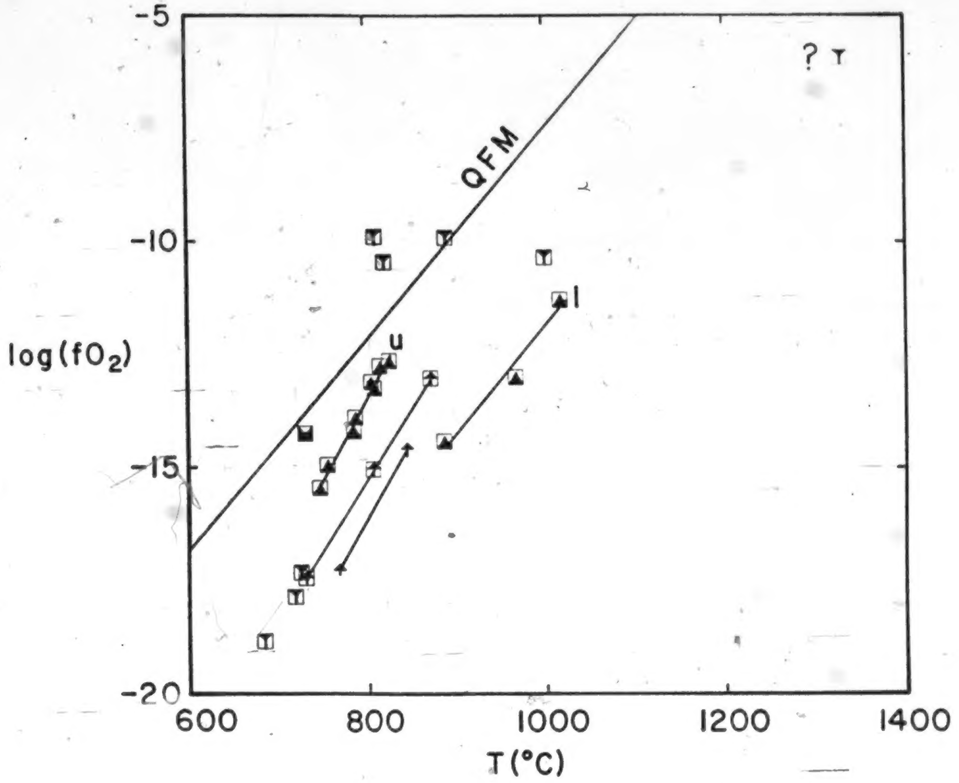

Fig. 23. T - fO_2 diagram from co-existing oxide pairs. Symbols used for each centre are listed in Table 1. u = upper Hyalo Ridge; l = lower Hyalo Ridge; ? = probably erroneous analysis. The temperatures calculated all lie near the QFM buffer, in the subsolidus region for basalts.

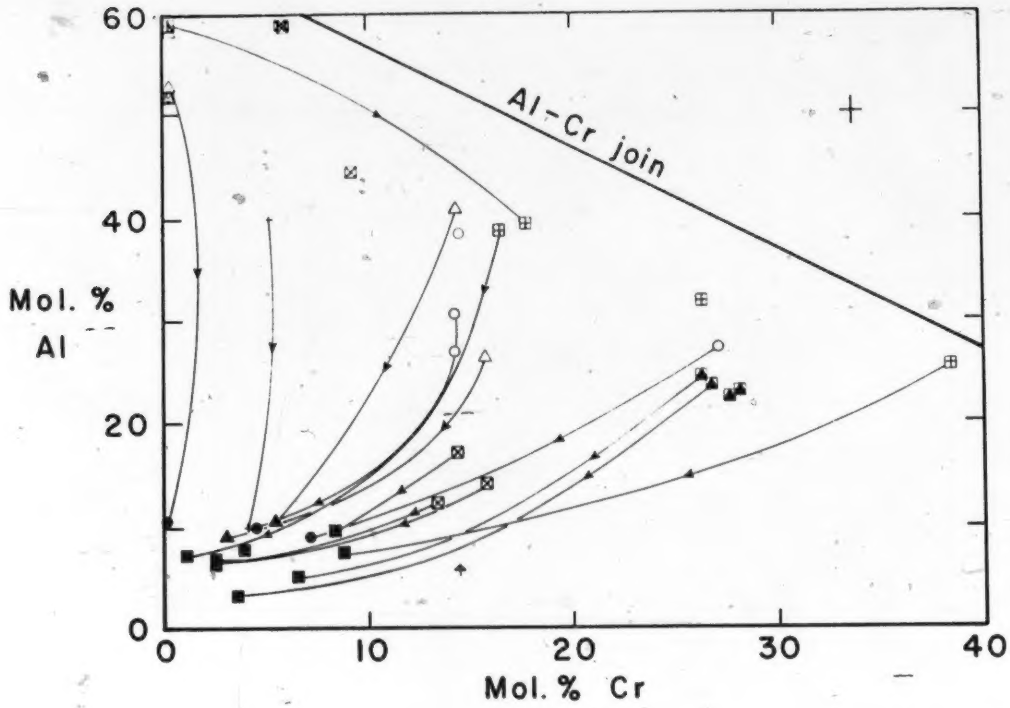

Fig. 24. Cr against Al for xenophyric and xenolith spinels. Symbols used for each centre are listed in Table 1. Incognate spinels are represented by open, groundmass overgrowths by closed, symbols. Error bars are given at the 2σ confidence level. One xenocryst shows zonation from an aluminous to chromiferous composition.

Spinels from the Dragon's Tongue are most enriched in Al and most depleted in Cr. Spinels from Kostal Lake and from Flourmill Centre exhibit a wide range in Cr and Al concentrations and are probably derived from a considerable depth range in the upper mantle. Three broad groupings exist, based on Cr concentration, but this may be the result of a low sample population. The Cr-poor spinel occuring in the Dragon's Tongue is poor in MgO and is therefore a hercynitic spinel.

One spinel xenocryst from Flourmill Centre is exceptional to the general trend of peripheral alteration and equilibration with the host magma. The xenocryst has an Al-rich core, zoned to a relatively Cr-rich rim. Such zoning is common (Haggerty 1976) and demonstrates a disequilibrium relationship within the xenocryst. Although such a zonation might imply that the spinel originated in an environment favouring the development of Al-rich spinel and was subsequently reequilibrated in an environment favouring Cr-spinel, it must be stressed that this is an isolated example of a disequilibrium texture and cannot be taken as indicative of a general case.

Orthopyroxene

Orthopyroxene occurs as xenocrysts in alkaline lavas from Flourmill, Spanish Lake, Pyramid Mountain and from the proximal portion of the Dragon's Tongue. Lavas from Hyalo Ridge do not contain orthopyroxene, even as a groundmass phase, although it is part of the normative assemblage in several samples (see Chapter 5). It is probable that all the alkaline lavas contain orthopyroxene xenocrysts.

All analyses of orthopyroxene are presented in Table B-9 in Appendix B. The analyses are recalculated after the method of Lindsley (1983) to give end member percentages.

Orthopyroxene compositions range from En_{56} to En_{90} and comprise three groups. The first type occurs in the Dragon's Tongue and at Flourmill Centre and has a composition of approximately En_{60}. The Flourmill orthopyroxene occurs in the microxenolith which hosts primary apatite inclusions in iron-rich clinopyroxene (Plates 12C, 12D, 12E). The second type consists of orthopyroxene of composition En_{71-72}, in association with aluminous clinopyroxene in the proximal portion of the Dragon's Tongue. The aluminous clinopyroxene is usually associated with aluminous spinel and, rarely, kaersutite. The third type comprises orthopyroxene with a compositional range from En_{88} to En_{90} and represents orthopyroxene from the Cr-spinel lherzolite assemblage. Orthopyroxene of this type was analysed in a xenolith from Spanish Lake and is also represented by xenocrysts from Spanish Mump.

Amphibole

The only amphibole present in lavas or xenoliths in the Wells Gray area occurs in a spinel clinopyroxenite xenolith found in the proximal portion of the Dragon's Tongue (Plates 12A, 12B). Compositions of the amphibole are listed in Table B-10 in Appendix B. No attempt has been made to recalculate Fe to obtain the Fe^{2+}/Fe^{3+} ratio. At least two other elements, Mn and Ti, can occur in states other than divalent and tetravalent, respectively (Hawthorne, 1981). Such uncertainty precludes recalculation on a stoichiometric basis. Uncertainties regarding site occupancies for each species further obstruct this method of calculation (Hawthorne, 1981). Microanalytical techniques for determination of Fe^{3+} were not used; inclusions of Fe-Ti oxides in the amphibole occur in such quantity and in such fine grain size as to render separation techniques impractical.

The amphibole is classified as a kaersutite, having an average formula, based on 23 oxygens, of a typical kaersutite (Hawthorne 1981). It has a moderately high TiO_2 content and MgO content (5.5% and 12% respectively).

The amphibole in the xenolith 14/8/9X1 exhibits a reaction texture with enclosing lava and, within the xenolith, exhibits a corrosion texture where the host lava has penetrated, the reaction forming iron-tianium oxide. Hercynitic spinel is also present in the xenolith. Sodic plagioclase occurs as an intersertal phase. All phases exhibit a reaction texture with the enclosing melt. The amphibole, however, exhibits a sutured, non-reaction margin with the clinopyroxene (Plates 12A, 12B).

Amphibolite or clinopyroxenite containing hercynitic spinel is a rare xenolith in the Wells Gray area. By contrast, nearly all the Quaternary lavas in the area contain xenocrysts and/or xenoliths dominantly composed of clinopyroxene with a composition similar to that in xenolith 14/8/9X1. Resorption of all phases from the xenoliths suggest that they are incognate at near-surface temperatures and pressures, although they may be in equilibrium with the magma at temperatures and pressures representative of the source region.

A crustal origin for the amphibole clinopyroxenite and, by association, all clinopyroxene xenocrysts and clinopyroxenites could be inferred, both by the presence of amphibole in this assemblage and by the presence of incognate, sodic plagioclase, observed at Dragonhead and in the older phase of activity (4/8/17X) in Flourmill Centre. The range of values of ^{87}Sr/^{86}Sr obtained from xenocrysts of aluminous clinopyroxene (A.D. Smith unpubl. data) suggests a component enriched in radiogenic Sr relative to the values obtained in this study (Chapter 6). However, textural and mineralogical features exist in 14/8/9XI which suggest that the xenolith and its associated assemblage are not derived from the crust. Firstly, the presence of hercynitic spinel, in association with plagioclase is remarkable; the aluminous spinel is indicative of a higher pressure environment consistent with that beneath the base of the crust. Secondly, the plagioclase is interpreted as a late stage, low pressure reaction product, probably formed during ascent as a reaction rim enclosing and isolating both the spinel and kaersutite. The effective source assemblage is therefore amphibole + spinel + clinopyroxene. Thirdly, the aluminous nature of the clinopyroxene (as much as 9% Al_2O_3) suggests that it is derived from considerable depth.

Incompatible elements have been analysed in both amphibole and host lavas; K, Na and Ti are not significantly concentrated in phases other than amphibole and liquid. The K/Na ratios of melt and kaersutite are identical within analytical error. An inverse correlation exists between K and Ti for the kaersutite and proximal lavas of the Dragon's Tongue (Fig.25). This suggests a cognate relationship at some stage of magmatic evolution.

Petrographic and chemical data indicate that the amphibole and the enclosing clinopyroxene were cognate with the melt at some temperature and pressure. The optically continuous remnants of amphibole in clinopyroxene indicate that amphibole was a major constituent of the xenolith. The dehydration reaction to clinopyroxene precludes fractionation of amphibole from the melt but implies that amphibole is at least one of the source phases for the Wells Gray lavas. It is proposed, therefore, that the generation, in terms of major elements be modelled as partial melting of zones of amphibolite in the subcordilleran upper mantle. Later melting of relict amphibole produced the reaction rim

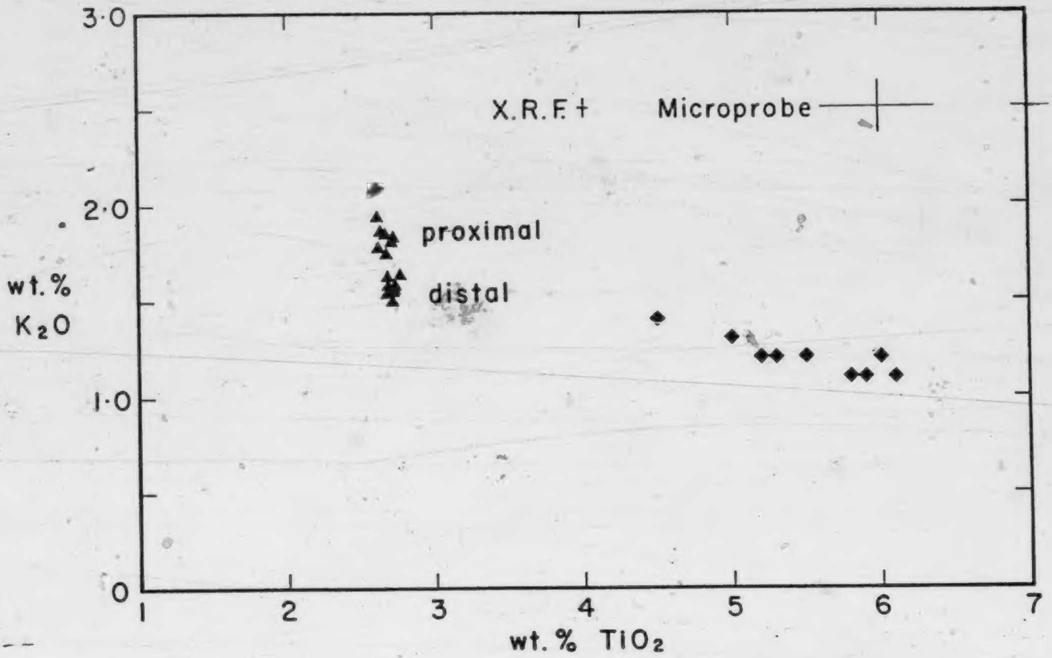

Fig. 25. TiO_2 against K_2O for the Dragonhead amphiboles. The amphibole compositions are represented by diamonds, those of the lavas by triangles. Error bars are given at the 2σ confidence level both for microprobe analyses of kaersutite and for X.R.F. whole rock analyses.

of sodic plagioclase. This hypothesis is discussed at greater length in Chapter 5.

Apatite

The single occurrence of apatite reported in Chapter 3 is in a microxenolith in the Flourmill Centre (Plates 12C to 12E). Analyses of the apatite are presented in Table B-11 in Appendix B. The mineral is stoichiometric and contains as much as 0.3 weight percentage Cl. Fluorine was not analysed quantitatively because of the difficulties of resolving the F peak on the energy dispersive system.

Sulphide minerals

Sulphide inclusions occur in clinopyroxene in xenocrysts and xenoliths from all the Recent centres. Sulphide compositions range from highly nickeliferous pyrrhotite in the Flourmill Centre to mildly nickeliferous pyrrhotite in the Dragon's Tongue. In a sample from Spanish Lake, an inclusion in spinel lherzolite, also in clinopyroxene exhibits exsolution of two sulphide phases. The first lies on the join FeS-NiS and is a high temperature phase. The second is stoichiometric chalcopyrite. The Ni-bearing phase has as much as 40 weight percent Ni. The effect of such sulphide phases on the Ni-MgO relationships in the sample suite will be to scatter any olivine control curve. This effect is noticeable in the trace element chemistry reported in Chapter 5. One 50 μm-diameter inclusion, of 40 weight percent Ni, in 1 gm of sample would be enough to change the Ni content by as much as 1 ppm.

C. Xenolith thermometry

Samples of xenoliths containing orthopyroxene and clinopyroxene or spinel and olivine are amenable to the application of geologic thermometers. Samples available for thermometry in the Wells Gray area are few in number where the present study is concerned; the initial sampling bias was towards xenolith-free rather than xenolith-rich samples. Nevertheless, small xenoliths, ranging in size from 0.5 cm to as much as 3 cm are ubiquitous in the alkaline lavas and the bias against xenoliths was reversed in selecting samples for microprobe analysis The suitability of such samples for accurate temperature measurements is uncertain, because of their small size; it is probable that some equilibration with the melt has taken place. The purpose of this section is, therefore, to make an estimate of the relative equilibration temperatures of the various xenolith types, rather than attempt to deduce accurate equilibration temperatures from unsuitable samples.

Several two-pyroxene thermometers are available. A discussion of these is given by Fujii and Scarfe (1982). For the purposes of this study, which are to provide a general comparision of the xenolith assemblages using limited data, the Wells (1977) thermometer was selected because it permits comparison of these data with those of Brearley *et al.* (1984) and Fujii and Scarfe (1982).

Orthopyroxene is absent in several of the xenoliths. In such cases, the two-pyroxene thermometer cannot be used. An alternative method is to use the spinel-olivine geothermometer of Fabriés (1979). This thermometer is unreliable (Fujii and Scarfe 1982) but results obtained using this method can be compared roughly to those obtained by the two-pyroxene method by application of both thermometers to the Spanish Lake Cr-spinel lherzolite.

Pyroxene pairs selected for temperature calculations are shown in Fig.19. Analyses on which the calculations are based are listed in Tables B-2 and B-9. Spanish Lake and Pyramid Mountain are represented by xenolith 24/8/13X and xenocrysts from hyaloclastite 13/8/10, respectively. The number of analyses collected is not large in either case but both assemblages are homogeneous and, apparently, are closely related These samples represent the Cr-spinel lherzolite assemblage. Temperatures calculated from these analyses are within error of each other; a best estimate of the equilibration temperature is 980±80°C, based upon the close agreement between the analyses from Pyramid Mountain (990°C) and from Spanish Lake (970°C).

The pyroxene pair analysed from Dragonhead is from 14/8/1X. The assemblage is from a small aggregate, poorly sampled, and includes a high-Al clinopyroxene; the analyses, although homogeneous, are for these two reasons not suitable for an accurate estimate of xenolith temperature. The calculated temperature, however, will provide a general estimate of the equilibration temperature relative to that of the Cr-spinel lherzolites. The estimated temperature is approximately 1100°.

The pyroxenes analysed from Flourmill Centre are from 2/8/6X3, the ferroan websterite hosting apatite. With the exception of clinopyroxene from the rim of the xenolith, the orthopyroxene and clinopyroxene analyses are both homogeneous, suggesting that the mineral pair is in equilibrium. The estimated equilibration temperature of this assemblage is 940±80°C. The three major groups of xenolith can, therefore, be compared by this method.

Temperatures calculated for 24/8/13X using the spinel-olivine thermometer are significantly lower (880°C) than those obtained using the two pyroxene thermometer. Analyses of mineral pairs to complement the two-pyroxene temperatures were not obtained; comparison of temperatures obtained by the two different methods is therefore semiquantitative at best. The temperature obtained for the spinel wehrlite from Ray Ridge was, nevertheless, 970°C, 90°C higher than the more magnesian Cr-spinel lherzolite assemblage. An estimate of the temperature relative to those obtained by the Wells two-pyroxene thermometer is therefore approximately 1070°C.

General estimates of temperatures from the small nodules in the Wells Gray area suggest that the compositional relationships in the Cr-spinel lherzolite assemblage and the implicit thermal regime extend throughout a considerable area beneath Wells Gray Park. Although preliminary estimates suggest that the high-Al assemblage and a ferroan spinel wehrlite assemblage may have higher equilibration temperatures, more data are needed for a definitive statement.

D. Summary

The Wells Gray lavas are olivine-clinopyroxene phyric and olivine-clinopyroxene xenophyric, with the exception of Hyalo Ridge, which has olivine-plagioclase phyric lavas with no significant xenocrysts or xenoliths. Olivine is the dominant phenocryst phase in both lava types. Two populations of olivine phenocryst composition occur, with compositions of approximately Fo_{82} and Fo_{75}, respectively. The latter composition is too poor in Mg to have equilibrated with normal mantle. These populations occur with plagioclase microphenocryst populations of compositions An_{70} and An_{59}, respectively. Clinopyroxene is titaniferous, strongly zoned and exhibits a well-defined compositional variation towards more Fe-rich compositions. Fe-Ti oxide pairs define cooling trends through T-fO_2 space, near to the QFM buffer. The low temperatures calculated from the oxide pairs may be due to enhanced cation diffusion in the presence of volatiles

Xenoliths and xenocrysts comprise four main assemblages. The first is a Cr-spinel bearing assemblage, usually spinel lherzolite, with pyroxene equilibration temperatures of approximately 980°C. This temperature lies within the range of values obtained for this assemblage in B.C. (Fujii and Scarfe 1981, Brearley *et al.* 1984).

The second type of xenolith is rare and is represented by a single spinel wehrlite with more ferroan olivine and clinopyroxene than the Cr-spinel assemblage. The xenolith has a poorly constrained equilibration temperature of 1070°C.

The third assemblage is represented by a websterite from Flourmill Centre which contains ferroan augite, hypersthene and primary apatite inclusions. The xenolith equilibrated at approximately 940°C, within error of the Cr-spinel lherzolite assemblage.

The fourth assemblage is high in Al, high in Fe relative to the Cr-spinel lherzolites, comprises spinel clinopyroxenites with rare lherzolites and websterites and can contain kaersutitic amphibole. A poorly-constrained equilibration temperature (two pyroxene) for this assemblage is 1100°C.

The kaersutite which occurs with the fourth assemblage is nearly identical in composition to poikilitic kaersutite reported by Best (1974) from the Grand Canyon (Sample 73, Best 1974). The Wells Gray kaersutite has a K/Na ratio similar to that of the host lava. Best interpreted the amphibole as a product of mantle metasomatism; a later publication (Dawson and Smith 1982) cite the circular problem of melt derivation from kaersutite as against the precipitation of kaersutite from an alkaline melt. The stable coexistence of Al-augite with kaersutite in 14/8/9X is interpreted as evidence for a primary origin for the kaersutite.

5.

WHOLE ROCK CHEMISTRY

The purpose of this part of the study is to determine the concentrations of major and selected trace elements in representative samples from each of the centres studied. The major element compositions of lavas from several of these centres (Fiesinger 1975, Fiesinger and Nicholls 1977) have already been determined and found to be alkaline. The present study will use the major and trace element compositions to evaluate the petrogenesis of the alkaline lavas. Previous work in the Anahim Belt, to the west of the Wells Gray area, has been carried out on the Rainbow Range shield volcano (Bevier 1978, 1983a, 1983b) and in the Stikine Belt on the Edziza (Souther and Hickson 1984) and Level Mountain (Hamilton 1981) complexes. In addition to Fiesinger's work on the Wells Gray lavas, Hickson (1987) has conducted chemical and isotopic analyses on the earlier, transitional lavas in the southern part of the area.

A. Analytical procedure

Sample selection

Samples from each of the eleven volcanic centres were examined petrographically; descriptions are given in Chapter 3. A total of 108 samples were selected for major and trace element analysis. Samples were selected to represent each of the eleven volcanic centres studied. Two or three samples only were selected from the smaller centres but the larger centres and the postglacial centres were sampled extensively in order to study the different phases of activity described in Chapter 2. Care was taken to ensure minimal contamination, from accidental inclusions of later lavas, from incognate material and from weathering.

Crustal material included in the lavas showed strong, narrow reaction rims isolating the material from the melt. Few crustal xenoliths exhibited soaking by the magmas. The lack of corrosion of crustal xenoliths suggests that little, if any, chemical modification took place by crustal contamination during ascent of the magmas to the surface.

Sample preparation

Details of sample powder preparation are given in Appendix C. Sample aliquots for trace element analysis were crushed using a rotary grinder with mullite plates and in an agate swing mill. Those aliquots for major element analysis were crushed using a tungsten carbide swing mill. Care was taken to minimise airborne contamination of the sample powders during preparation.

Whole rock chemical analysis

108 samples were analysed for SiO_2, TiO_2, ΣFe as FeO, MnO, MgO, CaO, Na_2O, K_2O and P_2O_5 using a Philips 1400 X-ray fluorescence spectrometer with a rhodium tube. Analyses were conducted by Midland Earth Science Associates of Nottingham, England. The method of analysis is described by Harvey and Atkin (1982). Samples analysed for major elements were prepared from powders using the fused disc method with a lithium tetraborate flux. Loss on ignition was reported for each sample. The trace elements S, Cl, Rb, Sr, Ba, Sc, Y, Zr, Nb, V, Cr, Co and Ni were analysed by the pressed disc method. Sc was also analysed by this method, using a tungsten tube because of absorption interference.

The concentrations of H_2O and CO_2 were not determined for whole rock samples, for several reasons. Firstly, water and carbon dioxide absorbed from the atmosphere are particularly high in concentration in finely ground samples. The only method of preventing this is by crushing and subsequent storage in a inert atmosphere. Heating of powdered samples to exclude H_2O^- invariably liberates some of the structurally bound water and carbon dioxide (Gitlin pers. comm. 1985). The losses on ignition reported by the Nottingham laboratory were conducted using sample aliquots which had equilibrated in a more humid atmosphere and could not be compared directly with analyses conducted at the University of Alberta.

Analytical precision and uncertainty

Analytical precision based on counting statistics cannot be evaluated in the absence of the raw data. Nine unmarked replicates and aliquots of U.S.G.S. standard rock powders BHVO-1, DNC-1 and W-2 were included with the samples. One replicate of the last standard was also included. Table C-1 lists the analytical results for replicates. Results for standards are presented in Table C-2 together with published values for comparison. On the basis of replicate analyses and comparison with published values of U.S.G.S. standards, errors were assigned for each element analysed. These are listed in Table C-3.

Determination of ferric iron

The method used to determine Fe^{3+} is described in detail in Appendix C. Briefly, the powdered samples were weighed and dissolved in hydrofluoric acid. Sufficient NH_4VO_3 was added to oxidise all the Fe^{2+} in the aliquot, an indicator was added and the solution was titrated with a solution of $(NH_4)_2Fe(SO_4)_2.6H_2O$ until the unused V^{5+} was used up.

B. Analytical results

Normative mineralogy and chemical classification

Normative analyses and classification after Irvine and Baragar (1971) were calculated using the BASIC programme NIGGLE, compiled by the author. C.I.P.W. norms for all samples are given in Table D-1. All samples analysed, with the exception of those taken from Hyalo Ridge, fall within the alkaline field defined by Irvine and Baragar, both in an elementary alkalies - silica plot (Fig.26) and in those authors' Ol'-Ne'-Q' ternary diagram. The discriminant function recommended for basic rocks did not discriminate effectively and was not used. Samples do, however plot within the alkaline field of Irvine and Baragar's Fig.5. The norms have as much as 13 weight percent normative nepheline.

All samples, including those from Hyalo Ridge, are sodic or K-poor. The alkaline samples range from alkali olivine basalt to nephelinite and hawaiite despite their restricted composition; Normative anorthite and colour index are close to the triple junction of Irvine and Baragar's Fig.10. Were some of the sodium to be assigned to pyroxene, a more realistic interpretation, all compositions would lie in the alkali olivine basalt - hawaiite fields. The names assigned on the basis of a simple normative

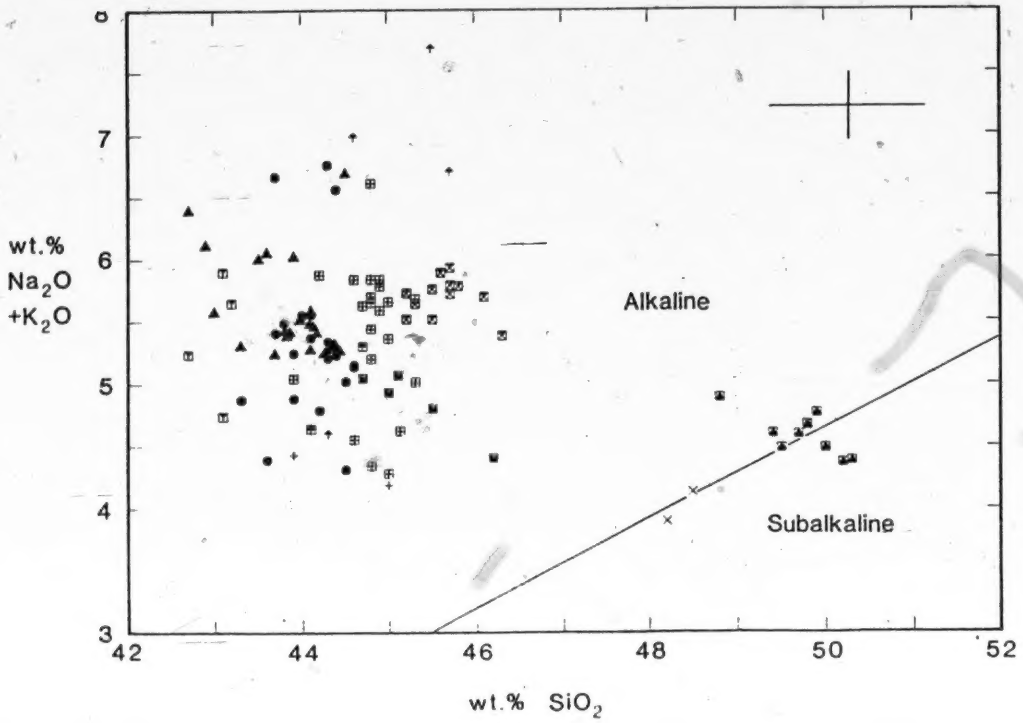

Fig. 26. Weight % SiO_2 against weight percent total alkalies. The dividing line between alkaline and subalkaline fields is drawn after Irvine and Baragar (1971). Symbols used for each centre are listed in Table 1. Error bars are given at the 2σ confidence level based on the maximum observed concentrations of each component. The majority of the lavas in Wells Gray Park are sodic basanitoids.

calculation are therefore misleading in their variety and do not imply inclusion in any continuous series.

Fiesinger's (1975) classification of the Flourmill lavas as ankaramites is based upon the abundance of phyric pyroxene. Many of these pyroxenes, as described in Chapter 3, are xenocrysts of several different varieties. The lavas erupted from Kostal Lake and the centres around Ray Lake are also richly pyroxene phyric and xenophyric and do not differ texturally from the Flourmill lavas. The alkaline lavas are therefore assigned *en masse* to the alkali olivine basalt - hawaiite suite and are classified as basanitoids.

Hyalo Ridge, the tuya in Spanish Creek, has a very uniform composition, enriched in silica with respect to the other lavas. The compositions of the Hyalo Ridge lavas are typical of the earlier lavas examined by Hickson (1987) and will be considered as part of the same group. Compositions of the basalts in the Hyalo Ridge centre range from subalkaline to the margin of the alkaline field; all save one sample have normative orthopyroxene; none is present in the modes. These lavas are therefore classified as transitional tholeiitic basalts.

Major elements

Major element compositions for each sample are given in Table D-1. SiO_2, Al_2O_3 and TiO_2 concentrations are typical of alkali basalts and are comparable with Bevier's (1979) compositional data for the Rainbow Range parental magmas. Bevier did not discover any evidence of crustal contamination and assumed the parental magmas to be near-primary in composition.

MgO, FeO and CaO values for the lavas studied have ranges of 6.3-13.5, 9.8-14.1 and 7.0-10.5 weight percent respectively. Plots of each major element against silica show a scatter of points with no clearly defined trends. A distinct separation of the older transitional basalts from the alkaline lavas (Fig.26) is the only remarkable feature. Silica contents of the Flourmill and Spanish Lake centres are slightly higher than those of the more easterly Kostal Lake and Dragonhead centres, possibly as a function of their high content of clinopyroxene xenocrysts.

MgO in all the lavas, including those from Hyalo Ridge, is inversely proportional to Al_2O_3 (Fig.27). Values for the lavas define a line which may be extended to the composition of the aluminous clinopyroxene or olivine described in Chapter 4 or to a composition representing a mixture of these two minerals. A plot of total iron against MgO (Fig.28) shows two possible chemical trends, the first being caused by contamination with xenophyric olivine, such as seen in the xenocryst-rich samples of Flourmill Centre. The trends joining the different phases of activity at Kostal Lake and Dragonhead are in slightly different directions. The differences in trends are due to differences in the bulk composition of the material accumulated or fractionated and probably reflect small differences in chemical or modal composition at or near the source. None of the observed variation requires greater than 10% fractionation or accumulation of a mafic phase.

Mg numbers for the Wells Gray volcanics, normalised to an $Fe^{3+}/\Sigma Fe$ of 0.15 (Frey *et al.* 1978), vary from as low as 0.49 in the later lavas on Ray Mountain and in the samples from Pointed Stick Cone to as high as 0.71 in olivine-xenophyric samples from the older phase of activity in the Flourmill Centre. In general, however, Mg numbers increase in the younger phases of activity for a given centre, unless there is a significant quantity of xenophyric material.

The Mg numbers of the lavas are not representative of primary liquids in equilibrium with a mantle composition represented by the Cr-spinel lherzolite assemblage, which is the most common assemblage in the Wells Gray lavas. Frey *et al.* (1978) cite Mg_{68} as the minimum value for a lava in equilibrium with a normal (Fo_{88-89}) mantle olivine (Palme and Nickel 1985).

The majority of the Wells Gray lavas have Mg numbers in the range 60 to 66; higher numbers are usually associated with a high phenocryst and xenocryst content. There is no evidence for significant crystal fractionation in the Wells Gray alkaline lavas. Rb/Sr ratios increase with increasing Mg/(Mg+Fe) in both the Dragonhead and Kostal Lake centres, which show the largest variation in trace element compositions. All lavas are porphyritic and contain abundant small ultramafic xenoliths, as described in Chapters 3 and 4, suggesting that their rate of ascent was sufficiently rapid as to preclude significant crystal fractionation.

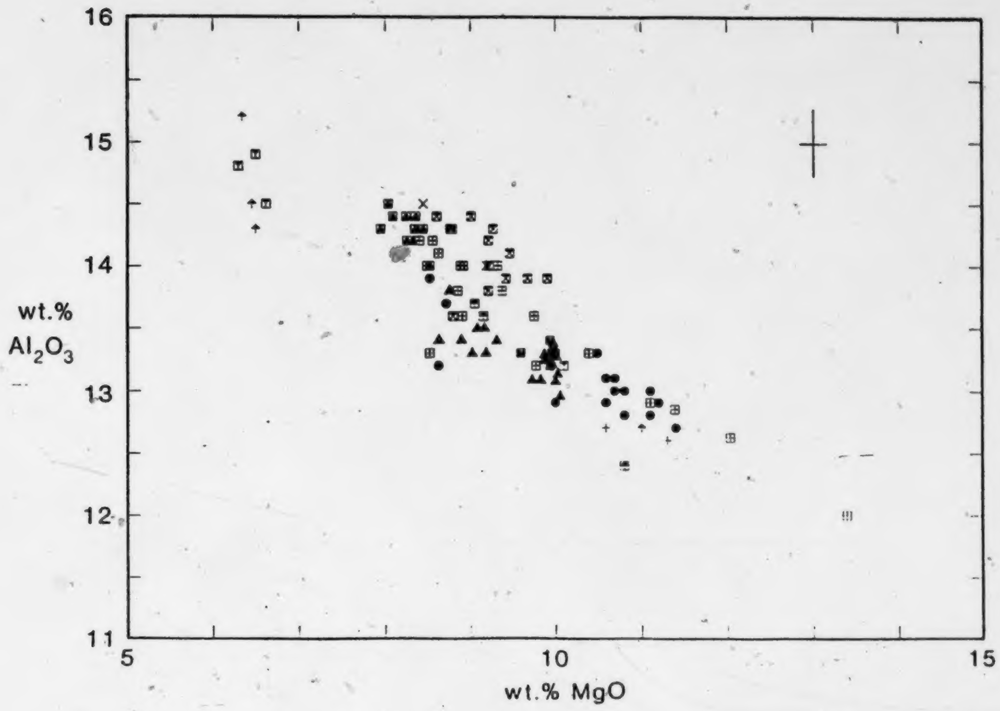

Fig. 27. Weight % MgO against weight % Al_2O_3. Symbols used for each centre are listed in Table 1. Error bars are given at the 2σ confidence level based on the maximum observed concentrations of each component. The lavas lie along a line which may be extended to the composition of aluminous clinopyroxene or olivine, suggesting accumulation of either or both of these phases during ascent, to dilute the lavas with an Al-poor composition.

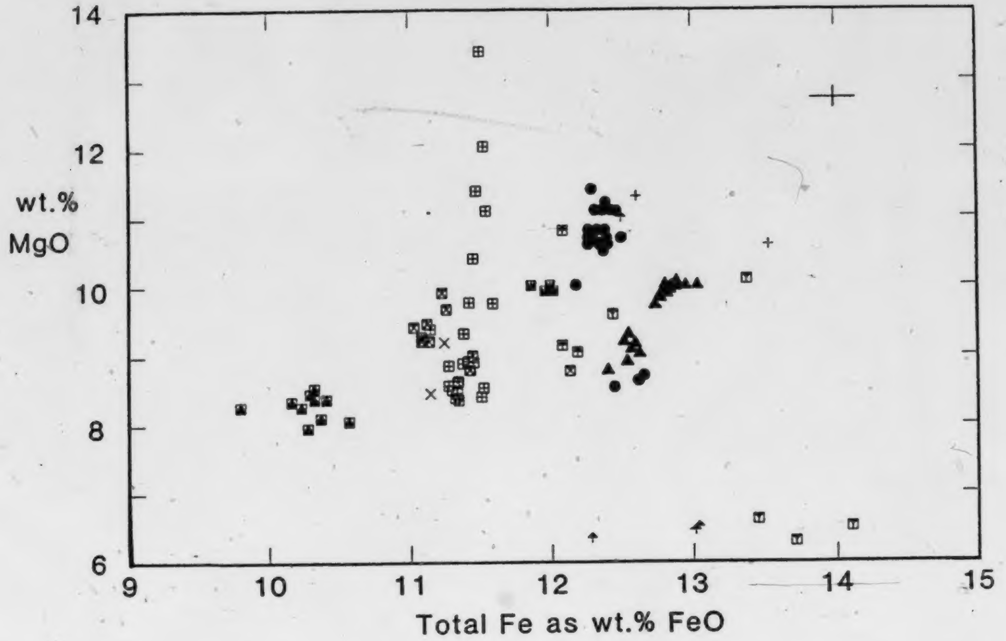

Fig. 28. Total Fe, as weight percent FeO, against MgO. Symbols used for each centre are listed in Table 1. Error bars are given at the 2σ confidence level based on the maximum observed concentrations of each component. Each sample suite has a discrete value for FeO and MgO, suggesting that each suite is independently generated.

A resolution of the problem of rapidly-ascended liquids with non-primary Mg numbers is to propose a source region, or regions, enriched in Fe, relative to Mg. Such heterogeneities have been proposed to account for the chemical and isotopic variation in ocean island basalts (Zindler *et al.* 1984) and are attributed to the presence, in the upper mantle, of ancient oceanic crust, which has become decoupled from its lithospheric mantle (Hofmann and White 1982). The heterogeneities are most evident in lavas inferred to be generated from a small source volume (Zindler *et al.* 1984). The Wells Gray lavas, of small erupted volume in a subduction environment are possibly generated in a similar manner, from heterogeneous mantle.

MgO, FeO and CaO are constant for each sample suite, except in the case already described, where olivine accumulation has occured. The decrease in CaO from earlier to later phases of activity in the Kostal Lake and Dragonhead centres can be accounted for by a maximum of 8% fractionation or accumulation of clinopyroxene. This is not consistent with the 30% fractionation required to account for trace element variations, described below. It is concluded, therefore, that the composition of the Wells Gray lavas is not controlled by significant fractionation of olivine and clinopyroxene during ascent. This conclusion is supported by the large quantities of ultramafic xenoliths in the lavas which indicate ascent velocities sufficiently rapid as to hinder efficient fractionation.

A graph of K_2O against Na_2O shows a covariance between the two elements which extends to the concentrations of these elements in the amphibole from the xenolith in the Dragon's Tongue (Chapter 3). This relationship is shown in Fig.29. The pargasite described by Brearley and Scarfe (1984) at Lightening Peak, British Columbia has a K/Na ratio which is incompatible with those of the Wells Gray lavas. The Dragonhead kaersutite falls in the middle of a range of K/Na ratios for mantle-derived amphiboles (Arai 1986) from 0.01 to 1.4. The agreement in K/Na values between the Dragonhead kaersutite and the host lava suggests that the amphibole represents a possible source composition. Dawson and Smith (1982), in their review of upper mantle amphiboles, state quite concisely that the converse holds true and that the kaersutite is most often interpreted as a reaction product of melt with xenoliths. The mutually interpenetrant clinopyroxene-kaersutite grain boundary (Plates 12A, 12B) is

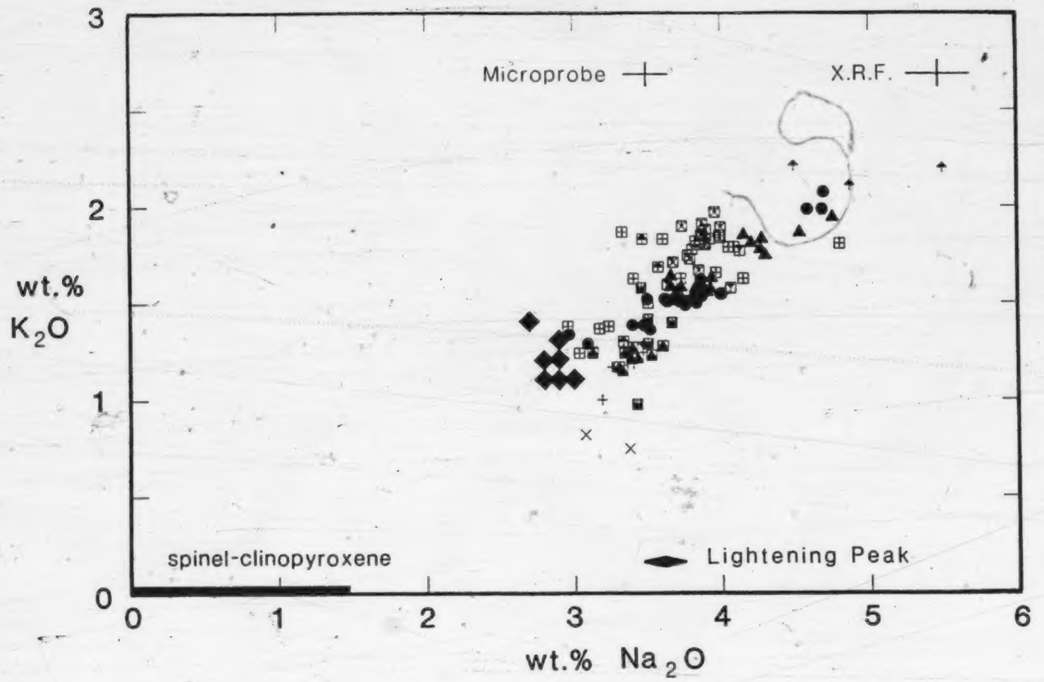

Fig. 29. Weight % K_2O against weight percent Na_2O. Symbols used for each centre are listed in Table 1; amphibole analyses (Table B-10) from a xenolith from the proximal portion of the Dragon's Tongue are represented by diamonds. Error bars are given at the 2σ confidence level based on the maximum observed concentrations of each component; separate error envelopes are given for microprobe and X.R.F. analyses. The lavas could be generated by melting of amphibole to produce a spinel clinopyroxenite residue. Note that the Lightening Peak amphibole (Brearley *et al*. 1984) does not lie along the line.

reemphasised here to support the interpretation of the kaersutite as a primary phase.

Trace element variation

Trace element compositions for 13 elements are available for 106 samples. These values are listed in Table D-1. The Wells Gray lavas, particularly the alkaline lavas, are typically enriched in incompatible elements such as Ba and Zr, to a much greater extent than any lavas in British Columbia (Bevier 1979, Souther and Hickson 1984, Hamilton 1981). The lavas from Hyalo Ridge are typical transitional tholeiitic lavas which are identical to those studied by Hickson (1987). This section will therefore deal mainly with the chemistry of the alkaline lavas.

The trace and minor elements are divided into four groups. The first group comprises the elements Mn, Sc, Y and Co. These elements are relatively low in concentration in the Wells Gray lavas and do not vary significantly with eruptive event or with centre. Mn and Co are siderophile, and are of equal concentration in olivine, pyroxene and whole rock. The absence of significant variation in Sc indicates that no significant amount of clinopyroxene fractionation or accumulation has taken place, even in strongly xenophyric lavas.

The second group comprises the chalcophile element Ni. Ni has been used, together with Mg, (Sato 1977) as a discriminant for primary magmas from the earth's mantle. However, the analyses (Chapter 4) of sulphide inclusions in clinopyroxene grains indicate that primary sulphur is present in these rocks in sufficient quantities as to "scrub" Ni from the silicate melt. A plot of MgO against Ni shows a positive covariance (Fig.30) but the range of Mg and Ni values in each centre is too small, compared to the error to make any inferences for any suite save that from the Flourmill Centre. Here, the slope of Ni against MgO (Fig.30) indicates accumulation of olivine with a Ni content of approximately 0.35 weight %. This suggests that the phyric olivine is nickeliferous and that the magmas are near-primary in composition.

A graph of Ni against S shows a scatter of values. Given that the sulphide inclusions occur in unpredictable and variable quantities and that a single inclusion 0.01 mm in diameter, with a 40% Ni content, can produce an increment of 1 ppm Ni in a 1 gm sample, the Ni and S values for the samples are, at present, not interpretable. A plot of

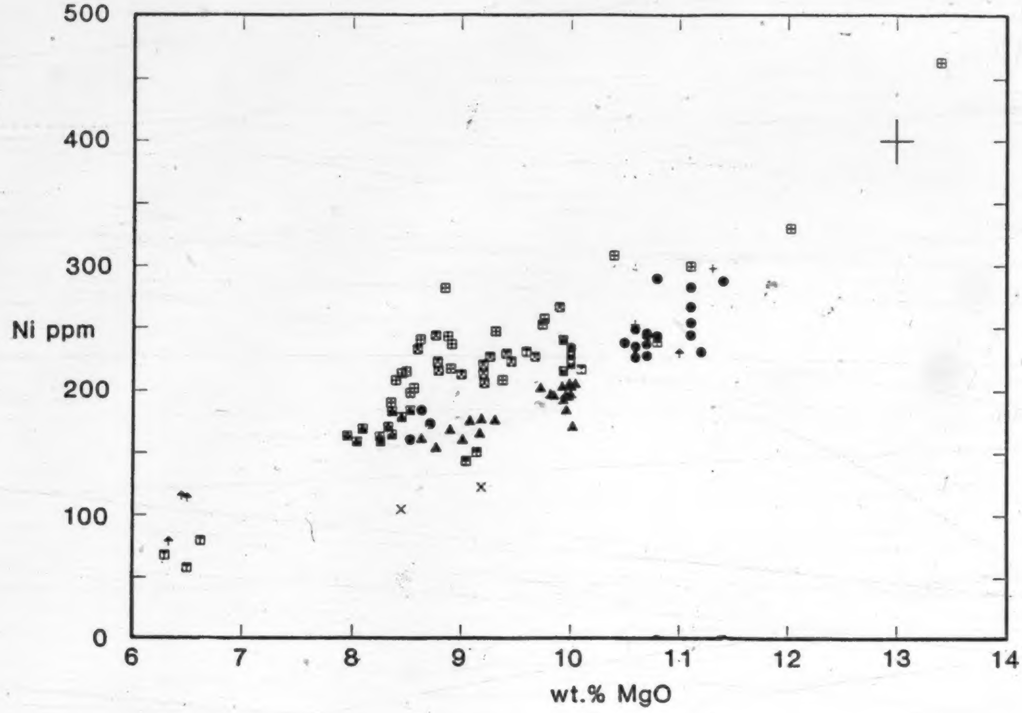

Fig. 30. MgO against Ni for the Wells Gray lavas. Symbols used for each centre are listed in Table 1. Error bars are given at the 2σ confidence level based on the maximum observed concentrations of each component. The two components show a linear covariance but there is no continuous change in composition except in the Flourmill centre. The enrichment in Mg and Ni is due to accumulation of xenophyric olivine. The Mg-depleted samples from the Ray Mountain area possibly represent the end products of olivine fractionation.

Ni against Co (not shown) is scattered.

The third group comprises the semi-compatible transition elements Ti, V and Cr. Chromium varies in the lavas from high concentrations in older lavas to lower concentrations in younger lavas. A plot of MgO against Cr (Fig.31) shows that for a given MgO value the Cr concentrations increase from Kostal Lake and Dragonhead to the Spanish Creek volcanoes and so to the transitional tholeiitic lavas of Hyalo Ridge. This suggests that the trace element compositions of the lavas are moving, with time, towards *less* refractory compositions, implying that the source region is also changing with time. Within the Dragonhead and Kostal Lake centres, however, later lavas have higher Cr and MgO concentrations, suggesting that their sources become more refractory with time.

Vanadium, also a member of this group, has been used as an indicator of magnetite fractionation (Duncan and Taylor 1968). A graph of total iron as FeO against V for the Wells Gray lavas shows a total absence of covariance, indicating that magnetite fractionation is not significant in producing the chemical variations observed in the lavas. A graph of CaO against V, however, shows a strong positive covariance (Fig.32) which indicates fractionation or accumulation of a mineral or minerals with compositions lying along the trend. Two candidates for such a process are clinopyroxene, which is enriched in CaO relative to the magmas, and olivine, which is depleted in both CaO and V relative to the magmas. It is probable that vanadium occurs in clinopyroxene as the V^{4+} ion, which has an ionic radius closer to that of the Cr^{3+} ion (Henderson 1982). Accumulation or fractionation of either mafic mineral will have a complementary effect on the CaO-V diagram, that is, fractionation of olivine is equivalent to accumulation of pyroxene. The total amount of mafic phases fractionated or accumulated cannot, however, exceed 10%, as discussed above.

The fourth, most interesting, group comprises the incompatible elements Rb, Sr, Ba, Zr and Nb. These elements show a common covariance, together with Cl and the major oxides K_2O and P_2O_5 (e.g. Fig.33). One explanation of this covariance would be that of different degrees of partial melting in the source. However, a difference of as much as 30% in partial melting would be required to produce the observed variation in these elements. This is inconsistent with the small variation required by the major

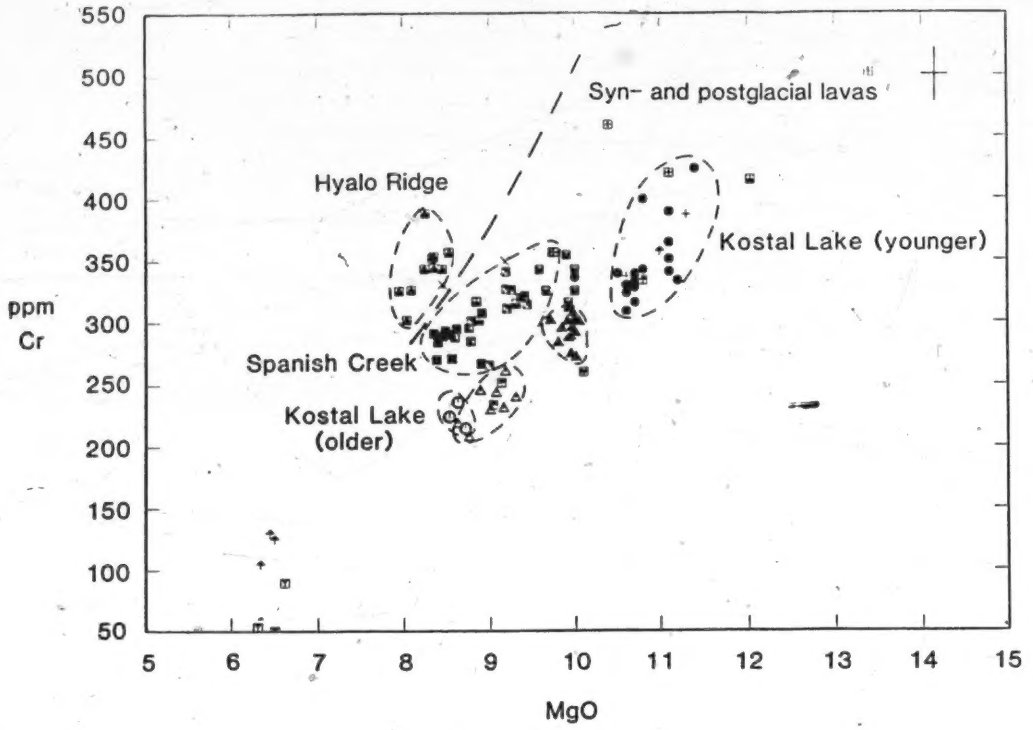

Fig. 31. Weight percent MgO against Cr for the Wells Gray lavas. Symbols used for each centre are listed in Table 1. Error bars are given at the 2σ confidence level based on the maximum observed concentrations of each component. The transitional olivine basalts from Hyalo Ridge are the most enriched in Cr for a given MgO concentration. The Dragonhead and Kostal Lake centres (triangles and circles) show enrichment in Cr and MgO in later phases of activity (filled symbols) relative to earlier (hollow).

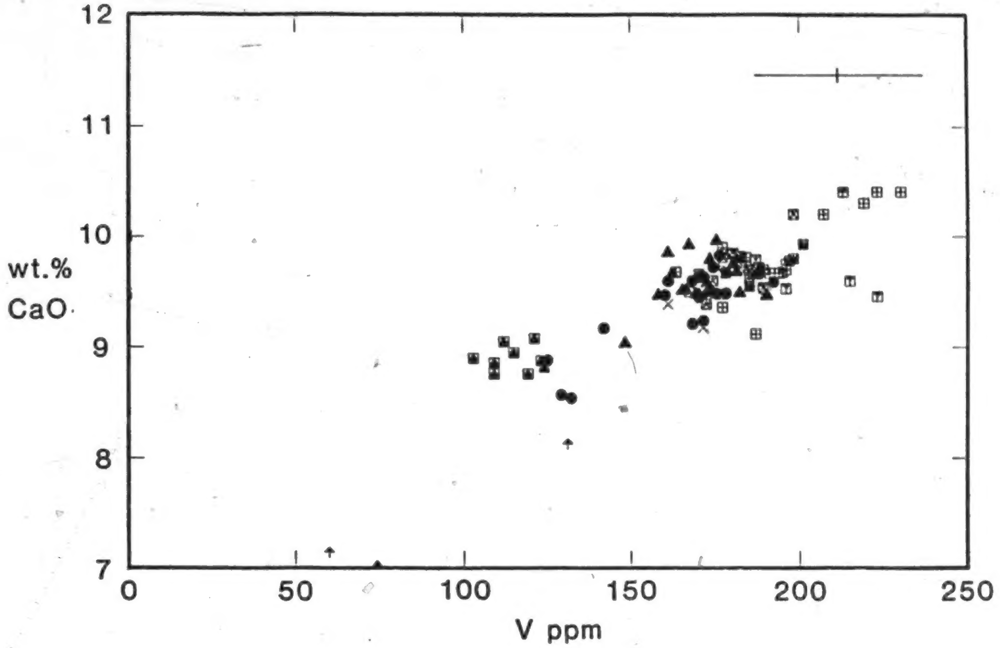

Fig. 32. CaO against V in the Wells Gray lavas. Symbols used for each centre are listed in Table 1. Error bars are given at the 2σ confidence level based on the maximum observed concentrations of each component. The two elements show a positive covariance, within analytical error. The range of values for Flourmill and for Kostal Lake suggests that small amounts of clinopyroxene have been accumulated during ascent.

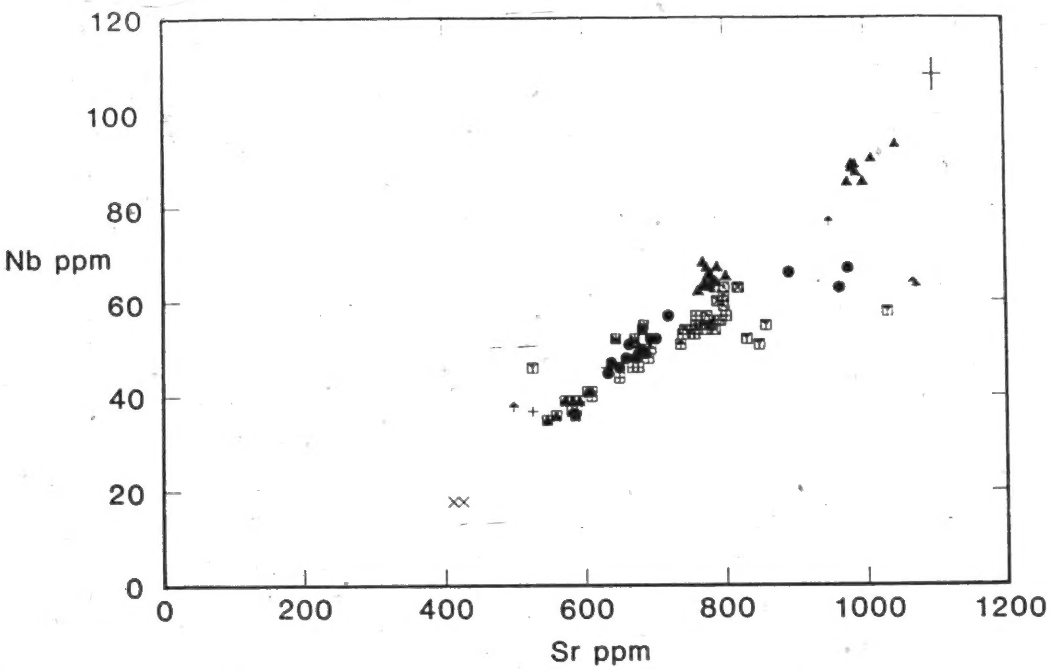

Fig. 33. Sr against Nb for the Wells Gray lavas. Symbols used for each centre are listed in Table 1. Error bars are given at the 2σ confidence level based on the maximum observed concentrations of each component. The observed covariance is common for all suites except Pointed Stick Cone, the later phase of activity on Ray Mountain and the earlier phase of activity at Kostal Lake.

network-modifying elements and by the CaO-V covariance (Fig.32). A more reasonable explanation would be that an initial episode of partial melting in the source depleted the latter in incompatible elements and produced an enriched melt. Successive episodes of melting in the same source produced correspondingly depleted lavas.

A plot of Ba against Sr (Fig.34) shows two covariant trends. The first includes the samples from Flourmill, Spanish Lake, Dragonhead, and the earlier phase of activity on Ray Mountain. Samples which form this trend are enriched in Ba relative to those of the second trend which includes the samples from Kostal Lake, Hyalo Ridge, Pyramid Mountain and the later phase of activity on Ray Mountain. Samples from Pointed Stick Cone do not fall on either trend and are interpreted as the possible result of crustal contamination.

The divergence of the Ba-Sr trends, which is not related to geographic area, is significant and indicates the presence of at least two unrelated sources of trace elements for the Wells Gray lavas. The Ba-enriched trend is designated Type 1 and the Ba-poor trend Type 2. This separation is also reflected in plots of Zr against Ba, Zr against Nb and Ba against Nb (Figs.35, 36 and 37). The Type 1 lavas are therefore depleted in Zr and enriched in Ba relative to the Type 2 lavas.

There is a general covariance of all incompatible elements elements with P_2O_5. The correlation of Sr with P_2O_5 (Fig.38) is particularly good, suggesting that the distribution of Sr in the source region is associated, at least in part, with P_2O_5 and possibly with a phosphate storage phase, such as apatite described in Chapter 3, at or near the source regions for the lavas.

In addition to the incompatible cations, Cl shows a positive covariance with P_2O_5 (Fig.39). The graph appears to be scattered but, for each sample suite, there is a cluster of samples defining a maximum concentration for that suite, while within-suite P_2O_5 concentrations are constant. The covariance between Cl(maximum) and P_2O_5 for the Wells Gray lavas is, therefore, quite good.

The maximum Cl for each sample suite defines a sharp covariance with other incompatible elements, such as Nb (Fig.40). The abundance of Cl in the Wells Gray lavas could be due to the presence of a phase rich in Cl and P_2O_5 in the source regions. The phase could be volatile; more probably it is a Cl-bearing phosphate.

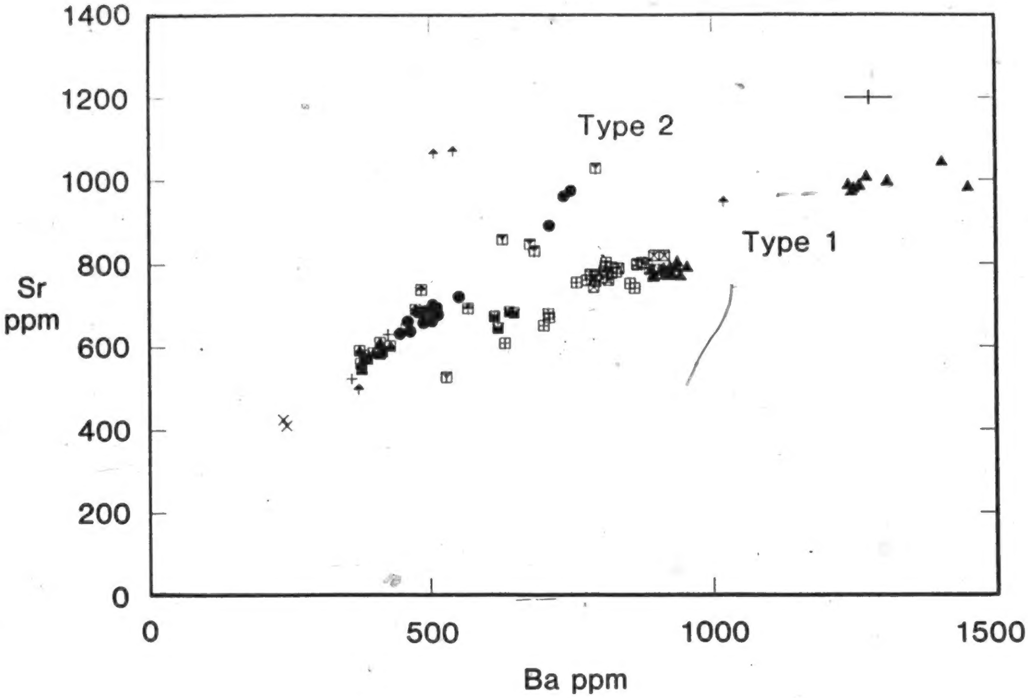

Fig. 34. Ba against Sr for the Wells Gray lavas. Symbols used for each centre are listed in Table 1. Error bars are given at the 2σ confidence level based on the maximum observed concentrations of each component. The lavas fall into two types; a Ba-enriched type (Type 1) including Dragonhead, the earlier phase of activity on Ray Mountain, Flourmill and Spanish Lake and a relatively Sr-enriched type (Type 2) including Kostal Lake, Spanish Bonk and the later phase of activity on Ray Mountain. The samples from Pointed Stick Cone are strongly enriched in Sr and are, apparently, unrelated to other lavas.

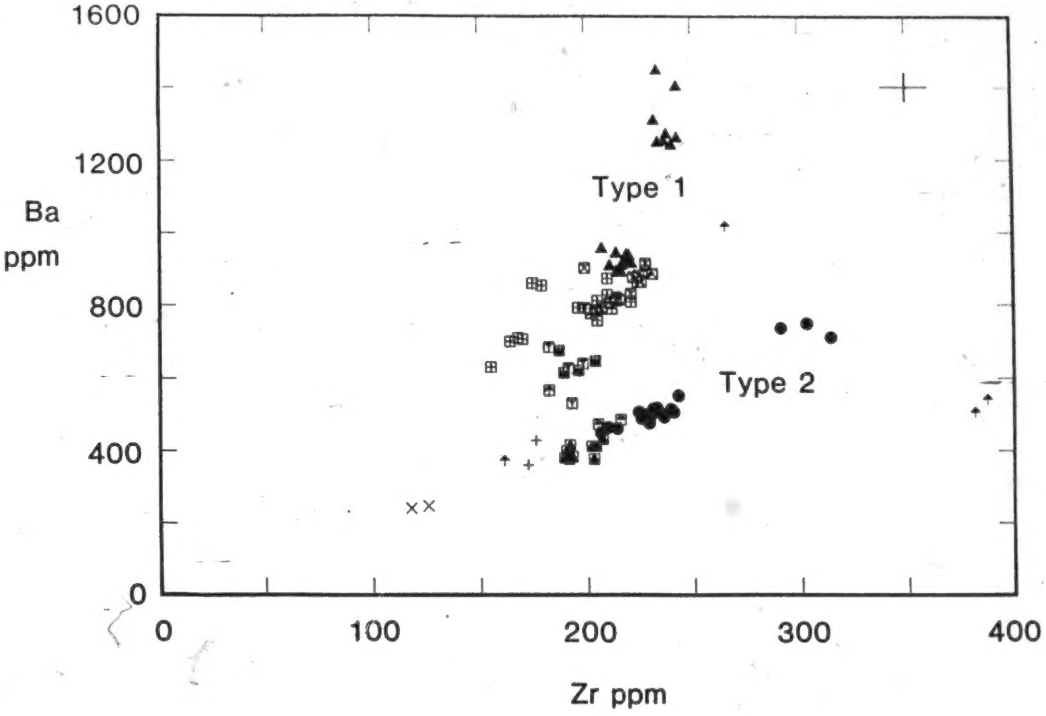

Fig. 35. Zr against Ba for the Wells Gray lavas. Symbols used for each centre are listed in Table 1. Error bars are given at the 2σ confidence level based on the maximum observed concentrations of each component. The lavas fall into the same types as on the previous diagram, with the exception of the Ray Mountain lavas. The Ba-enriched Type 1 is relatively depleted in Zr.

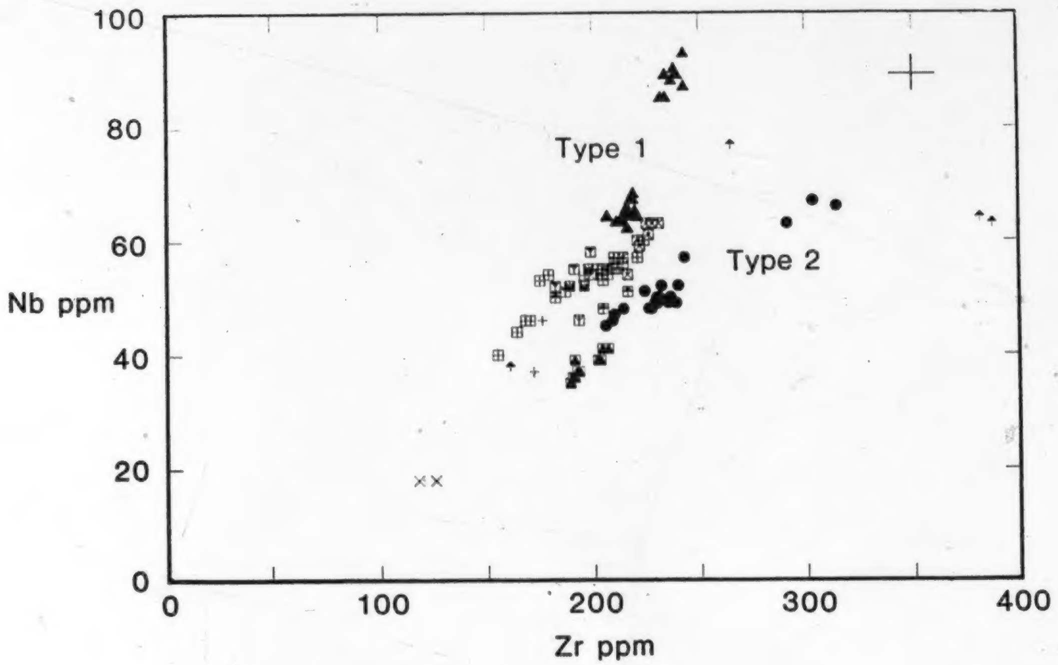

Fig. 36. Zr against Nb for the Wells Gray lavas. Symbols used for each centre are listed in Table 1. Error bars are given at the 2σ confidence level based on the maximum observed concentrations of each component. Type 2, with the exception of the later lavas on Ray Mountain, is enriched in Zr relative to Type 1.

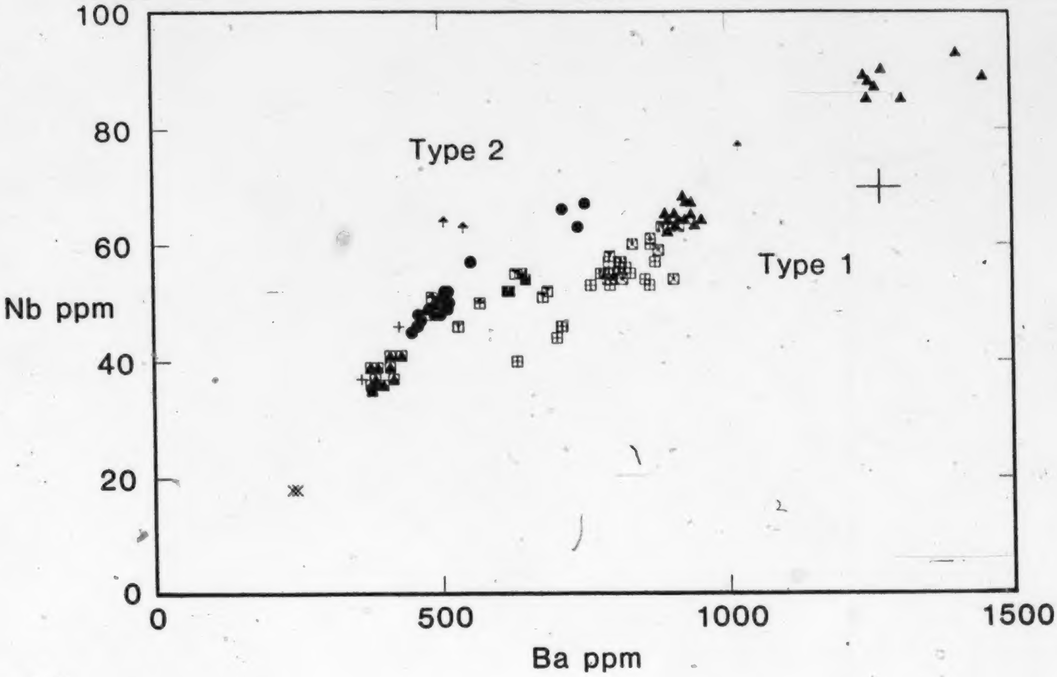

Fig. 37. Ba against Nb for the Wells Gray lavas. Symbols used for each centre are listed in Table 1. Error bars are given at the 2σ confidence level based on the maximum observed concentrations of each component. Types 1 and 2 appear to define separate linear trends.

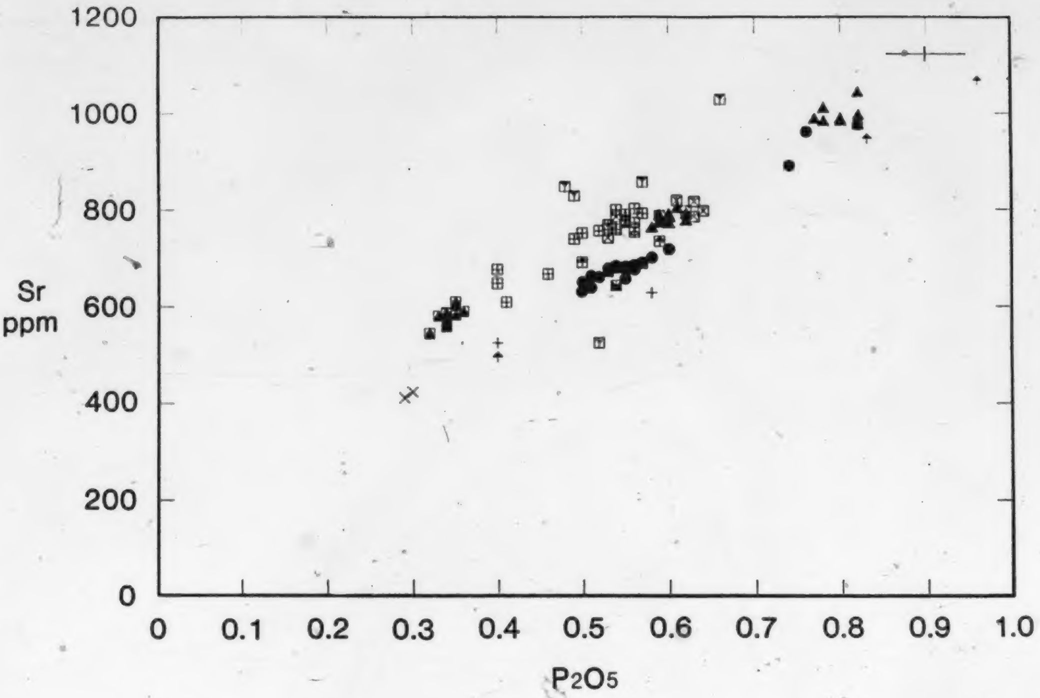

Fig. 38. Weight % P_2O_5 against Sr for the Wells Gray lavas. Symbols used for each centre are listed in Table 1. Error bars are given at the 2σ confidence level based on the maximum observed concentrations of each component. The covariance between these elements suggests that strontium may be associated with phosphorous in the source region, either in a phosphate phase or in a metasomatic fluid.

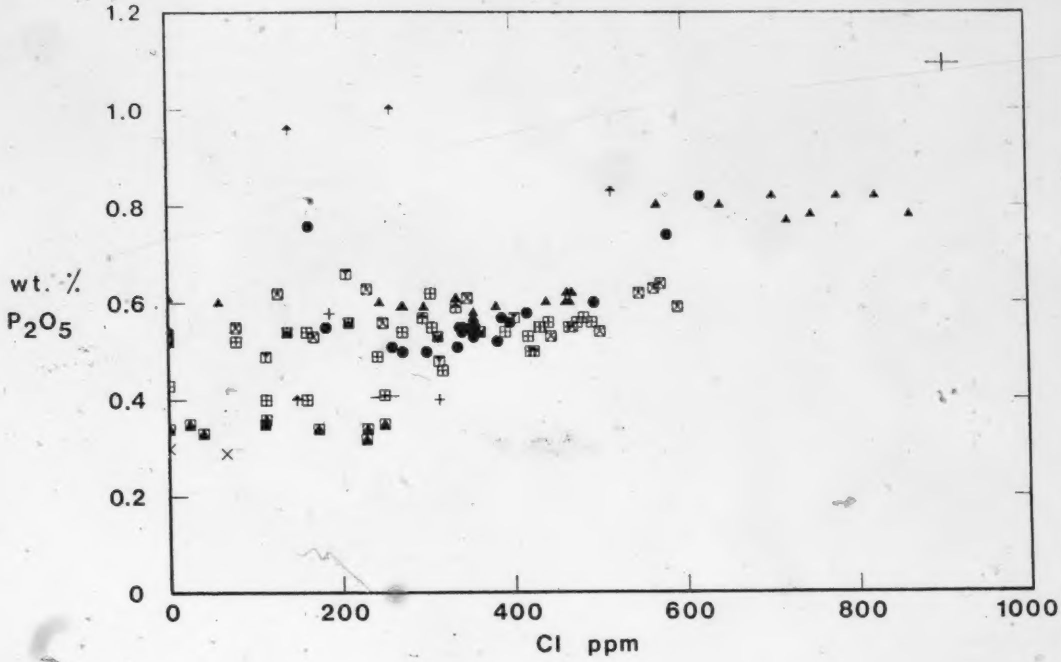

Fig. 39. Cl against P_2O_5 for the Wells Gray lavas. Symbols used for each centre are listed in Table 1. Error bars are given at the 2σ confidence level based on the maximum observed concentrations of each component. There is a strong covariance between the maximum Cl concentration in any sample suite and the mean P_2O_5 concentration for that suite. This suggests that the maximum Cl concentrations for each suite represent near-primary values; samples with values lower than the suite maximum have been degassed.

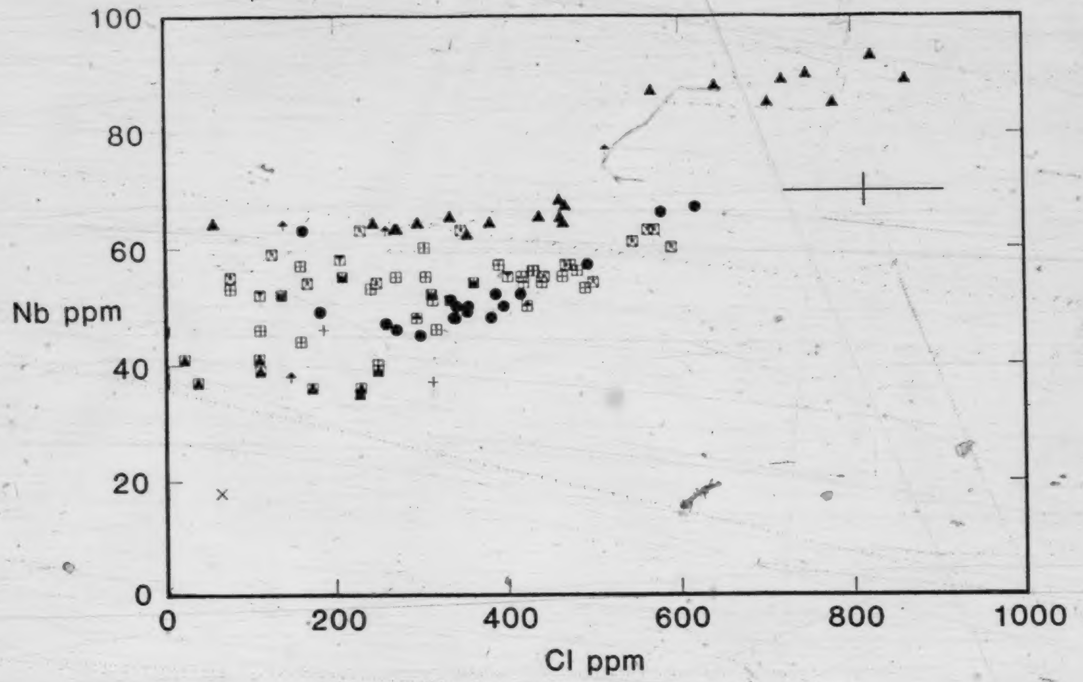

Fig. 40. Cl against Nb for the Wells Gray lavas. Symbols used for each centre are listed in Table 1. Error bars are given at the 2σ confidence level based on the maximum observed concentrations of each component. There is a strong covariance between the maximum Cl concentration in any sample suite, assumed to be the primary concentration in the lava, and the mean Nb concentration of that suite. This suggests that Nb is closely associated with Cl in the source region.

C. Generation of the Wells Gray lavas

The genesis of basaltic magma (Yoder 1976) takes place by the partial melting of either spinel lherzolite or garnet lherzolite in volatile-poor or volatile-rich conditions. Spinel lherzolite is the most common choice for the lavas of the Cordillera because of its abundance as a xenolith in cordilleran lavas. Asthenospheric mantle is present beneath the Canadian Cordillera at depths which lie well within the stability field of spinel. Garnet lherzolite xenoliths, by contrast, are absent from the assemblages found in cordilleran British Columbia.

Concentrations of rare earth elements determined for at least one sample of the alkaline lavas (A.D. Smith, unpubl. data) indicate that these lavas are strongly enriched in light rare-earth elements. This enrichment suggests that either amphibole or garnet is present in the source regions but is greater than can be accounted for by single stage melting of a chondritic garnet lherzolite unless very small degrees of partial melting are assumed (Harrison 1981). Although it may be possible (MacKenzie 1985) to separate as little as 0.1% partial melt from the source, it is more probable that the enrichment is the product of a process comprising at least two stages.

Takahashi and Kushiro (1983) conducted an equilibrium study of dry melting in a natural peridotite, concluding that a range of melt compositions could be derived from the dry xenoliths, the melt compositions becoming progressively more undersaturated with increasing pressure. The Wells Gray lavas could be generated, by their estimates, from a spinel lherzolite similar to that beneath Hawaii, under a pressure of approximately 20 kb. Equilibration calculations made by Hickson (pers. comm. 1987) indicate that the Wells Gray magmas were generated from discrete source regions.

The subcordilleran mantle of British Columbia has undergone three major subduction events in the past 150 Ma. The most recent is active subduction under the southern portion of the Canadian Cordillera (Keen and Hyndman 1979). It is probable therefore that the subcordilleran mantle contains appreciable quantities of volatile components. The presence of apatite and amphibole in mantle xenoliths and the vesicularity of volcanic glass from the hyaloclastite mounds suggest that water, carbon dioxide, phosphorous and chlorine are all present in significant amounts. Studies conducted by Wyllie (1977; 1978) and by Eggler (1976) indicate that the presence of

CO_2 depresses the solidus of peridotite and drives the composition of silicate melts towards SiO_2 - undersaturated values. H_2O also depresses peridotite solidi, enhances the solubility of CO_2 in silicate melts and drives magma compositions towards the SiO_2 - saturated field. Chlorine , as Cl^- depolymerises silicate melts (Burnham 1979) and phosphorous, as PO_4^{3-}, polymerises silicate melts (Mysen 1986). The relative proportions of these components in the source, and their predicted effect on magma compositions, even for synthetic systems are poorly known. Nevertheless, it is probable that a volatile-bearing phase has melted to release the flux necessary for partial melting.

A study recently conducted by Brearley and Scarfe (1984) in British Columbia describes amphibole in a spinel lherzolite located at Lightening Peak in the Intermontane Belt of the Cordillera. This occurrence was interpreted as primary amphibole. Gilbert *et al.* (1982) stated that, given a mixed volatile phase of H_2O and CO_2, a pargasitic amphibole would be stable at temperatures above 1100°C in the spinel stability field. A poorly-constrained temperature obtained for the aluminous assemblage in Chapter 4 is 1100°C. At such a temperature, a slight decompression, a change in the activities of volatile components, or a rise in temperature would initiate melting of the amphibole. Water thus liberated would further alter the volatile activities. Constraints upon the hypothetical conditions are, therefore, poor; nevertheless, melting of the amphibole would then proceed according to the following reaction:

2 amphibole + vapour → 3 diopside + 2 forsterite + spinel + liquid

The melting of pargasite at high pressure will produce a liquid close to nephelinite in composition (Jenkins 1983).

The Lightening Peak amphibole has a ratio of K_2O/Na_2O that is clearly incompatible with those of the Wells Gray lavas (Fig.29). However, the amphibole discovered in a spinel clinopyroxenite nodule in the Dragon's Tongue has a K/Na ratio similar to that of the host lava and represents a possible source composition. Textural relationships between the amphibole and the clinopyroxene-spinel assemblage resemble those reported by Arai (1986) for occurrences of amphibole in mantle xenoliths.

Partition coefficients for major elements between clinopyroxene and co-existing amphibole are presented in Table 2. Predicted values listed in the table are taken from Hawthorne (1981) and from Henderson (1982). Partition coefficients for the Lightening

Table 2

Predicted and observed partition coefficients (χ(amphibole)/χ(pyroxene)) for two xenoliths in British Columbia.

Element	Predicted	Dragon's Tongue	Lightening Peak
Si	n.a.	n.a.	n.a.
Ti	2.5+	4	4
Al	1.67+	1.77	2.19
Fe	1.5+	1.45	1.46
Mn	1	1	1
Mg	1	0.85	1.12
Ca	n.a.	0.57	0.51
Na	1-3.03	3.21	2.64

Predicted partition coefficients are based on data compiled by Henderson (1980) and by Hawthorne (1981). n.a. = data not available. Data on Lightening Peak are from Brearley and Scarfe (1984); those from the Dragon's Tongue are taken from this study.

Peak assemblage are calculated from Brearley and Scarfe (1984). Values for the Dragon's Tongue are listed in Tables B-2 and B-10, in Appendix B. All values for each element show very close agreement. The values indicate that clinopyroxene and amphibole are at least close to equilibrium for both assemblages.

We may consider the generation of melt in the source region as equilibrium melting approximating the reaction of Brearley and Scarfe (1984). Generation of magma from melting of an amphibole incorporates far fewer assumptions than its hypothetical generation from a spinel lherzolite or garnet lherzolite assemblage. The occurrence of xenocrysts of aluminous clinopyroxene in all alkaline lavas from Wells Gray Park implies that the aluminous assemblage described in Chapter 4 is involved.

Modelling of magma generation was carried out using the compositions listed in Table 3. The magma composition was assumed to be that of the Dragon's Tongue lavas enclosing the amphibole-bearing nodule. Compositional modification may have taken place in transit to the surface, by crystal fractionation or accumulation, but the magma composition is probably closest to that in equilibrium with the nodule at depth. Similarly the composition of the clinopyroxene and spinel co-existing with the amphibole were also used.

Melting of the amphibole was assumed to take place according to the reaction:

Amphibole → Liquid + Clinopyroxene + Spinel

The reaction is, naturally, simplified, excluding phosphate and many other significant components, but it serves as a model for the melting of amphibole alone. Calculations based on this reaction assume that all potassium from the melted amphibole will be partitioned into the melt. From this simplified assumption the solid/liquid ratio of the melted amphibole can be calculated. A similar procedure using Ca and Na yields the ratio of spinel to clinopyroxene. Once the relative proportions are calculated, the residual proportions of all other major oxides are calculated.

Calculations based on this reaction show that the amphibole will melt to a liquid composition resembling that of the proximal portion of the Dragon's Tongue and to an aluminous clinopyroxene and hercynitic spinel identical in composition to those in the nodule. All major oxides are accounted for by this model save for a slight residual excess in MgO and a major excess in TiO_2. The discrepancy in MgO can be accounted

Table 3

Concentrations of major elements in amphibole mass-balance calculation.

Phase	Amphibole (Mean of 14/8/9X-R)	Magma (Mean of proximal Dragon's Tongue)	Pyroxene (Mean of 14/8/9X-R)	Spinel (Mean of 14/8/9X-R)	Olivine
SiO_2	40.37	43.50	48.28	0.38	39.39
TiO_2	5.53	2.66	1.37	0.66	0
Al_2O_3	14.76	13.48	8.34	55.44	0
FeO	11.76	12.55	8.11	28.62	18.94
MgO	12.1	9.00	14.26	14.59	41.82
CaO	10.55	9.71	18.48	0.11	0
Na_2O	2.86	4.30	0.89	0	0
K_2O	1.18	1.81	0	0	0
% melt :					
+phenocrysts	n.a.	65.2	26.7	8.1	n.a.
-phenocrysts		67.8	24.3	7.9	4.0

Residual percentages	No fractionation, Ti included	No fractionation, Ti omitted	4% olivine fractionation, Ti omitted
SiO_2	-.914	-.866	-.778
TiO_2	3.38	3.38	3.41
Al_2O_3	-.746	-.793	-.434
FeO	-.906	-.926	-1.15
MgO	0.59	0.59	-.128
CaO	-.725	-.706	-.279
Na_2O	-.181	-.180	-.160

Analyses are averages of five or more analyses for each phase. Mean analyses of mineral phases are taken exclusively from 14/8/9X-R, the amphibole-bearing nodule and are listed in Tables B-2, B-8 and B-10. The magma composition is that of the proximal portion of the Dragon's Tongue which hosts the amphibole-bearing nodule. Analyses from which the mean is calculated are listed in Table D-1. Precisions for all mean values fall within the confidence limits given in Tables A-3 and C-3, as appropriate. The percentage of magma generated from the amphibole was calculated using mass balance of K_2O in amphibole and magma. The relative proportions of clinopyroxene and spinel were calculated by minimising the residual values of the major oxides after extraction of the three phases from the bulk composition. Residua after extraction of spinel and clinopyroxene from the remaining material are listed in the lower part of the table.

for by a slightly higher hypothetical MgO content of the primary magma. MgO was probably depleted in the magma by minor fractionation of olivine during ascent from the source region. Such fractionation would not disturb either the SiO_2 or ΣFe concentrations of the magma significantly because concentrations in the olivine are close to those of the magma. In fact, the process is probably more complex, but the above modelling is strongly suggestive of generation of the magma from a source composition approximately equivalent to amphibole.

The residual in TiO_2 poses a far greater problem. The amphibole is enriched in TiO_2, relative to the melt by a factor of at least 2. This is in accordance with published partition coefficients (Hawthorne 1981) but does not agree with the mass balance calculations. It is possible that TiO_2 is partitioned into another phase (e.g. ilmenite), but no petrographic evidence of this phase exists. It is, therefore, necessary to consider the site distribution of TiO_2 in amphibole, with respect to amphibole breakdown.

Fig.41 shows the structure of amphibole. Three types of octahedral site exist for metal cations; these are the M1, M2 and M3 sites. The M4 site is a large site, commonly hosting Ca^{2+} and Na^{+} cations. The M1, M2 and M3 sites commonly host Mg^{2+}, Fe^{2+}, Fe^{3+}, Cr^{3+} and Ti^{4+}.

It is probable (Hawthorne 1981) that Ti can also exist in trivalent form; in both cases it seems to be partitioned into the M1 site (Veblen and Buseck 1980) This site is close to the A site, housing K^{+} and Rb^{+} ions on the back of the tetrahedral chain. The amphibole analyses from the Dragon's Tongue show an inverse variance between TiO_2 and K_2O. This is interpreted as the effect of melt produced from the amphibole equilibrating with unmelted amphibole. Such equilibration would be fairly rapid, given the large size of the "channels" in the amphibole structure (Hawthorne 1981). Possibly the effect is so pronounced with TiO_2 alone because of its small ionic size and high field strength.

It is proposed, therefore, that an amphibole poorer in TiO_2 is the best candidate for a principal source phase in the generation of the alkaline lavas. The amphibole is of composition similar to that of a kaersutite from an ultramafic xenolith in the Grand Canyon area, described by Best (1974) and is similar to several analyses published by Dawson and Smith (1982) and by Arai (1986). Other phases, such as phosphate, will

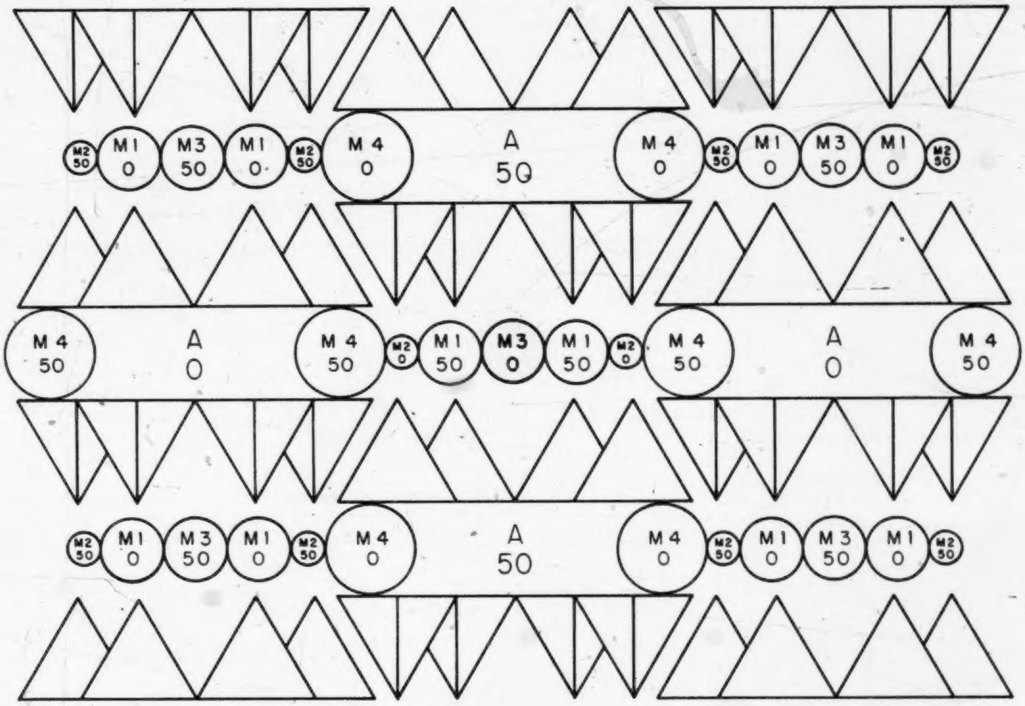
M2 50
M1 0
M3 50
M1 0
M2 50
M 4 0
A 50
M 4 0
M2 50
M1 0
M3 50
M1 0
M2 50
M 4 50
A 0
M 4 50
M2 0
M1 50
M3 0
M1 50
M2 0
M 4 50
A 0
M 4 50
M2 50
M1 0
M3 50
M1 0
M2 50
M 4 0
A 50
M 4 0
M2 50
M1 0
M3 50
M1 0
M2 50

Fig. 41. Structure of an amphibole, viewed along the z axis. Cation sites are labelled and assigned a percentage height in the unit cell above (001). Ti is partitioned into th M3 site, close to the A site which accepts K⁺ ions. Ti may exist as Ti^{3+} or Ti^{4+} in the amphibole; a coupled substitution could explain the inverse variance seen in Fig.25.

contribute to the incompatible element composition of the magma, and some assimilation of relatively refractory phases, such as clinopyroxene, will occur. It is also proposed that at least some of the Wells Gray lavas are produced by breakdown of small but significant quantities of this amphibole-rich assemblage in the subcordilleran mantle.

D. Summary

The whole rock chemistries of the Wells Gray lavas fall into a transitional tholeiitic and an alkaline group. The major element concentrations in each sample suite indicate that only minor crystal fractionation has taken place since generation and the presence of mantle xenoliths in most lavas indicates that the magmas' ascent was sufficiently rapid as to preclude efficient crystal fractionation. No clear pattern of increasing Rb/Sr ratios with decreasing Mg number is present, either for the entire suite or within individual centres. Each centre appears to have a discrete source reservoir with a major element composition differing from the other regions.

The high content of sulphur in the rocks renders Ni useless as a quantitative petrogenetic tool; nevertheless, the lavas have concentrations of Ni, Co and Cr which are characteristic of primary magmas. Mg numbers for most of the lavas range from 60 to 66, which is slightly low, unless the magmas were generated from iron-rich mantle.

The incompatible elements Ba, Zr and Sr define two covariant trends which are interpreted as evidence of two distinct trace element source regions. These source regions are not areally related. The first lava type, designated Type 1, is characterised by relatively Ba-rich and relatively Zr-poor concentrations. Type 2 is relatively Ba-poor and Zr-rich.

No correlation exists between these incompatible element concentrations and the major element concentrations in the lavas. Incompatible elements, such as Ba and Sr show as much as 30% variation which is not in agreement with the 10% fractional crystallisation permitted by variations in the major elements. The variation in trace elements is interpreted as a depletion in the source region of initial partial melting. Subsequent melts, for a given centre, are tapping a partially depleted source volume.

The great enrichment in all large ion lithophile elements in the Wells Gray lavas cannot occur without an enrichment during partial melting of approximately 500, relative to the analyses published by Smith (1986). A more probable mechanism is that of metasomatism of a depleted source rock, prior to initiation of partial melting. Phosphate and chloride are apparently major components of the fluid phase and probably formed the apatite described in Chapters 3 and 4. Small, discrete variations in the compatible element concentrations are reflected in the composition of the erupted lavas.

Calculations using the amphibole-bearing xenolith indicate that the clinopyroxene-magma-spinel assemblage can be generated by melting of a low-titanium kaersutite, with some accessory minerals, such as phosphate. An optimum 4% olivine fraction, when added to the host magma, will reduce the residuals of the calculation to minima.

It is proposed, therefore, that the alkaline lavas in Wells Gray Park were generated by melting of amphibole in discrete veins in the mantle source region. The veining was formed during a geologically recent metasomatic event which perturbed the distribution of the major elements and overprinted that of the incompatible elements. Successive batches of melting in the source region of a single centre depleted part of the source; that volume then formed part of a later source volume, contributing a more refractory component to the later magma.

6.

ISOTOPIC ANALYSIS

The isotopic ratios of strontium and neodymium were determined for twenty samples from the Quaternary alkaline lavas of the Wells Gray area. The purpose of these analyses is: firstly, to determine the isotopic characteristics of the source regions and to compare these with existing data on the subcordilleran mantle (Smith 1986); secondly, to determine the relationship, if any, between the source regions and to constrain the time of generation of the heterogeneities; and, thirdly, to identify, if possible, any evidence of contamination of the magmas by continental crust.

Neither ^{87}Sr/^{86}Sr nor ^{143}Nd/^{144}Nd have, to date, been reported from Quaternary alkali basalts in the Wells Gray area. A similar study (Hickson and Baadsgaard in prep.) was conducted, concurrently with the present study, on samples of pre- and synglacial transitional tholeiitic lavas in the south of the Wells Gray area; this study complemented a high-precision K/Ar age study (Hickson and Souther 1984, Hickson 1987). Hickson concluded that the lavas were derived from a source region previously depleted by at least one episode of partial melting and that no significant contamination by crustal material had taken place.

Isotopic work in the Anahim Belt was conducted by Bevier (1978, 1983a) who measured Sr and Pb isotopic ratios in Chilcotin Group basalts of the Rainbow Range. Bevier found no evidence of crustal contamination in the isotopic compositions of parental lavas, which have whole rock major element compositions similar to those of the syn- and postglacial lavas in the present study area. Significant chemical differences between the two areas have already been discussed, in the preceding chapter.

A. Analytical procedure

Sample selection

Twenty samples were selected for the isotopic study from those already analysed for whole rock major and trace element concentrations. Sample selection was based upon geological significance, comprising geographic and stratigraphic location; upon chemical significance, whether representative of a number of analyses from a major eruptive phase or of an unusual composition; upon a low degree of weathering and upon a high degree of volatile retention. Volatile retention was estimated from measured Cl concentrations. A positive correlation between P_2O_5 concentrations and maximum values for Cl within a sample suite suggests that the maximum Cl values are close to primary concentrations in the lavas at eruption. Samples with such concentrations are probably least altered.

Nine samples which were selected did not have maximum concentrations of Cl. Five of these exceptions were made for the purpose of having better stratigraphic control of the isotopic analyses. Three were the least weathered samples available from small, poorly sampled centres and had anomalous chemical compositions. One sample, W2-21/7/1-R, from the distal portion of the Dragon's Tongue, had been analysed in replicate four times, for whole rock major and trace element concentrations. Whole rock analyses of these nine samples showed no departure from the average non-volatile element concentrations of each appropriate unit.

Two samples of volcanic glass, from Spanish Mump and from Pyramid Mt. were also analysed. Microprobe data for major elements in these samples are reported in Table B-13, but trace element concentrations, determined by X.R.F. for whole rock samples, were not measured.

Sample preparation

A detailed account of sample preparation is given in Appendix C. Whole rock sample powders analysed were aliquots of powders prepared for major element analysis by X.R.F.. The two glass samples were first washed in dilute HCl in an ultrasonic bath to remove secondary calcite, then crushed to a grain size of approximately 0.5 mm. Weathered fragments of glass were then removed by hand-picking.

Isotopic ratios were measured using aliquots of approximately 0.5 g for the whole rock samples and approximately 0.2 g of each glass sample. Concentrations of Sm and Nd were determined for eight whole rock samples by the isotope dilution method, using a mixed ^{149}Sm-^{145}Nd spike solution.

The method used for sample dissolution and separation of Sr, Sm and Nd is that described by Smith (1986) and based on Dosso and Murthy (1980) and Cavell and

Baadsgaard (1986). Both Sr and Nd isotopic ratios were determined using a single aliquot of each sample; Sm and Nd concentrations also used a single, spiked, aliquot.

Isotopic analysis

Details of isotopic analysis are given in Appendix C. Separates for the determination of Sm, Nd and Sr isotopic ratios, in both spiked and unspiked aliquots, were loaded as chloride onto tantalum side filaments of a filament assembly bearing a rhenium centre filament. Sr separates were loaded onto double filament assemblies; Nd and Sm separates were loaded onto both double and triple filament assemblies. Isotopic ratios were measured in a VG Micromass 30 mass spectrometer with a 30.5 cm radius of curvature and a 90° sector magnet. All ^{143}Nd/^{144}Nd ratios were normalised to a ^{146}Nd/^{144}Nd ratio of 0.724127 and all ^{87}Sr/^{86}Sr ratios to an ^{88}Sr/^{86}Sr ratio of 8.373225.

Analytical precision and reproducibility

In-run precision for each isotopic analysis is listed in Table 4. Reproducibility of analyses over the course of the study was estimated from replicate analyses of ^{87}Sr/^{86}Sr in N.B.S. SRM 607 and of ^{143}Nd/^{144}Nd in the La Jolla standard. For this instrument, reproducibility is estimated as ±0.0002 for ^{87}Sr/^{86}Sr and ±0.00003 for ^{143}Nd/^{144}Nd (2σ). During the course of the study, 13 analyses of the N.B.S. standard SRM 987 gave a value for ^{87}Sr/^{86}Sr of 0.71026±2 (2σ) and 21 analyses of the La Jolla Nd standard gave a value for ^{143}Nd/^{144}Nd of 0.51105±2 (2σ).

B. Analytical results

Isotopic ratios of Sr and Nd

The ^{87}Sr/^{86}Sr and ^{143}Nd/^{144}Nd ratios determined in the lavas are listed in Table 4 and plotted on Fig.42. Samples analysed have values of ^{87}Sr/^{86}Sr and ^{143}Nd/^{144}Nd ranging between 0.7030 and 0.7041 and between 0.5119 and 0.5123 (ϵNd=+2.1 to +7.3 (±0.6, 2σ), respectively. All ratios are initial ratios; the oldest sample analysed is 0.3 Ma in age and the radiogenic increases in ^{87}Sr/^{86}Sr and ^{143}Nd/^{144}Nd since eruption lie within the in-run precision and are negligible.

Table 4

Results of isotopic analyses

Sample number	$\frac{^{87}\mathrm{Sr}^{1}}{^{86}\mathrm{Sr}}$	$\frac{^{143}\mathrm{Nd}^{1}}{^{144}\mathrm{Nd}}$	$\frac{\mathrm{Sm}}{\mathrm{Nd}}$	Sm ppm	Nd ppm
26/8/2-SM	0.70321 ±3	0.51214 ±3	n.a.	n.a.	n.a.
26/8/3-SB	0.70348 ±3	0.51214 ±3	n.a.	n.a.	n.a.
23/8/6-ST	0.70389 ±2	0.51198 ±2	0.2066 ±1	5.798 ±5	28.06 ±1
23/8/12-ST	0.70408 ±2	0.51196 ±2	0.1827 ±2	6.124 ±5	33.52 ±3
24/8/11-SL	0.70382 ±4	0.51204 ±2	0.1901 ±1	7.773 ±4	40.88 ±2
24/8/14-SL	0.70384 ±2	0.51197 ±2	0.1967 ±1	7.453 ±7	37.89 ±2
4/8/7-SC	0.70355 ±1	0.51205 ±1	n.a.	n.a.	n.a.
4/8/2-SC	0.70376 ±4	0.51201 ±2	n.a.	n.a.	n.a.
2/8/6-SC	0.70382 ±2	0.51199 ±1	n.a.	n.a.	n.a.
13/8/10-PY	0.70312 ±3	0.51220 ±3	n.a.	n.a.	n.a.
17/8/7-RM	0.70310 ±3	0.51209 ±2	0.2131 ±1	7.448 ±6	34.96 ±2
17/8/13-RM	0.70387 ±3	0.51200 ±1	0.1929 ±7	7.38 ±28	38.27 ±2
18/8/9-RR	0.70317 ±3	0.51222 ±2	n.a.	n.a.	n.a.
18/8/4-RC	0.70331 ±1	0.51221 ±3	n.a.	n.a.	n.a.
14/8/2-R	0.70369 ±2	0.51199 ±3	0.1739 ±7	9.111 ±7	52.39 ±7
14/8/5-R	0.70365 ±3	0.51199 ±1	n.a.	n.a.	n.a.
21/7/1-R	0.70362 ±2	0.51203 ±1	0.1883 ±3	7.711 ±4	40.95 ±2
29/7/3-KN	0.70309 ±2	0.51220 ±2	0.2133 ±3	7.090 ±9	33.25 ±2
29/7/6-KS	0.70306 ±3	0.51215 ±1	n.a.	n.a.	n.a.
29/7/7-KP	0.70310 ±3	0.51208 ±2	0.1954 ±1	9.232 ±6	47.25 ±3

Initial ratios for both Sr and Nd (1) were obtained for unspiked samples and are uncorrected because of the young age of the samples and their relatively low concentrations of Sm and Rb. Sm and Nd concentrations and Sm/Nd ratios were obtained using a mixed Nd-Sm spike. Analytical precisions are quoted as two sigma. n.a. = not analysed. Suite suffixes are listed in Table 1.

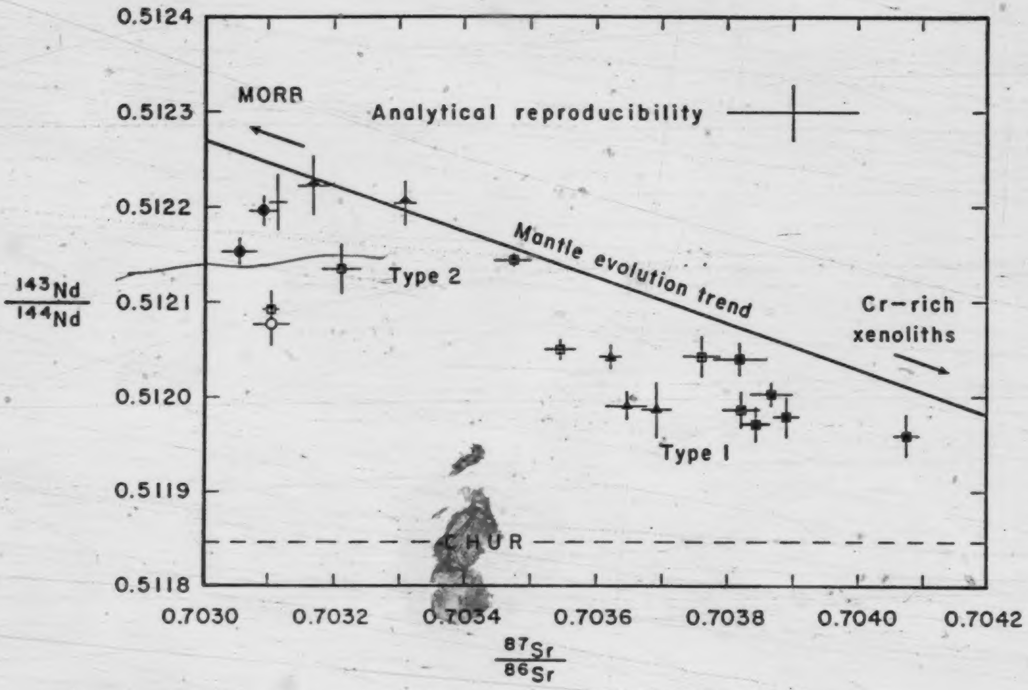

Fig. 42. Sr and Nd isotopic compositions in the Wells Gray lavas. The lava compositions lie subparallel to the mantle evolution line, intermediate between values for the Cr-rich ultramafic xenoliths (CHUR) and those for mid-ocean ridge basalts (MORB). The alkali basalts fall into the two groups identified in Fig.34; the Type 2 lavas are closer to the MORB field while the Type 1 lavas are closer to CHUR in isotopic composition. Symbols used for each centre are listed in Table 1. Error bars are given at the 2σ confidence level for each sample, based on replicate measurements. The error bar at the top of the diagram is a 2σ confidence envelope based on replicate analyses on N.B.S. SRM 607 for $^{87}Sr/^{86}Sr$ and the La Jolla standard for $^{143}Nd/^{144}Nd$ during the course of this study.

Neither the Rb-Sr nor the Sm-Nd isotopic systems give isochrons or pseudoisochrons for the Wells Gray lavas, indicating that the isotopic heterogeneities in the lavas, characteristic of the source compositions, were not formed by a single-stage process. The $^{87}Sr/^{86}Sr$ values are in radiogenic Sr and enriched in $^{143}Nd/^{144}Nd$ relative to the assumed bulk-earth value, which is determined from the chondritic uniform reservoir (CHUR; $^{143}Nd/^{144}Nd$=0.51187 and $^{87}Sr/^{86}Sr$ =0.7047). The source regions of the lavas have, therefore, suffered an overall depletion of Rb relative to Sr and of Nd relative to Sm, over a period of time which permitted the radioactive decay of ^{87}Rb and ^{147}Sm to change the $^{87}Sr/^{86}Sr$ and $^{143}Nd/^{144}Nd$ ratios to depleted and enriched values, respectively, relative to CHUR. No constraints exist for the timing or extent of such a Rb-Nd depletion, nor is there any evidence that the depletion occurred in a single event or over the entire source region of the lavas. Such a depletion will be referred to as a *time-integrated* depletion.

An inverse correlation between radiogenic Sr and Nd, for all samples analysed, lies subparallel to the mantle evolution curve (Figs.42 and 43). Values lie within error of the curve or towards $^{143}Nd/^{144}Nd$-depleted and $^{87}Sr/^{86}Sr$-depleted values. The values also lie within the accepted field (Henderson 1984) for ocean island and intraplate basalts such as Hawaii (Chen and Frey 1983, 1985), southern Australia (McDonough *et al.* 1985) and the Chilcotin Group basalts (Smith 1986) of British Columbia (Fig.43). The Geronimo Volcanic Field (Menzies *et al.* 1985) also lies in this region of the diagram. Smith (1986) reports low Rb concentrations, relative to Sr, Sm and Nd, in xenoliths of spinel lherzolite; it is possible that the low Rb/Sr ratios, relative to Sm/Nd, have caused a time-integrated depletion in $^{87}Sr/^{86}Sr$ rather than in $^{143}Nd/^{144}Nd$.

Two groups of isotopic ratios, for the alkalic lavas, correspond to the lava types identified by trace element chemistry. Type 1, high Ba lavas have higher $^{87}Sr/^{86}Sr$ and lower $^{143}Nd/^{144}Nd$, closer to the assumed bulk-earth values represented by CHUR. The Type 2, high Zr lavas have lower radiogenic Sr and higher radiogenic Nd, close to the field of mid-ocean ridge basalts. The transitional tholeiitic basalts of Hyalo Ridge have $^{143}Nd/^{144}Nd$ values which lie within the range of the alkaline lavas but are enriched in radiogenic Sr, although these values are still depleted relative to CHUR. The grouping is similar to that observed by McDonough *et al.* (1985) in the Newer Basalts of

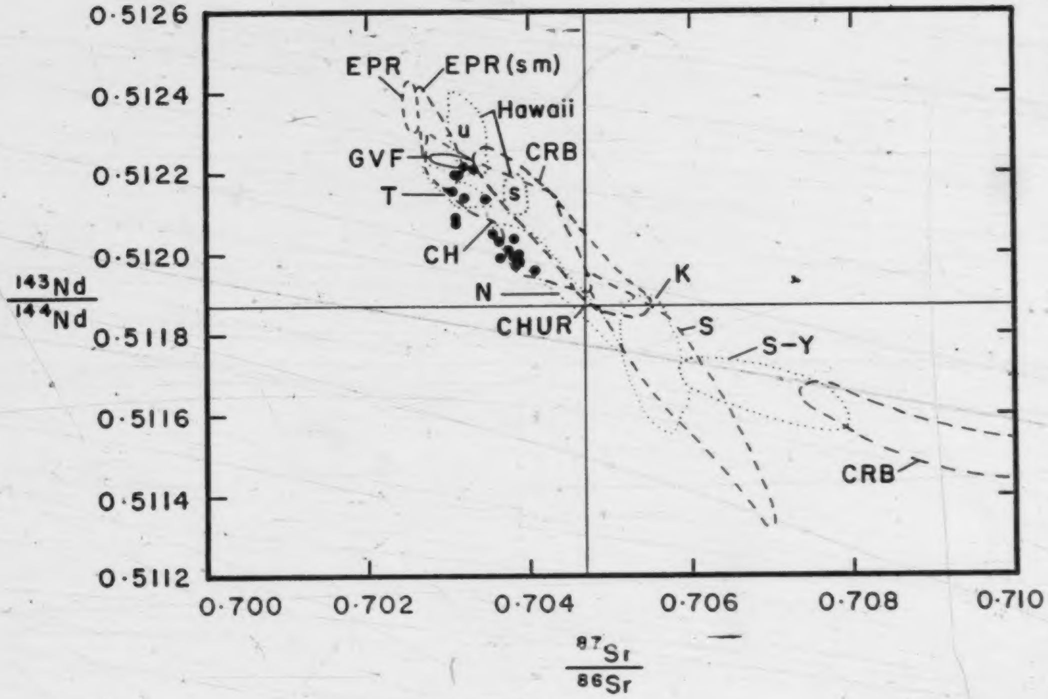

Fig. 43. Comparison of isotopic data with those from other basaltic rocks. The lava compositions lie subparallel to the mantle evolution line and are slightly depleted in $^{87}Sr/^{86}Sr$ and/or $^{143}Nd/^{144}Nd$ relative to the majority of basalts represented here. The two groups identified resemble the groupings obtained by (McDonough *et al.* 1985). EPR = East Pacific Rise and EPR(sm) = seamounts (White and Hoffmann 1982); s,u = saturated and undersaturated lavas from Hawaii (Chen and Frey 1985); GVF = Gerónimo Volcanic Field; S = Sierra Nevada; S-Y = Snake River Plain - Yellowstone (Menzies *et al.* 1985); N = Newer Basalts of South Australia and Victoria; T = Tasmanian basalts (McDonough *et al.* 1985); CH = Chilcotin Group basalts (Smith 1986); CRB = Columbia River basalts (Carlson *et al.* 1981); K = Kerguelen Islands (Zindler *et al.* 1984). The Wells Gray lavas are represented by circles. The two groups identified resemble the groupings obtained by (McDonough *et al.* 1985).

southeastern Australia and for the Tasmanian basalts. Chen and Frey (1985) report three groupings for the Honomanu, Kula and Haleakala Series from Hawaii in either case the more strongly undersaturated lavas lie closer to the MORB field. Such is not the case for the Wells Gray lavas. Although, within Types 1 and 2, there is a general trend towards the MORB field with progressive degrees of undersaturation, the isotopic range is quite small. Moreover, when the two groups are combined, it is evident that the Dragon's Tongue samples plot in the middle of the range of isotopic values.

The Newer basalts of Australia and the sequence of basalts observed in Hawaii are interpreted as the result of partial melting in a mantle plume-MORB environment (McDonough *et al.* 1985, Chen and Frey 1985). The Wells Gray lavas, firstly, are erupted from vents to one side of the Anahim lineament and may not represent plume-related volcanism. Secondly, the erupted volumes of the Wells Gray lavas are several orders of magnitude lower than either the Australian or the Hawaiian basalts studied. The comparatively large volume of source region sampled and homogenised in the lavas erupted in the two regions may result in dilution of small-scale heterogeneities which are amplified by the small erupted (and therefore small source) volumes of the Wells Gray lavas.

The isotopic difference between the groups is interpreted as the result of mixing between at least two source components. Carlson (1984), in a model for the isotopic evolution of the Columbia River Basalts identified five source components contributing to their petrogenesis. Two were inferred to be subducted oceanic crust, two to be enriched lithospheric mantle beneath the continental crust and one to be the continental crust itself. This study cannot distinguish between the two types of enriched lithospheric mantle; the mantle beneath British Columbia atypically lacks a lithospheric root (Berry and Forsyth 1975). Carlson's (1984) contaminated oceanic crust component has higher ^{87}Sr/^{86}Sr and/or ^{143}Nd/^{144}Nd relative to the mantle mixing curve; no clear evidence exists, therefore, for its presence in the Wells Gray source regions.

The possible contributors to the isotopic compositions of the Wells Gray lavas are, therefore, a MORB component (subducted oceanic crust, subducted oceanic mantle or both), and either a mantle component which has not suffered a time-integrated depletion of a continental crust component. The first two components, at least, are present in the source regions. Zindler *et al.* (1984) have shown that, in the ocean basins, the scale of isotopic heterogeneity in the mantle, relative to the scale of the source regions, controls the isotopic compositions of ocean island basalts. A similar model is probably appropriate for the subcordilleran mantle.

The contamination of ascending lavas by inclusion of, or isotopic equilibration with, radiogenic Sr and non-radiogenic Nd from the continental crust is a possible contributor to the isotopic diversity present in the Wells Gray lavas. Carlson (1984) identifies a C4 crustal component with a ^{87}Sr/^{86}Sr ratio of 0.711 and a ^{143}Nd/^{144}Nd ratio of 0.5108, values close to those from recent basalts and of spinel lherzolite nodules from B.C. (Smith 1986). The latter work indicates that enriched mantle is present near the source regions; however, there is no effective way of distinguishing between the enriched mantle component and a possible crustal component using isotopic data alone. The variation in isotopic compositions can, nevertheless, be accounted for by mixing of two possible mantle source components without significant contamination by continental crust.

For individual centres, and for the entire sample suite, there is no correlation between ^{87}Sr/^{86}Sr and the concentrations of SiO_2, Sr, or other incompatible elements, indicating that no significant melting of crustal xenoliths or wallrock has taken place during the rapid ascent of the magmas (c.f. McDonough *et al.* 1985). Although the possibility of isochoric isotopic exchange between lava and country rock exists, the lava ascent (in the instance of the alkaline lavas) was sufficiently rapid as to preclude significant isotopic exchange. The model developed by Menzies *et al.* (1985) for the Geronimo alkaline volcanics suggests that incompatible element enrichment would take place in the wallrock, rather than in the magma, in the presence of a CO_2-rich fluid. No explicit evidence exists, therefore, to indicate that continental crust was included in the petrogenesis of the Wells Gray lavas.

The ^{87}Sr/^{86}Sr values for different phases of activity in any given centre lie within error of each other. One exception to this observation is the two phases of activity on Ray Mountain, which are of different chemical types (Chapter 5) and significantly different eruption times (Chapter 2). Their isotopic and chemical relationship is enigmatic. Sr concentrations for the Wells Gray lavas exhibit a positive covariance with P_2O_5

(Fig.38). The Sr/P_2O_5 ratios of the Type 2 lavas appear slightly lower than those of the Type 1 lavas, approximating the grouping of Sm/Nd, but the two groups lie within error of each other on Fig.38; the slight difference in trends is therefore not significant. ^{87}Sr/^{86}Sr shows no covariance with P_2O_5. This implies that any phosphate phase contributing to the composition of the lava either does not contribute significantly to the Sr concentration of the lava or is isotopically similar to the lava or is in isotopic equilibrium with the lava.

The two groups of alkaline lavas have mean ^{87}Sr/^{86}Sr ratios of approximately 0.7031 and 0.7037 (Types 2 and 1, respectively). ^{87}Rb/^{86}Sr ratios derived from the Rb/Sr ratios of the lavas can be used to estimate the time necessary to evolve these different ratios from source regions of different Rb/Sr ratios and identical ^{87}Sr/^{86}Sr ratios. The time is calculated using the relationship:

$$T = (^{87}\mathrm{Sr}/^{86}\mathrm{Sr}_1 - {}^{87}\mathrm{Sr}/^{86}\mathrm{Sr}_2) \;/\; (\lambda^{87}\mathrm{Rb} \times (^{87}\mathrm{Rb}/^{86}\mathrm{Sr}_1 - {}^{87}\mathrm{Rb}/^{86}\mathrm{Sr}_2))$$

where λ^{87}Rb = 1.42×10^{-11} a^{-1}. This calculation assumes that the Rb/Sr ratio of the magmas is that of the source material. The age calculated is 1±0.3 Ga. Rb is, in fact, preferentially partitioned into the melt, relative to Sr; this age is therefore a minimum age of heterogeneous segregation for a dry peridotite mantle. A similar calculation, using ^{147}Sm/^{144}Nd$_1$, ^{147}Sm/^{144}Nd$_2$, ^{143}Nd/^{144}Nd$_1$, ^{143}Nd/^{144}Nd$_2$ and λ^{147}Sm ($=6.54 \times 10^{-12}$ a^{-1}) gives an age of 1.6±0.3 Ga. Nd is preferentially partitioned into the melt, relative to Sm; this age is therefore a maximum age of heterogeneity. Neither age can be more precisely estimated, within the limits of the data available; both ages are, however, significantly older than the age of the Cordillera and are of the same order of magnitude as those estimated by Menzies *et al.* (1985) for the mantle beneath the Geronimo volcanic field.

In a given centre, earlier lavas are enriched in incompatible elements and depleted in radiogenic Nd relative to later lavas, although major element concentrations are equivalent. The ^{143}Nd/^{144}Nd values show an inverse correlation with P_2O_5 but, in the Kostal Lake and Dragonhead centres, there are inverse correlations between the two variables (Figs.44 and 45) which regress to ^{143}Nd-depleted values.

The paucity of data and the restricted range in P_2O_5 concentrations preclude accurate estimates of the shape or slope of the correlations; nevertheless, the variations

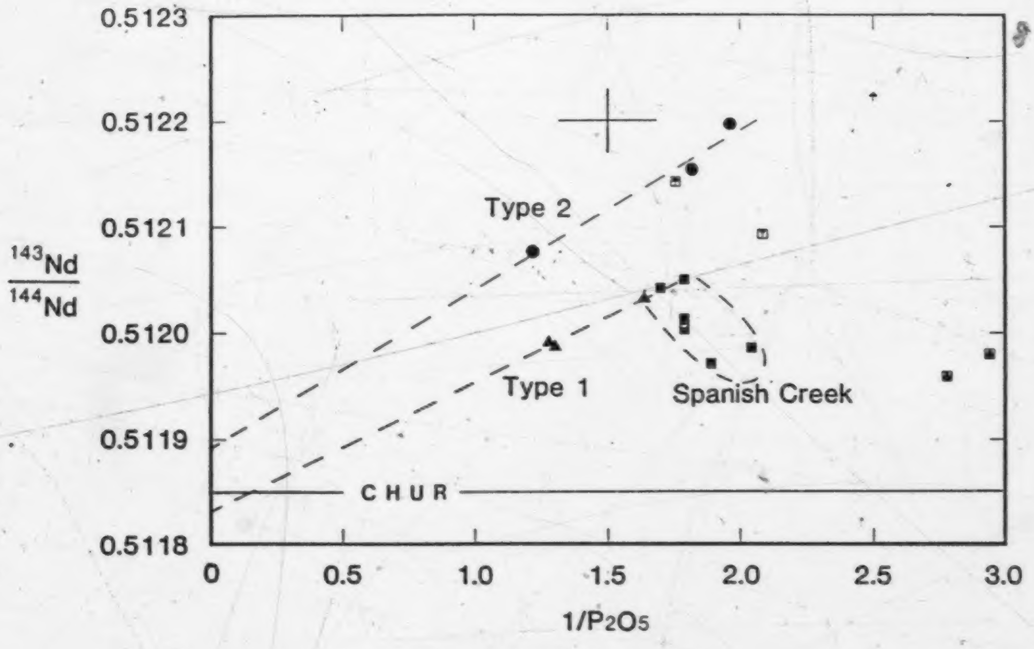

Fig. 44. 1/P_2O_5 against Nd isotopic composition. Type 1 and Type 2 lavas show independent covariances, regressing to undepleted mantle values of $^{143}Nd/^{144}Nd$ at P_2O_5 values corresponding to a phosphate mineral. The Spanish Lake and Flourmill lavas lie away from the Type 1 line, possibly as a result of accumulation of phosphate-poor material with an undepleted Nd isotopic signature. Symbols used for each centre are listed in Table 1. Solid squares represent samples from the Spanish Lake and Flourmill centres. Error bars are given at the 2σ confidence level based on the maximum observed concentrations in the case of P_2O_5 and on replicate analyses of the La Jolla standard in the case of $^{143}Nd/^{144}Nd$.

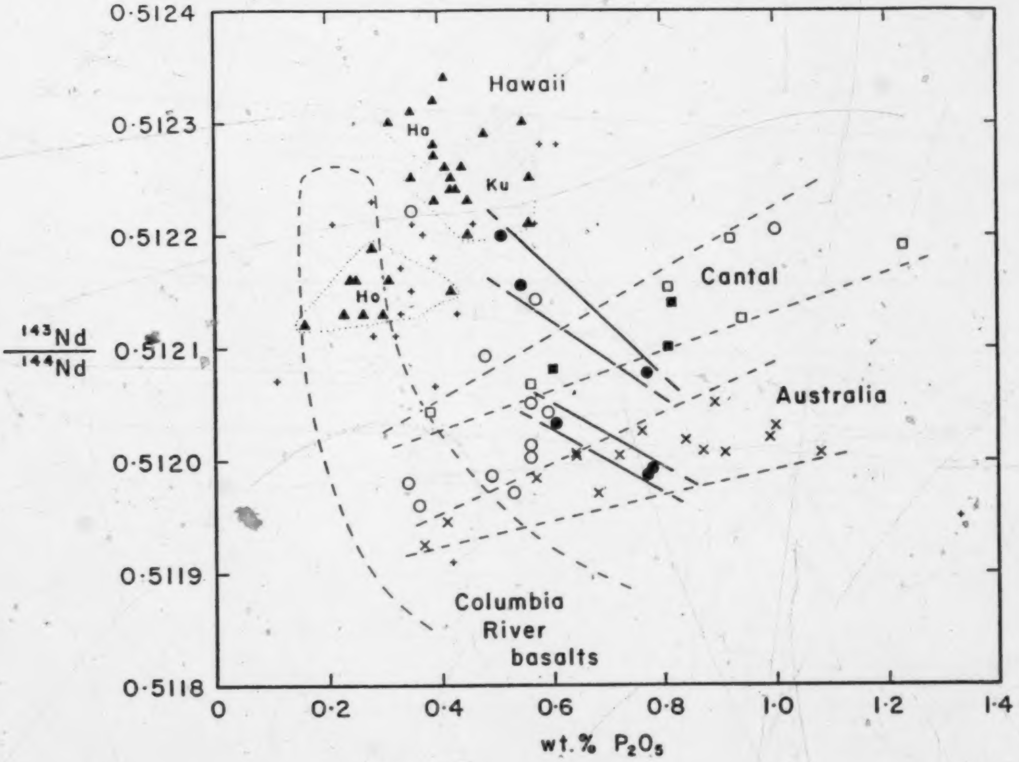

Fig. 45. P_2O_5 against Nd isotopic composition. $^{143}Nd/^{144}Nd$ and P_2O_5 values are from Chen and Frey (1985) for Hawaii (triangles); from Downes (1984) and from Chauvel and Jahn (1981) for Cantal in the Massif Central (closed and open squares, respectively); from McDonough *et al.* (1985) for the Newer Basalts of South Australia and Victoria (X) and from Smith (1986) for the Chilcotin Group basalts (+). Samples analysed from the Columbia River basalts (Carlson *et al.* 1981) are not shown, but the field of values is included for comparison. Ho = Honomanu Series; Ku = Kula Series; Ha = Haleakala Series Samples from this study are plotted as circles. Filled circles indicate samples from the the two centres with inverse correlations between $^{143}Nd/^{144}Nd$ and P_2O_5, contrary to the trends seen in Cantal, Hawaii and Australia.

lie outside analytical precision and are interpreted as real. Both correlations regress to high-phosphorous compositions near 0.51187, which is a bulk-earth value (ϵ_0) for ^{143}Nd/^{144}Nd. This value is significantly lower than those of the volcanics and may represent a source component which has not undergone a time-integrated depletion. The ^{143}Nd/^{144}Nd value for the refractory component, by extrapolation to a P_2O_5 value of 0, in the lavas is P_2O_5 estimated to lie between 0.5122 for Dragonhead (Type 1) and 0.5124 for Kostal Lake (Type 2); these values are close to the field of mid-ocean ridge basalts.

Data from Downes (1984), Chauvel and Jahn (1984), McDonough *et al.* (1985), Chen and Frey (1985), Carlson *et al.* (1981), Smith (1986) and this study were used to construct Fig.45. All four studies of intraplate basalts with alkaline affinities show a positive correlation with P_2O_5. The Chilcotin Basalts and Columbia River Basalts show somewhat more scattered distributions, but the Chilcotin Group still show a positive covariance. The Columbia River Basalts show a weak negative trend of P_2O_5 against ^{143}Nd/^{144}Nd which may be due in part to crustal contamination.

The Wells Gray lavas as a whole do not show a clear trend but two centres of small erupted volume exhibit the inverse correlation described above, which cuts across the observed trends for other alkaline provinces. It must be stressed here that the data are not necessarily contradictory. The Wells Gray area was sampled with the intention of studying small-scale variations in individual centres, rather than the regional variations in large areas such as southeastern Australia. The large erupted volumes of lava in such provinces may mask smaller scale heterogeneities within the source volumes.

The ^{87}Sr/^{86}Sr ratios of individual eruptive phases from a single centre lie within error of each other and are not dependent upon P_2O_5; the converse is true of ^{143}Nd/^{144}Nd. Spinel lherzolites, assumed to be representative of the subcordilleran mantle, have been analysed by Smith (1986). All samples analysed are strongly depleted in Rb relative to chondritic abundances, some samples by as much as one order of magnitude. Strontium, samarium and neodymium concentrations are near-chondritic. The historic depletion of Rb, relative to Sr indicates that the existing Sr isotopic ratios in the source regions received a significantly lower radiogenic contribution after the event which depleted Rb. Magma generated from such a source region would be of monotonous Sr isotopic composition. The presence of sufficient Sm in the source region, and the occurrence of phases which partition Sm and Nd differently would permit the development of Nd isotopic heterogeneities.

Graphs of $^{143}Nd/^{144}Nd$ against P_2O_5 or against Cl (Figs.44, 45 and 46) show, in addition to the inverse correlation between variables, a trend of decreasing $^{143}Nd/^{144}Nd$ with decreasing P_2O_5 and Cl. This trend is present in the Flourmill and Spanish Lake centres. Both centres are characterised by an abundance of xenophyric clinopyroxene which represents at least three different assemblages from the subcordilleran mantle. The trend towards a low-volatile, low $^{143}Nd/^{144}Nd$ component is therefore interpreted as an effect of the accumulation of xenophyric clinopyroxene, of one or more of the varieties described in Chapters 3 and 4. The clinopyroxene grains (A.D. Smith, unpubl. data) have $^{87}Sr/^{86}Sr$ values of approximately 0.705, characteristic of mantle which has not undergone a time-integrated depletion.. Nd was not analysed for these samples.

Sm and Nd concentrations

Samarium and neodymium concentrations and Sm/Nd values for the ten samples analysed by isotope dilution are presented in Table 4. The concentrations of samarium in the alkali basalts range from 7.0 to 9.5 ppm and in the transitional basalts between 5.5 and 6.5 ppm. Neodymium concentrations range from 33 to 53 ppm in the alkali basalts and from 28 to 34 ppm in the transitional basalts. Sm/Nd values range from 0.180 to 0.215 in both petrogenetic groups. The values from the alkaline lavas are comparable with values for Sm and Nd determined for alkali basalts from the Massif Central (Downes 1984, Chauvel and Jahn 1981); with Nd concentrations determined for the Newer Basalts of Victoria State, Australia (McDonough *et al.* 1985); with values for Sm and Nd determined for certain of the Columbia River Basalts (Carlson *et al.* 1981); with concentriations in lavas from the Geronimo volcanic field in Arizona (Menzies *et al.* 1985) and with values determined by Beswick and Carmichael (1978). The values show a range of enrichment factors, relative to chondritic abundances (Nakamura 1974), from 44 to 84 for Nd and from 27 to 47 for Sm. Sm/Nd ratios are comparable with those from other areas of alkali basalts but are significantly below those determined by Carlson *et al.* (1984) for the Columbia River Basalts. Both the low Sm/Nd values and the high enrichment of Nd and, to a lesser extent Sm, relative to chondritic abundances suggest

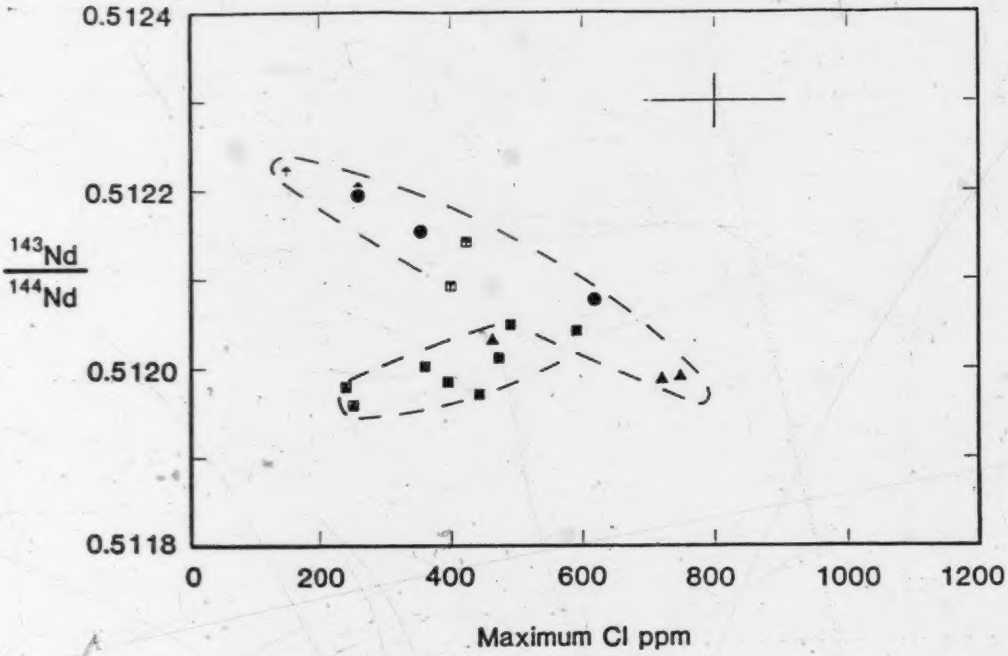

Fig. 46. Maximum Cl for a sample suite against Nd isotopic composition. The analyses indicate at least three possible sources for the Wells Gray lavas. The first is a Cl-rich, CHUR-like source, possibly a phosphate. The other two are Cl-poor and range in composition betweene CHUR and MORB. Symbols used for each centre are listed in Table 1. Solid squares represent samples from the Spanish Lake and Flourmill centres. Error bars are given at the 2σ confidence level based on the maximum observed concentrations in the case of Cl and on replicate analyses of the La Jolla standard in the case of $^{143}Nd/^{144}Nd$.

that the alkaline lavas are highly enriched in the light rare-earth elements. Published values for partition coefficients for phases in a lherzolite source rock (e.g. Harrison 1981) indicate that such an enrichment cannot take place during single-stage melting from lherzolite with a chondritic rare-earth pattern without impossibly small degrees of partial melting (less than one percent).

Calculations of partitioning for Sm and Nd during partial melting using the concentrations determined by Smith (1986) in spinel lherzolite nodules from B.C. require bulk partition coefficient (source rock/magma) of approximately 0.02 for either element. Published values for partition coefficients for the major minerals composing spinel lherzolite are summarised by Henderson (1982). Calculations using these partition coefficients indicate that the source rock could have no greater than 5% clinopyroxene in order to generate the observed Sm enrichment and no greater than 2% clinopyroxene in order to generate the observed Nd enrichment. These values are maximum values, assuming that the balance of the source rock comprises olivine, with no accessory phases. This modal composition is clearly inconsistent with the petrologic observations made by Fujii and Scarfe (1982), by Brearley *et al.* (1984) and by the present study.

The Sm and Nd concentrations determined by Smith (1986) for spinel lherzolite are normal or slightly depleted relative to chondritic abundances. The partial melting calculations are, therefore, interpreted as support for the hypothesis of melt generation from enriched regions in a subcordilleran spinel lherzolite mantle. Such enrichment could be chemical in nature or could cause mineralogical changes such as the formation of amphibole-rich veins.

Sr, Sm, and Nd concentrations in basalts of the Wells Gray area all show a positive correlation with P_2O_5 concentrations (Figs.38, 47 and 48). A plot of Sm/Nd ratios against P_2O_5 for the Wells Gray lavas shows three groups of areally unrelated values, two with an inverse correlation of Sm/Nd against P_2O_5 (Fig.49). In all three groups, Sm/Nd increases from older to younger phases of discrete centres which could indicate increasing depletion in the source region for each volcano with time.

The two analyses from the Hyalo Ridge transitional olivine basalts shows no significant change in phosphorous content with Sm/Nd although the younger sample has the higher Sm/Nd ratio. This relative depletion in P_2O_5 suggests that the the transitional

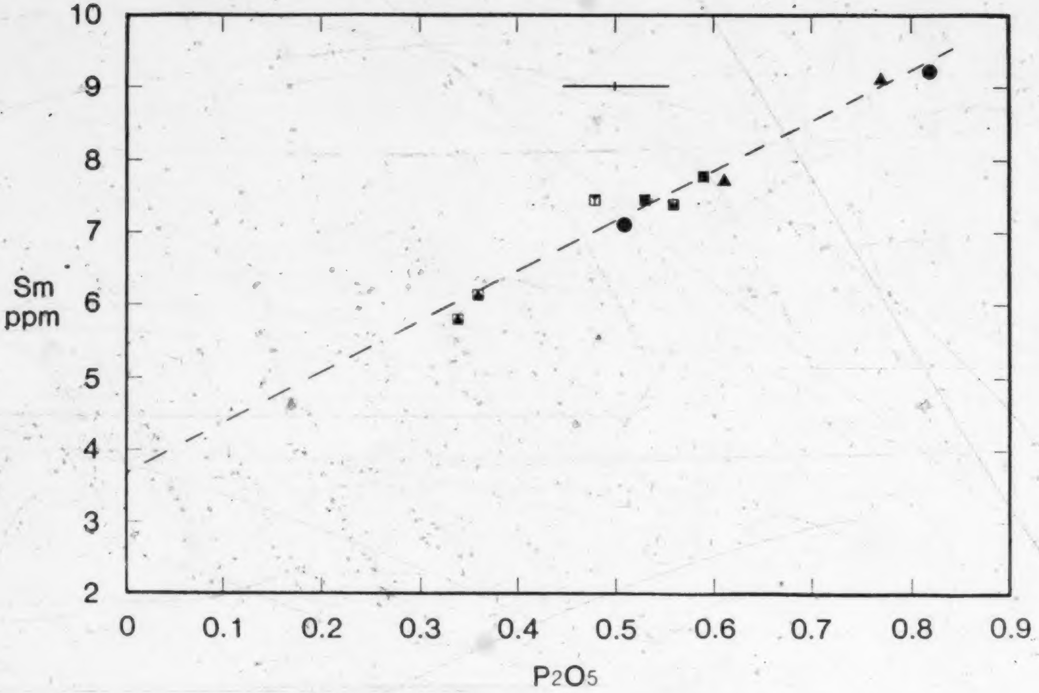

Fig. 47. P_2O_5 (wt.%) against Sm in the Wells Gray lavas. All samples, from all three suites, lie within error of a single regression line showing a positive covariance. Symbols used for each centre are listed in Table 1. Solid squares represent samples from the Spanish Lake Centre. Error bars are given at the 2σ confidence level based on the maximum observed concentrations of each component.

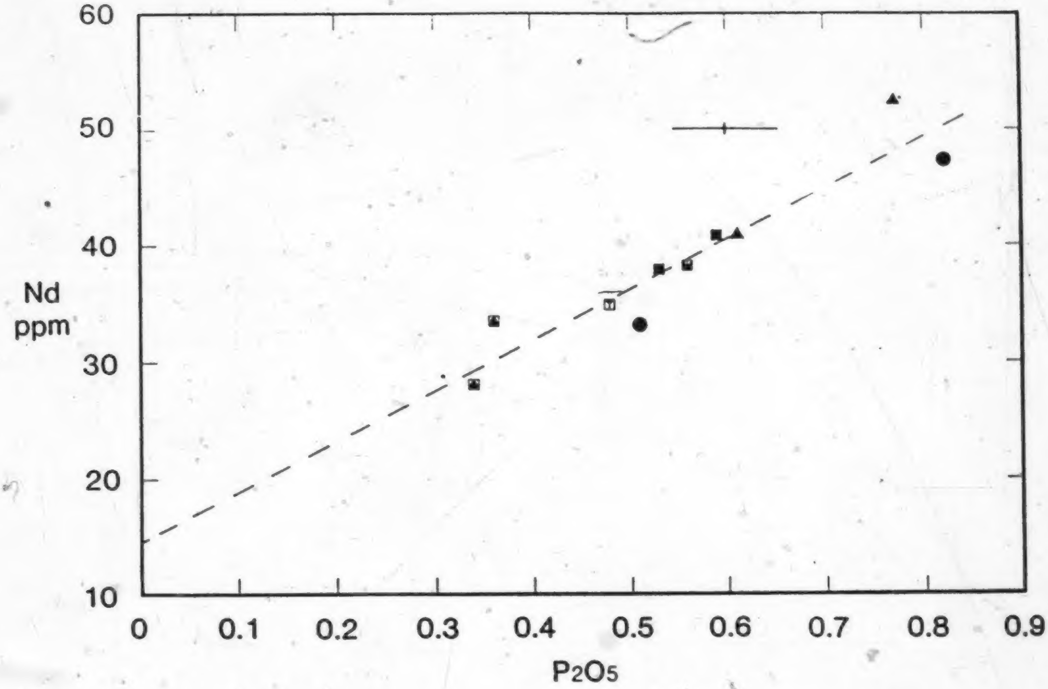

Fig. 48. P_2O_5 (wt.%) against Nd in the Wells Gray lavas. Samples from Kostal Lake have lower Nd concentrations, for a given P_2O_5 concentration, than lavas of equivalent composition from the Dragon's Tongue. Symbols used for each centre are listed in Table 1. Solid squares represent samples from the Spanish Lake Centre. Error bars are given at the 2σ confidence level based on the maximum observed concentrations of each component.

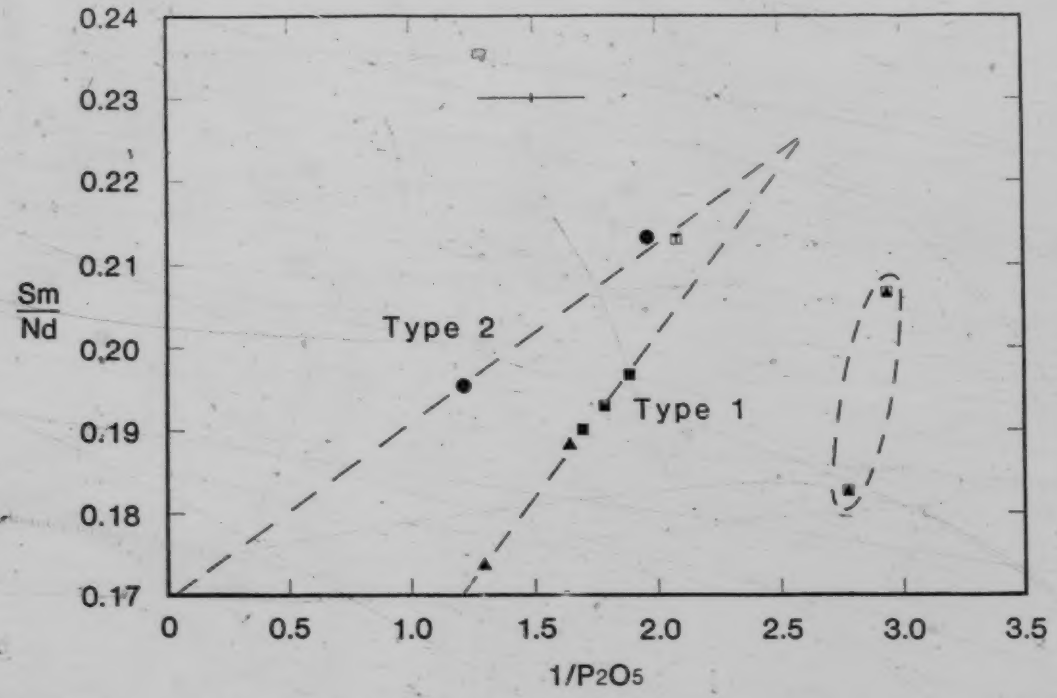

Fig. 49. $1/P_2O_5$ (wt.%) against Sm/Nd in the Wells Gray lavas. The Type 1 and Type 2 lavas lie on separate lines, each of which regresses to a value for phosphate representing a chemically undepleted REE source. Symbols used for each centre are listed in Table 1. Solid squares represent samples from the Spanish Lake Centre. Error bars are given at the 2σ confidence level based on the maximum observed concentrations of each component.

lavas are derived from a depleted source, possibly by a higher degree of partial melting than that inferred for the alkaline lavas.

The group comprising basanitoids of Spanish Lake, Dragon's Tongue and the earlier lavas on Ray Mountain, shows a positive correlation of Sm/Nd against $1/P_2O_5$ (Fig.49). The covariance appears to be linear, which suggests a mixing mechanism. This group is equivalent to the Sr-Ba-Zr Type 1 grouping noted in Chapter 5. The second group of basanitoids, from Kostal Lake and from the later lava flow at the summit of Ray Mountain, shows a similar correlation; this group is equivalent to the Type 2 lavas of Chapter 5. The shape of the latter trend is uncertain, due to the sparsity of data points from this group. The trends, if indeed linear, would converge at values of approximately 0.227 and 0.38 for Sm/Nd and P_2O_5, respectively. It is unlikely that this crossover point is significant; the disparity in high field strength element concentrations between the two groups suggests that each type is equilibrated with a different refractory component at or near its source. The refractory components both have low P_2O_5 concentrations and high Sm/Nd. A melt derived from a more refractory source will have a higher Sm/Nd ratio and lower concentrations of incompatible elements. Extrapolation of the two covariances to a value for $1/P_2O_5$ appropriate to that of phosphate (approximately 0.02) gives Sm/Nd values of 0.12 and 0.17 for Type 1 and Type 2, respectively.

Covariance of rare-earth elements and Sr with phosphorous is fairly common in alkaline lavas and is not in itself indicative of phosphate control in the source region of a magma suite. The observed variation in Sm/Nd and in $^{143}Nd/^{144}Nd$ suggesting that their distribution in the Wells Gray lavas is at least partly controlled by melting of, or by equilibration with, a phosphate phase in or near the source region. The concentrations of P_2O_5 in the lavas indicate that the phosphate is present in quantities comprising 1% (and not exceeding 2%) of the mode of the lavas. Implicit in this interpretation is the existence either of two sources of differing accessory phase and incompatible element composition or of significantly different partial melting processes in the source regions. The former hypothesis is preferred, because of the relative homogeneity in major element concentrations exhibited by most of the lavas.

Hofmann and Hart (1978) used published Sr diffusion data to estimate the elapsed time from an isotopically heterogeneous to an isotopically homogeneous source rock, given the physical conditions of the mantle and an appropriate rock type. For a fluid-rich mantle, Hofmann and Hart estimated that isotopic equilibrium would be attained at a maximum of 1-2 Ma. Sm diffusion coefficients are close to those of Sr (Sneeringer *et al.* 1984) suggesting that the two isotopic systems are coupled under mantle conditions. Little is known about the nature of the diffusion in the presence of phosphorous, chlorine, water and carbon dioxide; nevertheless, the time elapsed between generation of the isotopic heterogeneity and the generation of the lavas cannot have exceeded 2 Ma.

Data presented in Chapter 4 indicate two different incompatible element compositional trends in the alkaline lavas, indicated by the concentrations of Sr, Ba and Zr. The trends are absent for major and trace compatible elements, which show small significant differences in the lavas and do not indicate major differences in partial melting mechanisms. The variations, however, do suggest small differences in the compatible element concentrations in the respective source regions. The Sm and Nd concentrations, in addition to the incompatible element data, are therefore interpreted as the result of two different source types with respect to incompatible elements, overprinted on individual sources of differing compatible element chemistry.

C. Summary

^{87}Sr/^{86}Sr and ^{143}Nd/^{144}Nd isotopic ratios in the Wells Gray lavas define two groups, which correspond to the Type 1 and Type 2 groups defined in Chapter 5. The two groups lie on a trend subparallel to the mantle evolution trend, and lie between the MORB field and that assumed to represent undepleted mantle. Type 1 has higher ^{87}Sr/^{86}Sr and lower ^{143}Nd/^{144}Nd than Type 2, whose ^{87}Sr/^{86}Sr and ^{143}Nd/^{144}Nd values lie close to the MORB field.

The isotopic compositions of the lavas can be modelled by mixing between a MORB-type source component, either subducted oceanic crust or subducted oceanic mantle, and an undepleted subcordilleran mantle, identified by Smith (1986) and by Carlson (1984). No evidence exists for crustal contamination of the isotopic systems.

Individual centres within either type have very similar values of ^{87}Sr/^{86}Sr but ^{143}Nd/^{144}Nd is inversely correlated with P_2O_5 in lavas from Dragonhead (Type 1) and

Kostal Lake. This indicates that Nd isotopic ratios are controlled either by melting of, or by isotopic exchange with, a sublithospheric phosphate phase with an undepleted Nd isotopic signature. If such heterogeneity exists in the source region, it is short-lived; the event causing the heterogeneity cannot occur more than 2 Ma prior to generation of the magmas (Hofmann and Hart 1978). A similar relationship is seen in the data of Chauvel and Jahn (1984), from alkali basalts from the Massif Central.

Sm and Nd in alkaline lavas from the Wells Gray area both show a positive correlation with P_2O_5 which is similar to the trends observed by other workers (Beswick and Carmichael 1978, McDonough *et al.* 1985, Chauvel and Jahn 1984). Extrapolation of the trends for Sm and Nd, to P_2O_5 values appropriate for phosphate, gives values for the two elements of approximately 280 and 2000 ppm, respectively. This is consistent with the generalised value cited by Beswick and Carmichael (1978) of 15000 ppm for total LREE in apatite from a spinel lherzolite. Their Sm/Nd correlation with P_2O_5 is similar to that observed in this study; the Wells Gray lavas lie near the median of Beswick's and Carmichael's data.

Sm, Nd and Sr concentrations and ratios in both Wells Gray lava types may be controlled by a phosphate phase at or near the source region. Any Sr concentrated in the phosphate is in isotopic equilibrium with that in the melt. ^{143}Nd/^{144}Nd in the lavas, however, is controlled by the amount of phosphate contributed to the melt, either from the source or by sublithospheric contamination. Post-generation accumulation of xenophyric clinopyroxene has obscured this relationship in the Spanish Creek lavas.

7.

VOLATILE CONCENTRATIONS

The purpose of this part of the study is to measure the concentrations of H_2O and CO_2 present in the Wells Gray lavas, to compare the results from both alkaline and transitional lavas with each other, to compare both these values to those obtained for similar lavas elsewhere in the world and to interpret the results with respect to the petrogenetic history of the lavas.

It has been suggested from experimental work (Eggler 1973, 1974, 1978, Wyllie 1977, 1978, 1979, Brey and Green 1975) that volatile concentrations in the source regions of tholeiitic lavas are lower than in those of alkaline lavas; it was therefore proposed that CO_2 is a major flux in the generation of alkaline lavas. Given that these deductions are correct and that CO_2 is more soluble in alkalic lavas (Mysen *et al.* 1975, 1976, Mysen and Virgo 1980, Brey 1976, Sharma 1979, Sharma *et al.* 1979), CO_2 should therefore occur in significantly greater concentrations in the Wells Gray alkalic lavas than in the transitional tholeiitic series from Hyalo Ridge.

Two types of sample are appropriate for the determination of volatile concentrations in lavas. The first comprises samples of whole glass. Concentrations of H_2O and CO_2 have been determined for volcanic glasses in lavas from Kilauea, Hawaii (Harris and Anderson 1983), in seafloor basalts (Delaney 1977, Delaney *et al.* 1978) and in seamounts (Byers *et al.* 1984). No studies have, as yet, been conducted on glasses from the intraplate alkali basalts of the North American Cordillera.

The second type of glass sample is formed when the growth of phenocrysts in any lava entraps small volumes of melt; these are considered to represent the composition of the host magma at the time of their entrapment (Harris 1981a, 1981b). A review of the various inclusion types, analogous to fluid inclusions , is given by Roedder (1979). Melt inclusions are present in all samples collected from Wells Gray Park. Part of this study is therefore to determine their suitability for microdetermination of their volatile concentrations.

A. Analytical procedure

Sample selection

Samples were selected which had been rapidly quenched, by ice or by water, to form a pristine glass, yellow to brown in colour. Several localities in Wells Gray Park exhibit ice or water contact features where quenching has been rapid. Pyramid Mountain and Spanish Mump are both SUGMs (Hickson 1987). Hyalo Ridge is a tuya and Ray Mountain exhibits at least one ice contact horizon. The distal portion of the Dragon's Tongue contains at least one flow lobe which represents a water or ice contact with development of a near-pristine glass margin. These are the only localities at which samples suitable for study were found

Petrography of volcanic glass

Photomicrographs of volcanic glasses from the four localities listed above are shown in Plates 10A, 10C, 10D and 10E. Plate 10C shows a sample of hyaloclastite from the southern flank of Hyalo Ridge. A detailed description of the glass is given in Chapter 3. Briefly, the glass fragments range in size from 0.1 mm to as much as 5 mm and are blocky in shape. Vesicles are rare or absent. Rare microphenocrysts of olivine and plagioclase, as much as 5% of a whole shard, are present.

Pristine glass samples are rare in the alkalic lavas. All samples taken from lava flows or from cinders and agglutinate in any of the subaerial cones are devitrified. The only samples which retain glass other than intersertal residual glass are samples which have been quenched by contact with water or ice.

Even rapidly quenched samples are, in places, devitrified. At Pyramid Mountain one of the larger glass fragments is progressively oxidised as a function of depth into the fragment away from a holohyaline rim. The rim of brown glass is 2 cm thick. Devitrification of the glass is associated with the development of Fe-Ti oxide needles in the glass (Plate 10E). The small size of the needles precludes analysis by electron microbeam. Such development of microcrystalline oxide is common and only small samples of pristine glass are available. Such samples are, without exception, highly vesicular (Plates 10A, 10F). This suggests that increased concentrations of volatiles in the melt enhance ionic transfer and promote the formation of crystals.

Samples from Type 1 lavas (see Chapters 5 and 6) are all at least partly crystallised; the only exception is the ice contact feature in the proximal portion of the Dragon's Tongue. This sample contains pristine glass but is at least 10 km distal to the vent and is probably extensively degassed. The sample would not, therefore be comparable to those from locations proximal to a vent. Samples of this type available from Type 2 occurrences include Spanish Mump, Pyramid Mountain and the basal hyaloclastite from the second phase of activity at Ray Mountain. Samples from the transitional tholeiitic suite are represented by the hyaloclastite on Hyalo Ridge.

The vesicles in hyaloclastite from Pyramid Mountain contain gas under pressure; puncturing of the vesicles in oil permitted measurement of the relative diameters, and therefore the relative volumes, of the vesicle and of the gas contained, at atmospheric temperature and pressure. The gas contained in any vesicle expanded to a volume as much as 2.5 times that of the enclosing vesicle. Using the Ideal Gas Law and an assumed magma temperature of 1100°C, a pressure of entrapment of approximately 12 bars was calculated. The implication is that the vesicles formed, in the extruded lava, under a hydrostatic pressure consistent with that at the bottom of an intraglacial lake, at a depth of approximately 120 m. This supports Hickson's (1987) theory of formation for Pyramid Mountain.

Petrography of glass inclusions

Melt inclusions are present in all samples collected from Wells Gray Park. Three types were identified, after those described by Roedder (1979). The first, most common, type of melt inclusion comprises small portions of melt trapped during rapid skeletal growth of the olivine crystal, probably during cooling on the surface. These resemble those described in Fig.1A of Roedder's paper. The inclusions of this type in the Wells Gray lavas are, without exception, devitrified and are rarely sealed. Inclusions of this size do not exceed 150 μm in diameter; the total volatile content of an inclusion, therefore, is too small for the analytical range of the apparatus used.

The second type of inclusion is also described by Roedder, as Type E. Inclusions of this type, if larger than 200 μm in diameter, are within the analytical range of the apparatus and, like the first type, occur mainly in crystals of olivine, or, very rarely, clinopyroxene. Such inclusions are ellipsoidal to lobate in shape and range in size from 10 to 300 µm in diameter. Devitrification on quenching is almost ubiquitous and is accompanied by the formation of bubbles in the devitrified melt inclusions (Plate 12F), indicating that the melt was supersaturated with CO_2 and/or H_2O at the time of phenocryst formation. In many cases, the volatile phase has formed a neck in the melt inclusion (Plate 12F).

The bubbles are interpreted as originating as microvesicles in the ascending magma which acted as nucleation sites for phenocryst growth, such that a phenocryst grew around the vesicle. Such a process indicates that volatile contents measured in residual glass from any of the devitrified inclusions will represent, at best, a minimum estimate of their primary concentrations. Contraction and resultant cracking of phenocrysts has broken the seal on all but 5% of the inclusions. This is probably a result of decompression, differential cooling in the melt and expansion of the gas bubble in the melt inclusion.

Small (less than 0.01 mm in size) inclusions of fluid occur in olivine grains other than those associated with spinel lherzolite. Spinel lherzolite xenoliths are devoid of such inclusions. The inclusions are transparent and are almost certainly inclusions of fluid rich in CO_2.

Pristine glass inclusions occur only at Hyalo Ridge and at Pyramid Mountain. Glass inclusions in the distal portion of the Dragon's Tongue formed, as did the phenocrysts, after the eruption. In each case the crystals are in water or ice contact features at the margin of flows. The holohyaline melt inclusions do not exceed 150 µm in diameter. This size of inclusion does not exceed the lower detection limit of the vacuum fusion apparatus.

To conclude, those melt inclusions of size sufficient for analysis are devitrified and vesicular. Those at chill contacts are too small for the volatile concentrations to be measurable by the apparatus. Studies of the volatile concentrations in the lavas must, therefore, be restricted to those glassy samples formed by ice contact.

Sample preparation

Samples from each of the centres were hand-picked to select fragments of glass free from phenocrysts, weathered surfaces and unburst vesicles. The samples were mounted on glass slides, polished to optical flatness then turned over and the other side similarly polished to produce a wafer of glass 0.05 to 0.1 mm thick (thickness is not crucial). The samples were analysed by electron microprobe, using the standards listed in Table A-1 and using the techniques described in Chapter 3. Analytical results are presented in Table 5, together with analytical errors.

Apparatus

The analytical technique used to measure the concentrations of H_2O and CO_2 in small samples of glass is a modification of that used by Harris (1981b), using an apparatus constructed by J.T. Dunn. A detailed description of the apparatus and its use are given in Appendix E. The apparatus is designed to make use of the Ideal Gas Law which describes the behaviour of gases at low pressures thus:

$$PV=nRT$$

where P=pressure=ΣPartial pressures of component gases; V=volume; R=Universal Gas Constant; T=absolute temperature.

A diagram of the apparatus is shown in Fig.50. Briefly, the apparatus is made of pyrex and comprises a Kanthal wire furnace and temperature controller, a sample volume, a McLeod gauge, and a pumping system, the latter comprising a mercury diffusion pump augmented by a standard roughing pump.

The sample volume comprises a detachable sample tube, made from fused quartz, the end surrounded by the furnace during fusion. The remainder of the sample volume is made of pyrex, as is the rest of the apparatus. At the other end of the sample volume is a capacitance manometer for direct measurement of small variances in pressure. Half way down the sample volume, a U-bend permits freezing of CO_2 and H_2O by immersion in liquid nitrogen.

A valve (V1) isolates the capacitance manometer and U-bend from the sample tube. This isolated volume is referred to as the measuring volume. A second valve (V2), between the fused quartz tube and V1, connects the sample volume to the vacuum

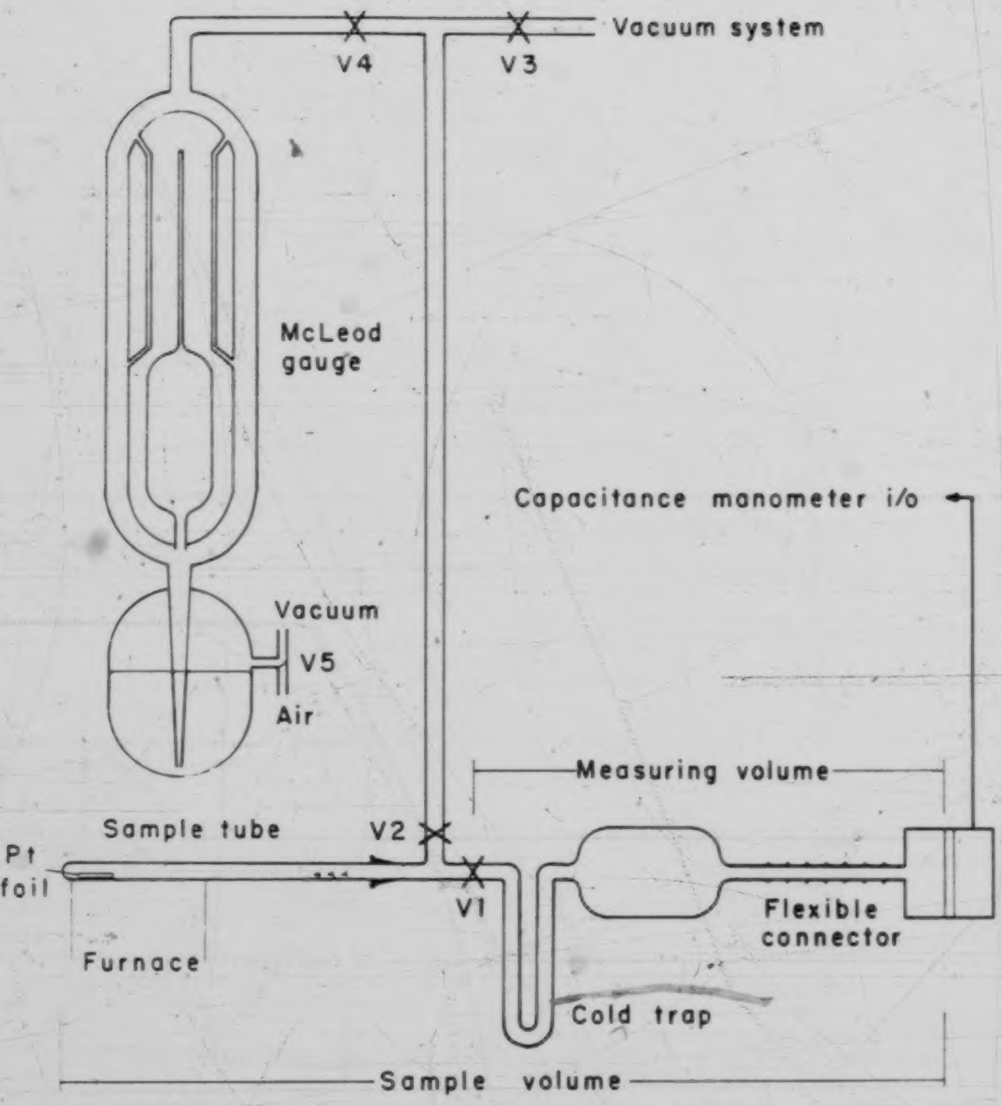
Vacuum system
V4
V3
McLeod gauge
Capacitance manometer i/o
Vacuum
V5
Air
Measuring volume
Sample tube
V2
Pt foil
V1
Flexible connector
Furnace
Cold trap
Sample volume

Fig. 50. Vacuum fusion apparatus used in volatile analysis. V1 to V5 are valves. The apparatus comprises a mercury diffusion pump, augmented by a roughing pump (described collectively on the diagram as 'vacuum system'); a McLeod gauge and the sample volume, isolated by V2. The cold trap is cooled by liquid nitrogen. The furnace is of Kanthal wire, linked to a temperature regulator. The transducer is connected to a CV23 power supply and digital readout. Transducer response can also be measured with a digital voltmeter. All glass parts are of pyrex, except for the sample tube, which is made of fused quartz.

system and the McLeod gauge. Details of sample cleaning and preparation are given in Appendix E. Samples are fused on platinum foil in the sample tube; the platinum foil is prepared by firing at 1200°C *in vacuo* in the apparatus with V2 open. V2 is then closed with the furnace still heating the foil in the tube and the furnace is then removed to allow the foil to cool in the isolated tube.

A sample pressure-time graph from an analytical run is presented in Fig.51. Blank runs are made before each analytical measurement, replicating run conditions in every detail except for fusion of the sample. The width of the tube permits as many as 6 samples to be analysed in one load, provided they are not confused in the tube.

Analytical precision and error

Analytical results are presented in Table 5, together with major oxide concentrations. Each analysis, of either major element or volatile concentrations is a mean of at least three analyses. Errors are based on replicate analyses, both for the probe data and for the vacuum fusion data and are given at the 2σ confidence level. Blank pressures measured during each run, for both H_2O and CO_2, were approximately 10 to 16% of pressures for that phase; in-run precision is therefore no more precise than two significant figures.

Only one widely-analysed standard was available for volatile analysis; this is the Juan de Fuca Ridge glass TT-152-21, analysed by Fine and Stolper (1985). No inter-laboratory standards of alkali basalt exist, at the time of writing. A mean of 0.27±0.018 weight percent H_2O and a mean of 0.043±0.02 weight percent CO_2 were obtained for this standard, compared with values of 0.37% H_2O and 0.024% CO_2 cited by Fine and Stolper (1985). The significantly lower water value is due to adsorption on to the walls of the measuring volume (Harris 1981b), and the high CO_2 value to adsorption on to the Pt foil and, to a lesser extent, on the samples immediately prior to the run. The absolute CO_2 contributions of the adsorption decrease in relative importance with increased sample size and CO_2 concentration; the rate of H_2O adsorption onto the walls of the measuring volume is a function of the partial pressure of that species in the volume and will remain significant until the sample volume is saturated.

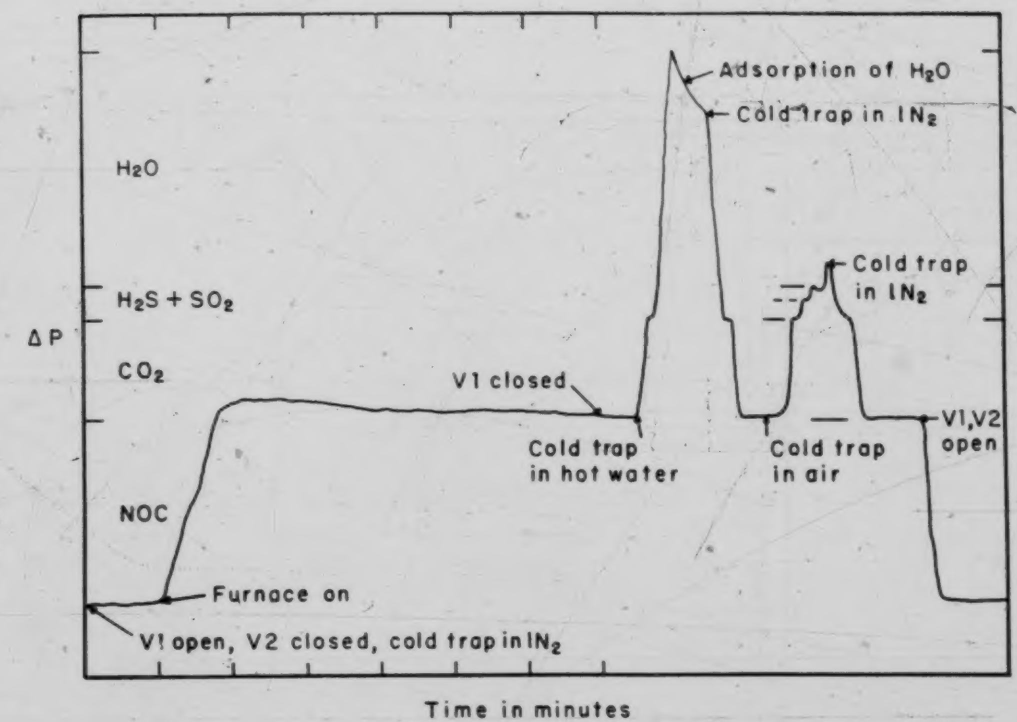

Fig. 51. Schematic time-pressure diagram of a vacuum fusion analysis. Samples are fused for 6 minutes at 1100°C, prior to isolation of the measuring volume. The total pressure of volatile species is measured first, the gas frozen back into the cold trap, and the latter warmed slowly in air. Sublimation "shelves" identify complete outgassing of a volatile species, in the order CO_2, H_2S, SO_2, H_2O. Repeat determinations of CO_2 and SO_2 are possible, due to their lack of adsorption onto the walls of the measuring volume. The total pressure of noncondensible gases is measured at the end of a run.

Table 5

Major oxide, H_2O and CO_2 concentrations in volcanic glasses.

Element	TT-152-21	23/8/2-ST	26/8/2-SM	13/8/10-PY
SiO_2	n.a.	52.2±0.11	48.28±0.04	47.54±0.01
TiO_2	n.a.	2.22±0.03	2.69±0.03	3.07±0.01
Al_2O_3	n.a.	14.73±0.09	16.37±0.04	16.32±0.03
FeO	n.a.	10.63±0.04	11.15±0.05	12.45±0.02
MnO	n.a.	0.11±0.02	0.13±0.01	0.13±0.01
MgO	n.a.	5.73±0.08	3.64±0.04	3.83±0.02
CaO	n.a.	9.29±0.01	7.07±0.04	7.73±0.02
Na_2O	n.a.	3.51±0.03	5.33±0.02	5.13±0.08
K_2O	n.a.	1.27±0.03	2.64±0.01	2.48±0.02
P_2O_5	n.a.	0.33±0.03	1.06±0.02	0.99±0.02
CO_2	0.043 ±0.02	0.012 ±0.006	0.09 ±0.02	0.10 ±0.01
H_2O	0.27 ±0.018	0.044 ±0.006	0.41 ±0.03	0.37 ±0.03

Element	17/8/1-RM	17/8/2-RM	17/8/3-RM
SiO_2	48.64±0.06	45.4±0.11	46.27±0.03
TiO_2	3.23±0.02	4.04±0.03	4.10±0.02
Al_2O_3	14.66±0.02	16.33±0.03	16.65±0.02
FeO	12.4±0.14	13.23±0.04	13.5±0.14
MnO	0.18±0.01	0.16±0.02	0.17±0.01
MgO	4.18±0.05	4.86±0.01	4.93±0.06
CaO	8.21±0.07	9.66±0.03	9.92±0.08
Na_2O	4.07±0.03	2.3±0.21	1.36±0.03
K_2O	2.54±0.08	2.06±0.01	1.76±0.02
P_2O_5	0.81±0.02	0.48±0.02	0.51±0.04
CO_2	0.102 ±0.007	0.037 ±0.006	0.031 ±0.004
H_2O	0.41 ±0.04	0.087 ±0.002	0.06 ±0.03

Volatile and major oxide concentrations are averages of at least three analyses per sample. Major oxides were analysed using the electron microprobe. H_2O and CO_2 were analysed by vacuum fusion. The East Pacific Rise glass TT-152-21 is included for comparison. Analytical precisions are given at the 1σ confidence level.

B. Analytical results

The analytical results shown in Table 5 fall into two groups. The first comprises the alkali basalts of Type 2, which form the Spanish Mump, Pyramid Mountain and upper Ray Mountain edifices. All these glasses have H_2O concentrations of at least 0.35 wt.% and CO_2 concentrations between 0.09 and 0.105 wt%; all samples lie within analytical error of others. The only exceptions to this are samples from higher in the section on Ray Mountain; devolatilisation of the glasses in these samples has resulted in low, erratic measurements. The sample from the bottom of the section, however, has volatile concentrations comparable with other glasses from Type 2.

The glass shards taken from the flanks of Hyalo Ridge have lower concentrations of both volatile species. The glass is non-vesicular and H_2O concentrations are as little as 0.044 wt.%, comparable to the East Pacific Rise glass TT-152-21 (0.27 wt.%) used as a comparative standard. CO_2 is barely detectable, an average value being 0.012±0.006 wt.%, the gas evolved, even from 500 μgm samples, being near the detection limit of the apparatus.

For each of the pristine samples in the Wells Gray lavas, the ratio of H_2O to CO_2 is approximately 4, regardless of enrichment in incompatible elements (Fig.52). The ratio is probably significant, given the widely disparate geomorphologic settings and quenching conditions of each of the hyaloclastites. The ratio is interpreted to represent the relative solubilities of the two components in the magmas under near-surface conditions.

Mysen (1977), in a summary of solubility data for H_2O and CO_2 solubilities in silicate melts, concluded that, while the solubility of H_2O in magmas is mainly dependent upon pressure, the solubility of CO_2 is dependent upon pressure, temperature and the composition of the magma, simplified as the ratio of non-bridging oxygen anions to tetrahedrallycoordinated (network-forming) cations (NBO/T). Although the latter value is fairly constant for the Wells Gray lavas, in the range 1.1 to 1.2, the composition of the coexisting volatile phase forming the vesicles is not known. In addition, the relatively high concentrations of Cl and P_2O_5 in the lavas precludes the treatment of the volatile solubilities in a simple H_2O - CO_2 system.

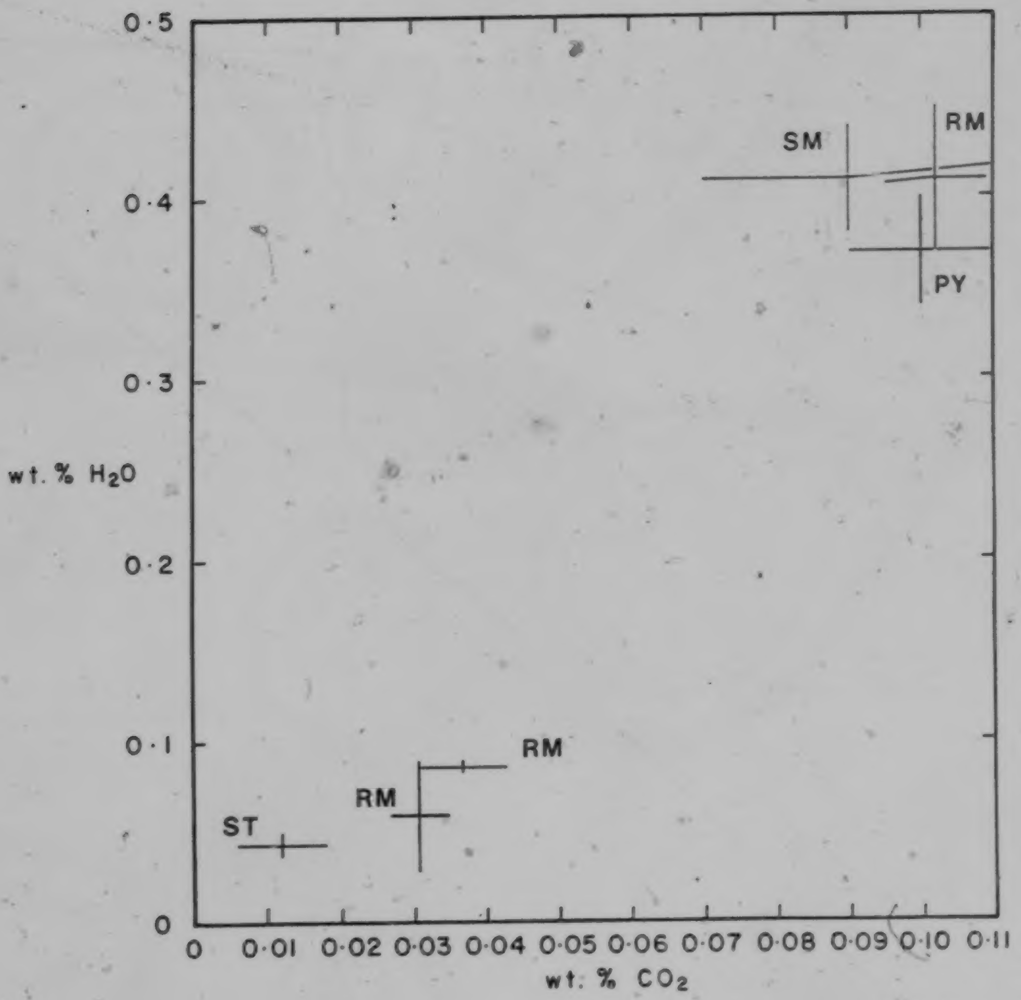

Fig. 52. CO_2 against H_2O for volcanic glasses. Suffixes used for each centre are listed in Table 1. Errors for P_2O_5 are given at the 1σ confidence level based on the maximum observed concentration. Errors for H_2O are given at the 1σ confidence level based on replicate determinations taken from several glass fragments.

The ratio of K_2O to H_2O in melt inclusions in Kilauean basalts was used by Harris and Anderson (1983) to determine the source phase for the water dissolved in the primary magmas. No such linear relationship exists for the Wells Gray lavas. This suggests that water may be stored in more than one phase in the various source regions beneath Wells Gray Park, an interpretation consistent with the hypothesis of mantle metasomatism, detailed in Chapter 5.

On a graph of H_2O against P_2O_5 for the Wells Gray lavas (Fig.53), neither group is sufficiently variable as to plot in a range which can be extrapolated to the origin with any confidence. A line constructed through both groups does not pass near the origin, suggesting either that the two groups did not have a common phosphate source phase, or that the source phase, or phases, was characterised by Cl^- or F^- as well as by hydroxyl groups. Concentrations of Cl in the lavas, determined by X.R.F., are as high as 0.03 weight percent, enough to move any linear correlation in Fig.53 closer to the origin.

C. Summary

Alkalic lavas from Wells Gray Park are typically enriched in the volatile species H_2O and CO_2 relative to the transitional lavas of Hyalo Ridge. Vesiculation has taken place during ascent, such that the vesicles have acted as nucleation sites for phenocrysts. Melt inclusions are commonly unsealed, devitrified and have exsolved a volatile phase. Glasses analysed do not show a linear trend of K_2O with H_2O but all have H_2O/CO_2 ratios near 4 and show a poor linear or curvilinear correlation with P_2O_5. This may be indicative of the composition of the fluid in equilibrium with the magmas at or near their source.

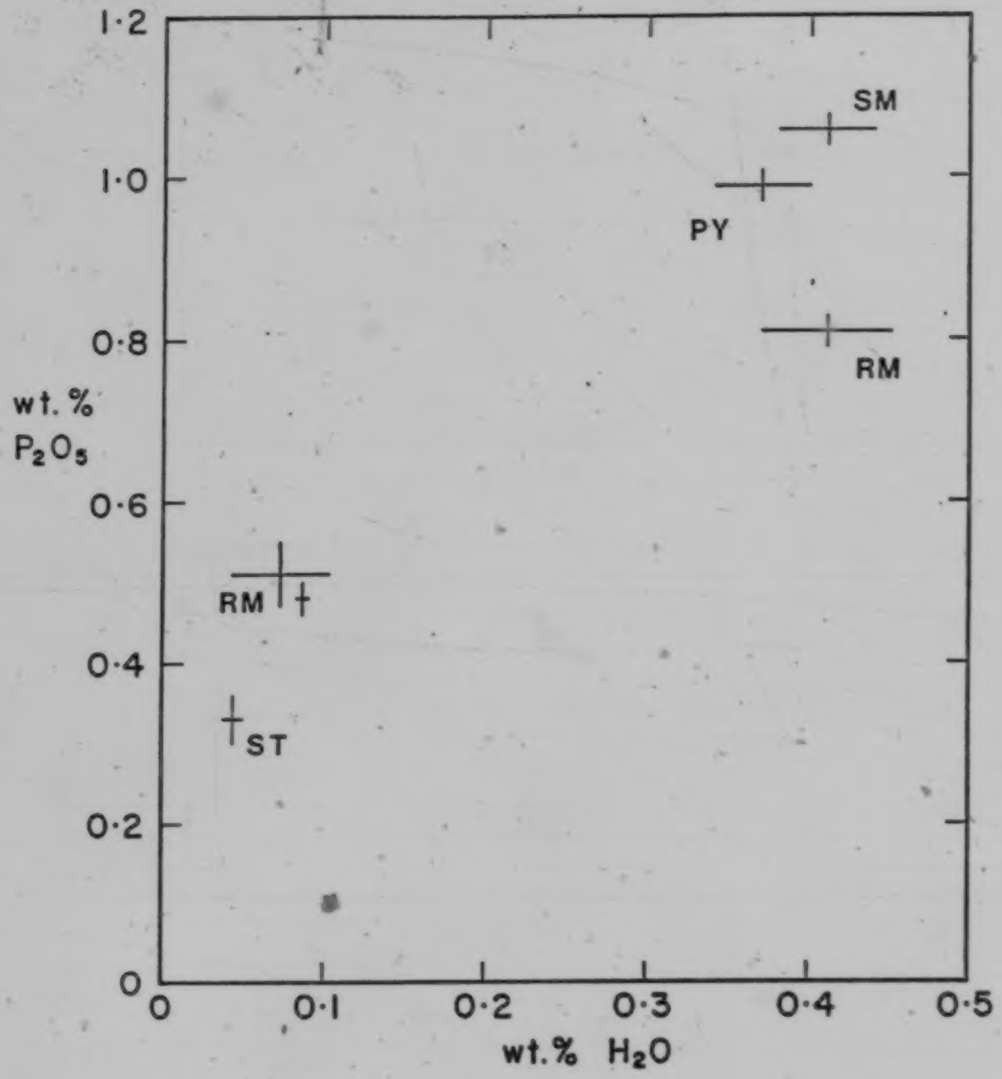

Fig. 53. H_2O against P_2O_5 for volcanic glasses. Suffixes used for each centre are listed in Table 1. Errors for P_2O_5 are given at the 1σ confidence level based on the maximum observed concentration. Errors for H_2O are given at the 1σ confidence level based on replicate determinations taken from several glass fragments.

8.

CONCLUSION

A. Results

The eleven volcanoes studied in the Wells Gray Park area were active over a period from 300 ka B.P. to the present day. One centre (Hyalo Ridge) is a tuya, two are sub-glacial mounds or SUGMs (Hickson 1987), two are glaciated cinder cones and one is a dissected fissure-type volcano. Four are post-glacial, complex cinder cones with two or more stages of activity. The eruptive phases in polygenetic centres are separated by tens or hundreds of years, with the exception of the two phases in the Ray Mountain centre which were separated by at least one glacial advance.

The lavas lie in two compositional fields; those from Hyalo Ridge are transitional tholeiitic basalts and represent the greater part of the lavas erupted in the park. The remainder lie in the compositional fields of alkali basalt, basanitoid and hawaiite. A further division of the alkaline lavas, on the basis of incompatible element concentrations, is possible, into a Ba-enriched Type 1 and a Zr-enriched Type 2.

The lavas from Hyalo Ridge are olivine ± plagioclase phyric and avesicular. The rest of the lavas are olivine ± clinopyroxene phyric, olivine ± clinopyroxene xenophyric and highly vesicular. Xenoliths of Cr-spinel lherzolite and Al-spinel clinopyroxenite are also abundant in the alkalic lavas.

Analyses of the two main phenocryst phases (olivine and clinopyroxene) indicate that each has three main compositional types. For olivine the compositional ranges are Fo_{90} to Fo_{91}, Fo_{84} to Fo_{72} and Fo_{74} to Fo_{60}. The first is a refractory composition, from a Cr-spinel lherzolite. The remaining types are found as phenocrysts, in the Type 1 and Type 2 lavas and as xenocrysts in the Type 2 and Type 1 lavas, respectively.

The three main types of clinopyroxene xenocryst are a mantle-derived chrome diopside, an aluminous augite and a ferroan augite. Phyric, titaniferous chrome-rich augite occurs as a phenocryst phase. The chrome diopside is part of the spinel lherzolite assemblage and the aluminous augite is part of the Al-spinel clinopyroxenite assemblage.

Primary volatile-bearing phases occur in ultramafic xenoliths in three of the recent centres. At Kostal Lake, phlogopite occurs as crystallographically controlled inclusions. Blebs of the mineral, 0.1 mm in size, occur in trains on the 001 face of clinopyroxene in wehrlite xenoliths. The trains run parallel to the b-axis of clinopyroxene and are interpreted as volatile-rich inclusions in the clinopyroxene.

At Dragonhead, a primary amphibole occurs in an aluminous spinel-bearing clinopyroxenite. The mineral occurs with clinopyroxene, showing at least one weakly sutured grain boundary . The kaersutite, at sealed grain boundaries, is in apparent equilibrium with the aluminous augite. At lower pressure, during ascent, sodic plagioclase has formed as a low-pressure reaction rim around the amphibole and spinel, The assemblage is interpreted as a possible source composition for the host lavas and resembles amphibole reported by Arai (1986) and by Best (1974).

At the Flourmill centre, primary inclusions of apatite, 20 μm in diameter, were discovered in a clinopyroxene grain comprising part of a websterite. The websterite fragment is 3 mm in size and is interpreted as part of a mantle assemblage enriched in Fe; xenoliths of similar composition were found at Ray Ridge. The apatite is chloriferous and represents the first description of an occurrence of this mineral in Canada as a primary constituent of an upper mantle assemblage.

The major element chemistry of each lava suite indicates that no significant fractionation has taken place within the suite. Major element concentrations for the majority of the lavas give Mg numbers which are near-primary (Frey *et al.* 1978). Each volcano is characterised by discrete values for Mg and ΣFe which suggest that each volcano tapped a different source region in the upper mantle. The homogeneity within each centre does not, however, preclude the possibility of fractionation at depth prior to final ascent. Fractionation trends are absent save in the Flourmill centre, where an accumulation trend of olivine causes MgO enrichment in the older lavas.

All lavas from the study area are enriched in incompatible elements, particularly the alkaline earth elements, relative to lavas in the Anahim Belt (c.f. Bevier 1978, 1983a). The incompatible elements, particularly the trace elements, show extensive variation, particularly in lavas from Kostal Lake and the Dragon's Tongue. At least 30% fractionation is required to account for such a range in concentrations; this is incompatible with the range in major element concentrations which permit a maximum of 10% fractionated material. It is more probable, therefore, that the range in trace elements is due to multiple phases of partial melting in the same source region, the first melting event depleting the source in incompatible elements.

Two types of magma are defined by ratios of trace incompatible elements. The first, designated Type 1, is represented by lavas from the Dragon's Tongue, Flourmill and Spanish Lake. These lavas are characteristically enriched in Ba. Type 2 (Kostal Lake) are enriched in Zr. The two magma types also differ in their $^{87}Sr/^{86}Sr$ and $^{143}Nd/^{144}Nd$ isotopic ratios, as summarised below.

A strong positive correlation exists between maximum Cl concentrations and Nb. The close correlation between these elements suggests that incompatible element enrichment occurred as a result of metasomatism in the source regions of the magmas. Niobium is usually partitioned into oxide and ferromagnesian minerals. Their strong covariance indicates, therefore, that little or no crystal fractionation involving ferromagnesian minerals has taken place since the enrichment event, throughout the subsequent generation and ascent of the Wells Gray magmas.

Strong enrichment of sulphur in the Wells Gray lavas precludes the use of Ni as an indicator of the primary nature of the magma. Small inclusions of sulphide, of varying Ni content, in clinopyroxene grains render the use of Sato's (1977) method of determination impractical.

Lavas from Wells Gray Park are typically enriched in the volatile species H_2O and CO_2, such that both commence exsolution from the magmas prior to eruption; the vesicles produced act as nucleation sites for crystals. Melt inclusions sufficiently large for analysis are commonly unsealed and devitrified and are not amenable to analysis. Glasses analysed do not show a linear trend of K_2O with H_2O but all have H_2O/CO_2 ratios near 4.

Twenty samples analysed for $^{87}Sr/^{86}Sr$ and $^{143}Nd/^{144}Nd$ in the study area lie in two isotopic groups, slightly below the mantle evolution curve. The group designated Type 1 is characterised by $^{87}Sr/^{86}Sr$ values ranging from 0.7036 to 0.7042 and by $^{143}Nd/^{144}Nd$ values ranging from 0.5119 to 0.5120. That designated Type 2 is characterised by ratios of 0.7030 to 0.7033 and 0.5120 to 0.5123, respectively. Both fields fall close to those of the Geronimo Volcanic Field (Menzies *et al.* 1985), Hawaii (Chen and Frey 1985) and the Australian basalts (McDonough *et al.* 1985), all of which are interpreted as the products of isotopic mixing between MORB and more enriched compositions.

For individual centres, such as Kostal Lake, the ^{87}Sr/^{86}Sr value does not vary significantly with the phase of activity. This is probably due to low concentrations of Rb in the source rocks, such that Sr isotopes are not significantly partitioned between phases. The ^{143}Nd/^{144}Nd value, however, displays a consistent increase from earlier to later phases within individual centres; this effect, while most pronounced in the Kostal Lake lavas, is observed in all the post-glacial centres.

An inverse correlation between P_2O_5 and ^{143}Nd/^{144}Nd in lavas from both Kostal Lake (Type 2) and from the Dragon's Tongue (Type 1) suggests that a phosphate phase in the source region is controlling the distribution of Sm and Nd and therefore of ^{143}Nd/^{144}Nd. Isotopic disequilibrium is present, either in the source regions of the lava or in the material accumulated after generation. The observed trends are consistent with a source comprising accessory phosphate with low Sm/Nd and (in both types) a ^{143}Nd/^{144}Nd value of approximately 0.51187, typical of "undepleted" mantle, with a refractory phase, probably clinopyroxene, characterised by high Sm/Nd and ^{143}Nd/^{144}Nd values of 0.5122 and 0.5124, for Type 1 and Type 2, respectively. This clear separation in isotopic composition between Type 1 and Type 2 indicates the presence of at least two different source components for the Wells Gray lavas. Isotopic equilibrium for Sr is present within each source region. Studies by Hofmann and Hart (1978) and by Sneeringer *et al*. (1984) indicate that the isotopic heterogeneity in the source region must form less thsn 2 Ma before onset of the volcanism.

In the Flourmill and Spanish Lake centres, departure from the trend of P_2O_5-^{143}Nd/^{144}Nd proportionality is observed, although these centres retain the correlation of their Sm/Nd ratios with P_2O_5 (both centres belong to Type 1). The departure is probably due to the accumulation of clinopyroxene xenocrysts, with low, possibly undepleted mantle, values of ^{143}Nd/^{144}Nd, during ascent. Values for ^{87}Sr/^{86}Sr of 0.7055 (A.D. Smith unpubl. data) indicate that the xenophyric clinopyroxene is the contaminant.

B. Possible sources for magma

The Wells Gray lavas are intraplate basaltic lavas with strongly enriched incompatible and light rare-earth element concentrations. Three models have been proposed for such volcanism in the Anahim Belt. (Bevier *et al.* 1979). The first is control of the volcanism by a deep crustal discontinuity such as a shear zone, running along the 52nd parallel. No geological evidence for such a discontinuity exists. The second involves the leading edge of the subducted Juan de Fuca plate. Frictional melting at this point is assumed to trigger the ascent and eruption of magmas. This model cannot account for the age progression of volcanoes in the Anahim Belt.

The third model, preferred by Bevier *et al.* (1979), is that of a hotspot in the upper mantle, stationary with respect to the asthenospheric mantle, being overridden by the North American plate. The trace of the supposed hotspot is in agreement with the sense and speed of the North American plate, but deviates from this trend at the eastern end of the Belt. The model nevertheless provides an explanation for the anomalies in mantle conductivity and natural seismicity at the eastern end of the Anahim Belt. The disadvantage of the model is that there is seismic evidence that the underthrust Juan de Fuca plate may lie at shallow levels beneath the crust, interposing itself between the locus of hot spot melting and the base of the continental lithosphere. Evidence for the presence of the slab is given by the shallow dip of the plate at the continental margin and by the presence of a high-velocity layer at approximately the depth required for the generation of alkali basalt magma. In addition, the spacing between the eastern end of the volcanic chain and the seismically active area at McNaughton Lake is 100 km; somewhat too great for the lithospheric thickness involved (Vogt 1974a, 1974b).

Possible sources for magma in the region of Wells Gray Park are depicted in Fig.54. The source region for the lavas lies in the spinel peridotite or garnet peridotite stability field. The inferred zone of incipient partial melting extends from almost at the base of the continental crust into the garnet peridotite stability field. Three subduction events have taken place on the western margin of North America; the mantle is therefore almost certainly heterogeneous. The high-velocity layer may be part of the subducted Juan de Fuca plate. The layer is at or near the boundary between spinel and garnet stability fields. The possible sources are therefore four: (1) undepleted or

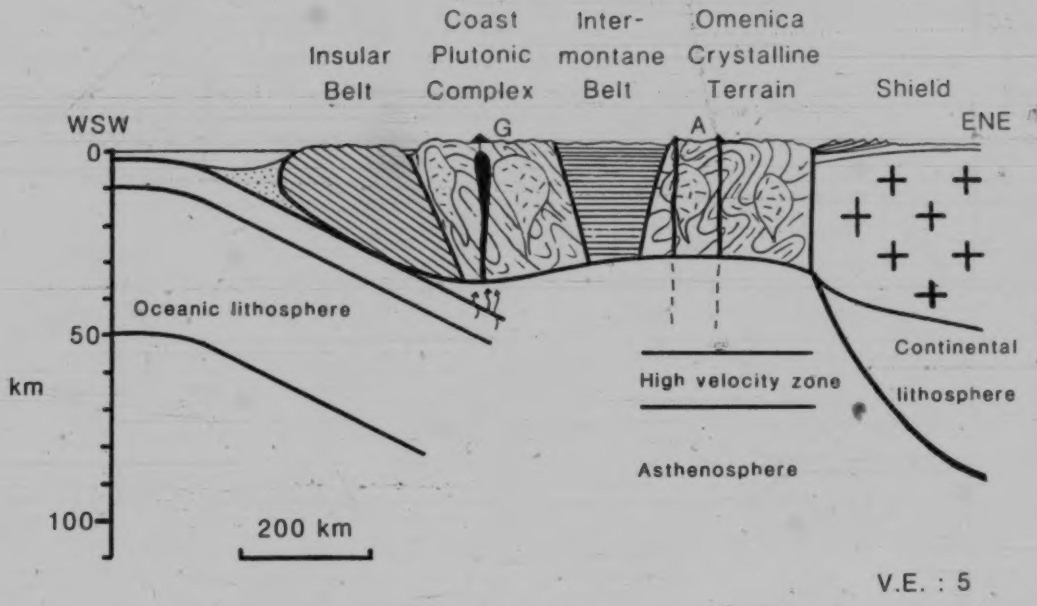
Insular Belt
Coast Plutonic Complex
Inter-montane Belt
Omenica Crystalline Terrain
Shield
WSW
ENE
G
A
0
50
100
km
Oceanic lithosphere
High velocity zone
Asthenosphere
Continental lithosphere
200 km
V.E. : 5

Fig. 54. The subcordilleran mantle of British Columbia. G = Garibaldi Belt, A = Anahim Belt. The diagram shows the anomalous asthenosphere, absence of lithospheric mantle and presence of a high-velocity seismic refractor beneath the Canadian Cordillera. The lithospheric mantle is either partially melted or has been decoupled and removed. The high-velocity layer may be subducted oceanic lithosphere.

MORB-like mantle, each in either the spinel or garnet stability fields.

C. Petrogenesis of the Wells Gray lavas

Fig.55 demonstrates three possible modes of magma formation for the Wells Gray lavas. The first invokes devolatilisation of a slab of oceanic lithosphere to provide fluid for propogation of metasomatic processes and eventually partial melting in the overlying mantle (Fig.55a). This model depends upon whether volatiles persist in the slab for long periods of time following subduction.

Thermal models of subduction zones have been developed by Hasebe *et al.* (1970), Turcotte and Schubert (1973) Andrews and Sleep (1974) and Anderson *et al.* (1976, 1978). Although the considerations of frictional heating, asthenospheric flow and heat transport were treated differently, the consensus of the authors is that endothermic dehydration reactions will absorb much of the heat generated by friction in the downgoing slab and that a low temperature regime may persist in the slab's interior to greater distances in the mantle than previously assumed. Dehydration of chlorite, epidote and (possibly) serpentine in Anderson *et al.*'s (1986) model will maintain sufficiently low temperatures in the slab as to stabilise amphibole to as great a distance as 400-500 km beneath the Cordillera, particularly if frictional heating is low; this last is suggested by aseismic subduction. However, greater knowledge of the chemistry of the fluid or fluids involved in this metasomatism is necessary for better understanding of the element partitioning and speciation during metasomatism and, consequently of isotopic systems in the petrogenesis of alkali basalts.

A second possible model proposes partial melting of the subducted oceanic crust or lithosphere, following heating by friction or simple conduction (Fig.55b). The magmas would have the isotopic character of MORB and would have to be reequilibrated with mantle material closer in isotopic composition to CHUR. This model obviates the necessity for considering isotopic disequilibrium in the source because the phosphate phase controlling the Nd isotopic ratios of the lavas would only be in contact with them for a short period.

The third possible model is a two-stage model for petrogenesis of the [illegible] which allows for the [illegible] enrichment in incompatible and light rare earth elements

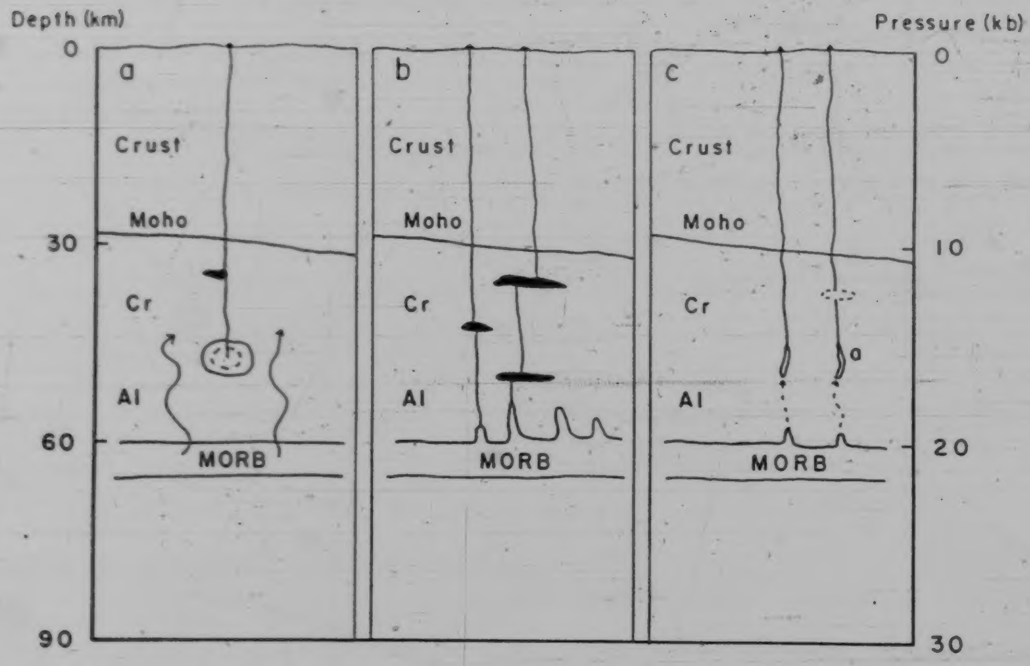

Fig. 55. Possible methods of generation of the Wells Gray lavas: a. Devolatilisation of a MORB reservoir, enriching a lherzolite source rock in incompatible elements. b. Melting of a MORB source rock and isotopic equilibration with a spinel lherzolite mantle in mantle magma chambers c. Two-stage model, with melting of a MORB source rock and crystallisation of the melt as amphibolite veins in a spinel lherzolite mantle. Bulk remelting of the veins (65% partial melting) followed, to produce the lavas and a spinel clinopyroxenite residuum. This last model allows for a garnetiferous source rock to produce an initial light rare-earth enrichment in the [illegible]

Partial melting of a garnetiferous assemblage with a MORB isotopic character could produce a strongly undersaturated melt which would ascend to crystallise as amphibole veins in the overlying mantle. Degassing of the melt upon ascent could metasomatise the host mantle close to the vein, enriching it in incompatible elements. Upon crystallisation, both the host mantle and the amphibole-rich vein would retain their isotopic character for a period not exceeding 2 Ma (Hofmann and Hart 1978, Sneeringer *et al* 1984). The concentrations of radioactive heat-producing elements in the amphibole would suffice to raise the temperature of the vein to melting point in approximately 1 Ma. Upon melting, the amphibole would increase the relative enrichment in Nd with respect to Sm still further and produce a residuum of clinopyroxene and spinel. Host mantle material surrounding the vein and clinopyroxene, residual from the earlier of two melting events, would contaminate the magma generated during the later event. Based upon the evidence of the presence, in the source regions, of apatite and amphibole, and the compositional relationship between amphibole, magma, clinopyroxene and spinel in the Dragon's Tongue, it is therefore proposed that akaline magmas erupted in Wells Gray Provincial Park are the products of such a two-stage process in the subcordilleran mantle.

LIST OF REFERENCES

ANDERSON, R.N., UYEDA, S. and MIYASHIRO, A. 1976. Geophysical and geochemical constraints at converging plate boundaries, part I: dehydration in the downgoing slab. Geophysical Journal of the Royal Astronomical Society **44**, pp.333-357.

------, DELONG, S.F. and SCHWARZ, W.M. 1978. Geophysical and geochemical constraints at converging plate boundaries, part II: a thermal model for subduction with dehydration in the downgoing slab. Journal of Geology **86**, pp.731-739.

ANDREWS, D.J. and SLEEP, N.H. 1974. Numerical modelling of tectonic flow behind island arcs. Geophysical Journal of the Royal Astronomical Society **38**, pp.3513-3536.

ARAI, S. 1986. K/Na variation in phlogopite and amphibole of upper mantle peridotites due to fractionation of the metasomatizing fluids. Journal of Geology **94**, pp.436-444.

BEAUMONT, C. 1979. On the rheological zonation of the lithosphere during flexure. Tectonophysics **59**, pp.347-365.

BERRY, M.J. and FORSYTH, D.A. 1975. Structure of the Canadian Cordillera from seismic refraction and other data. Canadian Journal of Earth Sciences **12**, pp.182-208.

BEST, M.G. 1974. Mantle-derived amphibole within inclusions in alkalic-basaltic lavas. Journal of Geophysical Research **79**, pp.2107-2113.

BESWICK, A.E. and CARMICHAEL, I.S.E. 1978. Constraints on mantle source compositions imposed by phosphorous and the rare-earth elements. Contributions to Mineralogy and Petrology **67**, pp.317-330.

BEVIER, M.L. 1978. Field relations and petrology of the Rainbow Range shield volcano, west-central British Columbia. Ph.D. thesis, University of British Columbia, 100p.

------ 1983a. Implications of chemical and isotopic composition for petrogenesis of Chilcotin Group basalts, British Columbia. Journal of Petrology **24**, pp.207-226.

------ 1983b. Regional stratigraphy and age of Chilcotin Group basalts, south-central British Columbia. Canadian Journal of Earth Sciences **20**, pp.515-524.

------, ARMSTRONG, R.L. and SOUTHER, J.C. 1979. Miocene peralkaline volcanism in west-central British Columbia - its temporal and plate-tectonics setting. Geology **7**, pp.389-392.

BINGHAM, D.K., INGHAM, M.R. and GOUGH, D.I. 1981. Anomalies in electrical conductivity in western Canada. EOS **62**, pp.844-845.

BOETTCHER, A.L. and O'NEIL, J.R. 1980. Stable isotope, chemical and petrographic studies of high-pressure amphiboles and micas: evidence for metasomatism in the mantle source regions of alkali basalts and kimberlites. American Journal of Science **280A**, pp.594-621.

BREARLEY, M. 1986. Ultramafic xenoliths from British Columbia, Canada: petrological and dissolution studies. Ph.D. thesis, University of Alberta, 168p.

------ and SCARFE, C.M. 1984. Amphibole in a spinel lherzolite xenolith: evidence for volatiles and partial melting in the upper mantle beneath southern British Columbia. Canadian Journal of Earth Sciences **21**, pp.1067-1072.

------, ------ and Fujii, T. 1984. The petrology of ultramafic xenoliths from Summit Lake, near Prince George, British Columbia. Contributions to Mineralogy and Petrology **88**, pp.53-63.

BREY, G. 1976. CO_2 solubility and solubility mechanisms in silicate melts at high pressures. Contributions to Mineralogy and Petrology **57**, pp.215-221.

------ and GREEN, D.H. 1975. The role of CO_2 in the genesis of olivine melilitite. Contributions to Mineralogy and Petrology **49**, pp.93-103.

BRYAN, W.B. 1976. Solubility of CO_2 in olivine melilitite at high pressures and role of CO_2 in the earth's upper mantle. Contributions to Mineralogy and Petrology **55**, pp.217-230.

------ 1977. Systematic study of liquidus phase relations in olivine melilitite+H_2O+CO_2 at high pressures and petrogenesis of an olivine melilitite magma. Contributions to Mineralogy and Petrology **61**, pp.141-162.

[illegible]

ferric-ferrous ratios of basalt, ferrobasalt, andesite, and rhyodacite glasses from the Galapagos 95.5°W propogating rift. Geochimica et Cosmochimica Acta **48**, pp.2239-2246.

CAMFIELD, P.A. and GOUGH, D.I. 1975. Anomalies in daily variation magnetic fields and structure under the northwestern United States and southwestern Canada. Geophysical Journal of the Royal Astronomical Society **41**, pp.193-218.

CAMPBELL, R.B. 1963a. Quesnel Lake, east half, British Columbia. Geological Survey of Canada Map 1-1963.

------ 1963b. Adams Lake, British Columbia. Geological Survey of Canada Map 48-1963.

------ 1967. Canoe River, British Columbia. Geological Survey of Canada Map 15-1967.

------ and TIPPER, H.W. 1971. Geology of the Bonaparte Lake map-area, British Columbia. Geological Survey of Canada Memoir 363, 100p.

CANER, B. 1971. Quantitative interpretation of geomagnetic depthsounding data in western Canada. Journal of Geophysical Research **76**, pp.7202-7216.

------, AULD, D.R., DRAGERT, H. and CAMFIELD, P.A. 1971. Geomagnetic depth-sounding and crustal structure in western Canada. Journal of Geophysical Research **76**, pp.7181-7201.

CARLSON, R.W. 1984. Isotopic constraints on Columbia River flood basalt genesis and the nature of the subcontinental mantle. Geochimica et Cosmochimica Acta **48**, pp.2357-2372.

------, LUGMAIR, G.W. and MacDOUGALL, J.D. 1981. Columbia River volcanism: the question of mantle heterogeneity or crustal contamination. Geochimica et Cosmochimica Acta **45**, pp.2483-2499.

CAVELL, P.A. and BAADSGAARD, H. 1986. Geochronology of the Big Spruce Lake alkaline intrusion. Canadian Journal of Earth Sciences **23**, pp.1-10.

CHANDRA, N.N. and CUMMING, G.L. 1972. Seismic refraction studies in western Canada. Canadian Journal of Earth Sciences **9**, pp.1099-1109.

CHAUVEL, C. and JAHN, B.-M. 1984. Nd-Sr isotope and REE geochemistry of alkali basalts from the Massif Central, France. Geochimica et Cosmochimica Acta **48**, pp.93-110.

CHEN, C.-Y. and FREY, F.A. 1983. Origin of Hawaiian tholeiite and alkalic basalt. Nature **302**, pp.785-789.

------ 1985. Trace element and isotopic geochemistry of lavas from Haleakala volcano, E. Maui, Hawaii: implications for the origin of Hawaiian basalts. Journal of Geophysical Research **90**, pp.8743-8768.

CLARK, S.P., Jr. and RINGWOOD, A.E. 1964. Density distribution and constitution of the mantle. Reviews of Geophysics **2**, pp.35-88.

CLOWES, R.M. 1980. Compilation of geophysical/geological data near Golden, B.C.. Earth Physics Branch Open File **80-14**, 41p.

COHEN, R.S. and O'NIONS, R.K. 1982. The lead, neodymium and strontium isotopic structure of ocean ridge basalts. Journal of Petrology **23**, pp.299-324.

CONEY, P.J., JONES, D.L. and MONGER, J.W.H. 1980. Cordilleran suspect terranes. Nature **288**, pp.329-333.

CUMMING, W.B., CLOWES, R.M. and ELLIS, R.M. 1979. Crustal structure from a seismic refraction profile across southern British Columbia. Canadian Journal of Earth Sciences **16**, pp.1024-1040.

DAWSON, J.B. and SMITH, J.V. 1982. Upper mantle amphiboles: a review. Mineralogical magazine **45**, pp.35-46.

DELANEY, J.R. 1977. Distribution of volatiles in the glassy rims of submarine pillow basalts. Ph.D. thesis, University of Arizona (Tuscon), 132p.

------, ANDERSON, D.H. and KARSTEN, J. 1978. Analysis of water in basaltic glasses using an ion microprobe mass analyser. EOS **59**, p.1117.

DETRICK, R.S. and CROUGH, S.T. 1978. Inland subsidence, hotspots and lithospheric thinning. Journal of Geophysical Research **83**, pp.1236-1244.

DOSSO, L. and MURTHY, V.R. 1980. A Nd isotopic study of the Kerguelen islands: inferences on enriched oceanic mantle sources. Earth and Planetary Science Letters **48**, pp.268-276.

DOWNES, H. 1984. Sr and Nd isotope geochemistry of coexisting alkaline magma series, Cantal, Massif Central, France. Earth and Planetary Science Letters **69**, pp.321-334.

[illegible] function analysis of a [illegible] pp.1089-1098.

DRAGERT, H. and CLARKE, G.K.C. 1977. A detailed investigation of the Canadian Cordillera geomagnetic transition anomaly. Journal of Geophysics **42**, pp.373-390.

DETRICK, R.S. and CROUGH, S.T. 1978. Inland subsidence, hotspots and lithospheric thinning. Journal of Geophysical Research **83**, pp.1236-1244.

DOSSO, L. and MURTHY, V.R. 1980. A Nd isotopic study of the Kerguelen islands: inferences on enriched oceanic mantle sources. Earth and Planetary Science Letters **48**, pp.268-276.

DUDA, A. and SCMINKE, H-U. 1985. Polybaric differentiation of alkali basaltic magmas: evidence from green-core clinopyroxenes (Eifel, F.R.G.). Contributions to Mineralogy and Petrology **91**, pp.340-353.

DUNCAN, A.R. and TAYLOR, S.R. 1968. Trace element analyses of magnetites from andesitic and dacitic lavas from the Bay of Plenty, New Zealand. Contributions to Mineralogy and Petrology **20**, pp.30-33.

EGGLER, D.H. 1973. Role of CO_2 in melting processes in the mantle. Carnegie Institute Yearbook **72**, pp.457-467.

------ 1974. Effect of CO_2 on the melting of peridotite. Carnegie Institute Yearbook **73**, pp.215-224.

------ 1975. CO_2 as a volatile component of the mantle: the system Mg_2SiO_4-SiO_2-H_2O-CO_2. Physics and Chemistry of the Earth **9**, pp.869-882.

------ 1976. Does CO_2 cause partial melting in the low-velocity layer of the mantle? Geology **4**, pp.69-72.

------ 1978. The effect of CO_2 upon partial melting of peridotite in the system Na_2O-CaO-Al_2O_3-MgO-SiO_2-CO_2 to 35 kb, with an analysis of melting in a peridotite-H_2O-CO_2 system. American Journal of Science **278**, pp.305-343.

------, KUSHIRO, I. and HOLLOWAY, J.R. 1976. Stability of carbonate minerals in a hydrous mantle. Carnegie Institute Yearbook **73**, pp.631-636.

ELLIS, R.M., SPENCE, G.D., CLOWES, R.M., WALDRON, D.A., JONES, I.F., GREEN, A.G., FORSYTH, D.A., MAIR, J.A., BERRY, M.J., MEREU, R.F., KANASEWICH, E.R., CUMMING, G.L., HAJNAL, Z., HYNDMAN, R.D., MCMECHAN, G.A. and LONGCAREVIC, B.D. 1983. The Vancouver Island seismic project: a CO-CRUST onshore-offshore study of a convergent margin. Canadian Journal of Earth Sciences **20**, pp.719-741.

FABRIES, J. 1979. Spinel-olivine geothermometry in peridotites from ultramafic complexes. Contributions to Mineralogy and Petrology **69**, pp.329-336.

FIESINGER, D.W. 1975. Petrology of the Quaternary volcanic centres in the Quesnel Highlands and Garibaldi Provincial Park areas, British Columbia. Ph.D. thesis, University of Calgary, 132p.

------ and NICHOLLS, J. 1977. Petrography and petrology of Quaternary volcanic rocks, Quesnel Lake region, east-central British Columbia. **In**: Volcanic Regimes in Canada, Geological Association of Canada Special Paper 16, pp.25-38.

FORSYTH, D.A. and BERRY, M.J. 1974. A refraction survey across the Canadian Cordillera at 54°N. Canadian Journal of Earth Sciences **11**, pp.533-548.

FRANCIS, D.M. 1976. The origin of amphibole in lherzolite xenoliths from Nunivak Island, Alaska. Journal of Petrology **17**, pp.357-378.

FREY, F.A. 1984. Rare earth element abundances in upper mantle rocks. **In**: Geochemistry of the REE Elements (ed., P. Henderson), pp. 153-203. Elsevier.

------ and GREEN, D.H. 1974. The mineralogy, geochemistry and origin of lherzolite inclusions in Victorian basanites. Geochimica et Cosmochimica Acta **38**, pp.1023-1059.

------, ------ and ROY, S.D. 1978. Integrated models of basalt petrogenesis: a study of quartz tholeiites to olivine melilitites from south eastern Australia utilising geochemical and experimental petrological data. Journal of Petrology **19**, pp. 463-513.

------, RODEN, M.F. and ZINDLER, A. 1980. Constraints on mantle source compositions imposed by phosphorous and the rare earth elements. Contributions to Mineralogy and Petrology **75**, pp.165-173.

FUJII, T. and SCARFE, C.M. 1982. Petrology of ultramafic nodules from West Kettle River, near Kelowna, southern British Columbia. Contributions to Mineralogy and Petrology **80**, pp.297-306.

GILBERT, M.C., HELT, R.T., POPP, R.K. and SPEAR, F.S. 1982. Experimental studies of amphibole stability. **In**: Veblen, D.R. and Ribbe, P.H., eds. Amphiboles: Petrology and experimental phase relations, Mineralogical Society of America Reviews of Mineralogy **9B**, pp.229-353.

GOUGH, D.I. 1986. Mantle upflow tectonics in the Canadian Cordillera. Journal of Geophysical Research **91**, pp.1909-1920.

------, BINGHAM, D.K., INGHAM, M.R. and ALABI, A.O. 1982. Conductive structures in southwestern Canada: a regional magnetometer array study. Canadian Journal of Earth Sciences **19**, pp.1680-1690.

GREEN, D.H. 1973a. Conditions of melting of basanite magma from garnet peridotite. Earth and Planetary Science Letters **17**, pp.456-465.

------ 1973b. Experimental melting studies on a model upper mantle composition at high pressure under water-saturated and water-undersaturated conditions. Earth and Planetary Science Letters **19**, pp.37-53.

------ and RINGWOOD, A.E. 1967. The generation of basaltic magmas. **in**: "The genesis of basaltic magma" Contributions to Mineralogy and Petrology **15**, pp.159-167.

HAGGERTY, S.E. 1976. Opaque mineral oxides in terrestrial igneous rocks. **in:** Rumble, D., ed. Oxide minerals, Mineralogical Society of America Reviews of Mineralogy **3**, pp.101-300.

HALES, A.L. and NATION, J.B. 1973. A seismic refraction survey in the northern Rocky Mountains: more evidence for an intermediate crustal layer. Geophysical Journal of the Royal Astronomical Society **35**, pp.381-399.

HAMILTON, T.S. 1981. Late Cenozoic volcanics of the Level Mountain range, northwestern British Columbia: geology, petrology and palaeomagnetism. Ph.D. thesis, University of Alberta, 490p.

------ and SCARFE, C.M. 1977. Preliminary report on the petrology of the Level Mountain volcanic centre, northwest British Columbia. Geological Survey of Canada Paper 77-1A, pp.429-433.

HARRIS, D.M. 1981a. The concentrations of H_2O, CO_2, S and Cl during pre-eruption crystallization of some mantle-derived magmas. implications for magma genesis and eruption mechanisms. Ph.D. thesis, University of Chicago, 217p.

------ 1981b. Microdetermination of H_2O, CO_2 and SO_2 in glass using a 1280°C microscope vacuum heating stage, cryopumping and vapour pressure measurements from 77K to 273K. Geochimica et Cosmichimica Acta **45**, pp.2023-2036.

------ and ANDERSON, A.T. 1983. Concentrations, sources and losses of H_2O, CO_2 and S in Kilauean basalt. Geochimica et Cosmichimica Acta, **47**, pp.1139-1150.

HART, W.K. 1985. Chemical and isotopic evidence for mixing between depleted and enriched mantle, northwestern USA. Geochimica et Cosmochimica Acta **49**, pp.131-144.

HARVEY, P.K. and ATKIN, B.P. 1982. Automated X-ray fluorescence analysis. Institute of Mining and Metallurgy special volume: Sampling and analysis for the minerals industry **17-26**.

HASEBE, K., FUJI, N. and UYEDA, S. 1970. Thermal processes under island arcs. Tectonophysics **10**, pp.335-355.

HAWTHORNE, F.C. 1981. Crystal chemistry of the amphiboles. **In:** Veblen, D.R., ed. Amphiboles and other hydrous pyriboles - mineralogy, Mineralogical Society of America Reviews of Mineralogy **9A**, pp.1-102.

HENDERSON, P. 1982 Inorganic geochemistry. Pergamon Press, 353p.

------ 1984 (ed.). Rare-earth element geochemistry. Elsevier, 510p.

HICKSON, C.J. 1987. Quaternary volcanism in the Wells Gray-Clearwater area, east-central British Columbia. Ph.D. thesis, University of British Columbia, 364p.

------ and SOUTHER, J.G. 1984. Late Cenozoic volcanic rocks of the Clearwater - Wells Gray area, British Columbia. Canadian Journal of Earth Sciences **21**, pp.267-277.

HOFMANN, A.W. and HART, S.R. 1978. An assessment of local and regional isotopic equilibrium in the mantle. Earth and Planetary Science Letters **38**, pp.44-62.

------ and WHITE, W.M. 1982. Mantle plumes from ancient oceanic crust. Earth and Planetary Science Letters **57**, pp.421-436.

HYNDMAN, R.D. 1976. Heat flow measurements in the inlets of southwestern British Columbia. Journal of Geophysical Research **81**, pp.337-349.

------, LEWIS, T.J., WRIGHT, J.A., BURGESS, M. CHAPMAN, D.S. and YAMANO, M. 1982. Queen Charlotte fault zone: heat flow measurements. Canadian Journal of Earth Sciences **19**, pp.1657-1669.

IRVINE, T.N. and BARAGAR, W.R.A. 1971. A guide to the chemical classification of the common volcanic rocks. Canadian Journal of Earth Sciences **8**, pp.523-548.

JENKINS, D.M. 1983. Experimental phase relations of hydrous peridotites modelled in the system H_2O-CaO-MgO-Al_2O_3-SiO_2. Contributions to Mineralogy and Petrology **77**, pp.166-176.

KEEN, C.E. and HYNDMAN, R.D. 1979. Geophysical review of the continental margins of eastern and western Canada. Canadian Journal of Earth Sciences **16**, pp.712-747.

KUSHIRO, I. 1970. Stability of amphibole and phlogopite in the upper mantle. Carnegie Institute of Washington Yearbook **68**, pp.245-247.

------ 1971. Effect of water on the composition of magmas formed at high pressures. Journal of Petrology **13**, pp.311-334.

------, SATAKE, H. and AKIMOTO, S. 1975. Carbonate-silicate reactions at high pressures and possible presence of dolomite and magnesite in the upper mantle. Earth and Planetary Science Letters **28**, pp.116-120.

LINDSLEY, D.H. Pyroxene thermometry. American Mineralogist **68**, pp.477-493.

LLOYD, F.E. and BAILEY, D.K. 1975. Light element metasomatism of the continental mantle: the evidence and the consequences. Physics and Chemistry of the Earth **9**, pp.389-416.

MATHEWS, W.H., 1947. "Tuyas," flat-topped volcanoes in northern British Columbia. American Journal of Science **245**, pp.560-570.

McDONOUGH, W.F., McCULLOCH, M.T. and SUN, S.-S. 1985. Isotopic and geochemical systematics in Tertiary-Recent basalts from southeastern Australia and implications for the evolution of the sub-continental lithosphere. Geochimica et Cosmochimica Acta **49**, pp.2051-2068.

McKENZIE, D. 1985. The extraction of magma from the crust and mantle. Earth and Planetary Science Letters **74**, pp.81-91.

MENZIES, M. 1983. Mantle ultramafic xenoliths in alkaline magmas: evidence for mantle heterogeneity modified by magmatic activity. **In**: Continental Basalts and Mantle Xenoliths (eds. C.J. Hawkesworth and, M.J. Norry), pp.111-138.

------ and MURTHY, V.R. 1980a. Nd and Sr isotope geochemistry of hydrous mantle nodules and their host alkali baalts: implications for local heterogeneities in metasomatically veined mantle. Earth and Planetary Science Letters **46**, pp.323-334.

------ and ------ 1980b. Mantle metasomatisation as a precursor to the genesis of alkaline magmas- isotopic evidence. American Journal of Science **280-A**, pp.622-638.

------, KEMPTON, P. and DUNGAN, M. 1985. Interaction of continental lithosphere and asthenospheric melts below the Geronimo volcanic field, Arizona, USA. Journal of Petrology **26**, pp.663-693.

MERCIER, J-C.C. and NICOLAS, A. 1975. Textures and fabrics of upper mantle peridotites as illustrated by xenoliths from basalts. Journal of Petrology **16**, pp.454-487.

MEREU, R.F., MAJUMDAR, S.C. and WHITE, R.E. 1977. The structure of the crust and upper mantle under the highest ranges of the Canadian Rockies from a seismic refraction survey. Canadian Journal of Earth Sciences **14**, pp.196-208.

MILNE, W.G., ROGERS, G.C., RIDDIHOUGH, R.P., MCMECHAN, G.A. and HYNDMAN, R.D. 1978. Seismicity of western Canada. Canadian Journal of Earth Sciences **15**, pp.1170-1193.

MONGER, J.W.H. 1977. Upper Palaeozoic rocks of the western Canadian Cordillera and their bearing on Cordilleran evolution. Canadian Journal of Earth Sciences **14**, pp.1832-1859.

------, SOUTHER, J.C. and GALBRIESE, H. 1972. Evolution of the Canadian Cordillera: a plate-tectonic model. American Journal of Science **272**, pp.577-602.

------ and PRICE, R.A. 1979. Geodynamic evolution of the Canadian Cordillera - progress and problems. Canadian Journal of Earth Sciences **16**, pp.770-791.

------, PRICE, R.A. and TEMPELMAN-KLUIT, D.J. 1982. Tectonic accretion and the origin of the two major metamorphic and plutonic welts in the Canadian Cordillera. Geology **10**, pp.70-75.

MYSEN, B.O. 1976. The role of volatiles in silicate melts: solubility of carbon dioxide and water in feldspar, pyroxene and feldspathoid melts to 30 kb and 1625°C. American Journal of Science **276**, pp.969-996.

------ 1977. The solubility of H_2O_2 and CO_2 under predicted magma genesis conditions and some petrological and geophysical implications. Reviews of Geophysics and

Space Physics **15**, pp.351-361.

------ 1979. Trace-element partitioning between garnet peridotite minerals and water-rich vapour: experimental data from 5 to 30 kb. American Mineralogist **64**, pp.274-287.

------ 1986. Structure and petrologically important properties of silicate melts relevant to natural magmatic liquids. **In:** Scarfe, C.M. (ed.) M.A.C. short course in silicate melts, Ottawa.

------, ARCULUS, R.J. and EGGLER, D. 1975. Solubility of carbon dioxide in melts of andesite, tholeiite and olivine nephelinite composition to 30 kb pressure. Contributions to Mineralogy and Petrology **53**, pp.227-239.

------ and BOETTCHER A.L. 1975a. Melting of a hydrous mantle: I. Phase relations of natural peridotite at high pressures and temperatures with controlled activities of water, carbon dioxide and hydrogen. Journal of Petrology **16**, pp.520-548.

------ 1975b. Melting of a hydrous mantle: II. Geochemistry of crystals and liquids formed by anatexis of mantle peridotite at high pressures and high temperatures as a function of controlled activities of water, hydrogen and carbon dioxide. Journal of Petrology **16**, pp.549-593.

------, EGGLER, D., SEITZ, M.G. and HOLLOWAY, J.R. 1976. Carbon dioxide in silicate melts and crystals, I. Solubility measurements. American Journal of Science **276**, pp.455-479.

------ and VIRGO, D. 1980. The solubility behaviour of CO_2 in melts on the join $NaAlSi_3O_8$-$CaAl_2Si_2O_8$-CO_2 at high pressures and temperatures: a Raman spectroscopic study. American Mineralogist **65**, pp.1166-1175.

NAKAMURA, N. 1974. Determination of REE, Ba, Fe, Mg, Na and K in carbonaceous and ordinary chondrites. Geochimica et Cosmochimica Acta **38**, pp.757-775.

NGOE, P.V. and BOYER, D. 1978. Propriétés électriques de l'écorce et du manteau supérieur sous une chaîne volcanique quaternaire de la Cordillère canadienne en relation avec l'expansion de la dorsale nord-est du Pacifique. Comptes Rendus des Séances de l'Académie des Sciences Série D (Sciences Naturelles) **287**, pp.199-202.

PALME, H. and NICKEL, K.G. 1985. Ca/Al ratio and composition of the Earth's upper mantle. Geochimica et Cosmochimica Acta **49**, pp.2123-2132.

PARSONS, B. and SCLATER, J.G. 1977. An analysis of the variation of ocean-floor bathymetry and heat flow with age. Journal of Geophysical Research **82**, pp.803-827.

PORATH, H., GOUGH, D.I. and CAMFIELD, P.A. 1971. Conductive structures in the northwestern United States and southwest Canada. Geophysical Journal of the Royal Astronomical Society **23**, pp.387-398.

PRICE, R.A., MONGER, J.W.H. and MULLER, J.E. 1981. Cordilleran cross-section - Calgary to Victoria **in:** Thompson, R.I. and Cook, D.G. (eds.) Field guides to geology and mineral deposits, Geological Association of Canada annual meeting, Calgary, pp.261-334.

RIDDIHOUGH, R.P. 1979. Gravity and structure of an active margin British Columbia and Washington. Canadian Journal of Earth Sciences **16**, pp.350-363.

------ amd HYNDMAN, R.D. 1976. Canada's active western margin: the case for subduction. Geoscience Canada **3**, pp.269-278.

ROEDDER, E. 1979. Origin and significance of magmatic inclusions. Bulletin Mineralogique **102**, pp.487-510.

ROGERS, G.C. 1976. A microearthquake survey in northwest British Columbia and southwest Alaska. Bulletin of the Seismological Society of America **66**, pp.1643-1655.

------ 1979. Earthquake fault plane solutions near Vancouver Island. Canadian Journal of Earth Sciences **16**, pp.523-531.

------ 1981. McNaughton Lake seismicity - more evidence for an Anahim hotspot? Canadian Journal of Earth Sciences **18**, pp.826-828.

------ and SOUTHER, J.G. 1975. Hotspots trace plate movements. Geos **12**, pp.10-13.

SATO, H. 1977. Nickel content of basaltic magmas: identification of primary magmas and a measure of the degree of olivine fractionation. Lithos **10**, pp.113-120.

SCHNEIDER, M.E. and EGGLER, D.H. 1986. Fluids in equilibrium with peridotite minerals: implications for mantle metasomatism. Geochimica et Cosmochimica Acta **50**, pp.711-724.

SLEEP, N.H. 1974 Segregation of a magma from a mostly crystalline mush. Bulletin of the Geological Society of America **85**, pp.1225-1232.

SMITH, A.D. 1986. Isotopic and chemical studies of Terrane I, south-central British Columbia. Ph.D. thesis, University of Alberta, 195p.

SMITH, D.G.W. and GOLD C.M. 1976. A scheme for fully quantitative energy dispersive microprobe analysis. Advances in X-Ray Analysis **19**, pp.191-201.

SNEERINGER, M., HART, S.R. and SHIMIZU, N. 1984. Strontium and samarium diffusion in diopside. Geochimica et Cosmochimica Acta **48**, pp.1589-1608.

SOUTHER, J.G. 1970. Volcanism and its relationship to recent crustal movements in the Canadian Cordillera. Canadian Journal of Earth Sciences **7**, pp.553-568.

------ 1977. Volcanism and tectonic environments in the Canadian Cordillera: a second look. **in**: Volcanic Regimes in Canada, Geological Association of Canada Special Paper 16, pp.3-24.

------ and HICKSON, C.J. 1984. Crystal fractionation of the basalt comendite series of the Mount Edziza volcanic complex, British Columbia: major and trace elements. Journal of Volcanological and Geothermal Research **21**, pp.79-106.

SHARMA, S.K. 1979. Structure and solubility of carbon dioxide in silicate glasses of diopside and sodium melilite compositions at high pressures from Raman spectroscopic data. Carnegie Institute of Washington Yearbook **78**, pp.532-537.

------, HOERING, T.C. and YODER, H.S. 1979.Quenched melts of akermanite composition with or without CO_2 - characterization by Raman spectroscopy and gas chromatography. Carnegie Institute of Washington Yearbook **78**, pp.537-542.

SPENCE, G.D., CLOWES, R.M. and ELLIS, R.M. 1977. Depth limits on the M-discontinuity in the southern Rocky Mountain Trench, Canada. Bulletin of the Seismological Society of America **67**, pp.543-546.

SPENCER, T.H. and LINDSLEY, D.H. 1981. A solution model for coexisting Fe-Ti oxides. American Mineralogist **66**, pp.1189-1201.

STACEY, R.A. 1973. Gravity anomalies, crustal structure and plate tectonics in the Canadian Cordillera. Canadian Journal of Earth Sciences **10**, pp.615-628.

STOLPER, E. 1982. Water in silicate glasses: an infrared spectroscopic study. Contributions to Mineralogy and Petrology **81**, pp.1-17.

SUN, M. 1985. Sr isotopic study of ultramafic nodules from Neogene alkaline lavas of British Columbia, Canada, and Josephine Peridotite, southwestern Oregon, USA. MSc. thesis, University of British Columbia, 133p.

SUN, S.-S. 1982. Chemical composition and origin of the Earth's primitive mantle. Geochimica et Cosmochimica Acta **46**, pp.179-192.

TAKAHASHI, E. and KUSHIRO, I. 1983. Melting of a dry peridotite at high pressures and basalt magma genesis. American Mineralogist **68**, pp.859-879.

TEMPELMAN-KLUIT, D.J. 1979. Transported cataclasite, ophiolite and granodiorite in Yukon: evidence of arc-continent collision. Geological Survey of Canada Paper **79-14**, 27pp.

------ and WANLESS, R.K. 1975. Potassium-argon age determinations of metamorphic and plutonic rocks in the Yukon Crystalline Terrane. Canadian Journal of Earth Sciences **12**, pp.1895-1909.

TURCOTTE, D.L. and SCHUBERT, G. 1973. Frictional heating of the descending lithosphere. Journal of Geophysical Research **78**, pp.5876-5886.

VEBLEN, D.R. and BUSECK, P.R. 1980. Microstructures and reaction mechanisms in biopyriboles. American Mineralogist **65**, pp.599-623.

VOGT, P.R. 1974a. Volcano spacing, fractures and thickness of the lithosphere. Earth and Planetary Science Letters **21**, pp.235-252.

------ 1974b. Volcano spacing, fractures and thickness of the lithosphere - a reply. Earth and Planetary Science Letters **23**, pp.162-163.

WASS, S.Y. 1979. Multiple origins of clinopyroxenes in alkali basaltic rocks. Lithos **12**, pp.115-132.

WATTS, A.B. and TALWANI, M. 1975. Gravity effect of downgoing lithospheric slabs beneath island arcs. Bulletin of the Geological Society of America **86**, pp.1-4.

WEICHERT, D.H. and HYNDMAN, R.D. 1981. Rates of motion on the boundaries of the western Canada continental margin. Bulletin of the Seismological Society of America **52**, p.70.

WELLS, P.R.A. 1977. Pyroxene thermometry in simple and complex systems. Contributions to Mineralogy and Petrology **62**, pp.129-139.

WHITE, W.M. and HOFMANN, A.W. 1982. Sr and Nd isotope geochemistry of oceanic basalts and mantle evolution. Nature **296**, pp.821-824.

WICKENS, A.J. 1971. Variations in lithospheric thickness in Canada. Canadian Journal of Earth Sciences **8**, pp.1154-1162.

------ 1977. The upper mantle of southern British Columbia. Canadian Journal of Earth Sciences **14**, pp.1100-1115.

WILSHIRE, H.G. 1984. Mantle metasomatism: the rare-earth story. Geology **2**, pp.395-398.

------ and TRASK, N.J. 1971. Structural and textural relationships of amphibole and phlogopite in peridotite inclusions, Dish Hill, California. American Mineralogist **56**, pp.240-255.

------ and SHERVAIS, J.W. 1975. Al-augite and Cr-diopside ultramafic xenoliths in basaltic rocks from the western United States. Physics and Chemistry of the Earth **9**, pp.257-272.

------, PIKE, J.E., MEYER, C.E. and SCHWARZMAN, E.L. 1980. Amphibole-rich veins in lherzolite xenoliths, Dish Hill and Deadman Lake, California. American Journal of Science **280A**, pp.576-593.

WYLLIE, P.J. 1977. Mantle fluid compositions buffered by carbonates in peridotite-CO_2-H_2O. Journal of Geology **85**, pp.187-207.

------ 1978. Mantle fluid compositions buffered in peridotite-CO_2-H_2O by carbonates, amphibole and phlogopite. Journal of Geology **86**, pp.687-713.

------ 1979. Magmas and volatile components. American Mineralogist **64**, pp.469-500.

------ and HUANG, W.L. 1976. High CO_2 solubilities in mantle magmas. Geology **4**, pp.21-24.

YODER, H.S. 1976. Generation of basaltic magma. National Academy of Sciences 265p.

ZINDLER A., STAUDIGEL H. and BATIZA R. 1984. Isotope and trace element geochemistry of young Pacific seamounts: implications for the scale of upper mantle heterogeneity. Earth and Planetary Science Letters **70**, pp.175-195.

PHOTOGRAPHIC PLATES

PLATE 1

A. Hyalo Ridge, seen from the south across Spanish Lake. Its structure is that of a tuya (Mathews 1947). The steep sides of the edifice comprise indurated hyaloclastite. A break of slope at the base of the lava cap is marked by a line of trees near the summit.

B. Section exposed on the east flank of Hyalo Ridge, in a cirque below the summit. Four of the flows forming the lava cap of the tuya are truncated by the cirque. The location of Plate 1C is at the extreme left of the plate, at the base of the lava cap.

C. View along the section through the Hyalo Ridge lava cap, showing the four flows capping the edifice. C.M. Elléon is standing by an exposure of distal pillow lavas, shown in detail in Plate 1D.

D. Pillow lavas in the distal portion of the basal flow on Hyalo Ridge.

E. Blast pit in the easternmost crater of the Spanish Lake centre. The photograph is taken from the original floor, at the level of the lava filling the crater.

F. Lava flow from a flank eruption in Spanish Lake centre The portion of the erupted lava seen here flowed back into the main crater, creating a lava lake. The resurgent dome is visible in the background.

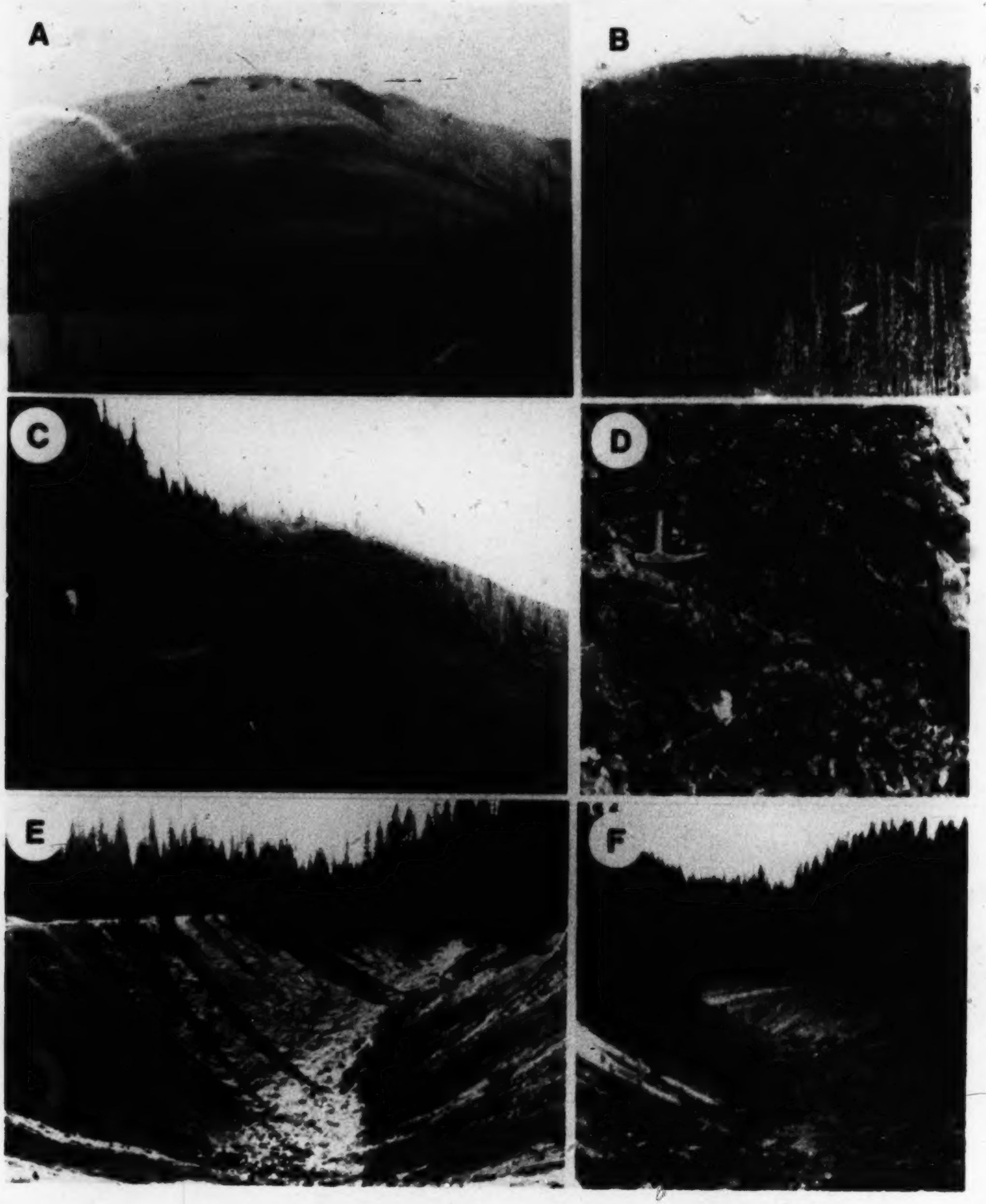
A
B
C
D
E
F

PLATE 2

Stereographic aerial photograph of the Spanish Lake centre, showing the three craters, resurgent dome and lava flows in the volcano and the pit crater of Peridot Lake, to the north of the cone. The locations and vistas of Plates 1E and 1F are shown by arrows. This plate is reproduced from aerial photographs BC7324-064 and BC7324-065 by courtesy of the Province of British Columbia. The photographs are copyright and no further reproductions may be made without permission from the B.C. Ministry of Environment and Parks.

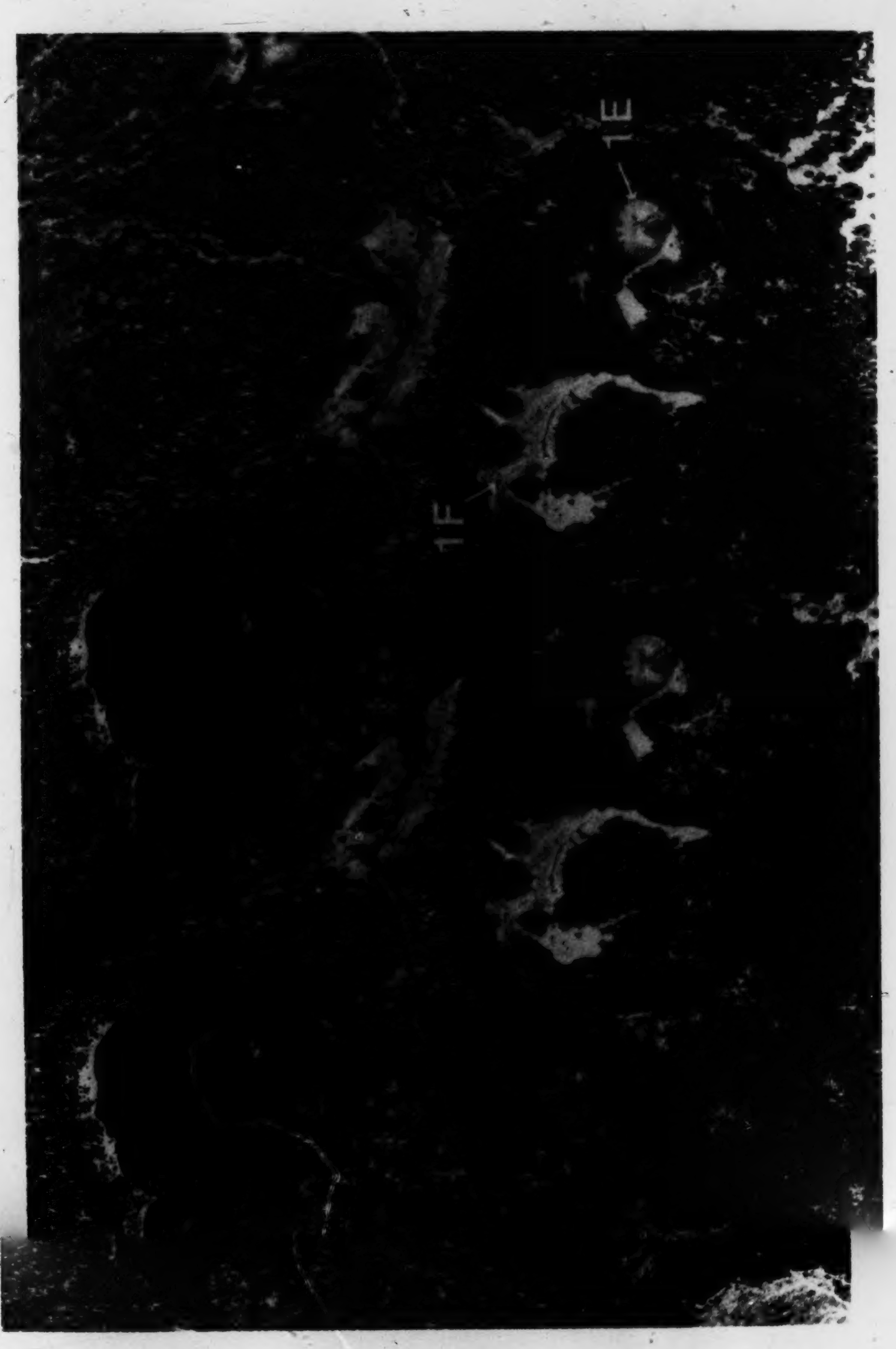
1E
1F

PLATE 3

Stereographic aerial photograph of the Flourmill centre, showing the three craters and lava flows. Note the layering of agglutinate in the youngest, northwest crater. The locations and vistas of Plates 4A to 4D are shown by arrows. This plate is reproduced from aerial photographs BC7323-221 and BC7323-222 by courtesy of the Province of British Columbia. The photographs are copyright and no further reproductions may be made without permission from the B.C. Ministry of Environment and Parks.

4D
4A
4B
4C

PLATE 4

A. Layered cinders and agglutinate in Flourmill centre (southwest crater). In the background are the lava beds filling the Spanish Creek valley.

B. Lava squeeze-up in the southwest crater of Flourmill centre.

C. Drained lava lake in the northwest crater of the Flourmill centre. Note the rafted blocks representing the collapsed crust of the lava lake. Foreground: J Gibbs, University of Alberta.

D. Explosion pit surrounded by a ring of scoria. This feature represents the last phase of activity in the Flourmill centre. Left to right J. Gibbs, C.M. Elleon, University of Alberta.

E. Volcanic bombs from the northwest part of the Flourmill centre.

F. Pyramid Mountain seen from the south. The edifice is described by Hickson (1987) as a SUGM, or SUbGlacial Mound; it comprises a hyaloclastite mound with a secondary summit (right), the latter interpreted by Hickson as a slumped summit; the original structure was supported by an intraglacial lake.

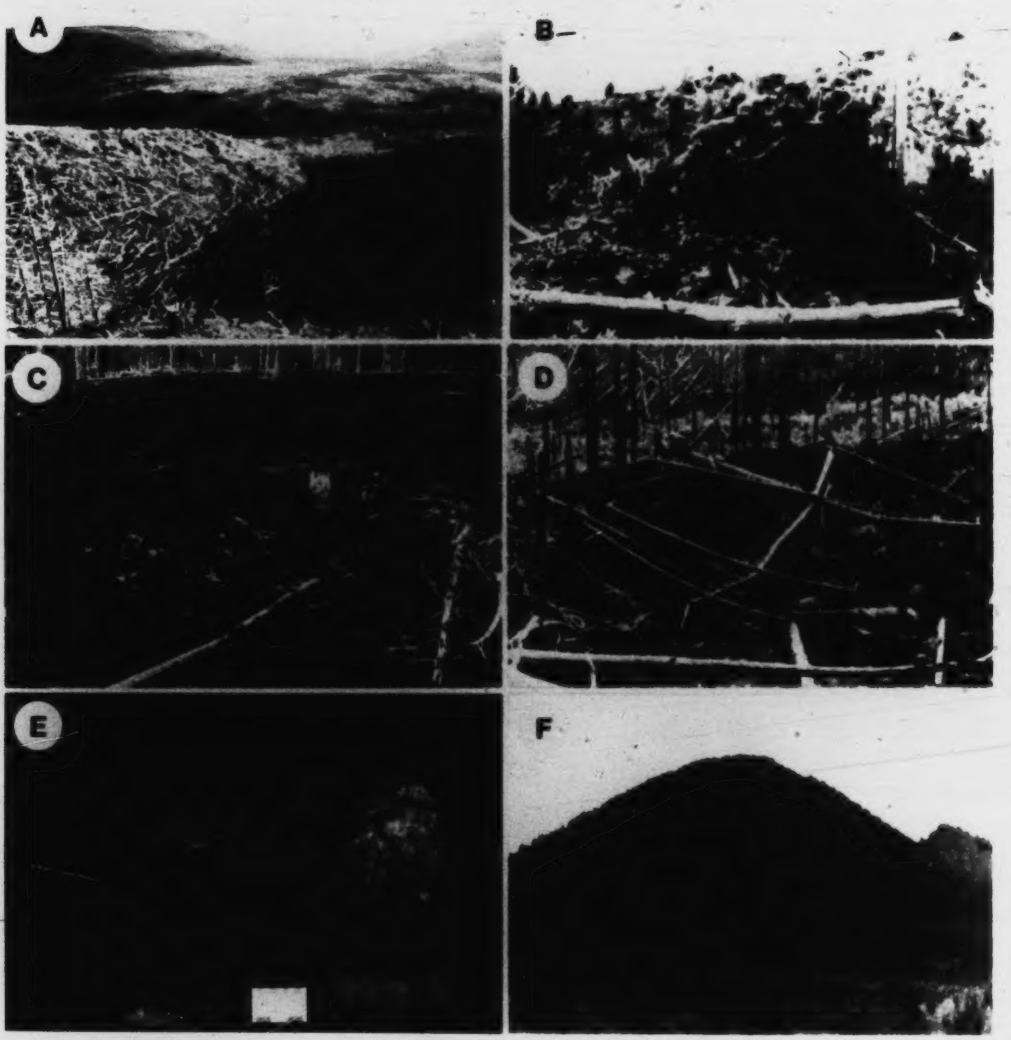
A
B
C
D
E
F

PLATE 5

A. The fissure structure in the Ray Mountain centre, showing the erupted lavas and the domes of the subvolcanic intrusions. Dykes extend from the margin of the main intrusion into the ejecta, to the left of the photograph. Both intrusive and extrusive rocks are from the earlier phase of activity on Ray Mountain. Photograph looking south towards Jack's Jump and the Helmcken Plateau.

B. View southward along the Ray Mountain fissure towards Key Puy, showing disturbance of the layering in the pyroclastic deposits near the fissure. Key Puy, a volcanic neck from the second phase of activity, intrudes country rocks at the right of the photograph. The summit of Ray Mountain is visible at the left, along the lava cliff seen in Plate 5E.

C. Dyke intruded during the earlier phase of activity at Ray Mountain. The dyke cuts subaerial ejecta from a previous eruption in the same phase of activity.

D. Basal contact of Ray Mountain hyaloclastite. the hyaloclastite overlies Shuswap quartz-feldspar-muscovite schist on the northern edge of the Ray Mountain centre. The hyaloclastite is the earliest deposit from the second phase of activity on Ray Mountain and is interpreted as the result of ice-lava contact.

E. Stratigraphic section through Ray Mountain, seen from Key Puy across the fissure. Subaerial ejecta from the earlier phase are overlain unconformably by hyaloclastite from the later phase. The contact is exposed at the right side of the photograph, beneath the summit of Ray Mountain. The hyaloclastite, which incorporates some subaerially-erupted volcanic bombs, is overlain by a lava flow and subaerial ejecta.

A

B

C

D

E

PLATE 6

Stereographic aerial photograph of the Dragonhead centre, showing the breached crater, landslide surface and lava flows coalescing in the valley. The locations and vistas of Plates 7A to 7C are shown by arrows. This plate is reproduced from aerial photographs BC5049-72 and BC5049-73 by courtesy of the Province of British Columbia. The photographs are copyright and no further reproductions may be made without permission from the B.C. Ministry of Environment and Parks.

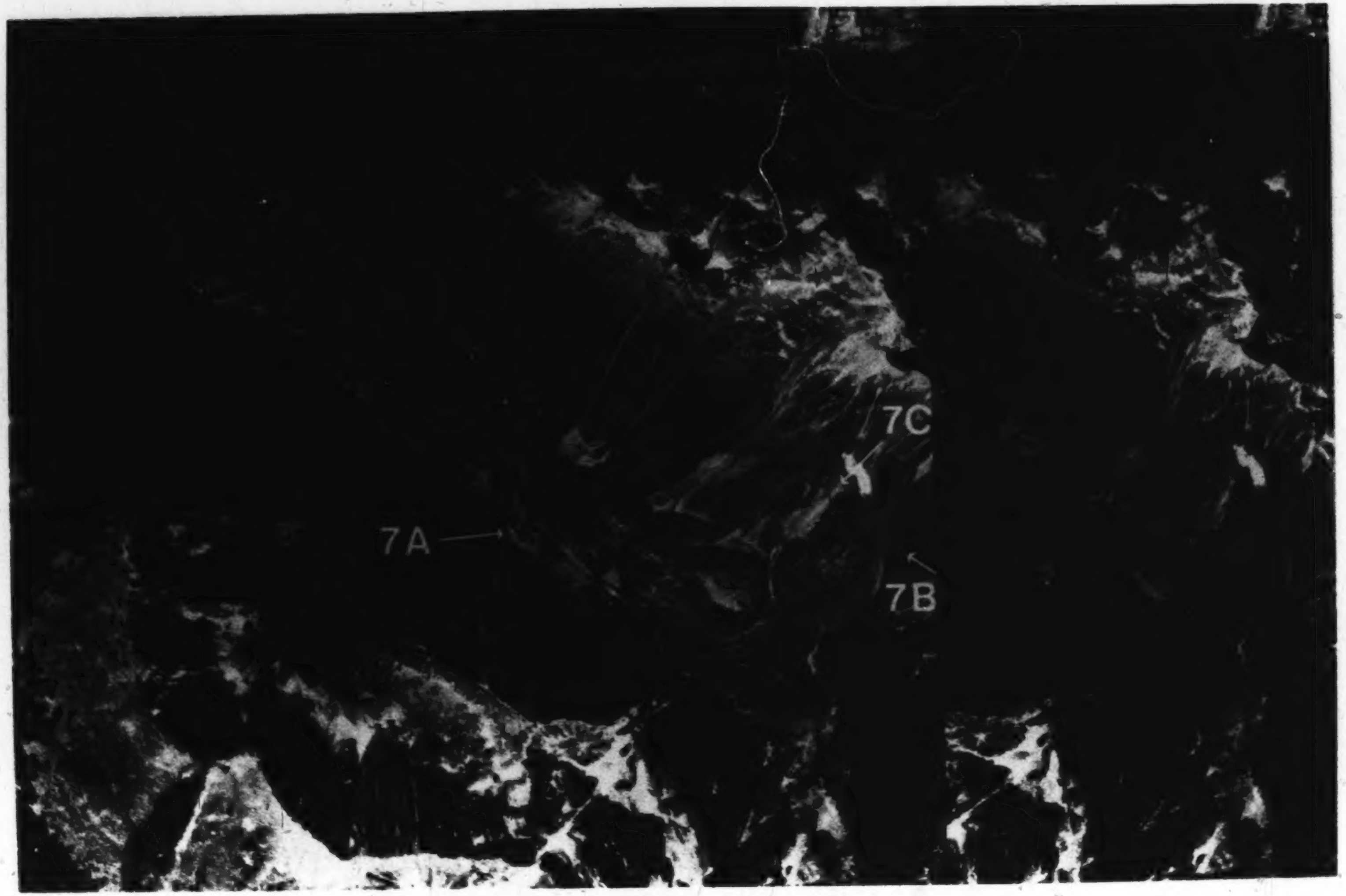
7C
7A
7B

PLATE 7

A. Dragonhead cone, from the air across the Falls Creek valley. The edifice is a simple cone, situated on the side of the valley. A landslide on the valley side permitted egress of two lava flows from the central crater.

B. Dragonhead cone from the northeast, showing slumping of the cone towards the Falls Creek valley. In the foreground of the photograph is a slope covered with a considerable, although unknown thickness of basaltic ash, formed from a lava fountain and driven by a prevailing southwest wind. The ash deposits are extensively weathered.

C. Breach in Dragonhead cone showing the slumped portion of the cone and the valley-filling flow beyond.

D. Vertical contact of distal Dragonhead flow with mica schist country rock. The lava flow filled an earlier stream canyon of Falls Creek, altering its course to the north.

E. Tree mould in the distal portion of the Dragonhead flow. The mould is one of several in the surface and at the base of the flow Bark impressions in one mould indicate that at least some of the trees were poplars. A mature forest had developed, therefore, after the last glaciation, before the lava flow was erupted.

F. Section from the base of the Dragonhead flow (distal portion). The flow rests on 3 to 5 cm of intercalated grey and brown silt. The silt covers a layer of carbon, relict from dead trees, which yielded a ^{14}C age of 7.5 ka. The basal unit comprises yellow micaceous sand, deposited by stream action.

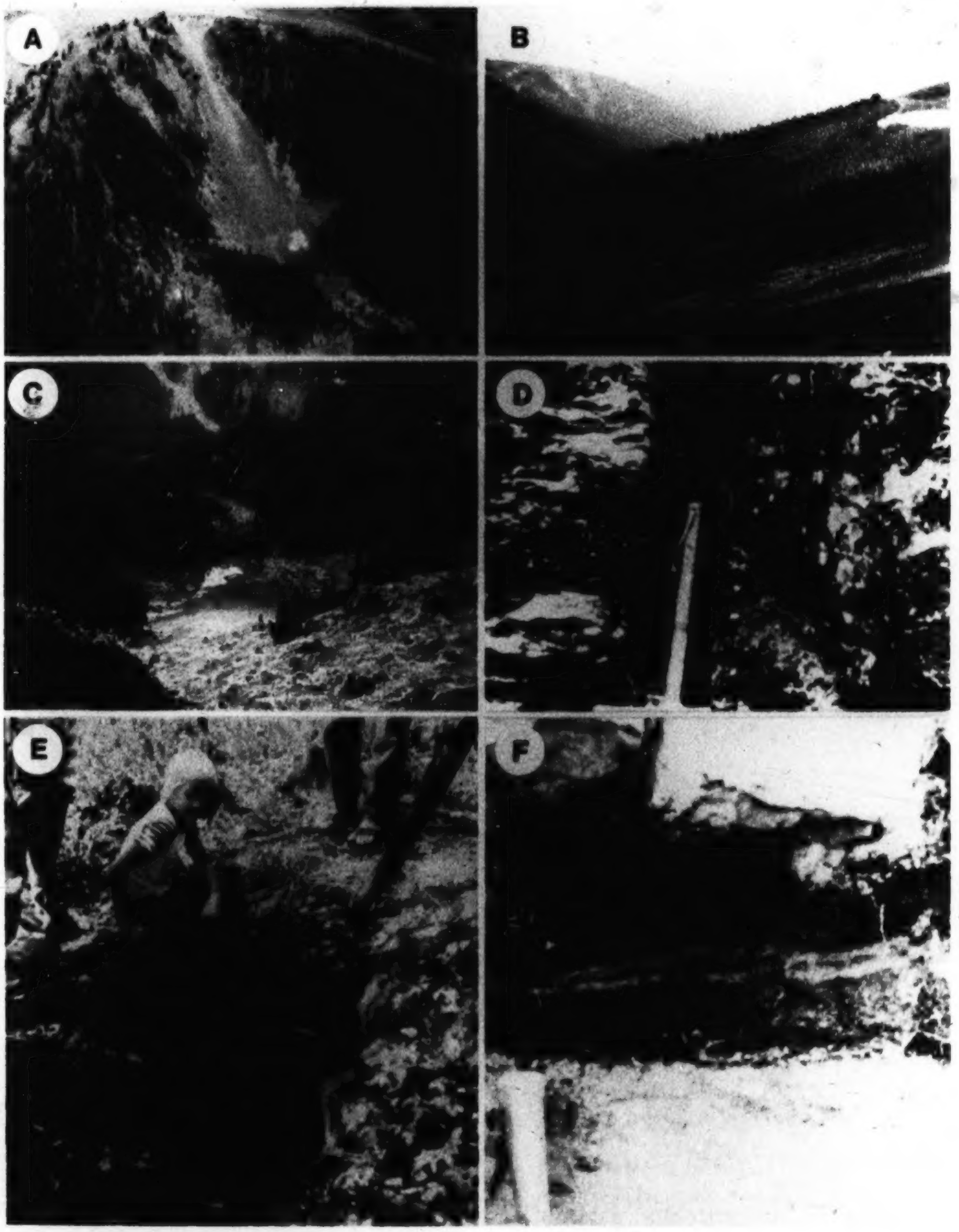
A
B
C
D
E
F

PLATE 8

Stereographic aerial photograph of the Kostal Lake centre, showing the two cones and the lava flows. Note the ponding of lava to the south of the south cone, damming the valley to form Kostal Lake. The locations and vistas of Plates 9A to 9F are shown by arrows. This plate is reproduced from aerial photographs BC1744-10 and BC1744-11 by courtesy of the Province of British Columbia. The photographs are copyright and no further reproductions may be made without permission from the B.C. Ministry of Environment and Parks.

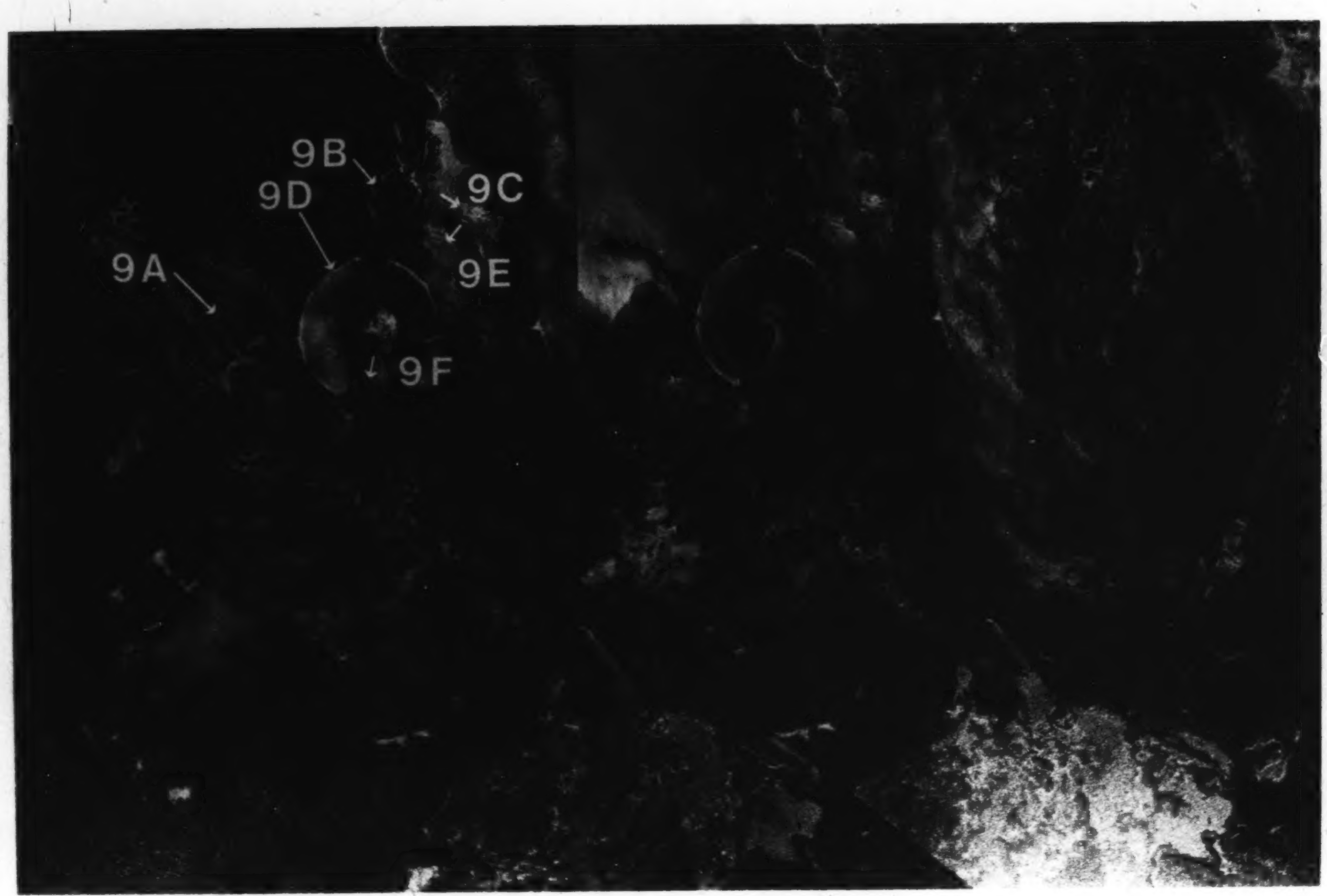
9B
9D
9C
9A
9E
9F

PLATE 9

A. Kostal Lake centre from the air, showing the older agglutinate mounds (top left), and the south cone (left). Lava draining through the breach formed the lava lake at the centre and lower right of the photograph. This lava lake abuts against the older lavas.

B. Kostal Lake centre from the air, showing the north cone (left centre) and flow (bottom), the flow from a lava tube (right centre) and a portion of the south cone (right). Photograph looking east.

C. View across the flow from the north cone at Kostal Lake, with the north cone in the background. The flow surface is of *aa*.

D. The south cone of the Kostal Lake centre, seen from the air. The small resurgent dome in the crater is visible at top centre.

E. The south cone of the Kostal Lake centre, viewed from the northwest across the flow from the lava tube. Pressure ridges are visible in the flow surface.

F. The breach in the south cone, showing collapse in the flow surface where the flow drains the crater. From left to right: C.J. Hickson, Geological Survey of Canada; D.R. Bull, University of Alberta; S. Bishop, University of British Columbia.

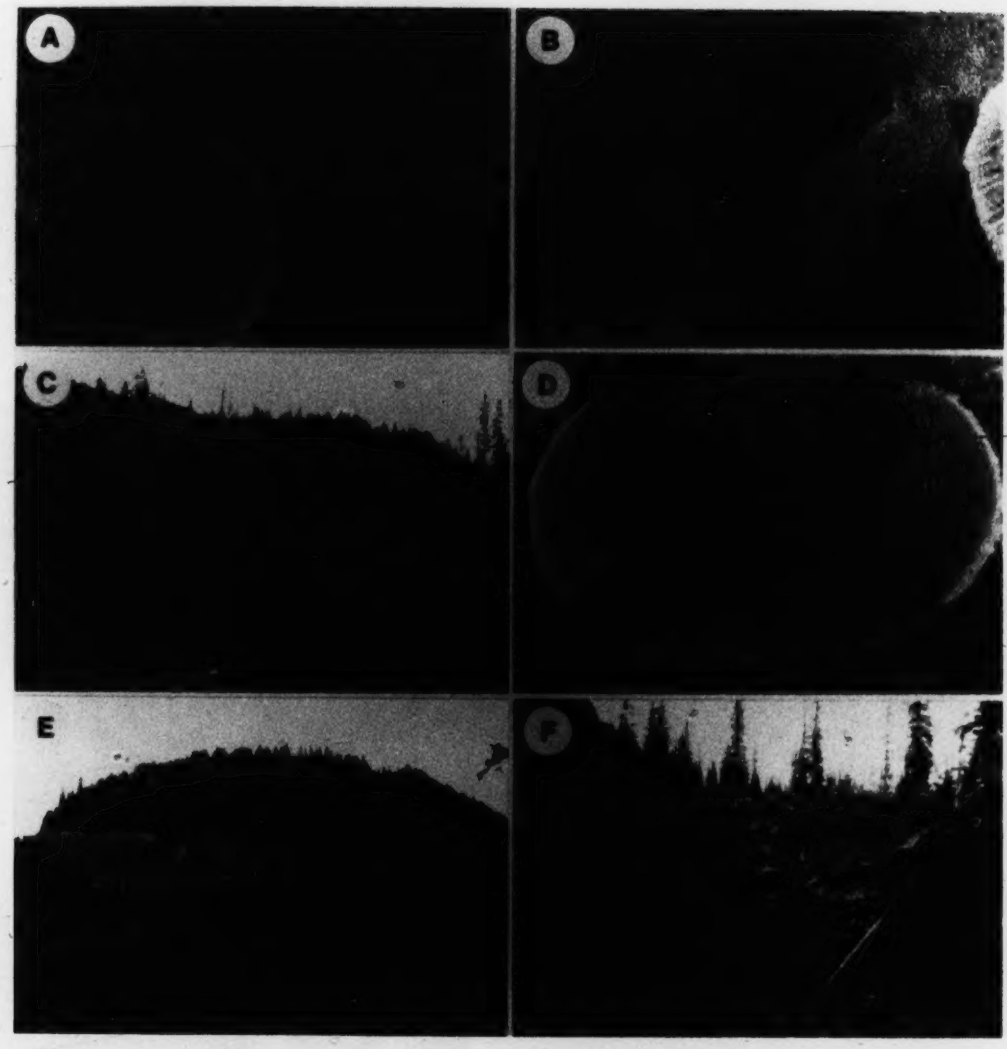
A
B
C
D
E
F

PLATE 10

A. Photomicrograph of hyaloclastite from Spanish Mump. Two fragments of glass, at lower centre and upper right are vesicular, with minor phenocrysts; the fragment in the upper right corner is the more glassy. An oxidised fragment of glass is present in the lower right of the photograph. On the left side of the photograph is a larger, partially crystallised fragment containing a xenophyric intergrowth of olivine and Cr-spinel. The Cr-spinel has been oxidised where it is in contact with the melt. Photomicrograph taken in plane polarised light.

B. Clinopyroxene xenocrysts in lava from Spanish Bonk. The xenocryst in the lower right of the photograph is of ferroan augite, that in the upper left is of aluminous augite. The former is pervasively corroded and lacks a phyric rim. The latter is peripherally corroded and weakly zoned, with a strongly zoned phyric rim. Photomicrograph taken between crossed polars.

C. Hyaloclastite from Hyalo Ridge. Three fragments of avesicular, light-coloured glass are present in the lower part of the photograph, matrix-suspended in a matrix of fine-grained hydrated glass with crystal fragments. On the left side of the photograph and in the lower right corner are oxidised of the same glass. Photomicrograph taken in plane polarised light.

D. Olivine xenocryst showing embayed margins. Photomicrograph taken in plane polarised light.

E. Glass fragment from Pyramid Mountain showing oxidation of glass, progressing from the margin of the fragment, at the lower right of the photograph, to the interior, at the upper left corner. increasing from lower left to upper right, with distance from the margin of the fragment. The larger phenocrysts in the glass, such as that in the upper right corner, are of olivine. Note the abundance of vesicles. Photomicrograph taken in plane polarised light.

Ei Enlargement of one of the crystal clusters visible in Plate 10E, surrounded by pristine glass. The small size of individual crystals precludes analysis by microbeam. The aggregate probably comprises an intergrowth of Fe-Ti oxide and plagioclase. Photomicrograph taken in plane polarised light.

F. Hyaloclastite from Ray Mountain. The photograph shows a globule of vesicular glass at right centre, with an oxidised centre, black in colour, and a hydrated rim, matrix-suspended in fragments of orange hydrated glass. Photomicrograph taken in plane polarised light.

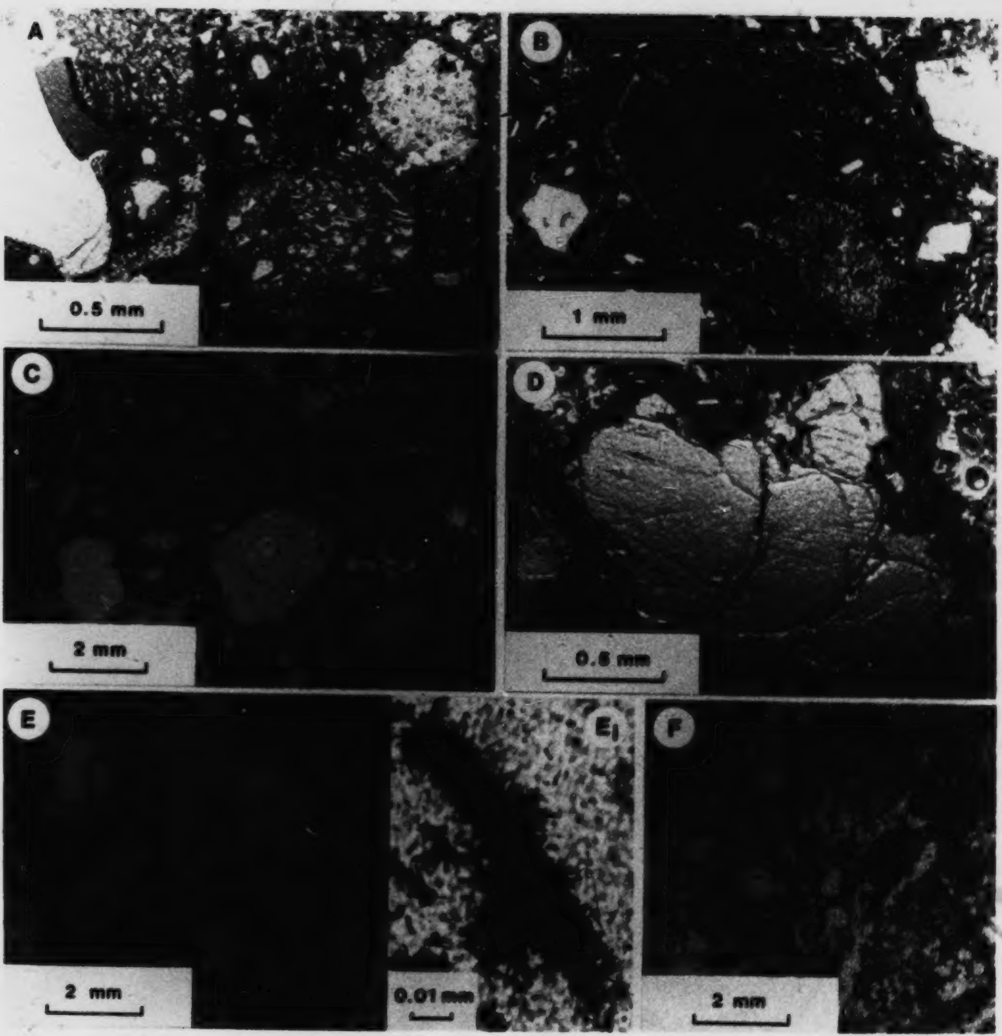
A
0.5 mm
B
1 mm
C
2 mm
D
0.5 mm
E
2 mm
E1
0.01 mm
F
2 mm

PLATE 11

A. Protoclastic aluminous spinel wehrlite from the Trophy Range, 10 km south of Wells Gray Park. The wehrlite comprises olivine and clinopyroxene, with accessory spinel. The large grains in the centre of the photograph are clinopyroxene; those on the right side of the field of view are olivine. The protoclastic texture has broken down in places into a fabric resembling a mortar or porphyroclastic texture. Photomicrograph taken between crossed polars.

B. Porphyroclastic Cr-spinel lherzolite from the distal portion of the Dragon's Tongue. The small grains at extinction in the lower centre of the photograph are Cr-spinel grains which have partially-formed vermicular texture. The light-coloured grains at the centre are strained olivine; the large dark grain at the top right is a strained clinopyroxene. Orthopyroxene is a minor phase. Photomicrograph taken between crossed polars.

C. Cr-spinel wehrlite, exhibiting tabular equigranular texture, from a locality on the Trophy Mountain range. The minerals shown comprise banded olivine and clinopyroxene. Photomicrograph taken between crossed polars.

D. Cr-spinel lherzolite, exhibiting mosaic equigranular texture, hosted by lava from the flank eruption at Spanish Lake Centre. The extinct grains at lower centre are Cr-spinel and exhibit vermicular texture. Olivine, orthopyroxene and clinopyroxene are all major constituents and exhibit 120° grain boundaries. Photomicrograph taken between crossed polars.

E. Protoclastic Al-spinel clinopyroxenite, from the proximal portion of the Dragon's Tongue. Spinel is an accessory phase in this xenolith. Clinopyroxene is the only phase shown and exhibits irregular zonation and mutually interpenetrant grain boundaries. Photomicrograph taken between crossed polars.

F. Porphyroclastic wehrlite, from the older parasitic cone at Spanish Lake Centre. The xenolith contains corroded clinopyroxene and fresh olivine, both phases exhibiting evidence of straining. Note the overgrowth of phyric clinopyroxene at top left. Photomicrograph taken between crossed polars.

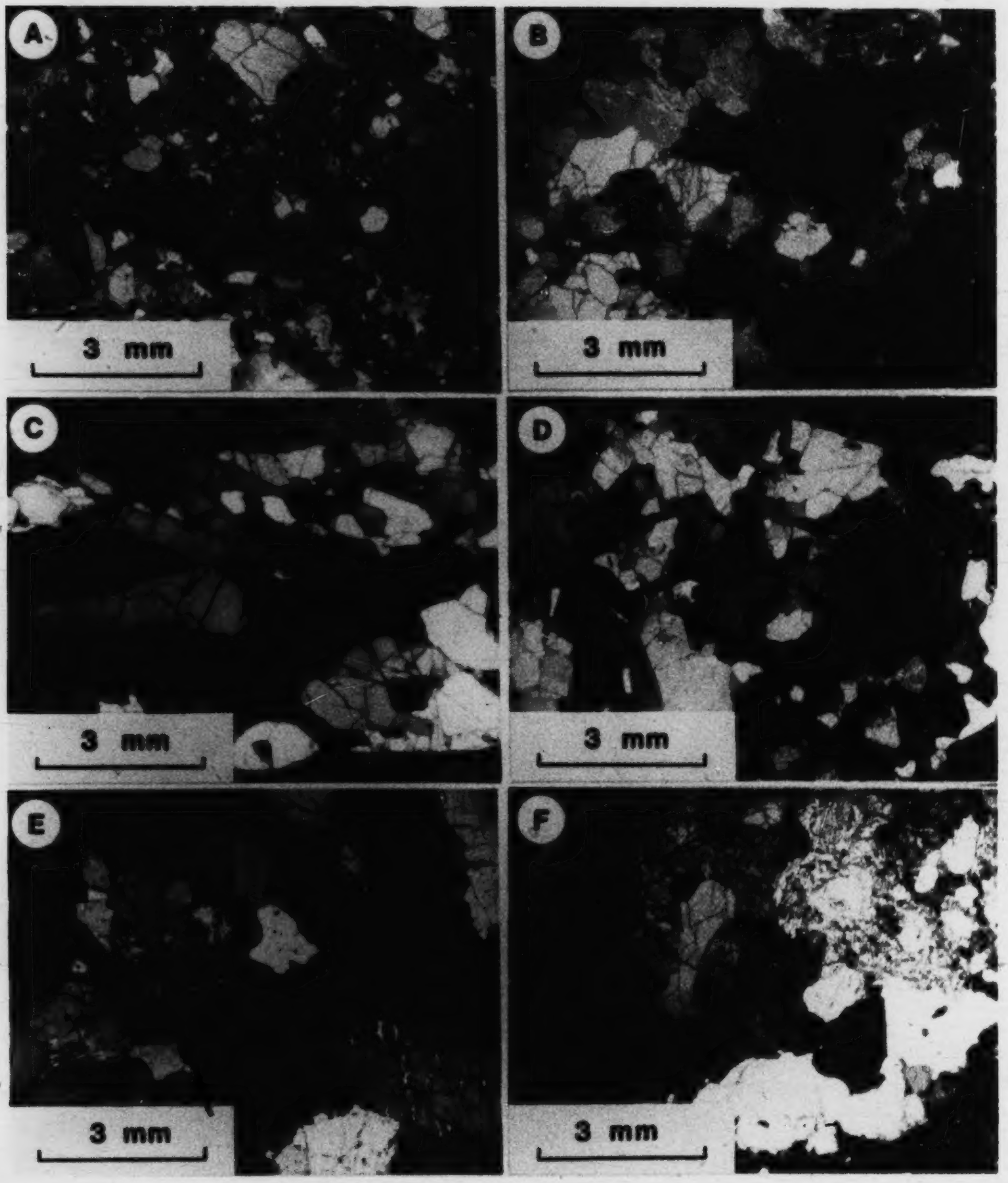
A
3 mm
B
3 mm
C
3 mm
D
3 mm
E
3 mm
F
3 mm

PLATE 12

A. Kaersutitic amphibole in an aluminous spinel clinopyroxenite from the proximal portion of the Dragon's Tongue. The amphibole (centre) occurs with aluminous spinel (lower left) and clinopyroxene (upper left, lower right). Note the development of oxides where the host melt has soaked into the xenolith. Photomicrograph taken in plane polarised light.

B. Kaersutitic amphibole in an aluminous spinel clinopyroxenite from the proximal portion of the Dragon's Tongue. The amphibole forms 120° grain boundaries with clinopyroxene and shows no reaction relationship; the clinopyroxene (dark grain at centre) exhibits mutual interpenetration with the amphibole. Where melt has invaded the xenolith, there is evidence of a reaction with the amphibole. Photomicrograph taken between crossed polars.

C. Websterite with primary apatite enclosed in clinopyroxene. The websterite is a small fragment from the earlier phase of activity in the Flourmill Centre, with a mosaic equigranular texture; the modal mineralogy of the parent rock in the mantle is therefore enigmatic. The apatite grains are enclosed in the darker fractured grain near the centre of the inclusion. Photomicrograph taken between crossed polars.

D. Primary apatite grains in clinopyroxene. At least two of the inclusions shown are still sealed. The inclusion on the far left is that exposed by polishing and subsequently analysed by electron microbeam. The inclusion is shown in Plate 12E. Photomicrograph taken in plane polarised light.

E. Electron photomicrograph of apatite grain analysed by energy dispersive analysis. Photograph taken using the output from the secondary electron detector on the department A.R.L. S.E.M.Q. microprobe while the electron beam was rastered over the area.

F. Devitrified melt inclusion in an olivine phenocryst. The melt inclusion was trapped during growth of the phenocryst, with synchronous or subsequent evolution of an exsolved volatile phase, forming a gas bubble in the centre of the inclusion. Devitrification of the enclosed melt formed microphenocrysts of clinopyroxene and felted intergrowths of plagioclase and Fe-Ti oxide. A lining of relatively fayalitic olivine formed on the walls of the inclusion. Photomicrograph taken in plane polarised light.

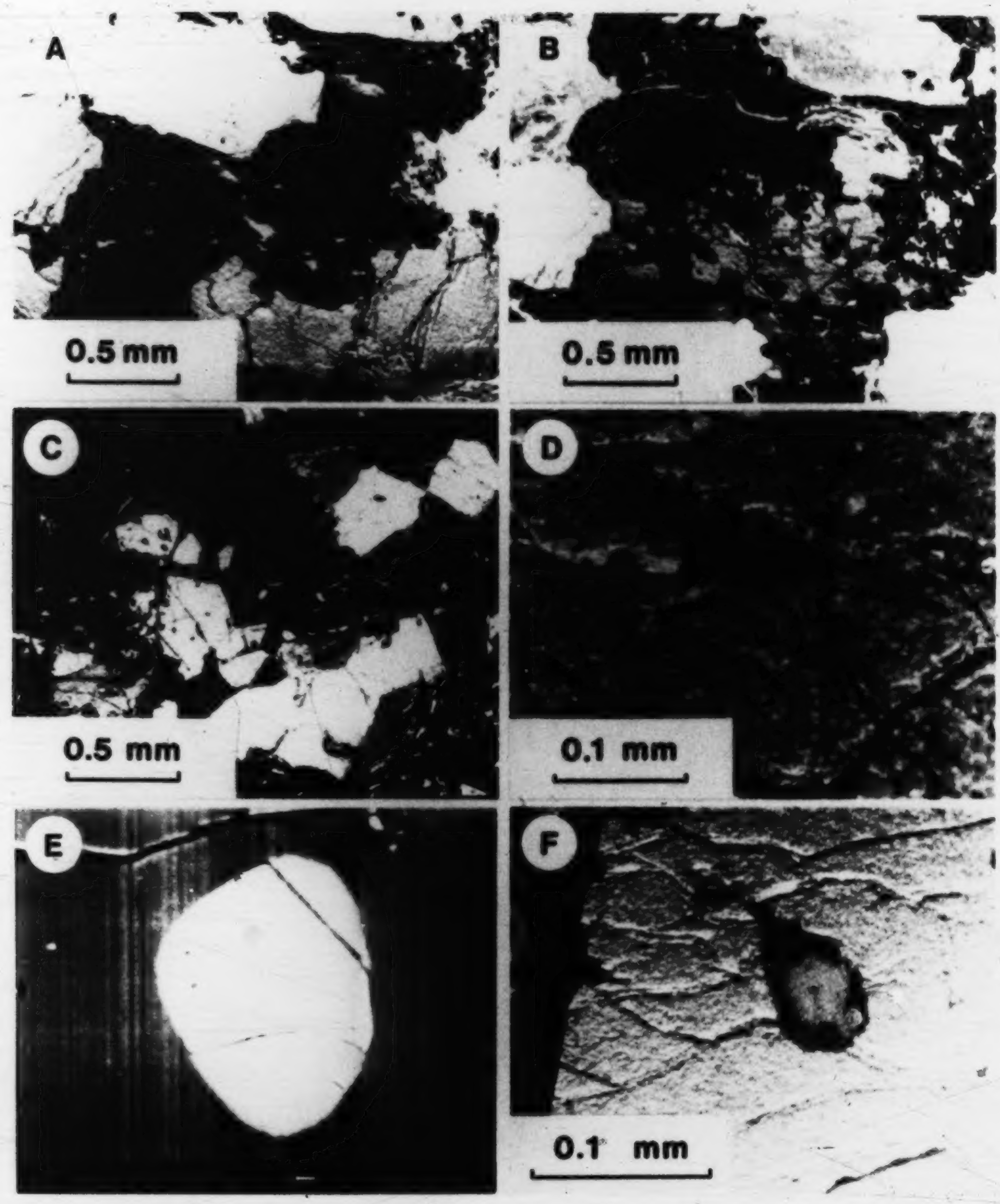
A
0.5 mm
B
0.5 mm
C
0.5 mm
D
0.1 mm
E
F
0.1 mm

APPENDIX A

ELECTRON MICROBEAM ANALYSIS

Sample selection

187 standard thin sections were examined prior to selection of samples for microbeam analysis. Sample selection, based on this examination was biased toward less weathered samples, also submitted for whole rock chemical analysis, and toward lavas relatively rich in phenocrysts and incognate material. Where more than one phase of activity could be identified, particularly in the postglacial centres, at least one representative sample was taken from each eruptive event.

Sample preparation

A total of 45 polished sections were prepared following the examination, representing phases of activity from nine of the eleven centres studied. Samples were prepared as polished thin sections, permitting detailed textural studies in addition to detailed chemical analysis by microbeam. The remaining two centres, Spanish Mump and Pyramid Mountain, are hyaloclastite mounds (SUGMs) and material from these centres was used to make grain mounts of whole glass. Material from Ray Mountain and Hyalo Ridge was also prepared in the same way.

Analytical procedure

Major mineral phases, accessory minerals and glass were analysed using an ARL SEMQ electron microprobe with an ORTEC energy dispersive system. Accelerating voltage during each run was 15 kV and the sample current was 0.39 nA. The ratio of sample current to aperture current was measured at the beginning and end of each run; aperture current was monitored throughout a run.

Minerals were identified in the microprobe using a combination of reflected light, transmitted light and back-scattered electron imagery, using large-scale photomicrographs taken during the course of petrographic analysis. The back-scattered electron imagery was also used to ensure that the beam was incident on a volume of material which was homogeneous and clean of inclusions, prior to each analysis.

Analytical standards, for each element analysed in each phase, are listed in Table A-1; element concentrations in each standard are given in Table A-2. Where possible, standards were chosen of a similar matrix to that of the phase to be analysed.

All spectra were collected over a period of four minutes live time. Olivine, pyroxene, oxide minerals and sulphide minerals were analysed using a point beam in a single location. Plagioclase was also analysed in this manner after measurements indicated that prolonged bombardment did not significantly alter the Na Kα counts obtained using a wavelength dispersive spectometer. For apatite and volcanic glass the spectra were obtained over several areas, using a 30 second (live time) acquisition period and a beam rastered over an area of 400 μm^2.

A minimum of 10^6 counts (full spectrum) were obtained for each sample analysed. Data were stored on floppy disc. Data processing was carried out with the EDATA2 data reduction programme of Smith and Gold (©1976).

Analytical results

Results were examined for totals and, where appropriate, stoichiometry Analyses deficient in either respect were discarded, with three exceptions. The first of these comprises the olivine analyses from Pointed Stick Cone and from Bathroom Bonk. All analyses from this run are consistently high in totals. The stoichiometry is, however, excellent; on these grounds it was considered justifiable to recalculate these analyses to 100%. Such a recalculation would not have been possible, nor justifiable, for pyroxene. The second exception made was the recalculation of all sulphide analyses to 100%. The sulphide analyses are semiquantitative and are included only to provide an estimate of their contribution to the chemistry of the enclosing lavas. The third exception made is where the analysis represents the only one obtained for a particular phase. In such cases, the analysis is marked in such a way as to identify it as suspect.

A total of 725 analyses was obtained for major phases, comprising clinopyroxene (186), olivine (204), plagioclase (104), oxide (174), orthopyroxene (14), amphibole (10), apatite (3), sulphide (9) and whole glass (21). All analyses are listed in Appendix B (Tables B-1 to B-13). Errors based on counting statistics and precisions of standard concentrations are listed, for each species, in Table A-3. In addition, the errors appropriate to each species are listed in the relevant tables in Appendix B.

Table A-1
Mineral standards used for analysis by electron microprobe

Element	Pyroxene	Olivine	Spinel	Magnetite	Ilmenite
Na	albite	n.a.	n.a.	n.a.	n.a.
Mg	diopside	diopside	diopside	diopside	diopside
Al	albite	D	chromite	chromite	chromite
Si	diopside	diopside	D	D	D
P	n.a.	n.a.	n.a.	n.a.	n.a.
S	n.a.	n.a.	n.a.	n.a.	n.a.
Cl	n.a.	n.a.	n.a.	n.a.	n.a.
K	n.a.	n.a.	n.a.	n.a.	n.a.
Ca	diopside	D	n.a.	D	D
Ti	ilmenite	ilmenite	ilmenite	ilmenite	ilmenite
Cr	chromite	D	chromite	chromite	chromite
Mn	willemite	willemite	willemite	willemite	willemite
Fe	ilmenite	ilmenite	haematite	haematite	haematite
Ni	n.a.	D	D	D	D
Cu	n.a.	n.a.	n.a.	n.a.	n.a.
Zn	n.a.	n.a.	willemite	willemite	willemite

Element	Plagioclase	Glass	Amphibole	Apatite	Sulphide
Na	albite	albite	albite	D	n.a.
Mg	n.a.	diopside	diopside	D	n.a.
Al	albite	albite	albite	D	n.a.
Si	albite	albite	albite	D	n.a.
P	n.a.	D	n.a.	apatite	n.a.
S	n.a.	D	n.a.	D	Sphalerite
Cl	n.a.	D	n.a.	apatite	n.a.
K	sanidine	sanidine	sanidine	D	n.a.
Ca	diopside	diopside	diopside	apatite	n.a.
Ti	ilmenite	ilmenite	ilmenite	D	ilmenite
Cr	n.a.	chromite	chromite	n.a.	D
Mn	willemite	willemite	willemite	D	willemite
Fe	ilmenite	ilmenite	ilmenite	D	ilmenite
Ni	n.a.	D	n.a.	n.a.	D
Cu	n.a.	n.a.	n.a.	n.a.	D
Zn	willemite	willemite	willemite	n.a.	willemite

D = default (no standard used); n.a. = element not analysed for mineral specified.

Table A-2
Chemical compositions of mineral standards used

Element	Franklin willemite	Cleveland Albite	Hohenfels sanidine	Wakefield diopside	Stillwater chromite
Na	n.a.	**8.579**	2.230	0.016	n.a.
Mg	0.074	n.a.	n.a.	**11.233**	**5.100**
Al	0.022	**10.338**	9.930	0.047	**6.680**
Si	13.121	**32.033**	30.230	**25.878**	n.a.
P	n.a.	n.a.	n.a.	n.a.	n.a.
S	n.a.	n.a.	n.a.	n.a.	n.a.
Cl	n.a.	n.a.	n.a.	n.a.	n.a.
K	n.a.	0.184	**10.050**	n.a.	n.a.
Ca	0.005	0.090	0.00	**18.390**	n.a.
Ti	n.a.	n.a.	0.00	0.051	0.480
Cr	n.a.	n.a.	n.a.	0.010	**27.910**
Mn	**3.733**	n.a.	n.a.	0.036	0.140
Fe	0.015	n.a.	0.140	0.040	27.430
Zn	**53.716**	n.a.	n.a.	n.a.	n.a.
			Includes: Ba (0.98)		Includes: V (0.14) Co (0.03) Ni (0.09)

Element	Obergaarden ilmenite	Elba haematite	Durango fluorapatite	Sphalerite
Na	n.a.	n.a.	0.170	n.a.
Mg	0.580	0.030	n.a.	n.a.
Al	0.010	0.010	0.040	n.a.
Si	0.00	n.a.	0.160	n.a.
P	n.a.	n.a.	**17.840**	n.a.
S	n.a.	n.a.	0.150	**32.60**
Cl	n.a.	n.a.	0.410	n.a.
K	n.a.	n.a.	n.a.	n.a.
Ca	n.a.	n.a.	**38.610**	n.a.
Ti	**25.590**	0.040	n.a.	n.a.
Cr	n.a.	n.a.	n.a.	n.a.
Mn	0.230	n.a.	n.a.	0.002
Fe	**38.690**	**69.860**	n.a.	0.08
Zn	0.010	n.a.	n.a.	**66.8**
	Includes: V (0.17)		Includes: La (0.38) Ce (0.44) Nd (0.22) Pr (0.10) Y (0.08) As (0.07) Sr (0.05)	Includes: Cd (0.105) Cu (0.002)

The compositions of all standards used in microprobe analysis are listed here. Errors are ± 0.1 weight percent. Values used in analytical work are in bold type.

Table A-3
Analytical precision in microprobe analysis

Element	Pyroxene	Olivine	Spinel	Magnetite	Ilmenite
Na	5.4	n.a.	n.a.	n.a.	n.a.
Mg	2.1	1.8	3.1	4.3	4.1
Al	2.2	i.c.	2.6	3.0	4.8
Si	0.9	1.0	4.1	4.5	i.c.
P	n.a.	n.a.	n.a.	n.a.	n.a.
S	n.a.	n.a.	n.a.	n.a.	n.a.
Cl	n.a.	n.a.	n.a.	n.a.	n.a.
K	n.a.	n.a.	n.a.	n.a.	n.a.
Ca	1.2	6.5	n.a.	6.3	i.c.
Ti	3.7	i.c.	3.0	1.3	1.0
Cr	3.7	i.c.	1.7	3.2	i.c.
Mn	12.0	12.0	5.9	5.9	7.8
Fe	2.0	1.7	1.1	0.8	1.2
Ni	n.a.	12.0	7.2	i.c.	i.c.
Cu	n.a.	n.a.	n.a.	n.a.	n.a.
Zn	n.a.	n.a.	i.c.	i.c.	i.c.

Element	Feldspar	Glass	Amphibole	Apatite	Sulphide
Na	3.7	3.6	3.6	7.1	n.a.
Mg	n.a.	2.5	2.5	4.6	n.a.
Al	1.9	2.0	2.0	4.0	n.a.
Si	0.7	0.9	0.9	1.5	n.a.
P	n.a.	5.9	n.a.	1.2	n.a.
S	n.a.	i.c.	n.a.	i.c.	0.5
Cl	n.a.	7.1	n.a.	4.0	n.a.
K	5.3	3.5	3.5	i.c.	n.a.
Ca	1.6	1.6	1.6	0.8	n.a.
Ti	i.c.	2.7	2.7	i.c.	i.c.
Cr	n.a.	i.c.	i.c.	n.a.	i.c.
Mn	i.c.	12.0	12.0	i.c.	i.c.
Fe	6.1	1.8	1.8	6.5	1.3
Ni	n.a.	i.c.	i.c.	n.a.	0.8[1]
Cu	n.a.	n.a.	n.a.	n.a.	1.0[1]
Zn	i.c.	i.c.	i.c.	n.a.	i.c.

Precisions are given, for every element analysed in each species, at the 99% confidence level, as a percentage of the total concentration of that element. n.a. = not analysed. i.c. = insufficient concentration present. [1] = precision based on the maximum concentration in that phase.

APPENDIX B

MINERAL CHEMISTRY

Table B-1
Major element concentrations in clinopyroxene

Clinopyroxene analyses comprise major oxide concentrations, cation numbers of each ionic species, recalculated on the basis of six oxygen anions and the molecular percentages of major end members. The latter, together with the percentage of Fe^{3+}, are calculated using the method of Lindsley (1983). Analyses are in the order given below; on each page is a subheading listing the centres described thereon. The source of each analysis is identified by the two-letter suffix, and is plotted on each diagram of this work with the appropriate symbol, as follows:

Suffix	Symbol	Unit
SM	⍐	Spanish Mump
SB	⍐	Spanish Bonk
ST	⍍	Hyalo Ridge
SL	☒	Spanish Lake Centre
SC	⊞	Flourmill Centre
PY	+	Pyramid Mountain
SP	X	Spahats (Second Canyon dyke)
RM	🅈	Ray Mountain
RR	⇞	Ray Ridge
RC	⇞	Pointed Stick Cone
R	Δ	Dragon's Tongue
RP	Δ	Dragon's Tongue (proximal)
RD	Δ	Dragon's Tongue (distal)
KL	O	Kostal Lake
KP	O	Kostal Lake (older lavas)
KN	O	Kostal Lake (north cone)
KS	O	Kostal Lake (south cone)
KT	O	Kostal Lake (lava tube)

Analytical precisions for every element analysed in clinopyroxene are listed below at the 99% confidence level, as a percentage of the total concentration of that element.

Na	5.4
Mg	2.1
Al	2.2
Si	0.9
Ca	1.2
Ti	3.7
Cr	3.7
Mn	12.0
Fe	2.0

Sample numbers comprise three parts, interpreted as follows :

26/8/3(X)	CP1(X)C,M,R	-SB
Sample number (X if xenolith)	ClinoPyroxene 1 (X if xenocryst) Core, Median or Rim	Suite suffix

Table B-1 (continued): **CLINOPYROXENE**
Spanish Bonk

Sample	26/8/3 CP1C-SB	26/8/3 CP1R-SB	26/8/3 CP2C-SB	26/8/3 CP2R-SB	26/8/3 CP3C-SB
Major oxides (wt.%)					
SiO_2	47.6	48.9	46.6	48.4	47.0
TiO_2	2.1	2.4	2.4	2.0	2.2
Al_2O_3	8.4	5.2	9.1	5.5	8.3
Fe_2O_3	2.5	2.4	2.7	3.2	3.5
FeO	5.8	4.8	5.4	4.0	4.6
MnO	0.1	0.1	0.0	0.1	0.1
MgO	13.1	13.2	12.4	13.0	12.6
CaO	19.4	22.4	20.3	22.3	20.2
Na_2O	1.1	0.8	1.1	0.9	1.3
Cr_2O_3	0.3	0.3	0.0	0.3	0.1
Total	100.5	100.8	100.0	99.8	99.9
Cations on the basis of 6 oxygens					
Si	1.755	1.808	1.730	1.803	1.744
Ti	0.058	0.067	0.067	0.056	0.063
Al (IV)	0.245	0.192	0.270	0.197	0.256
Al (VI)	0.120	0.033	0.128	0.046	0.109
Fe^{3+}	0.070	0.067	0.076	0.089	0.097
Fe^{2+}	0.180	0.150	0.168	0.125	0.143
Mn	0.003	0.005	0.000	0.002	0.003
Mg	0.722	0.728	0.687	0.723	0.698
Ca	0.768	0.886	0.806	0.889	0.804
Na	0.069	0.051	0.067	0.058	0.079
Cr	0.007	0.009	0.000	0.007	0.004
End member percentages					
Ac	6.9	5.1	6.7	5.8	7.9
Jd	0.0	0.0	0.0	0.0	0.0
TiCaTs	5.8	6.7	6.7	5.6	6.3
FeCaTs	0.1	1.6	0.8	3.1	1.8
CrCaTs	0.7	0.9	0.0	0.7	0.4
AlCaTs	12.0	3.3	12.8	4.6	10.9
Wo	29.1	38.0	30.1	37.4	30.5
En	36.1	36.4	34.4	36.1	34.9
Fs	9.0	7.5	8.4	6.3	7.1
Wo(tern)	39.2	46.4	41.3	46.9	42.1
En(tern)	48.7	44.4	47.1	45.3	48.1
Fs(tern)	12.1	9.1	11.5	7.8	9.8

Table B-1 (continued): **CLINOPYROXENE**
Spanish Bonk to Hyalo Ridge

Sample	26/8/3 CP3R-SB	26/8/3 CP4C-SB	26/8/3 CP4R-SB	26/8/3 CP5G-SB	23/8/12 CP1G-ST
Major oxides (wt.%)					
SiO_2	46.9	51.4	48.6	49.6	50.0
TiO_2	2.1	0.3	2.3	2.0	1.4
Al_2O_3	8.1	1.5	5.2	4.4	4.1
Fe_2O_3	2.1	2.5	3.3	1.8	0.0
FeO	5.4	12.9	4.2	5.4	7.9
MnO	0.1	0.5	0.1	0.1	0.0
MgO	13.0	12.0	13.1	13.2	15.2
CaO	20.6	18.4	22.2	22.1	19.4
Na_2O	0.7	0.8	1.0	0.9	0.1
Cr_2O_3	0.4	0.0	0.4	0.3	0.8
Total	99.7	100.4	100.5	100.1	99.0
Cations on the basis of 6 oxygens					
Si	1.749	1.947	1.803	1.845	1.869
Ti	0.060	0.010	0.064	0.057	0.040
Al (IV)	0.251	0.053	0.197	0.155	0.137
Al (VI)	0.105	0.013	0.029	0.037	0.043
Fe^{3+}	0.059	0.072	0.092	0.051	0.000
Fe^{2+}	0.167	0.410	0.129	0.167	0.248
Mn	0.002	0.017	0.004	0.003	0.000
Mg	0.723	0.679	0.723	0.730	0.847
Ca	0.824	0.746	0.880	0.882	0.776
Na	0.044	0.053	0.064	0.057	0.009
Cr	0.012	0.000	0.012	0.010	0.023
End member percentages					
Ac	4.4	5.3	6.4	5.1	0.0
Jd	0.0	0.0	0.0	0.6	0.9
TiCaTs	6.0	1.0	6.4	5.7	4.0
FeCaTs	1.5	2.0	2.8	0.0	0.0
CrCaTs	1.2	0.0	1.2	1.0	2.3
AlCaTs	10.5	1.3	2.9	3.1	3.4
Wo	31.6	35.1	37.4	39.2	34.0
En	36.2	33.9	36.1	36.5	42.4
Fs	8.3	20.5	6.5	8.4	12.4
Wo(tern)	41.5	39.2	46.7	46.6	38.3
En(tern)	47.5	37.9	45.2	43.4	47.7
Fs(tern)	11.0	22.9	8.1	9.9	14.0

Table B-1 (continued): **CLINOPYROXENE**
Hyalo Ridge

Sample	23/8/12 CP2G-ST	23/8/12 CP3G-ST	23/8/6 CP1G-ST	23/8/6 CP2G-ST	23/8/6 CP3G-ST
Major oxides (wt.%)					
SiO_2	50.8	49.4	50.6	52.8	51.9
TiO_2	1.5	1.9	1.4	1.0	0.9
Al_2O_3	2.6	5.4	2.4	2.0	5.8
Fe_2O_3	0.7	0.2	0.5	0.0	0.0
FeO	8.9	8.4	11.5	10.3	9.4
MnO	0.1	0.2	0.2	0.3	0.3
MgO	14.7	15.1	14.6	15.3	12.7
CaO	20.2	19.1	17.7	19.2	16.8
Na_2O	0.3	0.2	0.3	0.2	1.0
Cr_2O_3	0.2	0.5	0.0	0.0	0.0
Total	100.0	100.3	99.1	101.1	98.8
Cations on the basis of 6 oxygens					
Si	1.897	1.826	1.911	1.943	1.931
Ti	0.042	0.053	0.039	0.027	0.024
Al (IV)	0.103	0.174	0.089	0.065	0.119
Al (VI)	0.010	0.062	0.018	0.024	0.136
Fe^{3+}	0.019	0.004	0.014	0.000	0.000
Fe^{2+}	0.276	0.259	0.363	0.318	0.293
Mn	0.003	0.006	0.005	0.008	0.008
Mg	0.816	0.833	0.821	0.837	0.705
Ca	0.809	0.758	0.718	0.757	0.670
Na	0.017	0.012	0.022	0.012	0.064
Cr	0.007	0.013	0.000	0.000	0.000
End member percentages					
Ac	1.7	0.4	1.4	0.0	0.0
Jd	0.0	0.7	0.7	1.2	6.4
TiCaTs	4.2	5.3	3.9	2.7	2.4
FeCaTs	0.2	0.0	0.0	0.0	0.0
CrCaTs	0.7	1.3	0.0	0.0	0.0
AlCaTs	1.0	5.5	1.1	1.1	7.1
Wo	37.4	31.8	33.4	35.9	28.8
En	40.8	41.7	41.0	41.8	35.2
Fs	13.8	12.9	18.2	15.9	14.7
Wo(tern)	40.6	36.8	36.1	38.4	36.6
En(tern)	44.3	48.2	44.3	44.7	44.8
Fs(tern)	15.0	15.0	19.6	17.0	18.6

Table B-1 (continued): **CLINOPYROXENE**
Spanish Lake

Sample	24/8/13 CP1C-SL	24/8/13 CP1M-SL	24/8/13 CP1R-SL	24/8/13 CP2C-SL	24/8/13 CP2R-SL
Major oxides (wt.%)					
SiO_2	51.9	49.9	48.5	49.8	46.5
TiO_2	0.3	0.8	2.2	1.6	3.4
Al_2O_3	3.0	5.5	5.4	4.6	6.6
Fe_2O_3	1.5	1.6	2.1	1.3	2.1
FeO	8.2	8.9	5.7	5.0	6.5
MnO	0.2	0.1	0.1	0.0	0.0
MgO	13.3	12.7	13.8	14.6	12.0
CaO	21.1	19.6	22.0	22.3	22.2
Na_2O	0.8	0.9	0.4	0.4	0.6
Cr_2O_3	0.1	0.1	0.1	0.3	0.0
Total	100.3	100.1	100.4	99.9	99.9
Cations on the basis of 6 oxygens					
Si	1.928	1.862	1.800	1.843	1.746
Ti	0.009	0.022	0.062	0.044	0.095
Al (IV)	0.072	0.138	0.200	0.157	0.254
Al (VI)	0.058	0.102	0.035	0.046	0.040
Fe^{3+}	0.043	0.045	0.060	0.036	0.059
Fe^{2+}	0.253	0.277	0.177	0.154	0.204
Mn	0.005	0.004	0.004	0.000	0.000
Mg	0.738	0.706	0.763	0.806	0.670
Ca	0.840	0.782	0.873	0.883	0.895
Na	0.051	0.058	0.022	0.022	0.036
Cr	0.003	0.003	0.003	0.010	0.000
End member percentages					
Ac	4.3	4.5	2.2	2.2	3.6
Jd	0.7	1.2	0.0	0.0	0.0
TiCaTs	0.9	2.2	6.2	4.4	9.5
FeCaTs	0.0	0.0	3.8	1.4	2.4
CrCaTs	0.3	0.3	0.3	1.0	0.0
AlCaTs	5.1	9.0	3.5	4.6	4.0
Wo	38.9	33.3	36.8	38.5	36.8
En	36.9	35.3	38.1	40.3	33.5
Fs	12.7	13.9	8.8	7.7	10.2
Wo(tern)	43.9	40.4	43.9	44.5	45.7
En(tern)	41.7	42.8	45.5	46.6	41.6
Fs(tern)	14.3	16.8	10.6	8.9	12.7

Table B-1 (continued): **CLINOPYROXENE**
Spanish Lake

Sample	24/8/13 CP3C-SL	24/8/13 CP3R-SL	24/8/13 CP4G-SL	24/8/13 CP5G-SL	24/8/14 CP1C-SL
Major oxides (wt.%)					
SiO_2	47.1	45.1	49.3	46.2	47.6
TiO_2	2.5	3.8	1.9	3.4	2.4
Al_2O_3	7.4	8.5	5.0	7.0	7.0
Fe_2O_3	2.1	2.7	2.1	2.5	2.7
FeO	4.9	5.4	5.4	6.2	4.3
MnO	0.0	0.0	0.1	0.1	0.1
MgO	13.1	11.9	14.4	12.0	13.3
CaO	22.3	22.2	21.9	22.0	22.5
Na_2O	0.4	0.6	0.3	0.6	0.5
Cr_2O_3	0.5	0.1	0.3	0.0	0.5
Total	100.3	100.4	100.9	100.0	100.9
Cations on the basis of 6 oxygens					
Si	1.746	1.684	1.816	1.732	1.753
Ti	0.069	0.107	0.052	0.096	0.066
Al (IV)	0.254	0.316	0.184	0.268	0.247
Al (VI)	0.069	0.057	0.034	0.042	0.057
Fe^{3+}	0.058	0.076	0.059	0.072	0.075
Fe^{2+}	0.152	0.169	0.167	0.196	0.133
Mn	0.000	0.000	0.004	0.003	0.002
Mg	0.723	0.663	0.790	0.672	0.732
Ca	0.888	0.887	0.862	0.883	0.888
Na	0.025	0.036	0.021	0.037	0.031
Cr	0.014	0.004	0.008	0.000	0.015
End member percentages					
Ac	2.5	3.6	2.1	3.7	3.1
Jd	0.0	0.0	0.0	0.0	0.0
TiCaTs	6.9	10.7	5.2	9.6	6.6
FeCaTs	3.3	4.0	3.8	3.5	4.4
CrCaTs	1.4	0.4	0.8	0.0	1.5
AlCaTs	6.9	5.7	3.4	4.2	5.7
Wo	35.1	33.9	36.5	35.6	35.3
En	36.2	33.1	39.5	33.6	36.6
Fs	7.6	8.4	8.4	9.8	6.6
Wo(tern)	44.5	44.9	43.3	45.0	45.0
En(tern)	45.8	43.9	46.8	42.6	46.6
Fs(tern)	9.6	11.2	9.9	12.4	8.5

Table B-1 (continued): **CLINOPYROXENE**
Spanish Lake to Flourmill

Sample	24/8/14 CP1R-SL	24/8/14 CP2G-SL	24/8/14 CP3G-SL	24/8/14 CP4G-SL	2/8/6 CP1XC-SC
Major oxides (wt.%)					
SiO_2	49.7	49.5	48.0	46.6	46.6
TiO_2	1.9	2.1	2.7	2.7	2.4
Al_2O_3	4.3	3.9	5.0	7.4	8.7
Fe_2O_3	0.8	1.6	2.0	2.4	3.1
FeO	6.1	7.4	7.0	5.3	6.0
MnO	0.0	0.1	0.1	0.1	0.1
MgO	14.3	13.4	13.6	12.8	11.6
CaO	22.3	21.7	21.3	22.1	19.7
Na_2O	0.2	0.5	0.2	0.4	1.4
Cr_2O_3	0.2	0.0	0.0	0.5	0.0
Total	99.9	100.2	100.0	100.4	99.7
Cations on the basis of 6 oxygens					
Si	1.846	1.848	1.795	1.733	1.743
Ti	0.053	0.058	0.075	0.077	0.066
Al (IV)	0.154	0.152	0.205	0.267	0.257
Al (VI)	0.034	0.019	0.014	0.057	0.126
Fe^{3+}	0.023	0.044	0.057	0.067	0.089
Fe^{2+}	0.191	0.231	0.220	0.166	0.187
Mn	0.000	0.004	0.004	0.003	0.004
Mg	0.790	0.746	0.760	0.708	0.647
Ca	0.888	0.867	0.855	0.879	0.788
Na	0.014	0.028	0.015	0.025	0.090
Cr	0.006	0.000	0.000	0.014	0.000
End member percentages					
Ac	1.4	2.8	1.5	2.5	8.9
Jd	0.0	0.0	0.0	0.0	0.1
TiCaTs	5.3	5.8	7.5	7.7	6.6
FeCaTs	0.9	1.6	4.2	4.3	0.0
CrCaTs	0.6	0.0	0.0	1.4	0.0
AlCaTs	3.4	1.9	1.4	5.7	12.4
Wo	39.3	38.7	36.2	34.5	29.9
En	39.5	37.3	38.0	35.4	32.4
Fs	9.5	11.5	11.0	8.3	9.3
Wo(tern)	44.5	44.2	42.5	44.1	41.7
En(tern)	44.7	42.6	44.6	45.3	45.2
Fs(tern)	10.8	13.2	12.9	10.6	13.0

Table B-1 (continued): **CLINOPYROXENE**
Flourmill

Sample	2/8/6 CP1XR-SC	2/8/6 CP2XC-SC	2/8/6 CP2XM-SC	2/8/6 CP2XR-SC	2/8/6 CP3C-SC
Major oxides (wt.%)					
SiO_2	47.2	49.8	49.5	48.3	49.5
TiO_2	2.3	0.6	0.6	2.0	1.1
Al_2O_3	7.1	4.4	4.5	5.5	7.3
Fe_2O_3	2.5	2.7	2.9	2.6	2.0
FeO	4.5	8.6	9.4	4.4	5.4
MnO	0.1	0.3	0.4	0.1	0.1
MgO	13.4	12.7	13.1	14.2	15.7
CaO	22.0	19.3	17.7	21.7	18.2
Na_2O	0.4	0.9	1.0	0.5	0.8
Cr_2O_3	0.3	0.1	0.0	0.3	0.1
Total	100.0	99.6	99.1	99.6	100.2
Cations on the basis of 6 oxygens					
Si	1.755	1.875	1.870	1.798	1.810
Ti	0.064	0.017	0.018	0.055	0.030
Al (IV)	0.245	0.125	0.130	0.202	0.190
Al (VI)	0.065	0.071	0.072	0.039	0.123
Fe^{3+}	0.070	0.076	0.084	0.073	0.054
Fe^{2+}	0.138	0.272	0.297	0.136	0.165
Mn	0.003	0.010	0.011	0.003	0.003
Mg	0.742	0.714	0.737	0.790	0.856
Ca	0.877	0.779	0.718	0.865	0.712
Na	0.028	0.057	0.063	0.030	0.051
Cr	0.010	0.003	0.000	0.009	0.004
End member percentages					
Ac	2.8	5.7	6.3	3.0	5.1
Jd	0.0	0.0	0.0	0.0	0.0
TiCaTs	6.4	1.7	1.8	5.5	3.0
FeCaTs	4.2	1.9	2.1	4.3	0.3
CrCaTs	1.0	0.3	0.0	0.9	0.4
AlCaTs	6.5	7.1	7.2	3.9	12.3
Wo	34.8	33.5	30.3	35.9	27.6
En	37.1	35.7	36.9	39.5	42.8
Fs	6.9	13.6	14.9	6.8	8.2
Wo(tern)	44.1	40.5	37.0	43.7	35.1
En(tern)	47.1	43.1	44.9	48.1	54.4
Fs(tern)	8.8	16.4	18.1	8.2	10.5

Table B-1 (continued): **CLINOPYROXENE**
Flourmill

Sample	2/8/6 CP3R-SC	2/8/6 CP4C-SC	2/8/6 CP4R-SC	2/8/6 CP5G-SC	2/8/6 CP6G-SC
Major oxides (wt.%)					
SiO_2	46.1	47.5	44.8	49.8	46.7
TiO_2	2.4	2.2	3.6	1.4	2.6
Al_2O_3	8.3	7.0	7.9	4.3	5.9
Fe_2O_3	3.7	2.7	2.5	2.4	3.9
FeO	3.9	4.1	5.9	3.8	5.3
MnO	0.0	0.0	0.1	0.1	0.1
MgO	12.8	13.8	11.8	15.1	12.6
CaO	21.5	21.8	21.6	21.8	21.6
Na_2O	0.8	0.5	0.5	0.5	0.7
Cr_2O_3	0.3	0.0	0.2	0.6	0.1
Total	99.8	99.7	99.0	99.8	99.5
Cations on the basis of 6 oxygens					
Si	1.718	1.764	1.699	1.841	1.760
Ti	0.067	0.060	0.104	0.039	0.073
Al (IV)	0.282	0.236	0.301	0.159	0.240
Al (VI)	0.084	0.072	0.052	0.030	0.022
Fe^{3+}	0.103	0.075	0.071	0.067	0.109
Fe^{2+}	0.121	0.128	0.186	0.117	0.167
Mn	0.000	0.000	0.003	0.003	0.004
Mg	0.713	0.763	0.668	0.833	0.705
Ca	0.857	0.868	0.875	0.862	0.873
Na	0.047	0.031	0.034	0.033	0.041
Cr	0.009	0.000	0.006	0.016	0.003
End member percentages					
Ac	4.7	3.1	3.4	3.3	4.1
Jd	0.0	0.0	0.0	0.0	0.0
TiCaTs	6.7	6.0	10.4	3.9	7.3
FeCaTs	5.6	4.3	3.7	3.5	6.8
CrCaTs	0.9	0.0	0.6	1.6	0.3
AlCaTs	8.4	7.2	5.2	3.0	2.2
Wo	32.1	34.7	33.9	37.1	35.3
En	35.6	38.1	33.4	41.6	35.2
Fs	6.1	6.4	9.3	5.9	8.3
Wo(tern)	43.5	43.8	44.2	43.9	44.8
En(tern)	48.3	48.1	43.6	49.2	44.7
Fs(tern)	8.2	8.1	12.1	6.9	10.6

Table B-1 (continued): **CLINOPYROXENE**
Flourmill

Sample	4/8/7 CP1C-SC	4/8/7 CP1R-SC	4/8/7 CP2G-SC	4/8/7 CP3G-SC	4/8/7 CP4G-SC
Major oxides (wt.%)					
SiO_2	51.7	44.0	50.1	43.1	43.2
TiO_2	0.3	4.0	1.9	4.7	4.2
Al_2O_3	3.6	10.0	4.4	9.1	10.5
Fe_2O_3	1.3	3.7	1.7	4.1	4.4
FeO	5.3	4.5	5.4	6.6	4.0
MnO	0.1	0.1	0.1	0.1	0.0
MgO	14.7	11.9	14.5	10.8	11.5
CaO	23.3	21.9	22.5	21.1	22.0
Na_2O	0.1	0.5	0.3	0.7	0.7
Cr_2O_3	0.1	0.4	0.3	0.1	0.3
Total	100.8	101.1	101.5	100.5	100.9
Cations on the basis of 6 oxygens					
Si	1.897	1.632	1.835	1.626	1.607
Ti	0.009	0.111	0.051	0.133	0.117
Al (IV)	0.103	0.368	0.165	0.374	0.393
Al (VI)	0.053	0.067	0.026	0.031	0.066
Fe^{3+}	0.036	0.104	0.046	0.115	0.123
Fe^{2+}	0.163	0.140	0.165	0.208	0.125
Mn	0.005	0.003	0.002	0.004	0.000
Mg	0.805	0.655	0.789	0.609	0.638
Ca	0.915	0.872	0.883	0.851	0.877
Na	0.006	0.033	0.019	0.042	0.041
Cr	0.004	0.010	0.009	0.003	0.010
End member percentages					
Ac	0.6	3.3	1.9	4.2	4.1
Jd	0.0	0.0	0.0	0.0	0.0
TiCaTs	0.9	11.1	5.1	13.3	11.7
FeCaTs	3.0	7.0	2.7	7.3	8.2
CrCaTs	0.4	1.0	0.9	0.3	1.0
AlCaTs	5.3	6.7	2.6	3.1	6.6
Wo	41.0	30.7	38.5	30.5	30.1
En	40.3	32.8	39.4	30.4	31.9
Fs	8.2	7.0	8.3	10.4	6.3
Wo(tern)	45.9	43.6	44.6	42.8	44.1
En(tern)	45.0	46.5	45.8	42.7	46.7
Fs(tern)	9.1	9.9	9.6	14.6	9.2

Table B-1 (continued): **CLINOPYROXENE**
Flourmill

Sample	4/8/7	4/8/1	4/8/1	4/8/1	4/8/1
	CP5G-SC	CP1C-SC	CP1R-SC	CP2C-SC	CP2R-SC
Major oxides (wt.%)					
SiO_2	49.4	51.5	48.7	50.8	49.3
TiO_2	2.0	0.6	1.8	1.0	1.5
Al_2O_3	5.0	5.6	5.9	5.1	5.2
Fe_2O_3	2.1	1.0	1.6	2.1	2.5
FeO	5.4	4.9	5.3	4.0	4.1
MnO	0.0	0.1	0.1	0.1	0.1
MgO	14.5	17.2	14.2	15.6	14.4
CaO	22.0	19.0	21.9	21.2	22.1
Na_2O	0.4	0.5	0.2	0.6	0.5
Cr_2O_3	0.4	0.5	0.6	0.6	0.6
Total	101.2	101.1	100.5	101.0	100.4
Cations on the basis of 6 oxygens					
Si	1.813	1.859	1.798	1.846	1.817
Ti	0.056	0.016	0.049	0.026	0.042
Al (IV)	0.187	0.141	0.202	0.154	0.183
Al (VI)	0.030	0.096	0.056	0.065	0.045
Fe^{3+}	0.058	0.028	0.044	0.058	0.068
Fe^{2+}	0.166	0.148	0.164	0.121	0.127
Mn	0.000	0.004	0.003	0.003	0.003
Mg	0.791	0.923	0.780	0.845	0.793
Ca	0.864	0.733	0.866	0.826	0.872
Na	0.022	0.030	0.015	0.039	0.032
Cr	0.010	0.015	0.019	0.017	0.017
End member percentages					
Ac	2.2	2.8	1.5	3.9	3.2
Jd.	0.0	0.3	0.0	0.0	0.0
TiCaTs	5.6	1.6	4.9	2.6	4.2
FeCaTs	3.6	0.0	2.9	1.9	3.6
CrCaTs	1.0	1.5	1.9	1.7	1.7
AlCaTs	3.0	9.4	5.6	6.5	4.5
Wo	36.7	30.4	35.6	34.9	36.6
En	39.6	46.1	39.0	42.2	39.6
Fs	8.3	7.4	8.2	6.0	6.4
Wo(tern)	43.4	36.2	43.0	42.0	44.3
En(tern)	46.8	54.9	47.1	50.8	48.0
Fs(tern)	9.8	8.8	9.9	7.2	7.7

Table B-1 (continued): **CLINOPYROXENE**
Flourmill

Sample	4/8/1 CP3C-SC	4/8/1 CP3R-SC	4/8/1 CP3R-SC	4/8/1 CP4C-SC	4/8/1 CP4M-SC
Major oxides (wt.%)					
SiO_2	49.6	50.5	45.8	51.7	50.5
TiO_2	1.4	1.4	2.9	0.4	1.1
Al_2O_3	5.9	4.4	8.7	3.5	4.9
Fe_2O_3	1.8	1.5	3.3	1.3	1.5
FeO	4.8	5.1	4.7	8.9	4.6
MnO	0.1	0.1	0.1	0.2	0.0
MgO	14.7	15.1	12.5	13.3	15.4
CaO	21.5	22.0	22.0	20.9	21.6
Na_2O	0.4	0.3	0.5	0.6	0.4
Cr_2O_3	0.2	0.5	0.1	0.2	0.4
Total	100.6	101.2	100.6	100.9	100.6
Cations on the basis of 6 oxygens					
Si	1.819	1.847	1.697	1.913	1.848
Ti	0.038	0.038	0.080	0.010	0.031
Al (IV)	0.181	0.153	0.303	0.087	0.152
Al (VI)	0.076	0.038	0.078	0.064	0.060
Fe^{3+}	0.051	0.040	0.092	0.036	0.042
Fe^{2+}	0.148	0.157	0.145	0.276	0.139
Mn	0.004	0.003	0.003	0.006	0.000
Mg	0.805	0.823	0.690	0.734	0.838
Ca	0.846	0.864	0.873	0.829	0.848
Na	0.026	0.016	0.032	0.039	0.024
Cr	0.005	0.015	0.004	0.004	0.012
End member percentages					
Ac	2.6	1.6	3.2	3.6	2.4
Jd	0.0	0.0	0.0	0.3	0.0
TiCaTs	3.8	3.8	8.0	1.0	3.1
FeCaTs	2.4	2.4	6.0	0.0	1.8
CrCaTs	0.5	1.5	0.4	0.4	1.2
AlCaTs	7.6	3.8	7.8	6.1	6.0
Wo	35.2	37.4	32.5	37.7	36.3
En	40.2	41.2	34.5	36.7	41.9
Fs	7.4	7.8	7.3	13.8	7.0
Wo(tern)	42.5	43.3	43.8	42.7	42.6
En(tern)	48.6	47.6	46.4	41.6	49.2
Fs(tern)	8.9	9.1	9.8	15.6	8.2

Table B-1 (continued): **CLINOPYROXENE**
Flourmill

Sample	4/8/1 CP4R-SC	4/8/1 CP5C-SC	4/8/1 CP6G-SC	4/8/1 CP5R-SC	4/8/2 CP1C-SC
Major oxides (wt.%)					
SiO_2	46.9	48.5	46.8	46.7	51.6
TiO_2	2.2	2.3	2.4	2.5	0.9
Al_2O_3	7.6	4.8	7.7	7.7	4.9
Fe_2O_3	3.5	2.7	2.9	2.4	1.3
FeO	4.4	7.1	5.4	5.1	4.0
MnO	0.1	0.2	0.1	0.0	0.1
MgO	12.9	13.5	12.8	13.0	15.8
CaO	22.0	21.2	21.9	22.0	21.5
Na_2O	0.6	0.4	0.4	0.4	0.6
Cr_2O_3	0.3	0.2	0.4	0.6	0.2
Total	100.5	100.9	101.0	100.7	101.1
Cations on the basis of 6 oxygens					
Si	1.737	1.800	1.731	1.731	1.868
Ti	0.062	0.065	0.067	0.069	0.024
Al (IV)	0.263	0.200	0.269	0.269	0.132
Al (VI)	0.067	0.011	0.067	0.067	0.079
Fe^{3+}	0.098	0.076	0.081	0.068	0.035
Fe^{2+}	0.136	0.220	0.168	0.159	0.123
Mn	0.003	0.006	0.003	0.000	0.003
Mg	0.714	0.746	0.703	0.716	0.854
Ca	0.875	0.845	0.867	0.875	0.836
Na	0.035	0.023	0.025	0.022	0.036
Cr	0.010	0.006	0.012	0.017	0.005
End member percentages					
Ac	3.5	2.3	2.5	2.2	3.5
Jd	0.0	0.0	0.0	0.0	0.2
TiCaTs	6.2	6.5	6.7	6.9	2.4
FeCaTs	6.3	5.3	5.6	4.6	0.0
CrCaTs	1.0	0.6	1.2	1.7	0.5
AlCaTs	6.7	1.1	6.7	6.7	7.8
Wo	33.7	35.5	33.3	33.8	36.4
En	35.7	37.3	35.2	35.8	42.7
Fs	6.8	11.0	8.4	8.0	6.1
Wo(tern)	44.2	42.3	43.3	43.6	42.7
En(tern)	46.8	44.5	45.8	46.2	50.1
Fs(tern)	8.9	13.1	10.9	10.3	7.2

Table B-1 (continued): **CLINOPYROXENE**
Flourmill to Ray Mountain

Sample	4/8/2 CP1R-SC	4/8/2 CP2C-SC	4/8/2 CP2R-SC	4/8/2 CP3G-SC	17/8/7 CP2G-RM
Major oxides (wt.%)					
SiO_2	50.0	47.2	46.9	49.0	47.5
TiO_2	1.8	2.4	2.8	1.8	2.7
Al_2O_3	4.4	7.5	6.9	4.9	5.7
Fe_2O_3	1.8	2.8	2.1	2.7	3.3
FeO	5.4	4.4	6.6	4.9	5.7
MnO	0.0	0.1	0.1	0.1	0.1
MgO	14.3	13.1	12.3	14.3	12.0
CaO	22.4	22.3	21.8	21.8	22.2
Na_2O	0.5	0.5	0.4	0.4	0.9
Cr_2O_3	0.3	0.5	0.1	0.4	0.0
Total	100.9	101.0	100.2	100.5	100.2
Cations on the basis of 6 oxygens					
Si	1.839	1.741	1.752	1.812	1.779
Ti	0.050	0.065	0.078	0.051	0.077
Al (IV)	0.161	0.259	0.248	0.188	0.221
Al (VI)	0.031	0.066	0.057	0.023	0.031
Fe^{3+}	0.049	0.079	0.060	0.077	0.092
Fe^{2+}	0.166	0.137	0.207	0.151	0.178
Mn	0.000	0.003	0.003	0.003	0.004
Mg	0.786	0.719	0.686	0.790	0.668
Ca	0.881	0.880	0.873	0.863	0.891
Na	0.028	0.030	0.028	0.027	0.057
Cr	0.008	0.014	0.003	0.013	0.000
End member percentages					
Ac	2.8	3.0	2.8	2.7	5.7
Jd	0.0	0.0	0.0	0.0	0.0
TiCaTs	5.0	6.5	7.8	5.1	7.7
FeCaTs	2.2	4.8	3.2	5.0	3.6
CrCaTs	0.8	1.4	0.3	1.3	0.0
AlCaTs	3.1	6.6	5.7	2.3	3.1
Wo	38.5	34.3	35.2	36.3	37.3
En	39.3	35.9	34.3	39.5	33.4
Fs	8.3	6.8	10.3	7.6	8.9
Wo(tern)	44.7	44.5	44.1	43.5	46.9
En(tern)	45.6	46.6	43.0	47.4	41.9
Fs(tern)	9.7	8.9	13.0	9.1	11.2

Table B-1 (continued): **CLINOPYROXENE**
Ray Mountain

Sample	17/8/13 CP1XC-RM	17/8/13 CP1XR-RM	17/8/13 CP2XR-RM	17/8/13 CP3XC-RM	17/8/13 CP3XR-RM
Major oxides (wt.%)					
SiO_2	49.1	45.5	52.8	49.2	44.5
TiO_2	1.4	3.3	0.8	1.7	3.7
Al_2O_3	6.8	8.4	1.5	5.7	9.0
Fe_2O_3	2.6	2.8	1.7	2.8	3.7
FeO	4.2	5.3	5.9	4.4	4.7
MnO	0.1	0.1	0.1	0.1	0.0
MgO	14.8	12.4	14.4	14.5	12.0
CaO	21.1	22.1	22.3	22.1	22.1
Na_2O	0.5	0.4	0.9	0.4	0.5
Cr_2O_3	0.1	0.4	0.5	0.1	0.4
Total	101.0	100.9	101.0	101.1	100.7
Cations on the basis of 6 oxygens					
Si	1.794	1.690	1.943	1.802	1.657
Ti	0.040	0.094	0.021	0.048	0.103
Al (IV)	0.206	0.310	0.057	0.198	0.343
Al (VI)	0.086	0.056	0.008	0.049	0.052
Fe^{3+}	0.071	0.078	0.047	0.076	0.104
Fe^{2+}	0.127	0.165	0.181	0.135	0.148
Mn	0.003	0.003	0.004	0.003	0.000
Mg	0.805	0.685	0.789	0.790	0.668
Ca	0.826	0.880	0.877	0.868	0.882
Na	0.033	0.022	0.054	0.026	0.031
Cr	0.004	0.011	0.014	0.003	0.012
End member percentages					
Ac	3.3	2.2	4.7	2.6	3.1
Jd	0.0	0.0	0.7	0.0	0.0
TiCaTs	4.0	9.4	2.1	4.8	10.3
FeCaTs	3.7	5.5	0.0	5.0	7.3
CrCaTs	0.4	1.1	1.4	0.3	1.2
AlCaTs	8.6	5.6	0.1	4.9	5.2
Wo	33.0	33.2	42.1	35.9	32.1
En	40.3	34.2	39.4	39.5	33.4
Fs	6.4	8.2	9.1	6.7	7.4
Wo(tern)	41.5	43.8	46.5	43.7	44.0
En(tern)	50.6	45.3	43.5	48.1	45.8
Fs(tern)	8.0	10.9	10.0	8.2	10.1

Table B-1 (continued): **CLINOPYROXENE**
Ray Mountain

Sample	17/8/13 CP4C-RM	17/8/13 CP4R-RM	17/8/13 CP5C-RM	17/8/13 CP5R-RM	17/8/13 CP7G-RM
Major oxides (wt.%)					
SiO_2	52.3	49.3	51.8	48.5	47.7
TiO_2	0.6	2.0	0.3	2.0	3.1
Al_2O_3	2.6	4.5	2.7	5.5	5.7
Fe_2O_3	3.2	2.2	1.2	3.0	4.9
FeO	6.8	6.2	10.4	5.0	4.0
MnO	0.2	0.1	0.3	0.1	0.1
MgO	15.5	14.3	13.0	14.0	12.7
CaO	19.6	21.6	20.9	21.6	21.5
Na_2O	0.9	0.3	0.4	0.5	1.3
Cr_2O_3	0.1	0.2	0.1	0.4	0.0
Total	101.7	100.8	101.0	100.6	101.2
Cations on the basis of 6 oxygens					
Si	1.909	1.823	1.929	1.794	1.763
Ti	0.017	0.055	0.007	0.056	0.085
Al (IV)	0.091	0.177	0.071	0.206	0.237
Al (VI)	0.019	0.017	0.046	0.033	0.012
Fe^{3+}	0.087	0.061	0.033	0.082	0.137
Fe^{2+}	0.206	0.192	0.322	0.154	0.125
Mn	0.006	0.004	0.009	0.003	0.004
Mg	0.842	0.787	0.718	0.773	0.699
Ca	0.766	0.856	0.832	0.857	0.853
Na	0.053	0.017	0.026	0.031	0.083
Cr	0.003	0.007	0.003	0.011	0.000
End member percentages					
Ac	5.3	1.7	2.6	3.1	8.3
Jd	0.0	0.0	0.0	0.0	0.0
TiCaTs	1.7	5.5	0.7	5.6	8.5
FeCaTs	3.3	4.4	0.7	5.1	5.4
CrCaTs	0.3	0.7	0.3	1.1	0.0
AlCaTs	1.9	1.7	4.6	3.3	1.2
Wo	34.6	36.7	38.4	35.3	35.1
En	42.1	39.4	35.9	38.6	35.0
Fs	10.3	9.6	16.1	7.7	6.2
Wo(tern)	39.8	42.8	42.5	43.2	46.0
En(tern)	48.4	46.0	39.7	47.3	45.9
Fs(tern)	11.8	11.2	17.8	9.5	8.2

Table B-1 (continued): **CLINOPYROXENE**
Ray Mountain to Ray Ridge

Sample	17/8/1 CP1XC-RM	17/8/1 CP1XR-RM	19/8/1 CP1G-RM	19/8/1 CP2C-RM	18/8/9 CP1C-RR
Major oxides (wt.%)					
SiO_2	48.1	50.0	46.6	48.3	52.1
TiO_2	1.5	1.2	3.2	2.2	0.2
Al_2O_3	7.0	5.3	6.0	4.3	0.6
Fe_2O_3	3.0	2.1	2.1	1.9	0.5
FeO	5.1	5.3	6.8	6.9	14.6
MnO	0.1	0.1	0.1	0.2	0.9
MgO	14.6	15.6	12.3	12.3	11.9
CaO	20.0	19.5	21.8	22.2	17.9
Na_2O	0.5	0.6	0.4	0.5	0.7
Cr_2O_3	0.1	0.4	0.0	0.1	0.0
Total	100.1	100.3	99.4	99.1	99.3
Cations on the basis of 6 oxygens					
Si	1.777	1.836	1.760	1.830	1.996
Ti	0.043	0.034	0.090	0.062	0.005
Al (IV)	0.223	0.164	0.240	0.170	0.004
Al (VI)	0.082	0.064	0.026	0.022	0.023
Fe^{3+}	0.082	0.059	0.060	0.055	0.016
Fe^{2+}	0.156	0.164	0.214	0.219	0.468
Mn	0.005	0.004	0.005	0.005	0.029
Mg	0.805	0.857	0.693	0.694	0.681
Ca	0.791	0.768	0.881	0.901	0.734
Na	0.030	0.036	0.026	0.033	0.044
Cr	0.003	0.010	0.000	0.002	0.000
End member percentages					
Ac	3.0	3.6	2.6	3.3	1.6
Jd	0.0	0.0	0.0	0.0	2.9
TiCaTs	4.3	3.4	9.0	6.2	0.5
FeCaTs	5.2	2.2	3.4	2.2	0.0
CrCaTs	0.3	1.0	0.0	0.2	0.0
AlCaTs	8.2	6.4	2.6	2.2	-0.6
Wo	30.5	31.9	36.6	39.7	36.7
En	40.3	42.8	34.6	34.7	34.1
Fs	7.8	8.2	10.7	11.0	23.4
Wo(tern)	38.9	38.5	44.6	46.5	39.0
En(tern)	51.2	51.6	42.3	40.7	36.2
Fs(tern)	9.9	9.9	13.1	12.8	24.9

Table B-1 (continued): **CLINOPYROXENE**
Ray Ridge

Sample	18/8/9 CP1R-RR	18/8/9 CP2C-RR	18/8/9 CP3C-RR	18/8/9 CP3R-RR	18/8/9 CP4G-RR
Major oxides (wt.%)					
SiO_2	47.4	50.6	51.7	46.7	50.0
TiO_2	2.6	0.6	0.7	2.1	1.3
Al_2O_3	5.2	4.7	2.5	7.0	4.1
Fe_2O_3	2.6	1.1	2.4	3.0	1.4
FeO	5.5	4.4	5.3	4.1	5.6
MnO	0.1	0.0	0.1	0.0	0.1
MgO	12.9	15.8	15.5	13.1	15.2
CaO	21.9	20.1	20.4	21.9	20.8
Na_2O	0.6	0.7	0.8	0.6	0.4
Cr_2O_3	0.0	1.3	0.2	0.8	0.6
Total	98.8	99.3	99.8	99.3	99.5
Cations on the basis of 6 oxygens					
Si	1.792	1.867	1.914	1.748	1.858
Ti	0.073	0.018	0.020	0.060	0.036
Al (IV)	0.208	0.133	0.086	0.252	0.142
Al (VI)	0.024	0.073	0.021	0.059	0.036
Fe^{3+}	0.073	0.031	0.067	0.084	0.038
Fe^{2+}	0.175	0.136	0.164	0.127	0.175
Mn	0.003	0.000	0.005	0.000	0.004
Mg	0.729	0.871	0.855	0.730	0.841
Ca	0.888	0.794	0.810	0.879	0.828
Na	0.035	0.042	0.049	0.036	0.022
Cr	0.000	0.037	0.007	0.024	0.018
End member percentages					
Ac	3.5	3.1	4.9	3.6	2.2
Jd	0.0	1.1	0.0	0.0	0.0
TiCaTs	7.3	1.8	2.0	6.0	3.6
FeCaTs	3.8	0.0	1.8	4.8	1.6
CrCaTs	0.0	3.7	0.7	2.4	1.8
AlCaTs	2.4	6.2	2.1	5.9	3.6
Wo	37.7	33.9	37.2	34.4	36.1
En	36.5	43.5	42.8	36.5	42.0
Fs	8.8	6.8	8.2	6.4	8.7
Wo(tern)	45.4	40.2	42.2	44.5	41.5
En(tern)	44.0	51.7	48.5	47.2	48.4
Fs(tern)	10.6	8.1	9.3	8.2	10.0

Table B-1 (continued): **CLINOPYROXENE**
Pointed Stick Cone

Sample	18/8/4 CP1G-RC	18/8/4 CP2C-RC	18/8/4 CP2R-RC	18/8/4 CP3C-RC	18/8/4 CP3R-RC
Major oxides (wt.%)					
SiO_2	44.9	48.8	46.5	42.9	48.9
TiO_2	4.3	1.6	2.5	4.6	2.0
Al_2O_3	7.8	6.1	8.2	9.0	4.3
Fe_2O_3	2.9	2.3	2.4	5.1	1.2
FeO	6.2	6.6	6.4	4.7	7.5
MnO	0.0	0.1	0.0	0.1	0.1
MgO	11.4	13.7	12.5	10.5	13.2
CaO	21.7	18.8	19.1	22.1	21.4
Na_2O	0.8	1.1	1.1	0.9	0.4
Cr_2O_3	0.0	0.2	0.2	0.1	0.0
Total	100.0	99.6	99.2	99.9	99.3
Cations on the basis of 6 oxygens					
Si	1.690	1.818	1.745	1.625	1.843
Ti	0.122	0.046	0.072	0.130	0.058
Al (IV)	0.310	0.182	0.255	0.375	0.157
Al (VI)	0.035	0.088	0.108	0.026	0.034
Fe^{3+}	0.083	0.065	0.067	0.145	0.035
Fe^{2+}	0.195	0.204	0.202	0.148	0.236
Mn	0.000	0.003	0.001	0.003	0.004
Mg	0.641	0.763	0.699	0.591	0.739
Ca	0.875	0.752	0.769	0.896	0.865
Na	0.051	0.070	0.070	0.059	0.027
Cr	0.000	0.006	0.007	0.003	0.000
End member percentages					
Ac	5.1	6.5	6.7	5.9	2.7
Jd	0.0	0.5	0.3	0.0	0.0
TiCaTs	12.2	4.6	7.2	13.0	5.8
FeCaTs	3.2	0.0	0.0	8.6	0.8
CrCaTs	0.0	0.6	0.7	0.3	0.0
AlCaTs	3.5	8.4	10.4	2.6	3.4
Wo	34.3	30.8	29.3	32.5	38.3
En	32.0	38.2	35.0	29.5	36.9
Fs	9.7	10.2	10.1	7.4	11.8
Wo(tern)	45.1	38.9	39.4	46.8	44.0
En(tern)	42.1	48.2	47.0	42.5	42.5
Fs(tern)	12.8	12.9	13.6	10.7	13.6

Table B-1 (continued): **CLINOPYROXENE**
Dragon's Tongue (proximal)

Sample	14/8/1 CP1XR-RP	14/8/1 CP2C-RP	14/8/1 CP2R-RP	14/8/1 CP3C-RP	14/8/1 CP3R-RP
Major oxides (wt.%)					
SiO_2	45.9	48.0	48.1	48.9	44.3
TiO_2	2.7	0.4	0.5	0.6	3.5
Al_2O_3	6.7	6.4	6.4	5.1	8.0
Fe_2O_3	3.6	4.2	4.6	3.3	4.1
FeO	5.3	6.6	6.2	5.7	4.9
MnO	0.0	0.4	0.5	0.2	0.0
MgO	12.0	10.7	10.9	12.5	11.2
CaO	21.9	21.5	21.4	22.6	22.1
Na_2O	0.7	1.0	1.1	0.5	0.7
Cr_2O_3	0.0	0.0	0.0	0.0	0.0
Total	98.6	99.2	99.7	99.3	98.8
Cations on the basis of 6 oxygens					
Si	1.744	1.818	1.815	1.838	1.684
Ti	0.077	0.010	0.013	0.016	0.101
Al (IV)	0.256	0.182	0.185	0.162	0.316
Al (VI)	0.044	0.106	0.098	0.066	0.042
Fe^{3+}	0.102	0.120	0.130	0.095	0.118
Fe^{2+}	0.168	0.209	0.197	0.179	0.156
Mn	0.000	0.012	0.015	0.007	0.000
Mg	0.678	0.606	0.613	0.698	0.636
Ca	0.890	0.873	0.865	0.910	0.900
Na	0.042	0.064	0.069	0.030	0.047
Cr	0.000	0.000	0.000	0.000	0.000
End member percentages					
Ac	4.2	6.4	6.9	3.0	4.7
Jd	0.0	0.0	0.0	0.0	0.0
TiCaTs	7.7	1.0	1.3	1.6	10.1
FeCaTs	6.0	5.6	6.0	6.5	7.1
CrCaTs	0.0	0.0	0.0	0.0	0.0
AlCaTs	4.4	10.6	9.8	6.6	4.2
Wo	35.5	35.1	34.6	38.2	34.2
En	33.9	30.3	30.6	34.9	31.8
Fs	8.4	10.5	9.8	8.9	7.8
Wo(tern)	45.6	46.3	46.1	46.6	46.4
En(tern)	43.6	40.0	40.8	42.6	43.1
Fs(tern)	10.8	13.8	13.1	10.9	10.6

Table B-1 (continued): **CLINOPYROXENE**
Dragon's Tongue (proximal)

Sample	14/8/1 CP4C-RP	14/8/1 CP4R-RP	14/8/1 CP5G-RP	14/8/2 CP1C-RP	14/8/2 CP1R-RP
Major oxides (wt.%)					
SiO_2	52.1	45.8	41.9	52.0	47.2
TiO_2	0.0	2.6	4.7	0.2	2.4
Al_2O_3	2.6	7.4	9.7	2.9	6.6
Fe_2O_3	2.1	3.1	5.2	2.0	2.4
FeO	4.0	4.6	5.3	7.2	5.1
MnO	0.1	0.0	0.0	0.2	0.0
MgO	15.5	12.4	10.3	13.8	13.1
CaO	23.0	22.3	21.8	21.8	22.2
Na_2O	0.3	0.5	0.7	0.6	0.5
Cr_2O_3	0.0	0.3	0.0	0.0	0.4
Total	99.8	98.8	99.5	100.9	99.7
Cations on the basis of 6 oxygens					
Si	1.923	1.729	1.598	1.922	1.762
Ti	0.000	0.074	0.134	0.005	0.067
Al (IV)	0.077	0.271	0.402	0.078	0.238
Al (VI)	0.036	0.057	0.032	0.047	0.055
Fe^{3+}	0.059	0.088	0.148	0.057	0.067
Fe^{2+}	0.124	0.146	0.168	0.223	0.159
Mn	0.004	0.000	0.000	0.007	0.000
Mg	0.851	0.696	0.584	0.758	0.726
Ca	0.909	0.901	0.888	0.863	0.887
Na	0.017	0.030	0.047	0.037	0.028
Cr	0.000	0.008	0.000	0.000	0.012
End member percentages					
Ac	1.7	3.0	4.7	3.7	2.8
Jd	0.0	0.0	0.0	0.0	0.0
TiCaTs	0.0	7.4	13.4	0.5	6.7
FeCaTs	4.2	5.8	10.1	2.0	3.9
CrCaTs	0.0	0.8	0.0	0.0	1.2
AlCaTs	3.6	5.7	3.2	4.7	5.5
Wo	41.6	35.2	31.0	39.5	35.8
En	42.5	34.8	29.2	37.9	36.3
Fs	6.2	7.3	8.4	11.2	7.9
Wo(tern)	46.1	45.5	45.2	44.6	44.7
En(tern)	47.1	45.0	42.6	42.8	45.4
Fs(tern)	6.8	9.4	12.2	12.6	9.9

Table B-1 (continued): **CLINOPYROXENE**
Dragon's Tongue (proximal)

Sample	14/8/2 CP2C-RP	14/8/2 CP2R-RP	14/8/2 CP3C-RP	14/8/2 CP3R-RP	14/8/2 CP4XR-RP
Major oxides (wt.%)					
SiO_2	49.2	45.4	49.8	47.2	52.1
TiO_2	1.1	3.3	0.6	2.4	0.9
Al_2O_3	7.6	8.4	5.7	6.7	4.2
Fe_2O_3	2.6	3.0	3.0	3.7	0.0
FeO	4.2	4.9	4.3	3.9	9.9
MnO	0.1	0.0	0.0	0.1	0.3
MgO	14.8	12.2	14.4	13.3	16.1
CaO	19.8	22.3	21.5	22.5	16.1
Na_2O	0.9	0.5	0.7	0.6	0.5
Cr_2O_3	0.3	0.3	0.0	0.3	0.0
Total	100.8	100.4	99.9	100.8	100.2
Cations on the basis of 6 oxygens					
Si	1.793	1.692	1.838	1.746	1.914
Ti	0.031	0.094	0.017	0.068	0.026
Al (IV)	0.207	0.308	0.162	0.254	0.100
Al (VI)	0.120	0.062	0.084	0.040	0.081
Fe^{3+}	0.072	0.084	0.083	0.103	0.000
Fe^{2+}	0.126	0.154	0.133	0.121	0.304
Mn	0.004	0.000	0.000	0.003	0.008
Mg	0.806	0.675	0.790	0.730	0.883
Ca	0.774	0.890	0.852	0.889	0.635
Na	0.057	0.033	0.040	0.035	0.032
Cr	0.009	0.008	0.000	0.010	0.000
End member percentages					
Ac	5.7	3.3	4.0	3.5	0.0
Jd	0.0	0.0	0.0	0.0	3.2
TiCaTs	3.1	9.4	1.7	6.8	2.6
FeCaTs	1.5	5.0	4.3	6.8	0.0
CrCaTs	0.9	0.8	0.0	1.0	0.0
AlCaTs	12.0	6.2	8.4	4.0	4.9
Wo	29.9	33.8	35.4	35.2	28.0
En	40.3	33.7	39.5	36.5	44.1
Fs	6.3	7.7	6.6	6.0	15.2
Wo(tern)	39.1	44.9	43.4	45.3	32.1
En(tern)	52.7	44.8	48.5	47.0	50.5
Fs(tern)	8.3	10.2	8.1	7.8	17.4

Table B-1 (continued): **CLINOPYROXENE**
Dragon's Tongue (proximal) to Dragon's Tongue (distal)

Sample	14/8/2 CP4XR-RP	14/8/2 CP5G-RP	14/8/2 CP6G-RP	11/8/7 CP1G-RD	11/8/7 CP2G-RD
Major oxides (wt.%)					
SiO_2	45.4	48.3	48.6	43.6	46.3
TiO_2	3.1	1.7	2.1	3.7	2.7
Al_2O_3	8.2	8.8	4.7	8.8	6.7
Fe_2O_3	4.0	3.0	2.4	5.2	4.4
FeO	4.4	4.8	6.1	5.5	4.4
MnO	0.0	0.2	0.1	0.1	0.1
MgO	12.2	13.9	13.2	11.0	12.8
CaO	22.3	19.3	22.2	21.0	21.8
Na_2O	0.6	1.2	0.5	0.9	0.7
Cr_2O_3	0.2	0.0	0.0	0.1	0.4
Total	100.3	101.1	99.9	99.9	100.2
Cations on the basis of 6 oxygens					
Si	1.694	1.759	1.819	1.648	1.729
Ti	0.086	0.045	0.058	0.106	0.075
Al (IV)	0.306	0.241	0.181	0.352	0.271
Al (VI)	0.054	0.139	0.027	0.041	0.024
Fe^{3+}	0.112	0.083	0.067	0.149	0.124
Fe^{2+}	0.137	0.145	0.192	0.175	0.137
Mn	0.000	0.005	0.004	0.003	0.002
Mg	0.676	0.757	0.733	0.618	0.713
Ca	0.890	0.754	0.889	0.851	0.871
Na	0.039	0.072	0.029	0.054	0.040
Cr	0.007	0.000	0.000	0.004	0.013
End member percentages					
Ac	3.9	7.2	2.9	5.4	4.0
Jd	0.0	0.0	0.0	0.0	0.0
TiCaTs	8.6	4.5	5.8	10.6	7.5
FeCaTs	7.4	1.1	3.8	9.5	8.3
CrCaTs	0.7	0.0	0.0	0.4	1.3
AlCaTs	5.4	13.9	2.7	4.1	2.4
Wo	33.5	27.9	38.3	30.2	33.8
En	33.8	37.8	36.7	30.9	35.7
Fs	6.9	7.3	9.6	8.7	6.9
Wo(tern)	45.2	38.3	45.3	43.3	44.3
En(tern)	45.6	51.8	43.4	44.2	46.7
Fs(tern)	9.3	9.9	11.4	12.5	9.0

Table B-1 (continued): **CLINOPYROXENE**
Dragon's Tongue (distal) to Kostal Lake (older lavas)

Sample	11/8/7 CP3G-RD	31/8/8 CP1M-KP	31/8/8 CP1C-KP	31/8/8 CP1M-KP	31/8/8 CP2C-KP
Major oxides (wt.%)					
SiO_2	46.5	51.0	50.9	51.1	50.7
TiO_2	2.9	2.0	0.7	1.3	0.4
Al_2O_3	6.4	13.9	4.5	9.1	5.1
Fe_2O_3	3.1	0.0	1.3	0.0	2.9
FeO	5.6	10.5	5.4	6.6	6.5
MnO	0.0	0.1	0.1	0.0	0.3
MgO	12.7	8.3	15.7	11.9	12.8
CaO	21.7	12.7	20.7	17.8	20.0
Na_2O	0.5	2.1	0.4	1.2	1.4
Cr_2O_3	0.3	0.0	0.1	0.0	0.0
Total	99.6	100.6	100.0	99.0	100.0
Cations on the basis of 6 oxygens					
Si	1.747	1.842	1.872	1.876	1.882
Ti	0.081	0.054	0.020	0.035	0.010
Al (IV)	0.253	0.290	0.128	0.196	0.118
Al (VI)	0.031	0.302	0.069	0.198	0.106
Fe^{3+}	0.086	0.000	0.035	0.000	0.081
Fe^{2+}	0.176	0.318	0.165	0.202	0.202
Mn	0.000	0.003	0.003	0.000	0.009
Mg	0.712	0.445	0.860	0.651	0.708
Ca	0.873	0.489	0.815	0.701	0.797
Na	0.034	0.124	0.026	0.072	0.088
Cr	0.008	0.000	0.003	0.000	0.000
End member percentages					
Ac	3.4	0.0	2.6	0.0	8.1
Jd	0.0	12.4	0.0	7.2	0.7
TiCaTs	8.1	5.4	2.0	3.5	1.0
FeCaTs	5.3	0.0	0.9	0.0	0.0
CrCaTs	0.8	0.0	0.3	0.0	0.0
AlCaTs	3.1	17.8	6.9	12.6	9.9
Wo	35.0	12.9	35.7	27.0	34.4
En	35.6	22.3	43.0	32.5	35.4
Fs	8.8	15.9	8.3	10.1	10.1
Wo(tern)	44.1	25.3	41.1	38.8	43.0
En(tern)	44.8	43.6	49.4	46.7	44.3
Fs(tern)	11.1	31.1	9.5	14.5	12.7

Table B-1 (continued): **CLINOPYROXENE**
Kostal Lake (older lavas)

Sample	31/8/8 CP2M-KP	31/8/8 CP2R-KP	31/8/8 CP2R-KP	31/8/8 CP3C-KP	31/8/8 CP3M-KP
Major oxides (wt.%)					
SiO_2	50.5	49.1	47.6	46.6	46.0
TiO_2	0.3	1.7	2.5	1.5	1.7
Al_2O_3	5.0	5.0	5.6	7.9	8.4
Fe_2O_3	2.7	1.7	2.1	3.4	3.3
FeO	6.5	4.7	5.8	8.9	9.3
MnO	0.2	0.0	0.0	0.2	0.2
MgO	12.8	14.5	13.2	9.6	9.2
CaO	19.9	22.2	21.9	20.1	20.4
Na_2O	1.4	0.4	0.5	1.3	1.1
Cr_2O_3	0.1	0.4	0.2	0.1	0.0
Total	99.4	99.7	99.5	99.6	99.6
Cations on the basis of 6 oxygens					
Si	1.887	1.822	1.784	1.769	1.751
Ti	0.008	0.047	0.069	0.043	0.049
Al (IV)	0.113	0.178	0.216	0.231	0.249
Al (VI)	0.107	0.041	0.034	0.123	0.129
Fe^{3+}	0.076	0.047	0.059	0.098	0.093
Fe^{2+}	0.204	0.145	0.182	0.282	0.296
Mn	0.007	0.000	0.000	0.007	0.006
Mg	0.710	0.802	0.736	0.544	0.524
Ca	0.797	0.881	0.881	0.820	0.831
Na	0.088	0.022	0.030	0.079	0.072
Cr	0.003	0.012	0.007	0.003	0.000
End member percentages					
Ac	7.6	2.2	3.0	7.9	7.2
Jd	1.2	0.0	0.0	0.0	0.0
TiCaTs	0.8	4.7	6.9	4.3	4.9
FeCaTs	0.0	2.5	2.9	1.8	2.1
CrCaTs	0.3	1.2	0.7	0.3	0.0
AlCaTs	9.5	4.1	3.4	12.3	12.9
Wo	34.6	37.8	37.1	31.6	31.6
En	35.5	40.1	36.8	27.2	26.2
Fs	10.2	7.3	9.1	14.1	14.8
Wo(tern)	43.0	44.4	44.7	43.3	43.5
En(tern)	44.2	47.1	44.3	37.3	36.1
Fs(tern)	12.7	8.5	11.0	19.4	20.4

Table B-1 (continued): **CLINOPYROXENE**
Kostal Lake (older lavas)

Sample	31/8/8 CP3M-KP	31/8/8 CP3R-KP	31/8/8 CP3R-KP	31/8/8 CP4C-KP	31/8/8 CP4M-KP
Major oxides (wt.%)					
SiO_2	46.2	48.3	46.3	48.1	48.6
TiO_2	1.5	1.5	2.5	1.6	1.3
Al_2O_3	8.1	6.3	7.6	7.0	6.5
Fe_2O_3	3.6	2.1	2.4	2.2	2.0
FeO	8.6	3.9	4.4	4.3	4.6
MnO	0.2	0.0	0.0	0.1	0.0
MgO	9.3	13.7	12.7	13.9	14.3
CaO	20.3	22.3	22.3	22.2	21.2
Na_2O	1.3	0.6	0.5	0.3	0.5
Cr_2O_3	0.0	0.8	0.5	0.0	0.0
Total	99.2	99.4	99.3	100.0	99.2
Cations on the basis of 6 oxygens					
Si	1.762	1.796	1.734	1.778	1.807
Ti	0.044	0.042	0.071	0.045	0.037
Al (IV)	0.238	0.204	0.266	0.222	0.193
Al (VI)	0.128	0.071	0.069	0.085	0.094
Fe^{3+}	0.105	0.059	0.067	0.060	0.055
Fe^{2+}	0.275	0.120	0.137	0.134	0.143
Mn	0.006	0.000	0.000	0.003	0.000
Mg	0.528	0.760	0.711	0.766	0.794
Ca	0.832	0.890	0.896	0.882	0.845
Na	0.083	0.034	0.032	0.019	0.031
Cr	0.000	0.023	0.015	0.000	0.000
End member percentages					
Ac	8.3	3.4	3.2	1.9	3.1
Jd	0.0	0.0	0.0	0.0	0.0
TiCaTs	4.4	4.2	7.1	4.5	3.7
FeCaTs	2.2	2.5	3.5	4.2	2.5
CrCaTs	0.0	2.3	1.5	0.0	0.0
AlCaTs	12.8	7.1	6.9	8.5	9.4
Wo	31.9	36.4	35.3	35.6	34.5
En	26.4	38.0	35.6	38.3	39.7
Fs	13.7	6.0	6.8	6.7	7.2
Wo(tern)	44.3	45.3	45.4	44.1	42.4
En(tern)	36.7	47.3	45.8	47.5	48.8
Fs(tern)	19.1	7.5	8.8	8.3	8.8

Table B-1 (continued): **CLINOPYROXENE**
Kostal Lake (older lavas) to Kostal Lake (south cone)

Sample	31/8/8 CP4M-KP	31/8/8 CP4R-KP	29/7/6 CP1C-KS	29/7/6 CP1R-KS	29/7/6 CP2C-KS
Major oxides (wt.%)					
SiO_2	48.9	47.3	49.3	49.9	47.3
TiO_2	1.7	2.2	1.3	1.2	1.9
Al_2O_3	5.7	6.5	6.3	5.4	9.0
Fe_2O_3	2.0	2.0	1.9	2.0	1.8
FeO	4.3	5.3	4.3	4.1	6.2
MnO	0.0	0.0	0.1	0.0	0.1
MgO	14.2	13.1	14.7	14.9	12.7
CaO	22.4	22.1	21.3	21.7	19.3
Na_2O	0.4	0.4	0.5	0.6	1.1
Cr_2O_3	0.1	0.2	0.1	0.0	0.0
Total	100.1	99.5	100.0	99.7	99.4
Cations on the basis of 6 oxygens					
Si	1.808	1.771	1.814	1.840	1.761
Ti	0.046	0.063	0.036	0.033	0.052
Al (IV)	0.192	0.229	0.186	0.160	0.239
Al (VI)	0.058	0.059	0.088	0.074	0.155
Fe^{3+}	0.057	0.058	0.053	0.055	0.050
Fe^{2+}	0.133	0.165	0.133	0.128	0.194
Mn	0.000	0.000	0.004	0.000	0.004
Mg	0.785	0.730	0.805	0.817	0.704
Ca	0.886	0.888	0.840	0.859	0.771
Na	0.026	0.024	0.032	0.034	0.071
Cr	0.003	0.007	0.004	0.000	0.000
End member percentages					
Ac	2.6	2.4	3.2	3.4	5.0
Jd	0.0	0.0	0.0	0.0	2.0
TiCaTs	4.6	6.3	3.6	3.3	5.2
FeCaTs	3.1	3.3	2.1	2.1	0.0
CrCaTs	0.3	0.7	0.4	0.0	0.0
AlCaTs	5.8	5.9	8.8	7.4	13.4
Wo	37.4	36.3	34.5	36.6	29.2
En	39.2	36.5	40.2	40.9	35.2
Fs	6.6	8.3	6.7	6.4	9.7
Wo(tern)	44.9	44.8	42.4	43.6	39.4
En(tern)	47.1	45.0	49.4	48.7	47.5
Fs(tern)	8.0	10.2	8.2	7.6	13.1

Table B-2
Major element concentrations in incognate clinopyroxene

Clinopyroxene analyses comprise major oxide concentrations, cation numbers of each ionic species, recalculated on the basis of six oxygen anions and the molecular percentages of major end-members. The latter, together with the percentage of Fe^{3+}, are calculated using the method of Lindsley (1983). Analyses are in the order given below; on each page is a subheading listing the centres described thereon. The source of each analysis is identified by the two-letter suffix, and is plotted on each diagram of this work with the appropriate symbol, as follows:

Suffix	Symbol	Unit
SM	$\boxed{\ddagger}$	Spanish Mump
SB	$\boxed{\dagger}$	Spanish Bonk
ST	$\boxed{\Delta}$	Hyalo Ridge
SL	☒	Spanish Lake Centre
SC	⊞	Flourmill Centre
PY	+	Pyramid Mountain
SP	X	Spahats (Second Canyon dyke)
RM	$\boxed{Y}$	Ray Mountain
RR	‡	Ray Ridge
RC	†	Pointed Stick Cone
R	Δ	Dragon's Tongue
RP	Δ	Dragon's Tongue (proximal)
RD	Δ	Dragon's Tongue (distal)
KL	O	Kostal Lake
KP	O	Kostal Lake (older lavas)
KN	O	Kostal Lake (north cone)
KS	O	Kostal Lake (south cone)
KT	O	Kostal Lake (lava tube)

Analytical precisions for every element analysed in clinopyroxene are listed below at the 99% confidence level, as a percentage of the total concentration of that element.

Na	5.4
Mg	2.1
Al	2.2
Si	0.9
Ca	1.2
Ti	3.7
Cr	3.7
Mn	12.0
Fe	2.0

Sample numbers comprise three parts, interpreted as follows :

26/8/3(X)	CP1(X)C,M,R	-SB
Sample number (X if xenolith)	ClinoPyroxene 1 (X if xenocryst) Core, Median or Rim	Suite suffix

Table B-2 (continued): **CLINOPYROXENE**
Spanish Mump to Spanish Lake

Sample	26/8/2X CP1C-SM	26/8/2X CP2C-SM	26/8/2X CP3C-SM	26/8/2X CP4C-SM	24/8/13X CP1C-SL
Major oxides (wt.%)					
SiO_2	52.7	52.3	52.9	52.0	52.7
TiO_2	0.4	0.5	0.4	0.3	0.4
Al_2O_3	6.6	6.7	7.0	6.6	6.6
Fe_2O_3	0.5	0.0	1.0	0.5	0.6
FeO	2.3	2.6	2.1	2.5	2.3
MnO	0.1	0.1	0.1	0.1	0.1
MgO	14.8	14.7	14.8	15.2	15.2
CaO	20.4	19.9	19.9	20.1	20.2
Na_2O	2.0	2.1	2.3	1.7	2.0
Cr_2O_3	0.8	1.0	0.8	0.9	0.7
Total	101.1	100.1	101.6	100.4	100.8
Cations on the basis of 6 oxygens					
Si	1.891	1.894	1.888	1.879	1.891
Ti	0.010	0.013	0.010	0.009	0.010
Al (IV)	0.109	0.107	0.112	0.121	0.109
Al (VI)	0.172	0.178	0.181	0.162	0.170
Fe^{3+}	0.014	0.000	0.026	0.015	0.017
Fe^{2+}	0.070	0.079	0.061	0.075	0.071
Mn	0.002	0.003	0.003	0.003	0.002
Mg	0.793	0.792	0.789	0.820	0.816
Ca	0.784	0.771	0.760	0.778	0.776
Na	0.122	0.126	0.138	0.101	0.117
Cr	0.024	0.030	0.023	0.026	0.021
End member percentages					
Ac	1.4	0.0	2.6	1.5	1.7
Jd	10.8	12.6	11.1	8.6	10.1
TiCaTs	1.0	1.3	1.0	0.9	1.0
FeCaTs	0.0	0.0	0.0	0.0	0.0
CrCaTs	2.4	3.0	2.3	2.6	2.1
AlCaTs	6.4	5.2	6.9	7.6	7.0
Wo	34.3	33.8	32.9	33.3	33.8
En	39.6	39.6	39.4	41.0	40.8
Fs	3.5	4.0	3.1	3.7	3.5
Wo(tern)	44.3	43.7	43.6	42.7	43.3
En(tern)	51.2	51.2	52.3	52.5	52.2
Fs(tern)	4.5	5.1	4.1	4.8	4.5

Table B-2 (continued): **CLINOPYROXENE**
Spanish Lake

Sample	24/8/13X /OL CP1R-SL	24/8/13X CP1C-SL	24/8/13X /OP CP1R-SL	24/8/13X /SP2 CP2R-SL	24/8/13X CP2C-SL
Major oxides (wt.%)					
SiO_2	52.9	52.9	53.0	52.7	52.7
TiO_2	0.3	0.4	0.3	0.4	0.4
Al_2O_3	6.3	6.6	6.2	6.5	6.5
Fe_2O_3	0.2	0.7	0.1	0.4	0.8
FeO	2.8	2.4	2.9	2.8	2.2
MnO	0.0	0.0	0.0	0.1	0.1
MgO	15.6	15.4	15.7	15.7	15.4
CaO	20.2	20.3	19.9	19.9	20.2
Na_2O	1.8	1.9	1.8	1.7	1.9
Cr_2O_3	0.7	0.7	0.7	0.9	0.8
Total	100.6	101.2	100.8	101.3	101.1
Cations on the basis of 6 oxygens					
Si	1.900	1.890	1.903	1.885	1.887
Ti	0.008	0.010	0.009	0.010	0.010
Al (IV)	0.100	0.110	0.097	0.115	0.113
Al (VI)	0.166	0.168	0.167	0.160	0.161
Fe^{3+}	0.004	0.018	0.003	0.010	0.023
Fe^{2+}	0.085	0.071	0.086	0.083	0.065
Mn	0.000	0.000	0.000	0.003	0.003
Mg	0.833	0.819	0.838	0.837	0.824
Ca	0.778	0.777	0.766	0.764	0.776
Na	0.106	0.116	0.110	0.102	0.112
Cr	0.019	0.020	0.019	0.025	0.022
End member percentages					
Ac	0.4	1.8	0.3	1.0	2.3
Jd	10.2	9.8	10.7	9.1	8.9
TiCaTs	0.8	1.0	0.9	1.0	1.0
FeCaTs	0.0	0.0	0.0	0.0	0.0
CrCaTs	1.9	2.0	1.9	2.5	2.2
AlCaTs	6.4	7.0	6.0	6.9	7.1
Wo	34.3	33.8	33.9	33.0	33.7
En	41.7	41.0	41.9	41.9	41.2
Fs	4.3	3.5	4.3	4.1	3.2
Wo(tern)	42.8	43.2	42.3	41.8	43.1
En(tern)	51.9	52.3	52.3	53.0	52.8
Fs(tern)	5.3	4.5	5.4	5.2	4.1

Table B-2 (continued): **CLINOPYROXENE**
Spanish Lake to Flourmill

Sample	24/8/13X CP3C-SL	2/8/6X CP1C-SC	2/8/6X CP2C-SC	2/8/6X2 CP1C-SC	2/8/6X2 CP2C-SC
Major oxides (wt.%)					
SiO_2	52.7	47.3	46.1	51.3	51.8
TiO_2	0.4	1.4	2.5	0.5	0.5
Al_2O_3	6.6	9.0	8.0	5.2	4.7
Fe_2O_3	0.0	3.1	3.9	1.6	1.0
FeO	2.9	5.3	4.4	4.3	4.4
MnO	0.0	0.1	0.1	0.0	0.0
MgO	15.3	14.0	13.0	17.4	17.3
CaO	20.2	18.3	21.5	18.5	19.6
Na_2O	1.8	1.0	0.5	0.6	0.5
Cr_2O_3	0.7	0.0	0.0	0.6	0.6
Total	100.8	99.6	100.1	100.2	100.6
Cations on the basis of 6 oxygens					
Si	1.894	1.753	1.717	1.864	1.877
Ti	0.011	0.039	0.069	0.014	0.015
Al (IV)	0.108	0.247	0.283	0.136	0.123
Al (VI)	0.170	0.145	0.069	0.087	0.079
Fe^{3+}	0.000	0.086	0.109	0.043	0.028
Fe^{2+}	0.086	0.164	0.137	0.132	0.132
Mn	0.000	0.004	0.004	0.000	0.000
Mg	0.820	0.773	0.721	0.943	0.934
Ca	0.779	0.727	0.859	0.721	0.761
Na	0.105	0.063	0.033	0.039	0.029
Cr	0.021	0.000	0.000	0.017	0.017
End member percentages					
Ac	0.0	6.3	3.3	3.9	2.8
Jd	10.5	0.0	0.0	0.0	0.1
TiCaTs	1.1	3.9	6.9	1.4	1.5
FeCaTs	0.0	2.3	7.6	0.4	0.0
CrCaTs	2.1	0.0	0.0	1.7	1.7
AlCaTs	6.5	14.5	6.9	8.7	7.7
Wo	34.1	25.9	32.3	30.0	32.6
En	41.0	38.6	36.0	47.2	46.7
Fs	4.3	8.2	6.9	6.6	6.6
Wo(tern)	42.9	35.6	42.9	35.8	37.9
En(tern)	51.6	53.1	47.9	56.3	54.4
Fs(tern)	5.4	11.3	9.1	7.9	7.7

Table B-2 (continued): **CLINOPYROXENE**
Flourmill

Sample	2/8/6X3 /AP CP1C-SC	2/8/6X3 CP1C-SC	2/8/6X3 CP2C-SC	2/8/6X3 CP3R-SC	2/8/6X3 CP4C-SC
Major oxides (wt.%)					
SiO_2	51.9	52.0	52.0	52.2	51.9
TiO_2	0.0	0.2	0.2	0.0	0.2
Al_2O_3	2.1	2.2	2.2	2.2	2.2
Fe_2O_3	1.1	0.4	1.4	1.5	0.8
FeO	9.2	10.2	9.3	10.1	9.8
MnO	0.3	0.3	0.3	0.3	0.3
MgO	13.2	13.2	13.3	16.1	13.2
CaO	20.7	20.6	20.7	16.7	20.6
Na_2O	0.6	0.5	0.6	0.5	0.5
Cr_2O_3	0.2	0.2	0.2	0.0	0.1
Total	99.5	99.9	100.2	99.7	99.9
Cations on the basis of 6 oxygens					
Si	1.953	1.952	1.944	1.946	1.947
Ti	0.000	0.006	0.005	0.000	0.006
Al (IV)	0.047	0.048	0.056	0.054	0.053
Al (VI)	0.045	0.049	0.040	0.041	0.043
Fe^{3+}	0.032	0.012	0.039	0.041	0.023
Fe^{2+}	0.289	0.319	0.289	0.314	0.309
Mn	0.008	0.010	0.009	0.009	0.009
Mg	0.742	0.735	0.741	0.893	0.739
Ca	0.836	0.828	0.830	0.667	0.831
Na	0.035	0.030	0.037	0.028	0.030
Cr	0.005	0.006	0.005	0.000	0.004
End member percentages					
Ac	3.2	1.2	3.7	2.8	2.3
Jd	0.4	1.8	0.0	0.0	0.6
TiCaTs	0.0	0.6	0.5	0.0	0.6
FeCaTs	0.0	0.0	0.2	1.3	0.0
CrCaTs	0.5	0.6	0.5	0.0	0.4
AlCaTs	4.2	3.1	4.0	4.1	3.7
Wo	39.5	39.3	38.9	30.6	39.2
En	37.1	36.8	37.1	44.7	37.0
Fs	14.5	15.9	14.5	15.7	15.4
Wo(tern)	43.3	42.7	43.0	33.6	42.8
En(tern)	40.8	40.0	41.0	49.1	40.3
Fs(tern)	15.9	17.3	16.0	17.3	16.9

Table B-2 (continued): **CLINOPYROXENE**
Flourmill

Sample	4/8/17X CP1C-SC	4/8/17X CP2C-SC	4/8/17X CP3C-SC	4/8/4X CP1C-SC	4/8/4X CP2C-SC
Major oxides (wt.%)					
SiO_2	52.5	52.4	52.6	51.0	51.6
TiO_2	0.2	0.0	0.0	0.5	0.4
Al_2O_3	2.7	2.7	2.8	5.3	4.9
Fe_2O_3	2.2	2.5	3.1	0.1	0.4
FeO	2.3	2.1	1.8	5.5	5.4
MnO	0.1	0.1	0.1	0.1	0.0
MgO	17.2	17.1	17.5	17.0	17.6
CaO	21.0	21.1	20.3	18.4	18.0
Na_2O	0.7	0.8	0.9	0.4	0.6
Cr_2O_3	0.8	0.8	0.7	0.9	0.5
Total	100.0	99.6	99.8	99.4	99.5
Cations on the basis of 6 oxygens					
Si	1.916	1.920	1.916	1.871	1.887
Ti	0.004	0.000	0.000	0.013	0.012
Al (IV)	0.084	0.080	0.084	0.129	0.113
Al (VI)	0.034	0.035	0.034	0.099	0.099
Fe^{3+}	0.060	0.068	0.084	0.003	0.012
Fe^{2+}	0.070	0.064	0.056	0.169	0.164
Mn	0.004	0.005	0.003	0.002	0.000
Mg	0.933	0.930	0.953	0.932	0.956
Ca	0.821	0.827	0.794	0.725	0.704
Na	0.041	0.046	0.056	0.026	0.036
Cr	0.022	0.023	0.021	0.026	0.015
End member percentages					
Ac	4.1	4.6	5.6	0.3	1.2
Jd	0.0	0.0	0.0	2.3	2.4
TiCaTs	0.4	0.0	0.0	1.3	1.2
FeCaTs	2.0	2.2	2.8	0.0	0.0
CrCaTs	2.2	2.3	2.1	2.6	1.5
AlCaTs	3.4	3.5	3.4	7.6	7.5
Wo	37.1	37.3	35.5	30.5	30.1
En	46.7	46.5	47.6	46.6	47.8
Fs	3.5	3.2	2.8	8.5	8.2
Wo(tern)	42.5	42.9	41.3	35.6	35.0
En(tern)	53.5	53.5	55.4	54.5	55.5
Fs(tern)	4.0	3.7	3.2	9.9	9.5

Table B-2 (continued): **CLINOPYROXENE**
Flourmill to Pyramid Mountain

Sample	4/8/4X CP3C-SC	4/8/4X2 CP1C-SC	13/8/10 CP1C-PY	13/8/10 CP2C-PY	13/8/10 CP3C-PY
Major oxides (wt.%)					
SiO_2	52.2	51.4	52.1	52.9	52.3
TiO_2	0.5	0.6	0.5	0.3	0.5
Al_2O_3	4.6	5.0	7.2	6.9	7.1
Fe_2O_3	0.0	0.6	0.2	0.9	0.8
FeO	6.2	6.7	2.9	2.2	2.4
MnO	0.2	0.1	0.1	0.1	0.0
MgO	17.9	17.2	15.0	15.2	14.9
CaO	17.7	17.2	20.0	19.9	20.0
Na_2O	0.2	0.6	1.8	2.1	2.0
Cr_2O_3	0.3	0.3	1.0	0.8	0.9
Total	100.2	99.8	101.0	101.6	101.2
Cations on the basis of 6 oxygens					
Si	1.897	1.882	1.872	1.886	1.875
Ti	0.014	0.017	0.012	0.007	0.012
Al (IV)	0.111	0.118	0.128	0.114	0.125
Al (VI)	0.085	0.099	0.177	0.176	0.175
Fe^{3+}	0.000	0.016	0.004	0.025	0.022
Fe^{2+}	0.189	0.204	0.088	0.065	0.073
Mn	0.005	0.004	0.003	0.002	0.000
Mg	0.967	0.938	0.801	0.807	0.798
Ca	0.691	0.674	0.770	0.762	0.768
Na	0.012	0.038	0.107	0.125	0.121
Cr	0.010	0.008	0.028	0.024	0.024
End member percentages					
Ac	0.0	1.6	0.4	2.5	2.2
Jd	1.2	2.2	10.2	10.0	9.9
TiCaTs	1.4	1.7	1.2	0.7	1.2
FeCaTs	0.0	0.0	0.0	0.0	0.0
CrCaTs	1.0	0.8	2.8	2.4	2.4
AlCaTs	7.3	7.7	7.5	7.5	7.6
Wo	29.7	28.6	32.7	32.7	32.8
En	48.4	46.9	40.0	40.4	39.9
Fs	9.5	10.2	4.4	3.2	3.6
Wo(tern)	33.9	33.4	42.4	42.9	42.9
En(tern)	55.3	54.7	51.9	52.9	52.3
Fs(tern)	10.8	11.9	5.7	4.2	4.8

Table B-2 (continued): **CLINOPYROXENE**
Pyramid Mountain to Ray Ridge

Sample	13/8/10 CP4C-PY	19/8/1X CP1C-RM	19/8/1X CP2C-RM	18/8/9X CP1C-RR	18/8/9X CP2C-RR
Major oxides (wt.%)					
SiO_2	51.5	51.3	50.8	51.0	52.0
TiO_2	0.4	0.8	0.8	0.7	0.7
Al_2O_3	9.2	2.6	3.2	4.0	2.6
Fe_2O_3	1.1	0.1	1.8	1.5	0.6
FeO	2.4	9.5	8.4	3.5	4.3
MnO	0.1	0.2	0.2	0.0	0.1
MgO	14.0	12.8	13.2	15.8	15.8
CaO	20.0	21.9	21.1	21.6	21.9
Na_2O	2.2	0.4	0.6	0.5	0.5
Cr_2O_3	0.4	0.0	0.0	1.0	1.1
Total	101.3	99.6	100.2	99.9	99.7
Cations on the basis of 6 oxygens					
Si	1.840	1.929	1.898	1.874	1.914
Ti	0.010	0.024	0.024	0.020	0.020
Al (IV)	0.160	0.071	0.102	0.126	0.086
Al (VI)	0.230	0.046	0.038	0.049	0.028
Fe^{3+}	0.031	0.003	0.052	0.042	0.016
Fe^{3+}	0.072	0.298	0.263	0.107	0.131
Mn	0.003	0.005	0.008	0.000	0.002
Mg	0.744	0.717	0.737	0.865	0.869
Ca	0.767	0.882	0.843	0.850	0.864
Na	0.131	0.026	0.035	0.033	0.032
Cr	0.010	0.000	0.000	0.029	0.033
End member percentages					
Ac	3.1	0.3	3.5	3.3	1.6
Jd	10.0	2.2	0.0	0.0	1.6
TiCaTs	1.0	2.4	2.4	2.0	2.0
FeCaTs	0.0	0.0	1.7	0.9	0.0
CrCaTs	1.0	0.0	0.0	2.9	3.3
AlCaTs	13.0	2.4	3.8	4.9	1.2
Wo	30.8	41.8	38.3	37.2	39.9
En	37.2	35.8	36.9	43.2	43.4
Fs	3.6	14.9	13.2	5.4	6.6
Wo(tern)	43.0	45.2	43.3	43.4	44.4
En(tern)	51.9	38.7	41.8	50.4	48.3
Fs(tern)	5.0	16.1	14.9	6.2	7.3

Table B-2 (continued): **CLINOPYROXENE**
Ray Ridge to Dragon's Tongue (proximal)

Sample	18/8/9X CP3C-RR	13/8/1X CP1C-RP	13/8/1X CP1C-RP	13/8/1X CP1C-RP	13/8/1X CP1C-RP
Major oxides (wt.%)					
SiO_2	54.7	49.1	48.4	48.0	47.9
TiO_2	0.0	1.2	1.3	1.5	1.4
Al_2O_3	0.6	8.4	9.6	9.5	9.6
Fe_2O_3	0.5	3.2	3.4	3.3	3.3
FeO	3.7	5.6	5.7	5.8	5.5
MnO	0.1	0.1	0.2	0.2	0.2
MgO	19.1	14.7	14.8	14.3	14.0
CaO	18.8	17.6	17.2	17.6	17.8
Na_2O	0.9	1.3	1.2	1.2	1.3
Cr_2O_3	1.4	0.0	0.0	0.0	0.0
Total	99.7	101.3	102.1	101.3	101.0
Cations on the basis of 6 oxygens					
Si	1.987	1.784	1.746	1.746	1.746
Ti	0.000	0.032	0.035	0.041	0.039
Al (IV)	0.013	0.216	0.254	0.254	0.254
Al (VI)	0.013	0.145	0.153	0.155	0.161
Fe^{3+}	0.014	0.088	0.093	0.089	0.091
Fe^{2+}	0.111	0.169	0.173	0.176	0.169
Mn	0.002	0.005	0.006	0.005	0.005
Mg	1.033	0.794	0.798	0.775	0.761
Ca	0.730	0.687	0.667	0.686	0.695
Na	0.055	0.082	0.069	0.073	0.077
Cr	0.041	0.000	0.000	0.000	0.000
End member percentages					
Ac	1.4	8.2	6.9	7.3	7.7
Jd	4.1	0.0	0.0	0.0	0.0
TiCaTs	0.0	3.2	3.5	4.1	3.9
FeCaTs	0.0	0.6	2.4	1.6	1.4
CrCaTs	4.1	0.0	0.0	0.0	0.0
AlCaTs	-2.8	14.5	15.3	15.5	16.1
Wo	35.9	25.2	22.7	23.7	24.0
En	51.6	39.7	39.9	38.8	38.1
Fs	5.6	8.4	8.7	8.8	8.4
Wo(tern)	38.5	34.3	31.9	33.2	34.1
En(tern)	55.5	54.1	56.0	54.4	54.0
Fs(tern)	6.0	11.5	12.1	12.3	11.9

Table B-2 (continued): **CLINOPYROXENE**
Dragon's Tongue (proximal)

Sample	13/8/1X /SP CP2.1R-RP	13/8/1X CP2.2-RP	13/8/1X CP2.3-RP	13/8/1X CP2.4-RP	13/8/1X CP2.5-RP
Major oxides (wt.%)					
SiO_2	50.0	50.0	49.3	49.3	48.2
TiO_2	0.8	1.0	1.2	1.3	1.5
Al_2O_3	7.1	7.5	7.8	8.1	9.2
Fe_2O_3	3.4	2.6	2.7	2.9	2.9
FeO	9.0	8.8	8.0	7.6	6.3
MnO	0.2	0.2	0.2	0.2	0.1
MgO	17.9	16.9	16.0	15.4	13.3
CaO	12.3	13.8	15.1	15.9	18.3
Na_2O	0.9	0.9	1.0	1.1	1.3
Cr_2O_3	0.0	0.0	0.1	0.0	0.0
Total	101.6	101.9	101.4	101.8	101.1
Cations on the basis of 6 oxygens					
Si	1.809	1.805	1.793	1.786	1.763
Ti	0.023	0.027	0.032	0.035	0.040
Al (IV)	0.191	0.195	0.207	0.214	0.237
Al (VI)	0.110	0.126	0.126	0.132	0.158
Fe^{3+}	0.093	0.071	0.073	0.080	0.079
Fe^{2+}	0.271	0.267	0.244	0.231	0.194
Mn	0.007	0.007	0.005	0.005	0.004
Mg	0.963	0.911	0.868	0.834	0.727
Ca	0.477	0.535	0.589	0.617	0.716
Na	0.057	0.056	0.058	0.068	0.081
Cr	0.000	0.000	0.003	0.000	0.000
End member percentages					
Ac	5.7	5.6	5.8	6.8	7.9
Jd	0.0	0.0	0.0	0.0	0.2
TiCaTs	2.3	2.7	3.2	3.5	4.0
FeCaTs	3.6	1.4	1.4	1.3	0.0
CrCaTs	0.0	0.0	0.3	0.0	0.0
AlCaTs	11.0	12.6	12.6	13.2	15.6
Wo	15.4	18.4	20.7	21.9	26.0
En	48.1	45.5	43.4	41.7	36.3
Fs	13.5	13.4	12.2	11.5	9.7
Wo(tern)	20.0	23.8	27.1	29.1	36.0
En(tern)	62.4	58.9	56.9	55.5	50.5
Fs(tern)	17.6	17.3	16.0	15.4	13.5

Table B-2 (continued): **CLINOPYROXENE**
Dragon's Tongue (proximal)

Sample	13/8/1X CP2.6-RP	13/8/1X CP3-RP	13/8/1X CP4-RP	13/8/1X CP5-RP	14/8/9X CP1C-RP
Major oxides (wt.%)					
SiO_2	48.7	48.2	48.5	48.7	47.4
TiO_2	1.4	1.8	1.5	1.4	1.6
Al_2O_3	9.2	8.5	9.2	8.3	9.4
Fe_2O_3	2.9	2.8	2.4	2.8	2.0
FeO	7.0	7.1	6.7	7.2	6.2
MnO	0.2	0.1	0.1	0.2	0.1
MgO	14.1	12.9	14.1	13.6	13.5
CaO	17.1	18.3	17.8	17.9	18.9
Na_2O	1.3	1.4	1.1	1.2	0.9
Cr_2O_3	0.0	0.1	0.0	0.0	0.0
Total	101.9	101.5	101.6	101.3	100.1
Cations on the basis of 6 oxygens					
Si	1.765	1.766	1.764	1.782	1.751
Ti	0.038	0.050	0.041	0.038	0.043
Al (IV)	0.235	0.234	0.236	0.218	0.249
Al (VI)	0.158	0.136	0.157	0.141	0.161
Fe^{3+}	0.080	0.076	0.066	0.076	0.056
Fe^{2+}	0.212	0.219	0.202	0.219	0.193
Mn	0.005	0.004	0.004	0.005	0.004
Mg	0.764	0.705	0.765	0.744	0.741
Ca	0.663	0.720	0.694	0.702	0.747
Na	0.080	0.085	0.068	0.075	0.055
Cr	0.000	0.002	0.000	0.000	0.000
End member percentages					
Ac	8.0	7.6	6.6	7.5	5.5
Jd	0.0	0.9	0.2	0.0	0.0
TiCaTs	3.8	5.0	4.1	3.8	4.3
FeCaTs	0.0	0.0	0.0	0.1	0.2
CrCaTs	0.0	0.2	0.0	0.0	0.0
AlCaTs	15.8	12.6	15.5	14.1	16.1
Wo	23.3	27.0	24.9	26.1	27.1
En	38.2	35.3	38.2	37.2	37.0
Fs	10.6	10.9	10.1	11.0	9.6
Wo(tern)	32.3	36.9	34.0	35.2	36.7
En(tern)	53.0	48.1	52.2	50.1	50.2
Fs(tern)	14.7	14.9	13.8	14.7	13.1

Table B-2 (continued): **CLINOPYROXENE**
Dragon's Tongue (proximal)

Sample	14/8/9X CP2C-RP	14/8/9X CP3C-RP	14/8/9X CP4C-RP	14/8/1X CP1C-RP	14/8/1X CP1C-RP
Major oxides (wt.%)					
SiO_2	47.9	50.0	47.9	48.4	48.5
TiO_2	1.6	1.0	1.4	1.2	1.3
Al_2O_3	9.0	6.0	8.7	8.3	8.0
Fe_2O_3	1.8	2.2	1.7	2.4	2.7
FeO	6.8	5.5	5.7	6.3	6.0
MnO	0.1	0.2	0.2	0.1	0.2
MgO	13.5	16.0	13.4	13.9	15.0
CaO	18.5	18.7	19.9	18.4	17.5
Na_2O	1.0	0.6	0.8	1.0	1.0
Cr_2O_3	0.0	0.1	0.1	0.0	0.0
Total	100.4	100.4	99.9	100.1	100.1
Cations on the basis of 6 oxygens					
Si	1.765	1.829	1.769	1.784	1.783
Ti	0.044	0.027	0.040	0.035	0.035
Al (IV)	0.235	0.171	0.231	0.216	0.217
Al (VI)	0.158	0.089	0.149	0.146	0.130
Fe^{3+}	0.050	0.060	0.048	0.066	0.075
Fe^{2+}	0.209	0.167	0.176	0.194	0.185
Mn	0.004	0.005	0.005	0.004	0.005
Mg	0.740	0.871	0.741	0.763	0.823
Ca	0.732	0.733	0.787	0.728	0.688
Na	0.061	0.037	0.049	0.064	0.059
Cr	0.000	0.004	0.003	0.000	0.000
End member percentages					
Ac	5.0	3.7	4.8	6.4	5.9
Jd	1.1	0.0	0.1	0.0	0.0
TiCaTs	4.4	2.7	4.0	3.5	3.5
FeCaTs	0.0	2.4	0.0	0.1	1.7
CrCaTs	0.0	0.4	0.3	0.0	0.0
AlCaTs	14.6	8.9	14.9	14.6	13.0
Wo	27.1	29.4	29.8	27.3	25.3
En	37.0	43.5	37.0	38.2	41.1
Fs	10.4	8.4	8.8	9.7	9.3
Wo(tern)	36.3	36.2	39.4	36.4	33.4
En(tern)	49.7	53.5	49.0	50.7	54.3
Fs(tern)	14.0	10.3	11.6	12.9	12.2

Table B-2 (continued): **CLINOPYROXENE**
Dragon's Tongue (proximal)

Sample	14/8/1X CP2C-RP
Major oxides (wt.%)	
SiO_2	47.9
TiO_2	1.5
Al_2O_3	8.8
Fe_2O_3	2.7
FeO	6.3
MnO	0.2
MgO	14.5
CaO	17.5
Na_2O	0.9
Cr_2O_3	0.0
Total	100.4
Cations on the basis of 6 oxygens	
Si	1.760
Ti	0.041
Al (IV)	0.240
Al (VI)	0.142
Fe^{3+}	0.074
Fe^{2+}	0.195
Mn	0.006
Mg	0.796
Ca	0.688
Na	0.058
Cr	0.000
Endmember percentages	
Ac	5.8
Jd	0.0
TiCaTs	4.1
FeCaTs	1.6
CrCaTs	0.0
AlCaTs	14.2
Wo	24.5
En	39.8
Fs	9.7
Wo(tern)	33.1
En(tern)	53.8
Fs(tern)	13.2

Table B-3
Major element concentrations in olivine

Olivine analyses comprise major oxide concentrations, cation numbers of each ionic species, recalculated on the basis of four oxygen anions and the molecular percentages of end members. Analyses are in the order given below; on each page is a subheading listing the centres described thereon. The source of each analysis is identified by the two-letter suffix, and is plotted on each diagram of this work with the appropriate symbol, as follows:

Suffix	Symbol	Unit
SM	‡⃞	Spanish Mump
SB	‡⃞	Spanish Bonk
ST	▲⃞	Hyalo Ridge
SL	X⃞	Spanish Lake Centre
SC	+⃞	Flourmill Centre
PY	+	Pyramid Mountain
SP	X	Spahats (Second Canyon dyke)
RM	Y⃞	Ray Mountain
RR	‡	Ray Ridge
RC	ǂ	Pointed Stick Cone
R	Δ	Dragon's Tongue
RP	Δ	Dragon's Tongue (proximal)
RD	Δ	Dragon's Tongue (distal)
KL	O	Kostal Lake
KP	O	Kostal Lake (older lavas)
KN	O	Kostal Lake (north cone)
KS	O	Kostal Lake (south cone)
KT	O	Kostal Lake (lava tube)

Analytical precisions for every element analysed in olivine are listed below at the 99% confidence level, as a percentage of the total concentration of that element. i.c. = insufficient concentration.

Mg	1.8
Al	i.c.
Si	1.0
Ca	6.5
Ti	i.c.
Cr	i.c.
Mn	12.0
Fe	1.7
Ni	12.0

Sample numbers comprise three parts, interpreted as follows :

26/8/3(X)	OL 1(X)C,M,R	-SB
Sample number (X if xenolith)	OLivine 1 (X if xenocryst) Core, Median or Rim	Suite suffix

Table B-3 (continued): **OLIVINE**
Spanish Bank

Sample	26/8/3 OL1C-SB	26/8/3 OL1R-SB	26/8/3 OL2C-SB	26/8/3 OL2R-SB	26/8/3 OL3C-SB
Major oxides (wt.%)					
SiO_2	37.8	37.5	37.5	37.3	37.1
TiO_2	0.0	0.0	0.0	0.0	0.0
Al_2O_3	0.0	0.0	0.0	0.0	0.0
FeO	21.6	24.3	26.3	26.2	24.7
MnO	0.3	0.5	0.6	0.6	0.5
MgO	38.5	36.4	35.5	35.2	35.9
CaO	0.2	0.3	0.3	0.3	0.2
NiO	0.0	0.0	0.0	0.0	0.0
Total	98.4	99.0	100.1	99.7	98.4
Cations on the basis of 4 oxygens					
Si	0.998	0.997	0.995	0.996	0.996
Ti	0.000	0.000	0.000	0.000	0.000
Al	0.000	0.000	0.000	0.000	0.000
Fe^{2+}	0.477	0.542	0.583	0.586	0.554
Mn	0.006	0.012	0.013	0.013	0.011
Mg	1.516	1.444	1.404	1.401	1.436
Ca	0.005	0.009	0.009	0.009	0.006
Ni	0.000	0.000	0.000	0.000	0.000
End member percentages					
Fo	75.4	71.6	69.4	69.3	71.2
Fa	24.1	27.6	29.7	29.8	28.2
Mo	0.5	0.8	0.9	0.9	0.6

Table B-3 (continued): **OLIVINE**
Spanish Bonk

Sample	26/8/3 OL3R-SB	26/8/3 OL4C-SB	26/8/3 OL4C-SB	26/8/3 OL4R-SB	26/8/3 OL5C-SB
Major oxides (wt.%)					
SiO_2	36.9	38.9	38.9	37.2	37.4
TiO_2	0.0	0.0	0.0	0.0	0.0
Al_2O_3	0.0	0.0	0.0	0.0	0.0
FeO	25.3	16.2	16.2	24.6	23.8
MnO	0.6	0.2	0.2	0.5	0.5
MgO	35.2	43.0	43.0	35.9	36.7
CaO	0.3	0.3	0.3	0.3	0.3
NiO	0.0	0.0	0.0	0.0	0.0
Total	98.2	98.6	98.6	98.6	98.6
Cations on the basis of 4 oxygens					
Si	0.995	0.998	0.998	0.997	0.997
Ti	0.000	0.000	0.000	0.000	0.000
Al	0.000	0.000	0.000	0.000	0.000
Fe^{2+}	0.571	0.346	0.346	0.552	0.530
Mn	0.013	0.005	0.005	0.012	0.010
Mg	1.416	1.645	1.645	1.433	1.458
Ca	0.009	0.007	0.007	0.008	0.008
Ni	0.000	0.000	0.000	0.000	0.000
End member percentages					
Fo	70.0	81.7	81.7	71.1	72.3
Fa	29.1	17.5	17.5	28.1	26.9
Mo	0.9	0.7	0.7	0.8	0.8

Table B-3 (continued): **OLIVINE**
Spanish Bonk to Hyalo Ridge

Sample	26/8/3 OL5R-SB	23/8/2 OL1C-ST	23/8/2 OL1R-ST	23/8/2 OL2C-ST	23/8/2 OL2R-ST
Major oxides (wt.%)					
SiO_2	37.2	40.4	40.2	39.8	39.0
TiO_2	0.0	0.0	0.0	0.0	0.0
Al_2O_3	0.0	0.0	0.0	0.0	0.2
FeO	24.8	18.0	17.7	18.6	22.6
MnO	0.5	0.2	0.2	0.3	0.3
MgO	35.9	43.9	43.9	43.2	39.6
CaO	0.3	0.2	0.3	0.3	0.3
NiO	0.0	0.2	0.2	0.2	0.1
Total	98.7	102.9	102.4	102.3	102.2
Cations on the basis of 4 oxygens					
Si	0.996	0.999	0.998	0.993	0.993
Ti	0.000	0.000	0.000	0.000	0.000
Al	0.000	0.000	0.000	0.000	0.005
Fe^{2+}	0.556	0.372	0.367	0.389	0.483
Mn	0.012	0.005	0.004	0.006	0.007
Mg	1.431	1.617	1.622	1.607	1.505
Ca	0.008	0.006	0.007	0.008	0.010
Ni	0.000	0.003	0.004	0.004	0.001
End member percentages					
Fo	70.9	80.6	80.8	79.6	74.6
Fa	28.3	18.8	18.5	19.6	24.4
Mo	0.8	0.6	0.7	0.7	1.0

Table B-3 (continued): **OLIVINE**
Hyalo Ridge

Sample	23/8/12 OL1XC-ST	23/8/12 /CPX OL1XR-ST	23/8/12 OL2C-ST	23/8/12 OL2R-ST	23/8/12 OL3C-ST
Major oxides (wt.%)					
SiO_2	38.9	36.9	39.0	38.0	39.6
TiO_2	0.0	0.0	0.0	0.0	0.0
Al_2O_3	0.0	0.0	0.0	0.0	0.0
FeO	16.2	27.9	16.2	22.0	14.9
MnO	0.2	0.4	0.2	0.3	0.1
MgO	43.4	33.9	43.3	38.6	44.2
CaO	0.2	0.3	0.2	0.3	0.2
NiO	0.4	0.1	0.3	0.2	0.4
Total	99.2	99.5	99.2	99.4	99.4
Cations on the basis of 4 oxygens					
Si	0.993	0.995	0.995	0.995	1.002
Ti	0.000	0.000	0.000	0.000	0.000
Al	0.000	0.000	0.000	0.000	0.000
Fe^{2+}	0.345	0.629	0.346	0.481	0.314
Mn	0.004	0.009	0.005	0.007	0.003
Mg	1.651	1.361	1.646	1.508	1.666
Ca	0.005	0.009	0.006	0.009	0.005
Ni	0.008	0.002	0.007	0.005	0.008
End member percentages					
Fo	82.1	67.3	81.9	74.9	83.6
Fa	17.3	31.7	17.5	24.3	15.9
Mo	0.5	0.9	0.6	0.9	0.5

Table B-3 (continued): **OLIVINE**
Hyalo Ridge

Sample	23/8/12 OL3R-ST	23/8/12 OL4C-ST	23/8/12 OL4R-ST	23/8/12 OL5XC-ST	23/8/12 OL5XR-ST
Major oxides (wt.%)					
SiO_2	38.3	38.8	37.9	39.5	39.1
TiO_2	0.0	0.0	0.0	0.0	0.0
Al_2O_3	0.0	0.0	0.0	0.0	0.0
FeO	23.4	17.4	22.0	16.3	17.2
MnO	0.3	0.2	0.3	0.2	0.2
MgO	38.2	42.6	38.5	44.0	43.0
CaO	0.3	0.2	0.3	0.2	0.2
NiO	0.2	0.2	0.2	0.3	0.2
Total	100.8	99.4	99.2	100.4	99.9
Cations on the basis of 4 oxygens					
Si	0.996	0.993	0.995	0.995	0.994
Ti	0.000	0.000	0.000	0.000	0.000
Al	0.000	0.000	0.000	0.000	0.000
Fe^{2+}	0.510	0.373	0.484	0.344	0.366
Mn	0.006	0.005	0.006	0.004	0.004
Mg	1.478	1.627	1.508	1.651	1.629
Ca	0.010	0.007	0.008	0.006	0.007
Ni	0.004	0.003	0.004	0.005	0.005
End member percentages					
Fo	73.3	80.6	74.8	82.1	80.9
Fa	25.7	18.7	24.4	17.3	18.4
Mo	1.0	0.7	0.8	0.6	0.7

Table B-3 (continued): **OLIVINE**
Hyalo Ridge

Sample	23/8/12 OL6G-ST	23/8/12 OL7G-ST	23/8/6 OL1C-ST	23/8/6 OL1R-ST	23/8/6 OL2C-ST
Major oxides (wt.%)					
SiO_2	37.5	35.1	38.6	37.7	38.5
TiO_2	0.0	0.3	0.0	0.0	0.0
Al_2O_3	0.0	0.0	0.0	0.0	0.0
FeO	25.3	35.8	19.2	22.6	17.9
MnO	0.3	0.4	0.3	0.3	0.2
MgO	36.3	26.6	41.0	37.9	41.6
CaO	0.3	0.4	0.2	0.1	0.2
NiO	0.1	0.0	0.3	0.1	0.3
Total	99.9	98.7	99.6	98.8	98.7
Cations on the basis of 4 oxygens					
Si	0.993	0.994	0.995	0.996	0.995
Ti	0.000	0.007	0.000	0.000	0.000
Al	0.000	0.000	0.000	0.000	0.000
Fe^{2+}	0.560	0.849	0.415	0.501	0.387
Mn	0.007	0.010	0.006	0.008	0.005
Mg	1.435	1.126	1.577	1.493	1.606
Ca	0.010	0.013	0.006	0.004	0.007
Ni	0.003	0.000	0.006	0.003	0.006
End member percentages					
Fo	70.9	55.7	78.5	74.3	79.9
Fa	28.2	43.0	20.9	25.3	19.5
Mo	1.0	1.3	0.6	0.4	0.7

Table B-3 (continued): **OLIVINE**
Hyalo Ridge

Sample	23/8/6 OL3C-ST	23/8/6 OL3R-ST	23/8/6 OL4C-ST	23/8/6 OL4R-ST	23/8/6 OL5C-ST
Major oxides (wt.%)					
SiO_2	37.9	37.7	37.9	37.6	37.1
TiO_2	0.0	0.0	0.0	0.0	0.0
Al_2O_3	0.0	0.0	0.0	0.0	0.0
FeO	20.4	22.7	22.9	23.5	26.3
MnO	0.3	0.3	0.4	0.4	0.4
MgO	39.5	37.8	37.6	37.4	35.0
CaO	0.1	0.1	0.2	0.1	0.1
NiO	0.1	0.1	0.2	0.3	0.2
Total	98.4	98.8	99.1	99.2	99.1
Cations on the basis of 4 oxygens					
Si	0.995	0.997	1.000	0.995	0.996
Ti	0.000	0.000	0.000	0.000	0.000
Al	0.000	0.000	0.000	0.000	0.000
Fe^{2+}	0.449	0.501	0.506	0.519	0.591
Mn	0.007	0.007	0.008	0.009	0.008
Mg	1.548	1.491	1.477	1.474	1.402
Ca	0.004	0.003	0.006	0.004	0.004
Ni	0.003	0.003	0.004	0.005	0.003
End member percentages					
Fo	76.9	74.3	73.7	73.4	69.8
Fa	22.7	25.3	25.7	26.3	29.8
Mo	0.4	0.3	0.6	0.4	0.4

Table B-3 (continued): **OLIVINE**
Hyalo Ridge to Spanish Lake

Sample	23/8/6 OL5R-ST	23/8/6 OL6G-ST	23/8/6 OL7G-ST	24/8/13 OL1C-SL	24/8/13 OL2C-SL
Major oxides (wt.%)					
SiO_2	36.7	36.1	36.2	40.0	40.0
TiO_2	0.0	0.0	0.0	0.0	0.0
Al_2O_3	0.0	0.0	0.0	0.0	0.0
FeO	26.7	30.5	30.6	13.2	13.5
MnO	0.4	0.4	0.5	0.3	0.1
MgO	34.5	31.5	31.2	46.3	46.0
CaO	0.1	0.2	0.2	0.3	0.3
NiO	0.0	0.0	0.0	0.3	0.3
Total	98.4	98.7	98.6	100.4	100.2
Cations on the basis of 4 oxygens					
Si	0.995	0.993	0.998	0.995	0.996
Ti	0.000	0.000	0.000	0.000	0.000
Al	0.000	0.000	0.000	0.000	0.000
Fe^{2+}	0.605	0.702	0.706	0.274	0.282
Mn	0.009	0.010	0.011	0.005	0.003
Mg	1.393	1.295	1.280	1.717	1.710
Ca	0.004	0.007	0.006	0.008	0.007
Ni	0.000	0.000	0.000	0.006	0.006
End member percentages					
Fo	69.1	64.0	63.6	85.3	85.1
Fa	30.6	35.4	35.8	13.9	14.2
Mo	0.4	0.7	0.6	0.8	0.7

Table B-3 (continued): **OLIVINE**
Spanish Lake

Sample	24/8/13 OL2R-SL	24/8/13 OL3G-SL	24/8/13 OL4G-SL	24/8/13 OL5C-SL	24/8/14 OL1C-SL
Major oxides (wt.%)					
SiO_2	38.1	37.5	37.6	39.9	40.2
TiO_2	0.0	0.0	0.0	0.0	0.0
Al_2O_3	0.0	0.0	0.0	0.0	0.0
FeO	23.8	26.7	26.8	13.9	12.8
MnO	0.3	0.5	0.5	0.2	0.2
MgO	37.8	35.0	34.9	45.7	46.5
CaO	0.4	0.6	0.5	0.3	0.3
NiO	0.1	0.0	0.0	0.3	0.3
Total	100.7	100.3	100.3	100.2	100.2
Cations on the basis of 4 oxygens					
Si	0.994	0.996	0.999	0.996	0.998
Ti	0.000	0.000	0.000	0.000	0.000
Al	0.000	0.000	0.000	0.000	0.000
Fe^{2+}	0.520	0.593	0.596	0.290	0.267
Mn	0.007	0.011	0.011	0.004	0.004
Mg	1.469	1.387	1.380	1.702	1.720
Ca	0.012	0.016	0.015	0.008	0.007
Ni	0.003	0.000	0.000	0.005	0.006
End member percentages					
Fo	72.6	68.3	68.2	84.6	85.8
Fa	26.2	30.1	30.3	14.6	13.5
Mo	1.2	1.6	1.5	0.8	0.7

Table B-3 (continued): **OLIVINE**
Spanish Lake

Sample	24/8/14 OL1R-SL	24/8/14 OL2C-SL	24/8/14 OL3XC-SL	24/8/14 OL3XR-SL	24/8/14 OL4C-SL
Major oxides (wt.%)					
SiO_2	39.4	40.0	39.7	39.2	40.1
TiO_2	0.0	0.0	0.0	0.0	0.0
Al_2O_3	0.0	0.0	0.0	0.0	0.0
FeO	17.6	13.3	15.3	18.9	13.3
MnO	0.2	0.2	0.2	0.3	0.2
MgO	43.0	46.2	44.8	41.7	46.1
CaO	0.4	0.3	0.3	0.5	0.3
NiO	0.3	0.3	0.3	0.2	0.3
Total	100.9	100.2	100.5	100.8	100.3
Cations on the basis of 4 oxygens					
Si	0.994	0.996	0.996	0.996	0.997
Ti	0.000	0.000	0.000	0.000	0.000
Al	0.000	0.000	0.000	0.000	0.000
Fe^{2+}	0.371	0.278	0.320	0.402	0.278
Mn	0.005	0.004	0.005	0.007	0.004
Mg	1.618	1.714	1.672	1.581	1.710
Ca	0.011	0.007	0.007	0.013	0.008
Ni	0.006	0.006	0.005	0.004	0.007
End member percentages					
Fo	80.2	85.3	83.1	78.3	85.2
Fa	18.7	14.0	16.2	20.4	14.0
Mo	1.1	0.7	0.7	1.3	0.8

Table B-3 (continued): **OLIVINE**
Spanish Lake

Sample	24/8/14 OL4R-SL	24/8/14 OL5G-SL	24/8/14 OL6G-SL	24/8/14 OL7C-SL	24/8/14 OL7R-SL
Major oxides (wt.%)					
SiO_2	37.7	36.7	35.8	39.3	39.4
TiO_2	0.0	0.0	0.2	0.0	0.0
Al_2O_3	0.0	0.0	0.0	0.0	0.0
FeO	25.5	31.3	33.5	19.0	17.7
MnO	0.4	0.6	0.7	0.2	0.2
MgO	36.2	30.9	28.7	41.8	42.5
CaO	0.4	0.6	0.8	0.2	0.4
NiO	0.0	0.0	0.0	0.2	0.1
Total	100.2	100.1	99.7	100.8	100.2
Cations on the basis of 4 oxygens					
Si	0.996	0.999	0.994	0.998	1.000
Ti	0.000	0.000	0.004	0.000	0.000
Al	0.000	0.000	0.000	0.000	0.000
Fe^{2+}	0.563	0.714	0.777	0.404	0.375
Mn	0.009	0.013	0.016	0.005	0.004
Mg	1.425	1.256	1.187	1.584	1.610
Ca	0.011	0.019	0.023	0.006	0.010
Ni	0.000	0.000	0.000	0.004	0.002
End member percentages					
Fo	70.4	61.8	58.1	78.9	80.1
Fa	28.5	36.3	39.6	20.4	19.0
Mo	1.1	1.9	2.3	0.6	1.0

Table B-3 (continued): **OLIVINE**
Spanish Lake to Flourmill

Sample	3/8/4 OL1XC-SL	3/8/4 OL1XR-SL	3/8/4 OL2C-SL	2/8/6 OL1XC-SC	2/8/6 OL1XR-SC
Major oxides (wt.%)					
SiO_2	40.7	39.1	39.7	40.6	39.7
TiO_2	0.0	0.0	0.0	0.0	0.0
Al_2O_3	0.0	0.0	0.0	0.0	0.0
FeO	9.4	16.1	14.9	14.2	19.1
MnO	0.1	0.2	0.2	0.2	0.2
MgO	49.5	43.6	44.8	45.7	42.1
CaO	0.0	0.3	0.3	0.3	0.3
NiO	0.0	0.0	0.0	0.0	0.0
Total	99.7	99.3	99.9	100.9	101.4
Cations on the basis of 4 oxygens					
Si	0.998	0.995	0.998	1.005	1.001
Ti	0.000	0.000	0.000	0.000	0.000
Al	0.000	0.000	0.000	0.000	0.000
Fe^{2+}	0.192	0.342	0.313	0.294	0.403
Mn	0.003	0.005	0.004	0.004	0.004
Mg	1.810	1.654	1.679	1.686	1.583
Ca	0.000	0.008	0.008	0.007	0.008
Ni	0.000	0.000	0.000	0.000	0.000
End member percentages					
Fo	90.3	81.9	83.4	84.3	78.9
Fa	9.7	17.3	15.8	14.9	20.4
Mo	0.0	0.8	0.8	0.7	0.8

Table B-3 (continued): **OLIVINE**
Flourmill

Sample	2/8/6 OL2C-SC	2/8/6 OL2R-SC	2/8/6 OL3C-SC	2/8/6 OL3R-SC	2/8/6 OL4XC-SC
Major oxides (wt.%)					
SiO_2	40.5	39.4	40.0	39.6	40.3
TiO_2	0.0	0.0	0.0	0.0	0.0
Al_2O_3	0.0	0.0	0.0	0.0	0.0
FeO	13.6	16.9	13.8	17.3	16.5
MnO	0.2	0.2	0.2	0.2	0.2
MgO	45.3	43.0	45.3	42.8	44.2
CaO	0.3	0.3	0.3	0.3	0.3
NiO	0.0	0.0	0.0	0.0	0.0
Total	99.8	99.9	99.5	100.3	101.6
Cations on the basis of 4 oxygens					
Si	1.010	1.000	1.004	1.003	1.003
Ti	0.000	0.000	0.000	0.000	0.000
Al	0.000	0.000	0.000	0.000	0.000
Fe^{2+}	0.283	0.359	0.289	0.367	0.344
Mn	0.003	0.004	0.004	0.005	0.004
Mg	1.684	1.628	1.693	1.614	1.639
Ca	0.009	0.008	0.007	0.009	0.008
Ni	0.000	0.000	0.000	0.000	0.000
End member percentages					
Fo	84.6	81.0	84.6	80.5	81.8
Fa	14.5	18.2	14.7	18.6	17.4
Mo	0.9	0.8	0.7	0.9	0.8

Table B-3 (continued): **OLIVINE**
Flourmill

Sample	2/8/6 OL4XR-SC	2/8/6 OL5C-SC	2/8/6 OL5R-SC	2/8/6 OL6G-SC	4/8/1 OL1C-SC
Major oxides (wt.%)					
SiO_2	38.9	39.9	39.5	39.7	39.0
TiO_2	0.0	0.0	0.0	0.0	0.0
Al_2O_3	0.0	0.0	0.0	0.0	0.0
FeO	21.0	17.2	17.9	17.1	15.0
MnO	0.3	0.2	0.2	0.2	0.2
MgO	40.3	43.7	42.8	43.3	44.1
CaO	0.4	0.2	0.3	0.3	0.2
NiO	0.0	0.0	0.0	0.0	0.0
Total	101.0	101.2	100.7	100.5	98.5
Cations on the basis of 4 oxygens					
Si	0.997	1.000	0.999	1.001	0.995
Ti	0.000	0.000	0.000	0.000	0.000
Al	0.000	0.000	0.000	0.000	0.000
Fe^{2+}	0.449	0.361	0.378	0.360	0.320
Mn	0.006	0.003	0.004	0.004	0.004
Mg	1.539	1.630	1.612	1.626	1.679
Ca	0.012	0.006	0.009	0.009	0.006
Ni	0.000	0.000	0.000	0.000	0.000
End member percentages					
Fo	76.1	81.2	80.0	80.9	83.3
Fa	22.7	18.2	19.1	18.2	16.1
Mo	1.2	0.6	0.9	0.9	0.6

Table B-3 (continued): **OLIVINE**
Flourmill

Sample	4/8/1 OL1M-SC	4/8/1 OL1R-SC	4/8/1 OL3C-SC	4/8/1 OL3R-SC	4/8/1 OL4C-SC
Major oxides (wt.%)					
SiO_2	38.9	38.7	39.3	38.8	39.2
TiO_2	0.0	0.0	0.0	0.0	0.0
Al_2O_3	0.0	0.0	0.0	0.0	0.0
FeO	14.8	16.7	13.4	15.9	13.1
MnO	0.1	0.2	0.1	0.2	0.2
MgO	44.0	42.7	45.6	43.2	45.5
CaO	0.2	0.3	0.3	0.3	0.2
NiO	0.0	0.0	0.0	0.0	0.0
Total	98.1	98.7	98.7	98.4	98.1
Cations on the basis of 4 oxygens					
Si	0.997	0.995	0.994	0.996	0.996
Ti	0.000	0.000	0.000	0.000	0.000
Al	0.000	0.000	0.000	0.000	0.000
Fe^{2+}	0.318	0.359	0.283	0.341	0.277
Mn	0.003	0.005	0.003	0.005	0.004
Mg	1.681	1.636	1.719	1.654	1.721
Ca	0.006	0.009	0.007	0.007	0.005
Ni	0.000	0.000	0.000	0.000	0.000
End member percentages					
Fo	83.5	81.0	85.1	82.0	85.5
Fa	16.0	18.1	14.2	17.3	14.0
Mo	0.6	0.9	0.7	0.7	0.5

Table B-3 (continued): **OLIVINE**
Flourmill

Sample	4/8/1 OL4R-SC	4/8/1 OL5C-SC	4/8/1 OL5R-SC	4/8/7 OL1C-SC	4/8/7 OL1R-SC
Major oxides (wt.%)					
SiO_2	38.5	38.8	38.5	39.9	38.6
TiO_2	0.0	0.0	0.0	0.0	0.0
Al_2O_3	0.0	0.0	0.0	0.0	0.0
FeO	17.0	16.0	16.9	12.7	19.0
MnO	0.3	0.2	0.3	0.2	0.3
MgO	42.2	43.6	42.2	46.3	41.4
CaO	0.4	0.3	0.3	0.2	0.3
NiO	0.0	0.0	0.0	0.0	0.0
Total	98.4	98.9	98.2	99.3	99.6
Cations on the basis of 4 oxygens					
Si	0.995	0.993	0.996	0.998	0.993
Ti	0.000	0.000	0.000	0.000	0.000
Al	0.000	0.000	0.000	0.000	0.000
Fe^{2+}	0.368	0.342	0.366	0.266	0.410
Mn	0.006	0.004	0.006	0.003	0.006
Mg	1.626	1.662	1.628	1.729	1.589
Ca	0.011	0.008	0.009	0.005	0.009
Ni	0.000	0.000	0.000	0.000	0.000
End member percentages					
Fo	80.4	82.1	80.6	86.0	78.4
Fa	18.6	17.2	18.5	13.4	20.7
Mo	1.1	0.7	0.9	0.5	0.9

Table B-3 (continued): **OLIVINE**
Flourmill

Sample	4/8/7 OL2C-SC	4/8/7 OL2R-SC	4/8/7 OL3C-SC	4/8/7 OL3R-SC	4/8/2 OL1XC-SC
Major oxides (wt.%)					
SiO_2	38.0	37.3	39.7	39.2	39.2
TiO_2	0.0	0.0	0.0	0.0	0.0
Al_2O_3	0.0	0.0	0.0	0.0	0.0
FeO	15.7	18.3	12.9	15.7	15.0
MnO	0.2	0.3	0.2	0.2	0.2
MgO	42.6	39.8	46.1	43.5	43.6
CaO	0.3	0.3	0.3	0.3	0.3
NiO	0.0	0.0	0.0	0.0	0.0
Total	96.8	95.9	99.2	98.8	98.3
Cations on the basis of 4 oxygens					
Si	0.993	0.996	0.997	1.000	1.002
Ti	0.000	0.000	0.000	0.000	0.000
Al	0.000	0.000	0.000	0.000	0.000
Fe^{2+}	0.344	0.408	0.272	0.335	0.322
Mn	0.003	0.006	0.004	0.005	0.003
Mg	1.659	1.584	1.722	1.653	1.664
Ca	0.008	0.009	0.008	0.007	0.007
Ni	0.000	0.000	0.000	0.000	0.000
End member percentages					
Fo	82.0	78.4	85.4	82.3	83.0
Fa	17.3	20.6	13.8	17.0	16.3
Mo	0.8	0.9	0.8	0.7	0.7

Table B-3 (continued): **OLIVINE**
Flourmill

Sample	4/8/2 OL1XR-SC	4/8/2 OL2C-SC	4/8/2 OL2R-SC	4/8/2 OL3C-SC	4/8/2 OL3R-SC
Major oxides (wt.%)					
SiO_2	38.9	40.5	39.8	39.0	38.7
TiO_2	0.0	0.0	0.0	0.0	0.0
Al_2O_3	0.0	0.0	0.0	0.0	0.0
FeO	18.7	14.4	18.8	15.3	17.7
MnO	0.2	0.2	0.2	0.2	0.2
MgO	41.3	45.7	42.4	43.6	41.4
CaO	0.3	0.3	0.3	0.3	0.3
NiO	0.0	0.0	0.0	0.0	0.0
Total	99.4	101.0	101.4	98.4	98.4
Cations on the basis of 4 oxygens					
Si	1.000	1.003	1.001	0.999	1.002
Ti	0.000	0.000	0.000	0.000	0.000
Al	0.000	0.000	0.000	0.000	0.000
Fe^{2+}	0.402	0.297	0.396	0.327	0.384
Mn	0.004	0.004	0.004	0.004	0.005
Mg	1.585	1.686	1.589	1.664	1.599
Ca	0.009	0.007	0.009	0.008	0.008
Ni	0.000	0.000	0.000	0.000	0.000
End member percentages					
Fo	78.8	84.2	79.0	82.7	79.7
Fa	20.3	15.1	20.0	16.5	19.5
Mo	0.9	0.7	0.9	0.8	0.9

Table B-3 (continued): **OLIVINE**
Flourmill to Ray Mountain

Sample	4/8/2 OL4C-SC	4/8/2 OL4R-SC	4/8/2 OL5C-SC	4/8/2 OL5R-SC	17/8/3 OL1C-RM
Major oxides (wt.%)					
SiO_2	40.2	39.4	39.0	38.6	38.8
TiO_2	0.0	0.0	0.0	0.0	0.0
Al_2O_3	0.0	0.0	0.0	0.0	0.2
FeO	15.1	19.5	15.9	19.8	23.5
MnO	0.2	0.2	0.1	0.2	0.3
MgO	44.9	41.6	43.0	40.1	39.0
CaO	0.3	0.4	0.3	0.4	0.3
NiO	0.0	0.0	0.0	0.0	0.1
Total	100.6	101.3	98.2	99.2	102.1
Cations on the basis of 4 oxygens					
Si	1.003	0.999	1.002	1.002	0.992
Ti	0.000	0.000	0.000	0.000	0.000
Al	0.000	0.000	0.000	0.000	0.006
Fe^{2+}	0.314	0.414	0.341	0.429	0.503
Mn	0.004	0.005	0.002	0.005	0.006
Mg	1.668	1.571	1.645	1.550	1.488
Ca	0.009	0.011	0.007	0.012	0.008
Ni	0.000	0.000	0.000	0.000	0.002
End member percentages					
Fo	83.2	77.9	82.1	77.0	73.8
Fa	15.9	20.9	17.2	21.8	25.4
Mo	0.9	1.1	0.7	1.2	0.8

Table B-3 (continued): **OLIVINE**
Ray Mountain

Sample	17/8/3 OL1R-RM	17/8/7 OL1C-RM	17/8/7 OL1R-RM	17/8/7 OL2C-RM	17/8/7 OL2R-RM
Major oxides (wt.%)					
SiO_2	38.9	37.1	36.5	38.6	37.1
TiO_2	0.0	0.0	0.0	0.0	0.0
Al_2O_3	0.0	0.3	0.3	0.2	0.3
FeO	23.1	29.7	32.2	23.1	30.1
MnO	0.3	0.5	0.6	0.3	0.5
MgO	39.2	33.1	30.9	38.9	32.6
CaO	0.3	0.3	0.4	0.3	0.3
NiO	0.0	0.0	0.0	0.0	0.0
Total	101.7	100.9	100.9	101.5	100.9
Cations on the basis of 4 oxygens					
Si	0.997	0.992	0.991	0.993	0.994
Ti	0.000	0.000	0.000	0.000	0.000
Al	0.000	0.008	0.010	0.007	0.008
Fe^{2+}	0.495	0.664	0.730	0.498	0.676
Mn	0.006	0.012	0.014	0.006	0.012
Mg	1.499	1.319	1.248	1.491	1.302
Ca	0.007	0.009	0.011	0.009	0.009
Ni	0.000	0.000	0.000	0.000	0.000
End member percentages					
Fo	74.3	65.4	61.8	73.9	64.7
Fa	24.9	33.7	37.1	25.1	34.4
Mo	0.7	0.9	1.1	0.9	0.9

Table B-3 (continued): **OLIVINE**
Ray Mountain

Sample	17/8/7 OL3C-RM	17/8/7 OL3R-RM	17/8/7 OL4C-RM	17/8/7 OL4R-RM	17/8/7 OL6G-RM
Major oxides (wt.%)					
SiO_2	38.1	36.8	38.0	37.4	36.0
TiO_2	0.0	0.0	0.0	0.0	0.0
Al_2O_3	0.3	0.3	0.2	0.3	0.3
FeO	26.4	31.8	25.0	29.1	32.9
MnO	0.4	0.6	0.4	0.5	0.6
MgO	36.1	31.3	37.2	33.6	29.5
CaO	0.3	0.4	0.3	0.4	0.3
NiO	0.0	0.0	0.0	0.0	0.0
Total	101.6	101.2	101.1	101.3	99.5
Cations on the basis of 4 oxygens					
Si	0.994	0.993	0.991	0.993	0.995
Ti	0.000	0.000	0.000	0.000	0.000
Al	0.009	0.009	0.007	0.009	0.009
Fe^{2+}	0.578	0.717	0.546	0.646	0.761
Mn	0.009	0.014	0.008	0.011	0.014
Mg	1.403	1.259	1.445	1.332	1.213
Ca	0.010	0.011	0.009	0.012	0.010
Ni	0.000	0.000	0.000	0.000	0.000
End member percentages					
Fo	69.7	62.4	71.5	66.0	60.3
Fa	29.3	36.5	27.6	32.9	38.8
Mo	1.0	1.1	0.9	1.2	1.0

Table B-3 (continued): **OLIVINE**
Ray Mountain

Sample	17/8/13 OL 1C-RM	17/8/13 OL 1C-RM	17/8/13 OL 1R-RM	17/8/13 OL 1R-RM	17/8/13 OL2C-RM
Major oxides (wt.%)					
SiO_2	38.0	37.8	38.3	38.3	38.9
TiO_2	0.0	0.0	0.0	0.0	0.0
Al_2O_3	0.2	0.0	0.2	0.0	0.0
FeO	27.5	26.8	25.1	24.1	23.4
MnO	0.3	0.3	0.5	0.5	0.2
MgO	35.8	36.2	37.4	37.8	38.8
CaO	0.2	0.1	0.3	0.3	0.1
NiO	0.0	0.0	0.0	0.0	0.0
Total	102.1	101.2	101.9	100.8	101.5
Cations on the basis of 4 oxygens					
Si	0.992	0.992	0.992	0.996	1.000
Ti	0.000	0.000	0.000	0.000	0.000
Al	0.008	0.000	0.007	0.000	0.000
Fe^{2+}	0.601	0.587	0.543	0.524	0.504
Mn	0.007	0.007	0.012	0.011	0.005
Mg	1.392	1.417	1.442	1.465	1.488
Ca	0.006	0.004	0.009	0.007	0.004
Ni	0.000	0.000	0.000	0.000	0.000
End member percentages					
Fo	69.1	70.1	71.5	72.6	74.2
Fa	30.3	29.5	27.7	26.6	25.4
Mo	0.6	0.4	0.9	0.7	0.4

Table B-3 (continued): **OLIVINE**
Ray Mountain

Sample	17/8/13 OL2C-RM	17/8/13 OL2R-RM	17/8/13 OL2R-RM	17/8/13 OL3C-RM	17/8/13 OL3C-RM
Major oxides (wt.%)					
SiO_2	38.4	38.2	38.4	39.5	39.3
TiO_2	0.0	0.0	0.0	0.0	0.0
Al_2O_3	0.0	0.2	0.0	0.2	0.0
FeO	23.0	24.9	23.6	19.4	18.4
MnO	0.2	0.4	0.4	0.2	0.2
MgO	39.1	37.4	38.2	42.0	42.7
CaO	0.1	0.2	0.2	0.3	0.2
NiO	0.0	0.0	0.0	0.1	0.1
Total	101.0	101.4	100.9	101.7	101.0
Cations on the basis of 4 oxygens					
Si	0.993	0.994	0.997	0.996	0.994
Ti	0.000	0.000	0.000	0.000	0.000
Al	0.000	0.006	0.000	0.006	0.000
Fe^{2+}	0.498	0.541	0.513	0.409	0.389
Mn	0.005	0.010	0.009	0.004	0.005
Mg	1.508	1.447	1.478	1.577	1.609
Ca	0.004	0.006	0.006	0.007	0.006
Ni	0.000	0.000	0.000	0.003	0.003
End member percentages					
Fo	74.7	71.9	73.4	78.6	79.9
Fa	25.0	27.5	26.0	20.6	19.6
Mo	0.4	0.6	0.6	0.7	0.6

Table B-3 (continued): **OLIVINE**
Ray Mountain

Sample	17/8/13 OL3R-RM	17/8/13 OL3R-RM	17/8/13 OL4C-RM	17/8/13 OL4C-RM	17/8/13 OL4R-RM
Major oxides (wt.%)					
SiO_2	38.2	38.1	40.4	39.8	38.6
TiO_2	0.0	0.0	0.0	0.0	0.2
Al_2O_3	0.0	0.0	0.2	0.2	0.3
FeO	24.6	23.9	14.7	16.5	23.2
MnO	0.5	0.5	0.2	0.3	0.5
MgO	37.6	38.0	45.9	43.6	38.9
CaO	0.2	0.2	0.3	0.3	0.3
NiO	0.0	0.0	0.3	0.3	0.0
Total	101.2	100.6	102.0	100.9	102.0
Cations on the basis of 4 oxygens					
Si	0.994	0.993	0.995	0.997	0.989
Ti	0.000	0.000	0.000	0.000	0.003
Al	0.000	0.000	0.006	0.007	0.008
Fe^{2+}	0.535	0.520	0.303	0.346	0.498
Mn	0.011	0.010	0.004	0.005	0.011
Mg	1.459	1.478	1.681	1.632	1.487
Ca	0.007	0.006	0.008	0.007	0.009
Ni	0.000	0.000	0.005	0.005	0.000
End member percentages					
Fo	72.2	73.1	83.9	81.7	73.7
Fa	27.1	26.3	15.4	17.6	25.4
Mo	0.7	0.6	0.8	0.7	0.9

Table B-3 (continued): **OLIVINE**
Ray Mountain

Sample	17/8/13 OL4R-RM	17/8/13 OL5C-RM	17/8/13 OL5C-RM	17/8/13 OL5R-RM	17/8/13 OL5R-RM
Major oxides (wt.%)					
SiO_2	38.8	40.3	39.9	38.4	38.1
TiO_2	0.0	0.0	0.0	0.0	0.0
Al_2O_3	0.0	0.2	0.0	0.2	0.0
FeO	20.8	14.6	13.9	23.7	23.0
MnO	0.5	0.2	0.2	0.5	0.6
MgO	40.1	45.9	45.7	38.1	38.5
CaO	0.3	0.3	0.2	0.3	0.3
NiO	0.0	0.3	0.3	0.0	0.0
Total	100.5	101.9	100.1	101.2	100.4
Cations on the basis of 4 oxygens					
Si	0.999	0.993	0.996	0.993	0.993
Ti	0.000	0.000	0.000	0.000	0.000
Al	0.000	0.006	0.000	0.006	0.000
Fe^{2+}	0.449	0.301	0.290	0.513	0.500
Mn	0.010	0.004	0.003	0.011	0.012
Mg	1.536	1.686	1.703	1.471	1.493
Ca	0.008	0.008	0.006	0.009	0.009
Ni	0.000	0.006	0.007	0.000	0.000
End member percentages					
Fo	76.3	84.1	84.8	72.9	73.7
Fa	22.9	15.2	14.6	26.1	25.4
Mo	0.8	0.8	0.6	0.9	0.9

Table B-3 (continued): **OLIVINE**
Ray Mountain to Ray Ridge

Sample	17/8/13 OL6G-RM	17/8/13 OL7G-RM	18/8/9 OL1C-RR	18/8/9 OL1R-RR	18/8/9 OL2XC-RR
Major oxides (wt.%)					
SiO_2	38.3	38.2	37.2	37.0	38.3
TiO_2	0.0	0.0	0.0	0.0	0.0
Al_2O_3	0.2	0.2	0.0	0.0	0.0
FeO	24.1	25.1	27.4	29.0	21.4
MnO	0.6	0.5	0.5	0.5	0.3
MgO	37.9	37.2	34.5	33.1	39.7
CaO	0.3	0.3	0.4	0.3	0.3
NiO	0.0	0.0	0.0	0.0	0.0
Total	101.5	101.4	100.0	100.0	100.0
Cations on the basis of 4 oxygens					
Si	0.992	0.992	0.995	0.998	0.994
Ti	0.000	0.000	0.000	0.000	0.000
Al	0.007	0.006	0.000	0.000	0.000
Fe^{2+}	0.522	0.546	0.613	0.654	0.464
Mn	0.012	0.011	0.011	0.012	0.008
Mg	1.462	1.440	1.374	1.328	1.533
Ca	0.009	0.009	0.012	0.010	0.007
Ni	0.000	0.000	0.000	0.000	0.000
End member percentages					
Fo	72.5	71.4	67.8	65.8	75.8
Fa	26.6	27.8	31.1	33.2	23.5
Mo	0.9	0.9	1.2	1.0	0.7

Table B-3 (continued): **OLIVINE**
Ray Ridge

Sample	18/8/9 OL2XR-RR	18/8/9 OL3C-RR	18/8/9 OL3R-RR	18/8/9 OL4G-RR	18/8/9 OL5C-RR
Major oxides (wt.%)					
SiO_2	37.1	37.3	36.7	37.0	37.4
TiO_2	0.0	0.0	0.0	0.0	0.0
Al_2O_3	0.0	0.0	0.0	0.0	0.0
FeO	27.4	26.9	28.4	28.3	26.8
MnO	0.5	0.5	0.5	0.5	0.5
MgO	34.6	34.9	34.0	33.7	34.9
CaO	0.4	0.4	0.4	0.4	0.4
NiO	0.0	0.0	0.0	0.0	0.0
Total	100.0	100.0	100.0	100.0	100.0
Cations on the basis of 4 oxygens					
Si	0.992	0.994	0.986	0.994	0.997
Ti	0.000	0.000	0.000	0.000	0.000
Al	0.000	0.000	0.000	0.000	0.000
Fe^{2+}	0.613	0.601	0.640	0.637	0.598
Mn	0.012	0.011	0.012	0.011	0.010
Mg	1.380	1.389	1.365	1.351	1.386
Ca	0.011	0.010	0.011	0.011	0.012
Ni	0.000	0.000	0.000	0.000	0.000
End member percentages					
Fo	67.9	68.6	66.8	66.6	68.5
Fa	31.0	30.4	32.1	32.2	30.3
Mo	1.1	1.0	1.1	1.1	1.2

Table B-3 (continued): **OLIVINE**
Ray Ridge to Dragon's Tongue (proximal)

Sample	18/8/9 OL5R-RR	18/8/9 OL6C-RR	18/8/9 OL6R-RR	18/8/4 OL1C-RC	14/8/1 OL1XC-RP
Major oxides (wt.%)					
SiO_2	37.1	37.1	37.2	37.8	38.1
TiO_2	0.0	0.0	0.0	0.0	0.0
Al_2O_3	0.0	0.0	0.0	0.0	0.0
FeO	28.2	28.0	28.7	26.3	29.4
MnO	0.5	0.5	0.5	0.3	0.3
MgO	33.8	34.1	33.2	35.3	35.2
CaO	0.4	0.4	0.4	0.2	0.0
NiO	0.0	0.0	0.0	0.0	0.0
Total	100.0	100.0	100.0	100.0	103.0
Cations on the basis of 4 oxygens					
Si	0.995	0.995	1.000	1.004	0.994
Ti	0.000	0.000	0.000	0.000	0.000
Al	0.000	0.000	0.000	0.000	0.000
Fe^{2+}	0.633	0.627	0.646	0.584	0.640
Mn	0.012	0.011	0.012	0.007	0.007
Mg	1.354	1.361	1.330	1.396	1.366
Ca	0.011	0.011	0.011	0.006	0.000
Ni	0.000	0.000	0.000	0.000	0.000
End member percentages					
Fo	66.8	67.2	65.9	69.8	67.9
Fa	32.1	31.7	32.9	29.7	32.1
Mo	1.1	1.1	1.1	0.6	0.0

Table B-3 (continued): **OLIVINE**
Dragon's Tongue (proximal)

Sample	14/8/1 OL1XR-RP	14/8/1 OL2C-RP	14/8/1 OL2R-RP	14/8/1 OL3C-RP	14/8/1 OL3R-RP
Major oxides (wt.%)					
SiO_2	39.4	40.4	39.7	39.5	40.0
TiO_2	0.0	0.0	0.0	0.0	0.0
Al_2O_3	0.0	0.0	0.0	0.0	0.0
FeO	21.6	16.6	18.3	21.1	19.0
MnO	0.2	0.1	0.2	0.2	0.2
MgO	40.5	44.4	42.7	41.1	42.3
CaO	0.4	0.2	0.3	0.2	0.4
NiO	0.0	0.0	0.0	0.0	0.0
Total	102.2	101.6	101.1	102.1	101.9
Cations on the basis of 4 oxygens					
Si	0.999	1.003	1.001	0.998	1.003
Ti	0.000	0.000	0.000	0.000	0.000
Al	0.000	0.000	0.000	0.000	0.000
Fe^{2+}	0.457	0.344	0.385	0.446	0.398
Mn	0.005	0.003	0.004	0.004	0.005
Mg	1.529	1.642	1.602	1.548	1.582
Ca	0.011	0.004	0.007	0.005	0.010
Ni	0.000	0.000	0.000	0.000	0.000
End member percentages					
Fo	75.8	82.1	79.8	77.0	78.9
Fa	23.1	17.4	19.5	22.5	20.2
Mo	1.1	0.4	0.7	0.5	1.0

Table B-3 (continued): **OLIVINE**
Dragon's Tongue (proximal)

Sample	14/8/1 OL4C-RP	14/8/1 OL4R-RP	14/8/1 OL5C-RP	14/8/1 OL5R-RP	14/8/1 OL6G-RP
Major oxides (wt.%)					
SiO_2	40.0	39.4	39.6	39.4	39.4
TiO_2	0.0	0.0	0.0	0.0	0.0
Al_2O_3	0.0	0.0	0.0	0.0	0.0
FeO	17.8	20.9	18.1	20.0	19.8
MnO	0.2	0.2	0.2	0.2	0.2
MgO	43.4	40.8	42.4	41.3	41.3
CaO	0.3	0.3	0.2	0.3	0.3
NiO	0.0	0.0	0.0	0.0	0.0
Total	101.8	101.6	100.6	101.3	101.0
Cations on the basis of 4 oxygens					
Si	1.000	1.000	1.002	0.999	1.001
Ti	0.000	0.000	0.000	0.000	0.000
Al	0.000	0.000	0.000	0.000	0.000
Fe^{2+}	0.373	0.444	0.384	0.425	0.420
Mn	0.004	0.005	0.004	0.005	0.005
Mg	1.614	1.542	1.601	1.563	1.565
Ca	0.009	0.009	0.006	0.009	0.009
Ni	0.000	0.000	0.000	0.000	0.000
End member percentages					
Fo	80.2	76.7	80.0	77.6	77.8
Fa	18.9	22.4	19.4	21.5	21.3
Mo	0.9	0.9	0.6	0.9	0.9

Table B-3 (continued): **OLIVINE**
Dragon's Tongue (proximal) to Dragon's Tongue (distal)

Sample	14/8/2 OL1C-RP	14/8/2 OL1R-RP	14/8/2 OL2R-RP	14/8/1 OP1XR-RP	11/8/7 OL1C-RD
Major oxides (wt.%)					
SiO_2	40.3	39.3	37.5	38.7	40.0
TiO_2	0.0	0.0	0.0	0.0	0.0
Al_2O_3	0.0	0.0	0.0	0.0	0.0
FeO	16.5	19.7	19.3	21.9	16.9
MnO	0.2	0.2	0.2	0.3	0.2
MgO	44.3	41.1	39.1	40.1	44.2
CaO	0.2	0.3	0.4	0.3	0.3
NiO	0.0	0.0	0.0	0.0	0.2
Total	101.5	100.6	96.5	101.3	101.8
Cations on the basis of 4 oxygens					
Si	1.002	1.002	0.999	0.992	0.997
Ti	0.000	0.000	0.000	0.000	0.000
Al	0.000	0.000	0.000	0.000	0.000
Fe^{2+}	0.343	0.421	0.430	0.470	0.353
Mn	0.004	0.005	0.006	0.008	0.004
Mg	1.643	1.562	1.554	1.531	1.639
Ca	0.007	0.009	0.011	0.007	0.007
Ni	0.000	0.000	0.000	0.000	0.004
End member percentages					
Fo	81.9	77.8	77.1	75.6	81.6
Fa	17.4	21.3	21.8	23.7	17.8
Mo	0.7	0.9	1.1	0.7	0.7

Table B-3 (continued): **OLIVINE**
Dragon's Tongue (distal)

Sample	11/8/7 OL1R-RD	11/8/7 OL2C-RD	11/8/7 OL2R-RD	11/8/7 OL3C-RD	11/8/7 OL3R-RD
Major oxides (wt.%)					
SiO_2	39.5	39.8	39.5	39.9	39.7
TiO_2	0.0	0.0	0.0	0.0	0.0
Al_2O_3	0.0	0.2	0.0	0.0	0.0
FeO	18.5	18.0	18.5	17.6	18.4
MnO	0.3	0.2	0.3	0.2	0.3
MgO	42.4	43.4	42.9	43.5	42.8
CaO	0.4	0.3	0.3	0.3	0.4
NiO	0.1	0.2	0.1	0.1	0.0
Total	101.2	102.0	101.6	101.6	101.5
Cations on the basis of 4 oxygens					
Si	0.996	0.993	0.994	0.997	0.997
Ti	0.000	0.000	0.000	0.000	0.000
Al	0.000	0.006	0.000	0.000	0.000
Fe^{2+}	0.391	0.376	0.388	0.369	0.387
Mn	0.006	0.005	0.006	0.005	0.005
Mg	1.597	1.613	1.606	1.621	1.604
Ca	0.011	0.008	0.009	0.008	0.010
Ni	0.003	0.004	0.002	0.003	0.000
End member percentages					
Fo	79.1	80.2	79.5	80.6	79.5
Fa	19.8	19.0	19.6	18.6	19.6
Mo	1.1	0.8	0.9	0.8	1.0

Table B-3 (continued): **OLIVINE**
Dragon's Tongue (distal) to Kostal Lake (older lavas)

Sample	11/8/7	11/8/7	31/8/8	31/8/8	31/8/8
	OL4G-RD	OL5G-RD	OL1C-KP	OL1C-KP	OL1M-KP
Major oxides (wt.%)					
SiO_2	37.4	37.2	39.7	39.4	39.4
TiO_2	0.2	0.2	0.0	0.0	0.0
Al_2O_3	0.3	0.2	0.0	0.0	0.0
FeO	26.2	26.9	14.4	14.4	14.3
MnO	0.4	0.4	0.1	0.2	0.2
MgO	35.2	35.0	45.0	44.8	45.0
CaO	0.8	0.7	0.3	0.2	0.3
NiO	0.0	0.0	0.0	0.0	0.0
Total	100.5	100.6	99.5	99.0	99.3
Cations on the basis of 4 oxygens					
Si	0.989	0.987	0.999	0.997	0.996
Ti	0.005	0.004	0.000	0.000	0.000
Al	0.010	0.007	0.000	0.000	0.000
Fe^{2+}	0.579	0.597	0.303	0.304	0.303
Mn	0.010	0.009	0.003	0.003	0.004
Mg	1.388	1.382	1.690	1.692	1.694
Ca	0.022	0.019	0.007	0.006	0.007
Ni	0.000	0.000	0.000	0.000	0.000
End member percentages					
Fo	68.3	67.9	84.0	84.0	84.0
Fa	29.4	30.2	15.3	15.3	15.3
Mo	2.2	1.9	0.7	0.6	0.7

Table B-3 (continued): **OLIVINE**
Kostal Lake (older lavas)

Sample	31/8/8 OL1R-KP	31/8/8 OL2C-KP	31/8/8 OL2M-KP	31/8/8 OL2M-KP	31/8/8 OL2R-KP
Major oxides (wt.%)					
SiO_2	39.1	39.7	39.7	39.2	39.1
TiO_2	0.0	0.0	0.0	0.0	0.0
Al_2O_3	0.0	0.0	0.0	0.0	0.0
FeO	16.5	15.2	15.0	17.3	18.6
MnO	0.2	0.2	0.1	0.2	0.2
MgO	43.3	44.8	44.8	43.3	42.2
CaO	0.3	0.2	0.2	0.2	0.3
NiO	0.0	0.0	0.0	0.0	0.0
Total	99.4	100.1	99.8	100.2	100.4
Cations on the basis of 4 oxygens					
Si	0.996	0.997	0.998	0.993	0.996
Ti	0.000	0.000	0.000	0.000	0.000
Al	0.000	0.000	0.000	0.000	0.000
Fe^{2+}	0.352	0.319	0.315	0.367	0.396
Mn	0.004	0.004	0.003	0.004	0.005
Mg	1.643	1.677	1.681	1.637	1.601
Ca	0.008	0.006	0.005	0.007	0.007
Ni	0.000	0.000	0.000	0.000	0.000
End member percentages					
Fo	81.4	83.3	83.6	80.9	79.3
Fa	17.7	16.1	15.8	18.4	19.9
Mo	0.8	0.6	0.5	0.7	0.7

Table B-3 (continued): **OLIVINE**
Kostal Lake (older lavas)

Sample	31/8/8 OL3C-KP	31/8/8 OL3R-KP	31/8/8 OL4C-KP	31/8/8 OL4R-KP	31/8/8 OL5C-KP
Major oxides (wt.%)					
SiO_2	40.0	39.8	39.3	38.6	40.0
TiO_2	0.0	0.0	0.0	0.0	0.0
Al_2O_3	0.0	0.0	0.0	0.0	0.0
FeO	13.2	14.8	17.7	21.3	13.5
MnO	0.2	0.2	0.2	0.3	0.1
MgO	46.2	45.1	42.8	39.9	46.0
CaO	0.2	0.3	0.3	0.3	0.2
NiO	0.0	0.0	0.0	0.0	0.0
Total	99.8	100.2	100.3	100.3	99.9
Cations on the basis of 4 oxygns					
Si	0.999	0.998	0.997	0.996	0.998
Ti	0.000	0.000	0.000	0.000	0.000
Al	0.000	0.000	0.000	0.000	0.000
Fe^{2+}	0.275	0.309	0.375	0.459	0.282
Mn	0.004	0.004	0.005	0.006	0.003
Mg	1.718	1.684	1.618	1.533	1.713
Ca	0.006	0.008	0.008	0.009	0.006
Ni	0.000	0.000	0.000	0.000	0.000
End member percentages					
Fo	85.5	83.6	80.2	76.0	85.1
Fa	13.9	15.6	18.9	23.2	14.2
Mo	0.6	0.8	0.8	0.9	0.6

Table B-3 (continued): **OLIVINE**
Kostal Lake (older lavas) to Kostal Lake (south cone)

Sample	31/8/8 OL5R-KP	29/7/6 OL1C-KS	29/7/6 OL1M-KS	29/7/6 OL1M-KS	29/7/6 OL1R-KS
Major oxides (wt.%)					
SiO_2	39.3	38.1	38.5	39.2	39.4
TiO_2	0.0	0.0	0.0	0.0	0.0
Al_2O_3	0.0	0.0	0.0	0.0	0.0
FeO	17.3	22.7	21.6	16.3	16.3
MnO	0.2	0.3	0.3	0.1	0.2
MgO	43.2	38.9	40.0	43.7	43.5
CaO	0.3	0.1	0.1	0.2	0.3
NiO	0.0	0.0	0.0	0.0	0.0
Total	100.3	100.2	100.5	99.5	99.7
Cations on the basis of 4 oxygens					
Si	0.995	0.993	0.994	0.995	0.999
Ti	0.000	0.000	0.000	0.000	0.000
Al	0.000	0.000	0.000	0.000	0.000
Fe^{2+}	0.366	0.495	0.466	0.346	0.347
Mn	0.005	0.006	0.006	0.003	0.004
Mg	1.630	1.509	1.536	1.656	1.644
Ca	0.008	0.003	0.004	0.006	0.007
Ni	0.000	0.000	0.000	0.000	0.000
End member percentages					
Fo	80.7	74.8	76.2	82.1	81.8
Fa	18.4	24.9	23.5	17.3	17.5
Mo	0.8	0.3	0.4	0.6	0.7

Table B-3 (continued): **OLIVINE**
Kostal Lake (south cone)

Sample	29/7/6 OL2C-KS	29/7/6 OL2R-KS	29/7/6 OL3C-KS	29/7/6 OL3R-KS	29/7/6 OL4C-KS
Major oxides (wt.%)					
SiO_2	39.5	39.3	38.2	38.5	39.2
TiO_2	0.0	0.0	0.0	0.0	0.0
Al_2O_3	0.0	0.0	0.0	0.0	0.0
FeO	15.4	17.1	23.5	19.2	14.5
MnO	0.2	0.2	0.4	0.2	0.2
MgO	44.6	43.2	38.4	41.3	45.2
CaO	0.2	0.3	0.2	0.3	0.2
NiO	0.0	0.0	0.0	0.0	0.0
Total	99.9	100.1	100.6	99.6	99.3
Cations on the basis of 4 oxygens					
Si	0.994	0.995	0.994	0.993	0.990
Ti	0.000	0.000	0.000	0.000	0.000
Al	0.000	0.000	0.000	0.000	0.000
Fe^{2+}	0.325	0.363	0.512	0.413	0.307
Mn	0.004	0.005	0.008	0.005	0.004
Mg	1.676	1.634	1.488	1.587	1.704
Ca	0.006	0.007	0.005	0.009	0.005
Ni	0.000	0.000	0.000	0.000	0.000
End member percentages					
Fo	83.0	80.9	73.7	78.3	84.1
Fa	16.4	18.3	25.8	20.8	15.4
Mo	0.6	0.7	0.5	0.9	0.5

Table B-3 (continued): **OLIVINE**
Kostal Lake (south cone)

Sample	29/7/6 OL4R-KS	29/7/6 OL5C-KS	29/7/6 OL5R-KS
Major oxides (wt.%)			
SiO_2	38.9	39.2	39.0
TiO_2	0.0	0.0	0.0
Al_2O_3	0.0	0.0	0.0
FeO	16.1	15.9	17.1
MnO	0.1	0.2	0.2
MgO	43.8	43.9	42.8
CaO	0.2	0.3	0.3
NiO	0.0	0.0	0.0
Total	99.1	99.4	99.4
Cations on the basis of 4 oxygens			
Si	0.992	0.995	0.996
Ti	0.000	0.000	0.000
Al	0.000	0.000	0.000
Fe^{2+}	0.343	0.338	0.366
Mn	0.003	0.005	0.005
Mg	1.664	1.660	1.629
Ca	0.006	0.007	0.009
Ni	0.000	0.000	0.000
End member percentages			
Fo	82.2	82.2	80.6
Fa	17.2	17.1	18.4
Mo	0.6	0.7	0.9

Table B-4
Major element concentrations in incognate olivine

Olivine analyses comprise major oxide concentrations, cation numbers of each ionic species, recalculated on the basis of four oxygen anions and the molecular percentages of end members. Analyses are in the order given below; on each page is a subheading listing the centres described thereon. The source of each analysis is identified by the two-letter suffix, and is plotted on each diagram of this work with the appropriate symbol, as follows:

Suffix	Symbol	Unit
SM	⍐	Spanish Mump
SB	⍐	Spanish Bonk
ST	⍍	Hyalo Ridge
SL	⊠	Spanish Lake Centre
SC	⊞	Flourmill Centre
PY	+	Pyramid Mountain
SP	X	Spahats (Second Canyon dyke)
RM	Y	Ray Mountain
RR	⇞	Ray Ridge
RC	⇞	Pointed Stick Cone
R	Δ	Dragon's Tongue
RP	Δ	Dragon's Tongue (proximal)
RD	Δ	Dragon's Tongue (distal)
KL	O	Kostal Lake
KP	O	Kostal Lake (older lavas)
KN	O	Kostal Lake (north cone)
KS	O	Kostal Lake (south cone)
KT	O	Kostal Lake (lava tube)

Analytical precisions for every element analysed in olivine are listed below at the 99% confidence level, as a percentage of the total concentration of that element. i.c. = insufficient concentration.

Mg	1.8
Al	i.c.
Si	1.0
Ca	6.5
Ti	i.c.
Cr	i.c.
Mn	12.0
Fe	1.7
Ni	12.0

Sample numbers comprise three parts, interpreted as follows :

26/8/3(X)	OL1(X)C,M,R	-SB
Sample number (X if xenolith)	OLivine 1 (X if xenocryst) Core, Median or Rim	Suite suffix

Table B-4 (continued): **OLIVINE**
Spanish Mump to Spanish Lake

Sample	26/8/2X OL1C-SM	26/8/2X OL2C-SM	26/8/2X OL3C-SM	26/8/2X OL3R-SM	24/8/13X OL1C-SL
Major oxides (wt.%)					
SiO_2	41.3	41.9	41.7	41.9	40.7
TiO_2	0.0	0.0	0.0	0.0	0.0
Al_2O_3	0.0	0.0	0.0	0.0	0.0
FeO	10.7	9.7	10.3	10.2	10.0
MnO	0.2	0.2	0.1	0.1	0.1
MgO	49.0	50.0	49.9	50.1	49.4
CaO	0.1	0.0	0.0	0.1	0.1
NiO	0.4	0.5	0.5	0.4	0.4
Total	101.8	102.3	102.5	102.9	100.7
Cations on the basis of 4 oxygens					
Si	1.000	1.004	0.999	1.000	0.993
Ti	0.000	0.000	0.000	0.000	0.000
Al	0.000	0.000	0.000	0.000	0.000
Fe^{2+}	0.217	0.194	0.206	0.205	0.205
Mn	0.004	0.003	0.003	0.003	0.003
Mg	1.768	1.785	1.783	1.781	1.795
Ca	0.004	0.000	0.000	0.003	0.002
Ni	0.008	0.010	0.009	0.008	0.008
End member percentages					
Fo	88.6	90.1	89.5	89.3	89.5
Fa	11.0	9.9	10.5	10.4	10.3
Mo	0.4	0.0	0.0	0.3	0.2

Table B-4 (continued): **OLIVINE**
Spanish Lake to Pyramid Mountain

Sample	24/8/13X OP/ OL2R-SL	24/8/13X OL3C-SL	24/8/13X SP/ OL4R-SL	24/8/13X SP/ OL4R-SL	13/8/10X OL1C-PY
Major oxides (wt.%)					
SiO_2	40.8	40.9	40.3	41.0	42.0
TiO_2	0.0	0.0	0.0	0.0	0.0
Al_2O_3	0.0	0.0	0.0	0.0	0.0
FeO	10.0	10.0	10.1	10.1	9.9
MnO	0.2	0.2	0.2	0.2	0.2
MgO	49.1	49.3	47.4	49.4	50.3
CaO	0.1	0.1	0.1	0.1	0.0
NiO	0.4	0.5	0.5	0.5	0.4
Total	100.6	101.0	98.6	101.3	102.8
Cations on the basis of 4 oxygens					
Si	0.996	0.995	1.005	0.995	1.002
Ti	0.000	0.000	0.000	0.000	0.000
Al	0.000	0.000	0.000	0.000	0.000
Fe^{2+}	0.204	0.204	0.211	0.206	0.197
Mn	0.004	0.004	0.003	0.003	0.003
Mg	1.790	1.789	1.763	1.788	1.789
Ca	0.002	0.003	0.003	0.003	0.000
Ni	0.008	0.010	0.010	0.010	0.008
End member percentages					
Fo	89.4	89.4	88.9	89.3	90.0
Fa	10.3	10.4	10.8	10.4	10.0
Mo	0.2	0.3	0.3	0.3	0.0

Table B-4 (continued): **OLIVINE**
Pyramid Mountain to Ray Ridge

Sample	13/8/10X OL2C-PY	13/8/10X OL3C-PY	18/8/9X OL1C-RR	18/8/9X OL2C-RR	18/8/9X OL3C-RR
Major oxides (wt.%)					
SiO_2	41.9	42.2	39.8	39.5	40.2
TiO_2	0.0	0.0	0.0	0.0	0.0
Al_2O_3	0.0	0.0	0.0	0.0	0.0
FeO	10.4	9.0	18.4	18.7	15.8
MnO	0.2	0.1	0.2	0.3	0.2
MgO	49.9	51.0	43.1	42.6	45.1
CaO	0.0	0.0	0.1	0.3	0.1
NiO	0.4	0.4	0.3	0.2	0.4
Total	102.7	102.7	101.9	101.6	101.8
Cations on the basis of 4 oxygens					
Si	1.001	1.002	0.996	0.995	0.996
Ti	0.000	0.000	0.000	0.000	0.000
Al	0.000	0.000	0.000	0.000	0.000
Fe^{2+}	0.208	0.179	0.385	0.395	0.327
Mn	0.003	0.003	0.005	0.007	0.004
Mg	1.778	1.807	1.609	1.597	1.665
Ca	0.000	0.000	0.004	0.008	0.004
Ni	0.008	0.008	0.005	0.004	0.008
End member percentages					
Fo	89.4	90.9	80.2	79.3	83.2
Fa	10.6	9.1	19.4	20.0	16.5
Mo	0.0	0.0	0.4	0.8	0.4

Table B-5
Major element concentrations in plagioclase

Plagioclase analyses comprise major oxide concentrations, cation numbers of each ionic species, recalculated on the basis of eight oxygen anions and the molecular percentages of end members. Analyses are in the order given below; on each page is a subheading listing the centres described thereon. The source of each analysis is identified by the two-letter suffix, and is plotted on each diagram of this work with the appropriate symbol, as follows:

Suffix	Symbol	Unit
SM	↟⃞	Spanish Mump
SB	↟⃞	Spanish Bonk
ST	Δ⃞	Hyalo Ridge
SL	⊠	Spanish Lake Centre
SC	⊞	Flourmill Centre
PY	+	Pyramid Mountain
SP	X	Spahats (Second Canyon dyke)
RM	Y⃞	Ray Mountain
RR	↟	Ray Ridge
RC	↟	Pointed Stick Cone
R	Δ	Dragon's Tongue
RP	Δ	Dragon's Tongue (proximal)
RD	Δ	Dragon's Tongue (distal)
KL	O	Kostal Lake
KP	O	Kostal Lake (older lavas)
KN	O	Kostal Lake (north cone)
KS	O	Kostal Lake (south cone)
KT	O	Kostal Lake (lava tube)

Analytical precisions for every element analysed in plagioclase are listed below at the 99% confidence level, as a percentage of the total concentration of that element. i.c. = insufficient concentration. Analyses which are poor in quality but which give an approximate composition are labelled thus: ^{1}.

Na	3.7
Al	1.9
Si	0.7
K	5.3
Ca	1.6
Ti	i.c.
Mn	i.c.
Fe	6.1
Zn	i.c.

Sample numbers comprise three parts, interpreted as follows :

26/8/3(X)	PL1(X)C,M,R	-SB
Sample number (X if xenolith)	PLagioclase 1 (X if xenocryst) Core, Median or Rim	Suite suffix

Table B-5 (continued): **PLAGIOCLASE**
Spanish Bonk

Sample	26/8/3 PL1C-SB	26/8/3 PL1R-SB	26/8/3 PL2C-SB	26/8/3 PL2R-SB	26/8/3 PL3C-SB
Major oxides (wt.%)					
SiO_2	51.9	51.3	52.8	51.9	50.9
TiO_2	0.1	0.2	0.1	0.1	0.0
Al_2O_3	30.4	30.7	29.5	30.3	30.8
Fe_2O_3	0.6	0.6	0.7	0.7	0.6
FeO	0.0	0.0	0.0	0.0	0.0
MnO	0.0	0.0	0.0	0.0	0.0
CaO	13.1	13.5	12.3	13.0	13.9
Na_2O	4.6	4.2	4.9	4.3	4.1
K_2O	0.2	0.2	0.3	0.4	0.1
ZnO	0.1	0.2	0.3	0.2	0.2
Total	101.0	100.9	101.0	100.9	100.5
Cations on the basis of 8 oxygens					
Si	2.352	2.331	2.395	2.356	2.320
Ti	0.004	0.005	0.004	0.004	0.000
Al	1.625	1.645	1.576	1.621	1.659
Fe^{3+}	0.020	0.019	0.026	0.024	0.020
Fe^{2+}	0.000	0.000	0.000	0.000	0.000
Mn	0.000	0.000	0.000	0.000	0.000
Ca	0.635	0.659	0.597	0.632	0.678
Na	0.347	0.319	0.373	0.323	0.308
K	0.012	0.010	0.016	0.021	0.008
Zn	0.004	0.007	0.009	0.008	0.006
End member percentages					
An	64.0	66.9	60.9	65.1	68.4
Ab	34.8	32.1	37.5	32.8	30.8
Or	1.2	1.0	1.6	2.1	0.8

Table B-5 (continued): **PLAGIOCLASE**
Spanish Bonk to Hyalo Ridge

Sample	26/8/3 PL4G-SB	26/8/3 PL5G-SB	23/8/6 PL1G-ST	23/8/6 PL2C-ST	23/8/6 PL3C-ST
Major oxides (wt.%)					
SiO_2	52.0	51.5	56.1	53.1	53.1
TiO_2	0.1	0.2	0.2	0.1	0.1
Al_2O_3	30.2	30.4	25.8	28.2	28.4
Fe_2O_3	0.7	0.7	1.1	1.0	1.0
FeO	0.0	0.0	0.0	0.0	0.0
MnO	0.0	0.0	0.0	0.0	0.0
CaO	13.0	13.3	8.6	11.4	11.4
Na_2O	4.5	4.3	6.7	5.2	5.2
K_2O	0.2	0.2	0.7	0.5	0.5
ZnO	0.2	0.4	0.0	0.1	0.1
Total	101.0	101.0	99.2	99.6	99.9
Cations on the basis of 8 oxygens					
Si	2.358	2.340	2.570	2.436	2.432
Ti	0.005	0.006	0.006	0.005	0.004
Al	1.613	1.629	1.395	1.527	1.532
Fe^{3+}	0.024	0.024	0.038	0.033	0.035
Fe^{2+}	0.000	0.000	0.000	0.000	0.000
Mn	0.000	0.000	0.000	0.000	0.000
Ca	0.634	0.649	0.423	0.562	0.559
Na	0.342	0.323	0.509	0.395	0.398
K	0.010	0.009	0.043	0.031	0.032
Zn	0.008	0.013	0.000	0.003	0.003
End member percentages					
An	64.6	66.6	43.4	57.0	56.7
Ab	34.4	32.5	52.2	39.8	40.1
Or	1.0	0.9	4.4	3.2	3.2

Table B-5 (continued): **PLAGIOCLASE**
Hyalo Ridge

Sample	23/8/6 PL4C-ST	23/8/12 PL1G-ST	23/8/12 PL2G-ST	23/8/12 PL3C-ST	23/8/12 PL3R-ST
Major oxides (wt.%)					
SiO_2	53.2	52.5	52.7	52.9	53.9
TiO_2	0.0	0.0	0.1	0.0	0.1
Al_2O_3	28.7	28.7	28.8	28.6	27.6
Fe_2O_3	1.0	0.7	0.7	0.7	0.7
FeO	0.0	0.0	0.0	0.0	0.0
MnO	0.0	0.0	0.0	0.0	0.0
CaO	11.7	12.2	12.1	12.0	10.7
Na_2O	5.2	5.1	4.9	5.1	5.7
K_2O	0.5	0.3	0.4	0.3	0.3
ZnO	0.1	0.0	0.1	0.0	0.0
Total	100.4	99.5	99.8	99.6	99.1
Cations on the basis of 8 oxygens					
Si	2.426	2.412	2.413	2.427	2.479
Ti	0.000	0.000	0.004	0.000	0.004
Al	1.541	1.557	1.558	1.546	1.493
Fe^{3+}	0.036	0.024	0.023	0.023	0.025
Fe^{2+}	0.000	0.000	0.000	0.000	0.000
Mn	0.000	0.000	0.000	0.000	0.000
Ca	0.569	0.599	0.595	0.591	0.529
Na	0.394	0.390	0.371	0.386	0.436
K	0.028	0.020	0.020	0.020	0.020
Zn	0.003	0.000	0.003	0.000	0.000
End member percentages					
An	57.5	59.3	60.4	59.3	53.7
Ab	39.7	38.7	37.5	38.7	44.3
Or	2.8	2.0	2.1	2.0	2.0

Table B-5 (continued): **PLAGIOCLASE**
Hyalo Ridge to Spanish Lake

Sample	23/8/2 PL1G-ST	23/8/2 PL2G-ST	24/8/13 PL1C-SL	24/8/13 PL1R-SL	24/8/13 PL2G-SL
Major oxides (wt.%)					
SiO_2	54.1	54.0	52.5	52.5	52.4
TiO_2	0.0	0.0	0.2	0.2	0.1
Al_2O_3	29.3	29.4	29.9	30.0	30.2
Fe_2O_3	0.9	0.9	0.9	0.9	0.8
FeO	0.0	0.0	0.0	0.0	0.0
MnO	0.0	0.0	0.0	0.0	0.0
CaO	12.8	12.8	13.0	13.0	13.1
Na_2O	5.1	4.8	4.4	4.5	4.5
K_2O	0.2	0.3	0.4	0.4	0.4
ZnO	0.1	0.2	0.1	0.2	0.1
Total	102.5	102.4	101.4	101.7	101.7
Cations on the basis of 8 oxygens					
Si	2.415	2.414	2.371	2.370	2.362
Ti	0.000	0.000	0.006	0.006	0.004
Al	1.544	1.547	1.594	1.593	1.605
Fe^{3+}	0.029	0.031	0.031	0.031	0.028
Fe^{2+}	0.000	0.000	0.000	0.000	0.000
Mn	0.000	0.000	0.000	0.000	0.000
Ca	0.611	0.612	0.629	0.626	0.635
Na	0.379	0.359	0.329	0.339	0.339
K	0.014	0.016	0.023	0.025	0.022
Zn	0.004	0.005	0.005	0.005	0.004
End member percentages					
An	61.0	62.2	64.3	63.4	63.9
Ab	37.6	36.2	33.4	34.0	33.9
Or	1.3	1.6	2.3	2.5	2.2

Table B-5 (continued): **PLAGIOCLASE**
Spanish Lake

Sample	24/8/13 PL3G-SL	24/8/14 PL1G-SL	24/8/14 PL2G-SL	24/8/14 PL3C-SL	24/8/14 PL3R-SL
Major oxides (wt.%)					
SiO_2	51.7	51.7	51.4	51.7	50.8
TiO_2	0.1	0.1	0.2	0.2	0.2
Al_2O_3	30.7	30.7	30.5	29.4	30.7
Fe_2O_3	0.9	0.9	1.0	0.9	1.0
FeO	0.0	0.0	0.0	0.0	0.0
MnO	0.0	0.0	0.0	0.0	0.0
CaO	13.9	14.0	13.7	12.8	14.0
Na_2O	4.1	4.1	4.3	4.7	4.0
K_2O	0.4	0.3	0.4	0.4	0.4
ZnO	0.0	0.0	0.0	0.0	0.1
Total	101.8	101.7	101.5	100.0	101.2
Cations on the basis of 8 oxygens					
Si	2.331	2.331	2.328	2.370	2.309
Ti	0.003	0.004	0.005	0.006	0.005
Al	1.632	1.631	1.628	1.589	1.648
Fe^{3+}	0.030	0.029	0.034	0.030	0.034
Fe^{2+}	0.000	0.000	0.000	0.000	0.000
Mn	0.000	0.000	0.000	0.000	0.000
Ca	0.672	0.675	0.665	0.629	0.681
Na	0.311	0.306	0.328	0.361	0.306
K	0.020	0.020	0.022	0.023	0.020
Zn	0.000	0.000	0.000	0.000	0.004
End member percentages					
An	67.0	67.5	65.5	62.1	67.7
Ab	31.0	30.6	32.3	35.7	30.2
Or	2.0	2.0	2.1	2.3	2.0

Table B-5 (continued): **PLAGIOCLASE**
Flourmill

Sample	2/8/6 PL1C-SC	2/8/6 PL1R-SC	2/8/6 PL2C-SC	2/8/6 PL2R-SC	2/8/6 PL3C-SC
Major oxides (wt.%)					
SiO_2	51.8	52.2	50.9	51.9	50.2
TiO_2	0.1	0.1	0.0	0.1	0.1
Al_2O_3	29.6	29.4	30.0	29.7	30.8
Fe_2O_3	0.9	0.9	0.8	0.8	0.9
FeO	0.0	0.0	0.0	0.0	0.0
MnO	0.0	0.0	0.0	0.0	0.0
CaO	12.9	12.7	13.7	13.1	14.4
Na_2O	4.6	4.5	3.9	4.4	3.7
K_2O	0.4	0.4	0.3	0.4	0.3
ZnO	0.1	0.1	0.1	0.1	0.1
Total	100.4	100.3	99.7	100.6	100.5
Cations on the basis of 8 oxyggens					
Si	2.367	2.384	2.341	2.367	2.299
Ti	0.005	0.003	0.000	0.004	0.004
Al	1.594	1.583	1.626	1.595	1.661
Fe^{3+}	0.029	0.031	0.028	0.028	0.030
Fe^{2+}	0.000	0.000	0.000	0.000	0.000
Mn	0.000	0.000	0.000	0.000	0.000
Ca	0.632	0.620	0.674	0.640	0.706
Na	0.346	0.341	0.297	0.335	0.279
K	0.024	0.025	0.018	0.024	0.016
Zn	0.005	0.003	0.005	0.003	0.004
End member percentages					
An	63.2	63.0	68.3	64.2	70.6
Ab	34.4	34.5	29.9	33.4	27.8
Or	2.4	2.5	1.8	2.4	1.6

Table B-5 (continued): **PLAGIOCLASE**
Flourmill

Sample	4/8/1 PL1C-SC	4/8/1 PL1R-SC	4/8/1 PL2C-SC	4/8/1 PL3G-SC	4/8/1 PL4C-SC
Major oxides (wt.%)					
SiO_2	52.3	51.9	51.3	51.2	51.0
TiO_2	0.1	0.2	0.1	0.1	0.0
Al_2O_3	29.5	29.8	30.3	30.1	30.2
Fe_2O_3	0.8	1.0	1.1	1.4	1.0
FeO	0.0	0.0	0.0	0.0	0.0
MnO	0.0	0.0	0.0	0.0	0.0
CaO	12.8	12.9	13.9	13.6	13.8
Na_2O	4.6	4.4	3.9	4.1	3.9
K_2O	0.3	0.3	0.2	0.2	0.2
ZnO	0.1	0.2	0.1	0.2	0.2
Total	100.5	100.7	101.1	100.9	100.3
Cations on the basis of 8 oxygens					
Si	2.382	2.363	2.331	2.332	2.335
Ti	0.004	0.005	0.004	0.004	0.000
Al	1.585	1.599	1.625	1.616	1.630
Fe^{3+}	0.027	0.033	0.038	0.049	0.035
Fe^{2+}	0.000	0.000	0.000	0.000	0.000
Mn	0.000	0.000	0.000	0.000	0.000
Ca	0.624	0.631	0.676	0.664	0.674
Na	0.346	0.336	0.298	0.308	0.297
K	0.016	0.019	0.013	0.012	0.012
Zn	0.003	0.007	0.005	0.006	0.005
End member percentages					
An	63.4	64.2	68.6	67.7	68.8
Ab	34.9	33.9	30.0	31.2	30.0
Or	1.7	1.9	1.3	1.2	1.2

Table B-5 (continued): **PLAGIOCLASE**
Flourmill

Sample	4/8/1	4/8/2	4/8/2	4/8/2	4/8/7
	PL4R-SC	PL1R-SC	PL2C-SC[1]	PL3C-SC	PL1C-SC[1]
Major oxides (wt.%)					
SiO_2	50.9	51.1	51.4	53.3	51.2
TiO_2	0.0	0.1	0.0	0.2	0.1
Al_2O_3	30.4	30.2	30.1	28.6	30.3
Fe_2O_3	1.1	0.9	1.1	1.2	0.8
FeO	0.0	0.0	0.0	0.0	0.0
MnO	0.0	0.0	0.0	0.0	0.0
CaO	13.9	13.4	13.3	11.7	13.7
Na_2O	3.9	4.2	4.0	5.2	3.8
K_2O	0.1	0.2	0.3	0.4	0.3
ZnO	0.1	0.2	0.1	0.2	0.2
Total	100.4	100.4	100.4	100.9	100.5
Cations on the basis of 8 oxygens					
Si	2.324	2.338	2.348	2.421	2.335
Ti	0.000	0.003	0.000	0.007	0.005
Al	1.638	1.627	1.619	1.532	1.632
Fe^{3+}	0.038	0.032	0.037	0.040	0.028
Fe^{2+}	0.000	0.000	0.000	0.000	0.000
Mn	0.000	0.000	0.000	0.000	0.000
Ca	0.681	0.658	0.653	0.571	0.671
Na	0.294	0.320	0.306	0.395	0.287
K	0.009	0.014	0.017	0.025	0.018
Zn	0.004	0.006	0.005	0.005	0.007
End member percentages					
An	69.3	66.6	67.1	57.8	69.0
Ab	29.8	32.0	31.2	39.6	29.2
Or	0.9	1.4	1.7	2.6	1.9

Table B-5 (continued): **PLAGIOCLASE**
Flourmill to Pyramid Mountain

Sample	4/8/7 PL1R-SC[1]	4/8/7 PL2G-SC[1]	4/8/7 PL3G-SC[1]	13/8/10 PL1G-PY	13/8/10 PL2G-PY[1]
Major oxides (wt.%)					
SiO_2	50.9	51.3	51.2	55.4	55.7
TiO_2	0.0	0.2	0.0	0.2	0.2
Al_2O_3	30.5	30.3	30.1	28.2	27.9
Fe_2O_3	0.8	0.9	1.0	1.2	1.1
FeO	0.0	0.0	0.0	0.0	0.0
MnO	0.0	0.0	0.0	0.0	0.0
CaO	14.1	13.6	13.5	11.0	10.7
Na_2O	3.6	3.8	3.9	5.9	5.8
K_2O	0.3	0.3	0.3	0.5	0.5
ZnO	0.2	0.2	0.3	0.1	0.1
Total	100.4	100.7	100.2	102.5	102.1
Cations on the basis of 8 oxygens					
Si	2.324	2.335	2.343	2.471	2.489
Ti	0.000	0.005	0.000	0.006	0.005
Al	1.644	1.628	1.625	1.483	1.472
Fe^{3+}	0.029	0.032	0.034	0.039	0.037
Fe^{2+}	0.000	0.000	0.000	0.000	0.000
Mn	0.000	0.000	0.000	0.000	0.000
Ca	0.690	0.666	0.660	0.527	0.513
Na	0.271	0.286	0.295	0.436	0.431
K	0.018	0.020	0.019	0.029	0.030
Zn	0.007	0.008	0.009	0.004	0.004
End member percentages					
An	70.7	68.8	68.0	53.3	52.9
Ab	27.4	29.2	30.0	43.8	44.0
Or	1.8	2.0	1.9	2.9	3.1

Table B-5 (continued): **PLAGIOCLASE**
Ray Mountain

Sample	17/8/3 PL2G-RM	17/8/7 PL4C-RM	17/8/7 PL4R-RM	17/8/13 PL1G-RM	17/8/13 PL2C-RM
Major oxides (wt.%)					
SiO_2	52.9	51.6	53.3	51.8	53.1
TiO_2	0.2	0.1	0.2	0.1	0.1
Al_2O_3	29.3	29.5	28.8	30.3	29.9
Fe_2O_3	1.1	0.4	0.0	0.8	0.6
FeO	0.0	0.0	0.0	0.0	0.0
MnO	0.0	0.0	0.0	0.0	0.0
CaO	12.6	12.3	11.3	13.5	12.9
Na_2O	4.8	4.7	5.6	4.3	4.9
K_2O	0.3	0.3	0.4	0.2	0.3
ZnO	0.1	0.0	0.0	0.0	0.1
Total	101.3	98.9	99.5	101.1	101.8
Cations on the basis of 8 oxygens					
Si	2.393	2.382	2.440	2.346	2.387
Ti	0.006	0.004	0.008	0.005	0.005
Al	1.560	1.605	1.553	1.620	1.584
Fe^{3+}	0.037	0.015	0.000	0.029	0.019
Fe^{2+}	0.000	0.000	0.000	0.000	0.000
Mn	0.000	0.000	0.000	0.000	0.000
Ca	0.611	0.608	0.553	0.658	0.620
Na	0.363	0.361	0.424	0.321	0.365
K	0.017	0.017	0.021	0.014	0.016
Zn	0.005	0.000	0.000	0.000	0.002
End member percentages					
An	61.9	61.7	55.4	66.3	62.0
Ab	36.4	36.6	42.5	32.3	36.4
Or	1.7	1.7	2.1	1.4	1.6

Table B-5 (continued): **PLAGIOCLASE**
Ray Mountain

Sample	17/8/13 PL2R-RM	17/8/13 PL3G-RM	17/8/13 PL4G-RM	17/8/13 PL5G-RM	17/8/13 PL6C-RM
Major oxides (wt.%)					
SiO_2	52.3	52.1	52.3	52.1	51.8
TiO_2	0.0	0.0	0.1	0.1	0.1
Al_2O_3	30.2	30.8	30.8	30.9	31.3
Fe_2O_3	0.7	0.5	0.5	0.5	0.6
FeO	0.0	0.0	0.0	0.0	0.0
MnO	0.0	0.0	0.0	0.0	0.0
CaO	13.3	13.4	13.3	13.4	13.8
Na_2O	4.5	4.3	4.6	4.4	4.1
K_2O	0.2	0.2	0.2	0.2	0.3
ZnO	0.1	0.1	0.0	0.0	0.0
Total	101.3	101.4	102.0	101.8	102.0
Cations on the basis of 8 oxygens					
Si	2.362	2.350	2.349	2.342	2.325
Ti	0.000	0.000	0.005	0.005	0.004
Al	1.609	1.636	1.631	1.640	1.659
Fe^{3+}	0.025	0.017	0.017	0.019	0.019
Fe^{2+}	0.000	0.000	0.000	0.000	0.000
Mn	0.000	0.000	0.000	0.000	0.000
Ca	0.644	0.648	0.640	0.646	0.665
Na	0.337	0.324	0.346	0.331	0.305
K	0.013	0.014	0.014	0.012	0.015
Zn	0.005	0.003	0.000	0.000	0.000
End member percentages					
An	64.9	65.8	64.0	65.3	67.5
Ab	33.7	32.8	34.6	33.5	31.0
Or	1.3	1.4	1.4	1.2	1.5

Table B-5 (continued): **PLAGIOCLASE**
Ray Mountain to Ray Ridge

Sample	17/8/13	17/8/13	18/8/9	18/8/9	18/8/9
	PL6R-RM	PL6R-RM	PL1C-RR	PL1R-RR	PL3G-RR
Major oxides (wt.%)					
SiO_2	52.0	52.7	51.7	54.2	51.9
TiO_2	0.1	0.1	0.1	0.1	0.0
Al_2O_3	31.1	30.5	30.4	28.6	30.4
Fe_2O_3	0.6	0.6	0.8	0.6	0.7
FeO	0.0	0.0	0.0	0.0	0.0
MnO	0.0	0.0	0.0	0.0	0.0
CaO	13.6	13.0	13.5	11.2	13.3
Na_2O	4.4	4.6	4.4	5.7	4.5
K_2O	0.2	0.2	0.2	0.4	0.2
ZnO	0.0	0.0	0.0	0.2	0.1
Total	101.9	101.7	101.1	101.1	101.1
Cations on the basis of 8 oxygens					
Si	2.335	2.367	2.343	2.449	2.350
Ti	0.004	0.004	0.003	0.005	0.000
Al	1.646	1.615	1.626	1.525	1.626
Fe^{3+}	0.020	0.021	0.027	0.021	0.022
Fe^{2+}	0.000	0.000	0.000	0.000	0.000
Mn	0.000	0.000	0.000	0.000	0.000
Ca	0.653	0.625	0.655	0.542	0.648
Na	0.326	0.344	0.333	0.432	0.337
K	0.014	0.014	0.013	0.020	0.014
Zn	0.000	0.000	0.000	0.006	0.003
End member percentages					
An	65.7	63.6	65.4	54.8	65.0
Ab	32.9	35.0	33.2	43.2	33.6
Or	1.4	1.4	1.3	2.0	1.4

Table B-5 (continued): **PLAGIOCLASE**
Ray Ridge to Pointed Stick Cone

Sample	18/8/9 PL4G-RR	18/8/4 PL1C-RC	18/8/4 PL1R-RC	18/8/4 PL2C-RC	18/8/4 PL3G-RC
Major oxides (wt.%)					
SiO_2	51.3	55.0	54.9	56.2	56.1
TiO_2	0.2	0.0	0.2	0.2	0.2
Al_2O_3	30.1	28.3	28.3	27.5	27.3
Fe_2O_3	1.3	0.8	0.9	0.9	1.0
FeO	0.0	0.0	0.0	0.0	0.0
MnO	0.0	0.0	0.0	0.0	0.0
CaO	13.2	10.7	10.8	9.7	9.5
Na_2O	4.5	6.1	6.1	6.8	6.9
K_2O	0.2	0.3	0.3	0.4	0.3
ZnO	0.1	0.1	0.2	0.1	0.1
Total	100.9	101.5	101.7	101.7	101.4
Cations on the basis of 8 oxygens					
Si	2.336	2.474	2.466	2.516	2.519
Ti	0.006	0.000	0.007	0.006	0.008
Al	1.617	1.502	1.499	1.450	1.446
Fe^{3+}	0.043	0.027	0.031	0.030	0.034
Fe^{2+}	0.000	0.000	0.000	0.000	0.000
Mn	0.000	0.000	0.000	0.000	0.000
Ca	0.643	0.516	0.519	0.466	0.456
Na	0.345	0.456	0.456	0.509	0.514
K	0.012	0.020	0.017	0.021	0.019
Zn	0.004	0.005	0.005	0.003	0.004
End member percentages					
An	64.4	52.3	52.6	46.9	46.3
Ab	34.3	45.7	45.7	51.0	51.7
Or	1.2	2.0	1.7	2.1	1.9

Table B-5 (continued): **PLAGIOCLASE**
Dragon's Tongue (proximal)

Sample	14/8/1	14/8/1	14/8/1	14/8/2	14/8/2
	PL1C-RP	PL1R-RP	PL3C-RP	PL2G-RP	PL3G-RP
Major oxides (wt.%)					
SiO_2	54.1	54.4	54.5	54.8	53.8
TiO_2	0.3	0.4	0.3	0.4	0.3
Al_2O_3	28.6	28.2	28.3	27.7	29.0
Fe_2O_3	1.1	1.3	1.3	1.3	1.1
FeO	0.0	0.0	0.0	0.0	0.0
MnO	0.0	0.0	0.0	0.0	0.0
CaO	11.4	11.0	11.3	10.5	11.8
Na_2O	5.5	5.6	5.7	6.0	5.4
K_2O	0.5	0.6	0.5	0.6	0.4
ZnO	0.0	0.1	0.1	0.0	0.1
Total	101.4	101.5	101.9	101.2	101.8
Cations on the basis of 8 oxygens					
Si	2.437	2.450	2.446	2.473	2.418
Ti	0.009	0.012	0.010	0.014	0.009
Al	1.520	1.498	1.500	1.475	1.535
Fe^{3+}	0.039	0.045	0.043	0.043	0.038
Fe^{2+}	0.000	0.000	0.000	0.000	0.000
Mn	0.000	0.000	0.000	0.000	0.000
Ca	0.548	0.532	0.542	0.508	0.570
Na	0.416	0.424	0.423	0.447	0.402
K	0.027	0.033	0.030	0.033	0.021
Zn	0.000	0.002	0.004	0.000	0.005
End member percentages					
An	55.3	53.9	54.7	51.4	57.6
Ab	42.0	42.8	42.3	45.3	40.3
Or	2.8	3.3	3.0	3.3	2.1

Table B-5 (continued): **PLAGIOCLASE**
Dragon's Tongue (distal) to Kostal Lake (south cone)

Sample	11/8/7 PL1G-RD	11/8/7 PL2G-RD	11/8/7 PL3G-RD	29/7/6 PL1R-KL	29/7/6 PL2G-KL
Major oxides (wt.%)					
SiO_2	51.8	51.5	51.0	52.7	53.2
TiO_2	0.2	0.1	0.1	0.1	0.2
Al_2O_3	29.9	30.4	30.4	29.8	29.4
Fe_2O_3	1.0	1.1	0.9	1.0	1.1
FeO	0.0	0.0	0.0	0.0	0.0
MnO	0.0	0.0	0.0	0.0	0.0
CaO	13.1	13.6	13.7	12.9	12.3
Na_2O	4.4	4.1	4.1	4.8	5.1
K_2O	0.3	0.3	0.3	0.4	0.4
ZnO	0.2	0.2	0.1	0.0	0.0
Total	101.0	101.3	100.6	101.7	101.8
Cations on the basis of 8 oxygens					
Si	2.354	2.335	2.327	2.376	2.395
Ti	0.006	0.004	0.005	0.003	0.006
Al	1.603	1.623	1.636	1.582	1.563
Fe^{3+}	0.036	0.038	0.030	0.036	0.037
Fe^{2+}	0.000	0.000	0.000	0.000	0.000
Mn	0.000	0.000	0.000	0.000	0.000
Ca	0.637	0.659	0.668	0.624	0.595
Na	0.334	0.313	0.312	0.359	0.384
K	0.020	0.017	0.017	0.022	0.023
Zn	0.007	0.006	0.004	0.000	0.000
End member percentages					
An	64.5	66.8	67.1	62.1	59.4
Ab	33.5	31.4	31.2	35.7	38.3
Or	2.0	1.7	1.7	2.2	2.3

Table B-5 (continued): **PLAGIOCLASE**
Kostal Lake (south cone) to Kostal Lake (older lavas)

Sample	29/7/6 PL3G-KL	31/8/8 PL1C-KL	31/8/8 PL1R-KL	31/8/8 PL3G-KL
Major oxides (wt.%)				
SiO_2	53.0	52.7	53.8	53.1
TiO_2	0.2	0.2	0.3	0.2
Al_2O_3	29.3	29.9	29.3	29.9
Fe_2O_3	1.2	1.3	1.3	1.1
FeO	0.0	0.0	0.0	0.0
MnO	0.0	0.0	0.0	0.0
CaO	12.5	13.0	12.2	12.7
Na_2O	4.9	4.5	5.1	4.9
K_2O	0.3	0.4	0.5	0.4
ZnO	0.0	0.1	0.2	0.2
Total	101.4	102.2	102.6	102.6
Cations on the basis of 8 oxygens				
Si	2.394	2.368	2.405	2.375
Ti	0.006	0.007	0.009	0.008
Al	1.562	1.581	1.544	1.578
Fe^{3+}	0.040	0.045	0.043	0.038
Fe^{2+}	0.000	0.000	0.000	0.000
Mn	0.000	0.000	0.000	0.000
Ca	0.604	0.627	0.586	0.611
Na	0.370	0.339	0.377	0.367
K	0.019	0.021	0.029	0.024
Zn	0.000	0.004	0.005	0.006
End member percentages				
An	60.9	63.6	59.3	61.2
Ab	37.2	34.2	37.8	36.4
Or	1.9	2.2	2.9	2.4

Table B-6
Major element concentrations in incognate plagioclase

Plagioclase analyses comprise major oxide concentrations, cation numbers of each ionic species, recalculated on the basis of eight oxygen anions and the molecular percentages of end members. Analyses are in the order given below; on each page is a subheading listing the centres described thereon. Groundmass plagioclases from the host lavas are included for comparison. The source of each analysis is identified by the two-letter suffix, and is plotted on each diagram of this work with the appropriate symbol, as follows:

Suffix	Symbol	Unit
SM	$\boxed{\ddagger}$	Spanish Mump
SB	$\boxed{\ddagger}$	Spanish Bonk
ST	$\boxed{\Delta}$	Hyalo Ridge
SL	☒	Spanish Lake Centre
SC	⊞	Flourmill Centre
PY	+	Pyramid Mountain
SP	X	Spahats (Second Canyon dyke)
RM	$\boxed{Y}$	Ray Mountain
RR	‡	Ray Ridge
RC	‡	Pointed Stick Cone
R	Δ	Dragon's Tongue
RP	Δ	Dragon's Tongue (proximal)
RD	Δ	Dragon's Tongue (distal)
KL	O	Kostal Lake
KP	O	Kostal Lake (older lavas)
KN	O	Kostal Lake (north cone)
KS	O	Kostal Lake (south cone)
KT	O	Kostal Lake (lava tube)

Analytical precisions for every element analysed in plagioclase are listed below at the 99% confidence level, as a percentage of the total concentration of that element. i.c. = insufficient concentration. Analyses which are poor in quality but which give an approximate composition are labelled thus: ^{1}.

Na	3.7
Al	1.9
Si	0.7
K	5.3
Ca	1.6
Ti	i.c.
Mn	i.c.
Fe	6.1
Zn	i.c.

Sample numbers comprise three parts, interpreted as follows :

26/8/3(X)	PL1(X)C,M,R	-SB
Sample number (X if xenolith)	PLagioclase 1 (X if xenocryst) Core, Median or Rim	Suite suffix

Table B-6 (continued): **PLAGIOCLASE**
Flourmill

Sample	4/8/17X PL1C-SC[1]	4/8/17X PL1R-SC	4/8/17X PL2C-SC[1]	4/8/17X PL2M-SC	14/8/17X PL3C-SC
Major oxides (wt.%)					
SiO_2	60.8	58.3	59.8	55.9	59.4
TiO_2	0.0	0.0	0.0	0.0	0.1
Al_2O_3	25.0	26.6	24.7	28.3	25.9
Fe_2O_3	0.4	0.7	0.4	0.6	0.7
FeO	0.0	0.0	0.0	0.0	0.0
MnO	0.0	0.0	0.0	0.0	0.0
CaO	6.9	8.7	7.9	10.8	8.1
Na_2O	7.5	7.2	7.5	6.0	7.7
K_2O	1.0	0.8	0.8	0.6	0.8
ZnO	0.1	0.1	0.1	0.0	0.0
Total	101.8	102.5	101.3	102.2	102.8
Cations on the basis of 8 oxygens					
Si	2.693	2.586	2.670	2.492	2.623
Ti	0.000	0.000	0.000	0.000	0.004
Al	1.307	1.392	1.302	1.487	1.348
Fe^{3+}	0.013	0.022	0.013	0.020	0.024
Fe^{2+}	0.000	0.000	0.000	0.000	0.000
Mn	0.000	0.000	0.000	0.000	0.000
Ca	0.327	0.414	0.379	0.515	0.383
Na	0.552	0.530	0.558	0.445	0.564
K	0.056	0.047	0.048	0.036	0.048
Zn	0.003	0.004	0.004	0.000	0.000
End member percentages					
An	35.2	42.0	38.8	51.7	38.5
Ab	58.8	53.3	56.4	44.7	56.7
Or	6.0	4.7	4.8	3.6	4.8

Table B-6 (continued): **PLAGIOCLASE**
Flourmill

Sample	4/8/17 PL1G-SC[1]	4/8/17 PL2G-SC	4/8/4X PL1C-SC[1]	4/8/4X PL1R-SC	4/8/4X PL2C-SC
Major oxides (wt.%)					
SiO_2	52.3	53.4	56.2	56.4	55.5
TiO_2	0.1	0.3	0.2	0.3	0.3
Al_2O_3	30.7	29.2	27.8	28.0	28.2
Fe_2O_3	1.0	1.3	0.5	0.6	0.7
FeO	0.0	0.0	0.0	0.0	0.0
MnO	0.0	0.0	0.0	0.0	0.0
CaO	13.6	12.3	10.1	10.2	10.6
Na_2O	4.0	4.9	6.1	6.1	5.7
K_2O	0.4	0.6	0.7	0.8	0.7
ZnO	0.3	0.2	0.1	0.1	0.2
Total	102.3	102.2	101.6	102.4	101.7
Cations on the basis of 8 oxygens					
Si	2.344	2.398	2.514	2.509	2.485
Ti	0.005	0.010	0.006	0.009	0.009
Al	1.621	1.547	1.468	1.466	1.489
Fe^{3+}	0.033	0.043	0.016	0.020	0.022
Fe^{2+}	0.000	0.000	0.000	0.000	0.000
Mn	0.000	0.000	0.000	0.000	0.000
Ca	0.654	0.592	0.482	0.484	0.507
Na	0.295	0.367	0.454	0.452	0.429
K	0.023	0.035	0.042	0.043	0.038
Zn	0.010	0.006	0.005	0.004	0.005
End member percentages					
An	67.6	59.8	49.6	49.6	52.4
Ab	30.1	36.7	46.2	46.0	43.8
Or	2.4	3.5	4.3	4.4	3.8

Table B-6 (continued): **PLAGIOCLASE**
Flourmill to Dragon's Tongue (proximal)

Sample	4/8/4 PL1G-SC	4/8/4 PL1R-SC	4/8/4 PL2G-SC	14/8/9X PL1C-RP	14/8/9X PL1C-RP
Major oxides (wt.%)					
SiO_2	51.9	51.7	52.4	54.2	54.5
TiO_2	0.0	0.1	0.1	0.0	0.1
Al_2O_3	30.9	31.1	30.4	29.0	28.7
Fe_2O_3	0.7	0.8	0.9	0.4	0.4
FeO	0.0	0.0	0.0	0.0	0.0
MnO	0.0	0.0	0.0	0.0	0.0
CaO	13.8	13.9	13.2	11.3	11.1
Na_2O	4.1	4.0	4.4	5.4	5.6
K_2O	0.3	0.3	0.3	0.6	0.6
ZnO	0.1	0.2	0.1	0.1	0.1
Total	101.7	102.2	101.8	100.9	101.1
Cations on the basis of 8 oxygens					
Si	2.339	2.323	2.357	2.447	2.457
Ti	0.000	0.004	0.004	0.000	0.004
Al	1.639	1.647	1.611	1.544	1.528
Fe^{3+}	0.023	0.027	0.032	0.013	0.013
Fe^{2+}	0.000	0.000	0.000	0.000	0.000
Mn	0.000	0.000	0.000	0.000	0.000
Ca	0.665	0.670	0.639	0.547	0.538
Na	0.304	0.301	0.330	0.407	0.418
K	0.016	0.016	0.016	0.032	0.032
Zn	0.004	0.007	0.004	0.004	0.005
End member percentages					
An	67.6	68.2	65.1	55.7	54.6
Ab	30.8	30.3	33.4	41.1	42.1
Or	1.7	1.6	1.6	3.3	3.2

Table B-6 (continued): **PLAGIOCLASE**
Dragon's Tongue (proximal)

Sample	14/8/9X PL1C-RP	14/8/9X PL1R-RP	14/8/9X PL2C-RP	14/8/9X PL2R-RP	13/8/1X PL1C-RP
Major oxides (wt.%)					
SiO_2	52.8	54.2	56.5	54.3	55.0
TiO_2	0.1	0.0	0.0	0.0	0.0
Al_2O_3	29.8	29.0	27.4	28.9	29.4
Fe_2O_3	0.4	0.4	0.2	0.4	0.3
FeO	0.0	0.0	0.0	0.0	0.0
MnO	0.0	0.0	0.0	0.0	0.0
CaO	12.5	11.4	9.6	11.3	11.6
Na_2O	4.9	5.3	6.6	5.5	5.6
K_2O	0.4	0.6	0.7	0.5	0.4
ZnO	0.0	0.0	0.1	0.1	0.2
Total	101.0	100.9	101.1	100.9	102.4
Cations on the basis of 8 oxygens					
Si	2.390	2.449	2.541	2.452	2.449
Ti	0.004	0.000	0.000	0.000	0.000
Al	1.591	1.542	1.451	1.540	1.543
Fe^{3+}	0.015	0.015	0.007	0.012	0.009
Fe^{2+}	0.000	0.000	0.000	0.000	0.000
Mn	0.000	0.000	0.000	0.000	0.000
Ca	0.606	0.551	0.461	0.545	0.552
Na	0.366	0.401	0.491	0.413	0.413
K	0.026	0.033	0.043	0.029	0.022
Zn	0.000	0.000	0.003	0.003	0.005
End member percentages					
An	60.7	56.0	46.5	55.4	56.2
Ab	36.7	40.7	49.2	41.7	41.6
Or	2.6	3.3	4.3	2.9	2.2

Table B-6 (continued): **PLAGIOCLASE**
Dragon's Tongue (proximal)

Sample	13/8/1X PL1R-RP	13/8/1X PL2C-RP	13/8/1X PL2R-RP	13/8/1 PL1G-RP	13/8/1 PL2G-RP
Major oxides (wt.%)					
SiO_2	55.7	56.6	57.1	54.6	52.4
TiO_2	0.0	0.1	0.1	0.3	0.2
Al_2O_3	28.8	28.2	28.1	29.1	30.1
Fe_2O_3	0.3	0.3	0.5	1.0	1.0
FeO	0.0	0.0	0.0	0.0	0.0
MnO	0.0	0.0	0.0	0.0	0.0
CaO	10.8	10.1	9.9	11.4	12.8
Na_2O	6.0	6.5	6.6	5.5	4.6
K_2O	0.5	0.5	0.5	0.5	0.4
ZnO	0.2	0.1	0.2	0.1	0.0
Total	102.3	102.4	102.9	102.5	101.4
Cations on the basis of 8 oxygens					
Si	2.481	2.512	2.522	2.435	2.365
Ti	0.000	0.004	0.004	0.009	0.008
Al	1.509	1.477	1.463	1.530	1.602
Fe^{3+}	0.010	0.011	0.016	0.033	0.032
Fe^{2+}	0.000	0.000	0.000	0.000	0.000
Mn	0.000	0.000	0.000	0.000	0.000
Ca	0.516	0.479	0.467	0.543	0.621
Na	0.446	0.480	0.485	0.410	0.346
K	0.027	0.029	0.030	0.030	0.022
Zn	0.008	0.004	0.006	0.004	0.000
End member percentages					
An	52.5	48.7	47.9	55.4	62.8
Ab	44.8	48.4	49.1	41.5	35.0
Or	2.7	2.9	3.0	3.1	2.2

Table B-7
Major element concentrations in oxide

Oxide analyses comprise major oxide concentrations, cation numbers of each ionic species, recalculated on the basis of four or three oxygen anions, as appropriate, and the mole fractions of appropriate components. Analyses are in the order given below; on each page is a subheading listing the centres described thereon. The source of each analysis is identified by the two-letter suffix, and is plotted on each diagram of this work with the appropriate symbol, as follows:

Suffix	Symbol	Unit
SM	[ǂ]	Spanish Mump
SB	[ǂ]	Spanish Bonk
ST	[Δ]	Hyalo Ridge
SL	[X]	Spanish Lake Centre
SC	[+]	Flourmill Centre
PY	+	Pyramid Mountain
SP	X	Spahats (Second Canyon dyke)
RM	[Y]	Ray Mountain
RR	ǂ	Ray Ridge
RC	ǂ	Pointed Stick Cone
R	Δ	Dragon's Tongue
RP	Δ	Dragon's Tongue (proximal)
RD	Δ	Dragon's Tongue (distal)
KL	O	Kostal Lake
KP	O	Kostal Lake (older lavas)
KN	O	Kostal Lake (north cone)
KS	O	Kostal Lake (south cone)
KT	O	Kostal Lake (lava tube)

Analytical precisions for every element analysed in oxide are listed below at the 99% confidence level, as a percentage of the total concentration of that element. i.c. = insufficient concentration, n.a. = not analysed. Analyses which are poor in quality but which give an approximate composition are labelled thus: [1].

Element	Spinel	Magnetite	Ilmenite
Mg	3.1	4.3	4.1
Al	2.6	3.0	4.8
Si	4.1	4.5	i.c.
Ca	n.a.	6.3	i.c.
Ti	3.0	1.3	1.0
Cr	1.7	3.2	i.c.
Mn	5.9	5.9	7.8
Fe	1.1	0.8	1.2
Ni	7.2	i.c.	i.c.
Zn	i.c.	i.c.	i.c.

Sample numbers comprise three parts, interpreted as follows :

26/8/3(X)	OX1(X)C,M,R	-SB
Sample number (X if xenolith)	OXide 1 (X if xenocryst) Core, Median or Rim	Suite suffix

Table B-7 (continued): **OXIDE**
Spanish Mump to Spanish Bonk

Sample	26/8/2 OX1G-SM Spinel	26/8/2 OX2G-SM Spinel	26/8/2 OX3G-SM Spinel	26/8/2 OX4G-SM Spinel	26/8/3 OX1C-SB Ilmenite
Major oxides (wt.%)					
SiO_2	0.4	0.3	0.4	0.3	0.3
TiO_2	16.5	18.5	15.2	17.3	53.9
Al_2O_3	5.6	5.3	6.1	5.4	0.2
Fe_2O_3	31.0	28.9	30.4	31.0	3.2
FeO	39.2	40.8	38.0	39.3	35.0
MnO	0.2	0.3	0.4	0.3	1.0
MgO	5.4	5.3	5.4	5.6	7.1
CaO	0.2	0.2	0.2	0.3	0.2
Cr_2O_3	1.6	0.1	4.5	0.5	0.0
ZnO	0.0	0.0	0.0	0.0	0.0
NiO	0.0	0.0	0.0	0.0	0.0
Total	100.1	99.8	100.5	99.8	100.9
Cations on the basis of oxygen present					
Si	0.014	0.010	0.014	0.011	0.007
Ti	0.438	0.492	0.399	0.458	0.961
Al	0.232	0.221	0.250	0.225	0.007
Fe^{3+}	0.821	0.770	0.801	0.823	0.058
Fe^{2+}	1.154	1.207	1.111	1.158	0.693
Mn	0.007	0.008	0.011	0.008	0.020
Mg	0.284	0.281	0.283	0.293	0.250
Ca	0.006	0.007	0.007	0.010	0.005
Cr	0.044	0.004	0.123	0.013	0.000
Zn	0.000	0.000	0.000	0.000	0.000
Ni	0.000	0.000	0.000	0.000	0.000
Concentrations of trace components					
X(usp)	0.485	0.524	0.486	0.484	n.a.
x(ilm)	n.a.	n.a.	n.a.	n.a.	0.960

Table B-7 (continued): **OXIDE**
Spanish Bonk to Hyalo Ridge

Sample	26/8/3 OX2C-SB Ilmenite	26/8/3 OX1C-SB Ilmenite	26/8/3 OX2C-SB Ilmenite	26/8/3 OX2C-SB Spinel	23/8/2 OX1G-ST Spinel
Major oxides (wt.%)					
SiO_2	0.3	0.3	0.3	0.3	0.4
TiO_2	52.2	54.0	52.2	18.7	2.7
Al_2O_3	0.4	0.2	0.4	2.6	17.6
Fe_2O_3	5.6	4.5	6.6	29.2	14.4
FeO	35.7	33.9	34.8	42.6	19.6
MnO	0.7	1.0	0.7	0.5	0.4
MgO	5.9	7.7	6.4	3.6	11.0
CaO	0.3	0.2	0.3	0.2	0.4
Cr_2O_3	0.3	0.0	0.3	0.6	32.7
ZnO	0.0	0.0	0.0	0.0	0.1
NiO	0.0	0.0	0.0	0.0	0.0
Total	101.2	101.8	102.0	98.3	99.4
Cations on the basis of oxygen present					
Si	0.007	0.006	0.007	0.010	0.013
Ti	0.935	0.951	0.927	0.519	0.066
Al	0.010	0.007	0.010	0.113	0.665
Fe^{3+}	0.100	0.078	0.118	0.810	0.348
Fe^{2+}	0.711	0.664	0.687	1.311	0.525
Mn	0.014	0.020	0.014	0.015	0.011
Mg	0.210	0.269	0.227	0.196	0.526
Ca	0.007	0.005	0.007	0.006	0.014
Cr	0.005	0.000	0.005	0.018	0.828
Zn	0.000	0.000	0.000	0.000	0.003
Ni	0.000	0.000	0.000	0.000	0.000
Concentrations of trace components					
X(usp)	n.a.	n.a.	n.a.	0.530	0.642
x(ilm)	0.933	0.944	0.920	n.a.	n.a.

Table B-7 (continued): **OXIDE**
Hyalo Ridge

Sample	23/8/2 OX2G-ST Spinel	23/8/6 OX1C-ST Spinel	23/8/6 OX2C-ST Spinel	23/8/6 OX2C-ST Ilmenite	23/8/6 OX2C-ST Ilmenite
Major oxides (wt.%)					
SiO_2	0.4	0.4	0.3	1.1	1.1
TiO_2	2.4	10.0	9.8	48.5	48.5
Al_2O_3	18.4	2.6	2.7	0.7	0.7
Fe_2O_3	13.8	45.7	45.9	9.6	9.1
FeO	20.4	38.6	36.5	35.5	35.5
MnO	0.5	0.2	0.2	0.4	0.4
MgO	10.8	1.9	2.4	4.8	4.8
CaO	0.1	0.1	0.5	0.3	0.3
Cr_2O_3	33.6	2.2	1.9	0.2	0.2
ZnO	0.2	0.0	0.0	0.0	0.0
NiO	0.0	0.0	0.0	0.0	0.0
Total	100.6	101.7	100.4	101.2	100.8
Cations on the basis of oxygen present					
Si	0.014	0.015	0.011	0.027	0.027
Ti	0.057	0.274	0.270	0.875	0.878
Al	0.686	0.110	0.117	0.020	0.020
Fe^{3+}	0.329	1.250	1.267	0.173	0.165
Fe^{2+}	0.539	1.173	1.119	0.712	0.716
Mn	0.013	0.005	0.007	0.008	0.008
Mg	0.509	0.105	0.133	0.173	0.173
Ca	0.005	0.006	0.021	0.008	0.008
Cr	0.842	0.063	0.054	0.004	0.004
Zn	0.005	0.000	0.000	0.000	0.000
Ni	0.000	0.000	0.000	0.000	0.000
Concentrations of trace components					
X(usp)	0.665	0.307	0.282	n.a.	n.a.
x(ilm)	n.a.	n.a.	n.a.	0.888	0.893

Table B-7 (continued): **OXIDE**
Hyalo Ridge

Sample	23/8/6 OX3C-ST Spinel	23/8/6 OX4C-ST Spinel	23/8/6 OX4C-ST Ilmenite	23/8/6 OX5C-ST Spinel	23/8/6 OX5R-ST Spinel
Major oxides (wt.%)					
SiO_2	0.4	0.4	0.4	0.5	0.5
TiO_2	9.2	9.9	50.2	12.7	12.5
Al_2O_3	2.8	2.9	0.3	2.8	2.7
Fe_2O_3	46.3	44.0	8.0	36.5	35.9
FeO	36.4	37.1	36.0	38.6	38.0
MnO	0.2	0.3	0.5	0.3	0.4
MgO	2.6	2.4	4.9	3.3	3.2
CaO	0.2	0.2	0.3	0.2	0.3
Cr_2O_3	2.5	3.3	0.4	6.0	5.7
ZnO	0.0	0.0	0.0	0.2	0.0
NiO	0.0	0.0	0.0	0.0	0.0
Total	100.4	100.6	101.0	100.9	99.2
Cations on the basis of oxygen present					
Si	0.015	0.015	0.009	0.017	0.019
Ti	0.252	0.271	0.910	0.344	0.346
Al	0.119	0.124	0.007	0.118	0.116
Fe^{3+}	1.275	1.208	0.146	0.990	0.990
Fe^{2+}	1.114	1.134	0.725	1.164	1.166
Mn	0.006	0.010	0.010	0.008	0.011
Mg	0.140	0.133	0.176	0.176	0.177
Ca	0.008	0.009	0.009	0.008	0.011
Cr	0.072	0.096	0.008	0.170	0.166
Zn	0.000	0.000	0.000	0.005	0.000
Ni	0.000	0.000	0.000	0.000	0.000
Concentrations of trace components					
X(usp)	0.276	0.311	n.a.	0.411	0.411
x(ilm)	n.a.	n.a.	0.908	n.a.	n.a.

Table B-7 (continued): **OXIDE**
Hyalo Ridge

Sample	23/8/6 OX6C-ST Spinel	23/8/6 OX7G-ST Spinel	23/8/6 OX8C-ST Spinel	23/8/6 OX9C-ST Spinel	23/8/6 OX10C-ST Spinel
Major oxides (wt.%)					
SiO_2	0.5	0.5	0.5	0.4	0.4
TiO_2	8.9	15.9	12.8	10.4	8.6
Al_2O_3	2.4	2.2	2.8	2.6	2.8
Fe_2O_3	47.6	35.5	35.6	45.1	40.1
FeO	37.1	41.7	38.8	38.2	35.4
MnO	0.2	0.2	0.3	0.3	0.3
MgO	1.7	2.8	3.2	2.1	2.6
CaO	0.3	0.4	0.2	0.3	0.1
Cr_2O_3	0.9	0.2	6.0	1.4	8.4
ZnO	0.0	0.0	0.0	0.0	0.0
NiO	0.0	0.0	0.0	0.0	0.0
Total	99.5	99.5	100.2	100.9	98.6
Cations on the basis of oxygen present					
Si	0.018	0.019	0.017	0.015	0.014
Ti	0.249	0.440	0.350	0.287	0.240
Al	0.104	0.096	0.121	0.112	0.124
Fe^{3+}	1.335	0.980	0.973	1.242	1.122
Fe^{2+}	1.156	1.282	1.178	1.168	1.099
Mn	0.007	0.007	0.009	0.010	0.010
Mg	0.094	0.156	0.171	0.115	0.141
Ca	0.011	0.015	0.010	0.010	0.004
Cr	0.026	0.006	0.172	0.041	0.245
Zn	0.000	0.000	0.000	0.000	0.000
Ni	0.000	0.000	0.000	0.000	0.000
Concentrations of trace components					
X(usp)	0.264	0.441	0.424	0.306	0.342
x(ilm)	n.a.	n.a.	n.a.	n.a.	n.a.

Table B-7 (continued): OXIDE
Hyalo Ridge

Sample	23/8/6 OX11C-ST Spinel	23/8/6 OX12C-ST Spinel	23/8/6 OX13G-ST Spinel	23/8/12 SP1XC-ST Spinel	23/8/12 SP1XR-ST Spinel
Major oxides (wt.%)					
SiO_2	0.4	0.3	0.3	0.3	0.5
TiO_2	10.6	9.6	15.9	2.9	23.1
Al_2O_3	2.8	2.1	2.4	18.2	2.1
Fe_2O_3	42.2	45.7	34.2	13.5	18.1
FeO	37.5	38.8	41.7	28.2	49.6
MnO	0.3	0.2	0.3	0.4	0.4
MgO	2.6	1.2	3.3	5.9	2.0
CaO	0.3	0.1	0.1	0.2	0.3
Cr_2O_3	3.9	2.5	3.5	30.9	3.8
ZnO	0.0	0.0	0.0	0.1	0.0
NiO	0.0	0.0	0.0	0.0	0.0
Total	100.6	100.5	101.8	100.6	99.8
Cations on the basis of oxygen present					
Si	0.013	0.012	0.011	0.010	0.017
Ti	0.290	0.268	0.429	0.072	0.634
Al	0.122	0.093	0.101	0.704	0.090
Fe^{3+}	1.159	1.275	0.921	0.333	0.499
Fe^{2+}	1.144	1.202	1.250	0.772	1.517
Mn	0.008	0.008	0.010	0.010	0.013
Mg	0.140	0.066	0.175	0.290	0.110
Ca	0.011	0.004	0.005	0.008	0.012
Cr	0.112	0.072	0.099	0.800	0.109
Zn	0.000	0.000	0.000	0.002	0.000
Ni	0.000	0.000	0.000	0.000	0.000
Concentrations of trace components					
X(usp)	0.335	0.311	0.467	0.727	0.718
x(ilm)	n.a.	n.a.	n.a.	n.a.	n.a.

Table B-7 (continued): OXIDE
Hyalo Ridge

Sample	23/8/12 OX2C-ST Ilmenite	23/8/12 OX3C-ST Spinel	23/8/12 OX4C-ST Ilmenite	23/8/12 SP5XC-ST Spinel	23/8/12 SP5XR-ST Spinel
Major oxides (wt.%)					
SiO_2	0.3	0.5	0.3	0.5	0.5
TiO_2	49.6	24.5	51.8	2.7	21.7
Al_2O_3	0.4	1.2	0.2	19.1	3.5
Fe_2O_3	6.7	19.6	2.8	13.1	17.1
FeO	41.5	52.3	44.2	27.9	48.9
MnO	0.5	0.5	0.4	0.4	0.4
MgO	1.5	1.0	1.0	6.4	2.3
CaO	0.2	0.3	0.4	0.1	0.2
Cr_2O_3	0.0	0.0	0.0	30.6	6.9
ZnO	0.0	0.0	0.0	0.0	0.0
NiO	0.0	0.0	0.0	0.0	0.0
Total	100.7	99.9	101.2	100.9	101.4
Cations on the basis of oxygen present					
Si	0.008	0.017	0.007	0.016	0.017
Ti	0.924	0.682	0.963	0.066	0.582
Al	0.012	0.054	0.007	0.730	0.145
Fe^{3+}	0.125	0.547	0.052	0.320	0.460
Fe^{2+}	0.860	1.618	0.913	0.758	1.460
Mn	0.011	0.015	0.009	0.012	0.012
Mg	0.055	0.054	0.039	0.309	0.121
Ca	0.006	0.012	0.010	0.003	0.006
Cr	0.000	0.000	0.000	0.786	0.195
Zn	0.000	0.000	0.000	0.000	0.000
Ni	0.000	0.000	0.000	0.000	0.000
Concentrations of trace components					
X(usp)	n.a.	0.707	n.a.	0.731	0.733
x(ilm)	0.932	n.a.	0.972	n.a.	n.a.

Table B-7 (continued): **OXIDE**
Hyalo Ridge to Spanish Lake

Sample	23/8/12 SP5XR-ST Spinel	23/8/12 OX6G-ST Spinel	23/8/12 OX7C-ST Spinel	24/8/13 SP1XC-SL Spinel	24/8/13 SP1XC-SL Spinel
Major oxides (wt.%)					
SiO_2	0.6	1.1	0.4	1.5	0.4
TiO_2	24.9	24.7	26.3	7.8	16.3
Al_2O_3	2.5	1.5	2.3	12.9	6.8
Fe_2O_3	17.1	17.4	14.7	22.8	22.7
FeO	52.2	53.4	54.1	31.5	39.8
MnO	0.4	0.4	0.4	0.4	0.4
MgO	2.0	0.8	1.3	6.6	5.2
CaO	0.3	0.5	0.3	0.8	0.2
Cr_2O_3	1.7	0.0	1.7	16.3	9.1
ZnO	0.0	0.0	0.0	0.0	0.0
NiO	0.0	0.0	0.0	0.0	0.0
Total	101.7	99.9	101.6	100.6	100.9
Cations on the basis of oxygen present					
Si	0.021	0.042	0.014	0.051	0.015
Ti	0.670	0.684	0.714	0.196	0.424
Al	0.108	0.066	0.100	0.507	0.279
Fe^{3+}	0.461	0.482	0.399	0.571	0.593
Fe^{2+}	1.562	1.647	1.632	0.878	1.154
Mn	0.012	0.013	0.013	0.013	0.013
Mg	0.106	0.046	0.072	0.326	0.266
Ca	0.011	0.020	0.011	0.030	0.006
Cr	0.050	0.000	0.047	0.429	0.250
Zn	0.000	0.000	0.000	0.000	0.000
Ni	0.000	0.000	0.000	0.000	0.000
Concentrations of trace components					
X(usp)	0.741	0.735	0.782	0.543	0.611
x(ilm)	n.a.	n.a.	n.a.	n.a.	n.a.

Table B-7 (continued): **OXIDE**
Spanish Lake

Sample	24/8/13 SP1XR-SL Spinel	24/8/13 SP2XC-SL Spinel	24/8/13 SP2XR-SL Spinel	24/8/13 SP4XC-SL Spinel	24/8/13 OX5G-SL Spinel
Major oxides (wt.%)					
SiO_2	0.4	0.3	0.4	0.6	0.4
TiO_2	20.5	10.0	21.9	2.0	19.0
Al_2O_3	5.6	10.3	4.9	39.9	6.2
Fe_2O_3	20.8	22.5	21.0	13.3	20.5
FeO	44.4	33.1	45.8	17.3	42.8
MnO	0.4	0.5	0.5	0.3	0.5
MgO	4.6	6.0	4.4	15.1	4.9
CaO	0.2	0.2	0.2	0.1	0.2
Cr_2O_3	4.3	17.5	2.8	12.4	7.1
ZnO	0.0	0.0	0.0	0.1	0.0
NiO	0.0	0.0	0.0	0.3	0.0
Total	101.3	100.4	101.9	101.3	101.7
Cations on the basis of oxygen present					
Si	0.016	0.012	0.013	0.016	0.015
Ti	0.538	0.256	0.572	0.043	0.494
Al	0.228	0.415	0.203	1.325	0.254
Fe^{3+}	0.547	0.579	0.550	0.282	0.534
Fe^{2+}	1.295	0.943	1.335	0.406	1.237
Mn	0.013	0.013	0.015	0.007	0.015
Mg	0.238	0.305	0.226	0.633	0.251
Ca	0.007	0.007	0.009	0.003	0.007
Cr	0.118	0.471	0.076	0.277	0.193
Zn	0.000	0.000	0.000	0.002	0.000
Ni	0.000	0.000	0.000	0.006	0.000
Concentrations of trace components					
X(usp)	0.660	0.582	0.665	0.663	0.658
x(ilm)	n.a.	n.a.	n.a.	n.a.	n.a.

Table B-7 (continued): **OXIDE**
Spanish Lake

Sample	24/8/13 OX6G-SL Spinel	24/8/13 OX7G-SL Spinel	24/8/14CX IL1C-SL Ilmenite	24/8/14CX IL2C-SL Ilmenite	24/8/14 OX4G-SL Spinel
Major oxides (wt.%)					
SiO_2	0.4	0.5	0.5	0.5	0.5
TiO_2	20.9	24.1	53.8	51.8	20.7
Al_2O_3	5.6	4.3	0.5	0.3	5.0
Fe_2O_3	20.3	19.3	1.0	1.8	18.6
FeO	44.7	48.8	42.5	44.7	46.6
MnO	0.5	0.6	0.3	0.8	0.6
MgO	4.7	3.9	3.5	1.0	2.9
CaO	0.1	0.3	0.0	0.0	0.4
Cr_2O_3	4.2	0.9	0.0	0.0	5.2
ZnO	0.0	0.0	0.0	0.0	0.0
NiO	0.0	0.0	0.0	0.0	0.0
Total	101.4	102.7	102.0	100.9	100.4
Cations on the basis of oxygen present					
Si	0.014	0.018	0.011	0.013	0.020
Ti	0.547	0.629	0.974	0.967	0.555
Al	0.231	0.177	0.013	0.008	0.208
Fe^{3+}	0.532	0.505	0.017	0.033	0.498
Fe^{2+}	1.300	1.418	0.855	0.926	1.387
Mn	0.014	0.018	0.005	0.017	0.019
Mg	0.243	0.201	0.124	0.037	0.151
Ca	0.004	0.011	0.000	0.000	0.017
Cr	0.114	0.024	0.000	0.000	0.146
Zn	0.000	0.000	0.000	0.000	0.000
Ni	0.000	0.000	0.000	0.000	0.000
Concentrations of trace components					
X(usp)	0.669	0.699	n.a.	n.a.	0.702
x(ilm)	n.a.	n.a.	0.990	0.982	n.a.

Table B-7 (continued): **OXIDE**
Spanish Lake to Flourmill

Sample	24/8/14 OX5C-SL Spinel	24/8/14 OX5R-SL Spinel	4/8/2 SP1XC-SC Spinel	4/8/2 SP1XR-SC Spinel	4/8/2 OX2G-SC Spinel
Major oxides (wt.%)					
SiO_2	0.5	.6	0.4	0.5	0.5
TiO_2	13.8	.6	0.0	14.3	19.2
Al_2O_3	8.8	.2	20.8	5.4	3.3
Fe_2O_3	18.3	9.6	3.2	27.6	29.2
FeO	40.0	17.9	14.2	36.9	42.4
MnO	0.5	.7	0.4	0.7	0.7
MgO	3.5	.3	13.8	5.4	4.4
CaO	0.4	.4	0.1	0.3	0.3
Cr_2O_3	14.4	.7	47.2	9.4	0.0
ZnO	0.0	.0	0.0	0.0	0.0
NiO	0.0	.0	0.0	0.0	0.0
Total	100.2	9 .9	100.1	100.3	100.1
Cations on the basis of oxygen present					
Si	0.017	0 020	0.011	0.016	0.019
Ti	0.363	0 587	0.000	0.377	0.517
Al	0.362	0 178	0.756	0.222	0.140
Fe^{3+}	0.480	0 533	0.074	0.729	0.787
Fe^{2+}	1.169	1 447	0.365	1.083	1.269
Mn	0.015	0 020	0.012	0.020	0.020
Mg	0.182	0 122	0.631	0.280	0.235
Ca	0.014	0 017	0.003	0.010	0.013
Cr	0.399	0 076	1.149	0.262	0.000
Zn	0.000	0 000	0.000	0.000	0.000
Ni	0.000	0 000	0.000	0.000	0.000
Concentrations of trace component					
X(usp)	0.686	0 691	0.903	0.518	0.523
x(ilm)	n.a.	a.	n.a.	n.a.	n.a.

Table B-7 (continued): **OXIDE**
Flourmill

Sample	4/8/2 OX3G-SC Spinel	4/8/2 OX4R-SC Spinel	4/8/7 OX1G-SC Spinel	4/8/7 OX2G-SC Spinel	2/8/6 SP3XC-SC Spinel
Major oxides (wt.%)					
SiO_2	0.6	0.5	0.8	0.5	0.6
TiO_2	18.3	14.6	26.0	25.9	20.0
Al_2O_3	3.6	5.0	3.5	3.2	5.6
Fe_2O_3	30.3	31.0	15.4	16.2	24.3
FeO	41.5	38.0	53.1	52.6	45.5
MnO	0.7	0.6	0.6	0.7	0.5
MgO	4.4	4.7	2.1	2.1	3.7
CaO	0.3	0.2	0.4	0.3	0.3
Cr_2O_3	0.1	5.3	0.0	0.0	1.4
ZnO	0.0	0.0	0.0	0.0	0.0
NiO	0.0	0.0	0.0	0.0	0.0
Total	99.8	100.0	101.8	101.5	101.8
Cations on the basis of oxygen present					
Si	0.020	0.017	0.028	0.018	0.020
Ti	0.494	0.389	0.693	0.696	0.526
Al	0.150	0.210	0.146	0.136	0.230
Fe^{3+}	0.818	0.829	0.410	0.434	0.639
Fe^{2+}	1.245	1.128	1.578	1.572	1.329
Mn	0.023	0.019	0.019	0.021	0.014
Mg	0.235	0.251	0.111	0.111	0.192
Ca	0.012	0.008	0.013	0.012	0.011
Cr	0.003	0.148	0.000	0.000	0.040
Zn	0.000	0.000	0.000	0.000	0.000
Ni	0.000	0.000	0.000	0.000	0.000
Concentrations of trace components					
X(usp)	0.502	0.475	0.766	0.756	0.616
x(ilm)	n.a.	n.a.	n.a.	n.a.	n.a.

Table B-7 (continued): **OXIDE**
Flourmill

Sample	2/8/6 OX1G-SC Spinel	2/8/6 SP4XC-SC Spinel	2/8/6 SP4XR-SC Spinel	2/8/6 OX2G-SC Spinel	4/8/1 OX1C-SC Spinel
Major oxides (wt.%)					
SiO_2	0.6	0.4	0.4	0.6	0.5
TiO_2	19.5	2.1	20.2	20.6	26.9
Al_2O_3	5.5	33.3	5.0	5.1	2.9
Fe_2O_3	26.0	10.9	24.4	24.3	14.1
FeO	44.7	19.4	45.8	46.9	51.6
MnO	0.5	0.4	0.6	0.6	0.6
MgO	3.8	12.8	3.0	2.8	3.1
CaO	0.4	0.2	0.4	0.3	0.1
Cr_2O_3	1.0	21.3	1.2	0.2	0.0
ZnO	0.0	0.3	0.2	0.0	0.0
NiO	0.0	0.0	0.0	0.0	0.0
Total	102.0	101.0	101.2	101.4	99.8
Cations on the basis of oxygen present					
Si	0.020	0.011	0.014	0.020	0.017
Ti	0.512	0.046	0.539	0.548	0.730
Al	0.225	1.151	0.211	0.211	0.123
Fe^{3+}	0.682	0.241	0.650	0.647	0.384
Fe^{2+}	1.306	0.475	1.358	1.388	1.559
Mn	0.015	0.010	0.018	0.018	0.019
Mg	0.198	0.561	0.158	0.149	0.166
Ca	0.013	0.005	0.014	0.012	0.003
Cr	0.029	0.495	0.035	0.006	0.000
Zn	0.000	0.006	0.005	0.000	0.000
Ni	0.000	0.000	0.000	0.000	0.000
Concentrations of trace components					
X(usp)	0.588	0.733	0.619	0.623	0.779
x(ilm)	n.a.	n.a.	n.a.	n.a.	n.a.

Table B-7 (continued): **OXIDE**
Flourmill

Sample	4/8/1 OX1R-SC Spinel	4/8/1 SP1XC-SC Spinel	4/8/1 OX2G-SC Spinel	4/8/1 OX3G-SC Spinel	4/8/1 OX4G-SC Spinel
Major oxides (wt.%)					
SiO_2	0.5	0.4	0.7	0.6	0.5
TiO_2	27.4	1.1	20.5	23.3	23.0
Al_2O_3	2.2	27.3	3.6	2.1	2.4
Fe_2O_3	13.4	8.3	21.8	22.2	22.0
FeO	51.5	16.1	46.7	48.9	48.2
MnO	0.6	0.4	0.6	0.6	0.6
MgO	3.1	14.1	3.0	2.7	3.0
CaO	0.2	0.0	0.3	0.4	0.5
Cr_2O_3	0.0	33.8	4.6	0.7	1.4
ZnO	0.2	0.2	0.0	0.1	0.0
NiO	0.0	0.2	0.0	0.0	0.0
Total	99.3	101.9	101.8	101.5	101.6
Cations on the basis of oxygen present					
Si	0.020	0.013	0.026	0.020	0.017
Ti	0.749	0.025	0.545	0.626	0.617
Al	0.096	0.950	0.152	0.089	0.102
Fe^{3+}	0.366	0.185	0.579	0.599	0.590
Fe^{2+}	1.567	0.398	1.382	1.464	1.439
Mn	0.019	0.009	0.017	0.019	0.019
Mg	0.170	0.621	0.159	0.147	0.160
Ca	0.008	0.000	0.013	0.014	0.018
Cr	0.000	0.789	0.128	0.019	0.039
Zn	0.005	0.005	0.000	0.003	0.000
Ni	0.000	0.004	0.000	0.000	0.000
Concentrations of trace components					
X(usp)	0.788	0.772	0.655	0.657	0.658
x(ilm)	n.a.	n.a.	n.a.	n.a.	n.a.

Table B-7 (continued): **OXIDE**
Pyramid Mountain

Sample	13/8/10 SP1XC-PY Spinel	13/8/10 SP1XR-PY Spinel	13/8/10 OX2G-PY Spinel	13/8/10 OX3G-PY Spinel	13/8/10 OX4G-PY Spinel
Major oxides (wt.%)					
SiO_2	1.3	0.3	0.5	0.5	0.4
TiO_2	3.9	16.1	19.6	18.3	22.0
Al_2O_3	34.2	7.0	5.0	5.6	4.4
Fe_2O_3	18.7	28.2	27.7	28.3	23.7
FeO	23.6	37.9	42.5	41.1	44.2
MnO	0.3	0.3	0.4	0.3	0.4
MgO	12.0	6.2	5.3	5.2	5.4
CaO	0.2	0.1	0.2	0.2	0.2
Cr_2O_3	6.7	4.5	0.1	0.5	0.2
ZnO	0.2	0.0	0.0	0.0	0.0
NiO	0.0	0.0	0.0	0.0	0.0
Total	101.2	100.7	101.2	100.0	100.8
Cations on the basis of oxygen present					
Si	0.038	0.011	0.017	0.016	0.015
Ti	0.085	0.418	0.514	0.486	0.579
Al	1.184	0.285	0.207	0.232	0.183
Fe^{3+}	0.414	0.734	0.728	0.751	0.625
Fe^{2+}	0.580	1.096	1.240	1.212	1.294
Mn	0.006	0.009	0.011	0.009	0.011
Mg	0.525	0.318	0.273	0.272	0.282
Ca	0.007	0.005	0.008	0.009	0.008
Cr	0.156	0.123	0.002	0.013	0.005
Zn	0.004	0.000	0.000	0.000	0.000
Ni	0.000	0.000	0.000	0.000	0.000
Concentrations of trace components					
X(usp)	0.578	0.518	0.548	0.532	0.613
x(ilm)	n.a.	n.a.	n.a.	n.a.	n.a.

Table B-7 (continued): **OXIDE**
Ray Mountain

Sample	17/8/10 OX1C-RM Spinel	17/8/10 OX1R-RM Spinel	17/8/10 OX2G-RM Spinel	17/8/10 OX3G-RM Spinel	17/8/2 OX1G-RM Spinel
Major oxides (wt.%)					
SiO_2	0.5	0.4	0.4	0.4	0.4
TiO_2	17.1	18.8	22.4	19.3	16.7
Al_2O_3	11.5	9.3	5.7	6.9	8.3
Fe_2O_3	25.9	24.2	20.4	26.5	29.3
FeO	37.6	39.7	44.5	40.6	37.6
MnO	0.3	0.3	0.4	0.3	0.3
MgO	7.6	6.9	5.2	6.3	6.9
CaO	0.1	0.1	0.1	0.1	0.2
Cr_2O_3	0.0	0.2	0.0	0.0	1.0
ZnO	0.1	0.0	0.0	0.0	0.0
NiO	0.0	0.0	0.0	0.0	0.0
Total	100.7	100.1	99.0	100.2	100.5
Cations on the basis of oxygen present					
Si	0.017	0.015	0.014	0.012	0.012
Ti	0.430	0.483	0.596	0.502	0.430
Al	0.455	0.376	0.237	0.281	0.333
Fe^{3+}	0.653	0.622	0.543	0.690	0.754
Fe^{2+}	1.053	1.133	1.320	1.176	1.076
Mn	0.008	0.009	0.012	0.009	0.008
Mg	0.380	0.352	0.273	0.325	0.352
Ca	0.003	0.004	0.005	0.005	0.006
Cr	0.000	0.006	0.000	0.000	0.028
Zn	0.003	0.000	0.000	0.000	0.000
Ni	0.000	0.000	0.000	0.000	0.000
Concentrations of trace components					
X(usp)	0.546	0.582	0.663	0.555	0.497
x(ilm)	n.a.	n.a.	n.a.	n.a.	n.a.

Table B-7 (continued): **OXIDE**
Ray Mountain

Sample	17/8/2 OX2G-RM Spinel	17/8/2 OX3G-RM Spinel	17/8/3 OX1C-RM Spinel	17/8/3 OX2C-RM Spinel	17/8/3 OX3/1-RM Spinel
Major oxides (wt.%)					
SiO_2	0.3	0.3	0.3	0.3	0.4
TiO_2	18.3	17.2	1.5	1.8	3.4
Al_2O_3	6.5	7.8	2.4	2.5	3.2
Fe_2O_3	28.5	29.1	63.0	62.7	60.0
FeO	39.0	37.9	30.8	31.0	32.4
MnO	0.2	0.3	0.0	0.0	0.0
MgO	6.5	6.8	1.5	1.6	2.1
CaO	0.1	0.2	0.2	0.1	0.1
Cr_2O_3	0.0	0.6	0.2	0.1	0.2
ZnO	0.0	0.0	0.0	0.0	0.0
NiO	0.0	0.0	0.0	0.0	0.0
Total	99.5	100.2	100.0	100.1	101.8
Cations on the basis of oxygen present					
Si	0.011	0.011	0.012	0.011	0.014
Ti	0.480	0.446	0.043	0.049	0.093
Al	0.269	0.317	0.108	0.112	0.137
Fe^{3+}	0.748	0.755	1.777	1.764	1.644
Fe^{2+}	1.141	1.092	0.965	0.969	0.988
Mn	0.007	0.008	0.000	0.000	0.000
Mg	0.338	0.350	0.084	0.087	0.115
Ca	0.005	0.006	0.006	0.004	0.003
Cr	0.000	0.015	0.005	0.004	0.006
Zn	0.000	0.000	0.000	0.000	0.000
Ni	0.000	0.000	0.000	0.000	0.000
Concentrations of trace components					
X(usp)	0.516	0.502	0.041	0.048	0.092
x(ilm)	n.a.	n.a.	n.a.	n.a.	n.a.

Table B-7 (continued): **OXIDE**
Ray Mountain

Sample	17/8/3 OX3/2-RM Ilmenite	17/8/3 OX3/3-RM Spinel	17/8/3 OX3/4-RM Ilmenite	17/8/11 SP1XC-RM Spinel	17/8/11 SP1XR-RM Spinel
Major oxides (wt.%)					
SiO_2	0.4	0.4	0.4	0.2	0.2
TiO_2	39.3	6.1	38.4	0.9	0.9
Al_2O_3	5.2	4.1	5.2	52.5	52.2
Fe_2O_3	25.3	43.6	27.0	11.5	11.4
FeO	23.1	54.4	22.4	21.8	21.7
MnO	0.5	30.1	0.5	0.2	0.1
MgO	6.7	2.5	6.7	12.5	12.4
CaO	0.1	2.1	0.1	0.0	0.0
Cr_2O_3	0.0	0.4	0.1	0.3	0.3
ZnO	0.0	0.0	0.0	0.3	0.2
NiO	0.0	0.0	0.0	0.0	0.0
Total	100.7	101.6	100.8	100.2	99.4
Cations on the basis of oxygen present					
Si	0.008	0.013	0.009	0.007	0.006
Ti	0.695	0.166	0.679	0.018	0.018
Al	0.145	0.174	0.145	1.706	1.708
Fe^{3+}	0.448	1.457	0.477	0.238	0.237
Fe^{2+}	0.454	1.040	0.440	0.503	0.505
Mn	0.010	0.003	0.010	0.004	0.003
Mg	0.236	0.133	0.234	0.512	0.512
Ca	0.003	0.004	0.003	0.000	0.000
Cr	0.000	0.010	0.003	0.007	0.007
Zn	0.000	0.000	0.000	0.006	0.004
Ni	0.000	0.000	0.000	0.000	0.000
Concentrations of trace components					
X(usp)	n.a.	0.181	n.a.	0.750	0.751
x(ilm)	0.665	n.a.	0.644	n.a.	n.a.

Table B-7 (continued): **OXIDE**
Ray Mountain

Sample	17/8/11 OX3C-RM Spinel	17/8/11 OX4G-RM Spinel	17/8/11 OX5G-RM Spinel	17/8/7 OX1C-RM Spinel	17/8/7 OX3C-RM Spinel
Major oxides (wt.%)					
SiO_2	0.4	0.5	0.7	0.4	0.4
TiO_2	19.0	17.7	18.6	17.3	19.3
Al_2O_3	5.0	4.4	4.1	2.8	2.6
Fe_2O_3	27.7	28.5	28.9	31.5	28.1
FeO	41.2	42.1	43.8	43.2	45.3
MnO	0.4	0.5	0.7	0.5	0.5
MgO	5.2	4.2	3.5	2.4	2.3
CaO	0.2	0.3	0.3	0.3	0.2
Cr_2O_3	0.0	3.2	0.4	0.3	0.0
ZnO	0.0	0.0	0.0	0.0	0.0
NiO	0.0	0.0	0.0	0.0	0.0
Total	99.0	101.5	101.0	98.6	98.8
Cations on the basis of oxygen present					
Si	0.014	0.018	0.024	0.015	0.016
Ti	0.509	0.468	0.497	0.482	0.537
Al	0.212	0.184	0.173	0.122	0.114
Fe^{3+}	0.743	0.755	0.773	0.878	0.781
Fe^{2+}	1.227	1.239	1.301	1.338	1.399
Mn	0.013	0.016	0.020	0.016	0.016
Mg	0.276	0.220	0.186	0.131	0.129
Ca	0.006	0.011	0.013	0.012	0.008
Cr	0.000	0.090	0.012	0.007	0.000
Zn	0.000	0.000	0.000	0.000	0.000
Ni	0.000	0.000	0.000	0.000	0.000
Concentrations of trace components					
X(usp)	0.540	0.538	0.539	0.505	0.561
x(ilm)	n.a.	n.a.	n.a.	n.a.	n.a.

Table B-7 (continued): **OXIDE**
Ray Mountain

Sample	17/8/7 OX4C-RM Spinel	17/8/7 OX5C-RM Spinel	17/8/7 OX5C-RM Spinel	17/8/13 OX1C-RM Ilmenite	17/8/13[1] OX1C-RM Spinel
Major oxides (wt.%)					
SiO_2	0.4	0.4	0.4	0.3	0.4
TiO_2	20.4	16.5	18.8	51.7	12.0
Al_2O_3	2.5	2.6	2.4	0.3	3.2
Fe_2O_3	25.9	33.3	28.7	7.2	45.5
FeO	46.2	43.5	44.9	34.4	39.1
MnO	0.6	0.5	0.5	0.8	0.6
MgO	2.3	1.9	2.1	6.4	3.1
CaO	0.1	0.2	0.2	0.3	0.3
Cr_2O_3	0.3	0.4	0.4	0.0	0.8
ZnO	0.0	0.0	0.0	0.0	0.0
NiO	0.0	0.0	0.0	0.0	0.0
Total	98.7	99.3	98.4	101.2	105.0
Cations on the basis of oxygen present					
Si	0.014	0.014	0.013	0.007	0.015
Ti	0.569	0.459	0.526	0.925	0.313
Al	0.107	0.115	0.106	0.008	0.130
Fe^{3+}	0.720	0.926	0.803	0.128	1.191
Fe^{2+}	1.429	1.345	1.397	0.684	1.138
Mn	0.019	0.016	0.017	0.016	0.016
Mg	0.128	0.105	0.117	0.225	0.162
Ca	0.005	0.007	0.009	0.007	0.011
Cr	0.008	0.012	0.011	0.000	0.022
Zn	0.000	0.000	0.000	0.000	0.000
Ni	0.000	0.000	0.000	0.000	0.000
Concentrations of trace components					
X(usp)	0.596	0.487	0.553	n.a.	0.313
x(ilm)	n.a.	n.a.	n.a.	0.913	n.a.

Table B-7 (continued): **OXIDE**
Ray-Ridge to Pointed Stick Cone

Sample	18/8/9 OX1C-RR Spinel	18/8/9[1] OX2C-RR Ilmenite	18/8/9 OX2C-RR Spinel	18/8/9 OX5C-RC Ilmenite	18/8/4 OX1C-RC Spinel
Major oxides (wt.%)					
SiO_2	0.4	0.3	0.3	0.4	0.3
TiO_2	22.7	53.8	23.8	20.2	18.6
Al_2O_3	2.2	0.3	2.8	2.0	6.1
Fe_2O_3	23.4	3.0	19.8	60.0	28.9
FeO	47.3	40.7	49.6	11.3	42.2
MnO	0.6	0.5	0.4	0.6	0.5
MgO	3.2	4.0	2.4	3.6	5.0
CaO	0.2	0.2	0.2	0.2	0.0
Cr_2O_3	0.4	0.0	0.5	0.7	0.1
ZnO	0.0	0.0	0.0	0.0	0.0
NiO	0.0	0.0	0.0	0.0	0.0
Total	100.3	102.8	99.9	99.0	101.6
Cations on the basis of oxygen present					
Si	0.013	0.007	0.012	0.009	0.011
Ti	0.617	0.962	0.650	0.384	0.485
Al	0.095	0.008	0.121	0.060	0.250
Fe^{3+}	0.636	0.053	0.542	1.140	0.756
Fe^{2+}	1.431	0.810	1.509	0.238	1.225
Mn	0.018	0.011	0.013	0.013	0.014
Mg	0.175	0.143	0.132	0.137	0.257
Ca	0.006	0.005	0.007	0.006	0.000
Cr	0.010	0.000	0.013	0.013	0.002
Zn	0.000	0.000	0.000	0.000	0.000
Ni	0.000	0.000	0.000	0.000	0.000
Concentrations of trace components					
X(usp)	0.635	n.a.	0.696	n.a.	0.536
x(ilm)	n.a.	0.968	n.a.	0.286	n.a.

Table B-7 (continued): **OXIDE**
Pointed Stick Cone to Dragon's Tongue (proximal)

Sample	18/8/4 OX1R-RC Spinel	18/8/4 OX2C-RC Spinel	14/8/1 OX1C-RP Spinel	14/8/1 OX1R-RP Spinel	14/8/2 SP1XC-RP Spinel
Major oxides (wt.%)					
SiO_2	0.3	0.4	0.4	0.3	0.3
TiO_2	17.9	16.2	5.1	5.8	1.0
Al_2O_3	6.1	1.7	7.6	7.7	45.7
Fe_2O_3	29.2	34.6	51.2	50.1	18.3
FeO	41.0	41.5	33.5	32.4	23.5
MnO	0.4	0.2	0.2	0.2	0.3
MgO	4.9	2.8	2.7	3.7	10.7
CaO	0.1	0.1	0.0	0.0	0.0
Cr_2O_3	0.0	0.4	0.1	0.0	0.2
ZnO	0.1	0.0	0.0	0.0	0.2
NiO	0.0	0.0	0.0	0.0	0.0
Total	100.1	98.1	100.7	100.3	100.2
Cations on the basis of oxygen present					
Si	0.011	0.014	0.015	0.012	0.008
Ti	0.475	0.454	0.136	0.155	0.022
Al	0.254	0.075	0.318	0.324	1.541
Fe^{3+}	0.774	0.974	1.377	1.340	0.393
Fe^{2+}	1.208	1.299	1.002	0.963	0.563
Mn	0.013	0.008	0.007	0.005	0.007
Mg	0.259	0.158	0.142	0.199	0.456
Ca	0.004	0.004	0.000	0.000	0.000
Cr	0.000	0.013	0.003	0.000	0.004
Zn	0.002	0.000	0.000	0.000	0.005
Ni	0.000	0.000	0.000	0.000	0.000
Concentrations of trace components					
X(usp)	0.524	0.451	0.202	0.199	0.626
x(ilm)	n.a.	n.a.	n.a.	n.a.	n.a.

Table B-7 (continued): **OXIDE**
Dragon's Tongue (proximal)

Sample	14/8/2 SP1XR-RP Spinel	14/8/2 SP1XR-RP Spinel	14/8/2 IL1XC-RP Ilmenite	14/8/2 IL1XR-RP Spinel	14/8/2 OX1G-RP Spinel
Major oxides (wt.%)					
SiO_2	0.3	2.0	0.3	0.3	0.4
TiO_2	1.1	13.3	49.5	21.5	16.9
Al_2O_3	45.6	7.3	0.8	3.7	4.0
Fe_2O_3	18.3	31.9	10.7	26.2	32.9
FeO	23.5	38.9	33.1	43.8	40.8
MnO	0.3	0.6	0.7	0.7	0.7
MgO	10.7	4.9	6.1	5.1	4.1
CaO	0.0	0.2	0.1	0.1	0.3
Cr_2O_3	0.2	0.2	0.0	0.0	0.2
ZnO	0.2	0.0	0.1	0.0	0.0
NiO	0.0	0.0	0.0	0.0	0.0
Total	100.2	99.3	101.3	101.4	100.3
Cations on the basis of oxygen present					
Si	0.009	0.071	0.006	0.012	0.014
Ti	0.023	0.352	0.886	0.567	0.456
Al	1.537	0.303	0.022	0.151	0.169
Fe^{3+}	0.395	0.844	0.193	0.691	0.886
Fe^{2+}	0.562	1.142	0.660	1.285	1.221
Mn	0.007	0.016	0.014	0.021	0.021
Mg	0.458	0.258	0.215	0.267	0.216
Ca	0.000	0.008	0.003	0.006	0.012
Cr	0.004	0.005	0.000	0.000	0.005
Zn	0.005	0.000	0.002	0.000	0.000
Ni	0.000	0.000	0.000	0.000	0.000
Concentrations of trace components					
X(usp)	0.624	0.431	n.a.	0.578	0.469
x(ilm)	n.a.	n.a.	0.872	n.a.	n.a.

Table B-7 (continued): **OXIDE**
Dragon's Tongue (proximal)

Sample	14/8/2 OX2G-RP Spinel	14/8/2 OX3G-RP Spinel	14/8/2 OX4G-RP Spinel	14/8/2 OX5G-RP Spinel	14/8/2 IL1XC-RP Ilmenite
Major oxides (wt.%)					
SiO_2	0.4	0.5	0.4	0.4	0.3
TiO_2	16.9	17.1	17.6	18.4	49.5
Al_2O_3	3.7	3.5	4.3	3.9	0.8
Fe_2O_3	33.0	33.1	31.4	30.3	10.7
FeO	40.4	41.4	41.3	41.8	33.1
MnO	0.7	0.8	0.7	0.7	0.7
MgO	4.1	3.7	4.1	4.2	6.1
CaO	0.3	0.4	0.4	0.4	0.1
Cr_2O_3	0.0	0.1	0.1	0.0	0.0
ZnO	0.0	0.0	0.1	0.1	0.1
NiO	0.0	0.0	0.0	0.0	0.0
Total	99.5	100.6	100.3	100.2	101.3
Cations on the basis of oxygen present					
Si	0.016	0.018	0.016	0.015	0.006
Ti	0.457	0.460	0.471	0.495	0.886
Al	0.158	0.148	0.181	0.165	0.022
Fe^{3+}	0.896	0.891	0.843	0.815	0.193
Fe^{2+}	1.220	1.240	1.231	1.250	0.660
Mn	0.021	0.023	0.020	0.020	0.014
Mg	0.222	0.200	0.217	0.222	0.215
Ca	0.010	0.015	0.016	0.014	0.003
Cr	0.000	0.004	0.002	0.000	0.000
Zn	0.000	0.000	0.004	0.003	0.002
Ni	0.000	0.000	0.000	0.000	0.000
Concentrations of trace components					
X(usp)	0.463	0.469	0.491	0.509	n.a.
x(ilm)	n.a.	n.a.	n.a.	n.a.	0.872

Table B-7 (continued): **OXIDE**
Dragon's Tongue (proximal)

Sample	14/8/1 OX1G-RP Spinel	14/8/1 OX2G-RP Spinel	14/8/1 OX3G-RP Spinel	14/8/1 SP1XC-RP Spinel	14/8/1 SP1XR-RP Spinel
Major oxides (wt.%)					
SiO_2	0.4	0.3	0.5	0.5	0.6
TiO_2	18.3	15.5	14.9	1.7	15.3
Al_2O_3	5.8	6.5	7.0	36.0	7.4
Fe_2O_3	28.4	27.0	26.9	11.8	26.2
FeO	42.1	39.7	38.8	17.3	40.6
MnO	0.5	0.5	0.5	0.3	0.6
MgO	4.3	4.0	4.5	14.6	4.0
CaO	0.3	0.3	0.4	0.1	0.4
Cr_2O_3	0.0	5.0	6.1	18.9	5.9
ZnO	0.0	0.0	0.0	0.1	0.0
NiO	0.0	0.0	0.0	0.0	0.0
Total	100.1	98.7	99.5	101.3	100.8
Cations on the basis of oxygen present					
Si	0.015	0.012	0.017	0.013	0.021
Ti	0.486	0.417	0.395	0.036	0.401
Al	0.243	0.273	0.292	1.218	0.303
Fe^{3+}	0.755	0.729	0.715	0.255	0.690
Fe^{2+}	1.247	1.188	1.145	0.414	1.185
Mn	0.014	0.014	0.014	0.008	0.017
Mg	0.229	0.215	0.235	0.622	0.206
Ca	0.012	0.010	0.017	0.003	0.014
Cr	0.000	0.141	0.169	0.429	0.163
Zn	0.000	0.000	0.000	0.002	0.000
Ni	0.000	0.000	0.000	0.000	0.000
Concentrations of trace components					
X(usp)	0.540	0.548	0.542	0.698	0.564
x(ilm)	n.a.	n.a.	n.a.	n.a.	n.a.

Table B-7 (continued): **OXIDE**
Dragon's Tongue (proximal) to Dragon's Tongue (distal)

Sample	14/8/2 SP2XC-RP Spinel	14/8/2 SP2XC-RP Spinel	11/8/7 SP1XC-RD Spinel	11/8/7 SP1XR-RD Spinel	11/8/7 OX2G-RD Spinel
Major oxides (wt.%)					
SiO_2	0.3	0.5	0.8	0.6	0.6
TiO_2	1.1	1.0	5.4	17.9	19.3
Al_2O_3	46.5	48.6	20.9	6.5	5.8
Fe_2O_3	18.3	15.3	18.2	25.9	25.5
FeO	23.6	24.5	27.0	39.1	40.9
MnO	0.3	0.3	0.4	0.4	0.4
MgO	11.0	10.6	8.7	6.4	6.3
CaO	0.0	0.1	0.3	0.4	0.3
Cr_2O_3	0.1	0.1	18.7	3.4	2.3
ZnO	0.4	0.3	0.2	0.0	0.0
NiO	0.0	0.0	0.0	0.0	0.0
Total	101.6	101.1	100.5	100.5	101.5
Cations on the basis of oxygen present					
Si	0.010	0.013	0.025	0.020	0.020
Ti	0.023	0.020	0.130	0.464	0.500
Al	1.544	1.608	0.784	0.265	0.237
Fe^{3+}	0.387	0.323	0.435	0.674	0.660
Fe^{2+}	0.555	0.574	0.718	1.131	1.175
Mn	0.007	0.006	0.011	0.011	0.011
Mg	0.463	0.444	0.411	0.330	0.323
Ca	0.000	0.003	0.011	0.013	0.011
Cr	0.003	0.003	0.471	0.093	0.064
Zn	0.007	0.006	0.004	0.000	0.000
Ni	0.000	0.000	0.000	0.000	0.000
Concentrations of trace components					
X(usp)	0.627	0.687	0.617	0.550	0.567
x(ilm)	n.a.	n.a.	n.a.	n.a.	n.a.

Table B-7 (continued): **OXIDE**
Dragon's Tongue (distal) to Kostal Lake (south cone)

Sample	11/8/7 OX3G-RD Spinel	29/7/6 IL1XC-KS Ilmenite	29/7/6 IL1XR-KS Spinel	29/7/6 SP1XC-KS Spinel	29/7/6 SP1XR-KS Spinel
Major oxides (wt.%)					
SiO_2	0.4	0.3	0.4	0.0	0.2
TiO_2	18.7	53.3	24.2	1.1	17.5
Al_2O_3	6.2	0.4	4.1	46.3	7.2
Fe_2O_3	25.2	3.5	18.7	18.6	27.6
FeO	40.5	34.6	46.7	22.5	41.8
MnO	0.3	0.5	0.5	0.2	0.4
MgO	6.2	7.3	5.2	11.3	4.0
CaO	0.1	0.2	0.1	0.0	0.3
Cr_2O_3	3.5	0.7	2.0	0.2	0.2
ZnO	0.0	0.0	0.0	0.2	0.0
NiO	0.0	0.0	0.0	0.0	0.0
Total	101.0	100.9	102.0	100.4	99.2
Cations on the basis of oxygen present					
Si	0.013	0.007	0.014	0.000	0.008
Ti	0.485	0.949	0.630	0.024	0.469
Al	0.253	0.012	0.168	1.550	0.301
Fe^{3+}	0.656	0.063	0.488	0.397	0.739
Fe^{2+}	1.169	0.684	1.354	0.535	1.242
Mn	0.008	0.009	0.014	0.005	0.012
Mg	0.317	0.258	0.271	0.479	0.213
Ca	0.004	0.004	0.005	0.000	0.010
Cr	0.095	0.013	0.056	0.005	0.005
Zn	0.000	0.000	0.000	0.005	0.000
Ni	0.000	0.000	0.000	0.000	0.000
Concentrations of trace components					
X(usp)	0.574	n.a.	0.697	0.620	0.554
x(ilm)	n.a.	0.956	n.a.	n.a.	n.a.

Table B-7 (continued): **OXIDE**
Kostal Lake (south cone)

Sample	29/7/6 SP2XC-KS Spinel	29/7/6 SP2XC-KS Spinel	29/7/6 SP2XC-KS Spinel	29/7/6 OX1C-KS Spinel	29/7/6 OX1R-KS Spinel
Major oxides (wt.%)					
SiO_2	0.2	0.2	0.3	0.4	1.0
TiO_2	16.3	5.4	4.2	2.4	18.9
Al_2O_3	6.9	21.2	24.3	32.4	5.3
Fe_2O_3	26.2	20.8	18.7	12.9	22.1
FeO	40.6	25.3	25.1	20.7	44.7
MnO	0.4	0.3	0.4	0.4	0.5
MgO	4.2	9.3	8.9	11.8	3.1
CaO	0.2	0.1	0.2	0.2	0.6
Cr_2O_3	4.8	16.8	16.9	18.4	3.0
ZnO	0.0	0.1	0.2	0.1	0.1
NiO	0.0	0.0	0.0	0.0	0.0
Total	99.8	99.5	99.1	99.7	99.3
Cations on the basis of oxygen present					
Si	0.009	0.007	0.009	0.011	0.035
Ti	0.433	0.130	0.100	0.054	0.511
Al	0.286	0.799	0.910	1.144	0.225
Fe^{3+}	0.697	0.502	0.448	0.291	0.597
Fe^{2+}	1.200	0.678	0.666	0.520	1.340
Mn	0.013	0.008	0.010	0.010	0.014
Mg	0.222	0.445	0.422	0.528	0.164
Ca	0.007	0.004	0.006	0.005	0.024
Cr	0.134	0.425	0.425	0.435	0.086
Zn	0.000	0.003	0.005	0.002	0.003
Ni	0.000	0.000	0.000	0.000	0.000
Concentrations of trace components					
X(usp)	0.568	0.567	0.607	0.697	0.634
x(ilm)	n.a.	n.a.	n.a.	n.a.	n.a.

Table B-7 (continued): **OXIDE**
Kostal Lake (south cone) to Kostal Lake (older lavas)

Sample	29/7/6 OX2G-KS Spinel	29/7/6 OX3G-KS Spinel	31/8/8 SP1XC-KP Spinel	31/8/8 SP1XR-KP Spinel	31/8/8 OX1G-KP Spinel
Major oxides (wt.%)					
SiO_2	0.5	0.5	0.4	0.6	0.3
TiO_2	18.5	16.9	1.9	16.2	17.8
Al_2O_3	5.7	6.2	21.5	6.3	4.4
Fe_2O_3	25.9	27.7	11.2	24.0	30.2
FeO	43.1	40.7	23.2	38.9	42.8
MnO	0.5	0.4	0.5	0.5	0.5
MgO	3.8	4.7	8.9	5.4	3.3
CaO	0.4	0.4	0.1	0.3	0.4
Cr_2O_3	1.9	3.4	32.2	7.7	0.2
ZnO	0.1	0.1	0.1	0.0	0.0
NiO	0.0	0.0	0.0	0.0	0.0
Total	100.4	101.0	99.8	99.8	100.0
Cations on the basis of oxygen present					
Si	0.019	0.017	0.012	0.021	0.012
Ti	0.491	0.445	0.045	0.426	0.483
Al	0.237	0.253	0.806	0.262	0.187
Fe^{3+}	0.691	0.729	0.269	0.633	0.817
Fe^{2+}	1.276	1.188	0.617	1.142	1.288
Mn	0.016	0.013	0.014	0.015	0.016
Mg	0.201	0.244	0.421	0.280	0.177
Ca	0.015	0.015	0.003	0.010	0.014
Cr	0.052	0.093	0.810	0.213	0.007
Zn	0.002	0.002	0.002	0.000	0.000
Ni	0.000	0.000	0.000	0.000	0.000
Concentrations of trace components					
X(usp)	0.579	0.541	0.744	0.582	0.522
x(ilm)	n.a.	n.a.	n.a.	n.a.	n.a.

Table B-7 (continued): **OXIDE**
Kostal Lake (older lavas)

Sample	31/8/8 OX2G-KP Spinel	31/8/8 OX3G-KP Spinel	29/7/6 IL1XC-KS Ilmenite
Major oxides (wt.%)			
SiO_2	0.4	0.4	0.3
TiO_2	17.3	17.5	53.3
Al_2O_3	4.7	4.6	0.4
Fe_2O_3	30.4	30.5	3.5
FeO	41.2	42.5	34.6
MnO	0.5	0.5	0.5
MgO	4.2	3.5	7.3
CaO	0.3	0.3	0.2
Cr_2O_3	1.2	0.2	0.7
ZnO	0.0	0.0	0.0
NiO	0.0	0.0	0.0
Total	100.1	100.2	100.9
Cations on the basis of oxygen present			
Si	0.014	0.015	0.007
Ti	0.464	0.473	0.949
Al	0.196	0.195	0.012
Fe^{3+}	0.815	0.823	0.063
Fe^{2+}	1.229	1.274	0.684
Mn	0.014	0.015	0.009
Mg	0.223	0.186	0.258
Ca	0.011	0.013	0.004
Cr	0.034	0.006	0.013
Zn	0.000	0.000	0.000
Ni	0.000	0.000	0.000
Concentrations of trace components			
X(usp)	0.508	0.515	n.a.
x(ilm)	n.a.	n.a.	0.956

Table B-8
Major element concentrations in incognate oxide

Oxide analyses comprise major oxide concentrations, cation numbers of each ionic species, recalculated on the basis of four or three oxygen anions, as appropriate, and the mole fractions of appropriate components. Analyses are in the order given below; on each page is a subheading listing the centres described thereon. The source of each analysis is identified by the two-letter suffix, and is plotted on each diagram of this work with the appropriate symbol, as follows:

Suffix	Symbol	Unit
SM	[‡]	Spanish Mump
SB	[‡]	Spanish Bonk
ST	⍍	Hyalo Ridge
SL	⊠	Spanish Lake Centre
SC	⊞	Flourmill Centre
PY	+	Pyramid Mountain
SP	X	Spahats (Second Canyon dyke)
RM	[Y]	Ray Mountain
RR	†	Ray Ridge
RC	‡	Pointed Stick Cone
R	Δ	Dragon's Tongue
RP	Δ	Dragon's Tongue (proximal)
RD	Δ	Dragon's Tongue (distal)
KL	O	Kostal Lake
KP	O	Kostal Lake (older lavas)
KN	O	Kostal Lake (north cone)
KS	O	Kostal Lake (south cone)
KT	O	Kostal Lake (lava tube)

Analytical precisions for every element analysed in oxide are listed below at the 99% confidence level, as a percentage of the total concentration of that element. i.c. = insufficient concentration, n.a. = not analysed. Analyses which are poor in quality but which give an approximate composition are labelled thus: ^{1}.

Element	Spinel	Magnetite	Ilmenite
Mg	3.1	4.3	4.1
Al	2.6	3.0	4.8
Si	4.1	4.5	i.c.
Ca	n.a.	6.3	i.c.
Ti	3.0	1.3	1.0
Cr	1.7	3.2	i.c.
Mn	5.9	5.9	7.8
Fe	1.1	0.8	1.2
Ni	7.2	i.c.	i.c.
Zn	i.c.	i.c.	i.c.

Sample numbers comprise three parts, interpreted as follows :

26/8/3(X)	OX1(X)C,M,R	-SB
Sample number (X if xenolith)	OXide 1 (X if xenocryst) Core, Median or Rim	Suite suffix

Table B-8 (continued): **OXIDE**
Spanish Lake to Flourmill

Sample	24/8/13X SP1C-SL Spinel	8/13 2C-SL pinel	24/8/13X CPX/ SP2R-SL Spinel	24/8/13X OL/ SP2R-SL Spinel	2/8/6X[1] SP1C-SC Spinel
Major oxides (wt.%)					
SiO_2	0.3	0.2	0.2	0.2	0.4
TiO_2	0.1	0.1	0.0	0.1	0.7
Al_2O_3	57.4	8.4	58.6	58.4	58.9
Fe_2O_3	2.8	2.5	2.8	2.6	9.2
FeO	7.8	8.2	7.9	8.0	13.1
MnO	0.2	0.2	0.2	0.1	0.1
MgO	21.4	1.4	21.6	21.6	19.4
CaO	0.0	0.0	0.0	0.0	0.0
Cr_2O_3	8.8	8.9	8.8	8.7	0.0
ZnO	0.1	0.1	0.1	0.2	0.2
NiO	0.4	0.4	0.4	0.4	0.0
Total	99.5	00.3	100.6	100.2	102.1
Cations on the basis of oxygen prsent					
Si	0.007	.004	0.005	0.006	0.011
Ti	0.002	.002	0.000	0.002	0.014
Al	1.747	.760	1.760	1.760	1.775
Fe^{3+}	0.055	.047	0.054	0.049	0.177
Fe^{2+}	0.169	.175	0.168	0.171	0.279
Mn	0.004	.004	0.004	0.003	0.002
Mg	0.824	.817	0.821	0.822	0.739
Ca	0.000	.000	0.000	0.000	0.000
Cr	0.180	.180	0.176	0.176	0.000
Zn	0.003	.001	0.002	0.003	0.003
Ni	0.009	.009	0.009	0.008	0.000
Concentrations of trace componets					
X(usp)	0.903	.918	0.905	0.913	0.748
x(ilm)	n.a.	n.a.	n.a.	n.a.	n.a.

Table B-8 (continued): **OXIDE**
Flourmill to Ray Mountain

Sample	2/8/6X CP/ SP2C-SC Spinel	19/8/1X OX2C-RM Spinel	19/8/1X OX3C-RM Spinel	19/8/1 OX1XC-RM Spinel	19/8/1 OX2C-RM Ilmenite
Major oxides (wt.%)					
SiO_2	0.5	0.3	0.2	0.3	0.2
TiO_2	1.4	14.6	13.2	19.5	53.2
Al_2O_3	34.5	3.9	5.7	2.4	0.2
Fe_2O_3	9.5	37.8	37.5	30.5	3.8
FeO	14.8	42.0	39.8	46.5	37.7
MnO	0.3	0.4	0.3	0.5	0.8
MgO	15.8	2.3	2.8	2.3	5.3
CaO	0.0	0.1	0.0	0.0	0.2
Cr_2O_3	23.4	0.0	0.0	0.0	0.0
ZnO	0.1	0.0	0.0	0.0	0.0
NiO	0.0	0.0	0.0	0.0	0.0
Total	100.3	101.4	99.5	102.0	101.3
Cations on the basis of oxygen present					
Si	0.013	0.011	0.008	0.009	0.005
Ti	0.031	0.395	0.360	0.527	0.959
Al	1.171	0.163	0.241	0.101	0.005
Fe^{3+}	0.207	1.025	1.022	0.826	0.068
Fe^{2+}	0.356	1.266	1.205	1.397	0.755
Mn	0.007	0.013	0.011	0.017	0.016
Mg	0.680	0.123	0.153	0.123	0.188
Ca	0.000	0.003	0.000	0.000	0.004
Cr	0.534	0.000	0.000	0.000	0.000
Zn	0.002	0.000	0.000	0.000	0.000
Ni	0.000	0.000	0.000	0.000	0.000
Concentrations of trace components					
X(usp)	0.733	0.427	0.416	0.544	n.a.
x(ilm)	n.a.	n.a.	n.a.	n.a.	0.957

Table B-8 (continued): **OXIDE**
Ray Mountain to Ray Ridge

Sample	19/8/1 OX2C-RM Spinel	19/8/1 OX3C-RM Spinel	19/8/1 OX4C-RM Spinel	19/8/1 OX4C-RM Spinel	18/8/9X SP1C-RR Spinel
Major oxides (wt.%)					
SiO_2	0.3	0.9	0.3	0.3	0.5
TiO_2	13.4	12.3	11.7	12.2	15.0
Al_2O_3	2.8	3.2	3.5	3.2	3.9
Fe_2O_3	39.4	40.0	43.8	43.2	22.2
FeO	39.3	40.7	39.6	39.8	35.9
MnO	0.4	0.4	0.5	0.5	0.5
MgO	2.5	1.8	2.1	2.2	6.4
CaO	0.1	0.1	0.1	0.0	0.4
Cr_2O_3	0.0	0.0	0.1	0.1	15.6
ZnO	0.0	0.0	0.0	0.0	0.0
NiO	0.0	0.0	0.0	0.0	0.0
Total	98.1	99.4	101.8	101.4	100.3
Cations on the basis of oxygen present					
Si	0.010	0.033	0.011	0.009	0.018
Ti	0.376	0.341	0.317	0.332	0.394
Al	0.122	0.140	0.149	0.136	0.162
Fe^{3+}	1.108	1.112	1.190	1.178	0.585
Fe^{2+}	1.229	1.256	1.196	1.205	1.049
Mn	0.014	0.011	0.015	0.014	0.016
Mg	0.138	0.101	0.115	0.121	0.332
Ca	0.004	0.005	0.003	0.001	0.014
Cr	0.000	0.001	0.004	0.002	0.431
Zn	0.000	0.000	0.000	0.000	0.000
Ni	0.000	0.000	0.000	0.000	0.000
Concentrations of trace components					
X(usp)	0.381	0.373	0.338	0.347	0.590
x(ilm)	n.a.	n.a.	n.a.	n.a.	n.a.

Table B-8 (continued): OXIDE
Dragon's Tongue (proximal)

Sample	14/8/9X SP2C-RP Spinel	14/8/9X SP3C-RP Spinel	14/8/9X SP4C-RP Spinel	14/8/9X SP4C-RP Spinel	14/8/9X SP4C-RP Spinel
Major oxides (wt.%)					
SiO_2	0.4	0.4	0.3	0.3	0.4
TiO_2	0.3	0.6	0.7	0.7	0.7
Al_2O_3	56.1	55.5	54.7	54.8	54.5
Fe_2O_3	9.6	9.9	9.2	9.6	9.5
FeO	18.5	19.3	19.3	19.3	19.2
MnO	0.2	0.2	0.2	0.1	0.1
MgO	14.8	14.5	14.1	14.2	14.2
CaO	0.1	0.1	0.0	0.0	0.1
Cr_2O_3	0.1	0.1	0.1	0.1	0.1
ZnO	0.2	0.1	0.2	0.2	0.2
NiO	0.0	0.0	0.0	0.0	0.0
Total	100.4	100.7	98.8	99.3	99.1
Cations on the basis of oxygen present					
Si	0.010	0.010	0.009	0.009	0.011
Ti	0.006	0.012	0.014	0.014	0.015
Al	1.771	1.753	1.761	1.756	1.753
Fe^{3+}	0.194	0.200	0.190	0.196	0.195
Fe^{2+}	0.414	0.432	0.441	0.438	0.438
Mn	0.004	0.004	0.004	0.003	0.003
Mg	0.591	0.581	0.575	0.577	0.577
Ca	0.003	0.003	0.000	0.000	0.002
Cr	0.003	0.003	0.002	0.002	0.002
Zn	0.004	0.002	0.003	0.005	0.005
Ni	0.000	0.000	0.000	0.000	0.000
Concentrations of trace components					
X(usp)	0.771	0.768	0.782	0.775	0.775
x(ilm)	n.a.	n.a.	n.a.	n.a.	n.a.

Table B-8 (continued): **OXIDE**
Dragon's Tongue (proximal)

Sample	13/8/1X SP2C-RP Spinel	13/8/1X SP2R-RP Spinel	13/8/1X SP3C-RP Spinel	13/8/1X SP3C-RP Spinel	13/8/1X SP4C-RP Spinel
Major oxides (wt.%)					
SiO_2	0.4	0.4	0.4	0.4	0.4
TiO_2	0.6	0.7	0.7	0.6	0.8
Al_2O_3	53.8	53.8	55.9	56.0	55.1
Fe_2O_3	11.6	11.4	10.0	9.8	10.8
FeO	21.0	21.1	17.8	18.0	18.9
MnO	0.2	0.1	0.1	0.1	0.2
MgO	13.4	13.3	15.6	15.5	15.0
CaO	0.1	0.1	0.1	0.1	0.1
Cr_2O_3	0.1	0.3	0.1	0.1	0.2
ZnO	0.3	0.4	0.2	0.2	0.4
NiO	0.0	0.0	0.0	0.0	0.0
Total	101.5	101.6	100.9	100.9	102.0
Cations on the basis of oxygen present					
Si	0.012	0.011	0.010	0.011	0.012
Ti	0.012	0.014	0.014	0.013	0.017
Al	1.713	1.712	1.750	1.753	1.723
Fe^{3+}	0.236	0.232	0.200	0.197	0.215
Fe^{2+}	0.473	0.477	0.395	0.400	0.420
Mn	0.004	0.003	0.003	0.003	0.004
Mg	0.538	0.533	0.619	0.615	0.595
Ca	0.003	0.004	0.003	0.003	0.003
Cr	0.003	0.006	0.003	0.002	0.005
Zn	0.006	0.008	0.004	0.003	0.007
Ni	0.000	0.000	0.000	0.000	0.000
Concentrations of trace components					
X(usp)	0.741	0.746	0.758	0.762	0.746
x(ilm)	n.a.	n.a.	n.a.	n.a.	n.a.

Table B-8 (continued): **OXIDE**
Dragon's Tongue (proximal)

Sample	13/8/1X SP4C-RP Spinel
Major oxides (wt.%)	
SiO_2	0.4
TiO_2	0.9
Al_2O_3	55.2
Fe_2O_3	10.4
FeO	19.0
MnO	0.2
MgO	15.0
CaO	0.1
Cr_2O_3	0.2
ZnO	0.4
NiO	0.0
Total	101.9
Cations on the basis of oxygen present	
Si	0.012
Ti	0.018
Al	1.727
Fe^{3+}	0.208
Fe^{2+}	0.421
Mn	0.003
Mg	0.594
Ca	0.004
Cr	0.005
Zn	0.007
Ni	0.000
Concentrations of trace components	
X(usp)	0.754
x(ilm)	n.a.

Table B-9
Major element concentrations in incognate orthopyroxene

Orthopyroxene analyses comprise major oxide concentrations, cation numbers of each ionic species, recalculated on the basis of six oxygen anions and the molecular percentages of major end members. Analyses are in the order given below; on each page is a subheading listing the centres described thereon. The source of each analysis is identified by the two-letter suffix, and is plotted on each diagram of this work with the appropriate symbol, as follows:

Suffix	Symbol	Unit
SM	⍗	Spanish Mump
SB	⌸	Spanish Bonk
ST	⍍	Hyalo Ridge
SL	⊠	Spanish Lake Centre
SC	⊞	Flourmill Centre
PY	+	Pyramid Mountain
SP	X	Spahats (Second Canyon dyke)
RM	⍓	Ray Mountain
RR	♦	Ray Ridge
RC	‡	Pointed Stick Cone
R	Δ	Dragon's Tongue
RP	Δ	Dragon's Tongue (proximal)
RD	Δ	Dragon's Tongue (distal)
KL	O	Kostal Lake
KP	O	Kostal Lake (older lavas)
KN	O	Kostal Lake (north cone)
KS	O	Kostal Lake (south cone)
KT	O	Kostal Lake (lava tube)

Analytical precisions for every element analysed in orthopyroxene are listed below at the 99% confidence level, as a percentage of the total concentration of that element.

Na	5.4
Mg	2.1
Al	2.2
Si	0.9
Ca	1.2
Ti	3.7
Cr	3.7
Mn	12.0
Fe	2.0

Sample numbers comprise three parts, interpreted as follows :

26/8/3(X)	OP1(X)C,M,R	-SB
Sample number (X if xenolith)	OrthoPyroxene 1 (X if xenocryst) Core, Median or Rim	Suite suffix

Table B-9 (continued): **ORTHOPYROXENE**
Spanish Lake to Flourmill

Sample	24/8/13X OP1C-SL	24/ / 13X OP C-SL	24/8/13X /OL OP2R-SL	24/8/13X OP3C-SL	2/8/6X3 OP1C-SC
Major oxides (wt.%)					
SiO_2	55.5	5 .7	55.7	55.3	51.9
TiO_2	0.0	0	0.0	0.0	0.2
Al_2O_3	4.4	.2	4.3	4.4	1.4
Fe_2O_3	0.4	.4	0.5	0.3	1.8
FeO	6.0	.0	5.9	6.1	24.1
MnO	0.2	1	0.2	0.1	0.6
MgO	33.3	.3	33.4	33.2	20.3
CaO	0.6	.7	0.7	0.6	0.8
Na_2O	0.0	.0	0.0	0.0	0.0
Cr_2O_3	0.3	1.3	0.2	0.3	0.0
Total	100.9	0.8	100.9	100.2	101.5
Cations on the basis of 6 oxygens					
Si	1.900	1 006	1.904	1.903	1.938
Ti	0.000	000	0.000	0.000	0.005
Al (IV)	0.100	094	0.096	0.097	0.062
Al (VI)	0.079	077	0.076	0.081	0.001
Fe^{3+}	0.012	010	0.014	0.008	0.051
Fe^{2+}	0.172	072	0.169	0.175	0.753
Mn	0.004	104	0.005	0.004	0.018
Mg	1.698	001	1.701	1.702	1.130
Ca	0.022	025	0.025	0.023	0.034
Na	0.000	000	0.000	0.000	0.000
Cr	0.009	07	0.006	0.008	0.000
End member percentages					
Wo(tern)	1.2	4	1.4	1.3	1.8
En(tern)	89.5	.3	89.4	89.4	58.4
Fs(tern)	9.3	3	9.2	9.4	39.8

Table B-9 (continued): **ORTHOPYROXENE**
Flourmill to Dragon's Tongue (proximal)

Sample	2/8/6X3 OP2C-SC	13/8/10 OP1XC-PY	13/8/10 OP2XC-PY	13/8/10 OP3XC-PY	14/8/1X OP1C-RP
Major oxides (wt.%)					
SiO_2	51.8	56.3	56.2	56.0	51.4
TiO_2	0.2	0.1	0.1	0.1	0.5
Al_2O_3	1.4	4.6	4.4	5.3	5.2
Fe_2O_3	1.6	0.6	0.2	0.3	3.8
FeO	24.2	6.1	6.5	6.4	13.0
MnO	0.6	0.2	0.2	0.2	0.3
MgO	20.2	33.2	33.1	32.8	25.4
CaO	0.9	0.7	0.6	0.8	1.4
Na_2O	0.0	0.2	0.2	0.2	0.4
Cr_2O_3	0.0	0.5	0.4	0.4	0.0
Total	101.1	102.6	102.1	102.8	101.5
Cations on the basis of 6 oxygens					
Si	1.941	1.899	1.905	1.887	1.837
Ti	0.005	0.003	0.003	0.003	0.013
Al (IV)	0.059	0.101	0.095	0.113	0.163
Al (VI)	0.002	0.080	0.082	0.098	0.057
Fe^{3+}	0.046	0.016	0.005	0.009	0.103
Fe^{2+}	0.758	0.173	0.185	0.181	0.387
Mn	0.018	0.005	0.005	0.005	0.010
Mg	1.126	1.669	1.672	1.650	1.353
Ca	0.036	0.025	0.022	0.028	0.054
Na	0.000	0.012	0.009	0.010	0.023
Cr	0.000	0.013	0.009	0.011	0.000
End member percentages					
Wo(tern)	1.9	1.4	1.2	1.6	3.2
En(tern)	58.1	89.2	88.7	88.4	74.8
Fs(tern)	40.0	9.5	10.1	10.0	21.9

Table B-9 (continued): **ORTHOPYROXENE**
Dragon's Tongue (proximal)

Sample	14/8/1X OP1R-RP	14/8/1X OP2C-RP	14/8/1 OP1XC-RP	14/8/2 OP4XC-RP
Major oxides (wt.%)				
SiO_2	51.5	51.0	53.6	52.5
TiO_2	0.4	0.5	0.0	0.0
Al_2O_3	5.4	5.8	1.7	1.5
Fe_2O_3	2.7	3.3	1.4	2.5
FeO	14.0	13.5	15.7	22.1
MnO	0.3	0.3	0.3	0.9
MgO	25.3	25.1	26.5	21.2
CaO	1.4	1.3	0.6	0.8
Na_2O	0.2	0.3	0.0	0.2
Cr_2O_3	0.0	0.0	0.0	0.0
Total	101.1	101.1	99.9	101.9
Cations on the basis of 6 oxygens				
Si	1.844	1.830	1.944	1.939
Ti	0.012	0.013	0.000	0.000
Al (IV)	0.156	0.170	0.056	0.061
Al (VI)	0.071	0.075	0.017	0.004
Fe^{3+}	0.072	0.089	0.038	0.070
Fe^{2+}	0.419	0.406	0.478	0.683
Mn	0.010	0.008	0.010	0.027
Mg	1.351	1.340	1.432	1.165
Ca	0.053	0.052	0.025	0.033
Na	0.012	0.019	0.000	0.013
Cr	0.000	0.000	0.000	0.000
Endmember percentages				
Wo(tern)	3.1	3.1	1.3	1.8
En(tern)	73.5	74.0	73.6	61.0
Fs(tern)	23.4	22.9	25.1	37.2

Table B-10
Major element concentrations in amphibole

Amphibole analyses comprise major oxide concentrations only (see text) and are from a single occurrence in a nodule from the proximal portion of the Dragon's Tongue. Analytical precisions for every element analysed in amphibole are listed below at the 99% confidence level, as a percentage of the total concentration of that element. i.c. = insufficient concentration.

Na	3.6
Mg	2.5
Al	2.0
Si	0.9
K	3.5
Ca	1.6
Ti	2.7
Cr	i.c.
Mn	12.0
Fe	1.8
Ni	i.c.
Zn	i.c.

Sample numbers comprise three parts, interpreted as follows :

14/8/9(X)	AM1(X)C,M,R	-R
Sample number (X if xenolith)	AMphibole 1 (X if xenocryst) Core, Median or Rim	Suite suffix

Table B-10 (continued): **AMPHIBOLE**
Dragon's Tongue (proximal)

Sample	14/8/9X AM1C-RP	14/8/9X AM2C-RP	14/8/9X AM2C-RP	14/8/9X AM2C-RP	14/8/9X AM2C-RP
Major oxides (wt.%)					
SiO_2	40.9	40.5	40.6	40.6	40.6
TiO_2	4.5	5.2	5.8	5.9	5.5
Al_2O_3	15.2	14.8	14.8	14.7	14.8
FeO	11.9	11.8	11.8	11.7	11.7
MnO	0.0	0.1	0.0	0.0	0.1
MgO	12.4	12.2	12.2	12.1	12.2
CaO	10.7	10.7	10.6	10.5	10.6
Na_2O	2.7	2.9	2.9	3.0	2.9
K_2O	1.4	1.2	1.1	1.1	1.2
Total	99.8	99.4	99.8	99.6	99.6

Sample	14/8/9X AM3C-RP	14/8/9X AM4C-RP	14/8/9X AM5C-RP	14/8/9X AM6C-RP	14/8/9X AM7C-RP
Major oxides (wt.%)					
SiO_2	40.9	39.3	39.7	39.8	40.8
TiO_2	5.0	6.1	5.3	5.9	6.0
Al_2O_3	15.0	14.6	14.4	14.3	15.0
FeO	11.9	11.9	11.7	11.5	11.7
MnO	0.0	0.1	0.1	0.1	0.1
MgO	12.3	11.6	11.9	11.9	12.3
CaO	10.7	10.3	10.4	10.4	10.6
Na_2O	2.9	2.9	2.8	2.8	2.8
K_2O	1.3	1.1	1.2	1.1	1.2
Total	100.0	97.8	97.6	97.8	100.5

Table B-11
Major element concentrations in incognate apatite

Analyses are from the Flourmill centre only, as shown in the subheading. Analytical precisions for every element analysed in glass are listed below at the 99% confidence level, as a percentage of the total concentration of that element. i.c. = insufficient concentration.

Na	7.1
Mg	4.6
Al	4.0
Si	1.5
P	1.2
S	i.c.
Cl	4.0
K	i.c.
Ca	0.8
Ti	i.c.
Mn	i.c.
Fe	6.5

Sample numbers comprise three parts, interpreted as follows :

2/8/6(X)	AP1(X)	-SC
Sample number (X if a xenolith)	APatite 1 (X if a xenocryst)	Suite suffix

Flourmill

Sample	2/8/6X3 AP1C	2/8/6X3 AP1C	2/8/6X3 AP1R
Major oxides (wt.%)			
SiO_2	0.67	0.81	0.82
TiO_2	0.00	0.00	0.00
Al_2O_3	0.19	0.19	0.19
FeO	0.52	0.55	0.61
MnO	0.00	0.00	0.00
MgO	0.99	1.10	1.04
CaO	53.83	54.67	54.00
Na_2O	0.37	0.35	0.36
K_2O	n.d.	n.d.	n.d.
P_2O_5	41.83	42.23	41.82
Cl	0.24	0.19	0.31
Total	98.64	100.09	99.15

Table B-12
Major element concentrations in sulphide

Sulphide analyses are in the order given below; on each page is a subheading listing the centres described thereon. The source of each analysis is identified by the two-letter suffix, and is plotted on each diagram of this work with the appropriate symbol, as follows:

Suffix	Symbol	Unit
SM	♠⃞	Spanish Mump
SB	ǂ⃞	Spanish Bonk
ST	Δ⃞	Hyalo Ridge
SL	☒	Spanish Lake Centre
SC	⊞	Flourmill Centre
PY	+	Pyramid Mountain
SP	X	Spahats (Second Canyon dyke)
RM	Y⃞	Ray Mountain
RR	ǂ	Ray Ridge
RC	♠	Pointed Stick Cone
R	Δ	Dragon's Tongue
RP	Δ	Dragon's Tongue (proximal)
RD	Δ	Dragon's Tongue (distal)
KL	O	Kostal Lake
KP	O	Kostal Lake (older lavas)
KN	O	Kostal Lake (north cone)
KS	O	Kostal Lake (south cone)
KT	O	Kostal Lake (lava tube)

Analytical precisions for major elements analysed in sulphide are listed below at the 99% confidence level, as a percentage of the total concentration of that element. i.c. = insufficient concentration. [1] denotes precisions obtained from the maximum concentration of that element. All analyses are recalculated to 100%.

S	0.5
Ti	i.c.
Cr	i.c.
Mn	i.c.
Fe	1.3
Ni	0.8[1]
Cu	1.0[1]
Zn	i.c.

Sample numbers comprise three parts, interpreted as follows :

14/8/9(X) Sample number (X if xenolith)	SU1(X)C,M,R SUlphide 1 (X if xenocryst) Core, Median or Rim	-R Suite suffix

Table B-12 (continued): **SULPHIDE**
Hyalo Ridge, Spanish Lake, Flourmill and Dragon's Tongue

Sample	23/8/2 SU1G-ST	24/8/13X SU1.1-SL	24/8/13X SU2.1-SL	24/8/13X SU3.1-SL	24/8/13X SU3.2-SL
Major elements (wt.%)					
Si	0.9	0.7	0.7	0.6	0.7
Ti	0.2	0.0	0.0	0.0	0.0
Al	0.6	0.5	0.5	0.5	0.5
Fe	57.7	37.8	42.8	28.4	29.9
Mn	0.0	0.0	0.0	0.0	0.0
Mg	0.4	0.6	0.6	0.6	0.6
Ca	0.3	0.0	0.0	0.0	0.0
S	37.3	37.4	37.5	31.9	33.2
Zn	0.4	0.0	0.0	0.0	0.0
Ni	2.1	22.8	17.9	37.3	1.8
Cu	0.0	0.0	0.0	0.7	33.3
Total	100.0	100.0	100.0	100.0	100.0

Sample	4/8/4X SU1C-SC Inclusion in cpx	4/8/4X SU2C-SC Inclusion in cpx	14/8/1 SU1C-RP Inclusion in mt	14/8/9X SU1C-RP Inclusion in cpx
Major elements (wt.%)				
Si	0.9	0.8	0.6	0.7
Ti	0.1	0.1	0.2	0.7
Al	0.7	0.7	0.5	0.1
Fe	53.4	54.6	63.1	57.2
Mn	0.0	0.0	0.0	0.0
Mg	0.6	0.7	0.4	0.6
Ca	0.1	0.2	0.0	0.1
S	35.6	36.1	35.2	38.6
Zn	0.6	0.6	0.1	0.4
Ni	8.0	6.2	0.0	1.7
Cu	0.0	0.0	0.0	0.0
Total	100.0	100.0	100.0	100.0

Table B-13
Major element concentrations in whole glass

Analyses are in the order given below; on each page is a subheading listing the centres described thereon. The source of each analysis is identified by the two-letter suffix, and is plotted on each diagram of this work with the appropriate symbol, as follows:

Suffix	Symbol	Unit
SM	⊞	Spanish Mump
ST	⍍	Hyalo Ridge
PY	+	Pyramid Mountain
RM	🅈	Ray Mountain

Analytical precisions for every element analysed in glass are listed below at the 99% confidence level, as a percentage of the total concentration of that element. i.c. = insufficient concentration.

Na	3.6
Mg	2.5
Al.	2.0
Si	0.9
P	5.9
S	i.c
Cl	7.1
K	3.5
Ca	1.6
Ti	2.7
Cr	i.c.
Mn	12.0
Fe	1.8
Ni	i.c.
Zn	i.c.

Sample numbers comprise three parts, interpreted as follows :

26/8/2	GL1	-SM
Sample number	GLass 1	Suite suffix

Table B-13 (continued): **WHOLE GLASS**
Spanish Mump to Hyalo Ridge

Sample	26/8/2 GL1W-SM	26/8/2 GL2W-SM	26/8/2 GL3W-SM	23/8/2 GL1W-ST	23/8/2 GL2W-ST
Major oxides (wt.%)					
SiO_2	48.21	48.34	48.28	52.20	52.05
TiO_2	2.74	2.67	2.66	2.17	2.23
Al_2O_3	16.44	16.35	16.31	14.85	14.56
Fe_2O_3	4.24	4.17	4.16	3.67	3.73
FeO	7.29	7.50	7.36	7.26	7.25
MnO	0.14	0.12	0.13	0.08	0.13
MgO	3.60	3.72	3.61	5.87	5.60
CaO	7.15	7.02	7.03	9.30	9.30
Na_2O	5.32	5.36	5.30	3.52	3.56
K_2O	2.65	2.66	2.60	1.22	1.29
P_2O_5	1.03	1.08	1.07	0.31	0.30
Cl	0.11	0.12	0.13	0.00	0.00
Total	98.92	99.11	98.65	100.44	99.99
C.I.P.W. norm					
Q	0.0	0.0	0.0	1.1	1.1
C	0.0	0.0	0.0	0.0	0.0
Or	15.7	15.8	15.4	7.2	7.6
Ab	28.5	28.9	29.6	29.8	30.1
An	13.1	12.6	13.0	21.1	19.9
Lc	0.0	0.0	0.0	0.0	0.0
Ne	8.9	8.9	8.3	0.0	0.0
Ac	0.0	0.0	0.0	0.0	0.0
Wo(Di)	6.5	6.3	6.2	9.6	10.1
En(Di)	3.8	3.6	3.6	6.1	6.4
Fs(Di)	2.4	2.4	2.4	2.9	3.1
En(Hy)	0.0	0.0	0.0	8.5	7.6
Fs(Hy)	0.0	0.0	0.0	4.0	3.7
Fo	3.6	4.0	3.8	0.0	0.0
Fa	2.5	2.9	2.8	0.0	0.0
Mt	6.2	6.1	6.0	5.3	5.4
Hm	0.0	0.0	0.0	0.0	0.0
Il	5.2	5.1	5.1	4.1	4.2
Ap	2.3	2.4	2.3	0.7	0.7

Table B-13 (continued): WHOLE GLASS
Hyalo Ridge to Ray Mountain

Sample	23/8/2 GL3W-ST	13/8/10 GL1W-PY	13/8/10 GL2W-PY	13/8/10 GL3W-PY	17/8/1 GL1W-RM
Major oxides (wt.%)					
SiO_2	52.42	49.18	47.54	47.53	48.76
TiO_2	2.26	2.65	3.07	3.06	3.20
Al_2O_3	14.78	16.30	16.36	16.28	14.71
Fe_2O_3	3.76	4.15	4.57	4.56	4.70
FeO	7.33	6.87	7.37	7.32	7.94
MnO	0.12	0.10	0.12	0.14	0.16
MgO	5.74	3.28	3.85	3.81	4.12
CaO	9.26	7.11	7.71	7.75	8.19
Na_2O	3.46	5.27	5.23	5.04	4.02
K_2O	1.30	2.93	2.46	2.50	2.58
P_2O_5	0.38	1.15	1.02	0.97	0.81
Cl	0.00	0.13	0.11	0.10	0.00
Total	100.81	99.11	99.40	99.07	99.18
C.I.P.W. norm					
Q	1.7	0.0	0.0	0.0	0.0
C	0.0	0.0	0.0	0.0	0.0
Or	7.7	17.3	14.6	14.8	15.2
Ab	29.3	30.2	26.7	26.9	29.9
An	20.9	12.1	13.8	14.4	14.4
Lc	0.0	0.0	0.0	0.0	0.0
Ne	0.0	7.7	9.5	8.5	2.2
Ac	0.0	0.0	0.0	0.0	0.0
Wo(Di)	9.4	6.5	7.4	7.4	8.7
En(Di)	6.0	3.9	4.6	4.6	5.3
Fs(Di)	2.8	2.4	2.4	2.4	2.9
En(Hy)	8.4	0.0	0.0	0.0	0.0
Fs(Hy)	4.0	0.0	0.0	0.0	0.0
Fo	0.0	3.0	3.5	3.5	3.5
Fa	0.0	2.0	2.0	2.0	2.1
Mt	5.4	6.0	6.6	6.6	6.8
Hm	0.0	0.0	0.0	0.0	0.0
Il	4.3	5.0	5.8	5.8	6.1
Ap	0.8	2.5	2.2	2.1	1.8

Table B-13 (continued): **WHOLE GLASS**
Ray Mountain

Sample	17/8/1 GL2W-RM	17/8/1 GL3W-RM	17/8/2 GL1W-RM	17/8/2 GL2W-RM	17/8/2 GL3W-RM
Major oxides (wt.%)					
SiO_2	48.62	48.54	45.41	45.61	45.24
TiO_2	3.25	3.25	4.06	3.98	4.09
Al_2O_3	14.65	14.63	16.37	16.33	16.28
Fe_2O_3	4.75	4.75	5.56	5.48	5.59
FeO	8.39	8.07	8.21	8.25	8.28
MnO	0.20	0.19	0.18	0.13	0.18
MgO	4.14	4.27	4.88	4.86	4.85
CaO	8.10	8.34	9.61	9.65	9.71
Na_2O	4.05	4.13	2.28	2.67	1.96
K_2O	2.65	2.40	2.06	2.07	2.05
P_2O_5	0.85	0.78	0.47	0.46	0.52
Cl	0.00	0.00	0.00	0.00	0.00
Total	99.65	99.36	99.08	99.49	98.75
C.I.P.W. norm					
Q	0.0	0.0	0.0	0.0	0.8
C	0.0	0.0	0.0	0.0	0.0
Or	15.7	14.2	12.2	12.2	12.1
Ab	29.1	29.5	19.3	22.5	16.6
An	13.9	14.2	28.3	26.5	29.5
Lc	0.0	0.0	0.0	0.0	0.0
Ne	2.8	2.9	0.0	0.0	0.0
Ac	0.0	0.0	0.0	0.0	0.0
Wo(Di)	8.7	9.2	6.8	7.7	6.4
En(Di)	5.1	5.6	4.7	5.2	4.4
Fs(Di)	3.2	3.1	1.6	1.8	1.5
En(Hy)	0.0	0.0	5.8	0.6	7.8
Fs(Hy)	0.0	0.0	2.0	0.2	2.7
Fo	3.7	3.6	1.2	4.4	0.0
Fa	2.6	2.1	0.4	1.7	0.0
Mt	6.9	6.9	8.1	7.9	8.1
Hm	0.0	0.0	0.0	0.0	0.0
Il	6.2	6.2	7.7	7.6	7.8
Ap	1.8	1.7	1.0	1.0	1.1

Table B-13 (continued): **WHOLE GLASS**
Ray Mountain

Sample	17/8/3 GL1W-RM	17/8/3 GL2W-RM	17/8/3 GL4W-RM	17/8/10 GL1W-RM	17/8/10 GL2W-RM
Major oxides (wt.%)					
SiO_2	46.31	46.23	46.28	47.70	47.82
TiO_2	4.12	4.12	4.06	3.90	3.72
Al_2O_3	16.66	16.62	16.68	16.12	16.59
Fe_2O_3	5.62	5.62	5.56	5.40	5.22
FeO	8.58	8.50	8.17	8.03	7.63
MnO	0.18	0.17	0.15	0.15	0.11
MgO	4.85	4.89	5.04	4.25	4.08
CaO	10.08	9.81	9.87	8.48	8.68
Na_2O	1.31	1.42	1.34	1.63	1.85
K_2O	1.73	1.74	1.80	2.19	2.46
P_2O_5	0.58	0.52	0.44	0.68	0.64
Cl	0.00	0.00	0.00	0.00	0.00
Total	100.09	99.71	99.40	98.54	98.79
C.I.P.W. norm					
Q	5.3	4.9	4.9	7.0	5.0
C	0.0	0.0	0.0	0.0	0.0
Or	10.2	10.3	10.6	12.9	14.6
Ab	11.1	12.0	11.3	13.8	15.6
An	34.4	33.8	34.1	30.2	29.6
Lc	0.0	0.0	0.0	0.0	0.0
Ne	0.0	0.0	0.0	0.0	0.0
Ac	0.0	0.0	0.0	0.0	0.0
Wo(Di)	4.9	4.8	5.0	3.1	3.9
En(Di)	3.3	3.2	3.5	2.1	2.6
Fs(Di)	1.3	1.2	1.1	0.8	1.0
En(Hy)	8.8	9.0	9.1	8.5	7.6
Fs(Hy)	3.4	3.3	2.9	3.3	2.8
Fo	0.0	0.0	0.0	0.0	0.0
Fa	0.0	0.0	0.0	0.0	0.0
Mt	8.2	8.2	8.1	7.8	7.6
Hm	0.0	0.0	0.0	0.0	0.0
Il	7.8	7.8	7.7	7.4	7.1
Ap	1.3	1.1	1.0	1.5	1.4

Table ~~B-~~13 (continued): **WHOLE GLASS**
Ray Mountain

Sample	17/8/10 GL3W-RM
Major oxides (wt.%)	
SiO_2	47.45
TiO_2	3.74
Al_2O_3	16.84
Fe_2O_3	5.24
FeO	7.75
MnO	0.17
MgO	4.31
CaO	8.80
Na_2O	1.83
K_2O	2.44
P_2O_5	0.60
Cl	0.00
Total	99.16
C.I.P.W. norm	
Q	4.0
C	0.0
Or	14.4
Ab	15.5
An	30.5
Lc	0.0
Ne	0.0
Ac	0.0
Wo(Di)	3.9
En(Di)	2.6
Fs(Di)	1.0
En(Hy)	8.2
Fs(Hy)	3.1
Fo	0.0
Fa	0.0
Mt	7.6
Hm	0.0
Il	7.1
Ap	1.3

APPENDIX C

CHEMICAL AND ISOTOPIC ANALYSIS

A. Sample selection

Samples were selected from each of the ten volcanic centres studied. For the smaller centres only two or three samples were chosen but the larger and the postglacial centres were sampled extensively in order to study different phases of activity. Care was taken to ensure that as little contamination as possible was derived from later lavas, inclusions of crustal material and weathering. A total of 108 samples were selected for chemical analysis, 20 for isotopic analysis and eight for Sm amd Nd isotope dilution.

B. Sample preparation

Samples were trimmed of weathered surfaces using a trim saw, ground on all surfaces using silicon carbide grit to remove tramp steel, washed twice in an ultrasonic bath, the second time using distilled water, and dried in an oven at 120°C. Samples were then crushed to 2-3 cm size using a jaw crusher and visually examined to eliminate tramp steel acquired from the jaws. A clean aliquot of each sample was divided in two smaller aliquots The first was crushed in a tungsten carbide swing mill to -200 mesh. The second was first ground in a rotary grinder with mullite plates, then in an agate swing mill, to -200 mesh. Great care was taken to minimise airborne contamination of the sample powders during preparation.

C. Whole rock chemical analysis

108 samples were analysed for SiO_2, TiO_2, ΣFe as Fe_2O_3, MnO, MgO, CaO, Na_2O, K_2O and P_2O_5, using a Philips® PW1400 X-ray fluorescence spectrometer with a rhodium tube (Harvey and Atkin 1982). Analyses were conducted by Midland Earth Science Associates of Nottingham, England. Samples were prepared from powders ground in the tungsten carbide swing mill, using the fused disc method with a lithium tetraborate flux. Loss on ignition was reported for each sample and was negligible in all save two cases, where contamination from the plastic vial was encountered.

The trace elements S, Cl, Rb, Sr, Ba, Sc, Y, Zr, Nb, V, Cr, Co and Ni were analysed by the pressed disc method, using powders prepared from grinding in mullite and agate, as described above. Sc was analysed using a tungsten tube.

Nine unmarked replicates of thesis samples were included in the batch, together with aliquots of U.S.G.S. standard rock powders BHVO-1, DNC-1 and W-2. One replicate of W-2 was also included. Results for standards are presented in Table C-1 together with published values for comparison. The two sets of values are discussed in detail in Chapter 5.

Analytical results for the samples are shown in Table D-1 (Appendix D). A separate table (Table C-2) lists the analytical results for replicates

On the basis of replicate analyses and comparison with published values of U.S.G.S. standards, errors were assigned for each element analysed. These errors are listed in Table C-3.

Table C-1
Analytical results for U.S.G.S. whole rock standards

Element	BHVO-1 (This study)	BHVO-1 (Gladney and Goode 1983)	DNC-1 (This study)	DNC-1 (Gladney *et al.* 1983)
Major oxides (wt.%)				
SiO_2	49.67	49.9±0.8	**46.53**	**47.71**
TiO_2	2.72	2.65±0.09	0.48	0.48±0.03
Al_2O_3	**13.34**	**13.8±0.2**	18.34	18.0±0.76
Fe_2O_3	12.28	12.2±0.3	10.10	9.9±0.37
MnO	0.16	0.166±0.005	0.15	0.15±0.02
MgO	**7.43**	**7.1±0.2**	**10.51**	**10.16**
CaO	11.30	11.4±0.2	11.34	11.7±0.78
Na_2O	**2.44**	**2.21±0.08**	**1.97**	**1.7±0.11**
K_2O	0.53	0.55±0.08	0.23	0.23±0.01
P_2O_5	0.26	0.29±0.04	0.09	0.16±0.07
Trace elements (ppm)				
S	72	101	483	n.a.
Cl	**0**	**92±4**	**158**	**33**
Rb	11	10±2	**40**	**1.9-9.0**
Sr	385	440±70	**746**	**140-470**
Ba	130	142±18	**783**	**120±17**
Sc	**22**	**30±2**	**19**	**33±2**
Y	25	28±2	**27**	**19±2**
Zr	176	180±30	203	40-310
Nb	18	19±2	**53**	**2.2**
V	**263**	**314±12**	169	160±30
Cr	317	300±30	294	270±30
Co	40	45±1	47	54±4
Ni	127	117±18	233	190±40

Analytical results are compared with published values. Major oxide concentrations are in weight percent. Trace element concentrations are in parts per million by weight. Analytical precisions, unless otherwise specified, are given in Table C-3. Values which differ significantly (greater than 2σ) from published values are in bold type. n.a. = not analysed.

Table C-1 (continued).

Element	W-2 Rep. 1	W-2 Rep. 2	W-2 (Mean)	W-2 (Gladney *et al*. 1983)
Major oxides (wt.%)				
SiO_2	51.53	52.09	51.8±0.26	51.77
TiO_2	1.05	1.05	1.05±0.01	1.03±0.03
Al_2O_3	14.92	15.06	**14.99±0.07**	**15.4±0.11**
Fe_2O_3	10.96	11.03	11.00±0.04	10.7±0.56
MnO	0.17	0.16	0.17±0.01	0.17±0.02
MgO	6.56	6.71	**6.59±0.03**	**6.37**
CaO	10.93	10.90	10.92±0.02	10.9±0.56
Na_2O	2.45	2.43	**2.44±0.01**	**2.00±0.08**
K_2O	0.64	0.62	0.63±0.01	0.61
P_2O_5	0.14	0.12	0.13±0.01	0.15
Trace elements (ppm)				
S	138	137	**138±1**	**63**
Cl	41	47	**44±3**	**170**
Rb	23	21	22±1	23±2
Sr	192	192	192±1	155-350
Ba	213	210	212±2	200±40
Sc	29	30	**30±1**	**36±2**
Y	20	20	**20±1**	**25±2**
Zr	95	96	96±1	130±60
Nb	7	7	7±1	8
V	261	246	254±8	263±18
Cr	121	110	**116±6**	**91±4**
Co	39	38	39±1	43±3
Ni	74	69	72±3	70

Table C-2
Replicate whole rock analyses

Element	23/8/8-ST Rep. 1	23/8/8-ST Rep. 2	24/8/14-SL Rep. 1	24/8/14-SL Rep. 2
Major oxides (wt.%)				
SiO_2	49.96	48.45	46.36	46.37
TiO_2	1.73	1.72	2.51	2.50
Al_2O_3	14.37	13.86	14.45	14.47
Fe_2O_3	11.47	11.06	12.60	12.57
MnO	0.12	0.15	0.18	0.15
MgO	8.36	8.41	8.61	8.59
CaO	8.86	8.75	9.65	9.66
Na_2O	3.53	3.24	3.67	3.69
K_2O	1.23	1.20	1.71	1.70
P_2O_5	0.34	0.33	0.53	0.53
Trace elements (ppm)				
S	0	0	483	545
Cl	0	0	158	178
Rb	28	29	40	38
Sr	588	589	746	739
Ba	417	406	783	795
Sc	17	17	19	22
Y	18	18	27	24
Zr	192	192	203	205
Nb	37	38	53	54
V	109	130	169	170
Cr	344	354	294	281
Co	39	45	47	42
Ni	165	165	233	233

Table C-2 (continued).

Element	17/8/11-RM Rep. 1	17/8/11-RM Rep. 2	18/8/9-RR Rep. 1	18/8/9-RR Rep. 2
Major oxides (wt.%)				
SiO_2	44.53	44.93	43.30	44.47
TiO_2	2.50	2.51	2.14	2.15
Al_2O_3	13.12	13.33	12.73	12.77
Fe_2O_3	13.29	13.36	13.77	13.81
MnO	0.17	0.18	0.18	0.16
MgO	9.91	9.96	11.03	11.03
CaO	9.79	9.76	9.84	9.79
Na_2O	3.50	3.41	3.39	3.43
K_2O	1.58	1.58	1.19	1.18
P_2O_5	0.54	0.52	0.39	0.40
Trace elements (ppm)				
S	236	225	168	196
Cl	308	315	140	156
Rb	30	33	27	31
Sr	670	673	494	502
Ba	620	610	381	368
Sc	21	22	19	21
Y	24	22	22	22
Zr	188	190	159	162
Nb	53	50	38	37
V	205	189	196	164
Cr	307	317	358	355
Co	50	49	57	52
Ni	240	239	226	234

Table C-2 (continued).

Element	21/7/1-R Rep. 1	21/7/1-R Rep. 2	21/7/1-R Rep. 3	21/7/1-R Rep. 4
Major oxides (wt.%)				
SiO_2	43.71	43.80	44.33	43.35
TiO_2	2.69	2.68	2.70	2.67
Al_2O_3	13.18	13.10	13.22	12.92
Fe_2O_3	14.29	14.25	14.32	14.24
MnO	0.19	0.18	0.17	0.16
MgO	9.92	10.07	10.01	10.06
CaO	9.48	9.51	9.49	9.49
Na_2O	3.80	3.85	3.84	3.82
K_2O	1.56	1.61	1.57	1.59
P_2O_5	0.59		0.61	0.60
			0.62	
Trace elements (ppm)				
S	108	117	123	112
Cl	341	329	340	320
Rb	38	34	36	35
Sr	802	795	803	806
Ba	940	921	930	954
Sc	19	18	18	17
Y	23	23	22	24
Zr	225	213	217	225
Nb	65	65	64	67
V	180	173	184	191
Cr	277	264	272	272
Co	55	57	55	50
Ni	173	168	168	169

Table C-2 (continued).

Element	29/7/3-KN Rep. 1	29/7/3-KN Rep. 2	29/7/6-KS Rep. 1	29/7/6-KS Rep. 2
Major oxides (wt.%)				
SiO_2	43.74	44.21	44.59	44.20
TiO_2	2.61	2.61	2.63	2.61
Al_2O_3	12.90	13.05	13.18	13.09
Fe_2O_3	13.77	13.91	13.76	13.63
MnO	0.17	0.16	0.18	0.18
MgO	11.19	11.27	10.71	10.65
CaO	9.62	9.63	9.49	9.48
Na_2O	3.47	3.56	3.64	3.79
K_2O	1.36	1.36	1.52	1.50
P_2O_5	0.51	0.51	0.55	0.54
Trace elements (ppm)				
S	322	313	127	118
Cl	241	278	358	351
Rb	30	30	33	33
Sr	643	632	684	674
Ba	457	472	506	495
Sc	18	20	21	17
Y	22	19	21	21
Zr	212	208	229	231
Nb	47	47	49	50
V	169	170	172	178
Cr	344	323	328	332
Co	54	58	58	54
Ni	234	227	236	234

Table C-3
Analytical precision in whole rock analyses

Element	Standard deviation	Standard error
SiO_2	1.74	0.40
TiO_2	0.58	0.14
Al_2O_3	1.70	0.40
FeO	1.38	0.32
MnO	12.82	3.02
MgO	1.06	0.24
CaO	0.50	0.12
Na_2O	3.56	0.82
K_2O	1.90	0.44
P_2O_5	5.92	1.40
S	8.80	2.08
Cl	9.14	2.16
Rb	7.84	1.88
Sr	1.04	0.26
Ba	2.54	0.60
Sc	10.98	2.58
Y	7.70	1.82
Zr	2.56	0.60
Nb	3.04	0.72
V	9.94	2.34
Cr	4.80	1.12
Co	9.14	2.16
Ni	3.02	0.74

Standard deviations and standard errors for whole rock analyses by X-ray fluorescence spectrometry are based on deviances observed in unmarked replicates. Analytical precisions are quoted at 2σ, as percentages of total concentrations for each element or oxide.

D. Isotopic analysis

Sample preparation

Samples analysed for initial ratios of ^{87}Sr/^{86}Sr and ^{143}Nd/^{144}Nd were prepared using the method described by Smith (1986). The same aliquot was used for both Sr and Nd. Approximately 0.5 gm of powdered sample was dissolved in concentrated hydrofluoric and nitric acids (4:1 mixture), centrifuged and the supernatant discarded. The residue was dissolved in nitric acid and evaporated to dryness.

Two cycles of ammonia precipitation and fluorination were used to remove divalent cations and Fe, respectively. The residue was dissolved in dilute hydrochloric acid, refluxed for 1 hour and sufficient ammonium hydroxide was added to precipitate M_2O_3 complexes. The gel was centrifuged and the supernatant discarded. The residue was fluorinated using concentrated hydrofluoric acid and evaporated to near-dryness, then refluxed for 1 hour in a mixture of dilute hydrofluoric and hydrochloric acids. The mixture was centrifuged, the supernatant discarded, the residue dissolved in concentrated nitric acid and evaporated to dryness. The steps described in this paragraph were then repeated.

Ion exchange columns used for separation of Sr and rare earth elements were 24 x 0.6 cm in size (Smith 1986) and packed with BioRad AG 50-W-X8 cation exchange resin (-150 to -200 mesh) The columns were equilibrated with 2.3N hydrochloric acid. Samples were loaded in hydrochloric acid and eluted using 2.3N HCl; the fraction 35-55 ml being taken for Sr and the fraction 85-145 ml for Nd. The fractions taken were evaporated to dryness. Sr was purified using a second column, to reduce Ca further, before analysis by mass spectrometer.

Columns for the separation of Sm and Nd were 38 x 0.3 cm in size, packed with BioRad AG 50-W-X8 cation exchange resin (-150 to -200 mesh). The columns were equilibrated with 0.2M methylactic acid (pH=4.43). That fraction of sample containing rare earth elements was taken up in a single drop of 2.3N hydrochloric acid and loaded into a column. The fraction 50 to 70 ml was collected during elution, using a fractional collector, and evaporated to dryness. The fraction was then cleaned by passage through a third column, packed with BioRad AG 50-W-X8 cation exchange resin (-150 to -200 mesh) and equilibrated with 1N HCl; the sample was eluted with 1N and 2.3N HCl, stripped with 6N HCl and the last fraction evaporated to dryness.

Treatment for Sm and Nd isotope dilutions (9 in number) was identical save for the following. Samples of approximately the same size as for initial ratio determinations were carefully weighed and known quantities of mixed Sm and Nd spike were added. Dissolution was as for the initial ratio aliquots; only the rare earth element fraction was taken from the first column. The fractions 12 to 26 ml (for Sm) and 50 to 70 ml (for Nd) were taken from the second column and organic material was removed as for the initial ratio aliquots. Six of the samples were further purified of organic material by passage through a fourth (capillary) column with BioRad AG 50-W-X8 cation exchange resin (-150 to -200 mesh) similar to columns 1 and 3.

Blanks obtained for Sr and Nd concentrations during the period of analysis are a maximum of 36 ng, 3.51 ng and 9.56 ng for Sr, Sm and Nd, respectively (Smith 1986). Such blanks are at least three orders of magnitude lower in concentration than the minimum quantity of each element (A.D. Smith, pers. comm. 1986).

Mass spectrometry

Samples were analysed using an Aldermaston Micromass 30 mass spectrometer with a 30.5 cm radius of curvature and a 90° sector magnet. Sample concentrates for Sr analysis were loaded on to double rhenium filaments as a chloride. Those for Sm and Nd were loaded as metals either on to double rhenium filaments or on to triple filaments, the centre filament being of rhenium, the side (sample) filaments of tantalum.

The strength of the magnetic field was set at 3 kG for Sm and Nd runs and at 2 kG for Sr runs; filament currents were approximately 4.2/2.2 A and 3.1/1.0 A for rare earth elements and Sr, respectively. The accelerating voltage for all runs was set at 8.8 kV. Each analysis was conducted by peak switching with frequent measurements of background in several positions.

Measurements for the Sr runs were taken in the following order: ^{88}Sr, background (87-88), ^{86}Sr, background (86-87), ^{87}Sr-Rb, ^{86}Sr, ^{87}Sr-Rb, background (84-85), ^{85}(Rb) and background (85-86).

Measurements for the Nd isotope ratio runs were taken in the following order: ^{146}Nd, background (143-144), ^{143}Nd, background (143-144), ^{144}Nd, ^{143}Nd, ^{144}Nd, ^{147}Nd and background (146-147).

Measurements for Nd isotope dilution runs were taken in the following order: ^{146}Nd, background (145-146), ^{145}Nd, background (144-145), ^{142}Nd, background (142-143), ^{140}Ce, and background (140-142).

Measurements for Sm isotope dilution runs were taken in the following order: ^{147}Sm, background (147-148), ^{149}Sm, background (149-150), ^{152}Sm, background (153-154), ^{155}Gd, and background (153-154).

All Sr isotopic ratios are normalised to a value of 0.1194 for ^{86}Sr/^{88}Sr. All Nd isotopic ratios are normalised to a value of 0.724127 for ^{144}Nd/^{146}Nd. Twenty-one analyses of the La Jolla standard taken over the period of study give a value of 0.511053 ± 14 (2σ) for ^{143}Nd/^{144}Nd. Thirteen analyses of the standard N.B.S. SRM 987 for ^{87}Sr/^{86}Sr gave a value of 0.710261 ± 16 over the same time period. ^{87}Sr/^{86}Sr, ^{143}Nd/^{144}Nd and Sm and Nd concentrations measured for an aliquot of BCR-1 are, respectively, 0.70502 ± 4, 0.51184 ± 2, 6.637 ppm and 28.93 ppm.

APPENDIX D

WHOLE ROCK CHEMISTRY

Table D-1
Major oxide and trace element concentrations in samples of whole rock

Analyses are in the order given below; on each page is a subheading listing the centres described thereon. The source of each analysis is identified by the two-letter suffix, and is plotted on each diagram of this work with the appropriate symbol, as follows:

Suffix	Symbol	Unit
SB	⍐	Spanish Bonk
ST	⍍	Hyalo Ridge
SL	⊠	Spanish Lake Centre
SC	⊞	Flourmill Centre
PY	+	Pyramid Mountain
SP	X	Spahats (Second Canyon dyke)
RM	$\boxed{Y}$	Ray Mountain
RR	⇞	Bathroom Bonk
RC	⇞	Pointed Stick Cone
R	Δ	Dragon's Tongue
RP	Δ	Dragon's Tongue (proximal)
RD	Δ	Dragon's Tongue (distal)
KP	O	Kostal Lake (older lavas)
KN	O	Kostal Lake (north cone)
KS	O	Kostal Lake (south cone)
KT	O	Kostal Lake (lava tube)

Standard deviations and standard errors for whole rock analyses by X-ray fluorescence spectrometry, are based on deviances observed in eighteen unmarked replicates. Analytical precisions are quoted at one sigma, as percentages of total concentrations for each element or oxide. Ferric iron is recalculated to a value of 1.5%+TiO_2 (Irvine and Baragar 1971).

Element or oxide	Standard deviation	Standard error
SiO_2	1.74	0.40
TiO_2	0.58	0.14
Al_2O_3	1.70	0.40
FeO	1.38	0.32
MnO	12.82	3.02
MgO	1.06	0.24
CaO	0.50	0.12
Na_2O	3.56	0.84
K_2O	1.90	0.44
P_2O_5	5.92	1.40
S	8.80	2.08
Cl	9.14	2.16
Rb	7.96	1.88
Sr	1.14	0.26
Ba	2.54	0.60
Sc	10.98	2.58
Y	7.70	1.82
Zr	2.56	0.60
Nb	3.04	0.72
V	9.94	2.34
Cr	4.80	1.12
Co	9.14	2.16
Ni	3.12	0.74

Table D-1 (continued): Spanish Bonk to Hyalo Ridge

Sample	26/8/3-SB	26/8/4-SB	26/8/5-SB	23/8/3-ST	23/8/6-ST
Major oxides (wt.%)					
SiO_2	44.45	44.14	44.75	50.28	49.76
TiO_2	2.79	2.32	2.82	1.80	1.75
Al_2O_3	13.68	12.41	13.71	14.07	14.24
Fe_2O_3	4.29	3.82	4.32	3.30	3.25
FeO	8.22	8.65	8.30	7.35	7.23
MnO	0.17	0.18	0.15	0.13	0.15
MgO	9.14	10.81	9.04	8.53	8.33
CaO	9.68	10.49	9.70	8.76	8.88
Na_2O	3.58	3.34	3.47	3.13	3.35
K_2O	1.69	1.30	1.83	1.24	1.24
P_2O_5	0.57	0.50	0.59	0.32	0.34
Total	98.26	97.96	98.68	98.91	98.52
Trace elements (ppm)					
S	121	291	64	107	0
Cl	295	424	334	229	0
Rb	32	31	33	32	30
Sr	690	693	736	546	571
Ba	474	568	485	380	390
Sc	19	23	19	21	18
Y	24	22	26	18	19
Zr	205	182	216	189	191
Nb	48	50	51	35	39
V	195	213	189	109	123
Cr	251	334	233	356	352
Co	48	52	49	39	37
Ni	151	239	144	184	171
C.I.P.W. norm					
Q	0.0	0.0	0.0	0.0	0.0
C	0.0	0.0	0.0	0.0	0.0
Or	10.0	7.7	10.8	7.3	7.3
Ab	14.1	11.1	14.1	26.5	28.3
An	16.2	15.0	16.4	20.6	20.1
Lc	0.0	0.0	0.0	0.0	0.0
Ne	8.8	9.3	8.2	0.0	0.0
Ac	0.0	0.0	0.0	0.0	0.0
Wo(Di)	11.7	14.1	11.6	8.7	9.1
En(Di)	8.1	9.7	8.1	5.8	6.1
Fs(Di)	2.6	3.3	2.6	2.2	2.3
En(Hy)	0.0	0.0	0.0	9.1	4.6
Fs(Hy)	0.0	0.0	0.0	3.4	1.8
Fo	10.3	12.2	10.2	4.5	7.1
Fa	3.6	4.6	3.6	1.9	3.0
Mt	6.2	5.5	6.3	4.8	4.7
Hm	0.0	0.0	0.0	0.0	0.0
Il	5.3	4.4	5.4	3.4	3.3
Ap	1.2	1.1	1.3	0.7	0.7

Table D-1 (continued): Hyalo Ridge

Sample	23/8/8-ST	23/8/9-ST	23/8/10-ST	23/8/11-ST	23/8/12-ST
Major oxides (wt.%)					
SiO_2	49.96	48.85	49.46	50.36	49.89
TiO_2	1.73	1.77	1.86	1.85	1.88
Al_2O_3	14.37	14.25	14.39	14.48	14.49
Fe_2O_3	3.23	3.27	3.36	3.35	3.38
FeO	7.41	6.85	7.25	7.39	7.32
MnO	0.12	0.14	0.15	0.15	0.15
MgO	8.36	8.26	7.95	8.36	8.09
CaO	8.86	9.08	8.76	8.90	8.95
Na_2O	3.53	3.61	3.39	3.13	3.40
K_2O	1.23	1.28	1.21	1.25	1.27
P_2O_5	0.34	0.35	0.35	0.34	0.36
Total	99.14	97.71	98.13	99.56	99.18
Trace elements (ppm)					
S	0	67	215	218	99
Cl	0	111	251	231	113
Rb	28	30	31	29	30
Sr	588	610	583	559	592
Ba	417	412	412	378	377
Sc	17	15	18	19	19
Y	18	20	19	18	19
Zr	192	204	202	191	203
Nb	37	41	39	36	39
V	109	121	119	103	115
Cr	344	388	325	353	326
Co	39	37	44	37	33
Ni	165	159	164	183	169
C.I.P.W. norm					
Q	0.0	0.0	0.0	0.0	0.0
C	0.0	0.0	0.0	0.0	0.0
Or	7.3	7.6	7.2	7.4	7.5
Ab	29.8	28.9	28.7	26.5	28.7
An	19.7	18.9	20.4	21.7	20.5
Lc	0.0	0.0	0.0	0.0	0.0
Ne	0.0	0.9	0.0	0.0	0.0
Ac	0.0	0.0	0.0	0.0	0.0
Wo(Di)	9.2	10.0	8.7	8.4	9.0
En(Di)	6.1	6.8	5.8	5.6	6.0
Fs(Di)	2.4	2.4	2.2	2.2	2.3
En(Hy)	2.4	0.0	4.8	8.7	4.1
Fs(Hy)	1.0	0.0	1.9	3.3	1.6
Fo	8.7	9.7	6.5	4.6	7.1
Fa	3.8	3.7	2.8	1.9	3.0
Mt	4.7	4.7	4.9	4.9	4.9
Hm	0.0	0.0	0.0	0.0	0.0
Il	3.3	3.4	3.5	3.5	3.6
Ap	0.7	0.8	0.8	0.7	0.8

Table D-1 (continued): Hyalo Ridge to Spanish Lake

Sample	23/8/13-ST	23/8/16-ST	23/8/17-ST	24/8/3-SL	24/8/5-SL
Major oxides (wt.%)					
SiO_2	49.81	49.57	50.01	45.52	45.78
TiO_2	1.87	1.77	1.77	2.55	2.32
Al_2O_3	14.54	14.38	14.48	14.35	14.25
Fe_2O_3	3.37	3.27	3.27	4.05	3.82
FeO	7.53	7.34	7.29	8.49	7.64
MnO	0.13	0.12	0.14	0.17	0.15
MgO	8.04	8.45	8.25	8.76	9.20
CaO	8.82	8.95	9.05	9.69	9.60
Na_2O	3.44	3.31	3.33	3.93	3.96
K_2O	1.22	1.17	1.15	1.83	1.97
P_2O_5	0.35	0.34	0.33	0.53	0.63
Total	99.12	98.67	99.07	99.87	99.32
Trace elements (ppm)					
S	51	113	49	644	410
Cl	25	174	40	443	564
Rb	24	27	28	36	44
Sr	603	586	581	769	786
Ba	431	400	385	792	888
Sc	17	17	18	18	20
Y	18	16	18	25	23
Zr	207	190	193	207	231
Nb	41	36	37	55	63
V	124	115	112	185	174
Cr	302	343	343	296	327
Co	37	42	40	48	50
Ni	159	179	163	244	221
C.I.P.W. norm					
Q	0.0	0.0	0.0	0.0	0.0
C	0.0	0.0	0.0	0.0	0.0
Or	7.2	6.9	6.8	10.8	11.7
Ab	29.1	28.0	28.1	13.7	13.7
An	20.6	20.9	21.1	16.1	15.3
Lc	0.0	0.0	0.0	0.0	0.0
Ne	0.0	0.0	0.0	10.6	10.7
Ac	0.0	0.0	0.0	0.0	0.0
Wo(Di)	8.7	8.9	9.0	11.9	11.8
En(Di)	5.7	5.9	6.0	8.0	8.2
Fs(Di)	2.3	2.3	2.3	3.0	2.6
En(Hy)	4.1	4.6	5.5	0.0	0.0
Fs(Hy)	1.7	1.8	2.1	0.0	0.0
Fo	7.2	7.4	6.4	9.7	10.4
Fa	3.2	3.1	2.7	4.1	3.6
Mt	4.9	4.7	4.7	5.9	5.5
Hm	0.0	0.0	0.0	0.0	0.0
Il	3.6	3.4	3.4	4.8	4.4
Ap	0.8	0.7	0.7	1.2	1.4

Table D-1 (continued): Spanish Lake

Sample	24/8/6-SL	24/8/8-SL	24/8/9-SL	24/8/10-SL	24/8/11-SL
Major oxides (wt.%)					
SiO_2	45.38	46.15	45.52	45.77	45.28
TiO_2	2.31	2.32	2.58	2.31	2.34
Al_2O_3	14.07	14.39	14.39	14.10	13.87
Fe_2O_3	3.81	3.82	4.08	3.81	3.84
FeO	7.66	7.65	7.74	7.69	7.68
MnO	0.16	0.17	0.16	0.18	0.16
MgO	9.21	9.26	8.78	9.45	9.20
CaO	9.79	9.50	9.81	9.57	9.72
Na_2O	3.74	3.90	3.85	3.88	3.88
K_2O	1.90	1.80	1.67	1.91	1.85
P_2O_5	0.64	0.62	0.55	0.62	0.59
Total	98.67	99.58	99.13	99.29	98.41
Trace elements (ppm)					
S	428	356	238	358	398
Cl	571	128	78	547	591
Rb	42	41	35	42	42
Sr	799	798	774	798	789
Ba	884	879	784	866	833
Sc	22	20	20	22	20
Y	24	25	24	27	27
Zr	225	222	205	226	221
Nb	63	59	55	61	60
V	187	167	177	185	188
Cr	311	326	285	314	341
Co	45	42	52	49	40
Ni	206	227	223	223	214
C.I.P.W. norm					
Q	0.0	0.0	0.0	0.0	0.0
C	0.0	0.0	0.0	0.0	0.0
Or	11.2	10.6	9.9	11.3	10.9
Ab	13.5	16.1	15.5	14.0	13.4
An	16.0	16.4	17.0	15.4	14.9
Lc	0.0	0.0	0.0	0.0	0.0
Ne	9.8	9.2	9.3	10.2	10.5
Ac	0.0	0.0	0.0	0.0	0.0
Wo(Di)	11.9	11.1	11.7	11.7	12.3
En(Di)	8.2	7.7	8.2	8.1	8.5
Fs(Di)	2.6	2.5	2.6	2.6	2.7
En(Hy)	0.0	0.0	0.0	0.0	0.0
Fs(Hy)	0.0	0.0	0.0	0.0	0.0
Fo	10.4	10.8	9.6	10.8	10.1
Fa	3.7	3.8	3.3	3.8	3.6
Mt	5.5	5.5	5.9	5.5	5.6
Hm	0.0	0.0	0.0	0.0	0.0
Il	4.4	4.4	4.9	4.4	4.4
Ap	1.4	1.4	1.2	1.4	1.3

Table D-1 (continued): Spanish Lake

Sample	24/8/14-SL	24/8/15-SL	2/8/1-SL	3/8/1-SL	3/8/4-SL
Major oxides (wt.%)					
SiO_2	46.37	45.74	44.09	45.25	45.61
TiO_2	2.51	2.52	2.52	2.39	2.32
Al_2O_3	14.46	14.43	13.68	13.94	13.98
Fe_2O_3	4.01	4.02	4.02	3.89	3.82
FeO	7.72	7.83	7.81	7.72	7.59
MnO	0.17	0.18	0.17	0.17	0.16
MgO	8.60	9.00	8.79	9.90	9.41
CaO	9.66	9.54	10.20	9.53	9.39
Na_2O	3.68	3.87	3.78	3.79	4.00
K_2O	1.71	1.85	1.75	1.73	1.89
P_2O_5	0.53	0.55	0.54	0.56	0.63
Total	99.42	99.53	97.35	98.87	98.80
Trace elements (ppm)					
S	514	647	370	428	112
Cl	168	469	500	249	230
Rb	39	37	37	35	40
Sr	743	774	785	760	818
Ba	789	813	905	816	915
Sc	21	20	16	18	19
Y	26	23	22	24	24
Zr	204	214	199	216	228
Nb	54	57	54	54	63
V	170	189	198	189	172
Cr	288	265	301	354	321
Co	45	48	44	47	49
Ni	233	213	216	267	229
C.I.P.W. norm					
Q	0.0	0.0	0.0	0.0	0.0
C	0.0	0.0	0.0	0.0	0.0
Or	10.1	10.9	10.4	10.2	11.2
Ab	18.2	14.9	10.8	13.9	14.4
An	17.9	16.5	15.2	15.9	14.6
Lc	0.0	0.0	0.0	0.0	0.0
Ne	7.0	9.7	11.4	9.8	10.5
Ac	0.0	0.0	0.0	0.0	0.0
Wo(Di)	11.1	11.4	13.3	11.6	11.7
En(Di)	7.7	7.9	9.2	8.2	8.1
Fs(Di)	2.5	2.5	3.0	2.4	2.5
En(Hy)	0.0	0.0	0.0	0.0	0.0
Fs(Hy)	0.0	0.0	0.0	0.0	0.0
Fo	9.7	10.2	8.9	11.6	10.8
Fa	3.5	3.6	3.2	3.8	3.7
Mt	5.8	5.8	5.8	5.6	5.5
Hm	0.0	0.0	0.0	0.0	0.0
Il	4.8	4.8	4.8	4.5	4.4
Ap	1.2	1.2	1.2	1.2	1.4

Table D-1 (continued): Spanish Lake to Flourmill

Sample	3/8/7-SL	2/8/3-SC	4/8/2-SC	4/8/6-SC	4/8/8-SC
Major oxides (wt.%)					
SiO_2	45.87	44.86	44.95	45.32	44.84
TiO_2	2.30	2.33	2.53	2.57	2.54
Al_2O_3	13.97	13.84	14.35	13.34	14.28
Fe_2O_3	3.80	3.83	4.03	4.07	4.04
FeO	7.84	7.70	7.69	7.86	7.87
MnO	0.17	0.19	0.16	0.17	0.16
MgO	9.67	9.37	8.39	8.53	8.40
CaO	9.48	9.81	9.67	9.72	9.67
Na_2O	3.90	3.89	3.99	3.86	3.61
K_2O	1.88	1.81	1.85	1.82	1.83
P_2O_5	0.61	0.62	0.56	0.55	0.55
Total	99.49	98.25	98.17	97.81	97.79
Trace elements (ppm)					
S	197	253	626	53	107
Cl	347	305	474	430	431
Rb	44	37	37	37	37
Sr	819	797	802	777	790
Ba	896	866	874	821	822
Sc	18	23	16	23	19
Y	23	28	25	26	22
Zr	228	224	210	214	214
Nb	63	60	57	56	56
V	177	184	191	182	178
Cr	325	320	270	290	284
Co	48	45	48	47	47
Ni	227	208	179	198	208
C.I.P.W. norm					
Q	0.0	0.0	0.0	0.0	0.0
C	0.0	0.0	0.0	0.0	0.0
Or	11.1	10.7	10.9	10.8	10.8
Ab	14.3	12.2	13.6	15.1	14.5
An	15.0	14.9	15.7	13.7	17.3
Lc	0.0	0.0	0.0	0.0	0.0
Ne	10.1	11.2	10.9	9.5	8.7
Ac	0.0	0.0	0.0	0.0	0.0
Wo(Di)	11.7	12.4	11.9	12.9	11.3
En(Di)	8.1	8.6	8.2	8.9	7.7
Fs(Di)	2.6	2.7	2.7	3.0	2.7
En(Hy)	0.0	0.0	0.0	0.0	0.0
Fs(Hy)	0.0	0.0	0.0	0.0	0.0
Fo	11.2	10.4	8.9	8.7	9.3
Fa	4.0	3.6	3.2	3.2	3.5
Mt	5.5	5.6	5.8	5.9	5.9
Hm	0.0	0.0	0.0	0.0	0.0
Il	4.4	4.4	4.8	4.9	4.8
Ap	1.3	1.4	1.2	1.2	1.2

Table D-1 (continued): Flourmill

Sample	4/8/14-SC	25/8/3-SC	4/8/7-SC	4/8/9-SC	4/8/10-SC
Major oxides (wt.%)					
SiO_2	44.89	44.85	44.63	44.80	45.04
TiO_2	2.55	2.51	2.50	2.50	2.45
Al_2O_3	14.34	14.29	14.00	14.17	13.64
Fe_2O_3	4.05	4.01	4.00	4.00	3.95
FeO	7.68	7.66	7.81	7.74	7.89
MnO	0.16	0.16	0.18	0.15	0.16
MgO	8.45	8.56	8.91	8.62	8.90
CaO	9.67	9.63	9.70	9.36	9.68
Na_2O	4.00	4.80	4.05	3.83	3.86
K_2O	1.84	1.81	1.79	1.82	1.80
P_2O_5	0.55	0.57	0.56	0.54	0.56
Total	98.18	98.85	98.13	97.53	97.93
Trace elements (ppm)					
S	88	160	510	456	517
Cl	465	482	440	391	491
Rb	34	35	35	36	34
Sr	779	794	775	759	755
Ba	829	810	795	792	760
Sc	19	19	20	18	17
Y	24	23	26	25	24
Zr	210	211	207	212	205
Nb	55	56	54	57	53
V	194	185	186	177	163
Cr	289	271	307	295	267
Co	47	45	50	49	47
Ni	214	202	237	241	218
C.I.P.W. norm					
Q	0.0	0.0	0.0	0.0	0.0
C	0.0	0.0	0.0	0.0	0.0
Or	10.9	10.7	10.6	10.8	10.6
Ab	13.4	11.1	12.3	14.7	13.9
An	15.7	12.1	14.7	16.1	14.5
Lc	0.0	0.0	0.0	0.0	0.0
Ne	11.1	16.0	11.9	9.6	10.2
Ac	0.0	0.0	0.0	0.0	0.0
Wo(Di)	12.0	13.4	12.4	11.2	12.5
En(Di)	8.3	9.3	8.6	7.7	8.6
Fs(Di)	2.7	3.0	2.8	2.5	2.9
En(Hy)	0.0	0.0	0.0	0.0	0.0
Fs(Hy)	0.0	0.0	0.0	0.0	0.0
Fo	9.0	8.5	9.6	9.7	9.6
Fa	3.2	3.0	3.4	3.5	3.5
Mt	5.9	5.8	5.8	5.8	5.7
Hm	0.0	0.0	0.0	0.0	0.0
Il	4.8	4.8	4.8	4.8	4.7
Ap	1.2	1.2	1.2	1.2	1.2

Table D-1 (continued): Flourmill

Sample	3/8/10-SC	4/8/12-SC	4/8/13-SC	2/8/5-SC	2/8/6-SC
Major oxides (wt.%)					
SiO_2	44.70	44.98	44.98	44.87	43.97
TiO_2	2.53	2.56	2.53	2.21	2.42
Al_2O_3	14.03	14.38	14.05	12.93	13.24
Fe_2O_3	4.03	4.06	4.03	3.71	3.92
FeO	7.74	7.69	7.66	8.20	7.89
MnO	0.18	0.17	0.16	0.16	0.18
MgO	8.88	8.35	8.49	11.11	9.76
CaO	9.74	9.84	9.68	10.27	10.48
Na_2O	3.97	3.81	4.15	2.96	3.41
K_2O	1.66	1.78	1.63	1.38	1.63
P_2O_5	0.54	0.55	0.54	0.40	0.49
Total	98.00	98.17	97.90	98.20	97.39
Trace elements (ppm)					
S	277	103	142	276	278
Cl	272	306	161	160	242
Rb	34	37	35	28	34
Sr	764	783	801	649	740
Ba	812	808	811	701	863
Sc	16	21	19	23	21
Y	23	25	26	20	23
Zr	205	211	221	164	175
Nb	55	55	57	44	53
V	184	178	187	207	223
Cr	302	291	293	420	356
Co	46	49	48	58	57
Ni	243	190	215	299	257
C.I.P.W. norm					
Q	0.0	0.0	0.0	0.0	0.0
C	0.0	0.0	0.0	0.0	0.0
Or	9.8	10.5	9.6	8.2	9.6
Ab	13.6	14.2	14.8	13.0	9.9
An	15.5	16.8	14.9	17.9	16.0
Lc	0.0	0.0	0.0	0.0	0.0
Ne	10.8	9.8	11.0	6.5	10.2
Ac	0.0	0.0	0.0	0.0	0.0
Wo(Di)	12.2	11.9	12.4	12.7	13.7
En(Di)	8.5	8.2	8.6	8.9	9.6
Fs(Di)	2.7	2.7	2.8	2.8	3.0
En(Hy)	0.0	0.0	0.0	0.0	0.0
Fs(Hy)	0.0	0.0	0.0	0.0	0.0
Fo	9.6	8.9	8.9	13.2	10.4
Fa	3.4	3.2	3.2	4.5	3.6
Mt	5.8	5.9	5.8	5.4	5.7
Hm	0.0	0.0	0.0	0.0	0.0
Il	4.8	4.9	4.8	4.2	4.6
Ap	1.2	1.2	1.2	0.9	1.1

Table D-1 (continued): Flourmill

Sample	2/8/7-SC	3/8/8-SC	4/8/15-SC	4/8/16-SC	4/8/17-SC
Major oxides (wt.%)					
SiO_2	44.66	45.35	44.20	44.87	45.04
TiO_2	2.03	2.30	2.53	2.53	2.45
Al_2O_3	12.04	13.35	13.86	14.05	13.64
Fe_2O_3	3.53	3.80	4.03	4.03	3.95
FeO	8.32	8.03	7.65	7.75	8.03
MnO	0.16	0.18	0.17	0.17	0.17
MgO	13.47	10.41	8.85	9.31	9.74
CaO	9.12	10.36	9.70	9.90	10.46
Na_2O	3.18	3.51	4.09	3.33	3.73
K_2O	1.37	1.50	1.79	1.87	1.63
P_2O_5	0.41	0.46	0.53	0.52	0.50
Total	98.29	99.25	97.40	98.33	99.34
Trace elements (ppm)					
S	366	148	269	162	394
Cl	251	318	417	79	419
Rb	26	29	33	32	32
Sr	609	669	759	757	752
Ba	632	711	778	794	855
Sc	23	20	18	22	22
Y	16	20	28	23	23
Zr	155	168	202	196	179
Nb	40	46	55	53	54
V	187	219	196	177	230
Cr	501	459	317	315	356
Co	62	51	51	43	49
Ni	463	308	282	247	253
C.I.P.W. norm					
Q	0.0	0.0	0.0	0.0	0.0
C	0.0	0.0	0.0	0.0	0.0
Or	8.1	8.9	10.6	11.1	9.6
Ab	12.4	12.5	11.4	13.0	11.1
An	14.5	16.2	14.1	17.8	15.6
Lc	0.0	0.0	0.0	0.0	0.0
Ne	7.8	9.3	12.5	8.2	11.1
Ac	0.0	0.0	0.0	0.0	0.0
Wo(Di)	11.7	13.4	12.7	11.7	13.8
En(Di)	8.4	9.4	8.9	8.2	9.6
Fs(Di)	2.3	2.9	2.8	2.5	3.0
En(Hy)	0.0	0.0	0.0	0.0	0.0
Fs(Hy)	0.0	0.0	0.0	0.0	0.0
Fo	17.7	11.7	9.3	10.6	10.3
Fa	5.4	4.0	3.2	3.5	3.6
Mt	5.1	5.5	5.8	5.8	5.7
Hm	0.0	0.0	0.0	0.0	0.0
Il	3.9	4.4	4.8	4.8	4.7
Ap	0.9	1.0	1.2	1.1	1.1

Table D-1 (continued): Flourmill to Pyramid Mountain

Sample	4/8/1-SC	4/8/4-SC	10/8/8-SP	10/8/7-SP	13/8/9-PY
Major oxides (wt.%)					
SiO_2	45.00	45.13	48.56	48.25	45.01
TiO_2	2.13	2.18	1.75	1.72	2.28
Al_2O_3	12.62	12.85	14.55	14.00	12.68
Fe_2O_3	3.63	3.68	3.25	3.22	3.78
FeO	8.26	8.17	8.22	8.34	9.20
MnO	0.18	0.18	0.16	0.15	0.18
MgO	12.03	11.39	8.45	9.18	11.38
CaO	9.75	10.00	9.39	9.18	9.62
Na_2O	3.04	3.24	3.38	3.08	3.19
K_2O	1.24	1.38	0.75	0.82	1.00
P_2O_5	0.40	0.43	0.30	0.29	0.40
Total	98.28	98.63	98.76	98.24	98.72
Trace elements (ppm)					
S	209	0	23	275	48
Cl	113	0	0	67	314
Rb	31	0	11	16	26
Sr	677	0	425	412	525
Ba	708	0	241	248	361
Sc	19	0	21	19	21
Y	20	0	19	19	22
Zr	170	0	118	126	172
Nb	46	0	18	18	37
V	196	0	161	171	186
Cr	415	0	331	349	387
Co	53	0	41	49	53
Ni	330	0	105	123	298
C.I.P.W. norm					
Q	0.0	0.0	0.0	0.0	0.0
C	0.0	0.0	0.0	0.0	0.0
Or	7.3	8.2	4.4	4.9	5.9
Ab	14.5	13.4	28.6	26.0	16.7
An	17.1	16.4	22.3	21.9	17.3
Lc	0.0	0.0	0.0	0.0	0.0
Ne	6.1	7.6	0.0	0.0	5.6
Ac	0.0	0.0	0.0	0.0	0.0
Wo(Di)	12.0	12.7	9.3	9.1	11.6
En(Di)	8.4	8.9	6.0	5.9	7.9
Fs(Di)	2.5	2.7	2.8	2.6	2.9
En(Hy)	0.0	0.0	1.6	3.9	0.0
Fs(Hy)	0.0	0.0	0.7	1.7	0.0
Fo	15.2	13.7	9.5	9.3	14.4
Fa	5.0	4.6	4.9	4.5	5.8
Mt	5.3	5.3	4.7	4.7	5.5
Hm	0.0	0.0	0.0	0.0	0.0
Il	4.0	4.1	3.3	3.3	4.3
Ap	0.9	0.9	0.7	0.6	0.9

Table D-1 (continued): Pyramid Mountain to Ray Mountain

Sample	27/7/1-PY	17/8/5-RM	17/8/7-RM	17/8/11-RM	17/8/12-RM
Major oxides (wt.%)					
SiO_2	43.98	43.15	43.25	44.73	46.23
TiO_2	2.81	3.76	3.69	2.51	2.40
Al_2O_3	12.79	14.92	14.89	13.23	13.36
Fe_2O_3	4.31	5.26	5.19	4.01	3.90
FeO	9.66	9.37	9.04	8.41	8.93
MnO	0.17	0.15	0.17	0.18	0.17
MgO	10.68	6.50	6.30	9.94	9.59
CaO	9.73	9.60	9.46	9.78	9.56
Na_2O	3.26	3.47	4.07	3.46	3.43
K_2O	1.17	1.27	1.58	1.58	0.98
P_2O_5	0.58	0.49	0.48	0.53	0.52
Total	99.14	97.94	98.12	98.36	99.07
Trace elements (ppm)					
S	87	302	226	231	84
Cl	187	113	314	312	0
Rb	32	17	35	32	41
Sr	630	830	848	672	526
Ba	427	685	676	615	530
Sc	19	17	15	22	19
Y	24	19	18	23	24
Zr	176	182	187	189	193
Nb	46	52	51	52	46
V	176	215	223	197	185
Cr	337	51	54	312	342
Co	56	45	51	50	51
Ni	253	58	68	240	231
C.I.P.W. norm					
Q	0.0	0.0	0.0	0.0	0.0
C	0.0	0.0	0.0	0.0	0.0
Or	6.9	7.5	9.3	9.3	5.8
Ab	14.7	18.4	15.3	13.8	22.4
An	16.8	21.3	17.7	15.9	18.1
Lc	0.0	0.0	0.0	0.0	0.0
Ne	7.0	5.9	10.3	8.4	3.6
Ac	0.0	0.0	0.0	0.0	0.0
Wo(Di)	11.6	9.6	10.9	12.2	10.8
En(Di)	7.8	6.3	7.2	8.4	7.2
Fs(Di)	2.9	2.7	3.0	2.8	2.8
En(Hy)	0.0	0.0	0.0	0.0	0.0
Fs(Hy)	0.0	0.0	0.0	0.0	0.0
Fo	13.2	7.0	6.0	11.5	11.8
Fa	5.4	3.3	2.7	4.3	5.2
Mt	6.2	7.6	7.5	5.8	5.7
Hm	0.0	0.0	0.0	0.0	0.0
Il	5.3	7.1	7.0	4.8	4.6
Ap	1.3	1.1	1.0	1.2	1.1

Table D-1 (continued): Ray Mountain

Sample	17/8/13-RM	17/8/14-RM	17/8/15-RM	17/8/17-RM	19/8/1-RM
Major oxides (wt.%)					
SiO_2	45.09	45.51	45.19	42.76	43.13
TiO_2	2.53	2.49	2.50	2.76	3.34
Al_2O_3	13.39	13.35	13.43	13.23	14.56
Fe_2O_3	4.03	3.99	4.00	4.26	4.84
FeO	8.24	8.40	8.36	9.54	9.09
MnO	0.17	0.17	0.17	0.17	0.17
MgO	10.02	10.04	9.94	10.13	6.62
CaO	9.94	9.82	9.80	9.86	9.53
Na_2O	3.51	3.51	3.67	3.64	4.13
K_2O	1.42	1.29	1.40	1.60	1.77
P_2O_5	0.56	0.54	0.54	0.57	0.66
Total	98.90	99.11	99.00	98.52	97.84
Trace elements (ppm)					
S	62	20	53	305	188
Cl	209	138	361	401	207
Rb	35	38	39	40	39
Sr	684	645	682	857	1030
Ba	641	620	648	629	793
Sc	24	19	23	17	15
Y	21	22	22	20	22
Zr	198	196	204	191	199
Nb	55	52	54	55	58
V	201	182	198	180	196
Cr	325	342	316	260	90
Co	54	51	45	55	43
Ni	221	228	215	217	80
C.I.P.W. norm					
Q	0.0	0.0	0.0	0.0	0.0
C	0.0	0.0	0.0	0.0	0.0
Or	8.4	7.6	8.3	9.5	10.5
Ab	15.2	17.2	15.4	7.7	13.2
An	16.6	16.8	16.0	15.0	15.9
Lc	0.0	0.0	0.0	0.0	0.0
Ne	7.8	6.7	8.5	12.5	11.8
Ac	0.0	0.0	0.0	0.0	0.0
Wo(Di)	12.2	11.8	12.2	12.6	11.3
En(Di)	8.5	8.2	8.4	8.4	7.3
Fs(Di)	2.7	2.7	2.8	3.2	3.3
En(Hy)	0.0	0.0	0.0	0.0	0.0
Fs(Hy)	0.0	0.0	0.0	0.0	0.0
Fo	11.6	11.9	11.5	11.8	6.5
Fa	4.1	4.3	4.2	5.0	3.2
Mt	5.8	5.8	5.8	6.2	7.0
Hm	0.0	0.0	0.0	0.0	0.0
Il	4.8	4.7	4.8	5.2	6.3
Ap	1.2	1.2	1.2	1.2	1.4

Table D-1 (continued): Pointed Stick Cone to Dragon's Tongue

Sample	18/8/3-RC	18/8/4-RC	18/8/8-RC	18/8/9-RR	16/8/1-R
Major oxides (wt.%)					
SiO_2	44.65	45.50	45.77	44.39	44.57
TiO_2	2.99	2.94	2.66	2.15	2.61
Al_2O_3	14.32	14.53	15.23	12.75	13.85
Fe_2O_3	4.49	4.44	4.16	3.65	4.11
FeO	8.99	9.02	8.53	9.21	8.70
MnO	0.15	0.17	0.20	0.17	0.18
MgO	6.50	6.45	6.34	11.03	8.77
CaO	7.15	7.03	8.13	9.82	9.03
Na_2O	4.87	5.49	4.49	3.41	4.75
K_2O	2.11	2.20	2.21	1.19	1.94
P_2O_5	0.96	1.00	0.83	0.40	0.78
Total	97.18	98.77	98.55	98.17	99.29
Trace elements (ppm)					
S	109	129	97	182	427
Cl	141	260	514	148	862
Rb	42	45	47	29	43
Sr	1067	1071	947	498	981
Ba	507	541	1019	375	1450
Sc	12	16	16	20	17
Y	24	24	26	22	24
Zr	381	387	265	161	234
Nb	64	63	77	38	89
V	60	74	131	180	148
Cr	125	130	105	357	207
Co	36	42	36	55	48
Ni	114	116	79	230	154
C.I.P.W. norm					
Q	0.0	0.0	0.0	0.0	0.0
C	0.0	0.0	0.0	0.0	0.0
Or	12.5	13.0	13.1	7.0	11.5
Ab	21.3	21.0	19.8	12.8	11.8
An	11.0	8.5	14.8	15.9	10.7
Lc	0.0	0.0	0.0	0.0	0.0
Ne	10.7	13.8	9.8	8.7	15.4
Ac	0.0	0.0	0.0	0.0	0.0
Wo(Di)	7.6	8.3	8.4	12.6	12.1
En(Di)	4.8	5.1	5.2	8.4	8.1
Fs(Di)	2.4	2.7	2.7	3.2	3.2
En(Hy)	0.0	0.0	0.0	0.0	0.0
Fs(Hy)	0.0	0.0	0.0	0.0	0.0
Fo	8.0	7.7	7.5	13.4	9.7
Fa	4.4	4.4	4.3	5.7	4.2
Mt	6.5	6.4	6.0	5.3	6.0
Hm	0.0	0.0	0.0	0.0	0.0
Il	5.7	5.6	5.1	4.1	5.0
Ap	2.1	2.2	1.8	0.9	1.7

Table D-1 (continued): Dragon's Tongue

Sample	13/8/3-R	14/8/1-R	14/8/2-R	14/8/4-R	14/8/5-R
Major oxides (wt.%)					
SiO_2	42.94	43.60	43.91	43.03	43.67
TiO_2	2.72	2.67	2.70	2.68	2.62
Al_2O_3	13.40	13.54	13.50	13.37	13.40
Fe_2O_3	4.22	4.17	4.20	4.18	4.12
FeO	8.74	8.84	8.79	8.75	8.84
MnO	0.17	0.19	0.17	0.17	0.19
MgO	8.90	9.16	9.08	9.19	9.30
CaO	9.93	9.80	9.68	9.96	9.75
Na_2O	4.28	4.30	4.21	3.94	4.27
K_2O	1.83	1.75	1.81	1.63	1.78
P_2O_5	0.80	0.82	0.77	0.80	0.78
Total	97.93	98.84	98.82	97.70	98.72
Trace elements (ppm)					
S	250	337	282	203	209
Cl	641	702	720	568	747
Rb	39	36	40	38	38
Sr	980	996	986	987	1008
Ba	1249	1307	1240	1259	1271
Sc	19	18	18	20	16
Y	22	24	26	25	23
Zr	237	232	240	243	238
Nb	88	85	89	87	90
V	167	173	162	175	180
Cr	244	230	243	260	239
Co	58	47	55	47	51
Ni	168	165	175	176	175
C.I.P.W. norm					
Q	0.0	0.0	0.0	0.0	0.0
C	0.0	0.0	0.0	0.0	0.0
Or	10.8	10.4	10.7	9.6	10.5
Ab	7.7	9.5	10.5	9.9	9.3
An	11.9	12.4	12.6	14.0	12.1
Lc	0.0	0.0	0.0	0.0	0.0
Ne	15.4	14.5	13.6	12.7	14.5
Ac	0.0	0.0	0.0	0.0	0.0
Wo(Di)	13.4	12.9	12.7	12.6	13.0
En(Di)	9.0	8.6	8.5	8.5	8.7
Fs(Di)	3.4	3.3	3.2	3.1	3.3
En(Hy)	0.0	0.0	0.0	0.0	0.0
Fs(Hy)	0.0	0.0	0.0	0.0	0.0
Fo	9.3	10.0	9.9	10.1	10.2
Fa	3.9	4.2	4.1	4.1	4.3
Mt	6.1	6.0	6.1	6.1	6.0
Hm	0.0	0.0	0.0	0.0	0.0
Il	5.2	5.1	5.1	5.1	5.0
Ap	1.7	1.8	1.7	1.7	1.7

Table D-1 (continued): Dragon's Tongue

Sample	14/8/6-R	14/8/7-R	17/8/1-R	17/8/2-R	17/8/3-R
Major oxides (wt.%)					
SiO_2	43.56	42.73	44.16	44.37	44.43
TiO_2	2.66	2.63	2.71	2.72	2.70
Al_2O_3	13.48	13.32	13.33	13.35	13.31
Fe_2O_3	4.16	4.13	4.21	4.22	4.20
FeO	8.88	8.90	9.02	9.04	9.04
MnO	0.16	0.18	0.17	0.17	0.19
MgO	8.63	9.01	9.96	9.95	9.93
CaO	9.69	9.86	9.49	9.55	9.52
Na_2O	4.15	4.53	3.84	3.73	3.66
K_2O	1.85	1.86	1.57	1.58	1.60
P_2O_5	0.82	0.82	0.59	0.60	0.62
Total	98.04	97.97	99.05	99.28	99.20
Trace elements (ppm)					
S	320	365	167	208	244
Cl	822	777	270	466	467
Rb	39	35	35	35	36
Sr	1042	974	777	784	789
Ba	1405	1246	908	914	936
Sc	16	21	15	18	18
Y	25	23	22	22	21
Zr	243	234	211	221	219
Nb	93	85	63	64	67
V	181	161	169	173	166
Cr	218	229	274	289	287
Co	47	46	59	54	50
Ni	161	160	183	196	191
C.I.P.W. norm					
Q	0.0	0.0	0.0	0.0	0.0
C	0.0	0.0	0.0	0.0	0.0
Or	10.9	11.0	9.3	9.3	9.5
Ab	10.4	6.1	12.3	12.9	13.3
An	12.7	10.5	14.5	15.0	15.1
Lc	0.0	0.0	0.0	0.0	0.0
Ne	13.4	17.4	10.9	10.1	9.5
Ac	0.0	0.0	0.0	0.0	0.0
Wo(Di)	12.6	13.8	12.0	11.9	11.7
En(Di)	8.3	9.2	8.1	8.1	7.9
Fs(Di)	3.4	3.6	2.9	2.9	2.9
En(Hy)	0.0	0.0	0.0	0.0	0.0
Fs(Hy)	0.0	0.0	0.0	0.0	0.0
Fo	9.3	9.4	11.7	11.8	11.8
Fa	4.2	4.1	4.6	4.7	4.7
Mt	6.0	6.0	6.1	6.1	6.1
Hm	0.0	0.0	0.0	0.0	0.0
Il	5.1	5.0	5.1	5.2	5.1
Ap	1.8	1.8	1.3	1.3	1.4

Table D-1 (continued): Dragon's Tongue

Sample	17/8/4-R	17/8/5-R	17/8/6-R	11/8/7-R	11/8/8-R
Major oxides (wt.%)					
SiO_2	44.09	43.78	44.13	43.97	43.82
TiO_2	2.69	2.71	2.70	2.68	2.71
Al_2O_3	13.20	13.18	13.29	13.07	13.09
Fe_2O_3	4.19	4.21	4.20	4.18	4.21
FeO	9.11	9.16	9.04	9.08	8.95
MnO	0.16	0.16	0.16	0.17	0.19
MgO	9.97	9.99	9.87	10.00	9.72
CaO	9.58	9.51	9.54	9.49	9.47
Na_2O	3.90	3.87	3.90	3.93	3.82
K_2O	1.57	1.55	1.55	1.58	1.56
P_2O_5	0.62	0.60	0.61	0.60	0.60
Total	99.08	98.72	98.99	98.75	98.14
Trace elements (ppm)					
S	252	185	0	217	237
Cl	469	59	0	438	460
Rb	35	34	0	36	32
Sr	775	789	0	781	768
Ba	926	925	0	891	921
Sc	17	20	0	17	16
Y	22	22	0	23	23
Zr	218	219	0	215	219
Nb	67	64	0	65	68
V	172	165	0	172	175
Cr	296	302	0	291	301
Co	55	57	0	60	52
Ni	202	205	0	196	201
C.I.P.W. norm					
Q	0.0	0.0	0.0	0.0	0.0
C	0.0	0.0	0.0	0.0	0.0
Or	9.3	9.2	9.2	9.3	9.2
Ab	11.8	11.5	12.3	11.6	12.5
An	13.8	14.0	14.2	13.3	13.9
Lc	0.0	0.0	0.0	0.0	0.0
Ne	11.5	11.5	11.2	11.7	10.7
Ac	0.0	0.0	0.0	0.0	0.0
Wo(Di)	12.4	12.2	12.2	12.5	12.2
En(Di)	8.4	8.3	8.2	8.4	8.2
Fs(Di)	3.1	3.0	3.0	3.1	3.0
En(Hy)	0.0	0.0	0.0	0.0	0.0
Fs(Hy)	0.0	0.0	0.0	0.0	0.0
Fo	11.6	11.7	11.5	11.6	11.2
Fa	4.7	4.7	4.6	4.7	4.5
Mt	6.1	6.1	6.1	6.1	6.1
Hm	0.0	0.0	0.0	0.0	0.0
Il	5.1	5.1	5.1	5.1	5.1
Ap	1.4	1.3	1.3	1.3	1.3

Table D-1 (continued): Dragon's Tongue

Sample	11/8/9-R	11/8/1-R	11/8/2-R	11/8/3-R	2/9/1-R
Major oxides (wt.%)					
SiO_2	44.09	43.29	43.69	44.10	43.85
TiO_2	2.68	2.76	2.71	2.72	2.70
Al_2O_3	13.26	12.95	13.08	13.24	13.24
Fe_2O_3	4.18	4.26	4.21	4.22	4.20
FeO	9.05	9.05	8.99	8.97	9.06
MnO	0.17	0.20	0.15	0.16	0.18
MgO	10.00	10.05	9.81	9.85	9.92
CaO	9.47	9.77	9.46	9.49	9.48
Na_2O	3.71	3.66	3.74	4.03	3.86
K_2O	1.57	1.64	1.50	1.56	1.56
P_2O_5	0.60	0.59	0.59	0.58	0.59
Total	98.78	98.22	97.93	98.92	98.64
Trace elements (ppm)					
S	126	156	100	211	307
Cl	245	296	273	354	380
Rb	31	34	34	35	33
Sr	771	788	769	762	772
Ba	917	954	942	894	895
Sc	20	21	19	17	20
Y	21	24	23	22	21
Zr	218	207	214	216	214
Nb	64	64	63	62	64
V	158	180	190	170	175
Cr	301	300	283	295	300
Co	55	52	55	47	54
Ni	202	204	196	195	202
C.I.P.W. norm					
Q	0.0	0.0	0.0	0.0	0.0
C	0.0	0.0	0.0	0.0	0.0
Or	9.3	9.7	8.9	9.2	9.2
Ab	12.6	9.6	12.7	11.9	11.8
An	14.9	14.0	14.4	13.4	14.2
Lc	0.0	0.0	0.0	0.0	0.0
Ne	10.1	11.6	10.2	12.0	11.3
Ac	0.0	0.0	0.0	0.0	0.0
Wo(Di)	11.8	12.8	12.0	12.5	12.1
En(Di)	8.0	8.7	8.1	8.5	8.2
Fs(Di)	2.9	3.1	2.9	3.0	3.0
En(Hy)	0.0	0.0	0.0	0.0	0.0
Fs(Hy)	0.0	0.0	0.0	0.0	0.0
Fo	11.9	11.5	11.5	11.3	11.6
Fa	4.8	4.5	4.6	4.4	4.7
Mt	6.1	6.2	6.1	6.1	6.1
Hm	0.0	0.0	0.0	0.0	0.0
Il	5.1	5.2	5.1	5.2	5.1
Ap	1.3	1.3	1.3	1.3	1.3

Table D-1 (continued): Dragon's Tongue to Kostal Lake (older lavas)

Sample	11/8/6-R	21/7/1-R	29/7/7-KP	29/7/9-KP	31/8/8-KP
Major oxides (wt.%)					
SiO_2	44.25	43.80	44.48	44.32	43.73
TiO_2	2.73	2.69	2.75	2.85	2.82
Al_2O_3	13.37	13.13	13.94	13.76	13.28
Fe_2O_3	4.23	4.19	4.25	4.35	4.32
FeO	9.23	9.08	8.62	8.74	8.73
MnO	0.16	0.18	0.16	0.17	0.18
MgO	9.98	10.02	8.53	8.71	8.64
CaO	9.56	9.49	8.57	8.55	8.88
Na_2O	3.66	3.83	4.58	4.69	4.68
K_2O	1.58	1.58	1.98	2.07	1.98
P_2O_5	0.62	0.61	0.82	0.74	0.76
Total	99.37	98.60	98.68	98.95	98.00
Trace elements (ppm)					
S	243	115	403	464	202
Cl	462	333	619	579	163
Rb	34	36	40	42	38
Sr	776	801	975	891	962
Ba	907	936	750	710	738
Sc	19	18	18	13	18
Y	25	23	21	22	24
Zr	217	220	303	314	291
Nb	65	65	67	66	63
V	173	182	129	132	125
Cr	307	271	224	215	236
Co	53	54	44	51	52
Ni	194	170	161	173	184
C.I.P.W. norm					
Q	0.0	0.0	0.0	0.0	0.0
C	0.0	0.0	0.0	0.0	0.0
Or	9.3	9.3	11.7	12.2	11.7
Ab	12.7	11.5	14.2	12.4	11.1
An	15.4	13.9	11.6	10.4	9.4
Lc	0.0	0.0	0.0	0.0	0.0
Ne	9.9	11.3	13.3	14.8	15.4
Ac	0.0	0.0	0.0	0.0	0.0
Wo(Di)	11.7	12.2	10.7	11.4	12.4
En(Di)	7.9	8.2	7.2	7.7	8.3
Fs(Di)	2.9	3.0	2.7	2.8	3.1
En(Hy)	0.0	0.0	0.0	0.0	0.0
Fs(Hy)	0.0	0.0	0.0	0.0	0.0
Fo	11.9	11.8	9.9	9.9	9.3
Fa	4.9	4.7	4.1	4.0	3.9
Mt	6.1	6.1	6.2	6.3	6.3
Hm	0.0	0.0	0.0	0.0	0.0
Il	5.2	5.1	5.2	5.4	5.4
Ap	1.4	1.3	1.8	1.6	1.7

Table D-1 (continued): Kostal Lake (south cone)

Sample	29/7/5-KS	30/8/5-KS	31/8/9-KS	25/7/4-KS	25/7/6-KS
Major oxides (wt.%)					
SiO_2	44.35	44.56	44.63	44.68	44.30
TiO_2	2.61	2.68	2.66	2.64	2.61
Al_2O_3	13.18	13.13	13.34	13.14	13.00
Fe_2O_3	4.11	4.18	4.16	4.14	4.11
FeO	8.60	8.74	8.63	8.67	8.64
MnO	0.16	0.16	0.16	0.18	0.17
MgO	10.79	10.76	10.55	10.72	10.80
CaO	9.45	9.67	9.59	9.60	9.47
Na_2O	3.69	2.97	3.62	3.64	3.84
K_2O	1.52	1.34	1.52	1.51	1.50
P_2O_5	0.56	0.55	0.54	0.55	0.54
Total	99.02	98.74	99.40	99.47	98.98
Trace elements (ppm)					
S	158	123	158	162	0
Cl	354	183	353	340	0
Rb	32	28	34	30	0
Sr	677	683	685	674	0
Ba	510	478	501	498	0
Sc	21	21	21	21	0
Y	22	21	23	22	0
Zr	230	229	235	227	0
Nb	49	49	49	48	0
V	170	188	192	161	0
Cr	339	328	339	334	0
Co	54	53	56	53	0
Ni	237	246	238	243	0
C.I.P.W. norm					
Q	0.0	0.0	0.0	0.0	0.0
C	0.0	0.0	0.0	0.0	0.0
Or	9.0	7.9	9.0	8.9	8.9
Ab	12.6	16.0	13.2	13.1	12.1
An	14.9	18.5	15.6	15.0	13.8
Lc	0.0	0.0	0.0	0.0	0.0
Ne	10.1	4.9	9.4	9.6	11.0
Ac	0.0	0.0	0.0	0.0	0.0
Wo(Di)	11.8	10.8	11.9	12.1	12.4
En(Di)	8.3	7.5	8.3	8.4	8.6
Fs(Di)	2.6	2.4	2.6	2.7	2.7
En(Hy)	0.0	0.0	0.0	0.0	0.0
Fs(Hy)	0.0	0.0	0.0	0.0	0.0
Fo	13.1	13.6	12.7	12.9	12.9
Fa	4.5	4.7	4.4	4.5	4.4
Mt	6.0	6.1	6.0	6.0	6.0
Hm	0.0	0.0	0.0	0.0	0.0
Il	5.0	5.1	5.1	5.0	5.0
Ap	1.2	1.2	1.2	1.2	1.2

Table D-1 (continued): Kostal Lake (south cone) to Kostal Lake (north cone)

Sample	29/7/6-KS	29/7/11-KS	29/7/10-KS	29/7/8-KS	24/7/1-KN
Major oxides (wt.%)					
SiO_2	44.40	44.17	44.03	43.83	43.35
TiO_2	2.62	2.50	2.58	2.64	2.64
Al_2O_3	13.14	12.72	12.80	12.93	12.83
Fe_2O_3	4.12	4.00	4.08	4.14	4.14
FeO	8.56	8.69	8.60	8.45	8.66
MnO	0.18	0.16	0.18	0.16	0.16
MgO	10.68	11.43	10.87	10.06	10.83
CaO	9.49	9.21	9.48	9.18	9.73
Na_2O	3.72	4.01	4.00	3.87	3.48
K_2O	1.51	1.55	1.55	1.62	1.39
P_2O_5	0.55	0.56	0.57	0.60	0.50
Total	98.97	99.00	98.74	97.48	97.71
Trace elements (ppm)					
S	123	387	153	279	27
Cl	355	396	387	493	271
Rb	33	32	32	36	27
Sr	679	686	693	719	650
Ba	501	492	512	551	459
Sc	19	22	20	20	18
Y	21	22	20	21	22
Zr	230	236	232	243	209
Nb	50	50	52	57	46
V	175	168	160	142	174
Cr	330	424	399	336	342
Co	56	58	57	56	55
Ni	235	288	289	234	243
C.I.P.W. norm					
Q	0.0	0.0	0.0	0.0	0.0
C	0.0	0.0	0.0	0.0	0.0
Or	8.9	9.2	9.2	9.6	8.2
Ab	12.8	10.9	10.7	12.8	11.0
An	14.7	12.1	12.4	13.1	15.3
Lc	0.0	0.0	0.0	0.0	0.0
Ne	10.1	12.5	12.5	10.8	10.0
Ac	0.0	0.0	0.0	0.0	0.0
Wo(Di)	12.0	12.5	12.9	11.9	12.4
En(Di)	8.4	8.7	9.0	8.3	8.7
Fs(Di)	2.6	2.7	2.8	2.6	2.7
En(Hy)	0.0	0.0	0.0	0.0	0.0
Fs(Hy)	0.0	0.0	0.0	0.0	0.0
Fo	12.8	13.9	12.7	11.8	12.9
Fa	4.4	4.7	4.4	4.2	4.4
Mt	6.0	5.8	5.9	6.0	6.0
Hm	0.0	0.0	0.0	0.0	0.0
Il	5.0	4.8	4.9	5.0	5.0
Ap	1.2	1.2	1.2	1.3	1.1

Table D-1 (continued): Kostal Lake (north cone) to Kostal Lake (lava tube)

Sample	25/7/1-KN	29/7/3-KN	29/7/14-KN	30/8/2-KN	29/7/12-KT
Major oxides (wt.%)					
SiO_2	44.51	43.98	44.29	43.67	43.79
TiO_2	2.67	2.61	2.63	2.62	2.65
Al_2O_3	13.15	12.98	13.02	12.83	12.96
Fe_2O_3	4.17	4.11	4.13	4.12	4.15
FeO	8.66	8.69	8.77	8.72	8.61
MnO	0.17	0.17	0.16	0.16	0.17
MgO	10.69	11.23	11.19	11.16	10.60
CaO	9.65	9.63	9.68	9.83	9.60
Na_2O	3.50	3.52	3.40	3.10	3.87
K_2O	1.52	1.36	1.39	1.29	1.54
P_2O_5	0.51	0.51	0.52	0.50	0.55
Total	99.20	98.79	99.18	98.00	98.49
Trace elements (ppm)					
S	169	318	670	403	147
Cl	335	260	381	299	338
Rb	31	30	28	27	31
Sr	664	638	661	633	659
Ba	504	465	461	448	489
Sc	20	19	22	20	22
Y	20	21	21	21	21
Zr	224	210	214	206	226
Nb	51	47	48	45	48
V	171	170	178	176	168
Cr	324	334	341	364	309
Co	57	56	56	55	62
Ni	226	231	244	254	249
C.I.P.W. norm					
Q	0.0	0.0	0.0	0.0	0.0
C	0.0	0.0	0.0	0.0	0.0
Or	9.0	8.0	8.2	7.6	9.1
Ab	12.8	12.0	12.7	12.7	10.6
An	15.7	15.6	16.1	17.3	13.4
Lc	0.0	0.0	0.0	0.0	0.0
Ne	9.1	9.6	8.7	7.3	12.0
Ac	0.0	0.0	0.0	0.0	0.0
Wo(Di)	12.1	12.1	11.9	11.8	12.8
En(Di)	8.4	8.4	8.3	8.3	8.9
Fs(Di)	2.6	2.6	2.6	2.5	2.8
En(Hy)	0.0	0.0	0.0	0.0	0.0
Fs(Hy)	0.0	0.0	0.0	0.0	0.0
Fo	12.8	13.7	13.8	13.8	12.3
Fa	4.4	4.6	4.7	4.7	4.3
Mt	6.0	6.0	6.0	6.0	6.0
Hm	0.0	0.0	0.0	0.0	0.0
Il	5.1	5.0	5.0	5.0	5.0
Ap	1.1	1.1	1.1	1.1	1.2

Table D-1 (continued): Kostal Lake (lava tube)

Sample	29/7/13-KT	31/8/3-KT	31/8/5-KT
Major oxides (wt.%)			
SiO_2	44.34	43.92	44.14
TiO_2	2.62	2.67	2.56
Al_2O_3	13.04	12.85	12.83
Fe_2O_3	4.12	4.17	4.06
FeO	8.56	8.62	8.66
MnO	0.16	0.16	0.16
MgO	10.75	11.15	11.11
CaO	9.44	9.49	9.24
Na_2O	3.77	3.76	3.83
K_2O	1.51	1.49	1.54
P_2O_5	0.54	0.53	0.58
Total	98.85	98.81	98.71
Trace elements (ppm)			
S	124	296	408
Cl	340	354	416
Rb	29	32	34
Sr	681	678	701
Ba	514	513	506
Sc	22	21	21
Y	23	23	21
Zr	231	239	240
Nb	50	49	52
V	172	178	171
Cr	316	351	389
Co	58	56	50
Ni	228	267	282
C.I.P.W. norm			
Q	0.0	0.0	0.0
C	0.0	0.0	0.0
Or	8.9	8.8	9.1
Ab	12.6	11.1	12.0
An	14.2	13.8	13.2
Lc	0.0	0.0	0.0
Ne	10.5	11.2	11.1
Ac	0.0	0.0	0.0
Wo(Di)	12.2	12.5	12.0
En(Di)	8.5	8.8	8.4
Fs(Di)	2.6	2.6	2.6
En(Hy)	0.0	0.0	0.0
Fs(Hy)	0.0	0.0	0.0
Fo	12.9	13.4	13.6
Fa	4.4	4.4	4.6
Mt	6.0	6.0	5.9
Hm	0.0	0.0	0.0
Il	5.0	5.1	4.9
Ap	1.2	1.2	1.3

APPENDIX E

VACUUM FUSION APPARATUS

Construction

The apparatus used to measure the concentrations of H_2O and CO_2 in glass samples is similar to that used by Harris (1981b). The apparatus is shown in Fig.7-1. A vacuum on the order of 10^{-3} Torr is attained using a roughing pump; the vacuum is hardened using a mercury diffusion pump during analysis. A liquid nitrogen-cooled cold trap minimises back-diffusion of mercury vapour into the measuring volume during analysis.

The measuring volume of the apparatus comprises a pyrex tube 34.8 cm^{-3} in volume, isolated by a Kontes valve from a fused quartz sample tube and terminated, at the end furthest from the sample tube, by a Validyne AP20-10 pressure transducer. The latter is connected to a Validyne CD-23 transducer indicator, with output (0-10V) to a chart recorder. Heating of the sample tube is carried out using a Kanthal wire furnace with a Barber-Colman series 120 analogue temperature controller. Care is needed in controlling temperature, because the maximum output of the controller exceeds the maximum current tolerable by the furnace, resulting in failure of the furnace winding.

A second Kontes valve isolates the sample volume from the vacuum system and from a McLeod gauge, the latter used to calibrate the transducer. Save for the two valves in the sample volume, valves in the apparatus are standard bulb-backed stopcocks in the hard vacuum part of the system and simple ground glass stopcocks in the soft vacuum part of the system.

Problems in operation and sources of contamination

System operation originally used the following procedure. Pt sample containers were washed in HF, distilled water and dried in an oven prior to firing at 1 atmosphere in a furnace, at a temperature of 1200°C. Samples were washed in distilled water and dried at 120°C or were polished while mounted on a slide (in Canada balsam), then washed in acetone and distilled water before drying. Pumping after loading the apparatus was at first done with the roughing pump, then with the mercury diffusion pump.

Samples were run at 1200°C.

Initial runs using this method gave impossibly high CO_2 and H_2O values for glass from Pyramid Mountain and from the glass TT-152-21, from the East Pacific Rise. Step heating experiments showed a release of gas from the samples/tubes at 700 to 800°C and another at 1150+°C. Concentrations of noncondensible gases were particularly erratic and high in the latter range of temperature.

Contaminants included oil back-diffusion from the roughing pump, CO_2 escape from the vacuum system cold trap, adsorbed species on the Pt sample containers and (possibly) remnants of balsam on the polished samples. Adsorption of contaminants on to the walls of the measuring volume also occurred. The sources of this contamination were the mercury diffusion pump and the McLeod gauge; back-diffusion of Hg vapour from either source occurred when the measuring volume cold trap was immersed in liquid nitrogen and the sample volume was openles are to the vacuum system.

The high run temperatures caused excessive evolution of noncondensible gas from samples. Sources for the gases were cryptocrystalline oxide phases in the glass, which were reduced upon heating. A second, less significant source may have been reduction of the glass itself. A run temperature of 1100°C greatly reduces the problem.

Present operating procedure of the vacuum fusion system

Preparation and loading of samples

Back-diffusion of mercury vapour, oil and carbon dioxide is minimised by pumping the apparatus only through the cold trap and mercury diffusion pump. For the same reason, the cold trap is completely full at all times when a sample is in the apparatus. Samples are kept at 120°C prior to analysis and platinum sample containers are vacuum-fired immediately prior to an analytical run.

Sample containers are washed in HF and in distilled water, then dried in an oven at 120°C. Samples, after treatment, are similarly dried, at least overnight, then weighed using the Cahn balance with a calibration weight of 927.10^{-6} gm and returned to the oven. Fused quartz sample tubes are washed with reagent grade acetone, distilled water, HCl and distilled water, dried and fired to 1200°C in a furnace. The sample containers are then loaded into the sample tube, sealed to the apparatus, pumped down and fired *in vacuo* until an acceptably low volume of gas is evolved over a 6 minute heating period. The valve isolating the sample volume is then closed prior to removal of the furnace and the sample containers are allowed to cool *in vacuo* **without exposure to the pumping system.** This last is most important, given the problems with back-diffusion. The sample containers are brought up to atmospheric pressure and loaded with the samples, leaving one empty as a blank. The containers are reloaded into the tube with a magnetic steel clip for manoeuvring them and the sample tube is pumped down. Loading is carried out as quickly as possible.

Contamination of the platinum containers causes abnormally high blanks, for CO_2 particularly; a different technique is therefore used for small glass samples. This method is preferred for all save powdered samples because it enables the platinum lining of the tube to be fired *in vacuo* before and after a sample is run. A boat of platinum foil is loaded into the sample tube and remains in the fusion zone of the quartz sample tube throughout a set of analytical runs. Samples are prepared as described above but are loaded without the platinum boats, with a steel clip for manoeuvring them within the sample tube. During pre-heating, the glass samples remain in that part of the tube not being heated and the platinum foil is heated to 1200°C while pumping with Valve 2 open. After pre-heating, Valve 2 is closed **prior to removing the furnace** and the foil is allowed to cool without exposure to the pumping system. Blanks can be run, using this technique, before each sample is fused.

Analytical procedure

Each blank is measured in the following manner. The furnace is removed after pre-heating and the tube allowed to cool. The steel clip is then moved up the tube to the platinum foil as if it are pushing a glass sample, then returned to the "cold" end of the tube. The blank is measured after collection for 6 minutes at a fusion temperature of 1100°C. The gas evolved is then pumped out while the platinum foil is further heated to a temperature of 1200°C, to drive off any adsorbed volatiles.

A schematic diagram of the chart from a vacuum fusion run is presented in Fig.51. Samples are fused for 6 minutes at 1100°C if basalt. The sample volume is isolated during this period and the "U-bend" immersed in liquid nitrogen. At the end of the heating period, the measuring volume is isolated from the sample tube by closing Valve 1. The furnace removed and the U-bend is immersed in warm water. The temperature of the water is not crucial, so long as the measuring volume is brought quickly to room temperature. Two pressure peaks are often observed, the first representing the pressure peak of the water at its sublimation temperature, the second representing later thermal expansion. Adsorbtion is sufficiently rapid as to facilitate recognition of the first peak. The U-bend is then dried and re-immersed in liquid nitrogen.

Removal of the nitrogen and gradual warming in air suffices to identify the plateaux in pressure caused by CO_2 and the sulphur species H_2S and SO_2. For greater precision in measuring the transducer output, the chart recorder output is connected in parallel to a digital voltmeter; this is useful for small specimens or for low volatile contents. At the end of a fusion the U-bend is re-immersed in liquid nitrogen, both valves opened and the partial pressure of noncondensible gas is measured. The sample volume is then pumped out in preparation for the next sample, as described above.

Calibration of the transducer is carried out *after every run* using the McLeod gauge; at least six data points are accumulated while pumping down the sample tube after exposure to air. In a high turnover, it is convenient to combine calibration of the previous run with insertion of empty sample containers for firing, prior to the next run. Conversion of the transducer measurements to pressures and thence to molar quantities of gases is conducted using the program VACIII, compiled by the author. The program includes a routine for calculating weight percentages. Errors calculated by the program are based on a plus or minus 0.5 mm error in measurements on the McLeod gauge and on a plus or minus 0.002% error in reading the transducer indicator (in this case a digital voltmeter). Errors incurred in reading the lab temperature (plusminus 0.5°C) have a negligible effect on the measured error and are neglected. Errors incurred during weighing are treated as normal standard errors and are included in the error measurement.